
**Long Term Assessment of Dams Suffering from Alkali
Aggregate Reaction;
State of the Art Review**

COOPERATIVE AGREEMENT No. R18AC00055

JULY 29, 2020

MOHAMMAD AMIN HARIRI-ARDEBILI
VICTOR E. SAOUMA
University of Colorado, Boulder

Contents

1	Introduction	2
1.1	Document Preparation	2
1.2	Script tools	4
1.3	Creation of Web Site Based Search Engine	6
1.3.1	Introduction	6
1.4	Requirements	6
1.4.1	Install Instructions	6
1.4.2	Usage Instructions	7
1.4.2.1	Log in	7
1.4.2.2	Search	7
1.4.2.3	Visualization	9
1.4.2.4	PDF Publication and PDF Summaries	9
1.4.2.5	Publication URL	9
1.4.2.6	Register User	9
1.4.2.7	User Management	9
1.4.2.8	Adding Documents to the Search Engine	9
1.4.3	Technical Document	9
1.4.3.1	Overall Flow	9
1.4.3.2	Python Backend	11
1.4.3.3	ElasticSearch Backend	12
1.4.3.4	Web Frontend	13
2	Cross-References	15
2.1	Laboratory	15
2.2	Field	15
2.3	Cylinder	16
2.4	Blocks	17
2.5	Other	18
2.6	Expansion Assessment/monitoring	18
2.7	Reinforcement	22
2.8	Confined	23
2.9	Det. E	23
2.10	Det f't	25
2.11	Det f'c	25
2.12	Det Gf	26
2.13	Det K	26
2.14	Det. V	26

2.15	Det Bond	26
2.16	Quantified	26
2.17	Crack Index	27
2.18	Damage Rating Index	27
2.19	Petrography	28
2.20	Creep	29
2.21	Shrinkage	29
2.22	Temp 38oC (100oF)	29
2.23	Temp higher than 38	30
2.24	Capacity curve	30
2.25	Aggregate Grain size	31
2.26	SEM	32
2.27	Fiber reinforced polymer	32
2.28	Acoustic spectroscopy	32
2.29	Rehabilitation	32
2.30	Freeze-thaw	33
2.31	Radiation damage	33
2.32	Non Destructive Evaluation	33
2.33	Diagnosis	33
2.34	Performance testing	34
2.35	Micro	34
2.36	Meso	34
2.37	Mega	34
2.38	Multi scale	35
2.39	New constitutive model	35
2.40	Nonlinear	36
2.41	Coupled	37
2.42	Plasticity	37
2.43	Damage Mechanics	38
2.44	XFEM	38
2.45	Thermal analysis	38
2.46	Moisture analysis	39
2.47	Seismic	39
2.48	Sensitivity	40
2.49	Uncertainty	40
2.50	Parametric	40
2.51	Prognosis	40
2.52	Mathematical	41
2.53	Finite Element	42
2.54	Thermal equival.	44
2.55	Kinetic modeled	44
2.56	Literture survey	44
2.57	Poro-Mechanics	44
2.58	Chemical reaction	44
2.59	Petrography	45
2.60	Leaching	45
2.61	Gel	45
2.62	Fed-Agencies Reports	46

2.63	None	46
2.64	Gravity dam	46
2.65	Arch dam	48
2.66	Buttress dam	49
2.67	Buildings	49
2.68	Bridge	49
2.69	Nuclear power plants	50
2.70	Roads	50
2.71	Reclamation	50
2.72	ICAAR	50
2.73	Beams-Panels	50
2.74	Intake tower	51
2.75	Slot Cutting	51
2.76	Dams	51
2.77	Historical	51
3	References	52
3.1	Alnaggar, Mohammed and Cusatis, Gianluca and Di Luzio, Giovanni (2013)	52
3.2	Amberg, Francesco (2011)	56
3.3	Amberg, F (2012)	58
3.4	Amberg, F and Stucchi, R and Brizzo, N (2013)	61
3.5	Amberg, Francesco and Bremen, Roger and Droz, Patrice and Leroy, Raphaël and Maier, Johannes and Otto, Bastian (2017)	64
3.6	Nik-Azizan, N.Z. and Mandal, A. and Majid, T.A. and Maity, D. and Nazri, F.M. (2017)	65
3.7	Bach, Finn and Thorsen, Torsten S and Nielsen, MP (1993)	67
3.8	Bangert, F and Kuhl, D and Meschke, G (2004)	70
3.9	Batista, António Lopes and Piteira Gomes, J (2016)	72
3.10	Berube, Marc-Andre and Frenette, Jean and Pedneault, Annie and Rivest, Michel (2002)	74
3.11	Bérubé, Marc-André and Duchesne, J and Dorion, JF and Rivest, M (2002)	79
3.12	Bérubé, Marc-André and Smaoui, Nizar and Fournier, Benoit and Bissonnette, Benoit and Durand, Benoit (2005)	82
3.13	Blanco, A and Cavalaro, SHP and Segura, I and Segura-Castillo, L and Aguado, A (2018)	83
3.14	BOR (1941)	87
3.15	Capra, B and Bournazel, J-P (1998)	87
3.16	Capra, Bruno and Sellier, Alain (2003)	88
3.17	Carles-Gibergues, André and Cyr, Martin (2002)	89
3.18	Chen, Jun and Jayapalan, Amal R and Kim, Jin-Yeon and Kurtis, Kimberly E and Jacobs, Laurence J (2010)	91
3.19	Cima, J. and Reinicker, B. (year=2015)	92
3.20	Comby-Peyrot, Isabelle and Bernard, Fabrice and Bouchard, Pierre-Olivier and Bay, François and Garcia-Diaz, Eric (2009)	94
3.21	Comi, C and Fedele, R and Perego, U (2009)	95
3.22	Comi, Claudia and Kirchmayr, Beatrice and Pignatelli, Rossella (2012)	98
3.23	Coubard, G. and Sausse, J. (2017)	101
3.24	Criaud, A and Defossé, C (1995)	102

3.25	Crouch, RS and Wood, JGM (1990)	105
3.26	Chulliat, O. and Grimal, E. and Bourdarot, E. (2017)	106
3.27	Curtis, DD (1995)	109
3.28	Curtis, D. and Davis, B. and Rahman, S. and Powell, R. (2005)	111
3.29	Custódio, j. and Ferreira, j. and Silva, A. and Ribeiro, A.B. and Batista, A. (2017)	113
3.30	Diamond, S and Thaulow, N (1974)	115
3.31	Dolen, T. (2005)	116
3.32	Dolen, TP (2011)	120
3.33	Donghi, G. and Marcello, C. and Sainati, F. (year=2013)	123
3.34	Dunant, Cyrille F and Scrivener, Karen L (2010)	125
3.35	Dunant, Cyrille F and Scrivener, Karen L (2012)	126
3.36	Dunant, Cyrille F and Scrivener, Karen L (2012)	128
3.37	Dunant, Cyrille F and Scrivener, Karen L (2016)	130
3.38	Esposito, Rita and Anaç, Caner and Hendriks, Max AN and Çopuroğlu, Oğuzhan (2016)	130
3.39	Esposito, Rita and Hendriks, Max AN (2016)	135
3.40	Esposito, R and Hendriks, MAN (2017)	139
3.41	Fairbairn, Eduardo MR and Ribeiro, Fernando LB and Lopes, Luciana E and Toledo-Filho, Romildo D and Silvano, Marcos M (2006)	142
3.42	Fan, Shenfu and Hanson, John M (1998)	143
3.43	Ferche, Anca C and Panesar, Daman K and Sheikh, Shamim A and Vecchio, Frank J (2017)	145
3.44	Fernandes, Isabel and Noronha, Fernando and Teles, Madalena (2004)	147
3.45	Fernandes, Isabel and Noronha, Fernando and Teles, Madalena (2007)	148
3.46	Ferreira, Anna Paula Guida and Farage, Michèle Cristina Resende and Barbosa, Flávio de Souza (2013)	150
3.47	FHWA (2010)	151
3.48	FHWA (2013)	152
3.49	Fournier, Benoit and Bérubé, Marc-André (2000)	152
3.50	Fournier, Benoit and Ideker, Jason H and Folliard, Kevin J and Thomas, Michael DA and Nkinamubanzi, Pierre-Claver and Chevrier, Ray (2009)	156
3.51	Gao, Xiao Xiao and Multon, Stéphane and Cyr, Martin and Sellier, Alain (2011)	157
3.52	Gao, XX and Cyr, M and Multon, S and Sellier, A (2013)	159
3.53	Gao, XX and Cyr, M and Multon, S and Sellier, A (2013)	159
3.54	Gao, Xiao Xiao and Cyr, Martin and Multon, Stéphane and Sellier, Alain (2013)	160
3.55	Garcia-Diaz, E and Riche, J and Bulteel, D and Vernet, C (2006)	163
3.56	Gautam, Bishnu P and Panesar, Daman K (2017)	164
3.57	Gholizadeh-Vayghan, Asghar and Rajabipour, Farshad (2017)	168
3.58	Giaccio, G and Zerbino, R and Ponce, JM and Batic, Oscar R (2008)	169
3.59	Giorla, Alain B and Scrivener, Karen L and Dunant, Cyrille F (2015)	173
3.60	Gocevski, V. and Yildiz, E. (2017)	175
3.61	Godart, B and Mahut, B and Fasseu, P and Michel, M (2004)	179
3.62	Godart, Bruno and de Rooij, Mario Robert and Wood, Jonathan GM (2013)	179
3.63	Gong, Fuyuan and Takahashi, Yuya and Maekawa, Koichi (2017)	181
3.64	Grimal, 'Etienne and Sellier, Alain and Le Pape, Yann and Bourdarot, 'Eric (2008)	183
3.65	Guilloteau, T. and Martinot, F. and Sausse, J. (2017)	184
3.66	Gunn, R. and Scrivener, K. and Leemann, A. (2017)	186

3.67	Haha, M Ben and Gallucci, Emmanuel and Guidoum, Amor and Scrivener, Karen L (2007)	189
3.68	Hariri-Ardebili, Mohammad Amin and Saouma, Victor E and Merz, Christine (2018)	190
3.69	Hariri-Ardebili, Mohammad Amin and Saouma, Victor E (2018)	193
3.70	Hattingh, L. and Oosthuizen, C. and Tembe, I. and Mahlabela, C. (2017)	195
3.71	Hayes, Nolan Wesley and Gui, Qiang and Abd-Elssamd, Ammar and Le Pape, Yann and Giorla, Alain Benjamin and Le Pape, Sihem and Giannini, Eric R and Ma, Zhongguo John (2018)	197
3.72	Hefny, A and Lo, KY and Adeghe, L (2001)	199
3.73	Heidarzadeh, N and Samadzad, M and Shekarchi, M and Mirghaderi, SR (2017)	199
3.74	Helene, Paulo and Carvalho, Mariana and Pacheco, Jéssika (2017)	200
3.75	Herrador, Manuel F and Martínez-Abella, Fernando and Dopico, Juan Ramón Rabuñal (2008)	202
3.76	Huang, M and Pietruszczak, S (1996)	203
3.77	Huang, Maosong and Pietruszczak, S (1999)	205
3.78	Huang, H and Spencer, BW and Cai, G (2015)	208
3.79	Huang, Hai and Spencer, Benjamin W (2016)	209
3.80	Ichikawa, Tsuneki and Kimura, Takahide (2007)	210
3.81	Islam, Mohammad S and Ghafoori, Nader (2015)	212
3.82	Jensen, Viggo (2004)	214
3.83	Jensen, Viggo (2012)	216
3.84	Ju, Taeho and Achenbach, Jan D and Jacobs, Laurence J and Guimaraes, Maria and Qu, Jianmin (2017)	219
3.85	Kagimoto, Hiroyuki and Yasuda, Yukihiro and Kawamura, Mitsunori (2014)	220
3.86	Kobayashi, Kazuo and Inoue, Susumu and Yamasaki, Takao and Nakano, Kin-ichi (1988)	222
3.87	Kubat, Thamer and Al-Mahaidi, Riadh and Shayan, Ahmad (2016)	223
3.88	Lamea, M and Mirzabozorg, H (2015)	224
3.89	author="Lancon, H. and Piot, S. (2011)	226
3.90	Leemann, Andreas and Merz, Christine (2013)	227
3.91	Leemann, Andreas and Griffa, Michele (2013)	228
3.92	Leemann, A and Lura, P (2013)	229
3.93	author="Leroy, R. and Boldea, L.I. and Seignol, J.F. and Godart, B. (2011)	230
3.94	Leśnicki, Krzysztof J and Kim, Jin-Yeon and Kurtis, Kimberly E and Jacobs, Laurence J (2011)	233
3.95	Leśnicki, Krzysztof J and Kim, Jin-Yeon and Kurtis, Kimberly E and Jacobs, Laurence J (2013)	235
3.96	Liaudat, Joaquín and Martínez, A and López, CM and Carol, Ignacio (2015)	236
3.97	Liaudat, Joaquín and Carol, Ignacio and López, Carlos M and Saouma, Victor E (2017)	237
3.98	Lindgård, Jan and Nixon, Philip J and Borchers, Ingmar and Schouenborg, Björn and Wigum, Børge Johannes and Haugen, Marit and Åkesson, Urban (2010)	240
3.99	Lindgård, Jan and Andiç-Çakır, Özge and Fernandes, Isabel and Rønning, Terje F and Thomas, Michael DA (2012)	242
3.100	Lindgård, Jan and Sellevold, Erik J and Thomas, Michael DA and Pedersen, Bård and Justnes, Harald and Rønning, Terje F (2013)	245
3.101	Lindgård, Jan and Thomas, Michael DA and Sellevold, Erik J and Pedersen, Bård and Andiç-Çakır, Özge and Justnes, Harald and Rønning, Terje F (2013)	248

3.102Liu, Kai-Wei and Mukhopadhyay, Anol K (2015)	254
3.103Lu, Duyou and Zhou, Xiaoling and Xu, Zhongzi and Lan, Xianghui and Tang, Mingshu and Fournier, Benoit (2006)	255
3.104Marzouk, H and Langdon, S (2003)	255
3.105Merz, Christine and Leemann, Andreas (2013)	258
3.106Metalsi, Othman Omikrine and Seignol, Jean-François and Rigobert, Stéphane and Toutlemonde, François (2014)	260
3.107Miyagawa, Toyoaki and Seto, Kaoru and Sasaki, Kazunori and Mikata, Yasuhiro and Kuzume, Kazuhiro and Minami, Toshikazu (2006)	263
3.108Moranville-Regourd, Michelle (1997)	265
3.109Morenon, Pierre and Multon, Stéphane and Sellier, Alain and Grimal, Etienne and Hamon, François and Bourdarot, Eric (2017)	266
3.110Morenon, P. and Grimal, E. and Kolayer, P. and Sellier, A. and Multon, S. (year=2018)	269
3.111Mukhopadhyay, Anal and Shon, Chang-Seon and Zollinger, Dan (2006)	272
3.112Mullick, AK (1988)	273
3.113Multon, S and Seignol, J-F and Toutlemonde, F (2005)	274
3.114Multon, Stéphane and Seignol, Jean-François and Toutlemonde, François (2006)	276
3.115Multon, Stéphane and Toutlemonde, François (2006)	277
3.116Multon, Stéphane and Cyr, Martin and Sellier, Alain and Leklou, Nordine and Petit, Laurent (2008)	280
3.117Multon, Stéphane and Barin, François-Xavier and Godart, Bruno and Toutlemonde, François (2008)	282
3.118Multon, Stéphane and Sellier, Alain and Cyr, Martin (2009)	283
3.119Multon, Stéphane and Cyr, Martin and Sellier, Alain and Diederich, Paco and Petit, Laurent (2010)	284
3.120Na, Okpin and Xi, Yunping and Ou, Edward and Saouma, Victor E (2016)	285
3.121Noret, C. and Laliche, K. (2017)	287
3.122Orbovic, N. and Panesar, D. and Sheikh, S. and Vecchio, F. and Lamarche, C.P. and Blahoianu, A. (2015)	288
3.123Ostertag, Claudia P and Yi, ChongKu and Monteiro, Paulo JM (2007)	290
3.124Pan, JW and Feng, YT and Wang, JT and Sun, QC and Zhang, CH and Owen, DRJ (2012)	290
3.125Pan, JianWen and Feng, YunTian and Xu, YanJie and Jin, Feng and Zhang, ChuHan and Zhang, BingYin (2013)	291
3.126Pan, Jianwen and Feng, YT and Jin, Feng and Zhang, Chuhan (2013)	294
3.127Parvini, M and Pietruszczak, S and Gocevski, V (2001)	296
3.128Plusquellec, G and Geiker, MR and Lindgård, J and De Weerd, K (2018)	298
3.129Poyet, Stéphane and Sellier, Alain and Capra, Bruno and Thèvenin-Foray, Geneviève and Torrenti, Jean-Michel and Tournier-Cognon, Hélène and Bourdarot, Eric (2006)	300
3.130Rajabipour, Farshad and Giannini, Eric and Dunant, Cyrille and Ideker, Jason H and Thomas, Michael DA (2015)	302
3.131Reinicker, B. and Duke, W. and Cima, J. and Charlwood, R. (2010)	304
3.132Reinicker, B. and Abedzadeh, F. and Charlwood, R. and Cima, J. (2013)	306
3.133Rivard, Patrice and Fournier, Benoit and Ballivy, Gérard (2000)	307
3.134Rivard, Patrice and Fournier, Benoit and Ballivy, Gérard (2002)	308
3.135Rivard, Patrice and Saint-Pierre, François (2009)	309
3.136Rivard, Patrice and Ballivy, Gérard and Gravel, Clermont and Saint-Pierre, Francois (2010)	311

3.137	Sanchez, LFM and Fournier, B and Jolin, M and Bastien, J (2014)	313
3.138	Sanchez, LFM and Fournier, B and Jolin, M and Bastien, J (2015)	315
3.139	Sanchez, LFM and Fournier, B and Jolin, M and Duchesne, Josée (2015)	316
3.140	Sanchez, LFM and Fournier, B and Jolin, M and Bastien, J and Mitchell, D (2016)	320
3.141	Sanchez, LFM and Fournier, B and Jolin, M and Bedoya, MAB and Bastien, J and Duchesne, J (2016)	321
3.142	Sanchez, LFM and Fournier, B and Jolin, M and Mitchell, D and Bastien, J (2017)	324
3.143	Saouma, Victor and Perotti, Luigi (2006)	325
3.144	Saouma, Victor and Perotti, Luigi and Shimpo, Takashi (2007)	327
3.145	Saouma, Victor E and Hariri-Ardebili, Mohammad A (2014)	332
3.146	Saouma, Victor E and Martin, Ruth A and Hariri-Ardebili, Mohammad A and Katayama, Tetsuya (2015)	333
3.147	Saouma, Victor E and Hariri-Ardebili, Mohammad Amin and Le Pape, Yann and Balaji, Rajagopalan (2016)	335
3.148	Sargolzhahi, Maryam and Kodjo, Serge A and Rivard, Patrice and Rhazi, Jamal (2010)	338
3.149	Sausse, J and Fabre, JP (2011)	339
3.150	Sbarigia, M. and Zinetti, F. and Maugliani, V. and Palmitelli, G. and Mazzolani, S. (2013)	341
3.151	Sbarigia, M and Zinetti, F and Hernandez-Bagaglia, M (2016)	342
3.152	author="Scuero, A. and Vaschetti, G. (2011)	344
3.153	Seignol, Jean François and Godart, Bruno (2012)	345
3.154	Sellier, Alain and Bourdarot, Eric and Multon, Stéphane and Cyr, Martin and Grimal, Etienne (2009)	347
3.155	Shayan, Ahmad and Grimstad, Jack (2006)	350
3.156	Shayan, Ahmad (2016)	351
3.157	Helmuth, R. and Stark, D. and Diamond, S. and Moranville-Regourd, M. (2013)	352
3.158	Siegert, D and Multon, S and Toutlemonde, F (2005)	353
3.159	Smaoui, Nizar and Bérubé, Marc-André and Fournier, Benoit and Bissonnette, Benoit and Durand, Benoit (2004)	355
3.160	Smaoui, Nizar and Fournier, Benoit and Bérubé, Marc-André and Bissonnette, Benoit and Durand, Benoit (2004)	358
3.161	Smaoui, Nizar and Bérubé, Marc-André and Fournier, Benoit and Bissonnette, Benoit (2004)	361
3.162	Smaoui, N and Bérubé, MA and Fournier, Benoit and Bissonnette, B and Durand, B (2005)	363
3.163	Stanton, Thomas E (2008)	365
3.164	Steffens, Alexander and Li, Kefei and Coussy, Olivier (2003)	366
3.165	Swamy, RN and Al-Asali, MM (1986)	368
3.166	Swamy, R Narayan and Wan, WM Raymond (1993)	369
3.167	Takakura, Takeo and Masuda, Hirotaka and Murazumi, Yasuyuki and Takiguchi, Katsuki and Masuda, Yoshihiro and Nishiguchi, Isoharu (2007)	371
3.168	Talley, Kimberly G and Kapitan, Jacob G and Breen, John E (2016)	372
3.169	Tcherner, Julia and Aziz, T (2009)	374
3.170	Torii, Kazuyuki and Kubo, Tetsuji and Sannoh, Chikao and Kanitani, Maki (2016)	375
3.171	Ulm, Franz-Josef and Coussy, Olivier and Kefei, Li and Larive, Catherine (2000)	376
3.172	Šachlová, Šárka and Prikryl, Richard and Pertold, Zdeněk (2010)	379
3.173	Wald, David M and Allford, Morgan T and Bayrak, Oguzhan and Hrynyk, Trevor D (2017)	380

3.174	Wald, David and Martinez, Gloriana Arrieta and Bayrak, Oguzhan (2017)	382
3.175	Wallau, Wilma and Pirskawetz, Stephan and Volland, Katja and Meng, Birgit (2018)	384
3.176	Wang, Jian and Morikawa, Hidenori (2012)	386
3.177	Winnicki, Andrzej and Serkega, Szymon (2017)	387
3.178	Yang, Huaquan and Li, Pengxiang and Rao, Meijuan (2017)	389
3.179	Zhang, Chengzhi and Wang, Aiqin and Tang, Mingshu and Wu, Bingqin and Zhang, Ningsheng (1999)	390

List of Figures

1.1	Document preparation procedure	3
1.2	List of Keywords	4
1.3	Sample of a BibTeX entry	5
1.4	Sample entries in Bib-List.xlsx	5
1.5	Preliminaries	8
1.6	Bubbles	10
1.7	Registration Form	11
1.8	Request Access Form	11
1.9	User Management Panel	12
1.10	Search Engine Management	12
1.11	PyDocSen Flow	14
3.1	Axial strain evolution for: (a) Unrestrained specimens under 0 MPa, (b) Unrestrained specimens under 10 MPa, (c) Unrestrained specimens under 20 MPa, (d) 3-mm-Restrained specimens under 0 MPa, (e) 3-mm-Restrained specimens under 10 MPa, (f) 3-mm-Restrained specimens under 20 MPa, (g) 5-mm-Restrained specimens under 0 MPa, (h) 5-mm-Restrained specimens under 10 MPa, (i) 5-mm-Restrained specimens under 20 MPa	54
3.2	Radial strain evolution for: (a) Unrestrained specimens under 0 MPa, (b) Unrestrained specimens under 10 MPa, (c) Unrestrained specimens under 20 MPa, (d) 3-mm-Restrained specimens under 0 MPa, (e) 3-mm-Restrained specimens under 10 MPa, (f) 3-mm-Restrained specimens under 20 MPa, (g) 5-mm-Restrained specimens under 0 MPa, (h) 5-mm-Restrained specimens under 10 MPa, and (i) 5-mm-Restrained specimens under 20 MPa	55
3.3	All the studied dams; Amberg (2012)	60
3.4	Variation of static equilibrium due to internal expansion; Amberg (2012)	61
3.5	Volumetric expansion applied to the model; Amberg, Stucchi, and Brizzo (2013)	63
3.6	Calculated concrete expansion distribution at 2008; Amberg, Stucchi, and Brizzo (2013)	63
3.7	Computed closure of a slot during cutting; Amberg, Stucchi, and Brizzo (2013)	64
3.8	insert; Amberg et al. (2017)	65
3.9	Comparison on crest displacement; Nik-Azizan et al. (2017)	67
3.10	Maximum major principal stresses contour based on (Washa, Saemann, and Cramer, 1989); Nik-Azizan et al. (2017)	67
3.11	Characteristics of the test specimen; Bach, Thorsen, and Nielsen (1993)	69

3.12	Numerical simulation of a concrete beam affected by the ASR, columns left to right: distribution of the liquid saturation, the expansion rate, the expansion, and the damage parameter; Bangert, Kuhl, and Meschke (2004)	71
3.13	Numerical simulation of a concrete beam affected by the ASR, columns left to right: distribution of the liquid saturation, the expansion rate, the expansion, and the damage parameter; Bangert, Kuhl, and Meschke (2004)	72
3.14	Portuguese dams built with granite aggregates and affected by AAR; Batista and Piteira Gomes (2016)	74
3.15	Portuguese dams built with granite aggregates and affected by AAR; Average values of the monitored free strains by the stress-free Carlson strain-meters and strains obtained from geodetic leveling; Batista and Piteira Gomes (2016)	74
3.16	Laboratory assessment of the potential rate of ASR expansion members in service either already affected by ASR or not	77
3.17	Dams investigated, soluble alkali content, and estimated contributions by aggregates; Bérubé et al. (2002)	80
3.18	Dams investigated, soluble alkali content, and estimated contributions by aggregates; Bérubé et al. (2002)	81
3.19	Observed damages: (a) cracks in downstream face, (b) crack of upstream face, (c) cracks of strainway and loos of concrete, (d) corrosion of rebars, (e) erosion in diaphragm, (f) cracks in diaphragms, and (g) map cracking in the retaining walls of the dike; Blanco et al. (2018)	84
3.20	Maximum temperature reached in each point; Blanco et al. (2018)	85
3.21	Finite element analysis: (a) real crack pattern, (b) stresses in the diaphragm, and (c) crack pattern of the model; Blanco et al. (2018)	86
3.22	Details of the cores; Blanco et al. (2018)	86
3.23	Expansion in terms of R	88
3.24	Results of numerical simulations by Capra and Sellier (2003)	89
3.25	Typical expansion curves of concretes affected by AAR. X: visible part of expansion characterized by phenomenon independent of AAR	91
3.26	Results of AASHTO T 303 expansion and elastic modulus measurements; Chen et al. (2010)	92
3.27	Finite element model and calibration; Cima and Reinicker (2015)	93
3.28	Numerical simulation of a concrete cube affected by ASR, left: undamaged cut, right: 3D damaged pattern; Comby-Peyrot et al. (2009)	95
3.29	Evolution of the homogenized Young's modulus according to skeleton expansion; Comby-Peyrot et al. (2009)	95
3.30	Fontana Dam, left abutment: views of the cracked surface (a discontinuity in water flow pattern can be noticed in the photo) and inside the inspection gallery (after Ingraffea (1990)); Comi, Fedele, and Perego (2009)	96
3.31	Reaction extent and damage during AAR development; Comi, Fedele, and Perego (2009)	97
3.32	Reaction extent and damage during AAR development; Comi, Fedele, and Perego (2009)	98
3.33	Pattern of different quantities in the beam; Comi, Kirchmayr, and Pignatelli (2012)	99
3.34	Patterns of the reaction extent and damage after (a) 3, (b) 6 and (c) 60 years; Comi, Kirchmayr, and Pignatelli (2012)	100

3.35	Linear model and nonlinear model with concrete-to-rock joint on a swelling arch dam with thrust blocks; Stress reorientation and modification on the upstream face; Coubard and Sausse (2017)	102
3.36	Experimental results	104
3.37	Comparing the stiffness of cracked and uncracked specimen; Crouch and Wood (1990)	105
3.38	Comparison of measured and computed deformations in 3D modeling; Chulliat, Grimal, and Bourdarot (2017)	107
3.39	The tendons pattern (red) and drainage curtain seen from downstream; Chulliat, Grimal, and Bourdarot (2017)	108
3.40	The carbon fiber net seen from upstream; Chulliat, Grimal, and Bourdarot (2017)	108
3.41	Finite element models; Curtis (1995)	110
3.42	FE model and calibration results; Curtis et al. (2005)	112
3.43	Local spillway pier model mesh including trunnion pin and anchorage steel plate mesh; Curtis et al. (2005)	113
3.44	Miranda Dam: Results of quantitative analysis of vertical displacements at the top of the central buttress, obtained from geodetic leveling, between 1963 and 2014; Custódio et al. (2017)	114
3.45	Mechanical properties of different core samplings; Custódio et al. (2017)	115
3.46	Comparison of strength with modulus of elasticity in compression for mass concrete dams both with and without ASR	119
3.47	Comparison of the effects of aging and ASR on the tensile strength of mass concrete dams	119
3.48	Moving average of estimated percent bonded lift lines for mass concrete dams constructed from 1905 to 1993; Dolen (2011)	121
3.49	Estimate of percent bonded lift lines observed from drilled cores of Bureau of Reclamation concrete dams; Dolen (2011)	121
3.50	Direct tensile strength of parent mass concrete and bonded lift lines with and without AAR; Dolen (2011)	122
3.51	Direct shear, “break-bond”, and sliding friction properties of AAR affected lift lines and comparable unaffected mass concrete, 1925 to 1938; Dolen (2011)	122
3.52	Weighted average compressive strength and elastic properties of mass concrete, 1905 to 1993, and with or without alkali aggregate reaction, 1925 to 1938; Dolen (2011)	123
3.53	Sectional elevation, cross-section, and horizontal section of the Dam; Donghi, Marcello, and Sainati (2013)	124
3.54	Finite element model; Donghi, Marcello, and Sainati (2013)	124
3.55	Proposed model based on Dunant and Scrivener (2010)	126
3.56	Crack pattern of a numerical sample with a single inclusion in unloaded and loaded conditions. The cracks are mainly in the paste (dark grey), which is in tension as there are no other expanding aggregates to keep it in compression. The aggregate (light grey) is partly cracked around the gel pockets, from tension and also from cracks which propagated from the paste; Dunant and Scrivener (2012b)	128
3.57	Montage of the progressive formation of a crack network in a single inclusion. States at the bottom right show cracked paste; Dunant and Scrivener (2012a)	129
3.58	Results by Esposito et al. (2016)	133
3.59	Results by Esposito et al. (2016)	134
3.60	Experimental Results and Calculated Reference Values for Normalization Procedure; Esposito et al. (2016)	136
3.61	Variation of expansion dependent mechanical properties; Esposito et al. (2016)	136

3.62	Experimental data from the literature; a nonuniform scale for the expansion axis is used; Esposito et al. (2016)	137
3.63	Fitting adopting S-shaped curve (left column) and fitting adopting piecewise linear curve (right column); Esposito et al. (2016)	138
3.64	Overview of modelling approaches for ASR in concrete.	140
3.65	Models based on concrete expansion	141
3.66	Results for the ASR simulation: gel pressure for 40 years and the displacements at the crest of the dam; Fairbairn et al. (2006)	143
3.67	Comparison of cracking between; Fan and Hanson (1998)	144
3.68	Change in mechanical properties of reactive cylinders with ASR expansion; Fan and Hanson (1998)	145
3.69	Results of flexural loading tests; Fan and Hanson (1998)	145
3.70	Load-deformation responses of Fan and Hanson (1998) beam specimens; Ferche et al. (2017)	146
3.71	Different types of exudations from the top-level gallery. In the left panel, translucent droplets are present in the exudation; Fernandes, Noronha, and Teles (2004)	148
3.72	Schematic of the Alto Rabagao in Portugal (left); Concrete abutments (right); Fernandes, Noronha, and Teles (2007)	149
3.73	Gel pressure evolution in the concrete wall via the uncoupled (above) and the coupled (below) models; Ferreira, Farage, and Barbosa (2013)	151
3.74	Summer and winter relative humidity profiles in a bridge column exposed to arid desertic climate (from Stark 1990).	153
3.75	Effect of compressive stress on expansion due. to AAR (from ISE 1992)..	154
3.76	Field symptoms of AAR: (a) Severe spalling of a 20-year old median highway barrier under expansive thrust due to ASR; (b) relative movement of concrete pier caused by the expansive forces generated by the adjacent concrete section affected by ASR; (c) map-cracking in a wingwall of a 30-year old railway bridge affected by ASR; (d) longitudinal cracks on the edge of the deck and in the columns of a 20-year old highway bridge severely affected by ASR; (e) map-cracking due to AAR affecting the parapet wall of a 25 year-old highway.structure; (j) exudations of alkali-silica gel and efflorescence at the surface of a concrete foundation affected by ASR.	155
3.77	ASR expansions on prismatic specimens with siliceous limestone aggregate kept in NaOH solution; Gao et al. (2011)	158
3.78	Cracking patterns of specimens cast with siliceous limestone; Gao et al. (2011)	158
3.79	Three-step method for the recovery of aggregates and overall efficiency (for aggregate SL).; Gao et al. (2013a)	163
3.80	Schematic subdivision of the swelling curve; Garcia-Diaz et al. (2006)	164
3.81	DRI value versus longitudinal expansion for the reactive prisms in CPT and ACPT; Gautam and Panesar (2017)	165
3.82	Longitudinal expansion of concrete prisms in CPT and ACPT, original scales (left), different time scales (middle), and days required by reactive prisms in CPT and ACPT for identical expansion (right); Gautam and Panesar (2017)	166
3.83	Variation in dynamic modulus of elasticity of concrete over time using different time scales; Gautam and Panesar (2017)	167
3.84	Variation in modulus of rupture of concrete prism specimens over time using different time scales; Gautam and Panesar (2017)	168
3.85	Graphical demonstration of RSM data point selection for the 3 variables case ($\alpha = 1.682$); Gholizadeh-Vayghan and Rajabipour (2017)	169

3.86	Compression test results; Giaccio et al. (2008)	171
3.87	Results of flexural loading tests; Giaccio et al. (2008)	171
3.88	Variation of modulus of elasticity with age and expansion; Giaccio et al. (2008)	172
3.89	Variation of compressive strength with age and expansion; Giaccio et al. (2008)	172
3.90	Variation of the energy of fracture and characteristic length with age and expansion; Giaccio et al. (2008)	173
3.91	Microstructure and boundary conditions for the ASR simulation (dimensions in mm). Gel pockets are not represented. Grey level indicates the stiffness of the elements. The contrast has been enhanced in the mesh detail to highlight the distribution of the mechanical properties element by element; Giorla, Scrivener, and Dunant (2015)	174
3.92	Fraction of damage in the aggregates and the cement paste as a function of the degree of reaction (left); Damage progression as a function of degree of reaction and time (right); Giorla, Scrivener, and Dunant (2015)	175
3.93	Interruption of AAR's time-dependent properties for slot-cutting duration: (left) AAR expansion and (right) Elastic modulus degradation; Gocevski and Yildiz (2017)	176
3.94	The location of the 1972-73 slot-cutting and the concrete damage as a consequence of this intervention: (a) the increased macrocracking in the water passage of group A of the intake structure and (b) sheared stay vanes of units A and B following the slot-cutting at the junction of the intake structure and the right gravity dam; Gocevski and Yildiz (2017)	177
3.95	Slot-Cutting - between the units 35 and 36 (1980-1981); development of extensive concrete cracking in unit 36 five years after the slot-cutting in 1981; Gocevski and Yildiz (2017)	178
3.96	Calculation scheme for ASR gel generation and stress formation	182
3.97	Vertical swelling rates observed on dam n-18; Guilloteau, Martinot, and Sausse (2017)	185
3.98	Tangential and vertical strains modeled since the first impoundment on 30 dams; Guilloteau, Martinot, and Sausse (2017)	185
3.99	Schematic view of elements affecting the selection of AAR testing core samples; Gunn, Scrivener, and Leemann (2017)	187
3.100	Proposed strategic method for dam AAR identification, Extent and Prognosis Evaluations; Gunn, Scrivener, and Leemann (2017)	188
3.101	Image analysis sequence; Haha et al. (2007)	190
3.102	Image analysis sequence; Haha et al. (2007)	190
3.103	Predicting degradation of E and f_t based on optimization of experimental tests; Hariri-Ardebili, Saouma, and Merz (2018)	192
3.104	Domain of investigation for AAR expansion and the LHS based sampling approach; Hariri-Ardebili, Saouma, and Merz (2018)	192
3.105	Interpretation of probabilistic analyses results based on summarized curves; Hariri-Ardebili, Saouma, and Merz (2018)	193
3.106	Optimization-based curve fitting to find the future expansion and estimation of residual coefficients; Hariri-Ardebili and Saouma (2018)	194
3.107	Results of sensitivity analysis on concrete constitutive model, capacity curves (left) and Tornado diagram (right); Hariri-Ardebili and Saouma (2018)	195
3.108	Probabilistic presentation of capacity curves (left) and cumulative density functions (right); Hariri-Ardebili and Saouma (2018)	195
3.109	Cahora Bassa Dam: Carlson strain gauges: "Stress free" strain at the top of the dam wall above RL 300 m; Hattingh et al. (2017)	197

3.110	Variation of modulus of elasticity (left) and compressive strength (right); Hayes et al. (2018)	198
3.111	Signs of deterioration at the Paulo Guerra Bridge (left); severe steel corrosion (right); Helene, Carvalho, and Pacheco (2017)	201
3.112	Results of the modulus of elasticity tests and the compressive strength; Helene, Carvalho, and Pacheco (2017)	201
3.113	Typical values of ASR inhibition pressure; Herrador, Martínez-Abella, and Dopico (2008)	202
3.114	Map-like fissures on a concrete wall in the Belesar Dam; Herrador, Martínez-Abella, and Dopico (2008)	203
3.115	Contours of displacement components after 25 years of the reaction; Huang and Pietruszczak (1996)	205
3.116	Distribution of the stress intensity factor, β , after 25 years of continuing AAR; Huang and Pietruszczak (1996)	205
3.117	Distribution of damage factor $\bar{\beta}$ after 25 years of reaction; Huang and Pietruszczak (1999)	206
3.118	Geometry and finite element mesh of dam-foundation system; Huang and Pietruszczak (1999)	207
3.119	Distribution of Damage Factor $\bar{\beta}$ after 25 Years of Reaction with two types of thermal analyses; Huang and Pietruszczak (1999)	208
3.120	Comparison of displacements at crest of dam; Huang and Pietruszczak (1999)	208
3.121	Simulated results from ASR; Huang and Spencer (2016)	210
3.122	Percent loss in compressive strength (LICS) of concrete cylinders; Islam and Ghafoori (2015)	213
3.123	Statistical parameters of Eq. 3.11; Islam and Ghafoori (2015)	214
3.124	Statistical parameters of Eq. 3.12; Islam and Ghafoori (2015)	214
3.125	Percentage of cracked aggregates and the relation with the maximum crack width in the structure and the cracks in cement paste; Jensen (2004)	216
3.126	Reactive minerals and rock types; Jensen (2012)	217
3.127	Behaviours in concrete and microscopic characteristics; Jensen (2012)	218
3.128	Precautionary measures, cements (eq. Na ₂ O) and kg eq. Na ₂ O/m ³ concrete and additive replacement of cement contents; Jensen (2012)	218
3.129	Schematic subdivision of the swelling curve; Kagimoto, Yasuda, and Kawamura (2014)	221
3.130	Changes in compressive strength and modulus of elasticity with age in concretes; Kagimoto, Yasuda, and Kawamura (2014)	221
3.131	Failure modes; Kobayashi et al. (1988)	223
3.132	Comparison of displacements at crest of the Dam; Lamea and Mirzabozorg (2015)	225
3.133	Contours of the 1st principal stresses on downstream face for the time of 1800 days (L: Linear; A: AAR; NL: Joint); Lamea and Mirzabozorg (2015)	226
3.134	E-modulus as a function of Vickers hardness of the reaction product different loading levels (left); In the central area of three different aggregates tested with a load of 12 mN (right); Leemann and Lura (2013)	230
3.135	Deformation of a 2D-slice of the Dam after 40 years with upstream-downstream displacement mapping (navy blue represents upstream displacement above 20 mm); Leroy et al. (2011)	232
3.136	Views of the mesh, and Downstream displacement at the crest of the Dam; Leroy et al. (2011)	232

3.137	Transverse stress versus time at different heights (P1 is the top of the slot-cutting, P6 its bottom) and transverse displacement mapping just after slot-cutting; Leroy et al. (2011)	233
3.138	Experimental setup; Expansion of specimen and the measured nonlinearity; Leśnicki et al. (2011)	235
3.139	NIRAS results for accumulated damage; Leśnicki et al. (2013)	236
3.140	General view of the AARTM; Liaudat et al. (2017)	238
3.141	Results of the performed mechanical tests; Liaudat et al. (2017)	239
3.142	Compressive strength and modulus of elasticity of normal and high strength concretes; Marzouk and Langdon (2003)	257
3.143	Different phases of expansion during the residual expansion measurements in longitudinal and diametral directions of cores.	260
3.144	Geometrical characteristics of the idealized dam and finite element mesh including contact elements and boundary conditions; Metalssi et al. (2014)	262
3.145	Displacement and stress vs. time before and after sawing; Metalssi et al. (2014)	263
3.146	Chipping inspection of pier beam (left); Fractured steel bar (right); Miyagawa et al. (2006)	264
3.147	Factors influencing AAR related concrete expansion; Moranville-Regourd (1997)	266
3.148	Boundary conditions of theoretical tests; Morenon et al. (2017)	267
3.149	Comparison of strains and stresses in free swelling and restrained tests; Morenon et al. (2017)	268
3.150	Strains and damage (in loading direction) in loaded or restrained direction; Morenon et al. (2017)	268
3.151	ASR damage in the 3 MPa test (applied in one direction); Morenon et al. (2017)	269
3.152	Global methodology summary; Morenon et al. (2018)	271
3.153	Comparison of measured and computed deformations in 3D; Morenon et al. (2018)	271
3.154	Mechanical characteristics; Multon, Seignol, and Toutlemonde (2005)	275
3.155	Mean deflection of five beams at midspan; Multon, Seignol, and Toutlemonde (2005)	276
3.156	Characteristics of the 48 specimens including the steel rings and strain measurements by an automated device; Multon and Toutlemonde (2006)	278
3.157	Measured axial and radial strains of the reactive and reference specimens under axial loading only; Multon and Toutlemonde (2006)	279
3.158	Axial imposed strains versus radial imposed strains for the reactive specimens without restraint; Multon and Toutlemonde (2006)	279
3.159	Grading of aggregates of mortar mixtures; Multon et al. (2008a)	281
3.160	Effect of particle size of reactive aggregate on mortar expansion (M5 and M1) (left); Effect of the alkali contents on expansions of mortars M1 to M5 (right); Multon et al. (2008a)	281
3.161	Long-term expansion (t=500 days) versus aggregate radius (R) and initial alkali content (AC) in mortars, calculated using the asymptotic expansion model (data: $k=1$, $l_c=11 \mu\text{m}$, $\phi_{ref}^{gel} = 0.066$, $\phi^{void-mortar} = 0.17$, $AC_0=8.1 \text{ kg/m}^3$, $AC_{th}=3.5 \text{ kg/m}^3$).	285
3.162	Mechanical properties vs. immersion time; Na et al. (2016)	286
3.163	(left): Dam mesh: (1) Joint between two blocks, (2) Swelling areas, and (3) Joint along the dam footprint; (right): Cracking mechanism around swelling areas: (1) P4 Swelling area of P4, (2) Increase of the swelling bloc, (3) Shear stress at the origin of cracks, and (4) Plastic strain; Noret and Laliche (2017)	288
3.164	ASR effects on material tests; Orbovic et al. (2015)	289

3.165	Geometry and reinforcement of shear wall specimen; Orbovic et al. (2015)	289
3.166	AAR extent of the Fontana Dam; Pan et al. (2013a)	293
3.167	Comparison of crack patterns of Fontana Dam between field inspection and simulation; Pan et al. (2013a)	293
3.168	Yearly variation of crest displacement with time; Pan et al. (2013a)	294
3.169	Vertical displacements at the monitoring points; Pan et al. (2013b)	295
3.170	Distribution of the maximum principal stress (MPa) on the downstream and upstream faces; Pan et al. (2013b)	296
3.171	Predicted crack patterns of the Kariba Dam in 2012; Pan et al. (2013b)	296
3.172	Evolution of the stability factor; Parvini, Pietruszczak, and Gocevski (2001)	298
3.173	Distribution of the damage factor; Parvini, Pietruszczak, and Gocevski (2001)	298
3.174	Grading of aggregates of mortar mixtures; Plusquellec et al. (2018)	299
3.175	Photos of the Votna I Dam: a) map cracking at the rail of the Dam; b) map cracking inside the slab ; c) presence of ASR gel in a bore hole; d) humidity inside the slab; e) aggregates visible on the surface; f) upstream face after drilling; Plusquellec et al. (2018)	300
3.176	ASR expansion for constant RH (left); ASR expansions (right); Poyet et al. (2006)	302
3.177	Assumed cracking pattern; Reinicker et al. (2010)	306
3.178	Finite element simulation vs. measurement Reinicker et al. (2013)	307
3.179	Material properties with depth; Rivard and Saint-Pierre (2009)	310
3.180	Dynamic material properties and DRI with depth; Rivard and Saint-Pierre (2009)	311
3.181	Cross-section of investigated structure and P-waves velocity tomography; Rivard et al. (2010)	312
3.182	Responses of selected SDT output parameters versus the loading applied (% of the 28-day/design strength) for 25 MPa concrete mixtures (first row: Tx sand; second row: NM gravel); Sanchez et al. (2014)	314
3.183	Proposed procedure for concrete damage assessment using stiffness damage testing; Sanchez et al. (2016a)	321
3.184	AAR kinetics and material properties for the 35 MPa concrete mix; Sanchez et al. (2017)	325
3.185	Comparison of yearly vertical displacement, and principal stress fields in two models; Saouma and Perotti (2006)	327
3.186	Comparison of principal stress fields in two models; Saouma, Perotti, and Shimpo (2007)	329
3.187	Comparison between first guess analysis and final analysis with optimized parameters (left), Internal AAR-induced maximum principal stresses in MPa (right); Saouma, Perotti, and Shimpo (2007)	330
3.188	Crest vertical and horizontal displacements versus ATU; vertical versus horizontal displacements; Saouma, Perotti, and Shimpo (2007)	331
3.189	Correlation between AAR finite element simulation and observed cracks; Saouma, Perotti, and Shimpo (2007)	331
3.190	Proposed paradigms for proper aging management studies; Saouma and Hariri-Ardebili (2014)	333
3.191	Unrestrained (U), Restrained (R), and Fully Restrained (FR) boundary conditions for the Beam (B), Truncated Beam (TB), and Panel (P) models; (Single orb = vertex restriction; group of orbs = restriction in perpendicular direction on surface; single rod = edge restriction; group of rods = roller boundary conditions on surface); Saouma et al. (2016)	336

3.192	Boxplots for Shear Strength Increase in terms of each of the seven variables; Saouma et al. (2016)	337
3.193	Evolution of the mechanical characteristics of the RC and NRC with time; Sargolzhai et al. (2010)	339
3.194	Deformation of the crest of arch dams; Sausse and Fabre (2011)	340
3.195	The extension and the direction of the main crack; Sbarigia et al. (2013)	342
3.196	The slot cutting from downstream face. On the left, the kerb of the crest; on the right, the wire in the middle of the cutting; Sbarigia, Zinetti, and Hernandez-Bagaglia (2016)	344
3.197	Alphabetically sorted list of models to be included in compendium. Scales are denoted by μ (micro), M (material), and S (structure); AAR-effects can be represented by P (pressure) or E (prescribed expansion); nr stands for “not relevant”; Seignol and Godart (2012)	347
3.198	Global methodology summary; Sellier et al. (2009)	349
3.199	Principle of chemical advancement assessment; Sellier et al. (2009)	350
3.200	Finite element mesh (left plot); fitting of swelling amplitude on structural displacements (Point PC, direction yy), prediction for PC directions zz and xx, future extrapolation (middle plot); PA displacements, comparison with in-place observations and future prediction (right plot); Sellier et al. (2009)	350
3.201	Reduction in strength at different levels of expansion (left); Reduction in flexural strength at different levels of expansion (right); Shayan (2016)	352
3.202	Resonant frequency monitoring of the tested specimens (left); Measures of Young’s modulus (MPa) of the concrete specimens; Siegert, Multon, and Toutlemonde (2005)	355
3.203	Modulus of elasticity measured on cylinders during the first loading of the modified SDT test as a function of expansion due to ASR; Smaoui et al. (2004a)	356
3.204	Results of the modified SDT tests at different expansion levels for cylinders made with the Quebec City limestone; Smaoui et al. (2004a)	357
3.205	Relationships between the expansion of cylinders and the energy dissipated during the first cycle and the plastic strain accumulated after the five cycles of the modified SDT test; Smaoui et al. (2004a)	358
3.206	Diagrams illustrating the various types of specimens manufactured and the various types of measurements taken on each of them; Smaoui et al. (2004c)	362
3.207	Results of mechanical testing as a function of time; Smaoui et al. (2005)	364
3.208	Thomas Stanton of the California State Division of Highways and a Bridge Parapet Wall that is Showing Signs of Damage due to Alkali-Silica Reaction; From <i>Alkali-Aggregate Reactivity (AAR) Fact Book; (FHWA, 2013)</i>	365
3.209	Reactive concrete retaining wall and its finite element mesh; Steffens, Li, and Coussy (2003)	367
3.210	Variation of mechanical properties with time due to ASR; Swamy and Al-Asali (1986)	369
3.211	Effect of ASR expansion on pulse velocity and dynamic modulus; Swamy and Wan (1993)	370
3.212	Load-displacement comparison on the short face; Talley, Kapitan, and Breen (2016)	373
3.213	Effect of Expansion due to AAR on Elastic Modulus; Tchner and Aziz (2009)	375
3.214	Horizontal change in distance over time at the top of the tower; Torii et al. (2016)	376
3.215	Time dependent response of dam, ASR extent, and principal plastic strain vectors; Ulm et al. (2000)	378
3.216	ASR extent percent and longitudinal plastic strains in box girder; Ulm et al. (2000)	378

3.217	Specimen reinforcement layouts. (a) Three-layer uniaxial reinforcement; (b) Three-layer biaxial reinforcement; (c) Three-layer triaxial reinforcement; (d) Two-layer biaxial reinforcement (L1); (e) Two layer biaxial reinforcement (L2); (f) Combined two-layer/three-layer biaxial reinforcement (L3); Wald et al. (2017)	381
3.218	Axial expansions versus specimen age; Wald et al. (2017)	381
3.219	Instrumentation layout and monitoring zones; Measured directional expansions (calipers) versus specimen age; Wald, Martinez, and Bayrak (2017)	383
3.220	Mid-depth surface crack on x–z specimen face; Wald, Martinez, and Bayrak (2017)	384
3.221	Example curves of expansion approaches; Wallau et al. (2018)	385
3.222	Load-deflection curves of beams; Wang and Morikawa (2012)	387
3.223	Computational algorithm; Winnicki and Serkega (2017)	388
3.224	Cross section of Fontana Dam with foundation on subsoil; Winnicki and Serkega (2017)	388
3.225	Relative humidity and temperature field after 30 years; Winnicki and Serkega (2017)	389
3.226	Relative humidity and temperature field after 30 years; Winnicki and Serkega (2017)	389
3.227	Mortar expansion curves of the plagioclase granite (left), and weakly weathered granite (right); Yang, Li, and Rao (2017)	390

List of Tables

- 3.1 Classification of the Various Coefficients Proposed to Estimate the Potential Rate of ASR Expansion of Concrete Members in Service either already Affected by ASR or not, Based on Laboratory Test Results and Field Conditions. 78
- 3.2 Average compressive strength and elastic properties of concrete dams subject to aging 118

1 — Introduction

This document reports on the State of the Art review of dams suffering from Alkali Aggregate Reactions (AAR).

Given the breadth of the scope, an original approach was followed. First $\simeq 600$ publications were identified through [Google Scholar](#) with a variety of keywords. This list was then reduced to $\simeq 400$ on structures with existing AAR, and finally, after careful reading of the abstracts and conclusions, it was reduced to $\simeq 210$. This list was enriched by about 50 additional publications suggested by Reclamation.

Each of the retained documents was then summarized through bullet points, and then inserted in this report.

The process was highly automated by combining Matlab, L^AT_EX and B^IB_TE_X tools as described above.

Whereas this report constitutes the written part of our investigation, a full-text search engine (based on the Elastic-Search tool) was prepared [Sen4AAR](#) (Search Engine for AAR). The code uses a specially developed Python program, and then uses JavaScript for data visualization.

Finally, the structure of this report and the data-base is such that they are highly modular and can be relatively easily enriched with new documents.

1.1 Document Preparation

This section will describe the procedure followed for the preparation of the final document as illustrated by Fig. [1.1](#).

This literature survey focuses on

- Alkali Aggregate Reaction.
- Dams in general, but not exclusively.
- Emphasis on structural/component level (field, experimental and numerical).
- Avoided publications related to mitigation, mix design, determination of AAR presence.

The task was performed using an innovative approach that exploits modern tools, and was conducted as follows:

1. Collect relevant (.pdf) documents
 - Through Google Scholar.
 - From the author's pdf libraries.
2. Preliminary screening of ~ 400 documents, and retained ~ 200 for review.

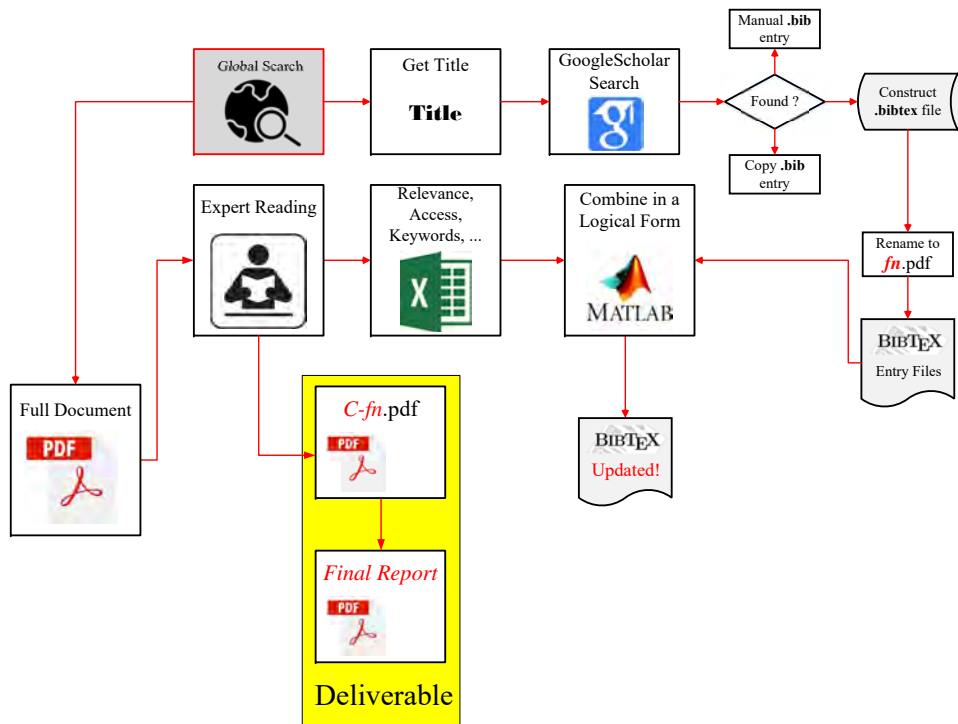


Figure 1.1: Document preparation procedure

3. Identified about 70 keywords with a numeric ID for subsequent tagging of documents, Fig. 1.2.
4. Each retained document was:
 - Assigned a tag id (typically first author last name, followed by year, and then first word of title; such as `stanton2008expansion`).
 - Full BibTeX entry entered in a `SOA-Final.bib` file, Fig. 1.3.
 - Update a spreadsheet file `Bib-List.xlsx`, Fig. 1.4, with includes:
 - tag id.
 - url address.
 - Flag indicating if full document is copyrighted or not.
 - Status (completed or not).
 - Initial of reviewer.
 - Each document was reviewed individually, and a corresponding “card” summarizing its finding (with figures when appropriate) was written `C-stanton2008expansion.tex`.

ID	Experimental	id	Numerical	ID2	Application
10	Laboratory;	50	Micro;	80	None;
11	Field;	51	Meso;	81	Gravity dam;
12	Cylinder;	52	Mega;	82	Arch dam;
13	Blocks;	53	Multi scale;	83	Buttress dam;
14	Other;	54	New constitutive model;	84	Buildings;
15	Expansion Assessment/monitoring	55	Nonlinear;	85	Bridge;
16	Reinforcement;	56	Coupled;	86	Nuclear power plants;
17	Confined;	57	Plasticity ;	87	Roads;
18	Det. E;	58	Damage Mechanics;	88	Reclamation;
19	Det f t;	59	XFEM;	89	ICAAR;
20	Det f c;	60	Thermal analysis;	90	Beams-Panels;
21	Det Gf;	61	Moisture analysis;	91	Intake tower;
22	Det K;	62	Seismic;	92	Slot Cutting;
23	Det. V;	63	Sensitivity;	93	Dams;
24	Det Bond;	64	Uncertainty;	94	Historical;
25	Quantified;	65	Parametric;		
26	Crack Index;	66	Prognosis;		
27	Damage Rating Index;	67	Mathematical;		
28	Petrography;	68	Finite Element;		
29	Creep;	69	Thermal equival.;		
30	Shrinkage;	70	Kinetic modeled;		
31	Temp 38oC (100oF);	71	Literture survey;		
32	Temp higher than 38;	72	Poro-Mechanics;		
33	Capacity curve;	73	Chemical reaction;		
34	Aggregate; Grain size	74	Petrography;		
35	SEM;	75	Leaching;		
36	Fiber reinforced polymer;	76	Gel;		
37	Acoustic spectrocopy;	77	Fed-Agencies Reports;		
38	Rehabilitation;				
39	Freeze-thaw;				
40	Radiation damage;				
41	Non Destructive Evaluation;				
42	Diagnosis;				
43	Performance testing				

Figure 1.2: List of Keywords

1.2 Script tools

Three matlab¹ based scripts were written to automate the process:

A `kwds_2_bibtex.m`

- Generates a consolidated 1-a and 1-b bib files into Temp.bib
- Generates a new Final.bib file that contains on top of the original tags:
 - Availability
 - Keywords
 - URL
- Note that
 - If there is an entry in the excel file with no corresponding entry in the .bib file an error is issued.

¹Though Python may have been a better environment, Matlab was selected because of its text recognition/editing capabilities, and the familiarity of the PIs

```

@Article{stanton40,
Title= {Expansion of Concrete Through Reaction Between Cement and Aggregate},
Author= {Stanton, T.E.},
Journal={Proceedings of ASCE},
Year={1940},
Pages={1781--1811},
Volume={66}
}

```

Figure 1.3: Sample of a BibTeX entry

Labels	Reviewer	Availability	Keywords							
alnaggar2013lattice	a	0	50	53	55	58	67	12		
azizan2017numerical	a	0	52	55	58	62	68	81		
bach1993load	a	0	10	13	16	33				
bangert2004chemo	a	0	52	56	58	65	68			
berube2002laboratory	v	0	10	15	31	34	66			
berube2002laboratory2	a	0	10	15	81	82				
berube2005evaluation	a	0	85	11	15	16	20			
blanco2018expansions	a	0	11	52	55	56	68	81		
capra1998modeling	v	0	10	61	76					
capra2003orthotropic	a	0	16	52	55	58	67	68	80	
carles2002interpretation	v	0	10	15	66					
chen2010rapid	a	0	10	15	18					
comby2009development	a	0	18	51	55	67	68	80		
comi2009chemo	a	0	52	54	60	61	67	68	81	
comi2012two	a	0	52	54	60	68	81			
criaud1995evaluating	v	0	10	31	32	75				

Figure 1.4: Sample entries in Bib-List.xlsx

- Not all Temp.bib file need to have a corresponding entry in the excel file.

B.Generate_C.tex.m

- Reads Final.bib
- Lists all .tex file in ./Cards
- For those entries in Final.bib without an existing Card, will create new ones and store them in Cards/New

C.Card_2_Report.m

- Reads Bib-List.xlsx to pull out the textual keywords
- Generates CU-USBR-1.tex file. Two parts
 - Identifies all entries associated with a keyword.
 - Compilation of all the cards to be printed.

1.3 Creation of Web Site Based Search Engine

1.3.1 Introduction

PyDocSen is a full-stack search engine writing in Python and facilitates ElasticSearch to search entire PDF documents, PDF summaries, as well as BibTex entries that contain keywords.

1.4 Requirements

- Docker
- Python 3
- Python Pip 3
- ElasticSearch 6.5.4

1.4.1 Install Instructions

To install, start with a fresh Ubuntu 18.04 docker image by running this command in the terminal:

```
docker pull image ubuntu
```

After completing the `docker pull` command, enter the following command to enter the interactive terminal of the `docker image`

```
docker container run -it ubuntu /bin/bash
```

In the interactive terminal, enter the following commands to install the search engine and run it in daemon-mode.

First upgrade the system to ensure latest dependencies and security patches.

```
apt-get update  
apt-get upgrade
```

Now install Python, Pip, and ElasticSearch:

```
apt-get install python3 python3-pip elasticsearch git
```

Enable ElasticSearch system service to make sure it runs at all times.

```
systemctl enable elasticsearch.service  
systemctl start elasticsearch.service
```

Now that ElasticSearch is installed, clone the project repository as follows:

```
git clone $GIT_REPOSITORY
```

Finally, install Python packages and run the daemon.

```
cd SEN4AAR/Program  
pip install -r requirements.txt  
flask -h 0.0.0.0 -p 443 -d
```

Now the program is running and can be accessed by navigating to the server's IP address or a domain name pointing to the server.

1.4.2 Usage Instructions

1.4.2.1 Log in

To login to the application, simply type in the username provided to you and the accompanying password. If your credentials are wrong, you will be redirected back to the login page. Otherwise, you will be redirected to the search page right away.

1.4.2.2 Search

To search for a specific term, simple enter a term in the search form and click search or hit **Enter**:

SEN4AAR

Sign In

Username

Password

If you have a .edu or .mil or .gov email, [click here](#) to get instant access.

(a) Sign-in Form

SEN4AAR

(b) Search Form

Figure 1.5: Preliminaries

1.4.2.3 Visualization

To view a bubble word frequency diagram, click on the **Bubble** button on any of the search results.

1.4.2.4 PDF Publication and PDF Summaries

To view the PDF publications behind a search result, it needs to be non-copyrighted. Otherwise, you need to be a super-user to access all PDF publications including copyrighted ones.

To view the PDF summaries, you simply need to be a regular user.

1.4.2.5 Publication URL

To view the publication URL of a search result, simply click the **URL** button and you will be automatically redirected to the respective directory.

1.4.2.6 Register User

To create an account to use PyDocSen, normal users will need to be approved by an administrator before they can use their account. If you have an email account TLD of edu, gov, or mil, you may request an instant account without waiting for approval you will simply get an email with a password you can use to login.

1.4.2.7 User Management

User management is simple in PyDocSen. Administrator powers include allowing or denying user applications, promoting to administrators, promoting to super users, as well as deleting users. Of course, the first administrator made is immune to deletion to make sure not to lock out the system from management.

Users can have 3 ranks. Normal users can only use the search facilities of the program. And super users are simply Normal users but with the ability to view all documents indexed in the system even if they are copyrighted. Finally administrators have access to the entire stack and can manage it.

1.4.2.8 Adding Documents to the Search Engine

To add documents to the search engine PyDocSen uses, an administrator can simply access the search engine management pane and simply upload, at a minimum, a bibtex file with entries that include keywords, and at most publications and cards to match. The publications need to be named the same as the label of the bibtex entries. And the summaries need to have the same of the publication PDF but with a "C-" prepended to the file name.

1.4.3 Technical Document

This section describes the architecture of the system, to give an idea for further improvement as well as keep a record of the inner workings of the system.

1.4.3.1 Overall Flow

The following flow chart describes the system as it is now:

Creep, shrinkage, and anisotropic damage in alkali-aggregate reaction swelling mechanism-Part I A constitutive model

Authors: Grimal, (E)tienne and Sellier, Alain and Le Pape, Yann and Bourdarot, (E)ric

Journal: ACI Materials Journal

Highlights:

"of the test (where α_0 was evaluated), and T is the current absolute temperature,"
 ", and drying creep."

"-J.; Coussy, O.; Kefei, L.; and Larive, C., "Thermo-ChemoMechanics of ASR Expansion in Concrete Structures"

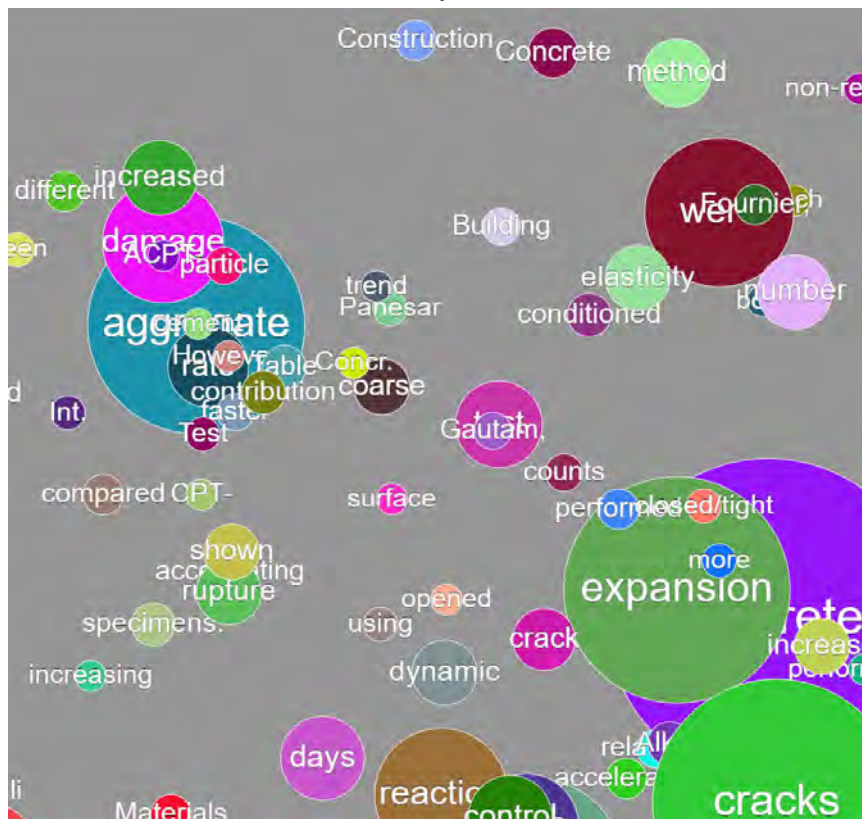
"Li, K., and Coussy, O., "Concrete ASR Degradation: From Material Modeling to Structure Assessment," Journal"

"; and Bourdarot, E., "Modeling of Alkali-Silica Reaction in Concrete, Part 2: Influence of Water on ASR"

(a) Bubble Visualization Button

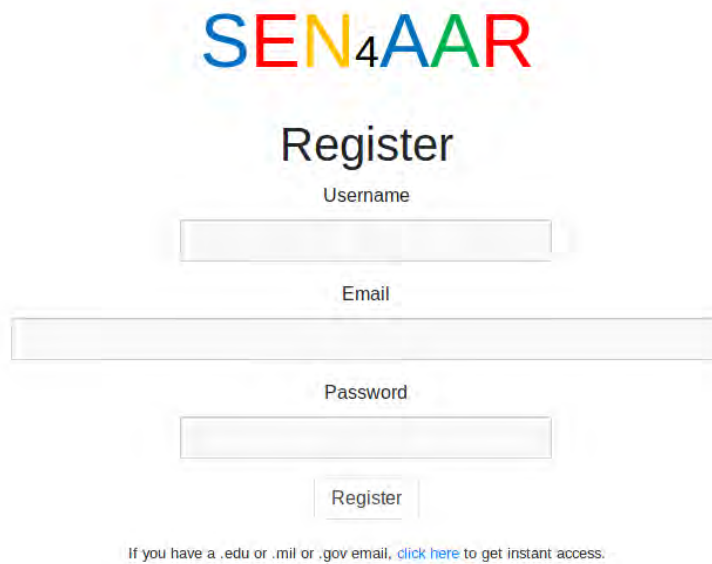
4/29/2019

gautam2017effect



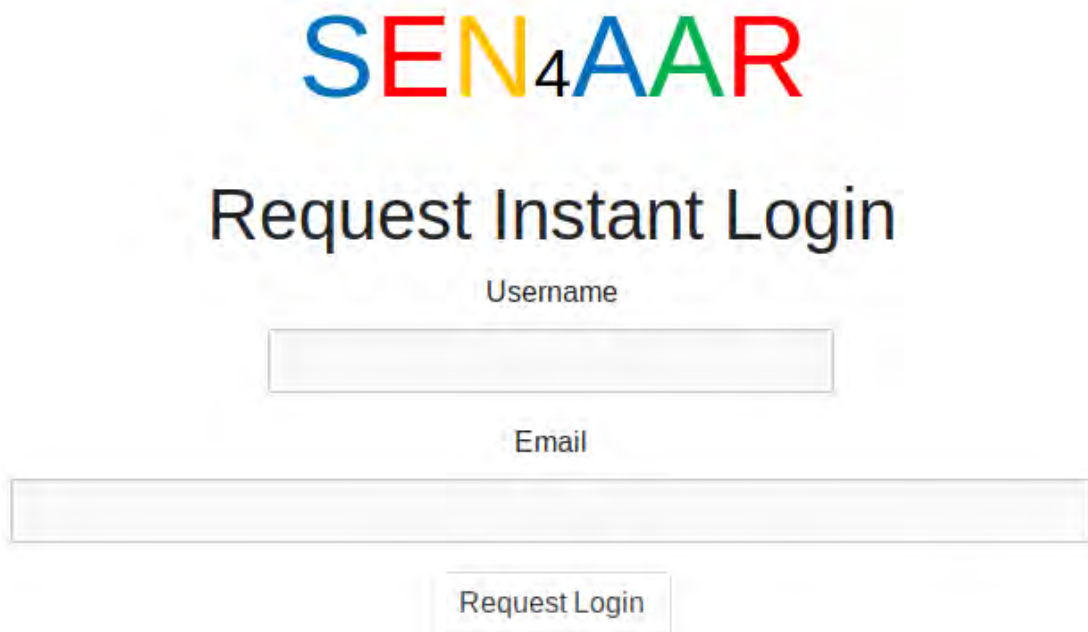
(b) Bubble Visualization Button

Figure 1.6: Bubbles



The registration form features the SEN4AAR logo at the top. Below it is the heading "Register". The form contains three input fields: "Username", "Email", and "Password". A "Register" button is positioned below the password field. A link is provided at the bottom: "If you have a .edu or .mil or .gov email, [click here](#) to get instant access."

Figure 1.7: Registration Form



The "Request Instant Login" form features the SEN4AAR logo at the top. Below it is the heading "Request Instant Login". The form contains two input fields: "Username" and "Email". A "Request Login" button is positioned below the email field.

Figure 1.8: Request Access Form

1.4.3.2 Python Backend

The backend is written in Python. The idea is to have readable code that can be improved upon by new developers without having to hassle with awkward syntax or a niche language. I am using Flask

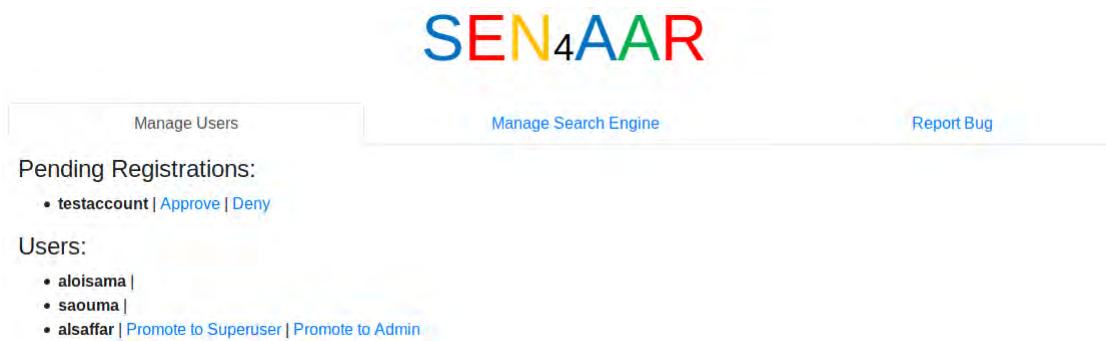


Figure 1.9: User Management Panel

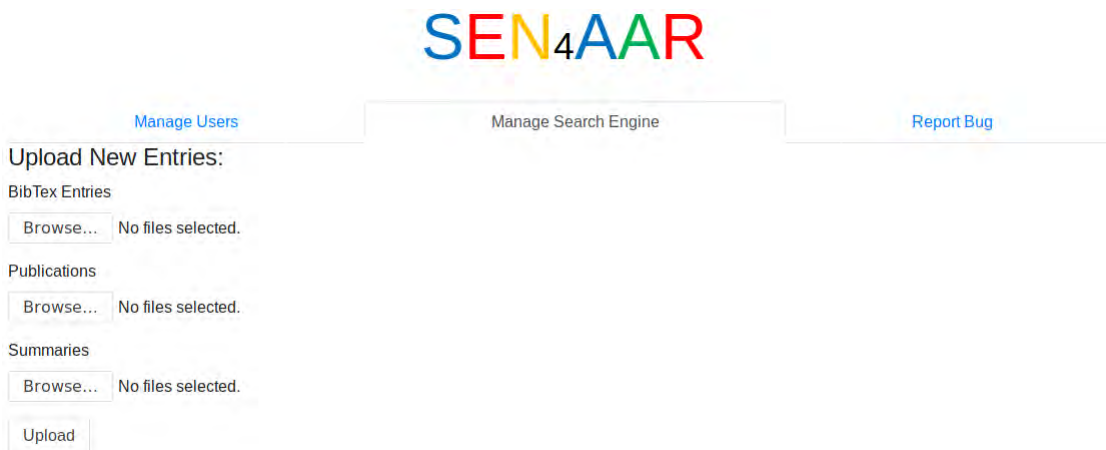


Figure 1.10: Search Engine Management

to drive the server side of the project because it is minimal and does not impose any requirements on the developer. The program is split into separate modules: authentication, administration, search engine, and visualization.

Authentication takes care of verifying user credentials, managing user registrations, sending emails for special email TLDs, and finally managing user roles by promotion/demotion. Administration takes care of any interfacing between administrators and the system; it adds allowing users, adding documents to the index, as well as gives information for reporting bugs. Search Engine simply interfaces with Elasticsearch and manages how results are sorted. Finally, visualization is responsible for preparing data from parsed documents to be visualized by JavaScript.

1.4.3.3 Elasticsearch Backend

Searching full-text is no easy task, and using Elasticsearch helps greatly with that. Elasticsearch allows us great flexibility in sorting search results as well as allowing certain operations such as and or or. Elasticsearch is only used as a search engine and not to store or serve any publications. That is done directly by WSGI.

1.4.3.4 Web Frontend

The web frontend is written in HTML, JavaScript, and CSS. I am using Flask's templating engine, Jinja2, to reuse pages and create reusable blocks and iterate over data easily. Javascript was also used to generate visualizations.

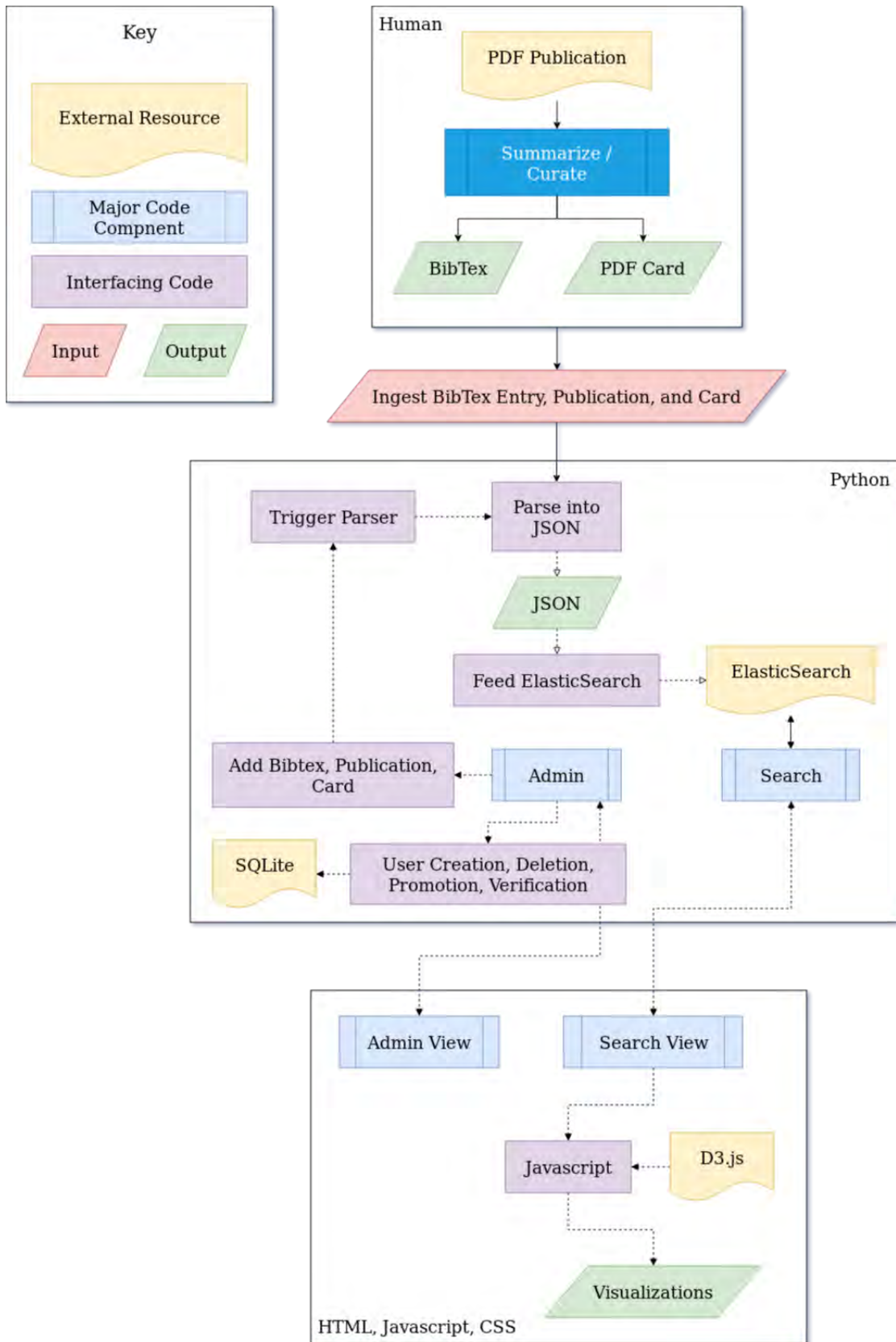


Figure 1.11: PyDocSen Flow

2— Cross-References

This chapter provides the reader with cross-referencing of all the reviewed documents. Each of the major keywords constitutes a section, followed by the corresponding document authors and sections. Internal hyperlinks make it easy for the reader to directly jump to the section of interest.

2.1 Laboratory

1. Fournier, Benoit and Bérubé, Marc-André (2000); Sect.: [3.49](#)
2. Godart, B and Mahut, B and Fasseu, P and Michel, M (2004); Sect.: [3.61](#)
3. Godart, Bruno and de Rooij, Mario Robert and Wood, Jonathan GM (2013); Sect.: [3.62](#)
4. Shayan, Ahmad and Grimstad, Jack (2006); Sect.: [3.155](#)
5. Yang, Huaquan and Li, Pengxiang and Rao, Meijuan (2017); Sect.: [3.178](#)
6. FHWA (2010); Sect.: [3.47](#)
7. Sbarigia, M and Zinetti, F and Hernandez-Bagaglia, M (2016); Sect.: [3.151](#)

2.2 Field

1. Bérubé, Marc-André and Smaoui, Nizar and Fournier, Benoit and Bissonnette, Benoit and Durand, Benoit (2005); Sect.: [3.12](#)
2. Esposito, Rita and Anaç, Caner and Hendriks, Max AN and Çopuroğlu, Oğuzhan (2016); Sect.: [3.38](#)
3. Herrador, Manuel F and Martínez-Abella, Fernando and Dopico, Juan Ramón Rabuñal (2008); Sect.: [3.75](#)
4. Lu, Duyou and Zhou, Xiaoling and Xu, Zhongzi and Lan, Xianghui and Tang, Mingshu and Fournier, Benoit (2006); Sect.: [3.103](#)
5. Miyagawa, Toyoaki and Seto, Kaoru and Sasaki, Kazunori and Mikata, Yasuhiro and Kuzume, Kazuhiro and Minami, Toshikazu (2006); Sect.: [3.107](#)
6. Mullick, AK (1988); Sect.: [3.112](#)
7. Plusquellec, G and Geiker, MR and Lindgård, J and De Weerdt, K (2018); Sect.: [3.128](#)
8. Rivard, Patrice and Saint-Pierre, François (2009); Sect.: [3.135](#)

9. Sanchez, LFM and Fournier, B and Jolin, M and Bastien, J (2015); Sect.: [3.138](#)
10. Saouma, Victor E and Hariri-Ardebili, Mohammad A (2014); Sect.: [3.145](#)
11. Shayan, Ahmad (2016); Sect.: [3.156](#)
12. Amberg, Francesco (2011); Sect.: [3.2](#)
13. Amberg, F and Stucchi, R and Brizzo, N (2013); Sect.: [3.4](#)
14. Donghi, G. and Marcello, C. and Sainati, F. (year=2013); Sect.: [3.33](#)
15. Morenon, P. and Grimal, E. and Kolayer, P. and Sellier, A. and Multon, S. (year=2018); Sect.: [3.110](#)
16. Sbarigia, M. and Zinetti, F. and Maugliani, V. and Palmitelli, G. and Mazzolani, S. (2013); Sect.: [3.150](#)
17. Batista, António Lopes and Piteira Gomes, J (2016); Sect.: [3.9](#)
18. Dolen, TP (2011); Sect.: [3.32](#)
19. Jensen, Viggo (2012); Sect.: [3.83](#)
20. Seignol, Jean François and Godart, Bruno (2012); Sect.: [3.153](#)
21. Custódio, j. and Ferreira, j. and Silva, A. and Ribeiro, A.B. and Batista, A. (2017); Sect.: [3.29](#)
22. Gunn, R. and Scrivener, K. and Leemann, A. (2017); Sect.: [3.66](#)
23. author="Leroy, R. and Boldea, L.I. and Seignol, J.F. and Godart, B. (2011); Sect.: [3.93](#)

2.3 Cylinder

1. Alnaggar, Mohammed and Cusatis, Gianluca and Di Luzio, Giovanni (2013); Sect.: [3.1](#)
2. Islam, Mohammad S and Ghafoori, Nader (2015); Sect.: [3.81](#)
3. Kubat, Thamer and Al-Mahaidi, Riadh and Shayan, Ahmad (2016); Sect.: [3.87](#)
4. Liu, Kai-Wei and Mukhopadhyay, Anol K (2015); Sect.: [3.102](#)
5. Multon, S and Seignol, J-F and Toutlemonde, F (2005); Sect.: [3.113](#)
6. Multon, Stéphane and Toutlemonde, François (2006); Sect.: [3.115](#)
7. Multon, Stéphane and Barin, François-Xavier and Godart, Bruno and Toutlemonde, François (2008); Sect.: [3.117](#)
8. Na, Okpin and Xi, Yunping and Ou, Edward and Saouma, Victor E (2016); Sect.: [3.120](#)
9. Poyet, Stéphane and Sellier, Alain and Capra, Bruno and Thèvenin-Foray, Geneviève and Torrenti, Jean-Michel and Tournier-Cognon, Hélène and Bourdarot, Eric (2006); Sect.: [3.129](#)

10. Sanchez, LFM and Fournier, B and Jolin, M and Mitchell, D and Bastien, J (2017); Sect.: [3.142](#)
11. Smaoui, Nizar and Bérubé, Marc-André and Fournier, Benoit and Bissonnette, Benoit and Durand, Benoit (2004); Sect.: [3.159](#)
12. Smaoui, Nizar and Bérubé, Marc-André and Fournier, Benoit and Bissonnette, Benoit (2004); Sect.: [3.161](#)
13. Wallau, Wilma and Pirskawetz, Stephan and Volland, Katja and Meng, Birgit (2018); Sect.: [3.175](#)
14. Dolen, TP (2011); Sect.: [3.32](#)
15. Custódio, j. and Ferreira, j. and Silva, A. and Ribeiro, A.B. and Batista, A. (2017); Sect.: [3.29](#)

2.4 Blocks

1. Bach, Finn and Thorsen, Torsten S and Nielsen, MP (1993); Sect.: [3.7](#)
2. Fournier, Benoit and Ideker, Jason H and Folliard, Kevin J and Thomas, Michael DA and Nkinamubanzi, Pierre-Claver and Chevrier, Ray (2009); Sect.: [3.50](#)
3. Gao, Xiao Xiao and Multon, Stéphane and Cyr, Martin and Sellier, Alain (2011); Sect.: [3.51](#)
4. Gao, XX and Cyr, M and Multon, S and Sellier, A (2013); Sect.: [3.52](#)
5. Hayes, Nolan Wesley and Gui, Qiang and Abd-Elssamd, Ammar and Le Pape, Yann and Giorla, Alain Benjamin and Le Pape, Sihem and Giannini, Eric R and Ma, Zhongguo John (2018); Sect.: [3.71](#)
6. Kagimoto, Hiroyuki and Yasuda, Yukihiro and Kawamura, Mitsunori (2014); Sect.: [3.85](#)
7. Liaudat, Joaquín and Carol, Ignacio and López, Carlos M and Saouma, Victor E (2017); Sect.: [3.97](#)
8. Marzouk, H and Langdon, S (2003); Sect.: [3.104](#)
9. Morenon, Pierre and Multon, Stéphane and Sellier, Alain and Grimal, Etienne and Hamon, François and Bourdarot, Eric (2017); Sect.: [3.109](#)
10. Multon, S and Seignol, J-F and Toutlemonde, F (2005); Sect.: [3.113](#)
11. Smaoui, Nizar and Bérubé, Marc-André and Fournier, Benoit and Bissonnette, Benoit (2004); Sect.: [3.161](#)
12. Wald, David M and Allford, Morgan T and Bayrak, Oguzhan and Hrynyk, Trevor D (2017); Sect.: [3.173](#)
13. Wang, Jian and Morikawa, Hidenori (2012); Sect.: [3.176](#)

2.5 Other

2.6 Expansion Assessment/monitoring

1. Berube, Marc-Andre and Frenette, Jean and Pedneault, Annie and Rivest, Michel (2002); Sect.: [3.10](#)
2. Bérubé, Marc-André and Duchesne, J and Dorion, JF and Rivest, M (2002); Sect.: [3.11](#)
3. Bérubé, Marc-André and Smaoui, Nizar and Fournier, Benoit and Bissonnette, Benoit and Durand, Benoit (2005); Sect.: [3.12](#)
4. Carles-Gibergues, André and Cyr, Martin (2002); Sect.: [3.17](#)
5. Chen, Jun and Jayapalan, Amal R and Kim, Jin-Yeon and Kurtis, Kimberly E and Jacobs, Laurence J (2010); Sect.: [3.18](#)
6. Crouch, RS and Wood, JGM (1990); Sect.: [3.25](#)
7. Crouch, RS and Wood, JGM (1990); Sect.: [3.25](#)
8. Diamond, S and Thaulow, N (1974); Sect.: [3.30](#)
9. Dunant, Cyrille F and Scrivener, Karen L (2012); Sect.: [3.35](#)
10. Dunant, Cyrille F and Scrivener, Karen L (2016); Sect.: [3.37](#)
11. Fan, Shenfu and Hanson, John M (1998); Sect.: [3.42](#)
12. Fernandes, Isabel and Noronha, Fernando and Teles, Madalena (2004); Sect.: [3.44](#)
13. Fernandes, Isabel and Noronha, Fernando and Teles, Madalena (2007); Sect.: [3.45](#)
14. Fournier, Benoit and Bérubé, Marc-André (2000); Sect.: [3.49](#)
15. Fournier, Benoit and Ideker, Jason H and Folliard, Kevin J and Thomas, Michael DA and Nkinamubanzi, Pierre-Claver and Chevrier, Ray (2009); Sect.: [3.50](#)
16. Gao, Xiao Xiao and Multon, Stéphane and Cyr, Martin and Sellier, Alain (2011); Sect.: [3.51](#)
17. Gao, XX and Cyr, M and Multon, S and Sellier, A (2013); Sect.: [3.52](#)
18. Gao, XX and Cyr, M and Multon, S and Sellier, A (2013); Sect.: [3.53](#)
19. Gautam, Bishnu P and Panesar, Daman K (2017); Sect.: [3.56](#)
20. Gholizadeh-Vayghan, Asghar and Rajabipour, Farshad (2017); Sect.: [3.57](#)
21. Haha, M Ben and Gallucci, Emmanuel and Guidoum, Amor and Scrivener, Karen L (2007); Sect.: [3.67](#)
22. Hayes, Nolan Wesley and Gui, Qiang and Abd-Elssamd, Ammar and Le Pape, Yann and Giorla, Alain Benjamin and Le Pape, Sihem and Giannini, Eric R and Ma, Zhongguo John (2018); Sect.: [3.71](#)

23. Hefny, A and Lo, KY and Adeghe, L (2001); Sect.: [3.72](#)
24. Helene, Paulo and Carvalho, Mariana and Pacheco, Jéssika (2017); Sect.: [3.74](#)
25. Herrador, Manuel F and Martínez-Abella, Fernando and Dopico, Juan Ramón Rabuñal (2008); Sect.: [3.75](#)
26. Huang, M and Pietruszczak, S (1996); Sect.: [3.76](#)
27. Huang, Maosong and Pietruszczak, S (1999); Sect.: [3.77](#)
28. Islam, Mohammad S and Ghafoori, Nader (2015); Sect.: [3.81](#)
29. Jensen, Viggo (2004); Sect.: [3.82](#)
30. Kagimoto, Hiroyuki and Yasuda, Yukihiro and Kawamura, Mitsunori (2014); Sect.: [3.85](#)
31. Kobayashi, Kazuo and Inoue, Susumu and Yamasaki, Takao and Nakano, Kin-ichi (1988); Sect.: [3.86](#)
32. Kubat, Thamer and Al-Mahaidi, Riadh and Shayan, Ahmad (2016); Sect.: [3.87](#)
33. Leemann, Andreas and Merz, Christine (2013); Sect.: [3.90](#)
34. Leemann, A and Lura, P (2013); Sect.: [3.92](#)
35. Leśnicki, Krzysztof J and Kim, Jin-Yeon and Kurtis, Kimberly E and Jacobs, Laurence J (2011); Sect.: [3.94](#)
36. Leśnicki, Krzysztof J and Kim, Jin-Yeon and Kurtis, Kimberly E and Jacobs, Laurence J (2013); Sect.: [3.95](#)
37. Liaudat, Joaquín and Carol, Ignacio and López, Carlos M and Saouma, Victor E (2017); Sect.: [3.97](#)
38. Lindgård, Jan and Andiç-Çakır, Özge and Fernandes, Isabel and Rønning, Terje F and Thomas, Michael DA (2012); Sect.: [3.99](#)
39. Lindgård, Jan and Sellevold, Erik J and Thomas, Michael DA and Pedersen, Bård and Justnes, Harald and Rønning, Terje F (2013); Sect.: [3.100](#)
40. Lindgård, Jan and Thomas, Michael DA and Sellevold, Erik J and Pedersen, Bård and Andiç-Çakır, Özge and Justnes, Harald and Rønning, Terje F (2013); Sect.: [3.101](#)
41. Liu, Kai-Wei and Mukhopadhyay, Anol K (2015); Sect.: [3.102](#)
42. Lu, Duyou and Zhou, Xiaoling and Xu, Zhongzi and Lan, Xianghui and Tang, Mingshu and Fournier, Benoit (2006); Sect.: [3.103](#)
43. Mukhopadhyay, Anal and Shon, Chang-Seon and Zollinger, Dan (2006); Sect.: [3.111](#)
44. Mullick, AK (1988); Sect.: [3.112](#)
45. Multon, S and Seignol, J-F and Toutlemonde, F (2005); Sect.: [3.113](#)
46. Multon, Stéphane and Seignol, Jean-François and Toutlemonde, François (2006); Sect.: [3.114](#)

47. Multon, Stéphane and Toutlemonde, François (2006); Sect.: [3.115](#)
48. Multon, Stéphane and Cyr, Martin and Sellier, Alain and Leklou, Nordine and Petit, Laurent (2008); Sect.: [3.116](#)
49. Multon, Stéphane and Barin, François-Xavier and Godart, Bruno and Toutlemonde, François (2008); Sect.: [3.117](#)
50. Multon, Stéphane and Cyr, Martin and Sellier, Alain and Diederich, Paco and Petit, Laurent (2010); Sect.: [3.119](#)
51. Na, Okpin and Xi, Yunping and Ou, Edward and Saouma, Victor E (2016); Sect.: [3.120](#)
52. Ostertag, Claudia P and Yi, ChongKu and Monteiro, Paulo JM (2007); Sect.: [3.123](#)
53. Poyet, Stéphane and Sellier, Alain and Capra, Bruno and Thèvenin-Foray, Geneviève and Torrenti, Jean-Michel and Tournier-Cognon, Hélène and Bourdarot, Eric (2006); Sect.: [3.129](#)
54. Rivard, Patrice and Saint-Pierre, François (2009); Sect.: [3.135](#)
55. Rivard, Patrice and Ballivy, Gérard and Gravel, Clermont and Saint-Pierre, Francois (2010); Sect.: [3.136](#)
56. Sanchez, LFM and Fournier, B and Jolin, M and Bastien, J (2014); Sect.: [3.137](#)
57. Sanchez, LFM and Fournier, B and Jolin, M and Bastien, J (2015); Sect.: [3.138](#)
58. Sanchez, LFM and Fournier, B and Jolin, M and Bastien, J and Mitchell, D (2016); Sect.: [3.140](#)
59. Sanchez, LFM and Fournier, B and Jolin, M and Bedoya, MAB and Bastien, J and Duchesne, J (2016); Sect.: [3.141](#)
60. Sanchez, LFM and Fournier, B and Jolin, M and Mitchell, D and Bastien, J (2017); Sect.: [3.142](#)
61. Sargolzahi, Maryam and Kodjo, Serge A and Rivard, Patrice and Rhazi, Jamal (2010); Sect.: [3.148](#)
62. Sausse, J and Fabre, JP (2011); Sect.: [3.149](#)
63. Sellier, Alain and Bourdarot, Eric and Multon, Stéphane and Cyr, Martin and Grimal, Etienne (2009); Sect.: [3.154](#)
64. Shayan, Ahmad and Grimstad, Jack (2006); Sect.: [3.155](#)
65. Siegert, D and Multon, S and Toutlemonde, F (2005); Sect.: [3.158](#)
66. Smaoui, Nizar and Bérubé, Marc-André and Fournier, Benoit and Bissonnette, Benoit and Durand, Benoit (2004); Sect.: [3.159](#)
67. Smaoui, Nizar and Fournier, Benoit and Bérubé, Marc-André and Bissonnette, Benoit and Durand, Benoit (2004); Sect.: [3.160](#)
68. Smaoui, Nizar and Bérubé, Marc-André and Fournier, Benoit and Bissonnette, Benoit (2004); Sect.: [3.161](#)

69. Smaoui, N and Bérubé, MA and Fournier, Benoit and Bissonnette, B and Durand, B (2005); Sect.: [3.162](#)
70. Swamy, R Narayan and Wan, WM Raymond (1993); Sect.: [3.166](#)
71. Talley, Kimberly G and Kapitan, Jacob G and Breen, John E (2016); Sect.: [3.168](#)
72. Torii, Kazuyuki and Kubo, Tetsuji and Sannoh, Chikao and Kanitani, Maki (2016); Sect.: [3.170](#)
73. Wald, David M and Allford, Morgan T and Bayrak, Oguzhan and Hrynyk, Trevor D (2017); Sect.: [3.173](#)
74. Wald, David and Martinez, Gloriana Arrieta and Bayrak, Oguzhan (2017); Sect.: [3.174](#)
75. Wallau, Wilma and Pirskawetz, Stephan and Volland, Katja and Meng, Birgit (2018); Sect.: [3.175](#)
76. Yang, Huaquan and Li, Pengxiang and Rao, Meijuan (2017); Sect.: [3.178](#)
77. FHWA (2013); Sect.: [3.48](#)
78. Amberg, Francesco (2011); Sect.: [3.2](#)
79. Amberg, F (2012); Sect.: [3.3](#)
80. Sbarigia, M. and Zinetti, F. and Maugliani, V. and Palmitelli, G. and Mazzolani, S. (2013); Sect.: [3.150](#)
81. Batista, António Lopes and Piteira Gomes, J (2016); Sect.: [3.9](#)
82. Dolen, TP (2011); Sect.: [3.32](#)
83. Jensen, Viggo (2012); Sect.: [3.83](#)
84. Swamy, RN and Al-Asali, MM (1986); Sect.: [3.165](#)
85. Tcherer, Julia and Aziz, T (2009); Sect.: [3.169](#)
86. Orbovic, N. and Panesar, D. and Sheikh, S. and Vecchio, F. and Lamarche, C.P. and Blahoiianu, A. (2015); Sect.: [3.122](#)
87. Guilloteau, T. and Martinot, F. and Sausse, J. (2017); Sect.: [3.65](#)
88. Gunn, R. and Scrivener, K. and Leemann, A. (2017); Sect.: [3.66](#)
89. Hattingh, L. and Oosthuizen, C. and Tembe, I. and Mahlabela, C. (2017); Sect.: [3.70](#)
90. author="Leroy, R. and Boldea, L.I. and Seignol, J.F. and Godart, B. (2011); Sect.: [3.93](#)
91. Sbarigia, M and Zinetti, F and Hernandez-Bagaglia, M (2016); Sect.: [3.151](#)
92. author="Scuero, A. and Vaschetti, G. (2011); Sect.: [3.152](#)
93. Wang, Jian and Morikawa, Hidenori (2012); Sect.: [3.176](#)

2.7 Reinforcement

1. Bach, Finn and Thorsen, Torsten S and Nielsen, MP (1993); Sect.: [3.7](#)
2. Bérubé, Marc-André and Smaoui, Nizar and Fournier, Benoit and Bissonnette, Benoit and Durand, Benoit (2005); Sect.: [3.12](#)
3. Fan, Shenfu and Hanson, John M (1998); Sect.: [3.42](#)
4. Ferche, Anca C and Panesar, Daman K and Sheikh, Shamim A and Vecchio, Frank J (2017); Sect.: [3.43](#)
5. Hayes, Nolan Wesley and Gui, Qiang and Abd-Elssamd, Ammar and Le Pape, Yann and Giorla, Alain Benjamin and Le Pape, Sihem and Giannini, Eric R and Ma, Zhongguo John (2018); Sect.: [3.71](#)
6. Heidarzadeh, N and Samadzad, M and Shekarchi, M and Mirghaderi, SR (2017); Sect.: [3.73](#)
7. Helene, Paulo and Carvalho, Mariana and Pacheco, Jéssika (2017); Sect.: [3.74](#)
8. Kobayashi, Kazuo and Inoue, Susumu and Yamasaki, Takao and Nakano, Kin-ichi (1988); Sect.: [3.86](#)
9. Kubat, Thamer and Al-Mahaidi, Riadh and Shayan, Ahmad (2016); Sect.: [3.87](#)
10. Miyagawa, Toyoaki and Seto, Kaoru and Sasaki, Kazunori and Mikata, Yasuhiro and Kuzume, Kazuhiro and Minami, Toshikazu (2006); Sect.: [3.107](#)
11. Multon, S and Seignol, J-F and Toutlemonde, F (2005); Sect.: [3.113](#)
12. Multon, Stéphane and Seignol, Jean-François and Toutlemonde, François (2006); Sect.: [3.114](#)
13. Talley, Kimberly G and Kapitan, Jacob G and Breen, John E (2016); Sect.: [3.168](#)
14. Torii, Kazuyuki and Kubo, Tetsuji and Sannoh, Chikao and Kanitani, Maki (2016); Sect.: [3.170](#)
15. Wald, David M and Allford, Morgan T and Bayrak, Oguzhan and Hrynyk, Trevor D (2017); Sect.: [3.173](#)
16. Wald, David and Martinez, Gloriana Arrieta and Bayrak, Oguzhan (2017); Sect.: [3.174](#)
17. Sbarigia, M. and Zinetti, F. and Maugliani, V. and Palmitelli, G. and Mazzolani, S. (2013); Sect.: [3.150](#)
18. Tchermer, Julia and Aziz, T (2009); Sect.: [3.169](#)
19. Chulliat, O. and Grimal, E. and Bourdarot, E. (2017); Sect.: [3.26](#)
20. Noret, C. and Laliche, K. (2017); Sect.: [3.121](#)
21. Sbarigia, M and Zinetti, F and Hernandez-Bagaglia, M (2016); Sect.: [3.151](#)
22. Wang, Jian and Morikawa, Hidenori (2012); Sect.: [3.176](#)

2.8 Confined

1. Hayes, Nolan Wesley and Gui, Qiang and Abd-Elssamd, Ammar and Le Pape, Yann and Giorla, Alain Benjamin and Le Pape, Sihem and Giannini, Eric R and Ma, Zhongguo John (2018); Sect.: [3.71](#)
2. Liaudat, Joaquín and Carol, Ignacio and López, Carlos M and Saouma, Victor E (2017); Sect.: [3.97](#)
3. Liu, Kai-Wei and Mukhopadhyay, Anol K (2015); Sect.: [3.102](#)
4. Miyagawa, Toyooki and Seto, Kaoru and Sasaki, Kazunori and Mikata, Yasuhiro and Kuzume, Kazuhiro and Minami, Toshikazu (2006); Sect.: [3.107](#)
5. Morenon, Pierre and Multon, Stéphane and Sellier, Alain and Grimal, Etienne and Hamon, François and Bourdarot, Eric (2017); Sect.: [3.109](#)
6. Multon, Stéphane and Toutlemonde, François (2006); Sect.: [3.115](#)
7. Ostertag, Claudia P and Yi, ChongKu and Monteiro, Paulo JM (2007); Sect.: [3.123](#)
8. Smaoui, Nizar and Bérubé, Marc-André and Fournier, Benoit and Bissonnette, Benoit (2004); Sect.: [3.161](#)
9. Wald, David M and Allford, Morgan T and Bayrak, Oguzhan and Hrynyk, Trevor D (2017); Sect.: [3.173](#)
10. Wald, David and Martinez, Gloriana Arrieta and Bayrak, Oguzhan (2017); Sect.: [3.174](#)
11. Tchermer, Julia and Aziz, T (2009); Sect.: [3.169](#)
12. Hattingh, L. and Oosthuizen, C. and Tembe, I. and Mahlabela, C. (2017); Sect.: [3.70](#)
13. Wang, Jian and Morikawa, Hidenori (2012); Sect.: [3.176](#)

2.9 Det. E

1. Chen, Jun and Jayapalan, Amal R and Kim, Jin-Yeon and Kurtis, Kimberly E and Jacobs, Laurence J (2010); Sect.: [3.18](#)
2. Crouch, RS and Wood, JGM (1990); Sect.: [3.25](#)
3. Dolen, T. (2005); Sect.: [3.31](#)
4. Esposito, Rita and Anaç, Caner and Hendriks, Max AN and Çopuroğlu, Oğuzhan (2016); Sect.: [3.38](#)
5. Giaccio, G and Zerbino, R and Ponce, JM and Batic, Oscar R (2008); Sect.: [3.58](#)
6. Hayes, Nolan Wesley and Gui, Qiang and Abd-Elssamd, Ammar and Le Pape, Yann and Giorla, Alain Benjamin and Le Pape, Sihem and Giannini, Eric R and Ma, Zhongguo John (2018); Sect.: [3.71](#)
7. Leemann, A and Lura, P (2013); Sect.: [3.92](#)

8. Leśnicki, Krzysztof J and Kim, Jin-Yeon and Kurtis, Kimberly E and Jacobs, Laurence J (2011); Sect.: [3.94](#)
9. Leśnicki, Krzysztof J and Kim, Jin-Yeon and Kurtis, Kimberly E and Jacobs, Laurence J (2013); Sect.: [3.95](#)
10. Liaudat, Joaquín and Carol, Ignacio and López, Carlos M and Saouma, Victor E (2017); Sect.: [3.97](#)
11. Marzouk, H and Langdon, S (2003); Sect.: [3.104](#)
12. Multon, S and Seignol, J-F and Toutlemonde, F (2005); Sect.: [3.113](#)
13. Na, Okpin and Xi, Yunping and Ou, Edward and Saouma, Victor E (2016); Sect.: [3.120](#)
14. Rivard, Patrice and Saint-Pierre, François (2009); Sect.: [3.135](#)
15. Sanchez, LFM and Fournier, B and Jolin, M and Bastien, J (2014); Sect.: [3.137](#)
16. Sanchez, LFM and Fournier, B and Jolin, M and Bastien, J (2015); Sect.: [3.138](#)
17. Sanchez, LFM and Fournier, B and Jolin, M and Bastien, J and Mitchell, D (2016); Sect.: [3.140](#)
18. Sanchez, LFM and Fournier, B and Jolin, M and Bedoya, MAB and Bastien, J and Duchesne, J (2016); Sect.: [3.141](#)
19. Sanchez, LFM and Fournier, B and Jolin, M and Mitchell, D and Bastien, J (2017); Sect.: [3.142](#)
20. Sargolzhahi, Maryam and Kodjo, Serge A and Rivard, Patrice and Rhazi, Jamal (2010); Sect.: [3.148](#)
21. Shayan, Ahmad (2016); Sect.: [3.156](#)
22. Siegert, D and Multon, S and Toutlemonde, F (2005); Sect.: [3.158](#)
23. Smaoui, Nizar and Bérubé, Marc-André and Fournier, Benoit and Bissonnette, Benoit and Durand, Benoit (2004); Sect.: [3.159](#)
24. Smaoui, N and Bérubé, MA and Fournier, Benoit and Bissonnette, B and Durand, B (2005); Sect.: [3.162](#)
25. Swamy, R Narayan and Wan, WM Raymond (1993); Sect.: [3.166](#)
26. Dolen, TP (2011); Sect.: [3.32](#)
27. Swamy, RN and Al-Asali, MM (1986); Sect.: [3.165](#)
28. Tcherer, Julia and Aziz, T (2009); Sect.: [3.169](#)
29. Orbovic, N. and Panesar, D. and Sheikh, S. and Vecchio, F. and Lamarche, C.P. and Blahoiianu, A. (2015); Sect.: [3.122](#)

2.10 Det f't

1. Dolen, T. (2005); Sect.: [3.31](#)
2. Esposito, Rita and Anaç, Caner and Hendriks, Max AN and Çopuroğlu, Oğuzhan (2016); Sect.: [3.38](#)
3. Marzouk, H and Langdon, S (2003); Sect.: [3.104](#)
4. Sanchez, LFM and Fournier, B and Jolin, M and Mitchell, D and Bastien, J (2017); Sect.: [3.142](#)
5. Shayan, Ahmad (2016); Sect.: [3.156](#)
6. Smaoui, N and Bérubé, MA and Fournier, Benoit and Bissonnette, B and Durand, B (2005); Sect.: [3.162](#)
7. Swamy, RN and Al-Asali, MM (1986); Sect.: [3.165](#)
8. Custódio, j. and Ferreira, j. and Silva, A. and Ribeiro, A.B. and Batista, A. (2017); Sect.: [3.29](#)

2.11 Det f'c

1. Bérubé, Marc-André and Smaoui, Nizar and Fournier, Benoit and Bissonnette, Benoit and Durand, Benoit (2005); Sect.: [3.12](#)
2. Dolen, T. (2005); Sect.: [3.31](#)
3. Esposito, Rita and Anaç, Caner and Hendriks, Max AN and Çopuroğlu, Oğuzhan (2016); Sect.: [3.38](#)
4. Giaccio, G and Zerbino, R and Ponce, JM and Batic, Oscar R (2008); Sect.: [3.58](#)
5. Hayes, Nolan Wesley and Gui, Qiang and Abd-Elssamd, Ammar and Le Pape, Yann and Giorla, Alain Benjamin and Le Pape, Sihem and Giannini, Eric R and Ma, Zhongguo John (2018); Sect.: [3.71](#)
6. Islam, Mohammad S and Ghafoori, Nader (2015); Sect.: [3.81](#)
7. Kagimoto, Hiroyuki and Yasuda, Yukihiro and Kawamura, Mitsunori (2014); Sect.: [3.85](#)
8. Marzouk, H and Langdon, S (2003); Sect.: [3.104](#)
9. Na, Okpin and Xi, Yunping and Ou, Edward and Saouma, Victor E (2016); Sect.: [3.120](#)
10. Rivard, Patrice and Saint-Pierre, François (2009); Sect.: [3.135](#)
11. Sanchez, LFM and Fournier, B and Jolin, M and Bastien, J and Mitchell, D (2016); Sect.: [3.140](#)
12. Sanchez, LFM and Fournier, B and Jolin, M and Bedoya, MAB and Bastien, J and Duchesne, J (2016); Sect.: [3.141](#)

13. Sanchez, LFM and Fournier, B and Jolin, M and Mitchell, D and Bastien, J (2017); Sect.: [3.142](#)
14. Sargolzhahi, Maryam and Kodjo, Serge A and Rivard, Patrice and Rhazi, Jamal (2010); Sect.: [3.148](#)
15. Shayan, Ahmad (2016); Sect.: [3.156](#)
16. Smaoui, N and Bérubé, MA and Fournier, Benoit and Bissonnette, B and Durand, B (2005); Sect.: [3.162](#)
17. Dolen, TP (2011); Sect.: [3.32](#)
18. Swamy, RN and Al-Asali, MM (1986); Sect.: [3.165](#)
19. Orbovic, N. and Panesar, D. and Sheikh, S. and Vecchio, F. and Lamarche, C.P. and Blahoiianu, A. (2015); Sect.: [3.122](#)
20. Custódio, j. and Ferreira, j. and Silva, A. and Ribeiro, A.B. and Batista, A. (2017); Sect.: [3.29](#)

2.12 Det Gf

1. Giaccio, G and Zerbino, R and Ponce, JM and Batic, Oscar R (2008); Sect.: [3.58](#)
2. Kagimoto, Hiroyuki and Yasuda, Yukihiro and Kawamura, Mitsunori (2014); Sect.: [3.85](#)

2.13 Det K

1. Siegert, D and Multon, S and Toutlemonde, F (2005); Sect.: [3.158](#)

2.14 Det. V

1. Shayan, Ahmad (2016); Sect.: [3.156](#)
2. Talley, Kimberly G and Kapitan, Jacob G and Breen, John E (2016); Sect.: [3.168](#)
3. Orbovic, N. and Panesar, D. and Sheikh, S. and Vecchio, F. and Lamarche, C.P. and Blahoiianu, A. (2015); Sect.: [3.122](#)

2.15 Det Bond

1. Miyagawa, Toyoaki and Seto, Kaoru and Sasaki, Kazunori and Mikata, Yasuhiro and Kuzume, Kazuhiro and Minami, Toshikazu (2006); Sect.: [3.107](#)

2.16 Quantified

1. Gao, Xiao Xiao and Multon, Stéphane and Cyr, Martin and Sellier, Alain (2011); Sect.: [3.51](#)
2. Gao, XX and Cyr, M and Multon, S and Sellier, A (2013); Sect.: [3.52](#)
3. Wald, David and Martinez, Gloriana Arrieta and Bayrak, Oguzhan (2017); Sect.: [3.174](#)

2.17 Crack Index

1. Fan, Shenfu and Hanson, John M (1998); Sect.: [3.42](#)
2. Gao, Xiao Xiao and Multon, Stéphane and Cyr, Martin and Sellier, Alain (2011); Sect.: [3.51](#)
3. Jensen, Viggo (2004); Sect.: [3.82](#)
4. Kagimoto, Hiroyuki and Yasuda, Yukihiro and Kawamura, Mitsunori (2014); Sect.: [3.85](#)
5. Kobayashi, Kazuo and Inoue, Susumu and Yamasaki, Takao and Nakano, Kin-ichi (1988); Sect.: [3.86](#)
6. Leemann, Andreas and Merz, Christine (2013); Sect.: [3.90](#)
7. Leśnicki, Krzysztof J and Kim, Jin-Yeon and Kurtis, Kimberly E and Jacobs, Laurence J (2011); Sect.: [3.94](#)
8. Leśnicki, Krzysztof J and Kim, Jin-Yeon and Kurtis, Kimberly E and Jacobs, Laurence J (2013); Sect.: [3.95](#)
9. Ostertag, Claudia P and Yi, ChongKu and Monteiro, Paulo JM (2007); Sect.: [3.123](#)
10. Plusquellec, G and Geiker, MR and Lindgård, J and De Weerd, K (2018); Sect.: [3.128](#)
11. Rivard, Patrice and Ballivy, Gérard and Gravel, Clermont and Saint-Pierre, Francois (2010); Sect.: [3.136](#)
12. Smaoui, Nizar and Bérubé, Marc-André and Fournier, Benoit and Bissonnette, Benoit and Durand, Benoit (2004); Sect.: [3.159](#)
13. Smaoui, Nizar and Fournier, Benoit and Bérubé, Marc-André and Bissonnette, Benoit and Durand, Benoit (2004); Sect.: [3.160](#)
14. Yang, Huaquan and Li, Pengxiang and Rao, Meijuan (2017); Sect.: [3.178](#)
15. Swamy, RN and Al-Asali, MM (1986); Sect.: [3.165](#)
16. Gunn, R. and Scrivener, K. and Leemann, A. (2017); Sect.: [3.66](#)

2.18 Damage Rating Index

1. Gautam, Bishnu P and Panesar, Daman K (2017); Sect.: [3.56](#)
2. Rivard, Patrice and Fournier, Benoit and Ballivy, Gérard (2000); Sect.: [3.133](#)
3. Rivard, Patrice and Fournier, Benoit and Ballivy, Gérard (2002); Sect.: [3.134](#)
4. Rivard, Patrice and Saint-Pierre, François (2009); Sect.: [3.135](#)
5. Sanchez, LFM and Fournier, B and Jolin, M and Bastien, J (2014); Sect.: [3.137](#)
6. Sanchez, LFM and Fournier, B and Jolin, M and Bastien, J (2015); Sect.: [3.138](#)

7. Sanchez, LFM and Fournier, B and Jolin, M and Bastien, J and Mitchell, D (2016); Sect.: [3.140](#)
8. Sanchez, LFM and Fournier, B and Jolin, M and Bedoya, MAB and Bastien, J and Duchesne, J (2016); Sect.: [3.141](#)
9. Sanchez, LFM and Fournier, B and Jolin, M and Mitchell, D and Bastien, J (2017); Sect.: [3.142](#)
10. Sargolzhahi, Maryam and Kodjo, Serge A and Rivard, Patrice and Rhazi, Jamal (2010); Sect.: [3.148](#)
11. Sargolzhahi, Maryam and Kodjo, Serge A and Rivard, Patrice and Rhazi, Jamal (2010); Sect.: [3.148](#)
12. Smaoui, Nizar and Bérubé, Marc-André and Fournier, Benoit and Bissonnette, Benoit and Durand, Benoit (2004); Sect.: [3.159](#)
13. Smaoui, Nizar and Bérubé, Marc-André and Fournier, Benoit and Bissonnette, Benoit (2004); Sect.: [3.161](#)

2.19 Petrography

1. Fernandes, Isabel and Noronha, Fernando and Teles, Madalena (2004); Sect.: [3.44](#)
2. Fernandes, Isabel and Noronha, Fernando and Teles, Madalena (2007); Sect.: [3.45](#)
3. Haha, M Ben and Gallucci, Emmanuel and Guidoum, Amor and Scrivener, Karen L (2007); Sect.: [3.67](#)
4. Jensen, Viggo (2004); Sect.: [3.82](#)
5. Leemann, Andreas and Merz, Christine (2013); Sect.: [3.90](#)
6. Leemann, A and Lura, P (2013); Sect.: [3.92](#)
7. Mukhopadhyay, Anal and Shon, Chang-Seon and Zollinger, Dan (2006); Sect.: [3.111](#)
8. Mullick, AK (1988); Sect.: [3.112](#)
9. Plusquellec, G and Geiker, MR and Lindgård, J and De Weerd, K (2018); Sect.: [3.128](#)
10. Rivard, Patrice and Fournier, Benoit and Ballivy, Gérard (2002); Sect.: [3.134](#)
11. Rivard, Patrice and Saint-Pierre, François (2009); Sect.: [3.135](#)
12. Rivard, Patrice and Ballivy, Gérard and Gravel, Clermont and Saint-Pierre, François (2010); Sect.: [3.136](#)
13. Sanchez, LFM and Fournier, B and Jolin, M and Bastien, J (2014); Sect.: [3.137](#)
14. Sanchez, LFM and Fournier, B and Jolin, M and Duchesne, Josée (2015); Sect.: [3.139](#)
15. Sanchez, LFM and Fournier, B and Jolin, M and Bastien, J and Mitchell, D (2016); Sect.: [3.140](#)

16. Sanchez, LFM and Fournier, B and Jolin, M and Bedoya, MAB and Bastien, J and Duchesne, J (2016); Sect.: [3.141](#)
17. Sargolzhai, Maryam and Kodjo, Serge A and Rivard, Patrice and Rhazi, Jamal (2010); Sect.: [3.148](#)
18. Shayan, Ahmad and Grimstad, Jack (2006); Sect.: [3.155](#)
19. Torii, Kazuyuki and Kubo, Tetsuji and Sannoh, Chikao and Kanitani, Maki (2016); Sect.: [3.170](#)
20. Yang, Huaquan and Li, Pengxiang and Rao, Meijuan (2017); Sect.: [3.178](#)
21. Batista, António Lopes and Piteira Gomes, J (2016); Sect.: [3.9](#)
22. Takakura, Takeo and Masuda, Hirotaka and Murazumi, Yasuyuki and Takiguchi, Katsuki and Masuda, Yoshihiro and Nishiguchi, Isoharu (2007); Sect.: [3.167](#)
23. Custódio, j. and Ferreira, j. and Silva, A. and Ribeiro, A.B. and Batista, A. (2017); Sect.: [3.29](#)
24. Gunn, R. and Scrivener, K. and Leemann, A. (2017); Sect.: [3.66](#)

2.20 Creep

1. Grimal, 'Etienne and Sellier, Alain and Le Pape, Yann and Bourdarot, 'Eric (2008); Sect.: [3.64](#)
2. Liaudat, Joaquín and Carol, Ignacio and López, Carlos M and Saouma, Victor E (2017); Sect.: [3.97](#)
3. Sausse, J and Fabre, JP (2011); Sect.: [3.149](#)
4. Winnicki, Andrzej and Serkega, Szymon (2017); Sect.: [3.177](#)

2.21 Shrinkage

1. Poyet, Stéphane and Sellier, Alain and Capra, Bruno and Thèvenin-Foray, Geneviève and Torrenti, Jean-Michel and Tournier-Cognon, Hélène and Bourdarot, Eric (2006); Sect.: [3.129](#)
2. Smaoui, N and Bérubé, MA and Fournier, Benoit and Bissonnette, B and Durand, B (2005); Sect.: [3.162](#)

2.22 Temp 38oC (100oF)

1. Berube, Marc-Andre and Frenette, Jean and Pedneault, Annie and Rivest, Michel (2002); Sect.: [3.10](#)
2. Criaud, A and Defossé, C (1995); Sect.: [3.24](#)
3. Dunant, Cyrille F and Scrivener, Karen L (2012); Sect.: [3.35](#)

4. Gao, Xiao Xiao and Multon, Stéphane and Cyr, Martin and Sellier, Alain (2011); Sect.: [3.51](#)
5. Gao, XX and Cyr, M and Multon, S and Sellier, A (2013); Sect.: [3.52](#)
6. Gautam, Bishnu P and Panesar, Daman K (2017); Sect.: [3.56](#)
7. Islam, Mohammad S and Ghafoori, Nader (2015); Sect.: [3.81](#)
8. Lu, Duyou and Zhou, Xiaoling and Xu, Zhongzi and Lan, Xianghui and Tang, Mingshu and Fournier, Benoit (2006); Sect.: [3.103](#)
9. Mukhopadhyay, Anal and Shon, Chang-Seon and Zollinger, Dan (2006); Sect.: [3.111](#)
10. Multon, Stéphane and Barin, François-Xavier and Godart, Bruno and Toutlemonde, François (2008); Sect.: [3.117](#)
11. Na, Okpin and Xi, Yunping and Ou, Edward and Saouma, Victor E (2016); Sect.: [3.120](#)
12. Poyet, Stéphane and Sellier, Alain and Capra, Bruno and Thèvenin-Foray, Geneviève and Torrenti, Jean-Michel and Tournier-Cognon, Hélène and Bourdarot, Eric (2006); Sect.: [3.129](#)
13. Siegert, D and Multon, S and Toutlemonde, F (2005); Sect.: [3.158](#)

2.23 Temp higher than 38

1. Criaud, A and Defossé, C (1995); Sect.: [3.24](#)
2. Gautam, Bishnu P and Panesar, Daman K (2017); Sect.: [3.56](#)
3. Kobayashi, Kazuo and Inoue, Susumu and Yamasaki, Takao and Nakano, Kin-ichi (1988); Sect.: [3.86](#)
4. Leemann, Andreas and Merz, Christine (2013); Sect.: [3.90](#)
5. Liu, Kai-Wei and Mukhopadhyay, Anol K (2015); Sect.: [3.102](#)
6. Marzouk, H and Langdon, S (2003); Sect.: [3.104](#)
7. Wallau, Wilma and Pirkawetz, Stephan and Volland, Katja and Meng, Birgit (2018); Sect.: [3.175](#)

2.24 Capacity curve

1. Bach, Finn and Thorsen, Torsten S and Nielsen, MP (1993); Sect.: [3.7](#)
2. Ferche, Anca C and Panesar, Daman K and Sheikh, Shamim A and Vecchio, Frank J (2017); Sect.: [3.43](#)
3. Giaccio, G and Zerbino, R and Ponce, JM and Batic, Oscar R (2008); Sect.: [3.58](#)
4. Kobayashi, Kazuo and Inoue, Susumu and Yamasaki, Takao and Nakano, Kin-ichi (1988); Sect.: [3.86](#)
5. Sanchez, LFM and Fournier, B and Jolin, M and Bastien, J (2014); Sect.: [3.137](#)
6. Talley, Kimberly G and Kapitan, Jacob G and Breen, John E (2016); Sect.: [3.168](#)

2.25 Aggregate Grain size

1. Berube, Marc-Andre and Frenette, Jean and Pedneault, Annie and Rivest, Michel (2002); Sect.: [3.10](#)
2. Diamond, S and Thaulow, N (1974); Sect.: [3.30](#)
3. Dunant, Cyrille F and Scrivener, Karen L (2012); Sect.: [3.36](#)
4. Fournier, Benoit and Bérubé, Marc-André (2000); Sect.: [3.49](#)
5. Gao, Xiao Xiao and Cyr, Martin and Multon, Stéphane and Sellier, Alain (2013); Sect.: [3.54](#)
6. Lu, Duyou and Zhou, Xiaoling and Xu, Zhongzi and Lan, Xianghui and Tang, Mingshu and Fournier, Benoit (2006); Sect.: [3.103](#)
7. Mukhopadhyay, Anal and Shon, Chang-Seon and Zollinger, Dan (2006); Sect.: [3.111](#)
8. Mullick, AK (1988); Sect.: [3.112](#)
9. Multon, Stéphane and Cyr, Martin and Sellier, Alain and Leklou, Nordine and Petit, Laurent (2008); Sect.: [3.116](#)
10. Multon, Stéphane and Barin, François-Xavier and Godart, Bruno and Toutlemonde, François (2008); Sect.: [3.117](#)
11. Multon, Stéphane and Sellier, Alain and Cyr, Martin (2009); Sect.: [3.118](#)
12. Ostertag, Claudia P and Yi, ChongKu and Monteiro, Paulo JM (2007); Sect.: [3.123](#)
13. Plusquellec, G and Geiker, MR and Lindgård, J and De Weerdt, K (2018); Sect.: [3.128](#)
14. Poyet, Stéphane and Sellier, Alain and Capra, Bruno and Thèvenin-Foray, Geneviève and Torrenti, Jean-Michel and Tournier-Cognon, Hélène and Bourdarot, Eric (2006); Sect.: [3.129](#)
15. Sanchez, LFM and Fournier, B and Jolin, M and Duchesne, Josée (2015); Sect.: [3.139](#)
16. Smaoui, Nizar and Bérubé, Marc-André and Fournier, Benoit and Bissonnette, Benoit and Durand, Benoit (2004); Sect.: [3.159](#)
17. Smaoui, Nizar and Bérubé, Marc-André and Fournier, Benoit and Bissonnette, Benoit (2004); Sect.: [3.161](#)
18. Swamy, R Narayan and Wan, WM Raymond (1993); Sect.: [3.166](#)
19. FHWA (2013); Sect.: [3.48](#)
20. Jensen, Viggo (2012); Sect.: [3.83](#)

2.26 SEM

1. Haha, M Ben and Gallucci, Emmanuel and Guidoum, Amor and Scrivener, Karen L (2007); Sect.: [3.67](#)
2. Helene, Paulo and Carvalho, Mariana and Pacheco, Jéssika (2017); Sect.: [3.74](#)
3. Herrador, Manuel F and Martínez-Abella, Fernando and Dopico, Juan Ramón Rabuñal (2008); Sect.: [3.75](#)
4. Jensen, Viggo (2004); Sect.: [3.82](#)
5. Leemann, Andreas and Merz, Christine (2013); Sect.: [3.90](#)
6. Leemann, A and Lura, P (2013); Sect.: [3.92](#)
7. Mullick, AK (1988); Sect.: [3.112](#)
8. Ostertag, Claudia P and Yi, ChongKu and Monteiro, Paulo JM (2007); Sect.: [3.123](#)
9. Plusquellec, G and Geiker, MR and Lindgård, J and De Weerd, K (2018); Sect.: [3.128](#)
10. Shayan, Ahmad and Grimstad, Jack (2006); Sect.: [3.155](#)
11. Smaoui, N and Bérubé, MA and Fournier, Benoit and Bissonnette, B and Durand, B (2005); Sect.: [3.162](#)

2.27 Fiber reinforced polymer

1. Kubat, Thamer and Al-Mahaidi, Riadh and Shayan, Ahmad (2016); Sect.: [3.87](#)

2.28 Acoustic spectroscopy

1. Leśnicki, Krzysztof J and Kim, Jin-Yeon and Kurtis, Kimberly E and Jacobs, Laurence J (2011); Sect.: [3.94](#)
2. Leśnicki, Krzysztof J and Kim, Jin-Yeon and Kurtis, Kimberly E and Jacobs, Laurence J (2013); Sect.: [3.95](#)
3. Shayan, Ahmad and Grimstad, Jack (2006); Sect.: [3.155](#)

2.29 Rehabilitation

1. Torii, Kazuyuki and Kubo, Tetsuji and Sannoh, Chikao and Kanitani, Maki (2016); Sect.: [3.170](#)
2. Amberg, Francesco (2011); Sect.: [3.2](#)
3. Amberg, F and Stucchi, R and Brizzo, N (2013); Sect.: [3.4](#)
4. Cima, J. and Reinicker, B. (year=2015); Sect.: [3.19](#)

5. Curtis, DD (1995); Sect.: [3.27](#)
6. Curtis, D. and Davis, B. and Rahman, S. and Powell, R. (2005); Sect.: [3.28](#)
7. Donghi, G. and Marcello, C. and Sainati, F. (year=2013); Sect.: [3.33](#)
8. Morenon, P. and Grimal, E. and Kolayer, P. and Sellier, A. and Multon, S. (year=2018); Sect.: [3.110](#)
9. Reinicker, B. and Duke, W. and Cima, J. and Charlwood, R. (2010); Sect.: [3.131](#)
10. Sbarigia, M. and Zinetti, F. and Maugliani, V. and Palmitelli, G. and Mazzolani, S. (2013); Sect.: [3.150](#)
11. Takakura, Takeo and Masuda, Hirotaka and Murazumi, Yasuyuki and Takiguchi, Katsuki and Masuda, Yoshihiro and Nishiguchi, Isoharu (2007); Sect.: [3.167](#)
12. Chulliat, O. and Grimal, E. and Bourdarot, E. (2017); Sect.: [3.26](#)
13. Gocevski, V. and Yildiz, E. (2017); Sect.: [3.60](#)
14. Guilloteau, T. and Martinot, F. and Sausse, J. (2017); Sect.: [3.65](#)
15. Noret, C. and Laliche, K. (2017); Sect.: [3.121](#)
16. Sbarigia, M and Zinetti, F and Hernandez-Bagaglia, M (2016); Sect.: [3.151](#)
17. author="Scuero, A. and Vaschetti, G. (2011); Sect.: [3.152](#)

2.30 Freeze-thaw

2.31 Radiation damage

1. Ichikawa, Tsuneki and Kimura, Takahide (2007); Sect.: [3.80](#)

2.32 Non Destructive Evaluation

2.33 Diagnosis

1. Godart, B and Mahut, B and Fasseu, P and Michel, M (2004); Sect.: [3.61](#)
2. Godart, Bruno and de Rooij, Mario Robert and Wood, Jonathan GM (2013); Sect.: [3.62](#)
3. Leemann, Andreas and Griffa, Michele (2013); Sect.: [3.91](#)
4. Lindgård, Jan and Andiç-Çakır, Özge and Fernandes, Isabel and Rønning, Terje F and Thomas, Michael DA (2012); Sect.: [3.99](#)
5. Lindgård, Jan and Sellevold, Erik J and Thomas, Michael DA and Pedersen, Bård and Justnes, Harald and Rønning, Terje F (2013); Sect.: [3.100](#)
6. Lindgård, Jan and Thomas, Michael DA and Sellevold, Erik J and Pedersen, Bård and Andiç-Çakır, Özge and Justnes, Harald and Rønning, Terje F (2013); Sect.: [3.101](#)

2.34 Performance testing

1. Lindgård, Jan and Nixon, Philip J and Borchers, Ingmar and Schouenborg, Björn and Wigum, Børge Johannes and Haugen, Marit and Åkesson, Urban (2010); Sect.: [3.98](#)
2. Lindgård, Jan and Andiç-Çakır, Özge and Fernandes, Isabel and Rønning, Terje F and Thomas, Michael DA (2012); Sect.: [3.99](#)
3. Lindgård, Jan and Sellevold, Erik J and Thomas, Michael DA and Pedersen, Bård and Justnes, Harald and Rønning, Terje F (2013); Sect.: [3.100](#)
4. Lindgård, Jan and Thomas, Michael DA and Sellevold, Erik J and Pedersen, Bård and Andiç-Çakır, Özge and Justnes, Harald and Rønning, Terje F (2013); Sect.: [3.101](#)
5. Merz, Christine and Leemann, Andreas (2013); Sect.: [3.105](#)

2.35 Micro

1. Dunant, Cyrille F and Scrivener, Karen L (2012); Sect.: [3.36](#)
2. Liaudat, Joaquín and Martínez, A and López, CM and Carol, Ignacio (2015); Sect.: [3.96](#)
3. Multon, Stéphane and Sellier, Alain and Cyr, Martin (2009); Sect.: [3.118](#)

2.36 Meso

1. Comby-Peyrot, Isabelle and Bernard, Fabrice and Bouchard, Pierre-Olivier and Bay, François and Garcia-Diaz, Eric (2009); Sect.: [3.20](#)
2. Morenon, Pierre and Multon, Stéphane and Sellier, Alain and Grimal, Etienne and Hamon, François and Bourdarot, Eric (2017); Sect.: [3.109](#)

2.37 Mega

1. Blanco, A and Cavalaro, SHP and Segura, I and Segura-Castillo, L and Aguado, A (2018); Sect.: [3.13](#)
2. Capra, Bruno and Sellier, Alain (2003); Sect.: [3.16](#)
3. Ferche, Anca C and Panesar, Daman K and Sheikh, Shamim A and Vecchio, Frank J (2017); Sect.: [3.43](#)
4. Hariri-Ardebili, Mohammad Amin and Saouma, Victor E and Merz, Christine (2018); Sect.: [3.68](#)
5. Pan, JianWen and Feng, YunTian and Xu, YanJie and Jin, Feng and Zhang, ChuHan and Zhang, BingYin (2013); Sect.: [3.125](#)
6. Pan, Jianwen and Feng, YT and Jin, Feng and Zhang, Chuhan (2013); Sect.: [3.126](#)
7. Saouma, Victor E and Hariri-Ardebili, Mohammad Amin and Le Pape, Yann and Balaji, Rajagopalan (2016); Sect.: [3.147](#)

8. Sellier, Alain and Bourdarot, Eric and Multon, Stéphane and Cyr, Martin and Grimal, Etienne (2009); Sect.: [3.154](#)
9. Amberg, F and Stucchi, R and Brizzo, N (2013); Sect.: [3.4](#)
10. Cima, J. and Reinicker, B. (year=2015); Sect.: [3.19](#)
11. Curtis, DD (1995); Sect.: [3.27](#)
12. Curtis, D. and Davis, B. and Rahman, S. and Powell, R. (2005); Sect.: [3.28](#)
13. Donghi, G. and Marcello, C. and Sainati, F. (year=2013); Sect.: [3.33](#)
14. Gocevski, V. and Yildiz, E. (2017); Sect.: [3.60](#)

2.38 Multi scale

1. Alnagar, Mohammed and Cusatis, Gianluca and Di Luzio, Giovanni (2013); Sect.: [3.1](#)
2. Dunant, Cyrille F and Scrivener, Karen L (2010); Sect.: [3.34](#)
3. Esposito, Rita and Hendriks, Max AN (2016); Sect.: [3.39](#)

2.39 New constitutive model

1. Comi, C and Fedele, R and Perego, U (2009); Sect.: [3.21](#)
2. Comi, Claudia and Kirchmayr, Beatrice and Pignatelli, Rossella (2012); Sect.: [3.22](#)
3. Esposito, Rita and Hendriks, Max AN (2016); Sect.: [3.39](#)
4. Ferche, Anca C and Panesar, Daman K and Sheikh, Shamim A and Vecchio, Frank J (2017); Sect.: [3.43](#)
5. Giorla, Alain B and Scrivener, Karen L and Dunant, Cyrille F (2015); Sect.: [3.59](#)
6. Huang, M and Pietruszczak, S (1996); Sect.: [3.76](#)
7. Huang, Maosong and Pietruszczak, S (1999); Sect.: [3.77](#)
8. Moranville-Regourd, Michelle (1997); Sect.: [3.108](#)
9. Saouma, Victor and Perotti, Luigi (2006); Sect.: [3.143](#)
10. Saouma, Victor E and Martin, Ruth A and Hariri-Ardebili, Mohammad A and Katayama, Tetsuya (2015); Sect.: [3.146](#)
11. Steffens, Alexander and Li, Kefei and Coussy, Olivier (2003); Sect.: [3.164](#)
12. Reinicker, B. and Abedzadeh, F. and Charlwood, R. and Cima, J. (2013); Sect.: [3.132](#)

2.40 Nonlinear

1. Alnagar, Mohammed and Cusatis, Gianluca and Di Luzio, Giovanni (2013); Sect.: [3.1](#)
2. Nik-Azizan, N.Z. and Mandal, A. and Majid, T.A. and Maity, D. and Nazri, F.M. (2017); Sect.: [3.6](#)
3. Blanco, A and Cavalaro, SHP and Segura, I and Segura-Castillo, L and Aguado, A (2018); Sect.: [3.13](#)
4. Capra, Bruno and Sellier, Alain (2003); Sect.: [3.16](#)
5. Comby-Peyrot, Isabelle and Bernard, Fabrice and Bouchard, Pierre-Olivier and Bay, François and Garcia-Diaz, Eric (2009); Sect.: [3.20](#)
6. Dunant, Cyrille F and Scrivener, Karen L (2012); Sect.: [3.36](#)
7. Fairbairn, Eduardo MR and Ribeiro, Fernando LB and Lopes, Luciana E and Toledo-Filho, Romildo D and Silvano, Marcos M (2006); Sect.: [3.41](#)
8. Giorla, Alain B and Scrivener, Karen L and Dunant, Cyrille F (2015); Sect.: [3.59](#)
9. Hariri-Ardebili, Mohammad Amin and Saouma, Victor E and Merz, Christine (2018); Sect.: [3.68](#)
10. Hariri-Ardebili, Mohammad Amin and Saouma, Victor E (2018); Sect.: [3.69](#)
11. Huang, M and Pietruszczak, S (1996); Sect.: [3.76](#)
12. Huang, Maosong and Pietruszczak, S (1999); Sect.: [3.77](#)
13. Lamea, M and Mirzabozorg, H (2015); Sect.: [3.88](#)
14. Metalssi, Othman Omikrine and Seignol, Jean-François and Rigobert, Stéphane and Toutlemonde, François (2014); Sect.: [3.106](#)
15. Morenon, Pierre and Multon, Stéphane and Sellier, Alain and Grimal, Etienne and Hamon, François and Bourdarot, Eric (2017); Sect.: [3.109](#)
16. Pan, JianWen and Feng, YunTian and Xu, YanJie and Jin, Feng and Zhang, ChuHan and Zhang, BingYin (2013); Sect.: [3.125](#)
17. Pan, Jianwen and Feng, YT and Jin, Feng and Zhang, Chuhan (2013); Sect.: [3.126](#)
18. Parvini, M and Pietruszczak, S and Gocevski, V (2001); Sect.: [3.127](#)
19. Saouma, Victor and Perotti, Luigi (2006); Sect.: [3.143](#)
20. Saouma, Victor and Perotti, Luigi and Shimpo, Takashi (2007); Sect.: [3.144](#)
21. Saouma, Victor E and Hariri-Ardebili, Mohammad Amin and Le Pape, Yann and Balaji, Rajagopalan (2016); Sect.: [3.147](#)
22. Steffens, Alexander and Li, Kefei and Coussy, Olivier (2003); Sect.: [3.164](#)
23. Ulm, Franz-Josef and Coussy, Olivier and Kefei, Li and Larive, Catherine (2000); Sect.: [3.171](#)

24. Curtis, D. and Davis, B. and Rahman, S. and Powell, R. (2005); Sect.: [3.28](#)
25. Donghi, G. and Marcello, C. and Sainati, F. (year=2013); Sect.: [3.33](#)
26. Ferreira, Anna Paula Guida and Farage, Michèle Cristina Resende and Barbosa, Flávio de Souza (2013); Sect.: [3.46](#)
27. Morenon, P. and Grimal, E. and Kolayer, P. and Sellier, A. and Multon, S. (year=2018); Sect.: [3.110](#)
28. Reinicker, B. and Abedzadeh, F. and Charlwood, R. and Cima, J. (2013); Sect.: [3.132](#)
29. Winnicki, Andrzej and Serkega, Szymon (2017); Sect.: [3.177](#)
30. Huang, Hai and Spencer, Benjamin W (2016); Sect.: [3.79](#)
31. Coubard, G. and Sausse, J. (2017); Sect.: [3.23](#)
32. Chulliat, O. and Grimal, E. and Bourdarot, E. (2017); Sect.: [3.26](#)
33. Noret, C. and Laliche, K. (2017); Sect.: [3.121](#)
34. Wang, Jian and Morikawa, Hidenori (2012); Sect.: [3.176](#)

2.41 Coupled

1. Bangert, F and Kuhl, D and Meschke, G (2004); Sect.: [3.8](#)
2. Blanco, A and Cavalaro, SHP and Segura, I and Segura-Castillo, L and Aguado, A (2018); Sect.: [3.13](#)
3. Esposito, Rita and Hendriks, Max AN (2016); Sect.: [3.39](#)
4. Metalssi, Othman Omikrine and Seignol, Jean-François and Rigobert, Stéphane and Toutlemonde, François (2014); Sect.: [3.106](#)
5. Multon, Stéphane and Cyr, Martin and Sellier, Alain and Leklou, Nordine and Petit, Laurent (2008); Sect.: [3.116](#)
6. Ferreira, Anna Paula Guida and Farage, Michèle Cristina Resende and Barbosa, Flávio de Souza (2013); Sect.: [3.46](#)

2.42 Plasticity

1. Parvini, M and Pietruszczak, S and Gocevski, V (2001); Sect.: [3.127](#)
2. Ulm, Franz-Josef and Coussy, Olivier and Kefei, Li and Larive, Catherine (2000); Sect.: [3.171](#)

2.43 Damage Mechanics

1. Alnaggar, Mohammed and Cusatis, Gianluca and Di Luzio, Giovanni (2013); Sect.: [3.1](#)
2. Nik-Azizan, N.Z. and Mandal, A. and Majid, T.A. and Maity, D. and Nazri, F.M. (2017); Sect.: [3.6](#)
3. Bangert, F and Kuhl, D and Meschke, G (2004); Sect.: [3.8](#)
4. Capra, Bruno and Sellier, Alain (2003); Sect.: [3.16](#)
5. Dunant, Cyrille F and Scrivener, Karen L (2016); Sect.: [3.37](#)
6. Giorla, Alain B and Scrivener, Karen L and Dunant, Cyrille F (2015); Sect.: [3.59](#)
7. Grimal, 'Etienne and Sellier, Alain and Le Pape, Yann and Bourdarot, 'Eric (2008); Sect.: [3.64](#)
8. Pan, JianWen and Feng, YunTian and Xu, YanJie and Jin, Feng and Zhang, ChuHan and Zhang, BingYin (2013); Sect.: [3.125](#)
9. Pan, Jianwen and Feng, YT and Jin, Feng and Zhang, Chuhan (2013); Sect.: [3.126](#)
10. Sellier, Alain and Bourdarot, Eric and Multon, Stéphane and Cyr, Martin and Grimal, Etienne (2009); Sect.: [3.154](#)
11. Steffens, Alexander and Li, Kefei and Coussy, Olivier (2003); Sect.: [3.164](#)
12. Ferreira, Anna Paula Guida and Farage, Michèle Cristina Resende and Barbosa, Flávio de Souza (2013); Sect.: [3.46](#)
13. Morenon, P. and Grimal, E. and Kolayer, P. and Sellier, A. and Multon, S. (year=2018); Sect.: [3.110](#)
14. Huang, Hai and Spencer, Benjamin W (2016); Sect.: [3.79](#)
15. Gocevski, V. and Yildiz, E. (2017); Sect.: [3.60](#)

2.44 XFEM

1. Metalssi, Othman Omikrine and Seignol, Jean-François and Rigobert, Stéphane and Toutlemonde, François (2014); Sect.: [3.106](#)

2.45 Thermal analysis

1. Comi, C and Fedele, R and Perego, U (2009); Sect.: [3.21](#)
2. Comi, Claudia and Kirchmayr, Beatrice and Pignatelli, Rossella (2012); Sect.: [3.22](#)
3. Lamea, M and Mirzabozorg, H (2015); Sect.: [3.88](#)
4. Pan, JianWen and Feng, YunTian and Xu, YanJie and Jin, Feng and Zhang, ChuHan and Zhang, BingYin (2013); Sect.: [3.125](#)

5. Pan, Jianwen and Feng, YT and Jin, Feng and Zhang, Chuhan (2013); Sect.: [3.126](#)
6. Saouma, Victor and Perotti, Luigi (2006); Sect.: [3.143](#)
7. Saouma, Victor and Perotti, Luigi and Shimpou, Takashi (2007); Sect.: [3.144](#)
8. Steffens, Alexander and Li, Kefei and Coussy, Olivier (2003); Sect.: [3.164](#)
9. Ulm, Franz-Josef and Coussy, Olivier and Kefei, Li and Larive, Catherine (2000); Sect.: [3.171](#)
10. Amberg, F and Stucchi, R and Brizzo, N (2013); Sect.: [3.4](#)
11. Cima, J. and Reinicker, B. (year=2015); Sect.: [3.19](#)
12. Curtis, DD (1995); Sect.: [3.27](#)
13. Winnicki, Andrzej and Serkega, Szymon (2017); Sect.: [3.177](#)
14. Huang, Hai and Spencer, Benjamin W (2016); Sect.: [3.79](#)

2.46 Moisture analysis

1. Capra, B and Bournazel, J-P (1998); Sect.: [3.15](#)
2. Comi, C and Fedele, R and Perego, U (2009); Sect.: [3.21](#)
3. Grimal, 'Etienne and Sellier, Alain and Le Pape, Yann and Bourdarot, 'Eric (2008); Sect.: [3.64](#)
4. Huang, H and Spencer, BW and Cai, G (2015); Sect.: [3.78](#)
5. Lindgård, Jan and Sellevold, Erik J and Thomas, Michael DA and Pedersen, Bård and Justnes, Harald and Rønning, Terje F (2013); Sect.: [3.100](#)
6. Lindgård, Jan and Thomas, Michael DA and Sellevold, Erik J and Pedersen, Bård and Andić-Çakır, Özge and Justnes, Harald and Rønning, Terje F (2013); Sect.: [3.101](#)
7. Multon, Stéphane and Seignol, Jean-François and Toutlemonde, François (2006); Sect.: [3.114](#)
8. Curtis, DD (1995); Sect.: [3.27](#)
9. Winnicki, Andrzej and Serkega, Szymon (2017); Sect.: [3.177](#)
10. Huang, Hai and Spencer, Benjamin W (2016); Sect.: [3.79](#)

2.47 Seismic

1. Nik-Azizan, N.Z. and Mandal, A. and Majid, T.A. and Maity, D. and Nazri, F.M. (2017); Sect.: [3.6](#)
2. Lamea, M and Mirzabozorg, H (2015); Sect.: [3.88](#)
3. Parvini, M and Pietruszczak, S and Gocevski, V (2001); Sect.: [3.127](#)
4. Tchermer, Julia and Aziz, T (2009); Sect.: [3.169](#)

2.48 Sensitivity

1. Hariri-Ardebili, Mohammad Amin and Saouma, Victor E and Merz, Christine (2018); Sect.: [3.68](#)
2. Hariri-Ardebili, Mohammad Amin and Saouma, Victor E (2018); Sect.: [3.69](#)
3. Saouma, Victor E and Hariri-Ardebili, Mohammad Amin and Le Pape, Yann and Balaji, Rajagopalan (2016); Sect.: [3.147](#)
4. author="Leroy, R. and Boldea, L.I. and Seignol, J.F. and Godart, B. (2011); Sect.: [3.93](#)

2.49 Uncertainty

1. Gholizadeh-Vayghan, Asghar and Rajabipour, Farshad (2017); Sect.: [3.57](#)
2. Hariri-Ardebili, Mohammad Amin and Saouma, Victor E and Merz, Christine (2018); Sect.: [3.68](#)
3. Hariri-Ardebili, Mohammad Amin and Saouma, Victor E (2018); Sect.: [3.69](#)
4. Moranville-Regourd, Michelle (1997); Sect.: [3.108](#)

2.50 Parametric

1. Bangert, F and Kuhl, D and Meschke, G (2004); Sect.: [3.8](#)
2. Lamea, M and Mirzabozorg, H (2015); Sect.: [3.88](#)
3. Metalssi, Othman Omikrine and Seignol, Jean-François and Rigobert, Stéphane and Toutlemonde, François (2014); Sect.: [3.106](#)
4. Morenon, Pierre and Multon, Stéphane and Sellier, Alain and Grimal, Etienne and Hamon, François and Bourdarot, Eric (2017); Sect.: [3.109](#)
5. Saouma, Victor and Perotti, Luigi and Shimpo, Takashi (2007); Sect.: [3.144](#)
6. Saouma, Victor E and Hariri-Ardebili, Mohammad Amin and Le Pape, Yann and Balaji, Rajagopalan (2016); Sect.: [3.147](#)
7. author="Leroy, R. and Boldea, L.I. and Seignol, J.F. and Godart, B. (2011); Sect.: [3.93](#)

2.51 Prognosis

1. Berube, Marc-Andre and Frenette, Jean and Pedneault, Annie and Rivest, Michel (2002); Sect.: [3.10](#)
2. Carles-Gibergues, André and Cyr, Martin (2002); Sect.: [3.17](#)
3. Godart, B and Mahut, B and Fasseu, P and Michel, M (2004); Sect.: [3.61](#)
4. Godart, Bruno and de Rooij, Mario Robert and Wood, Jonathan GM (2013); Sect.: [3.62](#)

5. Saouma, Victor E and Hariri-Ardebili, Mohammad A (2014); Sect.: [3.145](#)
6. Sellier, Alain and Bourdarot, Eric and Multon, Stéphane and Cyr, Martin and Grimal, Etienne (2009); Sect.: [3.154](#)
7. FHWA (2010); Sect.: [3.47](#)

2.52 Mathematical

1. Alnagar, Mohammed and Cusatis, Gianluca and Di Luzio, Giovanni (2013); Sect.: [3.1](#)
2. Capra, Bruno and Sellier, Alain (2003); Sect.: [3.16](#)
3. Comby-Peyrot, Isabelle and Bernard, Fabrice and Bouchard, Pierre-Olivier and Bay, François and Garcia-Diaz, Eric (2009); Sect.: [3.20](#)
4. Comi, C and Fedele, R and Perego, U (2009); Sect.: [3.21](#)
5. Dunant, Cyrille F and Scrivener, Karen L (2010); Sect.: [3.34](#)
6. Esposito, Rita and Anaç, Caner and Hendriks, Max AN and Çopuroğlu, Oğuzhan (2016); Sect.: [3.38](#)
7. Garcia-Diaz, E and Riche, J and Bulteel, D and Vernet, C (2006); Sect.: [3.55](#)
8. Gholizadeh-Vayghan, Asghar and Rajabipour, Farshad (2017); Sect.: [3.57](#)
9. Giorla, Alain B and Scrivener, Karen L and Dunant, Cyrille F (2015); Sect.: [3.59](#)
10. Islam, Mohammad S and Ghafoori, Nader (2015); Sect.: [3.81](#)
11. Liaudat, Joaquín and Carol, Ignacio and López, Carlos M and Saouma, Victor E (2017); Sect.: [3.97](#)
12. Moranville-Regourd, Michelle (1997); Sect.: [3.108](#)
13. Mukhopadhyay, Anal and Shon, Chang-Seon and Zollinger, Dan (2006); Sect.: [3.111](#)
14. Multon, Stéphane and Seignol, Jean-François and Toutlemonde, François (2006); Sect.: [3.114](#)
15. Multon, Stéphane and Toutlemonde, François (2006); Sect.: [3.115](#)
16. Multon, Stéphane and Cyr, Martin and Sellier, Alain and Leklou, Nordine and Petit, Laurent (2008); Sect.: [3.116](#)
17. Pan, JianWen and Feng, YunTian and Xu, YanJie and Jin, Feng and Zhang, ChuHan and Zhang, BingYin (2013); Sect.: [3.125](#)
18. Pan, Jianwen and Feng, YT and Jin, Feng and Zhang, Chuhan (2013); Sect.: [3.126](#)
19. Saouma, Victor E and Martin, Ruth A and Hariri-Ardebili, Mohammad A and Katayama, Tetsuya (2015); Sect.: [3.146](#)
20. Amberg, F (2012); Sect.: [3.3](#)
21. Seignol, Jean François and Godart, Bruno (2012); Sect.: [3.153](#)

2.53 Finite Element

1. Nik-Azizan, N.Z. and Mandal, A. and Majid, T.A. and Maity, D. and Nazri, F.M. (2017); Sect.: [3.6](#)
2. Bangert, F and Kuhl, D and Meschke, G (2004); Sect.: [3.8](#)
3. Blanco, A and Cavalaro, SHP and Segura, I and Segura-Castillo, L and Aguado, A (2018); Sect.: [3.13](#)
4. Capra, Bruno and Sellier, Alain (2003); Sect.: [3.16](#)
5. Comby-Peyrot, Isabelle and Bernard, Fabrice and Bouchard, Pierre-Olivier and Bay, François and Garcia-Diaz, Eric (2009); Sect.: [3.20](#)
6. Comi, C and Fedele, R and Perego, U (2009); Sect.: [3.21](#)
7. Comi, Claudia and Kirchmayr, Beatrice and Pignatelli, Rossella (2012); Sect.: [3.22](#)
8. Esposito, Rita and Hendriks, Max AN (2016); Sect.: [3.39](#)
9. Fairbairn, Eduardo MR and Ribeiro, Fernando LB and Lopes, Luciana E and Toledo-Filho, Romildo D and Silvano, Marcos M (2006); Sect.: [3.41](#)
10. Ferche, Anca C and Panesar, Daman K and Sheikh, Shamim A and Vecchio, Frank J (2017); Sect.: [3.43](#)
11. Giorla, Alain B and Scrivener, Karen L and Dunant, Cyrille F (2015); Sect.: [3.59](#)
12. Grimal, 'Etienne and Sellier, Alain and Le Pape, Yann and Bourdarot, 'Eric (2008); Sect.: [3.64](#)
13. Hariri-Ardebili, Mohammad Amin and Saouma, Victor E and Merz, Christine (2018); Sect.: [3.68](#)
14. Hariri-Ardebili, Mohammad Amin and Saouma, Victor E (2018); Sect.: [3.69](#)
15. Huang, M and Pietruszczak, S (1996); Sect.: [3.76](#)
16. Huang, Maosong and Pietruszczak, S (1999); Sect.: [3.77](#)
17. Huang, H and Spencer, BW and Cai, G (2015); Sect.: [3.78](#)
18. Lamea, M and Mirzabozorg, H (2015); Sect.: [3.88](#)
19. Metalssi, Othman Omikrine and Seignol, Jean-François and Rigobert, Stéphane and Toutlemonde, François (2014); Sect.: [3.106](#)
20. Moranville-Regourd, Michelle (1997); Sect.: [3.108](#)
21. Morenon, Pierre and Multon, Stéphane and Sellier, Alain and Grimal, Etienne and Hamon, François and Bourdarot, Eric (2017); Sect.: [3.109](#)
22. Pan, JW and Feng, YT and Wang, JT and Sun, QC and Zhang, CH and Owen, DRJ (2012); Sect.: [3.124](#)

23. Pan, JianWen and Feng, YunTian and Xu, YanJie and Jin, Feng and Zhang, ChuHan and Zhang, BingYin (2013); Sect.: [3.125](#)
24. Pan, Jianwen and Feng, YT and Jin, Feng and Zhang, Chuhan (2013); Sect.: [3.126](#)
25. Parvini, M and Pietruszczak, S and Gocevski, V (2001); Sect.: [3.127](#)
26. Saouma, Victor and Perotti, Luigi (2006); Sect.: [3.143](#)
27. Saouma, Victor and Perotti, Luigi and Shimpo, Takashi (2007); Sect.: [3.144](#)
28. Saouma, Victor E and Hariri-Ardebili, Mohammad A (2014); Sect.: [3.145](#)
29. Saouma, Victor E and Hariri-Ardebili, Mohammad Amin and Le Pape, Yann and Balaji, Rajagopalan (2016); Sect.: [3.147](#)
30. Sellier, Alain and Bourdarot, Eric and Multon, Stéphane and Cyr, Martin and Grimal, Etienne (2009); Sect.: [3.154](#)
31. Steffens, Alexander and Li, Kefei and Coussy, Olivier (2003); Sect.: [3.164](#)
32. Ulm, Franz-Josef and Coussy, Olivier and Kefei, Li and Larive, Catherine (2000); Sect.: [3.171](#)
33. Amberg, F and Stucchi, R and Brizzo, N (2013); Sect.: [3.4](#)
34. Cima, J. and Reinicker, B. (year=2015); Sect.: [3.19](#)
35. Curtis, DD (1995); Sect.: [3.27](#)
36. Curtis, D. and Davis, B. and Rahman, S. and Powell, R. (2005); Sect.: [3.28](#)
37. Donghi, G. and Marcello, C. and Sainati, F. (year=2013); Sect.: [3.33](#)
38. Ferreira, Anna Paula Guida and Farage, Michèle Cristina Resende and Barbosa, Flávio de Souza (2013); Sect.: [3.46](#)
39. Morenon, P. and Grimal, E. and Kolayer, P. and Sellier, A. and Multon, S. (year=2018); Sect.: [3.110](#)
40. Reinicker, B. and Abedzadeh, F. and Charlwood, R. and Cima, J. (2013); Sect.: [3.132](#)
41. Sbarigia, M. and Zinetti, F. and Maugliani, V. and Palmitelli, G. and Mazzolani, S. (2013); Sect.: [3.150](#)
42. Winnicki, Andrzej and Serkega, Szymon (2017); Sect.: [3.177](#)
43. Seignol, Jean François and Godart, Bruno (2012); Sect.: [3.153](#)
44. Huang, Hai and Spencer, Benjamin W (2016); Sect.: [3.79](#)
45. Coubard, G. and Sausse, J. (2017); Sect.: [3.23](#)
46. Chulliat, O. and Grimal, E. and Bourdarot, E. (2017); Sect.: [3.26](#)
47. Gocevski, V. and Yildiz, E. (2017); Sect.: [3.60](#)
48. Gunn, R. and Scrivener, K. and Leemann, A. (2017); Sect.: [3.66](#)

49. author="Leroy, R. and Boldea, L.I. and Seignol, J.F. and Godart, B. (2011); Sect.: [3.93](#)
50. Noret, C. and Laliche, K. (2017); Sect.: [3.121](#)
51. Wang, Jian and Morikawa, Hidenori (2012); Sect.: [3.176](#)

2.54 Thermal equival.

2.55 Kinetic modeled

1. Dunant, Cyrille F and Scrivener, Karen L (2010); Sect.: [3.34](#)
2. Grimal, 'Etienne and Sellier, Alain and Le Pape, Yann and Bourdarot, 'Eric (2008); Sect.: [3.64](#)
3. Moranville-Regourd, Michelle (1997); Sect.: [3.108](#)
4. Multon, Stéphane and Toutlemonde, François (2006); Sect.: [3.115](#)
5. Saouma, Victor and Perotti, Luigi (2006); Sect.: [3.143](#)
6. Sausse, J and Fabre, JP (2011); Sect.: [3.149](#)

2.56 Literture survey

1. Esposito, R and Hendriks, MAN (2017); Sect.: [3.40](#)
2. Stanton, Thomas E (2008); Sect.: [3.163](#)
3. Helmuth, R. and Stark, D. and Diamond, S. and Moranville-Regourd, M. (2013); Sect.: [3.157](#)

2.57 Poro-Mechanics

1. Gong, Fuyuan and Takahashi, Yuya and Maekawa, Koichi (2017); Sect.: [3.63](#)
2. Liaudat, Joaquín and Martínez, A and López, CM and Carol, Ignacio (2015); Sect.: [3.96](#)

2.58 Chemical reaction

1. Multon, Stéphane and Sellier, Alain and Cyr, Martin (2009); Sect.: [3.118](#)
2. Rajabipour, Farshad and Giannini, Eric and Dunant, Cyrille and Ideker, Jason H and Thomas, Michael DA (2015); Sect.: [3.130](#)

2.59 Petrography

1. Leemann, Andreas and Griffa, Michele (2013); Sect.: [3.91](#)
2. Lindgård, Jan and Nixon, Philip J and Borchers, Ingmar and Schouenborg, Björn and Wigum, Børge Johannes and Haugen, Marit and Åkesson, Urban (2010); Sect.: [3.98](#)
3. Merz, Christine and Leemann, Andreas (2013); Sect.: [3.105](#)
4. Saouma, Victor E and Martin, Ruth A and Hariri-Ardebili, Mohammad A and Katayama, Tetsuya (2015); Sect.: [3.146](#)
5. Stanton, Thomas E (2008); Sect.: [3.163](#)

2.60 Leaching

1. Criaud, A and Defossé, C (1995); Sect.: [3.24](#)
2. Fournier, Benoit and Bérubé, Marc-André (2000); Sect.: [3.49](#)
3. Leemann, Andreas and Griffa, Michele (2013); Sect.: [3.91](#)
4. Lindgård, Jan and Andiç-Çakır, Özge and Fernandes, Isabel and Rønning, Terje F and Thomas, Michael DA (2012); Sect.: [3.99](#)
5. Lindgård, Jan and Sellevold, Erik J and Thomas, Michael DA and Pedersen, Bård and Justnes, Harald and Rønning, Terje F (2013); Sect.: [3.100](#)
6. Merz, Christine and Leemann, Andreas (2013); Sect.: [3.105](#)
7. Sanchez, LFM and Fournier, B and Jolin, M and Bedoya, MAB and Bastien, J and Duchesne, J (2016); Sect.: [3.141](#)

2.61 Gel

1. Capra, B and Bournazel, J-P (1998); Sect.: [3.15](#)
2. Esposito, R and Hendriks, MAN (2017); Sect.: [3.40](#)
3. Fournier, Benoit and Bérubé, Marc-André (2000); Sect.: [3.49](#)
4. Gao, XX and Cyr, M and Multon, S and Sellier, A (2013); Sect.: [3.53](#)
5. Gong, Fuyuan and Takahashi, Yuya and Maekawa, Koichi (2017); Sect.: [3.63](#)
6. Grimal, 'Etienne and Sellier, Alain and Le Pape, Yann and Bourdarot, 'Eric (2008); Sect.: [3.64](#)
7. Leemann, Andreas and Griffa, Michele (2013); Sect.: [3.91](#)
8. Lindgård, Jan and Andiç-Çakır, Özge and Fernandes, Isabel and Rønning, Terje F and Thomas, Michael DA (2012); Sect.: [3.99](#)

9. Lindgård, Jan and Sellevold, Erik J and Thomas, Michael DA and Pedersen, Bård and Justnes, Harald and Rønning, Terje F (2013); Sect.: [3.100](#)
10. Lindgård, Jan and Thomas, Michael DA and Sellevold, Erik J and Pedersen, Bård and Andić-Çakır, Özge and Justnes, Harald and Rønning, Terje F (2013); Sect.: [3.101](#)
11. Multon, Stéphane and Sellier, Alain and Cyr, Martin (2009); Sect.: [3.118](#)
12. Ostertag, Claudia P and Yi, ChongKu and Monteiro, Paulo JM (2007); Sect.: [3.123](#)
13. Pan, JW and Feng, YT and Wang, JT and Sun, QC and Zhang, CH and Owen, DRJ (2012); Sect.: [3.124](#)
14. Rajabipour, Farshad and Giannini, Eric and Dunant, Cyrille and Ideker, Jason H and Thomas, Michael DA (2015); Sect.: [3.130](#)
15. Rivard, Patrice and Fournier, Benoit and Ballivy, Gérard (2000); Sect.: [3.133](#)
16. Rivard, Patrice and Fournier, Benoit and Ballivy, Gérard (2002); Sect.: [3.134](#)
17. Sanchez, LFM and Fournier, B and Jolin, M and Duchesne, Josée (2015); Sect.: [3.139](#)
18. Saouma, Victor E and Martin, Ruth A and Hariri-Ardebili, Mohammad A and Katayama, Tetsuya (2015); Sect.: [3.146](#)
19. Šachlová, Šárka and Příklad, Richard and Pertold, Zdeněk (2010); Sect.: [3.172](#)
20. FHWA (2013); Sect.: [3.48](#)

2.62 Fed-Agencies Reports

1. BOR (1941); Sect.: [3.14](#)
2. FHWA (2010); Sect.: [3.47](#)

2.63 None

1. Capra, Bruno and Sellier, Alain (2003); Sect.: [3.16](#)
2. Comby-Peyrot, Isabelle and Bernard, Fabrice and Bouchard, Pierre-Olivier and Bay, François and Garcia-Diaz, Eric (2009); Sect.: [3.20](#)

2.64 Gravity dam

1. Nik-Azizan, N.Z. and Mandal, A. and Majid, T.A. and Maity, D. and Nazri, F.M. (2017); Sect.: [3.6](#)
2. Bérubé, Marc-André and Duchesne, J and Dorion, JF and Rivest, M (2002); Sect.: [3.11](#)
3. Blanco, A and Cavalaro, SHP and Segura, I and Segura-Castillo, L and Aguado, A (2018); Sect.: [3.13](#)

4. Comi, C and Fedele, R and Perego, U (2009); Sect.: [3.21](#)
5. Comi, Claudia and Kirchmayr, Beatrice and Pignatelli, Rossella (2012); Sect.: [3.22](#)
6. Fairbairn, Eduardo MR and Ribeiro, Fernando LB and Lopes, Luciana E and Toledo-Filho, Romildo D and Silvano, Marcos M (2006); Sect.: [3.41](#)
7. Fernandes, Isabel and Noronha, Fernando and Teles, Madalena (2007); Sect.: [3.45](#)
8. Herrador, Manuel F and Martínez-Abella, Fernando and Dopico, Juan Ramón Rabuñal (2008); Sect.: [3.75](#)
9. Huang, M and Pietruszczak, S (1996); Sect.: [3.76](#)
10. Huang, Maosong and Pietruszczak, S (1999); Sect.: [3.77](#)
11. Huang, H and Spencer, BW and Cai, G (2015); Sect.: [3.78](#)
12. Lu, Duyou and Zhou, Xiaoling and Xu, Zhongzi and Lan, Xianghui and Tang, Mingshu and Fournier, Benoit (2006); Sect.: [3.103](#)
13. Metalssi, Othman Omikrine and Seignol, Jean-François and Rigobert, Stéphane and Toutlemonde, François (2014); Sect.: [3.106](#)
14. Moranville-Regourd, Michelle (1997); Sect.: [3.108](#)
15. Mullick, AK (1988); Sect.: [3.112](#)
16. Parvini, M and Pietruszczak, S and Gocevski, V (2001); Sect.: [3.127](#)
17. Rivard, Patrice and Ballivy, Gérard and Gravel, Clermont and Saint-Pierre, Francois (2010); Sect.: [3.136](#)
18. Sausse, J and Fabre, JP (2011); Sect.: [3.149](#)
19. Sellier, Alain and Bourdarot, Eric and Multon, Stéphane and Cyr, Martin and Grimal, Etienne (2009); Sect.: [3.154](#)
20. Shayan, Ahmad and Grimstad, Jack (2006); Sect.: [3.155](#)
21. Ulm, Franz-Josef and Coussy, Olivier and Kefei, Li and Larive, Catherine (2000); Sect.: [3.171](#)
22. Yang, Huaquan and Li, Pengxiang and Rao, Meijuan (2017); Sect.: [3.178](#)
23. Amberg, Francesco (2011); Sect.: [3.2](#)
24. Amberg, F (2012); Sect.: [3.3](#)
25. Amberg, Francesco and Bremen, Roger and Droz, Patrice and Leroy, RaphaËL and Maier, Johannes and Otto, Bastian (2017); Sect.: [3.5](#)
26. Curtis, D. and Davis, B. and Rahman, S. and Powell, R. (2005); Sect.: [3.28](#)
27. Ferreira, Anna Paula Guida and Farage, Michèle Cristina Resende and Barbosa, Flávio de Souza (2013); Sect.: [3.46](#)

28. Reinicker, B. and Duke, W. and Cima, J. and Charlwood, R. (2010); Sect.: [3.131](#)
29. Reinicker, B. and Abedzadeh, F. and Charlwood, R. and Cima, J. (2013); Sect.: [3.132](#)
30. Sbarigia, M. and Zinetti, F. and Maugliani, V. and Palmitelli, G. and Mazzolani, S. (2013); Sect.: [3.150](#)
31. Winnicki, Andrzej and Serkega, Szymon (2017); Sect.: [3.177](#)
32. Batista, António Lopes and Piteira Gomes, J (2016); Sect.: [3.9](#)
33. Dolen, TP (2011); Sect.: [3.32](#)
34. Huang, Hai and Spencer, Benjamin W (2016); Sect.: [3.79](#)
35. Chulliat, O. and Grimal, E. and Bourdarot, E. (2017); Sect.: [3.26](#)
36. Gocevski, V. and Yildiz, E. (2017); Sect.: [3.60](#)
37. Guilloteau, T. and Martinot, F. and Sausse, J. (2017); Sect.: [3.65](#)
38. author="Lancon, H. and Piot, S. (2011); Sect.: [3.89](#)
39. author="Leroy, R. and Boldea, L.I. and Seignol, J.F. and Godart, B. (2011); Sect.: [3.93](#)
40. Sbarigia, M and Zinetti, F and Hernandez-Bagaglia, M (2016); Sect.: [3.151](#)
41. author="Scuero, A. and Vaschetti, G. (2011); Sect.: [3.152](#)

2.65 Arch dam

1. Bérubé, Marc-André and Duchesne, J and Dorion, JF and Rivest, M (2002); Sect.: [3.11](#)
2. Fernandes, Isabel and Noronha, Fernando and Teles, Madalena (2004); Sect.: [3.44](#)
3. Fernandes, Isabel and Noronha, Fernando and Teles, Madalena (2007); Sect.: [3.45](#)
4. Lamea, M and Mirzabozorg, H (2015); Sect.: [3.88](#)
5. Plusquellec, G and Geiker, MR and Lindgård, J and De Weerdt, K (2018); Sect.: [3.128](#)
6. Saouma, Victor and Perotti, Luigi (2006); Sect.: [3.143](#)
7. Saouma, Victor and Perotti, Luigi and Shimpo, Takashi (2007); Sect.: [3.144](#)
8. Sausse, J and Fabre, JP (2011); Sect.: [3.149](#)
9. Amberg, Francesco (2011); Sect.: [3.2](#)
10. Amberg, F (2012); Sect.: [3.3](#)
11. Amberg, F and Stucchi, R and Brizzo, N (2013); Sect.: [3.4](#)
12. Amberg, Francesco and Bremen, Roger and Droz, Patrice and Leroy, RaphaËL and Maier, Johannes and Otto, Bastian (2017); Sect.: [3.5](#)

13. Cima, J. and Reinicker, B. (year=2015); Sect.: [3.19](#)
14. Morenon, P. and Grimal, E. and Kolayer, P. and Sellier, A. and Multon, S. (year=2018); Sect.: [3.110](#)
15. Batista, António Lopes and Piteira Gomes, J (2016); Sect.: [3.9](#)
16. Coubard, G. and Sausse, J. (2017); Sect.: [3.23](#)
17. Guilloteau, T. and Martinot, F. and Sausse, J. (2017); Sect.: [3.65](#)
18. Gunn, R. and Scrivener, K. and Leemann, A. (2017); Sect.: [3.66](#)
19. Hattingh, L. and Oosthuizen, C. and Tembe, I. and Mahlabela, C. (2017); Sect.: [3.70](#)
20. author="Lancon, H. and Piot, S. (2011); Sect.: [3.89](#)
21. Noret, C. and Laliche, K. (2017); Sect.: [3.121](#)

2.66 Buttress dam

1. Sausse, J and Fabre, JP (2011); Sect.: [3.149](#)
2. Donghi, G. and Marcello, C. and Sainati, F. (year=2013); Sect.: [3.33](#)
3. Batista, António Lopes and Piteira Gomes, J (2016); Sect.: [3.9](#)
4. Custódio, j. and Ferreira, j. and Silva, A. and Ribeiro, A.B. and Batista, A. (2017); Sect.: [3.29](#)
5. Guilloteau, T. and Martinot, F. and Sausse, J. (2017); Sect.: [3.65](#)

2.67 Buildings

1. Heidarzadeh, N and Samadzad, M and Shekarchi, M and Mirghaderi, SR (2017); Sect.: [3.73](#)
2. Parvini, M and Pietruszczak, S and Gocevski, V (2001); Sect.: [3.127](#)

2.68 Bridge

1. Hariri-Ardebili, Mohammad Amin and Saouma, Victor E and Merz, Christine (2018); Sect.: [3.68](#)
2. Helene, Paulo and Carvalho, Mariana and Pacheco, Jéssika (2017); Sect.: [3.74](#)
3. Jensen, Viggo (2004); Sect.: [3.82](#)
4. Miyagawa, Toyooki and Seto, Kaoru and Sasaki, Kazunori and Mikata, Yasuhiro and Kuzume, Kazuhiro and Minami, Toshikazu (2006); Sect.: [3.107](#)
5. Sanchez, LFM and Fournier, B and Jolin, M and Bastien, J (2015); Sect.: [3.138](#)
6. Ulm, Franz-Josef and Coussy, Olivier and Kefei, Li and Larive, Catherine (2000); Sect.: [3.171](#)
7. Šachlová, Šárka and Přikryl, Richard and Pertold, Zdeněk (2010); Sect.: [3.172](#)

2.69 Nuclear power plants

1. Huang, H and Spencer, BW and Cai, G (2015); Sect.: [3.78](#)
2. Ichikawa, Tsuneki and Kimura, Takahide (2007); Sect.: [3.80](#)
3. Saouma, Victor E and Hariri-Ardebili, Mohammad A (2014); Sect.: [3.145](#)
4. Takakura, Takeo and Masuda, Hirotaka and Murazumi, Yasuyuki and Takiguchi, Katsuki and Masuda, Yoshihiro and Nishiguchi, Isoharu (2007); Sect.: [3.167](#)
5. Tcherer, Julia and Aziz, T (2009); Sect.: [3.169](#)

2.70 Roads

1. Steffens, Alexander and Li, Kefei and Coussy, Olivier (2003); Sect.: [3.164](#)

2.71 Reclamation

2.72 ICAAR

2.73 Beams-Panels

1. Fan, Shenfu and Hanson, John M (1998); Sect.: [3.42](#)
2. Ferche, Anca C and Panesar, Daman K and Sheikh, Shamim A and Vecchio, Frank J (2017); Sect.: [3.43](#)
3. Gao, Xiao Xiao and Multon, Stéphane and Cyr, Martin and Sellier, Alain (2011); Sect.: [3.51](#)
4. Gao, XX and Cyr, M and Multon, S and Sellier, A (2013); Sect.: [3.52](#)
5. Gao, Xiao Xiao and Cyr, Martin and Multon, Stéphane and Sellier, Alain (2013); Sect.: [3.54](#)
6. Giaccio, G and Zerbino, R and Ponce, JM and Batic, Oscar R (2008); Sect.: [3.58](#)
7. Hariri-Ardebili, Mohammad Amin and Saouma, Victor E (2018); Sect.: [3.69](#)
8. Kobayashi, Kazuo and Inoue, Susumu and Yamasaki, Takao and Nakano, Kin-ichi (1988); Sect.: [3.86](#)
9. Multon, S and Seignol, J-F and Toutlemonde, F (2005); Sect.: [3.113](#)
10. Multon, Stéphane and Seignol, Jean-François and Toutlemonde, François (2006); Sect.: [3.114](#)
11. Saouma, Victor and Perotti, Luigi and Shimpo, Takashi (2007); Sect.: [3.144](#)
12. Saouma, Victor E and Hariri-Ardebili, Mohammad Amin and Le Pape, Yann and Balaji, Rajagopalan (2016); Sect.: [3.147](#)
13. Siegert, D and Multon, S and Toutlemonde, F (2005); Sect.: [3.158](#)
14. Swamy, R Narayan and Wan, WM Raymond (1993); Sect.: [3.166](#)

15. Talley, Kimberly G and Kapitan, Jacob G and Breen, John E (2016); Sect.: [3.168](#)
16. Wald, David and Martinez, Gloriana Arrieta and Bayrak, Oguzhan (2017); Sect.: [3.174](#)
17. Orbovic, N. and Panesar, D. and Sheikh, S. and Vecchio, F. and Lamarche, C.P. and Blahoianu, A. (2015); Sect.: [3.122](#)

2.74 Intake tower

1. Torii, Kazuyuki and Kubo, Tetsuji and Sannoh, Chikao and Kanitani, Maki (2016); Sect.: [3.170](#)
2. Curtis, DD (1995); Sect.: [3.27](#)
3. Gocevski, V. and Yildiz, E. (2017); Sect.: [3.60](#)

2.75 Slot Cutting

1. Hefny, A and Lo, KY and Adeghe, L (2001); Sect.: [3.72](#)

2.76 Dams

1. Dolen, T. (2005); Sect.: [3.31](#)
2. Hefny, A and Lo, KY and Adeghe, L (2001); Sect.: [3.72](#)
3. Leemann, Andreas and Griffa, Michele (2013); Sect.: [3.91](#)
4. Rivard, Patrice and Fournier, Benoit and Ballivy, Gérard (2000); Sect.: [3.133](#)

2.77 Historical

1. Helmuth, R. and Stark, D. and Diamond, S. and Moranville-Regourd, M. (2013); Sect.: [3.157](#)

3 — References

3.1 Alnaggar, Mohammed and Cusatis, Gianluca and Di Luzio, Giovanni (2013)

URL

```
@article{
alnaggar2013lattice},
label={alnaggar2013lattice},
title={Lattice discrete particle modeling (LDPM) of alkali silica reaction (ASR)
deterioration of concrete structures},
author={Alnaggar, Mohammed and Cusatis, Gianluca and Di Luzio, Giovanni},
journal={Cement and Concrete Composites},
volume={41},
pages={45--59},
year={2013},
publisher={Elsevier}
Keywords={}
```

- The ASR effect is implemented within the framework of the Lattice Discrete Particle Model (LDPM) which simulates concrete heterogeneous character at the scale of coarse aggregate pieces.
- Main features include: volumetric expansion; expansion anisotropy under applied loading; non-uniform cracking distribution; concrete strength and stiffness degradation; alkali ion concentration effect; and temperature effects.
- The proposed LDPM-ASR model is calibrated using experimental results obtained by Multon and Toutlemonde (2006):
 - Experiments were performed using sealed cylindrical specimens (240 mm length and 130 mm in diameter).
 - Three different cases were considered: (1) free expansion; (2) restrained expansion by using a 3 mm thick steel ring; and (3) restrained expansion by using a 5 mm thick steel ring.
 - For each case, three loading conditions were considered: axial stresses of 0, 10, and 20 MPa.
 - The tests were characterized over a duration of 450 days after curing the specimens for 28 days at room temperature.

- Axial strains corresponding to the total expansion of specimens were averaged from 14 measurements regularly spaced over the perimeter.
 - For radial strains, diameter variations were measured at three levels of the cylinders at 10 regularly spaced angular locations.
- The experimental results show shrinkage of about 0.25% for the control nonreactive specimens. Also, there exists a considerable amount of creep. The formulated meso-scale model, however, does not include shrinkage and/or creep.
- A simplified approach was taken by adding basic creep and shrinkage strains macroscopically to the LDPM averaged responses.
- Figures 3.1 and 3.2 show the axial and radial strain evolution for the three models:
 - Simulated 1: excluding the effect of creep and shrinkage
 - Simulated 2: including creep and total shrinkage calibrated on companion specimen data
 - Simulated 3: including creep and estimated autogenous shrinkage

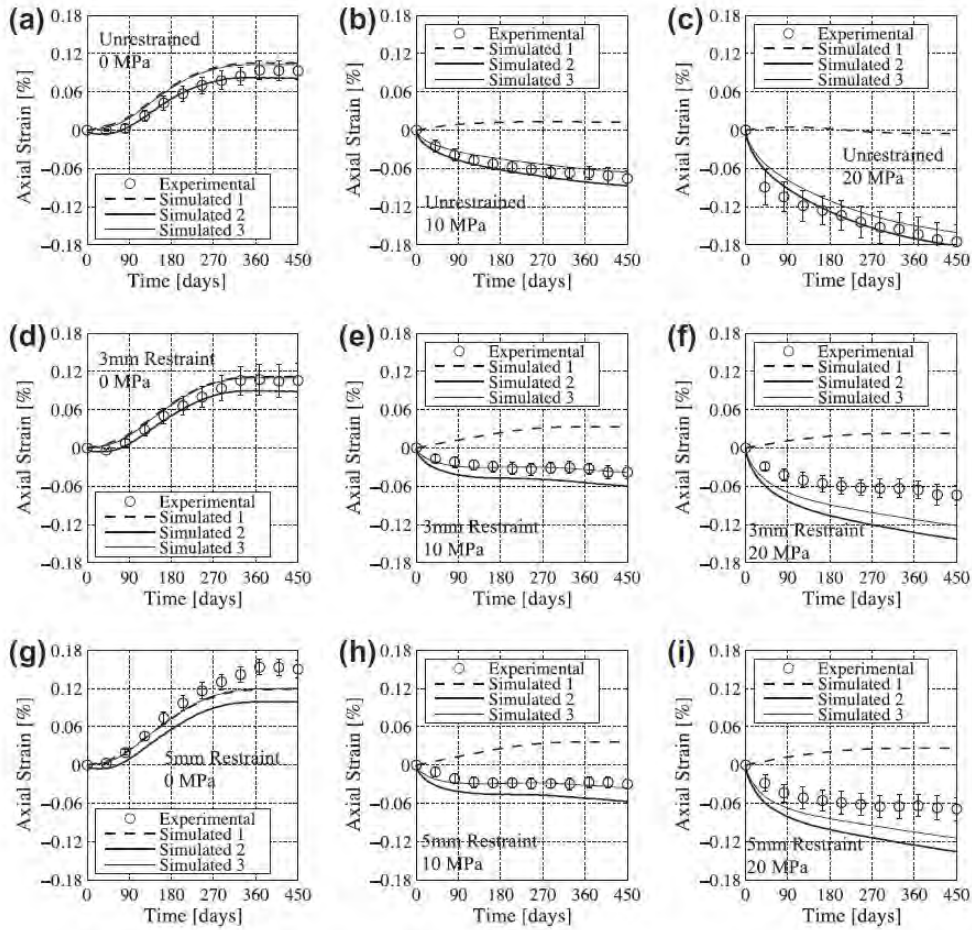


Figure 3.1: Axial strain evolution for: (a) Unrestrained specimens under 0 MPa, (b) Unrestrained specimens under 10 MPa, (c) Unrestrained specimens under 20 MPa, (d) 3-mm-Restrained specimens under 0 MPa, (e) 3-mm-Restrained specimens under 10 MPa, (f) 3-mm-Restrained specimens under 20 MPa, (g) 5-mm-Restrained specimens under 0 MPa, (h) 5-mm-Restrained specimens under 10 MPa, (i) 5-mm-Restrained specimens under 20 MPa

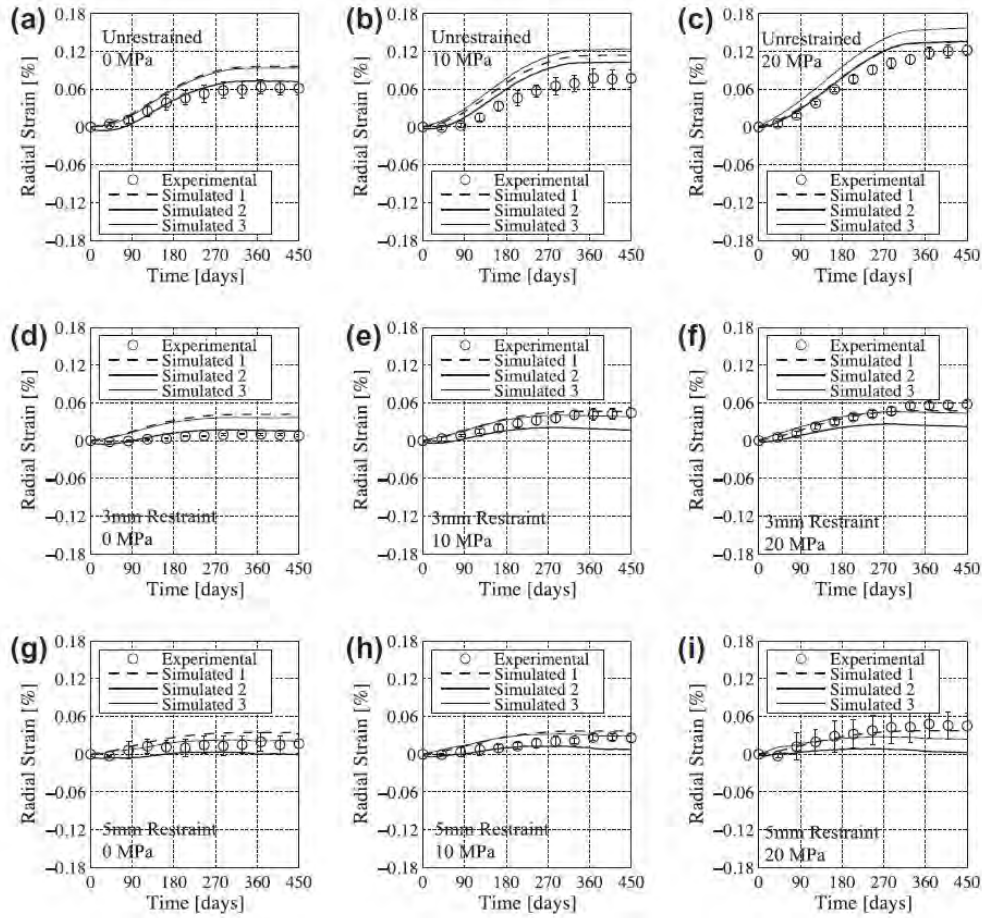


Figure 3.2: Radial strain evolution for: (a) Unrestrained specimens under 0 MPa, (b) Unrestrained specimens under 10 MPa, (c) Unrestrained specimens under 20 MPa, (d) 3-mm-Restrained specimens under 0 MPa, (e) 3-mm-Restrained specimens under 10 MPa, (f) 3-mm-Restrained specimens under 20 MPa, (g) 5-mm-Restrained specimens under 0 MPa, (h) 5-mm-Restrained specimens under 10 MPa, and (i) 5-mm-Restrained specimens under 20 MPa

3.2 Amberg, Francesco (2011)

```
@article{
  amberg2011performance},
label={amberg2011performance},
title={Performance of dams affected by expanding concrete},
author={Amberg, Francesco},
journal={Dams and Reservoirs under Changing Challenges},
pages={115--122},
year={2011},
publisher={CRC Press}
Keywords={}
```

- The most common chemical reactions causing concrete swelling are alkali aggregate reaction (AAR) and sulfate reaction (ISA). These reactions can also appear in combined form.
- According to the ICOLD Bulletin 97 (1991), the term AAR includes three types of reactions: the most common alkali-silica reaction (ASR), the slow rate alkali-silicate reaction (ASR), and the least frequent alkali-carbonate reaction (ACR).
- The concrete swelling leads to an increase in dam crest elevation.
- The value of rising allows a direct estimation of the expansion rate. This can vary from 5 mm/m/year up to 200 mm/m/year.
- Swelling of concrete might also occur more rapidly, but these cases have generally been able to be detected before dam construction.
- In some particular cases, a crest rising is more difficult to detect - even if the presence of concrete expansion is confirmed.
- The expansion rate in the vertical direction is often not uniform over the dam height.
- In arch dams, the presence of expansive phenomena induces an upstream drift.
- In straight gravity dams, an upstream drift can be observed, but in these cases the mentioned drift is due to nonuniform expansion within the wall thickness. In gravity dams, the drift might also be directed downstream.
- The current behavior of dams affected by extremely slow expansive phenomena is generally satisfactory since the swelling is at its initial state of progress, but small cracks do typically develop in those dams.
- It is possible to distinguish between two types of cracks: cracks induced directly by differential swelling and cracks induced indirectly by the structural response to the concrete expansion.
- Cracks produced directly by differential swelling are visible in particular in the inspection galleries. These cracks are characterized by a relative continuity along the gallery, but they are often not visible or are less visible on both dam faces.
- On the contrary, the typical diffuse cracking at the surface of structures affected by swelling is not visible in many dams.

- Structural cracks, produced indirectly by expansion, appear typically along structural discontinuities.
- The upstream drift in arch dams produces tensile stress at the downstream dam toe in case of low reservoir.
- Typical phenomena observed in concrete dams with expansion are:
 - Rising of dam height and horizontal permanent displacements (often upstream of drift).
 - Greater expansion in the upper part of the dam.
 - Nonuniform expansion within the dam body, causing cracks in galleries which are less visible at both dam faces.
 - Structural cracks due to the new equilibrium induced by permanent displacements.
- For the extremely slow rate of expansive phenomena in dams, i.e. less than 30 mm/m/year, it appears that the effect of moisture is of secondary importance for the reaction kinetics.
- The presence of internal cracks, observed in the inspection galleries but which were not found at the faces, clearly indicate a greater expansion near the surface than in the internal part of a dam.
- The most probable reason is that the reaction at the faces is accelerated by the higher temperatures. Many dams located in south facing slopes are strongly subjected to solar radiation.
- The average yearly temperature downstream can be 4-5°C higher than at the upstream face, and the maximum temperature in summer might be even more than 10°C higher.
- The temperature dependency could explain the greater expansion observed in the upper part relative to the lower part of many dams. In fact, in the upper, thinner part, the concrete reaches higher temperatures.
- Additional factor which explain a greater expansion near the faces of a dam than within the structure:
 - A facing concrete with higher cement content, and thus higher alkali content.
 - A higher content of oxygen near the faces exposed to air, which is favorable for the ISA reaction.
- In gravity dams, the mitigating effect of compressive stress on the expansion can clearly be observed.
- The horizontal expansion is clearly hindered by the structure and, therefore, an increase of compressive stress is expected.
- Since the chemical expansion is a slow load condition, creep is included in the structural behavior where it plays an important role.
- The safety assessment for the actual condition and the evaluation of the static equilibrium for medium and long term behavior thus becomes of primary importance for optimizing the maintenance.

- The simulation of the reaction in laboratory and the identification of the main parameters influencing the expansion rate in the dam have to take into account different factors, such as:
 - The already mentioned temperature, moisture, and constraint.
 - The alkali content in the concrete.
 - The dimension of the aggregates.
 - The dimension and thickness of the structure; moisture needs more time to penetrate through a thick structure than in a thin one. For a dam, it must also be considered that the water firstly infiltrates along cracks and joints and only subsequently diffuses through the concrete mass.
- Remedial works can be categorized into two parts:
 - Mitigate any expansion phenomenon
 - * Installation of an impervious membrane on the upstream dam face. The effect of this type of intervention is uncertain.
 - * Reduction of temperature, for example through watering. Nevertheless, the effect of this measure is limited.
 - * Increase of compressive stress by means of anchorages or additional masses. Theoretically a possible solution, but it is not feasible in practice since the forces required to limit the expansion in a dam would be very high.
 - Mitigate the effects of the reaction
 - * Grouting of the cracks with cement grout or epoxy resins to enhance the structural continuity, reduce leakage, or increase sliding safety on the lift joints.
 - * Improve the drainage and/or the grouting curtains to reduce uplift pressure and seepage.
 - * Sealing the upstream face with a membrane to avoid possible water inflow through cracks.
 - * Reinforcing using anchorages to assure the stability of a damaged dam.
 - * Slot cutting to relieve the compressive stresses on the downstream face.

3.3 Amberg, F (2012)

```
@inproceedings{
  amberg2012review},
  label={amberg2012review},
  title={A. review of expanding concrete cases and consequences on dam performance},
  author={Amberg, F},
  booktitle={Hydro 2012 Conference, Bilbao},
  year={2012}
  Keywords={}
```

- The paper highlights typical behaviors and phenomena observed in dams affected by expanding concrete.
- The behavior of four dams is presented anonymously, Figure 3.3.

- Gravity dam No.1
 - It is a 22 m high gravity dam built between 1951 and 1952.
 - In plan view, the gravity dam has a slight curvature.
 - In the beginning of the 1970s, a drift upstream began to occur, and vertical displacements were observed.
 - The recorded measures indicated at crest level an upstream drift of 0.2 mm/year and a rising of about 0.3 mm/year.
 - The expansion at the downstream face was greater than upstream, creating a rotation in upstream direction.
 - The greater expansion near the downstream face might be explained with higher temperatures.
 - Within the gallery, on both side walls, cracks were observed. The cracks on the downstream side open about 0.04 mm/year.
 - The crack does not reach the downstream face, demonstrating the hypothesis of a local greater expansion might be correct. Thus, the downstream face is in compression in the vertical direction.

- Arch gravity dam No.2
 - It is a 45 m high dam built in 1960, and the effects of concrete expansion have been observed since 1970.
 - Currently, the upstream drift is 2.0 mm/year at crest level.
 - At the beginning of the 1980s, cracks appeared on both sides of the upper gallery and developed into two continuous cracks. Both cracks are not visible on the dam faces.
 - In order to analyze the dam behavior, a structural analysis was performed assuming uniform expansion.
 - The fact that the crack does not reach the downstream face indicates that the compressive stress within the arches does not significantly exceed 1 MPa.

- Arch dam No.3
 - This is a thin arch dam built in 1965. Since around 1990, a drift in the upstream direction has been observed.
 - At crest elevation, the drift amounts to 1.4 mm/year.
 - To obtain the measured permanent displacement, a variable expansion over the height and different values for the vertical and the horizontal expansion have to be considered, Figure 3.4.
 - It appears that the vertical expansion is greater than the horizontal one.

- Gravity dam No.4
 - This dam was built in two phases: the first in 1926 and the second in 1943.
 - The dam is located at an elevation where the environment is quite cold.
 - Since 1960-65 the dam behavior shows the effect of concrete expansion.

- Observed are a crest rising, a horizontal drift displacement, and cracks.
- In plan view, the gravity dam has a straight part and a curved part in the highest portion of the dam. The behavior of these two parts is different.
- In the 1970s, a crack occurred on the downstream face, 6.5 m below the crest. Today, the opening rate of this crack is 0.7 mm/year.
- The fact that for this gravity dam a greater expansion occurs on the upstream than on the downstream face is confirmed by the behavior of the straight part.

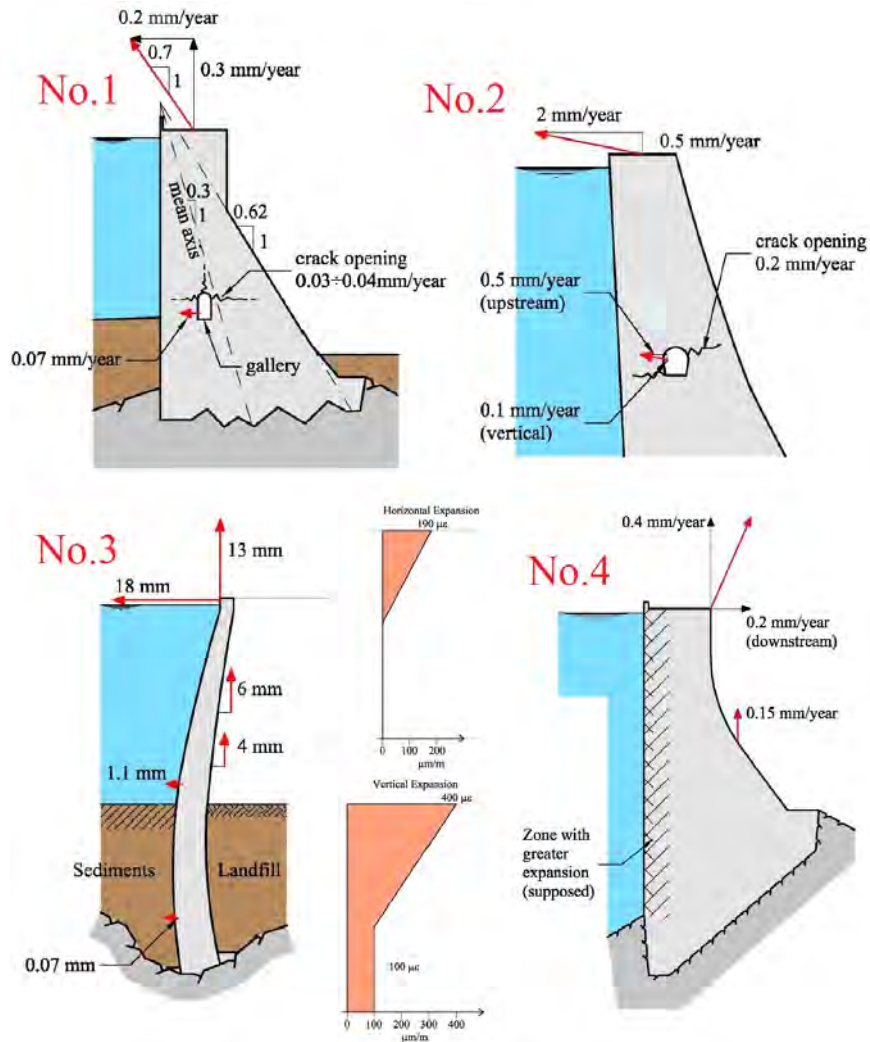


Figure 3.3: All the studied dams; Amberg (2012)

- All the case studies demonstrate that concrete expansion is not uniform within the structure, but varies mainly as a function of temperature and stress state.
- For the same structure, formed by three beams, three different loading cases are taken into account, producing practically the same displacement of the common node towards the left hand side.

- For Case 1, an expansion only in the horizontal beam is considered. Since its free expansion is partially hindered by the stiffness of both of the sub-vertical beams, a compressive stress might result in the horizontal beam. Since the two other beams are pushed towards the left-hand side, a tensile stress is obtained in the right beam and a compressive stress in the left one.
- For Case 2, an expansion occurs only in the right sub-vertical beam. The elongation of this beam is somehow hindered by the left sub-vertical beam, and, due to their interaction, a rotation and deformation towards the left hand side occurs. Both the horizontal and the left sub-vertical beams are in traction, while the right sub-vertical beam is in compression.
- Case 3 shows the combination of 1 and 2 where finally no stresses are induced within the structure.

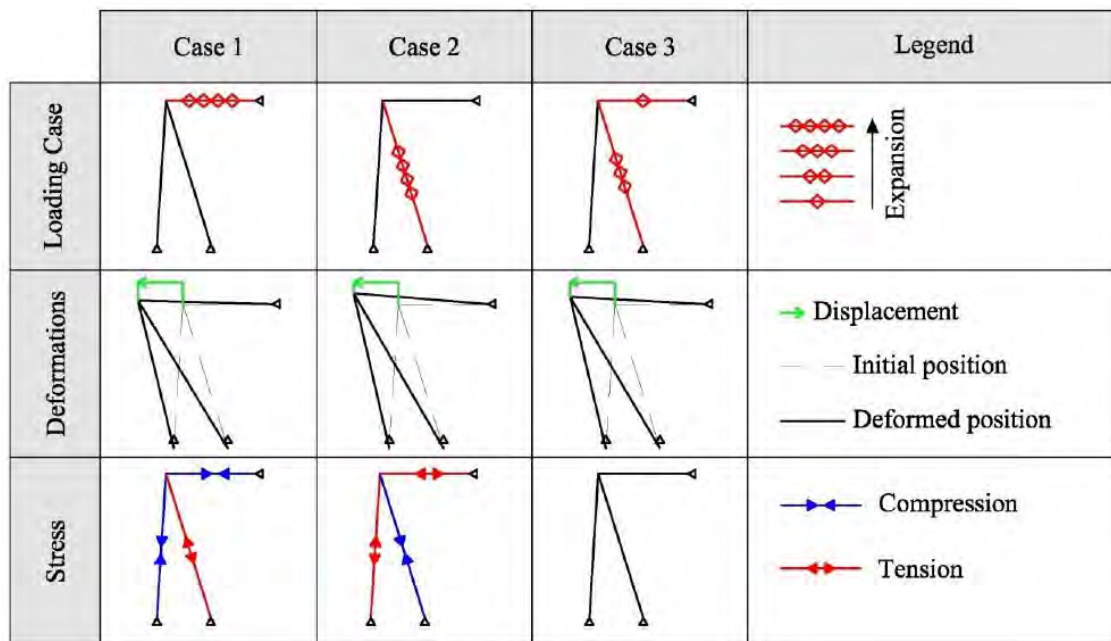


Figure 3.4: Variation of static equilibrium due to internal expansion; Amberg (2012)

3.4 Amberg, F and Stucchi, R and Brizzo, N (2013)

```
@inproceedings{
  amberg2013effect},
  label={amberg2013effect},
  title={The effect of temperature on the development of the Alkali Aggregate
    Reaction at the Pian Telessio dam},
  author={Amberg, F and Stucchi, R and Brizzo, N},
  booktitle={9th ICOLD European Club Symposium},
  year={2013}
  Keywords={}
```


- The effect of temperature on the development of the AAR at the Pian Telesio Dam is studied.
- It is an arch gravity dam located in Northern Italy.
- Since the second half of the 1970s, approximately 20 years after its completion, the Dam is showing an upstream drift caused by concrete expansion due to AAR.
- In 2008, rehabilitation works by means of vertical slot cuttings in the upper half of the Dam were performed in order to reduce the effects of the concrete expansion.
- The Dam's actual behavior during the rehabilitation diverged from the estimations based on the structural analysis performed during the design of the rehabilitation works.
- The downstream displacement of the Dam was lower than estimated.
- The analysis performed prior to rehabilitation works considered the effect of compressive stress and of humidity on the AAR development. However, these considerations were not sufficient.
- Thus, new analyses were performed to account for the temperature effects.
- The new model predicted the response with improved accuracy.
- In the new analyses, the stress state is compatible with the crack location, peripheral joint openings, cutting slot closure measures, and the results of flat jack tests performed during the rehabilitation works.
- In 2008, in order to evaluate the temperature effect on AAR, long term laboratory tests (2-3 years of duration) on concrete specimens (prism $7 \times 7 \times 28$ cm) were performed.
- Since the laboratory test results are unsuitable to be directly applied to the real structure, a back analysis aimed to identify the required parameters was performed. The analysis focused on the three parameters (τ_l , τ_c , and ε_∞) leaving the others unchanged.
- The calibration is done on the permanent upstream displacement, recorded by four pendulums distributed along the Dam.
- In order to obtain the correct time evolution of the AAR, four reference dates are considered. The total number of target parameters is 32.
- In order to evaluate the permanent displacement due to AAR, the expansion distribution along the Dam's thickness is applied to a 3D model.
- Figure 3.5 shows the concrete expansion applied to the model as a function of the Dam's elevation for the four reference dates.
- The nonuniform drift distribution observed for the Dam, which is more relevant at the crest than in the lower part, is obtained with uniform material properties and with constant expansion parameters within the Dam.
- Calculated concrete expansion distribution for the year 2008 is shown in Figure 3.6, with reference to the central block of the Dam. The nonlinearity of the expansion along the Dam's thickness is clear. Linearized distributions are plotted with a dashed line.

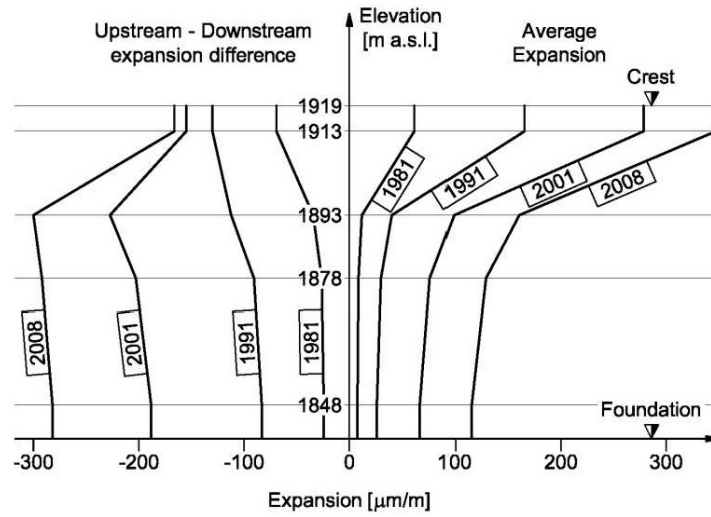


Figure 3.5: Volumetric expansion applied to the model; Amberg, Stucchi, and Brizzo (2013)

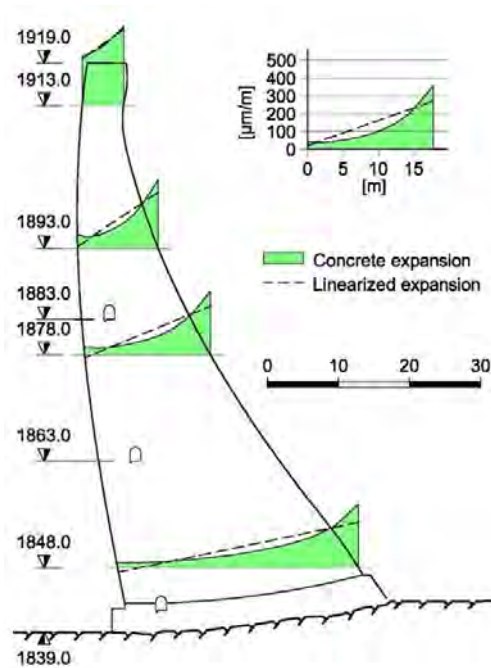


Figure 3.6: Calculated concrete expansion distribution at 2008; Amberg, Stucchi, and Brizzo (2013)

- The highest expansion is observed along the downstream face as well as in the upper, thin Dam part.
- The objective of slot cutting is to release the horizontal compressive stresses generated in the arches by the AAR expansion. Thus, a displacement in the downstream direction is expected.
- Figure 3.7 shows the closure of a principal slot as predicted by the new analysis.
- The slot closure is not uniform. Summing up the closure at the crest of all principal and secondary slots, the total computed closure at the crest reaches 51 mm upstream and 83 mm

downstream. The measured values are 56 mm and 66 mm, respectively.

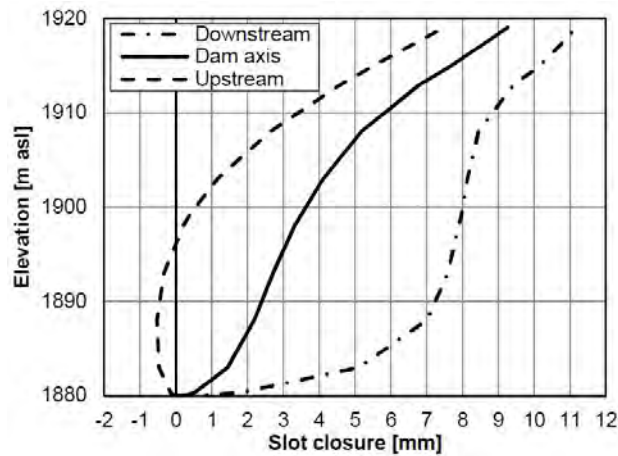


Figure 3.7: Computed closure of a slot during cutting; Amberg, Stucchi, and Brizzo (2013)

3.5 Amberg, Francesco and Bremen, Roger and Droz, Patrice and Leroy, Raphaël and Maier, Johannes and Otto, Bastian (2017)

```
@article{
  amberg2017swelling},
label={amberg2017swelling},
title={Swelling Dams in Switzerland},
author={Amberg, Francesco and Bremen, Roger and Droz, Patrice and Leroy,
  Rapha{\`E}L and Maier, Johannes and Otto, Bastian},
journal={Swelling Concrete in Dams and Hydraulic Structures: DSC 2017},
pages={40},
year={2017},
publisher={John Wiley \& Sons}
Keywords={}
```

- The paper summarizes the research on the current situation in Switzerland related to expansive phenomena in concrete dams.
- The behavior of a dam affected by this type of chemical reaction is characterized by trends, with both horizontal and vertical non-reversible displacements.
- The presence of trends have therefore been identified, analyzed, and compared on various structures.
- Among 154 dams, a relevant number, roughly 50%, is concerned by the problem. The expansions are quite low with average rates up to 30 $\mu\text{m}/\text{m}/\text{year}$.
- These 154 dams are classified in three groups:

- Class I: 74 dams (50%), H_i 40 m, or H_i 10 m and V_i 1 Mm³
 - Class II: 35 dams (25%), H_i 25 m, or H_i 15 m and V_i 50,000 m³, or H_i 10 m and V_i 0.1 Mm³, or H_i 5 m and V_i 0.5 Mm³
 - Class III: 35 dams (25%), smaller dams, in particular up to 25 m high but with small reservoir volumes
- Four categories of instrumentation were considered:
 - Horizontal displacements
 - * Pendulum
 - * Others devices, typically geodetic measurements. In many dams, the measurement interval is 5 years.
 - Vertical displacements
 - * Levelling: levelling together with geodetic measurements is the most commonly used monitoring device to record the vertical displacements.
 - * Invar wires, extensometers, and other devices.
 - The behavior of Swiss dams is defined as “In arch dams an upstream drift and a progressive crest rising is expected, while in gravity dams the horizontal drift might also be in downstream direction.” Subsequently, the identification of the presence of such tendencies became the focus.
 - Five answers are considered: yes, probably yes, situation unknown, probably no, and no.
 - Figure 3.8 shows the situation for all 74 concrete dams of class I (left), and the right plot is 90% of all dams including class II and III, as well.

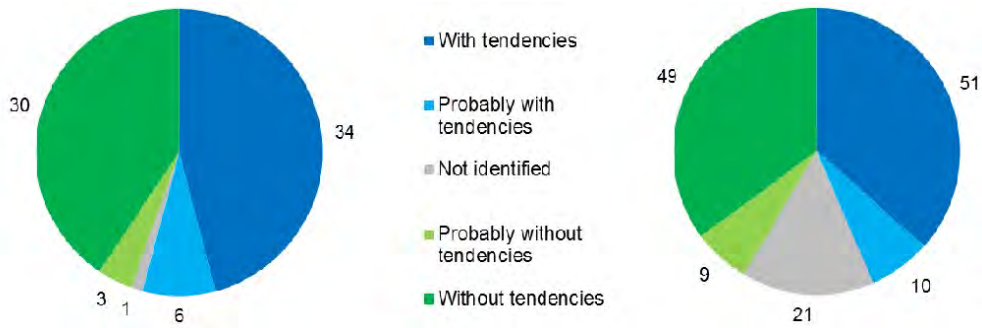


Figure 3.8: insert; Amberg et al. (2017)

•

3.6 Nik-Azizan, N.Z. and Mandal, A. and Majid, T.A. and Maity, D. and Nazri, F.M. (2017)

URL

```

@article{
azizan2017numerical},
label={azizan2017numerical},
title={Numerical prediction of stress and displacement of ageing concrete dam due
to alkali-aggregate and thermal chemical reaction},
author={Nik-Azizan, N.Z. and Mandal, A. and Majid, T.A. and Maity, D. and Nazri,
F.M.},
journal={Structural Engineering and Mechanics},
volume={64},
number={6},
pages={793--802},
year={2017}
Keywords={Laboratory; Reinforcement; Mega; New Const. Model; Capacity curve;
Finite Element; Beams-Panels }

```

- AAR damage analysis of Koyna gravity dam is performed to predict the stresses and displacements.
- Two-dimensional plane strain simulation is used.
- The extent of damage in concrete is computed using the orthotropic damage index proposed by Ghrib and Tinawi (1995). The ratio of degradation lies between 0 and 1, where zero represents no degradation and one corresponds to fully degraded material.
- Total porosity, ϕ , of concrete is considered as a measure to determine the degradation parameter:

$$\phi = \phi_0 + \phi_c + \phi_m \quad (3.1)$$

where ϕ_0 is the initial porosity, ϕ_c is the chemical porosity resulting from skeleton dissolution, and ϕ_m is the apparent mechanical porosity.

- Larive curve is used to present the volumetric expansion.
- Degradation of the modulus of elasticity and tensile strength is considered with an AAR damage factor:

$$\frac{E}{E_0} = \frac{f_t}{f_{t0}} = 1 - \frac{\varepsilon_{AAR}}{\varepsilon_{AAR} + 0.003} \quad (3.2)$$

- Using curve fitting on some data from 52 years old Kariba arch dam (Pan et al., 2013b), the following empirical expansion equation was proposed:

$$\varepsilon_{AAR} = 0.00435t^{1.1163} \quad (3.3)$$

- For the seismic analyses, the rigid foundation assumption with empty reservoir is considered.
- Moreover, two series of data were used to develop empirical material degradation models: Washa, Saemann, and Cramer (1989) and Dolen (2005b). Subsequently, the results of finite element simulations are developed separately for each one.

$$f_c(t_a) = 2.54 \ln t_a + f_{c0} \quad (3.4)$$

$$E(t_a) = 0.0175t_a^3 - 3.4054t_a^2 + 29.807t_a + E \quad (3.5)$$

- Finite element simulations were performed at three times: after completion, 50 years later, and 100 years later.
- The crest displacement of dam increased over time, Figure 3.9.

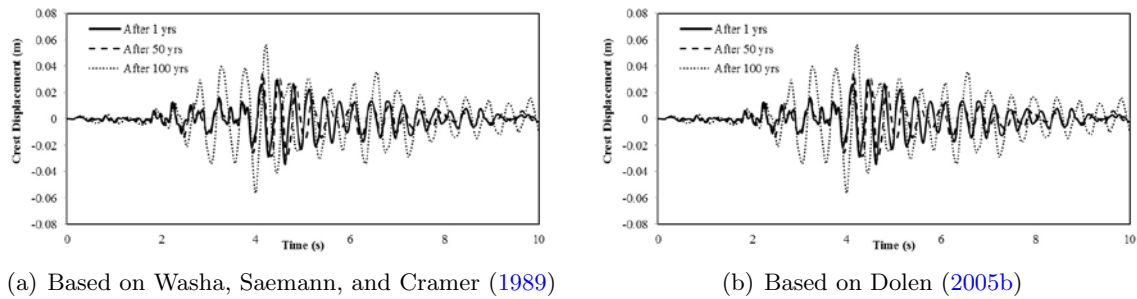


Figure 3.9: Comparison on crest displacement; Nik-Azizan et al. (2017)

- On the other hand, the contour plots revealed that the major principal stress at the neck reduced over time. These findings are attributed to the smaller modulus of elasticity in the aged dam and more flexible behavior.

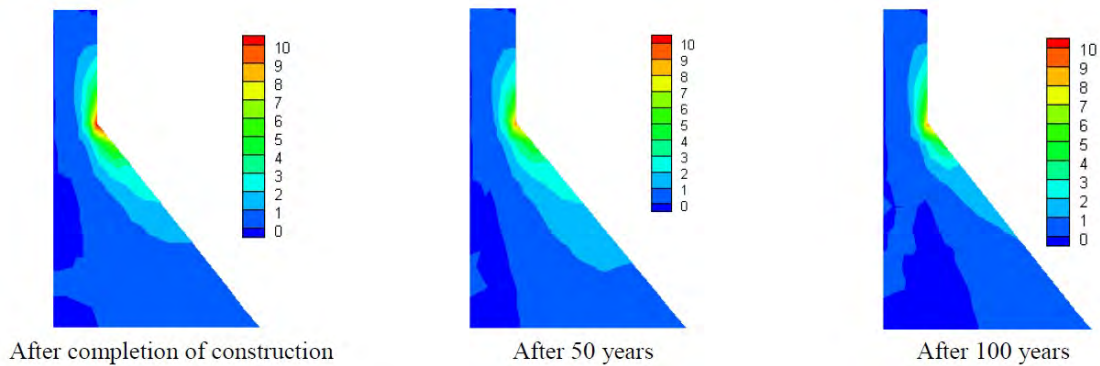


Figure 3.10: Maximum major principal stresses contour based on (Washa, Saemann, and Cramer, 1989); Nik-Azizan et al. (2017)

3.7 Bach, Finn and Thorsen, Torsten S and Nielsen, MP (1993)

[URL](#)

```
@article{
bach1993load},
label={bach1993load},
title={Load-carrying capacity of structural members subjected to alkali-silica
reactions},
author={Bach, Finn and Thorsen, Torsten S and Nielsen, MP},
journal={Construction and Building Materials},
volume={7},
number={2},
pages={109--115},
year={1993},
publisher={Elsevier}
Keywords={}
```

- The influence of ASR on load-carrying capacity of four types of structural members is investigated.
- Those four test series are listed below with the geometry, reinforcement, and loading protocol summarized in Figure 3.11.
 - Series A: Shear test on beams without shear reinforcement
 - Series C: Anchorage tests on beams
 - Series D: Anchorage tests on pull-out specimens
 - Series E: Punching tests on slabs
- All the specimens were cast with alkaline-susceptible aggregates and subjected to accelerated ASR.
- For the evaluation of the deterioration, a grading scale ranging from 0 to 4 is used: 0 corresponds to no deterioration, and 4 signifies deterioration to the point where “safety against failure is dubious or eliminated.”
- The structural and micro-structural analysis of cores from the beams shows a crack system parallel to the surfaces moving inward. The beams are thus subdivided into a damaged outer zone and a relatively undamaged inner zone.
- From the inspection of the beams, the following general observations are made:
 - On the beam faces, two to four continuous cracks are generally seen. The cracks run parallel to, and usually near, the edges.
 - The crack widths vary from 0.1 to 3.0 mm.
 - On the top face, one continuous crack is generally seen. The crack width is always 3.0 mm.
 - The fine cracks only penetrate the surface layer. The wider cracks go deeper and probably through the beam.
 - On all the faces of the beam, 10-15 pop-outs per 100 cm² (diameter 5-15 mm) are typical. A reacted grain is seen in the bottom of each pop-out.
 - White, threadlike salt precipitations are seen on most of the beams.

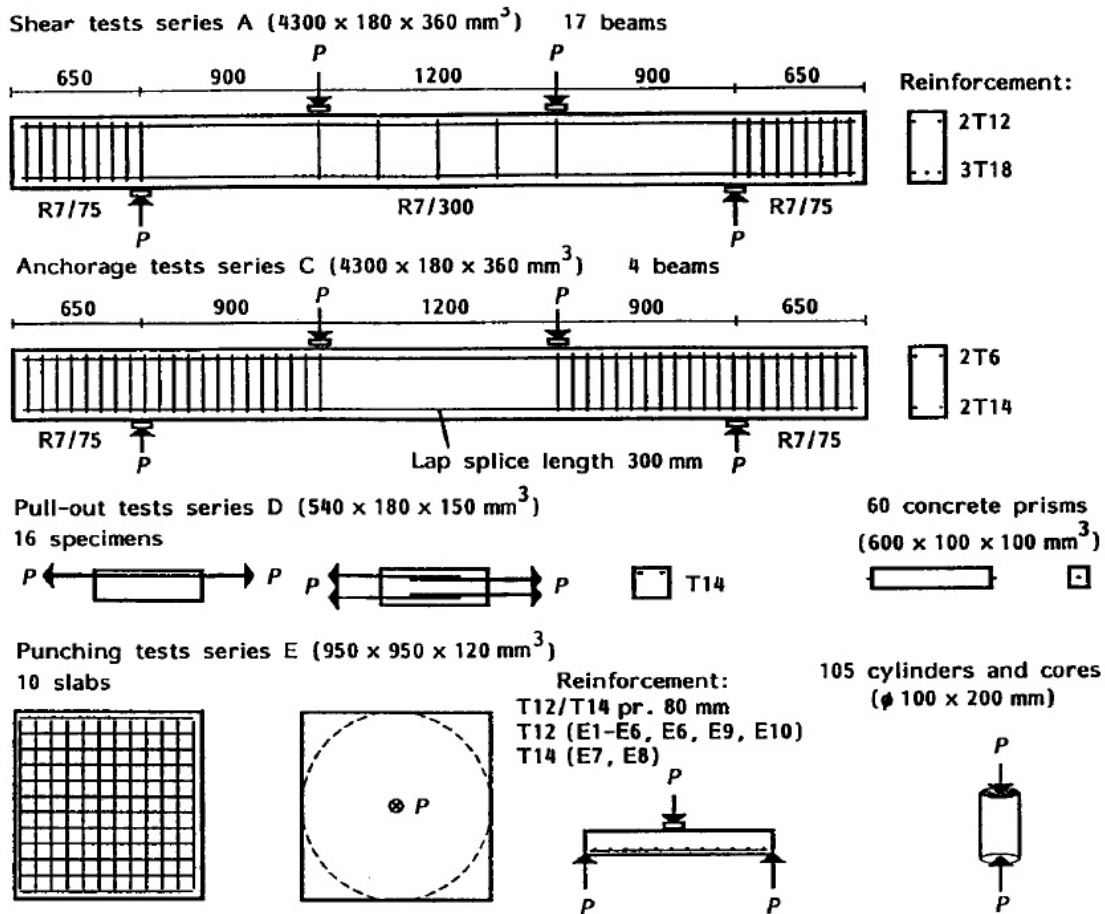


Figure 3.11: Characteristics of the test specimen; Bach, Thorsen, and Nielsen (1993)

- The following main conclusions are drawn from the shear, punching, and anchorage tests:
 - The shear strength of beams without shear reinforcement and the punching shear strength of slabs are not reduced by serious ASR deterioration.
 - Estimates of the shear capacity of ASR-damaged beams and the punching shear capacity of ASR-damaged slabs on the basis of the compressive strength of drilled cores underestimate the failure loads by approximately 20%.
 - The ASR-damaged beams and slabs show more ductility than the corresponding undamaged specimens, and the ASR-damaged specimens show more extensive cracking before failure.
 - ASR deterioration reduces the anchorage strength. The relatively few tests indicate a reduction of 20-30% in anchorage strength.
- Two hypotheses for shear strength increase were proposed:
 - The extensive fine cracking due to ASR leads to a higher ductility and, thereby, to the possibility of a more efficient stress distribution (arch action) in the shear zone.
 - The shear capacity is increased because the expansions lead to a pre-stressing of the reinforcement.

3.8 Bangert, F and Kuhl, D and Meschke, G (2004)

URL

```
@article{
  bangert2004chemo},
  label={bangert2004chemo},
  title={Chemo-hygro-mechanical modelling and numerical simulation of concrete
    deterioration caused by alkali-silica reaction},
  author={Bangert, F and Kuhl, D and Meschke, G},
  journal={International Journal for Numerical and Analytical Methods in
    Geomechanics},
  volume={28},
  number={7-8},
  pages={689--714},
  year={2004},
  publisher={Wiley Online Library}
  Keywords={Laboratory; Expansion monitoring; Petrography; SEM }
```

- The three-point bending test is performed on a 2D beam with a length of 64 cm and a height of 16 cm.
- Numerical simulations are performed in plane strain mode.
- The beam is subjected to a time-dependent hygral loading, as well as boundary conditions for 300 days.
- Figure 3.12 shows the time-dependent behavior of the beam with four characteristics:
 - $t = 20$ days corresponds to the end of the initial drying process. Due to the drying at the surface, the ASR shifts to the more humid inner parts.
 - Subsequently, the inner part of the beam is subjected to compression while the outer part is subjected to tension. These tensile stresses cause cracking along the surface.
 - $t = 40$ to 120 days corresponds to the wetting process characterized by a moisture transport oriented from the bottom toward the top.
 - $t = 140$ to 300 days corresponds to hygral unloading. Since only marginal changes of the damage state are observed, the ASR has almost completely come to an end.
- The evolution of the ASR expansion in three points along the axis of symmetry, as well as the capacity curves for the sound and ASR-affected beams, are shown in Figure 3.13.
- This shows that the ASR-induced expansion (and, consequently, the deterioration of concrete structures caused by the ASR) strongly depends on the moisture content and on the hygral loading history.
- The beam is subjected to the time-dependent hygral loading, as well as boundary conditions, for 300 days.
- At the end of $t = 300$ days, the structural stiffness is reduced by $1 - \frac{E_{300}}{E_0} = 55\%$ due to the ASR.

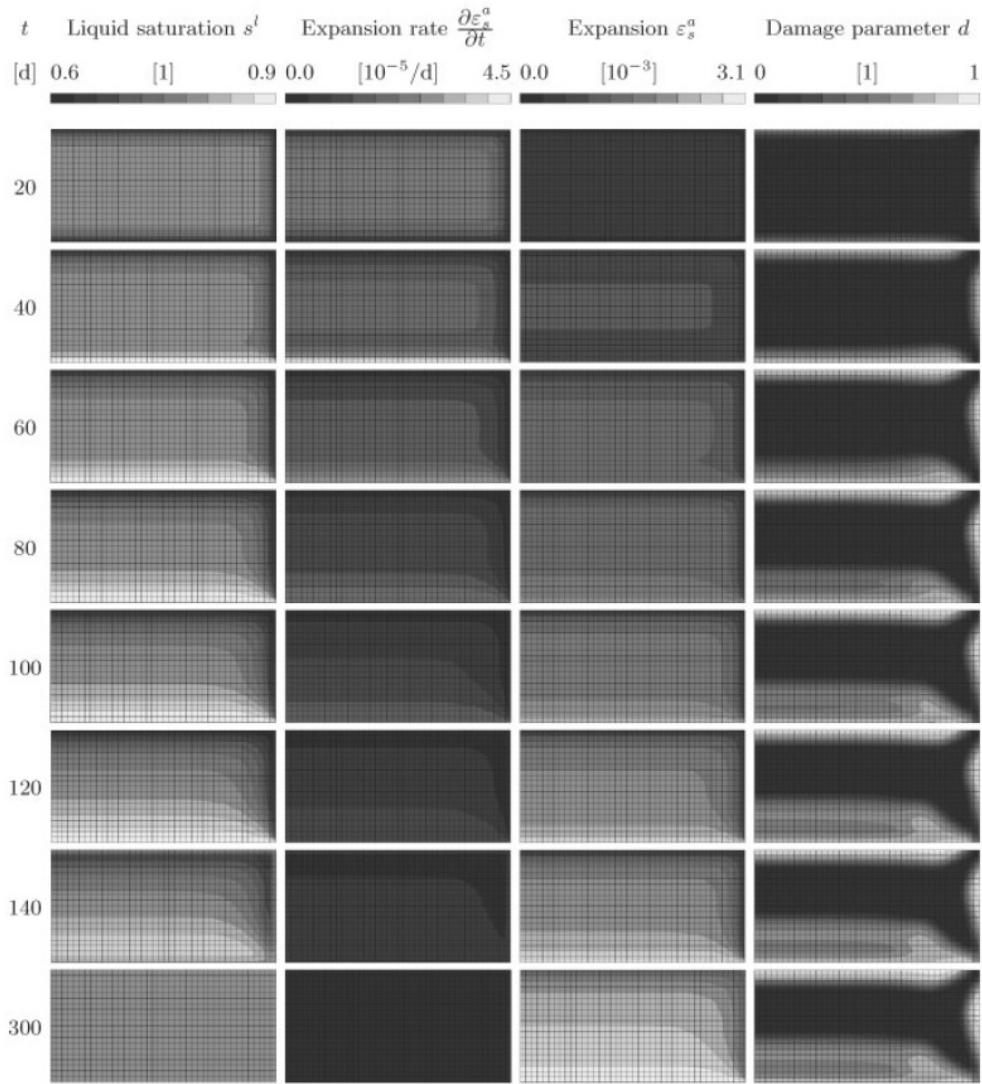


Figure 3.12: Numerical simulation of a concrete beam affected by the ASR, columns left to right: distribution of the liquid saturation, the expansion rate, the expansion, and the damage parameter; Bangert, Kuhl, and Meschke (2004)

- The beam is subjected to the time-dependent hygral loading, as well as boundary conditions, for 300 days.
- From load-displacement curves, the ultimate load is decreased by $1 - \frac{R_{300}^u}{R_0^u} = 27\%$.
- Furthermore, at $t = 300$ days, a more brittle structural response is observed in the very early post-peak regime.

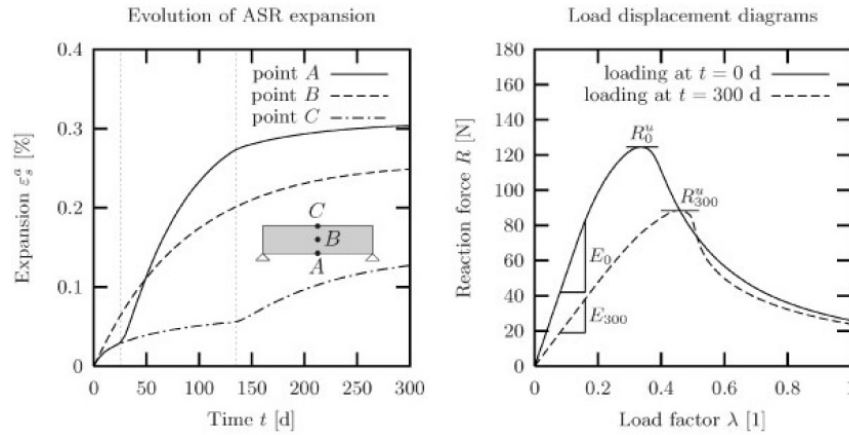


Figure 3.13: Numerical simulation of a concrete beam affected by the ASR, columns left to right: distribution of the liquid saturation, the expansion rate, the expansion, and the damage parameter; Bangert, Kuhl, and Meschke (2004)

3.9 Batista, António Lopes and Piteira Gomes, J (2016)

```
@article{
batista2016characteristic},
label={batista2016characteristic},
title={Characteristic behaviour of the Portuguese large concrete dams built with
granite aggregates and affected by ASR},
author={Batista, Ant{\'}nio Lopes and Piteira Gomes, J},
year={2016},
publisher={IBRACON/UNESP},
Keywords={Laboratory; Field; Expansion Assessment/monitoring Petrography; Gravity
dam; Arch dam; Buttress dam; },
DisplayPdF={0},
```

- Out of about 60 large concrete dams monitored in Portugal, 19 are affected by identified swelling processes.
- There are 13 dams (built between about 1940 and 1980) affected by ASR which exhibit a behavior characterized by very low expansion rates during the first 20 to 30 years but showing, since then, increasing rates of expansion.
- The monitoring results of these dams were obtained with specific devices. They show accumulated expansions of about 200×10^{-6} and current average free swelling rates of about 10×10^{-6} per year in most of the dams.
- Since the swelling magnitude values are moderate, no problems related with serviceability and safety are expected in the near future. The standard tests of accelerated expansion performed on samples taken from the body of some of these dams, however, showed a much lower growth potential than the one recorded on site.
- More specifically, three typical cases are investigated:

- Miranda Dam
 - * The Miranda Dam is a buttress structure, 80 m high, founded on a granite and schist rock mass.
 - * It was completed in 1961.
 - * Evidences of the swelling phenomenon were identified about 20 years after the construction by the detection of progressive vertical displacements upwards and vertical sliding on the central contraction joints.
 - * Linear and mapping cracking was detected on specific zones of the galleries and on the downstream surface.
 - * Mechanical and chemical tests (modulus of elasticity, compressive and tensile strengths, stiffness damage test, mineralogical analysis, petrographic characterization, cement, sulphate, alkali and silica contents, and residual expansion) were ongoing on samples taken from the Dam's body.
- Covao do Meio Dam
 - * The Covao do Meio Dam is a thin arch dam, 28 m high, founded on a granite rock mass.
 - * It was completed in 1953.
 - * The first signs of the swelling phenomenon were identified about 40 years after the construction, by the observation of progressive displacements, vertical upwards and radial upstream.
 - * Linear cracking on the downstream surface was detected in recent years.
 - * Mechanical and chemical tests were performed on samples taken from the Dam's body.
- Cabril Dam
 - * The Cabril Dam is a thin arch structure, 132 m high, located in a narrow V-shaped valley.
 - * It was completed in 1954.
 - * Abnormal behavior was observed during the first filling of the reservoir, characterized by horizontal cracking formation near the top on the downstream surface due to the high stiffness of the crest arch.
 - * Linear and mapping cracking was detected on specific zones of the galleries and on the downstream surface.
 - * Laboratory testing for AAR evaluation, including petrographic, chemical, and expansion tests, were also performed.
- The following Figures summarize the main results of the comparative analysis conducted about the concrete swelling of the 13 dams built with granite aggregates and affected by AAR.

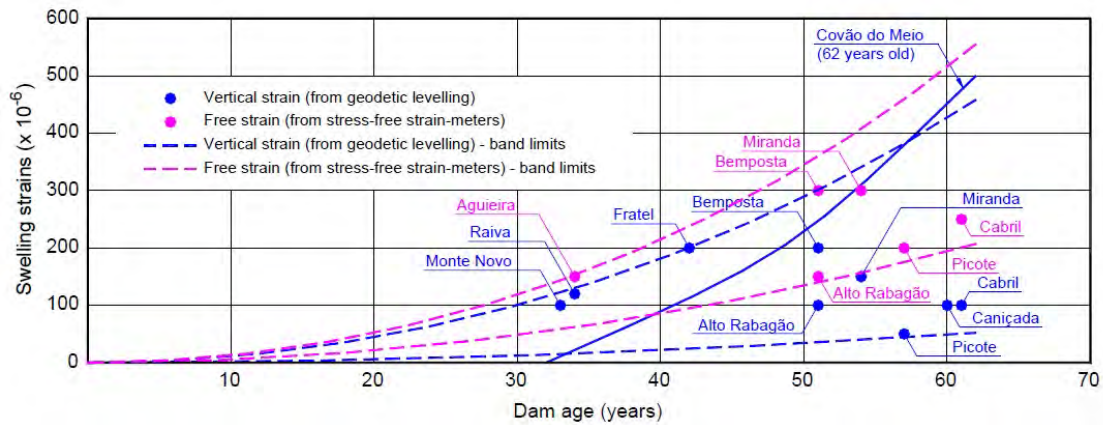


Figure 3.14: Portuguese dams built with granite aggregates and affected by AAR; Batista and Piteira Gomes (2016)

Dam	Age in 2015 (years)	Stress-free Carlson strain-meters		Geodetic levelling at the crest	
		Average value of the accumulated free strain ($\times 10^{-6}$)	Average annual rate in the last 5 years ($\times 10^{-6}$)	Average value of the accumulated vertical strain ($\times 10^{-6}$)	Average annual rate in the last 5 years ($\times 10^{-6}$)
Penide	66	-	-	150 (last 16 years)	10
Covão do Meio	62	-	-	500 (last 30 years)	25
Cabril	61	250	10	100	5
Caniçada	60	200 (last 25 years)	10	100	5
Picote	57	200	5	50	< 5
Miranda	54	300	10	150	5
Alto Rabagão	51	150	10	100	5
Bemposta	51	300	15	200	10
Caia	48	-	-	50 (12 years, 1996-2008)	5 (2003-2008)
Fratel	42	-	-	200	10
Agueira	34	150	5	(not directly related)	(not directly related)
Raiva	34	-	-	120	5
Monte Novo	33	-	-	100	10

Figure 3.15: Portuguese dams built with granite aggregates and affected by AAR; Average values of the monitored free strains by the stress-free Carlson strain-meters and strains obtained from geodetic leveling; Batista and Piteira Gomes (2016)

3.10 Berube, Marc-Andre and Frenette, Jean and Pedneault, Annie and Rivest, Michel (2002)

URL

```

@article{
berube2002laboratory,
label={berube2002laboratory},
title={Laboratory assessment of the potential rate of ASR expansion of field
concrete},
author={Berube, Marc-Andre and Frenette, Jean and Pedneault, Annie and Rivest,
Michel},
journal={Cement, concrete and aggregates},
volume={24},
number={1},
pages={13--19},
year={2002},
publisher={ASTM International},
Keywords={},
DisplayPdf={0},
url={http://www.astm.org/DIGITAL_LIBRARY/JOURNALS/CEMENT/PAGES/CCA10486J.htm}

```

- One of the few publications that addresses residual expansions of field concrete.
- ASR and related expansion and deterioration will continue in an affected concrete structure as long as the reactive mineral phases within the aggregate particles are not completely consumed, and if the two other essential conditions are still satisfied, i.e. high humidity and high alkali concentration in the concrete pore solution.
- The risk of expansion and damage due to ASR can be reasonably assessed in the laboratory from:
 1. The inherent expansivity of the concrete under study (**EXP**) , which is determined by testing core samples in air at 100% RH and 38°C.
 2. The residual absolute reactivity of the aggregates (**ABR**) present in the concrete under study, which can be determined by testing core samples in 1N NaOH solution at 38°C or, even better for coarse aggregates, by testing aggregates extracted from cores through the Concrete Prism Method CSA A23.2-14A-94;
 3. The amount of alkalis (**ALK**) that are still active in the concrete, e.g. in the pore solution, which is estimated by a hot-water extraction method on ground concrete.
 4. Humidity (**HUM**), temperature (**TEM**), and stress conditions (**STR**) (confinement, reinforcement, pretensioning, postensioning, ...) in service.
- Risk indices corresponding to each of the above parameters are combined to determine the potential rate of ASR expansion (**PRE**) of concrete members in service, either already affected by ASR or not.
- **PRE** takes a zero value when at least one of the three necessary conditions for ASR is not satisfied, e.g. when the aggregates are not reactive, when the concrete alkali content is low, or when the humidity conditions in service are low. Also, it can predict the anisotropic expansion in members whose different parts are exposed to different humidity, temperature and/or stress conditions.
- **PRE** does not predict for how long the expansion will continue in the concrete structure but just gives an indication of the maximum current or future rate of expansion due to ASR.

- PRE is mostly based on laboratory results. In the final evaluation, all other relevant available informations such as the age of the structure, the present state and the progress of deteriorations, the rates of expansion and defonnation, the behaviors of similar structures made with the same types of aggregates, and modelling studies, have to be considered.
- Long-term monitoring is the only way to obtain relevant information on the current rates of expansion, which can then be extrapolated.

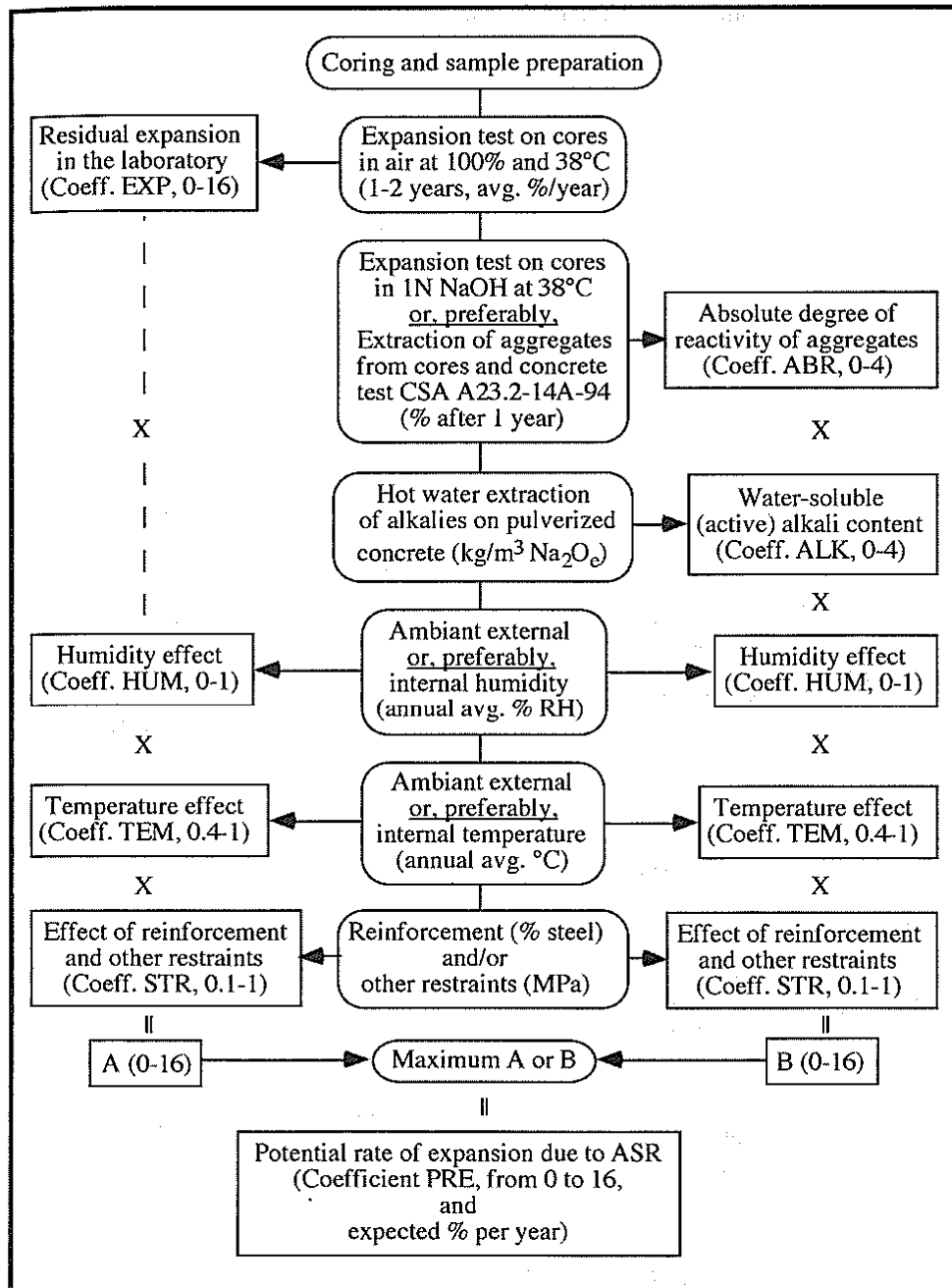


Fig. 1: Laboratory assessment of the potential rate of ASR expansion of concrete

Figure 3.16: Laboratory assessment of the potential rate of ASR expansion members in service either already affected by ASR or not

Coefficient EXP: Residual expansion in the laboratory (core testing in air at >95% RH and 38°C)					
% exp./year ¹	Residual exp. ¹	EXP ¹	% exp./year ¹	Residual exp. ¹	EXP ¹
< 0.003	negligible	0	0.015 to 0.02	moderate	6
0.003 to 0.005	very low	1	0.02 to 0.025	high	9
0.005 to 0.01	low	2	0.025 to 0.03	high	12
0.01 to 0.015	moderate	4	> 0.03	very high	16
Coefficient ABS: Absolute reactivity of aggregates (core testing in 1N NaOH at 38°C or Concrete Prism Test CSA A23.2-14A on aggregates extracted from cores)					
% exp. at 1 year ¹	Reactivity ¹	ABR ¹	% exp. at 1 year ¹	Reactivity ¹	ABR ¹
< 0.04	negligible	0	0.12 to 0.20	high	3
0.04 to 0.08	low	1	> 0.20	very high	4
0.08 to 0.12	moderate	2			
Coefficient ALK: Water-soluble alkali content (hot-water extraction method)					
kg/m ³ Na ₂ O _e	Alkali content	ALK	kg/m ³ Na ₂ O _e	Alkali content	ALK
< 1.0	very low	0	2.0 to 2.5	high	3
1.0 to 1.5	low	1	> 2.5	very high	4
1.5 to 2.0	moderate	2			
Coefficient HUM: Humidity conditions in service (internal or external)					
Internal humidity	"Humidity risk"	HUM	Internal humidity	"Humidity risk"	HUM
< 80% RH	very low	0	90-95% RH	high	0.75
80-85% RH	low	0.25	95-100% RH	very high	1
85-90% RH	moderate	0.5			
External (ambient) humidity		Thin element (<0.5 m)		Thick element (>0.5 m)	
		"Humidity risk"	HUM	"Humidity risk"	HUM
Indoor	• <70% RH	very low	0	low	0.5
	• 70-80% RH	low	0.25	moderate	0.75
	• 80-90% RH	moderate	0.5	high	1
	• 90-95% RH	high	0.75	very high	1
	• 95-100% RH or immersed	very high	1	"	1
Outdoor in deserts	• Not in contact with the ground	very low	0	moderate	0.5
	• In contact with the ground	low	0.25	high	0.75
Outdoor in other areas in North America					
• Not exposed to rain nor in contact with the ground		moderate	0.5	high	0.75
• Not exposed to rain but in contact with the ground		high	0.75	very high	1
• Exposed to rain, immersed or buried		very high	1	"	1
Coefficient TEM: Temperature conditions in service					
Annual avg. temp. (°C)	TEM	Annual avg. temp. (°C)	TEM	Annual avg. temp. (°C)	TEM
< 0	0.4	10 to 20	0.7	> 30	1.0
0 to 10	0.55	20 to 30	0.85		
Coefficient STR: Reinforcement and other restraints in service (in the direction(s) of rebars or restraints)					
% of steel	STR	% of steel	STR	Restraint (MPa)	STR
0	1.0	1	0.3	0	1.0
0.25	0.75	2	0.25	0.25	0.85
0.5	0.55	≥ 3	0.2	0.5	0.7
0.75	0.4			0.75	0.55
					1
					1.5
					2
					≥ 3
					0.1
Coefficient PRE: Potential rate of ASR expansion in concrete members in service					
PRE	Qualification	PRE	Qualification	PRE	Qualification
0	negligible	1 to 2	low	>6 to 12	high
> 0 to 1	very low	2 to 6	moderate	>12 to 16	very high

¹ After mass equilibrium when testing cores; the value is considered a minimum if the concrete cores were abnormally fissured or porous compared to the overall concrete member under study (coefficients EXP and ABS) or quite impermeable to the alkaline solution (coefficient ABS).

Table 3.1: Classification of the Various Coefficients Proposed to Estimate the Potential Rate of ASR Expansion of Concrete Members in Service either already Affected by ASR or not, Based on Laboratory Test Results and Field Conditions.

3.11 Bérubé, Marc-André and Duchesne, J and Dorion, JF and Rivest, M (2002)

URL

```
@article{
berube2002laboratory2,
label={berube2002laboratory2},
title={Laboratory assessment of alkali contribution by aggregates to concrete and
application to concrete structures affected by alkali--silica reactivity},
author={B{\`e}rub{\'e}, Marc-Andr{\'e} and Duchesne, J and Dorion, JF and Rivest,
M},
journal={Cement and Concrete Research},
volume={32},
number={8},
pages={1215--1227},
year={2002},
publisher={Elsevier}
Keywords={}
```

- The water-soluble alkali content of mass concrete elements from many dams was measured using a hot water extraction method shown in Figure 3.17.
- The results obtained for the core samples taken at different depths in a number of concrete elements are shown in Figure 3.18.
- In most cases, large variations with depth in the water-soluble alkali content are observed.
- Globally, the soluble alkali content tends to slightly decrease from the top to the bottom of the vertical drill holes made in the plots of the Beauharnois dam. This may be attributed to the fact that the average yearly temperature is slightly higher at depth in concrete. The higher temperature accelerates ASR.
- The values obtained often largely exceed the soluble alkali content expected to be released by the cement used.
- The soluble alkali content in the near-surface concrete (0.5 m or less from the surface) is often significantly lower (although sometimes higher) than at depth.
- It is recommended to always perform measurements on concrete samples taken at a minimum depth of about 0.5 m or more inside the concrete element under study.

Hydraulic dams	Sampled elements	Core number (number of samples analyzed)	Nature of aggregates		Measured soluble Na ₂ O _e (kg/m ³) ^a	Cement content (kg/m ³) ^b	Percent Na ₂ O _e in the cement ^b	Expected soluble Na ₂ O _e (kg/m ³) ^c	Aggregate contribution (kg/m ³) ^d
			Coarse	Fine					
Castor	?	1,2,3 (1)	gran. gn.	gran. sand	2.36	(275)	(1.0)	1.65	0.71
Melville	Pillar 7	11 (4)	gran. gn.	gran. sand	3.50	(275)	(1.0)	1.65	1.85
Melville	Pillar 9	15 (4)	gran. gn.	gran. sand	4.34	(275)	(1.0)	1.65	2.70
Melville	Pillar 12	19 (3)	gran. gn.	gran. sand	3.04	(275)	(1.0)	1.65	1.39
La Gabelle	left dam	27 (1)	gran. gn.	gran. sand	0.20	(275)	(1.0)	1.65	0
Rapides 7	Pillar 13	7,8 (1)	gran. gn.	gran. sand	4.30	(275)	(1.0)	1.65	2.65
St-Narcisse	Pillar	5 cores (1)	gran. gn.	gran. sand	1.40	(275)	(1.0)	1.65	0
Farmers	Cursor 27	22 (1)	gran. grav.	gran. sand	2.48	(275)	(1.0)	1.65	0.83
	Cursor 7	28 (1)	gran. grav.	gran. sand	4.01	(275)	(1.0)	1.65	2.36
	Cursor 1	34 (1)	gran. grav.	gran. sand	3.54	(275)	(1.0)	1.65	1.89
	Pillar 5	31 (5)	gran. grav.	gran. sand	2.46	(275)	(1.0)	1.65	0.81
	Pillar 14	24 (5)	gran. grav.	gran. sand	3.03	(275)	(1.0)	1.65	1.38
Hemmings	?	2 (1)	lith. grav.	lith. sand	2.59	(275)	(1.0)	1.65	0.94
	?	3 (1)	lith. grav.	lith. sand	1.39	(275)	(1.0)	1.65	0
Mitis 2	?	B (1)	lith. grav.	lith. sand	1.70	(275)	(1.0)	1.65	0.05
Lac Mitis	?	1 (2)	lith. grav.	lith. sand	1.62	(275)	(1.0)	1.65	0
Mistigou,	?	1 (2)	lith. grav.	lith. sand	1.88	(275)	(1.0)	1.65	0.23
	?	B (1)	lith. grav.	lith. sand	1.70	(275)	(1.0)	1.65	0.05
Rapides 15	Pillar 5	5 (1)	lith. grav.	lith. sand	3.00	(275)	(1.0)	1.65	1.35
Up. Salmon	?	1 (1)	diorite	lith. sand	2.69	(275)	(1.0)	1.65	1.04
	?	2 (1)	diorite	lith. sand	3.21	(275)	(1.0)	1.65	1.56
	?	3 (1)	diorite	lith. sand	2.53	(275)	(1.0)	1.65	0.88
Sartigan	Pillar 19	1 (2)	rhyol. tuff	lith. sand	3.10	(275)	1.3	2.15	0.95
	upst. wall	3 (2)	rhyol. tuff	lith. sand	2.79	(275)	1.3	2.15	0.65
	Pillar 8	7 (1)	rhyol. tuff	lith. sand	2.75	(275)	1.3	2.15	0.60
	Pillar 6	9 (2)	rhyol. tuff	lith. sand	3.08	(275)	1.3	2.15	0.94
	Pillar 5	10 (1)	rhyol. tuff	lith. sand	2.98	(275)	1.3	2.15	0.84
Mercier	?	9,10 (1)	dol. + gr.gn.	gran. sand	1.69	(275)	(1.0)	1.65	0.04
Coteau 3	Pillar 15	34 (5)	dolostone	gran. sand	2.69	(275)	(1.0)	1.65	1.04
Coteau 2	Pillar 2	20 (4)	dolostone	lith. sand	2.60	(275)	(1.0)	1.65	0.95
Coteau 1	Pillar 17	4 (4)	dolostone	sil. sandst.	2.23	(275)	(1.0)	1.65	0.58
Les Cèdres	intake	1 (1)	dolostone	gran. sand	1.35	(275)	(1.0)	1.65	0
	evacuator	17 (1)	dolostone	gran. sand	2.70	(275)	(1.0)	1.65	1.05
	aspirator	3 (1)	sil. sandst.	gran. sand	2.43	(275)	(1.0)	1.65	0.78
Riv. Prairie	Pillar 8	11 (1)	sil. lim.	gran. sand	0.24	(275)	(1.0)	1.65	0
	gr. 7, spier	16 (1)	sil. lim.	gran. sand	1.32	(275)	(1.0)	1.65	0
	ev. pil. 2	19,19A (1)	sil. lim.	gran. sand	1.75	(275)	(1.0)	1.65	0.10
	left dam	18 (1)	sil. lim.	gran. sand	1.83	(275)	(1.0)	1.65	0.18
	overflow	8 (1)	sil. lim.	gran. sand	2.21	(275)	(1.0)	1.65	0.56
	Pillar 26	10 (1)	sil. lim.	gran. sand	2.63	(275)	(1.0)	1.65	0.98
	gr. 2, wall	2,2A (1)	sil. lim.	gran. sand	2.96	(275)	(1.0)	1.65	1.31
	ev. pil. 12	20,20A (1)	sil. lim.	gran. sand	3.60	(275)	(1.0)	1.65	1.95
	ev., border	21 (1)	sil. lim.	gran. sand	4.66	(275)	(1.0)	1.65	3.01
Pont-Rouge	?	1 (1)	sil. lim.	gran. sand	0.40	(275)	(1.0)	1.65	0
Juillet 1	Pillar 4	2 (5)	sil. sandst.	gran. sand	3.11	(275)	(1.0)	1.65	1.46
Juillet 2	Pillar 3	7 (7)	sil. sandst.	gran. sand	3.10	(275)	(1.0)	1.65	1.45
Beauharnois	Plot 2	C (6)	sil. sandst.	sil. sandst.	1.57	(275)	(1.0)	1.65	0
		D (7)	sil. sandst.	sil. sandst.	1.85	(275)	(1.0)	1.65	0.20
	Plot 4	A (7)	sil. sandst.	sil. sandst.	1.25	(275)	(1.0)	1.65	0
		B (7)	sil. sandst.	sil. sandst.	1.08	(275)	(1.0)	1.65	0

^a Corrected for aggregate contribution in the test method.

^b Estimated values between brackets.

^c Assuming no aggregate contribution and 40% of cement alkalis in hydrates, which are not leached in the test.

^d Measured soluble Na₂O_e content – expected soluble Na₂O_e from the cement.

Figure 3.17: Dams investigated, soluble alkali content, and estimated contributions by aggregates; Bérubé et al. (2002)

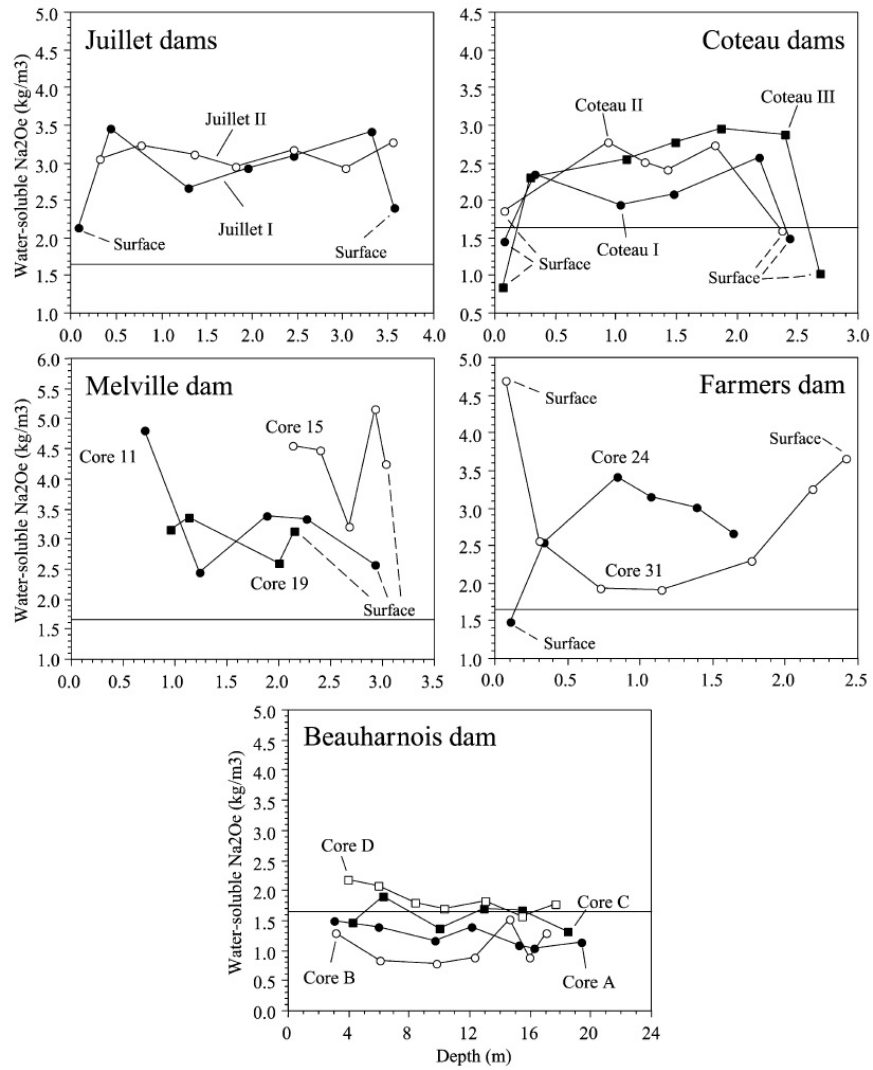


Figure 3.18: Dams investigated, soluble alkali content, and estimated contributions by aggregates; Bérubé et al. (2002)

3.12 Bérubé, Marc-André and Smaoui, Nizar and Fournier, Benoit and Bissonnette, Benoit and Durand, Benoit (2005)

URL

```
@article{
berube2005evaluation},
label={berube2005evaluation},
title={Evaluation of the expansion attained to date by concrete affected by
alkali--silica reaction. Part III: Application to existing structures},
author={B{\'}rub{\'}, Marc-Andr{\'} and Smaoui, Nizar and Fournier, Benoit and
Bissonnette, Benoit and Durand, Benoit},
journal={Canadian Journal of Civil Engineering},
volume={32},
number={3},
pages={463--479},
year={2005},
publisher={NRC Research Press}
Keywords={Laboratory; Blocks; Expansion monitoring; Reinforcement; Confined; Det.
E; Det f'c; }
```

- Three highway bridges in the Quebec City area (affected by various degrees of ASR and all incorporating similar alkali-silica reactive coarse limestone aggregates) were investigated.
 - Du-Vallon Bridge, built in 1966
 - * This bridge is made of a deck resting on reinforced concrete Y-shaped columns. The columns are supported by a massive concrete foundation.
 - * Concrete delamination and steel corrosion at the deck level is observed.
 - * Map cracking, sealing, disaggregation, and pop-outs affecting the massive concrete foundation are related to the presence of ASR.
 - * On average, the estimated volumetric expansion of the columns is 0.072%.
 - * The vertical expansion is smaller than the horizontal expansion due to loading and restraint.
 - * On the other hand, a global estimated volumetric expansion for the foundation is 0.130%.
 - Pere-Lelievre Bridge, built in 1972
 - * This bridge is composed of prestressed concrete beams resting on prestressed concrete pile caps.
 - * Each cap is supported by two reinforced concrete piles linked by a concrete wall.
 - * Each beam shows a major crack parallel to the prestressed cables.
 - * Major cracking is observed at the surface of all beams, pile caps, and piles.
 - * On average, beams present an estimated volumetric expansion of 0.049%.
 - St-David Bridge, built in 1972
 - * This bridge is made of prestressed concrete beams resting on circular reinforced concrete columns and mass concrete abutments. Both the abutments and columns show visual signs related to ASR (e.g. map cracking and exudation of siliceous gel).

- * Signs of steel corrosion and localized spalling are also observed.
- * On average, the abutment wall presents an estimated volumetric expansion of 0.069%, and this expansion is nearly similar in horizontal and vertical directions.
- In 2001, several Y-shaped columns and two massive foundations of the Du-Vallon bridge were repaired using a sealing technique.
- The columns and foundations were wrapped with composite material. These composite materials are either: conventional concrete, wet shotcrete, or self-compacting concrete (either reinforced or not reinforced).
- ASR in three highway bridges is already described including various signs and observations.
- Several samples were cored from the bridges and tested in the lab.
- A compression test, a splitting test, and a direct tension test were performed.
- The modulus of elasticity and the direct tensile strength are more affected by ASR than the uniaxial compressive strength and the indirect (splitting) tensile strength.

3.13 Blanco, A and Cavalaro, SHP and Segura, I and Segura-Castillo, L and Aguado, A (2018)

URL

```
@article{
blanco2018expansions},
label={blanco2018expansions},
title={Expansions with different origins in a concrete dam with bridge over
spillway},
author={Blanco, A and Cavalaro, SHP and Segura, I and Segura-Castillo, L and
Aguado, A},
journal={Construction and Building Materials},
volume={163},
pages={861--874},
year={2018},
publisher={Elsevier}
Keywords={Laboratory; Field; Det. E; Det f't; Det f'c; Mathematical; }
```

- A 62-year-old concrete gravity dam was investigated with signs of deterioration due to expansive reactions.
- Evidence of damage in the main elements of the dam can be summarized as:
 - Spillway
 - * Downstream face: Horizontal cracks without signs of infiltration
 - * Upstream face: Horizontal cracks
 - Bridge
 - * Structure of stairway: Loss of concrete cover, corrosion and deformation of the reinforcement

- * Deck: No signs of severe damage
- * Diaphragms: Surface erosion, corrosion of reinforcement and cracking
- Dikes
 - * Retaining walls: Map cracking



Figure 3.19: Observed damages: (a) cracks in downstream face, (b) crack of upstream face, (c) cracks of strainway and loos of concrete, (d) corrosion of rebars, (e) erosion in diaphragm, (f) cracks in diaphragms, and (g) map cracking in the retaining walls of the dike; Blanco et al. (2018)

- Multiple tests were performed on the samples extracted from the dam: (1) X-ray diffraction, (2) scanning electron microscope with energy dispersive spectroscopy mode, and (3) petrography.
- Comprehensive diagnosis of the dam revealed two different expansive reactions: (1) delayed ettringite formation and (2) alkali-silica reaction.
- High temperatures during construction led to delayed ettringite formation.
- A model based on finite differences was prepared to simulate heat transfer phenomena.
- The dam is modeled at a sectional level per length unit.
- The maximum time interval was set to 5 min, meaning that each year requires approximately 105,000 time steps.

- The construction procedure is defined as casting of consecutive layers.
- Once cast, the layer is unprotected and exchanges with atmospheric air may occur, as well as the diffusion with the bottom and lateral layers.
- Two scenarios were assumed for construction: fast and slow.
- The results of the thermal modeling for the fast scenario are presented in Figure 3.20 which plots the maximum temperatures reached in the cross section of the dam.
- This Figure reveals that the highest temperature occurs in the center of each of the different layers.
- Thermal modeling of the construction process confirms concrete temperatures can reach over 70°C.

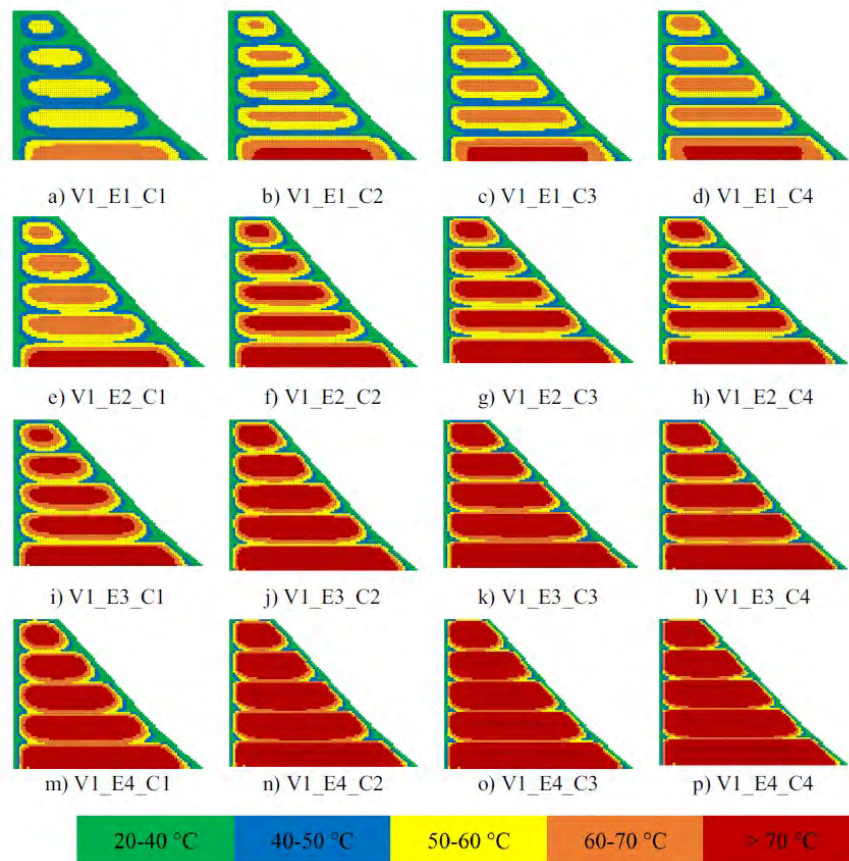


Figure 3.20: Maximum temperature reached in each point; Blanco et al. (2018)

- For crack analysis of the dam, the finite element software ATENA was used.
- Nonlinear fracture mechanics with the crack band method and smeared cracking is assumed for the behavior of concrete in tension.
- The behavior of the reinforcement in the piles is defined according to a bilinear model.

- The loads considered in the simulation are the weight of the pile and spillway and the expansion in the spillway.
- Figure 3.21 shows the crack pattern observed in the diaphragms.
- This pattern suggests that the cause of the cracks may be a volumetric expansion in the spillway.
- This figure also illustrates the tension stresses that would be generated in the diaphragms if an expansion did occur in the spillway.
- If those tension stresses reach the tensile strength of concrete, the cracks would appear perpendicularly to the direction of the tension, as observed in the real crack pattern.

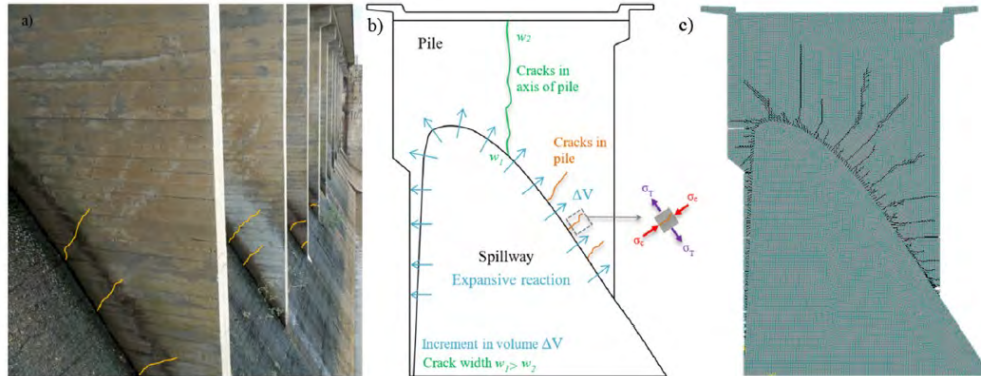


Figure 3.21: Finite element analysis: (a) real crack pattern, (b) stresses in the diaphragm, and (c) crack pattern of the model; Blanco et al. (2018)

- Microstructural analyses were conducted on aggregate samples from the quarry located near the dam and on mortar samples obtained from concrete cores.
- Seven cores were drilled from different elements of the dam, illustrated in Figure 3.22. Results of compressive strength and also the modulus of elasticity shows considerable spatial dispersion (i.e. heterogeneity).

Notation	Location	Diameter (mm)	Length (mm)	Compressive strength (MPa)	Elastic modulus (GPa)
M1	Wall in stairway structure	93.4	170	32.7	-
P1	Diaphragm of bridge	93.5	250	29.7	18.7
P2	Diaphragm of bridge	73.5	180	29.8	-
T1	Retaining wall	93.0	350	30.8	12.4
T2	Retaining wall	93.2	350	28.3	13.4
V1	Spillway	93.5	850	14.9	7.4
V2	Spillway	99.3	750	22.8	15.4

Figure 3.22: Details of the cores; Blanco et al. (2018)

- The mechanical tests were performed according to the standard UNIT-NM 69:1998.
- The compression test was subsequently corrected according to ACI 214R-11.

3.14 BOR (1941)

```
@techreport{
bor1941},
title={Alkalies in Cement and Their Effect on Aggregates and Concretes},
author={BOR},
institution={U.S. Department of the Interior, Bureau of Reclamation, and
Representatives of Cement Manufacturers and Other Interested Agencies},
year={1941}
keyword={Historical}
```

Probably the first conference dedicated exclusively to ASR.
Of historical relevance.

3.15 Capra, B and Bournazel, J-P (1998)

URL

```
@article{
capra1998modeling,
label={capra1998modeling},
title={Modeling of induced mechanical effects of alkali-aggregate reactions},
author={Capra, B and Bournazel, J-P},
journal={Cement and Concrete Research},
volume={28},
number={2},
pages={251--260},
year={1998},
publisher={Elsevier},
Keywords={},
DisplayPdf={0},
url={https://www.sciencedirect.com/science/article/pii/S0008884697002615}
```

- “classic paper” as it was the first to propose a quantitative relationship between ASR expansion and the relative humidity.

$$\varepsilon^{AAR} = H^m \varepsilon_{100} \quad (m=8) \quad (3.6)$$

- Other coverage is by now obsolete.

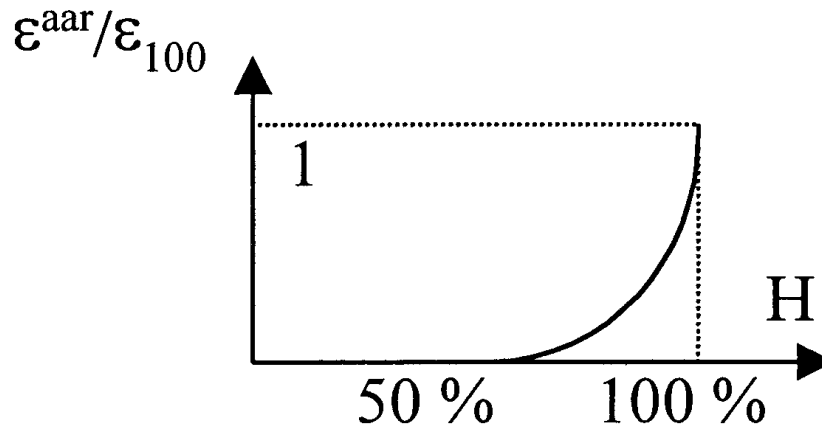


Figure 3.23: Expansion in terms of R

where H is the relative humidity and ϵ_{100} the free expansion at 100% relative humidity.

3.16 Capra, Bruno and Sellier, Alain (2003)

URL

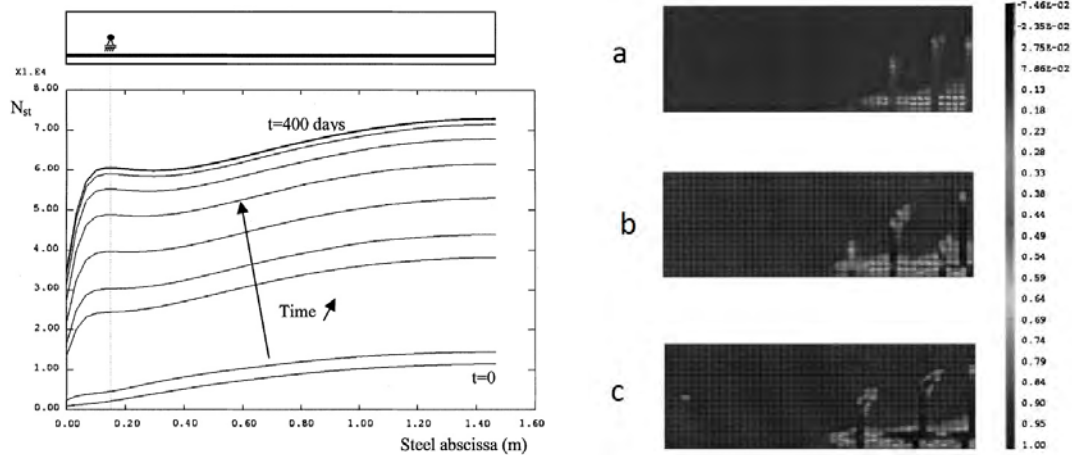
```
@article{
capra2003orthotropic},
label={capra2003orthotropic},
title={Orthotropic modelling of alkali-aggregate reaction in concrete structures:
numerical simulations},
author={Capra, Bruno and Sellier, Alain},
journal={Mechanics of materials},
volume={35},
number={8},
pages={817--830},
year={2003},
publisher={Elsevier}
Keywords={}
```

- A reinforced concrete beam subjected to AAR was simulated.
- The finite element code CASTEM2000 developed by the CEA (Commissariat à l'Energie Atomique) in France was used.
- The length of the beam is 1.0 m, height is 0.3 m and width is 0.25 m. One layer of two rebars is located at the distance of 0.05 m from the bottom of the beam.
- For the steel rebars: $E = 210$ GPa, $\nu = 0.3$, and $\rho = 7850$ kg/m³.
- For the concrete with AAR: elastic modulus $E = 30$ MPa, $\nu = 0.2$ and $\rho = 2500$ kg/m³.
- The dead weight of concrete is considered. The concrete of the beam is subjected to AAR.
- The finite element mesh used for the simulation is a plane stress of the half-beam.

1. Cracks are considered to open only by Mode I, account (Fig. 88 5).

2. The free expansion (ϵ_{100}) is proportional to the volume (V_g), therefore, this involves a time t where

- The concrete shows signs of minor damage under the ASR expansion, and the evolution of the tensile strength along steel bar is shown in Figure 3.24(a) for 400 days of expansion.



(a) Evolution of tensile strength along bar

(b) Principal damage fields (a) sound concrete, (b) AAR with humidity gradient, (c) AAR without humidity gradient

Figure 3.24: Results of numerical simulations by Capra and Sellier (2003)

- Next, the classic three-point bending test is applied to the model (with and without ASR).
- Figure 3.24(b) illustrates the principal damage fields in the beam.
- The beam without AAR shows a classical pattern of cracks which developed from the middle to the edge of the beam.
- The simulation of a beam subjected to AAR with a gradient of humidity shows a non-classical result: the first crack appears in the middle of the beam but jumps to the neighboring element before it continues to propagate.
- The crack spacing is also changed between the ASR affected and the sound concrete.

3.17 Carles-Gibergues, André and Cyr, Martin (2002)

[URL](#)

```

@article{
carles2002interpretation,
label={carles2002interpretation},
title={Interpretation of expansion curves of concrete subjected to accelerated
alkali--aggregate reaction (AAR) tests},
author={Carles-Gibergues, Andr{\`e} and Cyr, Martin},
journal={Cement and concrete research},
volume={32},
number={5},
pages={691--700},
year={2002},
publisher={Elsevier},
Keywords={},
DisplayPdf={0},
url={https://www.sciencedirect.com/science/article/pii/S0008884601007475}

```

- Based on long-term expansion results for concretes subjected to accelerated AAR tests show that, in some cases, the expansion continues for a long time after AAR has stopped.
- For these cases, the overall concrete swelling is certainly not only caused by AAR, and the expansion continuation probably reveals the swelling behavior of concrete when it is placed in saturated moisture conditions.
- Considering that this part of swelling, named the primary expansion, is not negligible compared to the limit expansions fixed by standard AAR tests (2×10^{-4} at 90 days
- It is important to evaluate this effect to avoid a wrong interpretation of the laboratory test.
- The primary expansion is not characteristic of AAR and may not occur in field conditions (temperature between 15 and 20°C and RH < 90% in temperate climates), the calculation of primary expansion could allow for some cases to avoid the inappropriate rejection of an aggregate that does not present any true risk for structures.
- It is commonly assumed that the expansion curve of a concrete prism affected by AAR, the general form of which is represented below (curve 1), can be characterized by three successive phases: an initial phase where swelling begins (OA), followed by a phase of significant expansion at a nearly constant rate (AB), and ended by a decrease in the expansion rate to reach a final plateau (B1).
- Another form of expansion curve is also found (curve 2), where the initial phase is not clearly separated from the expansion phase.
- Our curves clearly present other forms (curves 1' and 2'). They start like curves 1 and 2 but end with a final slope different from zero. These results do not seem to be in accordance with the results usually found, so they lead to a difficult problem of interpretation.
- Extensive analysis of the long-term expansion curves reported by many authors shows that many of them are similar to curves 1' and 2'.
- Estimates for the final slope are tabulated.

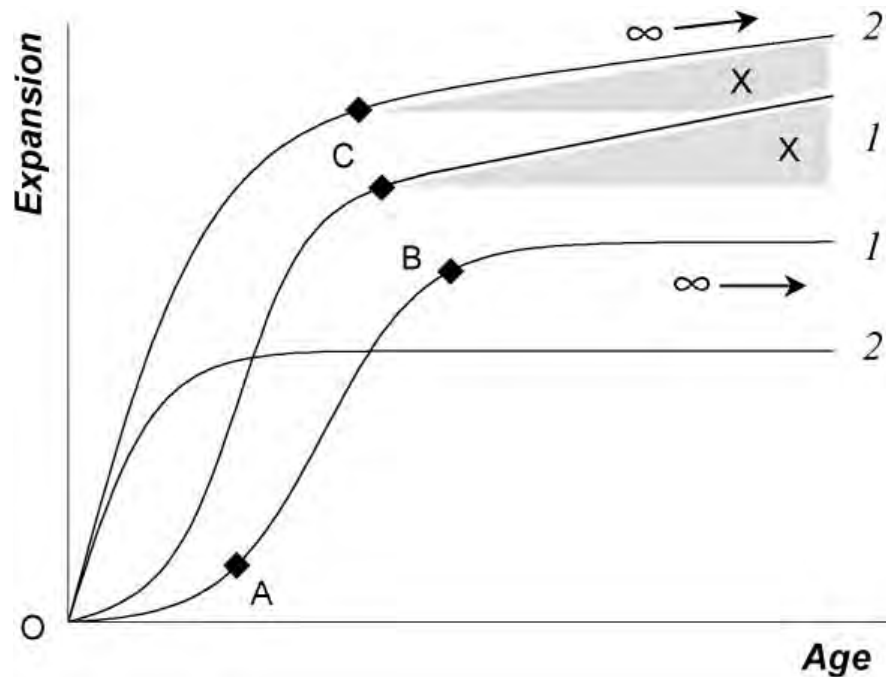


Figure 3.25: Typical expansion curves of concretes affected by AAR. X: visible part of expansion characterized by expansion characterized by AAR. Phenomenon independent of AAR.

3.18 Chen, Jun and Jayapalan, Amal R and Kim, Jin-Yeon and Kurtis, Kimberly E and Jacobs, Laurence J (2010) The form of expansion curve is also found (curve 2 of Fig. 6),

URL

```
@article{
  chen2010rapid},
  label={chen2010rapid},
  title={Rapid evaluation of alkali--silica reactivity of aggregates using a
    nonlinear resonance spectroscopy technique},
  author={Chen, Jun and Jayapalan, Amal R and Kim, Jin-Yeon and Kurtis, Kimberly E
    and Jacobs, Laurence J},
  journal={Cement and Concrete Research},
  volume={40},
  number={6},
  pages={914--923},
  year={2010},
  publisher={Elsevier}
  Keywords={}
```

(curves 1' and 2' shown on Fig. 6). They start like curves

- The nonlinear impact of resonance acoustic spectroscopy is used to characterize the alkali reactivity of different aggregates.
 - Several months samples from some aggregate types were used.
- At first, these results do not seem to be in accordance with the results usually found, so they lead to a difficult problem of interpretation. An analysis of the literature would clarify this situation. 91

In actual fact, an extensive analysis of the long-term expansion curves reported by many authors shows that many of them are similar to curves 1' and 2' of Fig. 6. Table 3 gives the calculated approximate slopes for the

It can be

- in the l
- curves
- mixture
- many y
- this sw
- dication
- that AA
- this sw

This analy
related to or
directly linke

3.4. Possible

There are
dimensional
changes can
(temperature)
ion or seco
(ion). Among
concrete exp
accelerated t

Table 3

Final expansion

Reference

Duchesne and
Bérubé [3]

Fournier et al. [

Ramlochan
et al. [8]

- Expansion of those samples, as well as the variation of the elastic modulus with respect to exposure time, are shown in Figure 3.26.

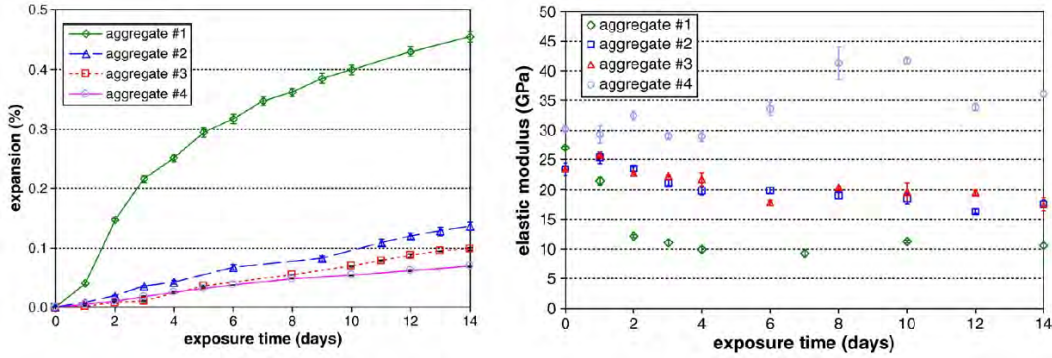


Figure 3.26: Results of AASHTO T 303 expansion and elastic modulus measurements; Chen et al. (2010)

- In general, the measured modulus of elasticity decreases with exposure time for the potentially reactive aggregates and increases (presumably due to continued cement hydration) for the innocuous aggregate #4.
- The modulus of the highly reactive aggregate #1 is seen to decrease most rapidly during the first 4 days when compared to that of the other aggregates.
- Although such tests might provide an indication of the influence of the ASR damage on the mechanical response, the mechanical measurements of elastic modulus are not suitable as a practical method for distinguishing among aggregate of moderate to marginal reactivity.

3.19 Cima, J. and Reinicker, B. (year=2015)

```
@article{
cimaconcrete15},
label={cimaconcrete15},
author={Cima, J. and Reinicker, B.},
title={Managing Concrete Growth at Roanoke Rapis Dam},
journal={Hydro Review},
year=2015
Keywords={Bridge; Field; Expansion monitoring; Reinforcement; Det f'c; }
```

- Roanoke Rapids Dam, located in North Carolina and completed in 1955, is classified as “high hazard potential” under FERC guidelines by virtue of potential loss of life and extensive property damage downstream should a failure occur.
- Following the routine monitoring and inspection of the structure, it is revealed that deformation occurred over time due to ASR.
- The Dam’s structure includes a gravity south non-overflow section, a service bay and power-house section, an interior gravity non-overflow section, gated spillway and emergency spillway sections, and a north non-overflow section.

- According to 2008-2009 design evaluation of several blocks using FERC’s Engineering Guidelines for the Evaluation of Hydropower Projects, it was concluded that the critical loading case controlling stability of the affected dam blocks is the probable maximum flood condition. Subsequently, deep, multistrand rock anchors were designed to stabilize these blocks.
- Due to a concern that partial block movement could create additional damage during anchor installation and loading, grouting of the ASR cracking was the first step in the remediation design.
- A finite element model was also developed to better understand the behavior of the structure.
- This 3D model was developed to include the major geometric features of the entire Dam’s structure but did not include galleries or other powerhouse openings.
- The advanced FEM model included several important and key features:
 - Transient thermal analysis;
 - Temperature-dependent ASR expansion rates;
 - Anisotropic stress-dependent ASR expansion rates;
 - Visco-elastic creep behavior with creep function and effective modulus of elasticity; and
 - Separation/opening along preexisting cracks.
- In stage II, the model was updated to include the entrance gallery, refining the geometry and increasing the model mesh density, the crack fill grouting, and the post-tensioned anchors, Figure .
- Finally, the model was updated to account for the observed changes in instrumentation after post-tensioned anchor installation (Stage III).
- Calibration of the model before and after post-tensioning is shown in Figure 3.27.
- It is evident that, since completion of the anchoring project, the trend of rapidly increasing downstream movement has been arrested, and only smaller seasonal temperature variations are observed.

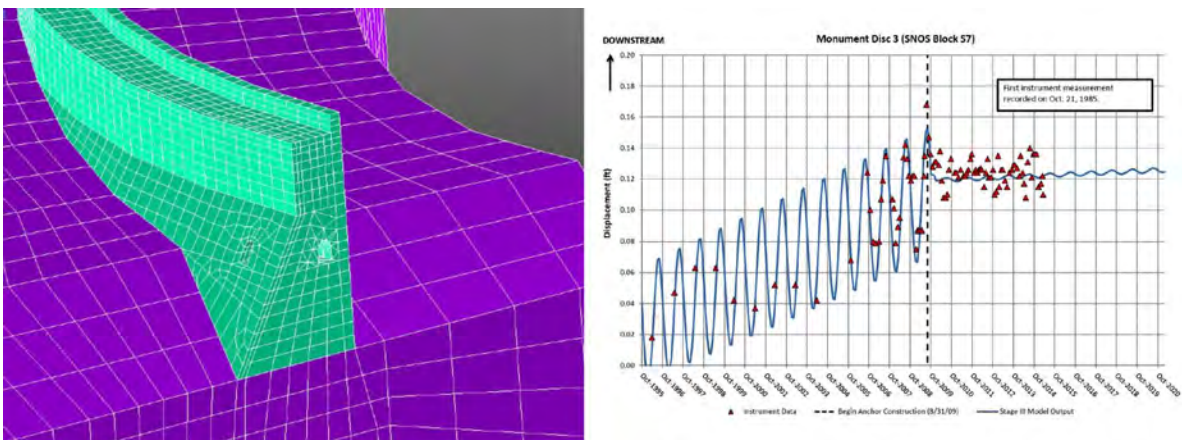


Figure 3.27: Finite element model and calibration; Cima and Reinicker (2015)

3.20 Comby-Peyrot, Isabelle and Bernard, Fabrice and Bouchard, Pierre-Olivier and Bay, François and Garcia-Diaz, Eric (2009)

URL

```
@article{
comby2009development},
label={comby2009development},
title={Development and validation of a 3D computational tool to describe concrete
behaviour at mesoscale. Application to the alkali-silica reaction},
author={Comby-Peyrot, Isabelle and Bernard, Fabrice and Bouchard, Pierre-Olivier
and Bay, Fran{\c{c}}ois and Garcia-Diaz, Eric},
journal={Computational Materials Science},
volume={46},
number={4},
pages={1163--1177},
year={2009},
publisher={Elsevier}
Keywords={}
```

- A tool for finite element analysis of quasi-brittle and heterogeneous materials (like concrete) was developed.
- The method is capable of considering a 3D biphasic material composed of coarse aggregates embedded in mortar.
- ASR is characterized at the mesoscale by a swelling of the reactive granular skeleton.
- $7 \times 7 \times 28$ cm parallelepipedic samples were simulated at 60°C (controlled temperature) and 100% RH to accelerate the reaction. The samples have been stored in autoclaves after seven days of hardening.
- Only half of the aggregates were reactive. Completely uniform random reactive aggregates were simulated inside the specimen.
- The nature of the swelling was assumed to be isotropic.
- Figure 3.28 (left) shows a cut plane in the sample after 14 days. Aggregates (dark) are purely elastic and, consequently, totally undamaged. Damage tends to be more important when it reaches the sample faces.
- In reality, where damage increases progressively inside, a cracking map at concrete surface is observed. Typically the crack pattern develops irregular polygonal forms. This is also shown in Figure 3.28 (right).
- The decrease of the Young's modulus is captured with such a modeling. In order to reach this goal, a compression test was performed after various times of swelling.
- Figure 3.29 presents the evolution of the ratio E/E_0 according to granular skeleton expansion. The global decrease is correctly described by the numerical modeling. The differences at the beginning are probably due to the cement hardening after 7 days.

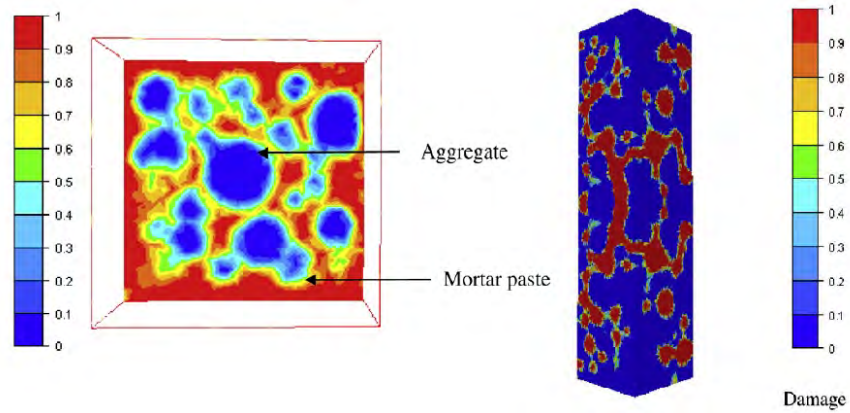


Figure 3.28: Numerical simulation of a concrete cube affected by ASR, left: undamaged cut, right: 3D damaged pattern; Comby-Peyrot et al. (2009)

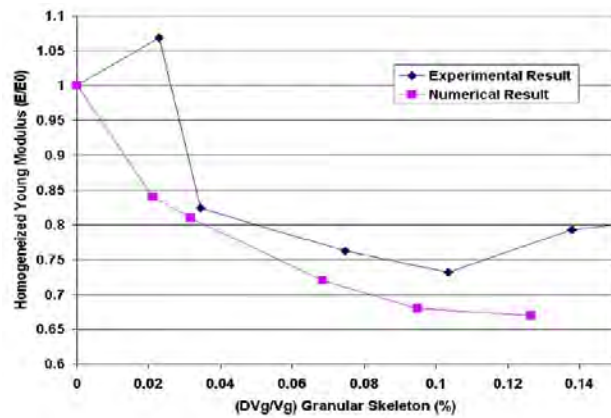


Figure 3.29: Evolution of the homogenized Young's modulus according to skeleton expansion; Comby-Peyrot et al. (2009)

3.21 Comi, C and Fedele, R and Perego, U (2009)

URL

```
@article{
  comi2009chemo},
  label={comi2009chemo},
  title={A chemo-thermo-damage model for the analysis of concrete dams affected by
    alkali-silica reaction},
  author={Comi, C and Fedele, R and Perego, U},
  journal={Mechanics of Materials},
  volume={41},
  number={3},
  pages={210--230},
  year={2009},
  publisher={Elsevier}
  Keywords={}
```

- Fontana Dam was completed in 1946 in North Carolina.
- Only 3 years later, in 1949, a pattern of cracking was first observed, as well as an upstream movement of the structure.
- In late 1972, inspectors found a large longitudinal crack near the left abutment in both the upstream and downstream walls of the foundation drainage gallery inside the dam.

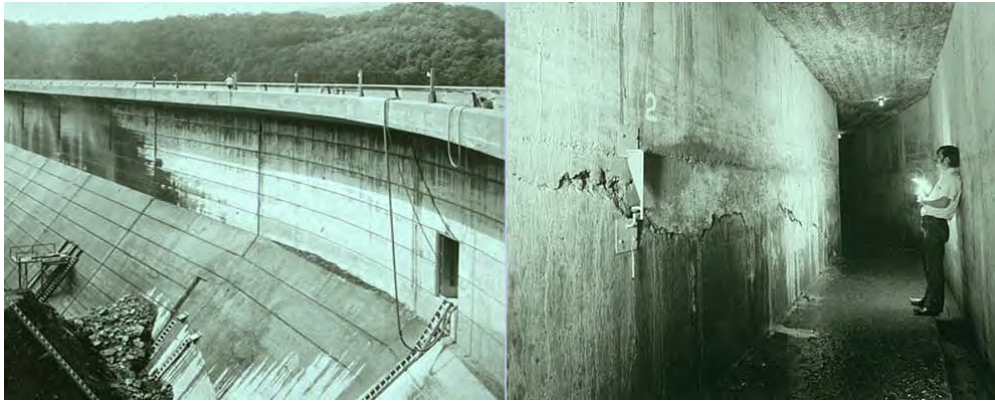


Figure 3.30: Fontana Dam, left abutment: views of the cracked surface (a discontinuity in water flow pattern can be noticed in the photo) and inside the inspection gallery (after Ingraffea (1990)); Comi, Fedele, and Perego (2009)

- Figure 3.30 shows a large crack. After inspections and monitoring activities, an accurate petrographic exam revealed the presence of AAR (Alkali Aggregate Reaction).
- Several retrofitting provisions were applied: spraying cold water on the downstream face to lower the temperature, post-tensioning the crack area by anchor rods and grouting, and cutting expansion slots across the upper portion of the dam.
- Progressive extensions of the large crack were estimated by diagnostic techniques and are documented in (Ingraffea, 1990): a schematic representation of the crack trajectory concerning one of the damaged dam monoliths.
- A chemo-thermo-damage model is proposed to simulate the swelling and the deterioration of local stiffness and strength in concrete due to AAR.
- AAR affected concrete is conceived as a two-phase heterogeneous material constituted by the expanding gel and by the homogenized concrete skeleton.
- The micro-cracking produced by the gel expansion is taken into account by means of an isotropic damage model based on the definition of two scalar damage variables (tension and compression).
- The finite element code Abaqus is used to implement the model and simulate the response of two concrete gravity dams.
- Models are 2D and strain is plane.
- The first case study is Koyna Dam which is analyzed with and without AAR for 16 years under accelerated conditions.

- The dam body is assumed to have uniform moisture. Thus, the main factor driving the AAR is the temperature history.
- Harmonically varying temperature is assumed for air and water. Foundation temperature is kept constant.
- Figure 3.31 illustrates the development of the AAR and its mechanical consequences within the considered dam, i.e. Spatial patterns of the reaction extent and of the tensile damage.

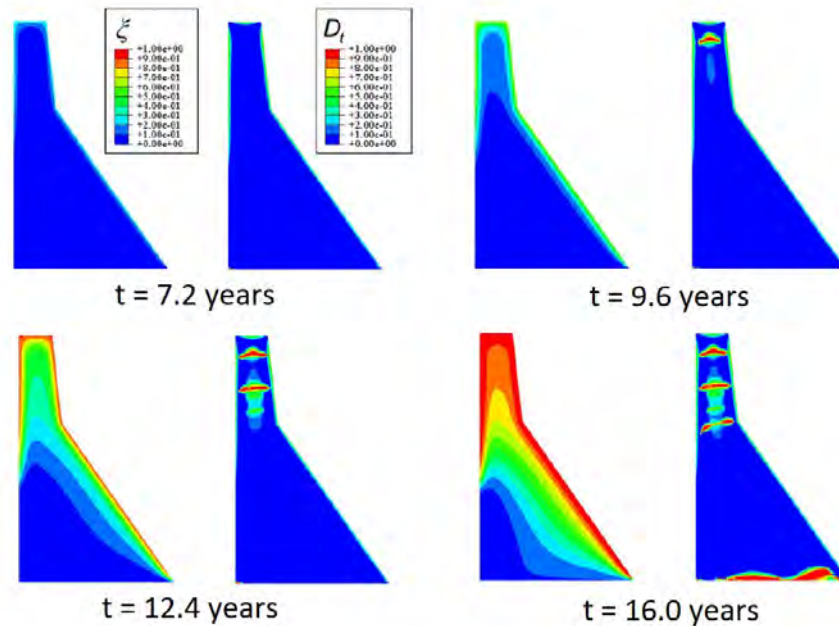


Figure 3.31: Reaction extent and damage during AAR development; Comi, Fedele, and Perego (2009)

- At the beginning of the AAR, the swelling is restricted to a thin “stripe” along the boundary exposed to air where the mean temperatures are higher. As a consequence of strain compatibility, the internal core of the dam is subjected to tensile stresses, whereas the external skin is compressed.
- In less than 4 years, several sub-horizontal cracks develop at about 15 m from each other along the vertical direction, starting in the upper part and then shifting toward the center of the dam volume.
- After about 16 years of AAR activity, a macroscopic horizontal crack develops also in the lower part of the dam.
- The second case study is Fontana dam which was completed in 1946 in North Carolina.
- Only 3 years later, in 1949, a pattern of cracking was first observed, together with an upstream movement of the structure (all due to AAR).
- The cracked section of dam is analyzed in order to assess the pattern of damage.

- Due to the peculiar dam geometry and loading conditions, the discretized domain includes part of the back-fill soil and part of the rock foundation.
- Figure 3.32 shows the reaction extent and tensile damage pattern at different times of the analysis. At the third year, a highly localized damage zone forms at the high-left corner of the drainage gallery, and it develops quickly reaching the downstream face. Starting about at $t = 4$ years, this new crack rapidly extends through the whole dam thickness.

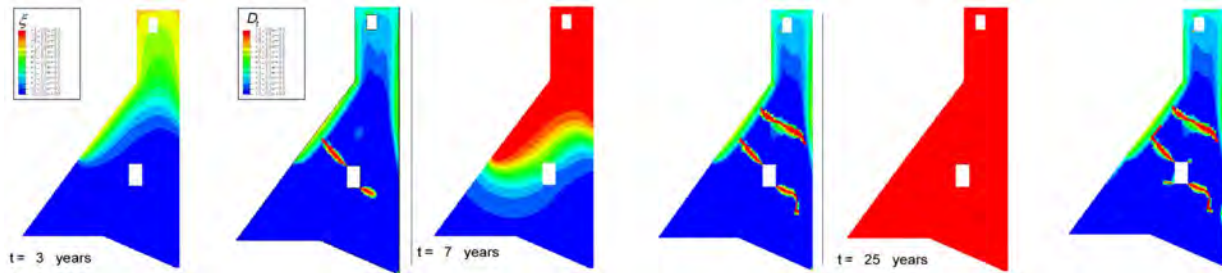


Figure 3.32: Reaction extent and damage during AAR development; Comi, Fedele, and Perego (2009)

3.22 Comi, Claudia and Kirchmayr, Beatrice and Pignatelli, Rossella (2012)

URL

```
@article{
  comi2012two},
  label={comi2012two},
  title={Two-phase damage modeling of concrete affected by alkali--silica reaction
    under variable temperature and humidity conditions},
  author={Comi, Claudia and Kirchmayr, Beatrice and Pignatelli, Rossella},
  journal={International Journal of Solids and Structures},
  volume={49},
  number={23-24},
  pages={3367--3380},
  year={2012},
  publisher={Elsevier}
  Keywords={}
```

- In this work the concrete affected by ASR is represented as a two-phase material made of a solid skeleton and a wet expanding gel.
- The mechanical degradation induced by the ASR is described by a phenomenological isotropic damage model.
- The proposed model has been validated by simulating the experimental tests performed by Multon and Toutlemonde (2010) on reactive plain and reinforced concrete beams. The aim is to investigate the effects of varying humidity conditions on the ASR development: After curing under aluminium sealing, the lower face of the beam was immersed in water, while

the upper face was dried with air at 30% RH for 14 months and then submitted to a delayed water supply for 9 months.

- The constitutive model has been implemented in the commercial code Abaqus.
- Exploiting symmetries, only one quarter of the beams have been modeled.
- Figure 3.33 shows the computed patterns of degree of saturation, reaction extent, as well as the contour plot of damage in the plain and reinforced beam after 14 and 23 months, respectively.
- The reaction starts in the lower part of the beam, where humidity is higher, and then develops in the upper part after water is supplied. Then a chemo-mechanical analysis was performed with the proposed model. The presence of reinforcement reduces the damage level.

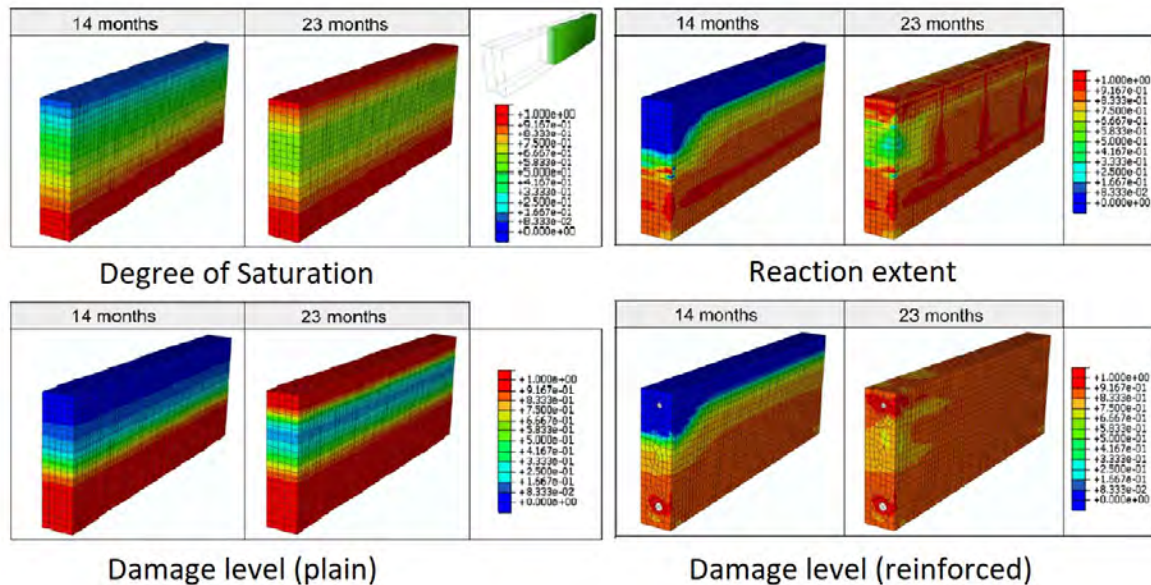


Figure 3.33: Pattern of different quantities in the beam; Comi, Kirchmayr, and Pignatelli (2012)

- They used the right gravity dam of the Beauharnois power plant (Québec, Canada) which was completed in 1941.
- This dam displayed cracks due to ASR, so the grouting of those cracks started in 1947. Afterwards, several retrofitting provisions were taken, including the adoptions of post-tension cables, the repair of surface concrete, and some expansion slots were cut in the structure to release the stresses.
- A period of 60 years after the construction is considered in the analysis.
- The chemical and mechanical properties of concrete are assumed homogeneously distributed in the dam.
- The modulus of elasticity, compressive strength, and tensile splitting strength of the concrete were determined from 45 years of field measurements.

- In order to determine the initial values, it was assumed that compressive strength does not change over time. Thus, the concrete was determined grade C40; the modulus of elasticity and tensile strength were roughly estimated.
- There was a reported a reduction of 28% for the Young's modulus and a reduction in the range 3-50% for the tensile strength.
- Since the final ASR expansion was unknown, various analyses were performed with variable values of the asymptotic axial ASR expansion.
- Plane-strain mesh with triangular elements with one Gauss point has been employed.
- Figure 3.34 shows the reaction extent and the damage at three different time steps. At the beginning the damage appears only on the external skin of the structure since it is the only area affected by the external humidity conditions.

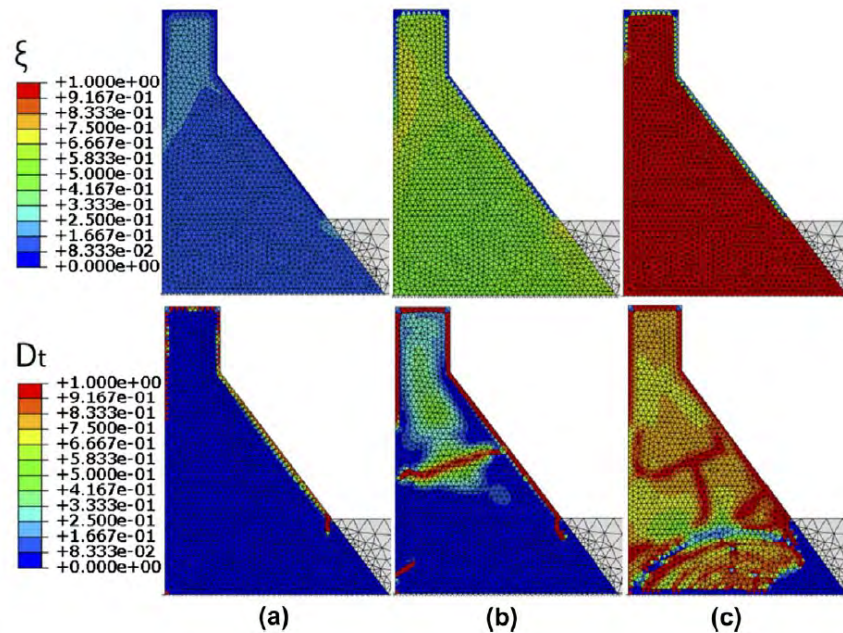


Figure 3.34: Patterns of the reaction extent and damage after (a) 3, (b) 6 and (c) 60 years; Comi, Kirchmayr, and Pignatelli (2012)

- The first macroscopic crack in the body of the dam and visible on the surface of the structure appears six years post-construction.
- The horizontal crest displacement rates after the first decade were computed as between 0.5 and 0.8 mm/year. According to measurements, the displacement rates were constant over two decades and equal to 2.2 mm/year in the horizontal upstream direction for a particular section and equal to 0.6 mm/year for another section of the dam.
- A right gravity dam of the Beauharnois power plant (Québec, Canada) which was completed in 1941 was studied.

- Some values were known: the measured modulus of elasticity (18 GPa), the compressive strength (44 MPa), and the tensile splitting strength (1.6-3.4 MPa) after 45 years of field measurements.
- In order to determine the initial values, the compressive strength was assumed to not change over time. Thus, the concrete was determined grade C40. Consequently, the modulus of elasticity ($36 \text{ GPa} \times 0.7 = 25 \text{ GPa}$), the coefficient 0.7 accounts for the aggregate type (sandstone), and tensile strength ($\sigma_t = 3.5 \text{ MPa}$) were roughly estimated.
- There was a reported reduction of 28% for the Young's modulus, and a reduction in the range 3-50% for the tensile strength.

3.23 Coubard, G. and Sausse, J. (2017)

```
@incollection{
coubard2017swelling},
label={coubard2017swelling},
booktitle={Swelling Concrete in Dams and Hydraulic Structures: DSC 2017},
editor={Sellier, Alain and Grimal, {\`E}tienne and Multon, St{\`e}phane and
Bourdarot, Eric},
year={2017},
title={Swelling Arch Dams with Thrust Blocks},
author={Coubard, G. and Sausse, J.},
publisher={John Wiley \& Sons},
Keywords={Mega; Nonlinear; Finite Element; Arch dam; },
DisplayPdf={0},
```

- The safety reassessment of arch dams with thrust blocks subject to swelling phenomena raises the issue of the stability of these thrust blocks.
- Classical analysis methods were conducted to low stability coefficients that could result in expensive and unnecessary reinforcement works.
- A methodology of calculation is made up of the following steps:
 - Analysis of the initial design and associated loadings.
 - Linear finite element model taking into account the arch and the thrust block. Simulation of concrete swelling by thermal analogy in a primary approach, accounting for a slight concrete creep due to swelling itself.
 - Classical stability analysis of the thrust block with resultant forces determined using the linear model and conservative parameters (low shear strength, no lateral abutment).
 - If a low stability coefficient is obtained, implementation of a nonlinear model with joint elements at the concrete-to-rock interface with a Mohr-Coulomb law. Evaluation of the irreversible displacements is obtained.
 - Comparison of these irreversible displacements with monitoring measures.
 - If necessary, monitoring device reinforcement of thrust block.

- If necessary, realization of site investigations in order to estimate the effectiveness of lateral abutment, shear strength and stress levels.
- If necessary, development of a more sophisticated non-linear model able to describe the behavior of swelling concrete.

- Figure 3.35 shows the swelling response of an arch dam.

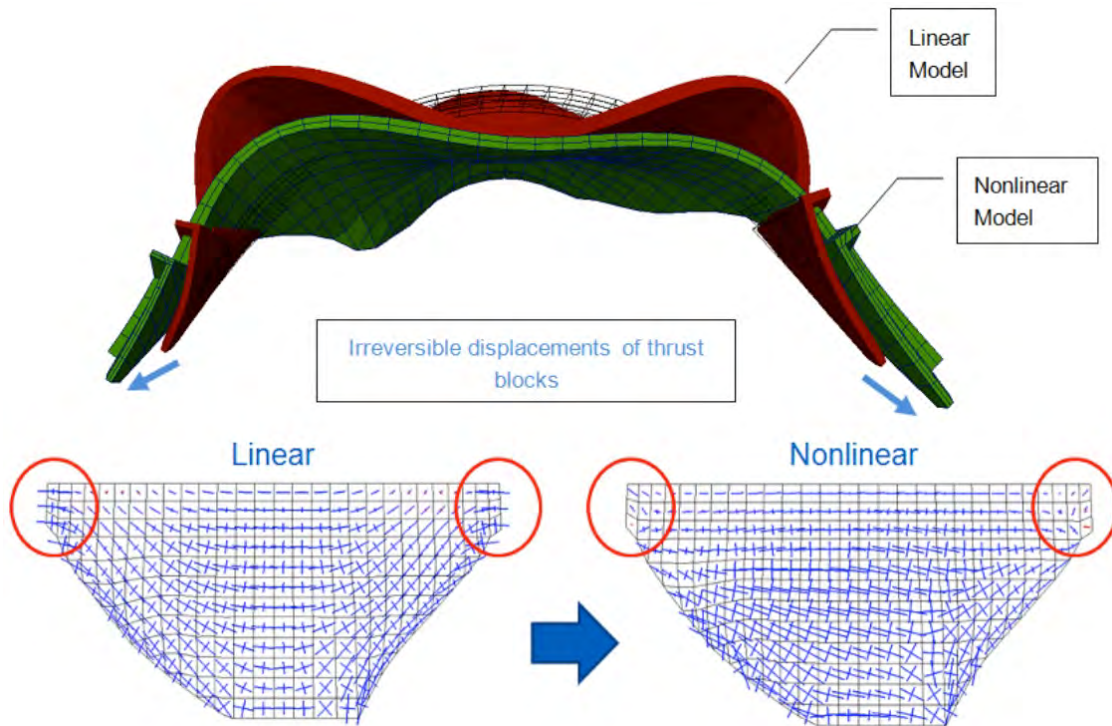


Figure 3.35: Linear model and nonlinear model with concrete-to-rock joint on a swelling arch dam with thrust blocks; Stress reorientation and modification on the upstream face; Coubard and Sausse (2017)

- For arch dams with thrust blocks submitted to swelling phenomena, the sum of actions highlights an increase in thrust block loading with time.
- Classical stability analyses can lead to conclude that sliding stability coefficients are low. This primary analysis can be seen as conservative, mostly because it neglects the nonlinear phenomena that occur within hyper-static structures such as arch dams.
- Indeed, nonlinear models demonstrate that millimetric displacements of thrust blocks are sufficient to reach a new acceptable equilibrium state.

3.24 Criaud, A and Defossé, C (1995)

URL

```

@article{
criaud1995evaluating,
label={criaud1995evaluating},
title={Evaluating the reaction of actual compositions of concrete with respect to
alkali-aggregate reactions preliminary testing at 110$\circ$ C and 150$\circ$
C},
author={Criaud, A and Defoss{\`e}, C},
journal={Materials and Structures},
volume={28},
number={1},
pages={32--42},
year={1995},
publisher={Springer},
Keywords={},
DisplayPdf={0},
url={https://link.springer.com/article/10.1007/BF02473289}

```

- Different curing methods at 110°C and 150°C were tested on concrete prisms of various compositions in order to develop a rapid expansion test to evaluate the risk of AAR in actual concrete compositions.
- No significant expansion occurred at 110°C (in water or water vapour).
- Expansion values in the range 0-0.35% for concrete prisms cured at 150°C in water or in alkaline solution during 3-5 weeks.
- For both curing methods at 150°C the highest expansion values are obtained for potentially reactive aggregates and high alkali levels in the concrete, whereas the lowest expansions correspond to the concrete mixes containing only non-reactive aggregates or having a total alkali content of less than 2.5 kg/m³.
- Alkaline treatment accounts better for the effectiveness of mineral admixtures and, in general, for the reactivity of the concrete compositions, than curing in water. From the correlations obtained with data at 38°C or 60°C and 100% RH after 12 and 4 months, respectively, alkaline curing for 3 weeks at 150°C shows a reasonable potential for predicting accurately the influence of the total alkali content, nature of the aggregates, water/cement ratio and effectiveness of mineral admixtures on concrete expansion.

the expansion data at 38°C appear in general to be low with respect to their 150°C counterparts. The reactivity of mixes containing silica fume (Nos 53 and 54) or microsilica (Nos 57, 58 and 87, 88) cannot be judged on the basis of the expansion values measured so far at 38°C (see Table 3). In Fig. 5, this series presents a systematic

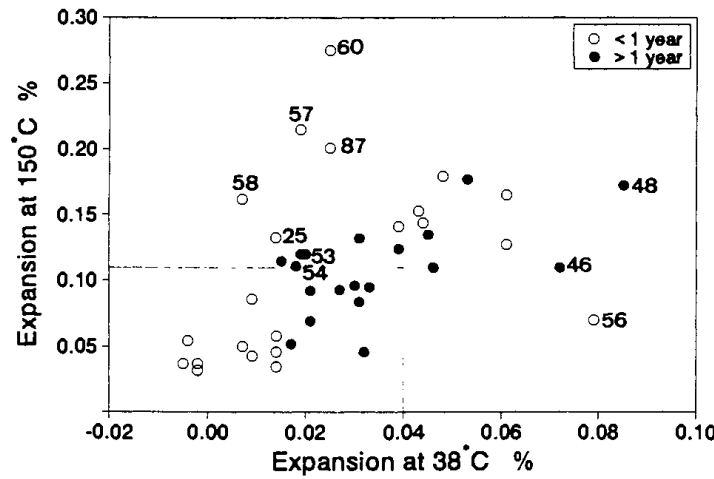


Fig. 5 Correlation between the expansion values (%) at 38°C and 100% RH (duration as indicated) and the expansions obtained by alkaline curing after 3 weeks.

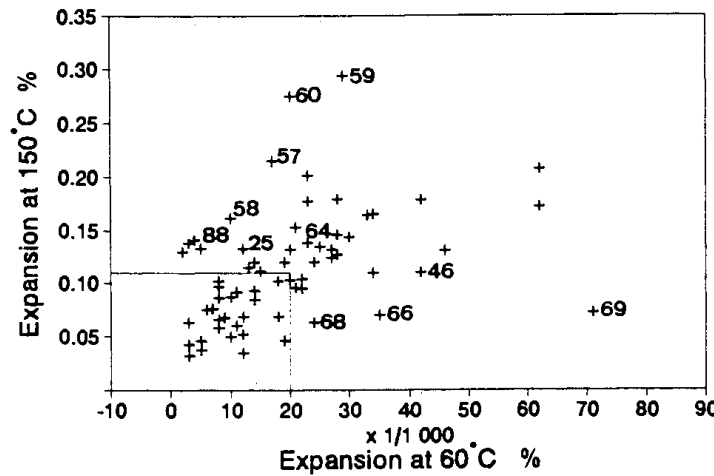


Fig. 6 Correlation between the expansion values (%) at 60°C and 100% RH (duration as indicated) and the expansions obtained by alkaline curing after 3 weeks.

aggregate-based concrete with lost some weight. No tent proposed for mix 69. Mixes MgO cement, and the result likely to be overestimated, hydration.

6. CONCLUSIONS AND TEST METHOD

The absence of expansion at several factors. First, the reorganize, with partial crystallization water. The Aft and Afm porosity of the material accommodate greater amount at 60°C. Moreover, the alkali-accelerated kinetics, is possible OH⁻ concentration within temperature rise and ASR [27] as well at 150°C under steam the increase of temperature lead to a further extension at 3–5 weeks, despite the re therefore generate a measure the presence of certain admixtures, the OH⁻ concentration high to keep the alkali-aggregate Curing the concrete prisms supplies enough alkalinity to these limitations but causes into the porosity of the prism. alkaline treatment, the expansion to result from several causes discussed elsewhere [28].

The correlations obtained or 60°C and 100% RH and the curing indicate a common cause the greater expansions do correspond highly reactive aggregates and the low values to sound concrete method thus shows a reasonable

Figure 3.36: Experimental results

3.25 Crouch, RS and Wood, JGM (1990)

URL

```
@article{
crouch1990damage},
label={crouch1990damage},
title={Damage evolution in AAR affected concretes},
author={Crouch, RS and Wood, JGM},
journal={Engineering Fracture Mechanics},
volume={35},
number={1-3},
pages={211--218},
year={1990},
publisher={Elsevier}
Keywords={}
```

- Over one hundred cores were removed from an AAR deteriorating concrete structure. More than half of these cores have been removed from nominally uncracked regions; the remainder coming from nominally cracked zones.
- The cores were tested under cyclic uniaxial compression. The loading range was 0.5-5.5 MPa.
- Figure 3.37 shows a histogram of the recorded Young's Moduli for the 117 cores.

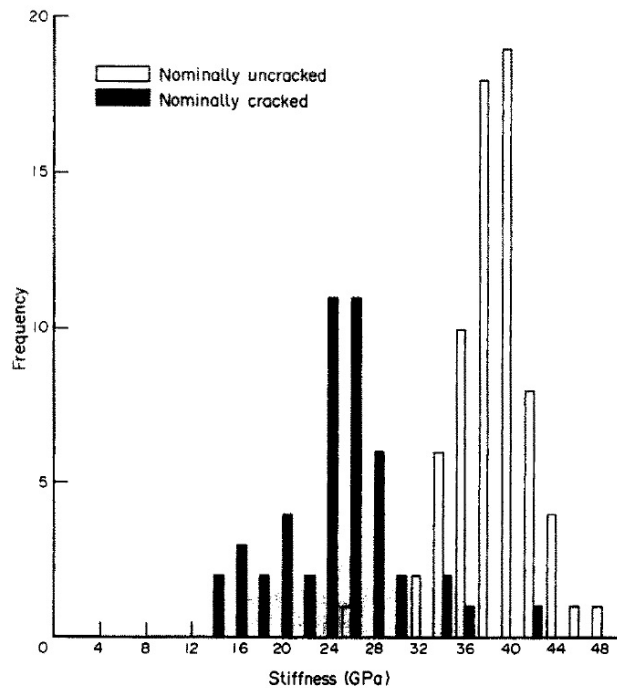


Figure 3.37: Comparing the stiffness of cracked and uncracked specimen; Crouch and Wood (1990)

- There is a clear drop (36%) in the mean stiffness for the cracked cores; however, these damaged specimens showed no obvious signs of macrocracking on their surfaces.

- Dissipated energy (or stress-strain hysteresis) offers an even more sensitive measure of distributed fracturing.

3.26 Chulliat, O. and Grimal, E. and Bourdarot, E. (2017)

```
@incollection{
culliat2017chambon},
label={culliat2017chambon},
booktitle={Swelling Concrete in Dams and Hydraulic Structures: DSC 2017},
editor={Sellier, Alain and Grimal, {\'}E}tienne and Multon, St{\'}e}phane and
    Bourdarot, Eric},
year={2017},
title={Chambon Dam},
author={Chulliat, O. and Grimal, E. and Bourdarot, E.},
publisher={John Wiley \& Sons},
Keywords={Field; Reinforcement; Rehabilitation; Finite Element; Gravity dam;
    Nonlinear; },
DisplayPdf={0},
```

- The Chambon Dam was completed in 1934. It is a concrete gravity dam.
- The right bank and the central sections are straight, while the left bank section (where the spillway was located) is curved.
- Its crest is 294 m long and 5 m wide. The downstream face is $H/V=0.75/1$ and the upstream face is vertical.
- The Chambon Dam suffers from severe AAR expansion, causing several pathologies, mainly resulting in shear stress zones in the structure and significant structural cracking, likely to affect its integrity under earthquake conditions.
- New reinforcement works were performed in 2013-2014, continuing those completed in the 1990s:
 - Installation of 415 prestressed upstream to downstream tendons crossing the structure, supplemented with a carbon fiber composite net on the upstream face,
 - Realization of 7 vertical diamond wire slot cuts
 - Replacement of the existing watertightness geomembrane
- The new multi-scales swelling law for concrete implemented in ASTER computer code was used for numerical simulation. It provided a very good fitting with the monitored dam behavior, Figure 3.38
- The FEM calculations showed that the benefits of the slot cuts done in the 1990's still remain in the upper part of the structure, confirmed by the monitoring of the deformations in the curved right wing. They, nevertheless, displayed noticeable stresses parallel to the abutments.

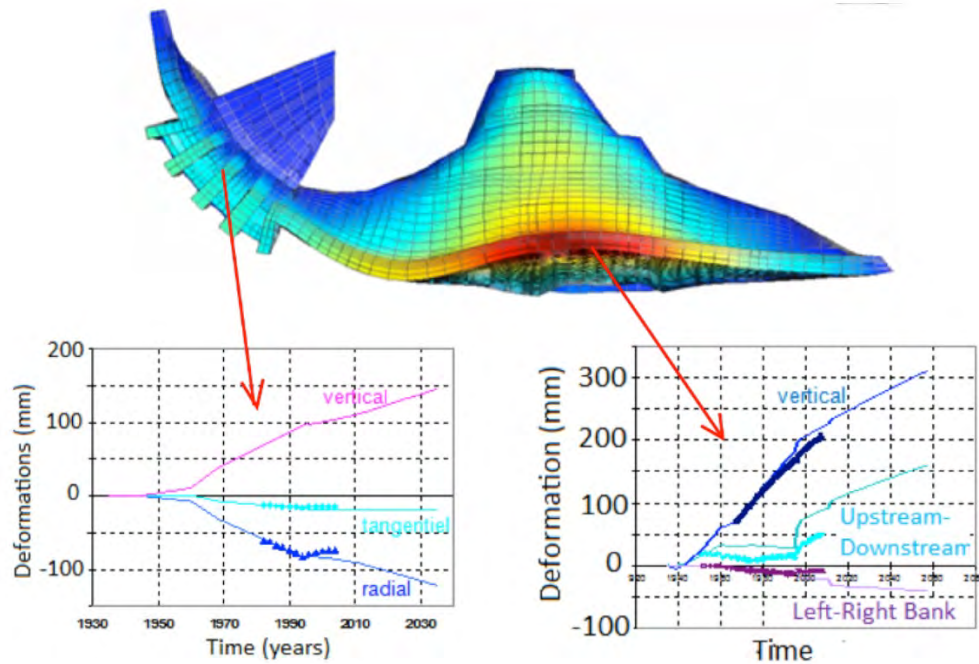


Figure 3.38: Comparison of measured and computed deformations in 3D modeling; Chulliat, Grimal, and Bourdarot (2017)

- The main objectives of the reinforcement are to maintain the integrity of the upper part of the dam and to prevent any upstream block falling that could lead damage the membrane, Figure 3.39.
- Consisting of horizontal cables, with greased sheathed strands type T15, crossing the structure from upstream to downstream, they were pretensioned and non-grouted.
- In addition to tendons, a carbon fiber composite net is added on the upstream face. It consists in the sticking of 6,000 m carbon fiber-strips.
- The 20×30 cm wide strips link the tendon heads, along vertical, horizontal and diagonal lines, Figure 3.40. The carbon fiber net serves confinement of small blocks that could escape the tendons' action.
- Strips of composite material (carbon strips glued with epoxy resin), glued to the concrete surface previously sand blasted, are designed to form a “chainstitch” and to resist tensile stress due to earthquake.

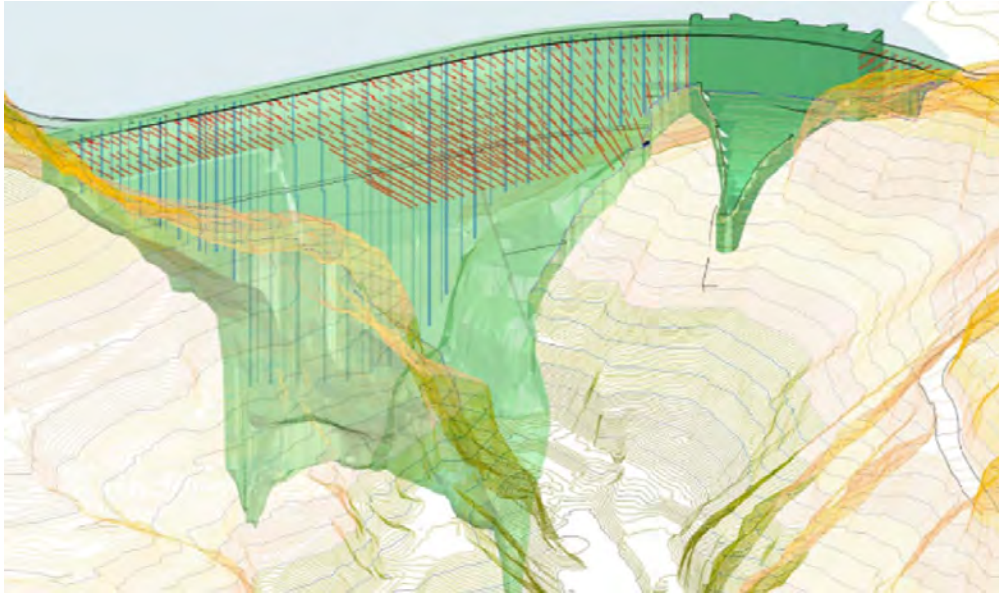


Figure 3.39: The tendons pattern (red) and drainage curtain seen from downstream; Chulliat, Grimal, and Bourdarot (2017)

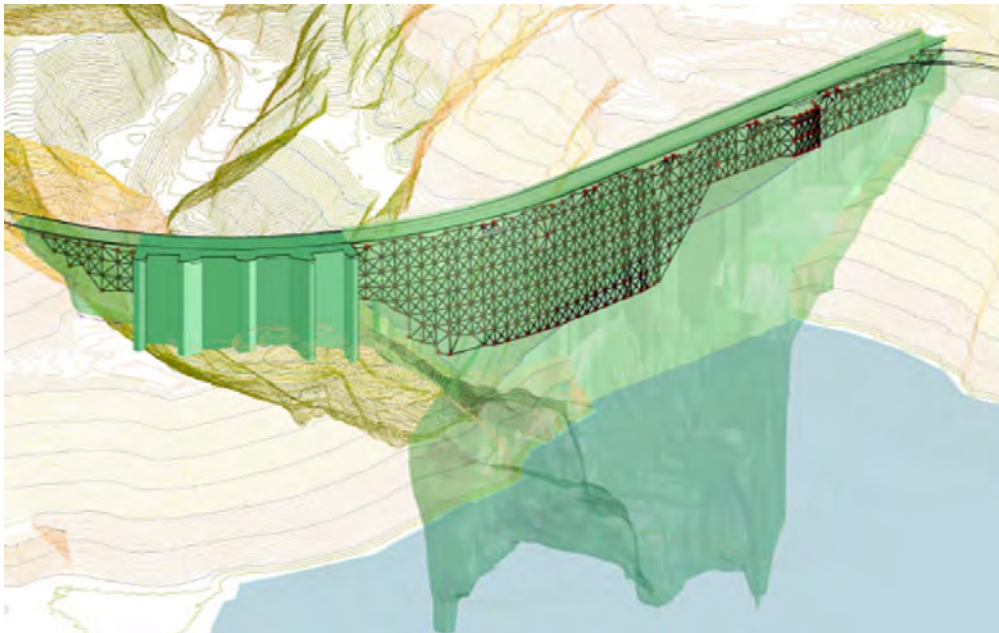


Figure 3.40: The carbon fiber net seen from upstream; Chulliat, Grimal, and Bourdarot (2017)

3.27 Curtis, DD (1995)

```
@techreport{
curtis1995modeling},
label={curtis1995modeling},
title={Modeling of AAR affected structures using the GROW3D FEA program},
author={Curtis, DD},
year={1995},
institution={Committee on Large Dams, Denver, CO (United States)}
Keywords={}
```

- The paper proposes a rational and practical methodology for finite element stress analysis of AAR affected structures.
- The paper is based on code GROW3D, a program which simulates the long term effects of AAR expansion and the effects of remedial repairs, such as slot cutting and/or anchoring.
- GROW3D uses an anisotropic expansion strain function and the following concrete properties:
 - Concrete growth expansion rates dependent on the stress vectors at each point
 - Concrete growth rate variation due to changes in moisture content and temperature
 - Time-dependent, enhanced creep behavior
- An analysis begins with a simulation of construction conditions. The results are used as the initial stress conditions in the time-dependent AAR analysis.
- The AAR analysis proceeds in a step-by-step fashion, thereby updating stresses and growth rates in the three principal stress directions as a function of current state of the structure.
- The program also allows a nonlinear analysis of the effects of concrete cracking and sliding on horizontal construction joints.
- The results of Mactaquac Station is presented for intake, diversion sluiceway, and powerhouse, Figure 3.41.
- The analysis results are used to identify potential structural problems and the need and timing of remedial measures.
- The local factors of safety are computed for several modes of failure including crushing, cracking, shear, and sliding on horizontal construction joints.
- The analysis of the intake structure used a 2D longitudinal slice through the upstream portion of the structure. The back-analysis of the intake was performed to further confirm the model before applying it to the diversion sluiceway. The foundation rock is modeled with spring elements.
- The model was used to estimate displacements and stresses in the intake in two conditions: pre-slot (1968-1988), and 1988 slot cut.
- The slot cut analyses were performed using a strategy similar to that used in numerical modeling of rock excavations:

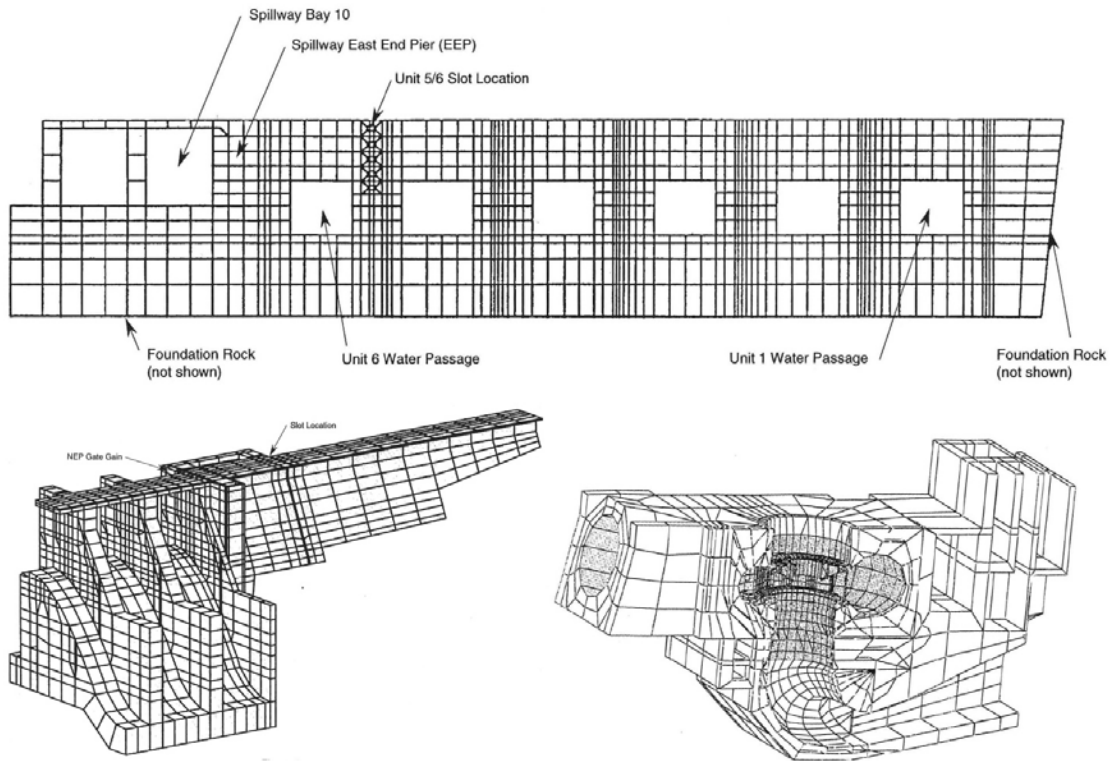


Figure 3.41: Finite element models; Curtis (1995)

- Select elements to be excavated corresponding to slot cut sequence.
 - Reduce the stiffness of elements to be excavated and apply a reverse initial stress load corresponding to the current stresses carried by these elements.
 - Compute displacement and stress change caused by excavation of selected slot elements.
 - Add displacement and stress changes to pre-slot conditions.
 - Iterate solution for closed slots.
 - Store results for post-processing.
- Next, the GROW3D model was applied to the diversion sluiceway and the west-end pier of the spillway.
 - A 3D FE model of the diversion sluiceway was developed to determine the state of stress in the north-end pier (NEP) of the structure, Figure 3.41.
 - The geometry is such that expansion of the gravity section of structure causes the NEP to tilt into the sluiceway and large shear stresses develop at the NEP/sluiceway roll-way junction.
 - The stiffness of the foundation rock is simulated using springs applied in the three global directions.
 - The computed displacement rates compared well to site measurements.
 - Finally, the powerhouse is simulated. The best calibration with unit and structure deformation data was achieved by assuming the powerhouse is free to separate from the rock at the elevation -29 ft gallery and above.

- Overall, the computed concrete stresses agreed very well with the overcoring measurements at nearly all locations, including areas in the vicinity of transverse slot locations.

3.28 Curtis, D. and Davis, B. and Rahman, S. and Powell, R. (2005)

```
@inproceedings{
curtisupdated2005},
label={curtisupdated2005},
title={Updated Assessment of Concrete Growth Effects on a TVA Dam},
author={Curtis, D. and Davis, B. and Rahman, S. and Powell, R.},
booktitle={USSD 2005 Conference, Salt Lake City, UT, June},
year={2005}
Keywords={}
```

- This paper investigates a 307 ft high concrete gravity dam which was completed in 1940 and consists of a non-overflow gravity dam, a spillway with seven bays, an intake, and a two-unit powerhouse.
- The finite element program ANSYS was used for analyses, employing a nonlinear stress-dependent concrete model and an enhanced creep model to capture AAR-affected concrete.
- The AAR-induced stresses have caused cracking at several locations, mainly along the horizontal construction joints at both ends of the dam.
- The non-overflow blocks adjacent to the spillway have deflected into the spillway opening, causing the spillway gates to bind.
- As a result, the goal was to monitor by instrumentation, finite element based investigations, and a slot-cutting program.
- The ANSYS model was calibrated to field measurements and then used to predict the future conditions in the dam and in the spillway.
- The model was also used to assess the behavior of slots (cut in the dam in the early 1990s) and to assess the effects of concrete growth on the sliding stability of the dam.
- In 1991, a 3D linear elastic analysis was performed on the dam with a simple thermal expansion. Subsequently, remedial works were recommended including: post-tensioning of the dam, cutting of expansion joints in the bridge, and cutting of four transverse slots.
- In 2002, the FE analyses were renewed in global and local levels.
- A mesh in Figure 3.42 is used to perform the time-dependent nonlinear concrete growth analyses.
- The material model from GROW3D was transferred into ANSYS.
- The model was stepped through time (using one-year time increments) to determine the effects of continued concrete growth.

- The finite element model was calibrated with vertical displacement survey data.
- Figure 3.42 shows the calibration to the Block 14 plumb line data (top-right). The results of comparison between the measured and computed spillway closure from the EDM survey is shown in the bottom-left plot. The slot closure measurements at Block 16/17 are also shown in the bottom-right figure. All of these results demonstrate a good agreement between the numerical model and the field measurements.

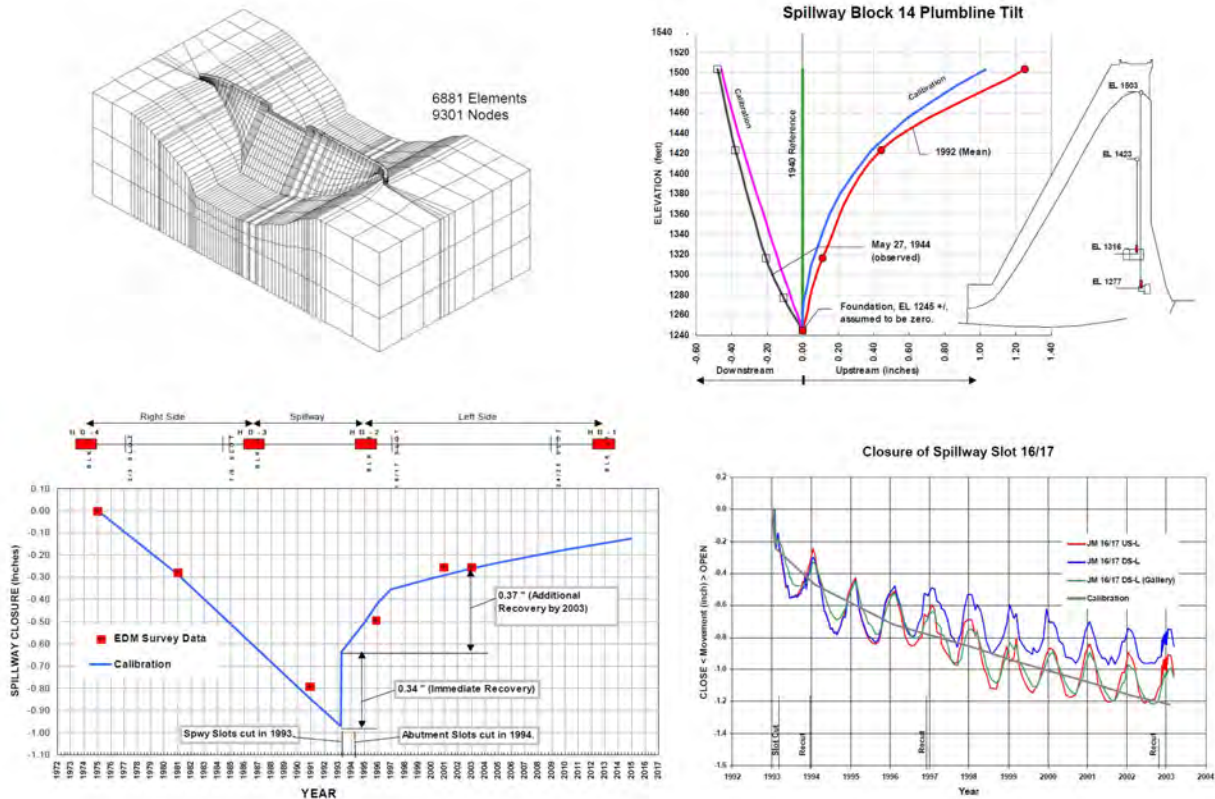


Figure 3.42: FE model and calibration results; Curtis et al. (2005)

- Investigation of the mechanisms of crack formation revealed that the cracking in the curved abutment blocks is due to the interaction of the longitudinal compression and the curved geometry of the dam at these locations.
- Because the spillway piers were not included in the global FE model, a local model of one spillway pier (including the trunnion anchorage steel) was developed in order to investigate their condition.
- The model of a typical pier is shown in Figure 3.43 (left), and the model of trunnion pin and anchorage steel is shown in the right plot.
- The anchorage steel restrains the concrete, and the restrained concrete expansion leads to higher horizontal concrete compressive stresses in the vicinity of the anchorage steel.
- The concrete above and below the trunnion pin anchorage steel expands horizontally at a greater rate than the concrete in the immediate vicinity of the trunnion anchorage steel.

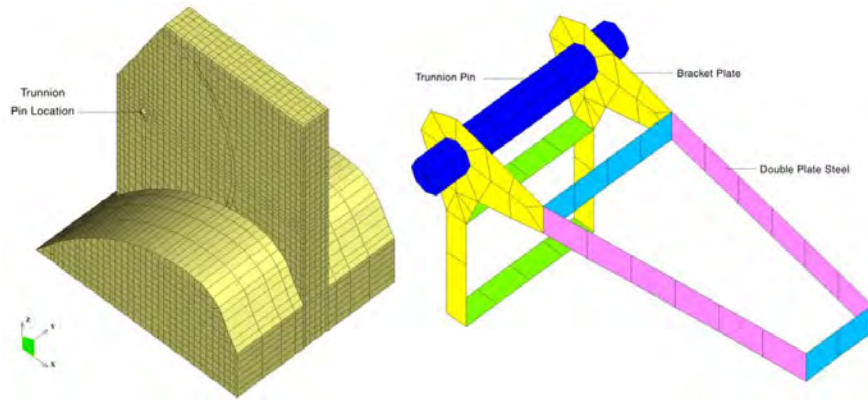


Figure 3.43: Local spillway pier model mesh including trunnion pin and anchorage steel plate mesh; Curtis et al. (2005)

3.29 Custódio, j. and Ferreira, j. and Silva, A. and Ribeiro, A.B. and Batista, A. (2017)

```
@incollection{
custodio2017disgnosis},
label={custodio2017disgnosis},
booktitle={Swelling Concrete in Dams and Hydraulic Structures: DSC 2017},
editor={Sellier, Alain and Grimal, {\'}E}tienne and Multon, St{\'}e}phane and
Bourdarot, Eric},
year={2017},
title={The diagnosis and prognosis of ASR and ISR in Miranda dam, Portugal},
author={Cust{\'}o}dio, j. and Ferreira, j. and Silva, A. and Ribeiro, A.B. and
Batista, A.},
publisher={John Wiley \& Sons},
Keywords={Laboratory; Field; Cylinder; Det f't; Det f'c; Buttress dam;
Petrography; },
DisplayPdF={0},
```

- In the last decades, a significant number of problems related to concrete deterioration were detected in large concrete structures in Portugal, the leading cause being ASR.
- The Miranda Dam is a buttress structure, 80 m high.
- The Dam was constructed in 1961. The monitoring system, installed during the construction, allows the evaluation of the actions and of the thermal, structural, and hydraulic responses.
- At the time the Dam was constructed, the aggregate was considered to be alkali non-reactive.
- Different types of concrete have been used in the Dam.
- Evidences of the Dam's swelling phenomenon were detected 20 years after construction by the progressive vertical displacements upwards, vertical sliding on the central contraction joints near the top, and the increase of strains measured in the stress-free strain-meters, Figure 3.44.

- Linear and map cracking was detected on specific zones of the galleries and on the downstream surface.

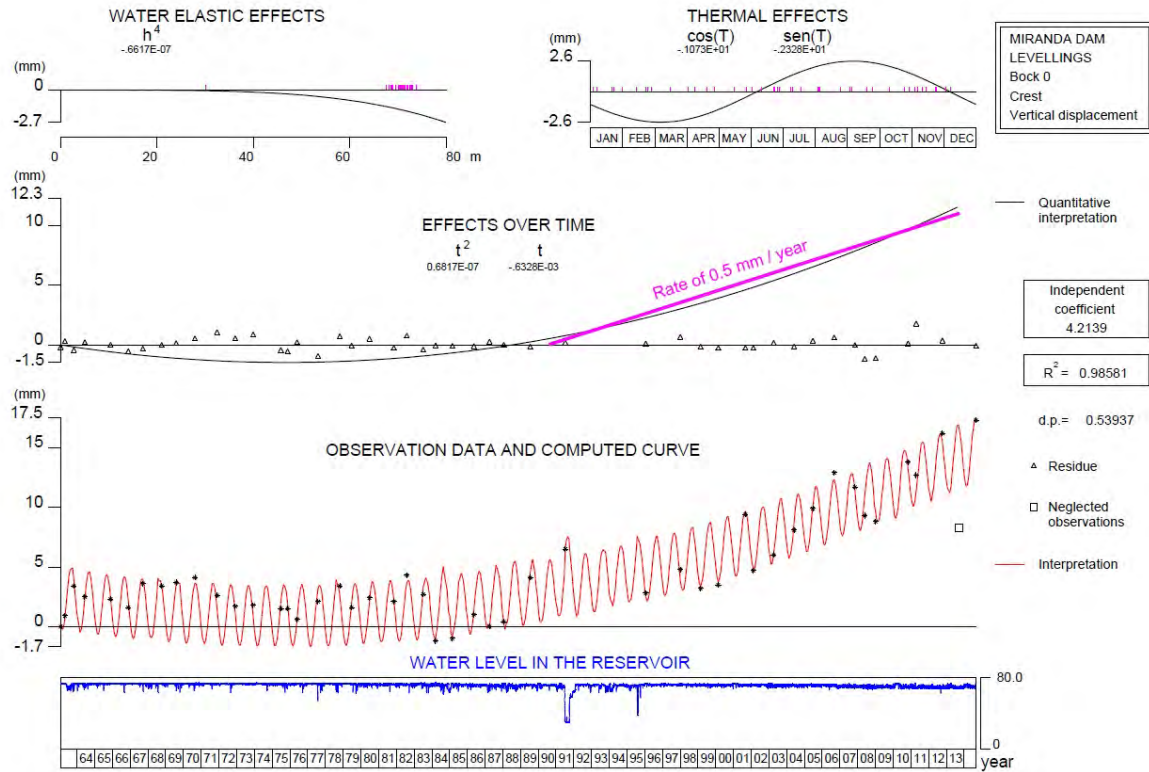


Figure 3.44: Miranda Dam: Results of quantitative analysis of vertical displacements at the top of the central buttress, obtained from geodetic leveling, between 1963 and 2014; Custódio et al. (2017)

- The laboratory test campaign was performed on 114 cores extracted from the Dam and on aggregates collected from a quarry, presumably the one used during the Dam's construction.
- The test campaign comprised the petrographic and mineralogical analysis of the concrete, chemical analysis of the concrete (determination of the cement, sulfate, alkali and silica contents) and the aggregate, evaluation of the aggregate potential alkali reactivity, evaluation of the potential for further expansion due to ASR and ISR, and the mechanical testing of the concrete (compressive and tensile strengths and stiffness damage test).
- In terms of the ASR, the residual expansion individual test results for all cores ranged from 0.001% to 0.008%, indicating a negligible to low potential for continued expansion due to ASR.
- Mechanical Testing
 - Compressive Strength: the cylindrical test results are shown in Figure 3.45. The graph also displays the strength estimate made from the compressive strength of cores extracted on the dam during its construction.

- The results show that there is a great variability on the condition of the concrete sampled throughout the structure, with the individual values ranging from 20.0 to 47.8 MPa.
- Tensile splitting strength: The individual values obtained varied from 1.7 to 4.1 MPa.
- Stiffness Damage Test: When comparing the experimental values with the correspondent estimated values for sound concrete, it is observed that the stiffness is below what was expected in five locations.

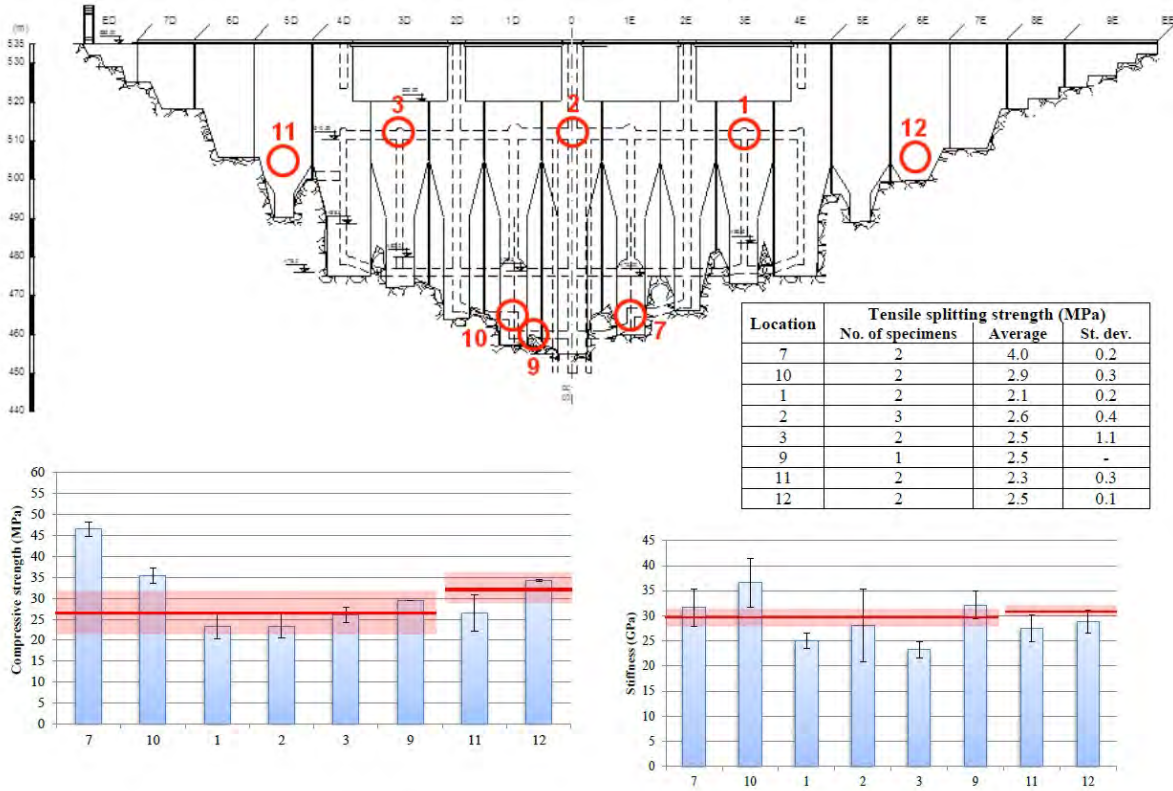


Figure 3.45: Mechanical properties of different core samplings; Custódio et al. (2017)

3.30 Diamond, S and Thaulow, N (1974)

URL

```

@article{
diamond1974study,
label={diamond1974study},
title={A study of expansion due to alkali-silica reaction as conditioned by the
      grain size of the reactive aggregate},
author={Diamond, S and Thaulow, N},
journal={Cement and Concrete Research},
volume={4},
number={4},
pages={591--607},
year={1974},
publisher={Elsevier},
Keywords={},
DisplayPdf={0},
url={https://www.sciencedirect.com/science/article/pii/000888467490009X}

```

- Influence of the size of the reactive aggregate within the range 125 μm and 20 μm on the extent and pattern of expansion due to alkalisilica reaction was explored.
- Opal characterized by physicochemical methods and carefully sized into seven fractions within this overall range was used as the reactive component of the aggregate.
- Mortars incorporating 5 and 10 percent of opal by weight of aggregate were prepared with a high-alkali cement.
- Large expansions were detected for opal of all size fractions, even as fine as 30 μm - 20 μm .
- Finer fractions yielded sudden and rapidly completed expansions of up to 2.5 percent.
- Coarser size ranges yielding slower, more prolonged expansions of almost the same order.
- The extent of microcracking observed was much less than had been expected, and the combined crack widths seemed to be significantly less than the total expansion.
- It is established that the presence of reactive aggregate in sizes passing the No. 300 sieve (< 53 μm) can lead to serious expansion when the aggregate is present in appropriate proportions, and fineness of size is no guarantee that such material will be innocuous.

3.31 Dolen, T. (2005)

URL

```

@article{
dolen05,
title={Materials Properties Model of Aging Concrete},
author={Dolen, T.},
institution={U.S. Department of the Interior, Bureau of Reclamation, Materials
      Engineering and Research Laboratory, 86-68180 },
year={2005},
number={Report DSO-05-05},
url={https://www.usbr.gov/ssle/damsafety/TechDev/DSOTechDev/DSO-05-05.pdf}
}

```

- Excellent and unique report.
- A database model of aging concrete was developed to identify the changes in materials properties over time for Bureau of Reclamation (Reclamation) mass concrete dams.
- Materials properties data on mass concrete were input to the Reclamation Aging Concrete Information System (ACIS).
- The data were analyzed for trends in the deterioration of concretes subject to aging, including alkali aggregate reaction (AAR) and general aging of early twentieth century concrete with high water-to cement ratios.
- The aging concretes were compared to dams of similar age, but not suffering from aging processes.
- The aging concretes were also compared to known good quality concretes that were manufactured after about 1948 to specifically resist deterioration from AAR, freezing and thawing (FT), and sulfate attack.
- Trends were established for comparing the compressive strength, splitting and direct tensile strength, and elastic properties of aging and non-aging dams.
- The strength and elastic properties of aging mass concrete differed significantly from those of comparable non-aging concretes.
- Both spatial variations within a structure and long-term changes in strength and elastic properties were identified.
- The ACIS database can be used to track the long-term materials properties behavior of dams through comprehensive concrete coring and testing programs.
- Laboratory core test data are included for dams ranging from about 10 to more than 83 years old. These data provide the necessary supporting documentation for the Dam Safety Office Comprehensive Facilities Review evaluation process and for dams in need of corrective action.

The following is extracted from [Numerical Modeling of AAR](#) by Saouma in reference to this report

Elastic properties

As pointed out earlier, the reaction is accompanied by a degradation of both the elastic modulus and tensile strength. In the absence of test results from recovered cores, it may be worthwhile to consult the extensive database assembled by the Bureau of Reclamation on properties of old dams measured over many years. This source could serve as an excellent starting point for preliminary analysis.

A database model of aging concrete was developed by the Bureau of Reclamation in order to identify the changes in material properties over time. Data on mass concrete material properties were input into the *Aging Concrete Information System* (ACIS), where they were analyzed for trends in the deterioration of concretes subject to aging, including the alkali aggregate reaction (AAR) and general aging of early 20th-century concrete with high water-to-cement ratios.

These aging concrete samples were then compared to dams from a similar period, yet without any adverse effects from aging processes. The aging concretes were also compared to known high

quality concretes mixed after circa 1948 specifically to resist deterioration from AAR, freezing and thawing (FT), and sulfate attack. Trends were established so as to compare the compressive strength, splitting and direct tensile strength, and elastic properties of both aging and non-aging dams.

The strength and elastic properties of aging mass concrete differed significantly from those of comparable non-aging specimens. Both the spatial variations within a structure and long-term changes in strength and elastic properties could be identified.

Three Bureau of Reclamation concrete dams have sustained significant deterioration attributable to AAR, and in particular ASR. Parker Dam, built in 1937-38, was the first Reclamation dam to be identified with ASR. American Falls Dam, which dates back to 1927, was actually the first Reclamation facility to experience deterioration caused by ASR and was ultimately replaced in 1977. Seminole Dam was constructed in 1938 and has gradually deteriorated over time. Both Parker and Seminole Dams feature comparable “reference” dams, i.e. built using similar materials and mixtures at about the same time with little deterioration.

Effect of confinement

Confinement plays an important role in reducing the elastic properties of concrete. Samples taken above 20 feet differ markedly from those extracted below the 20-foot level due to the (beneficial) effect of confinement. Table 3.2 clearly illustrates this effect. These data are to be compared

	Test Age years	Compressive strength lb/in ²	Modulus of Elasticity 10 ⁶ lb/in ²	Poisson's ratio
AAR-affected dams*	53.1	3,695	2.28	0.20
AAR cores from above 20 ft	48.0	3,180	2.09	0.20
AAR cores from below 20 ft	49.0	4,090	2.35	0.10
ACIS aging dams (1902 to 1920)*	79.7	2,490	2.59	0.23

*The average is weighted by the number of tests for a given sample set.

Table 3.2: Average compressive strength and elastic properties of concrete dams subject to aging with the non-ASR-affected concrete modulus value of approx. 5.410⁶ lb/in².

Compressive strength

Figure 3.46 shows the relationship between compressive strength and modulus of elasticity for all concrete cores both with and without ASR. Although the correlation coefficient for these equations is poor, the trend lines have been added to indicate the demarcation between the two classes of concrete. Individual correlations between compressive strength and modulus of elasticity are typically much better for individual dams using the same types of aggregate. These trends reveal that the strength-to-modulus of elasticity relationship provides a good indicator of ASR and may be used to develop failure criteria for predictive models.

Tensile strength

Tensile strength is becoming more critical in the structural analysis of concrete dams, particularly in the case of dynamic analyses involving earthquakes. Tensile strength tests were not normally performed until the 1970's, and tensile strength development in dams built before this era is unknown. The results of direct and splitting tensile strength tests on high quality concrete

and aging/ASR-affected concrete specimens are shown in Figure 3.47. Tensile strength data have typically been entered into the database as average values from just a few tests for each mixture. The aging data also include

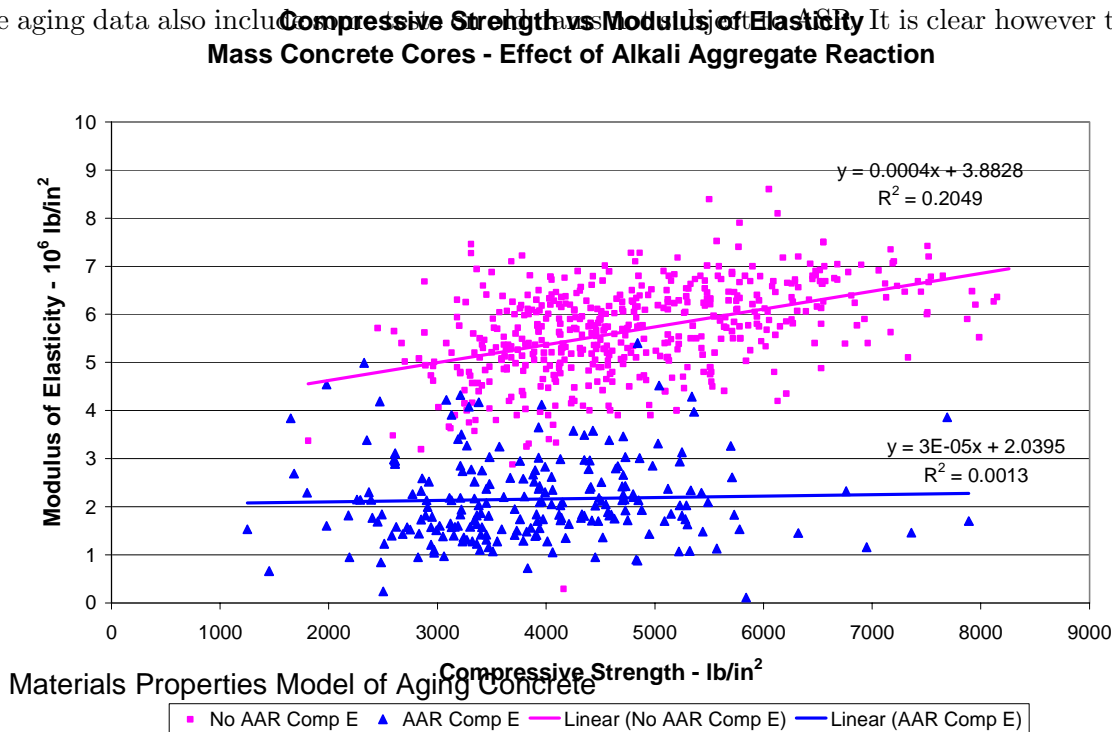


Figure 3.46: Comparison of strength to modulus of elasticity in compression for mass concrete dams with and without ASR. **Effects of Alkali Aggregate Reaction / Aging**

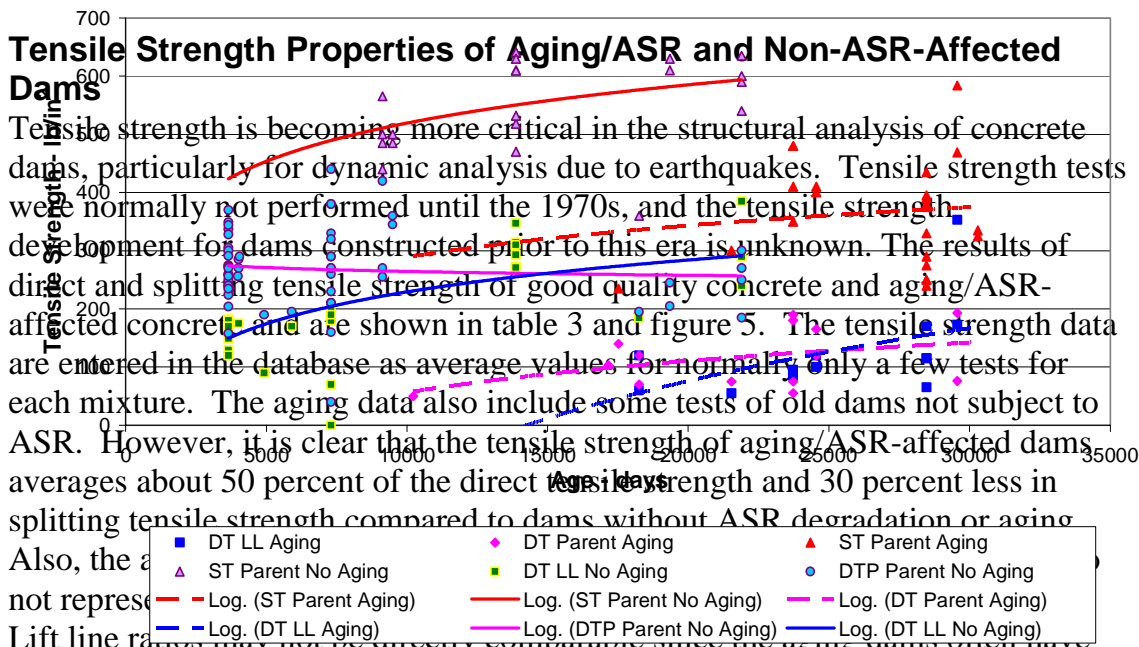


Figure 3.47: Comparison of the effects of aging and ASR on tensile strength of mass concrete dams.

Table 3.—Effect of aging on tensile strength of mass concrete cores expressed as a percentage of average compressive strength,¹ based on data from the ACIS concrete materials database

Tensile strength, lb/in ² (%) ²	
No aging ³	With aging ³

tensile strength of aging/ASR-affected dams is averaged at about 50 percent of the direct tensile strength and 30 percent less in splitting tensile strength, when compared to dams without ASR degradation or aging. Also, aging concrete data are often based solely on “testable” concrete and do not represent the condition of the deteriorated concrete that could not be tested. Lift line ratios may not be directly comparable since aging dams often contain more debonded lift lines. This input parameter has been added to more recent testing programs and constitutes a factor for some older and newer dams. Shear bond properties are not included in this dataset and moreover have not yet been analyzed due to insufficient records.

3.32 Dolen, TP (2011)

```
@inproceedings{
dolen2011selecting},
label={dolen2011selecting},
title={Selecting strength input parameters for structural analysis of aging
concrete dams},
author={Dolen, TP},
booktitle={Proceedings of the 31st USSD Annual Conference},
year={2011},
Keywords={Laboratory; Field; Cylinder; Expansion Assessment/monitoring Det. E; Det
f’c; Gravity dam; },
DisplayPdF={0},
```

- The Bureau of Reclamation Dam Safety Program performs periodic examinations and risk analysis of all of their dams.
- The probability of failure is estimated, often considering average, high, and low strength properties of mass concrete.
- Not all dams have a complete history of construction and the strength properties must be assumed.
- A database of mass concrete core tests from the past 50 years was analyzed to determine bond strength input parameters. The average direct tension and shear properties of lift lines were compared for different state-of-the-practice construction methods.
- The properties were estimated for three primary construction eras and separately for dams suffering from ASR.
- Concrete materials properties are estimated from the aging concrete information system (ACIS) database of historical mass concrete core test results.
- The percent of bonded lift lines was estimated based on the available records from the number of lift lines obtained intact compared to the total number of lift lines intercepted. Figure 3.48 shows the change in percent of bonded lift lines over time.
- Figure 3.49 summarizes the lower and upper bounds.

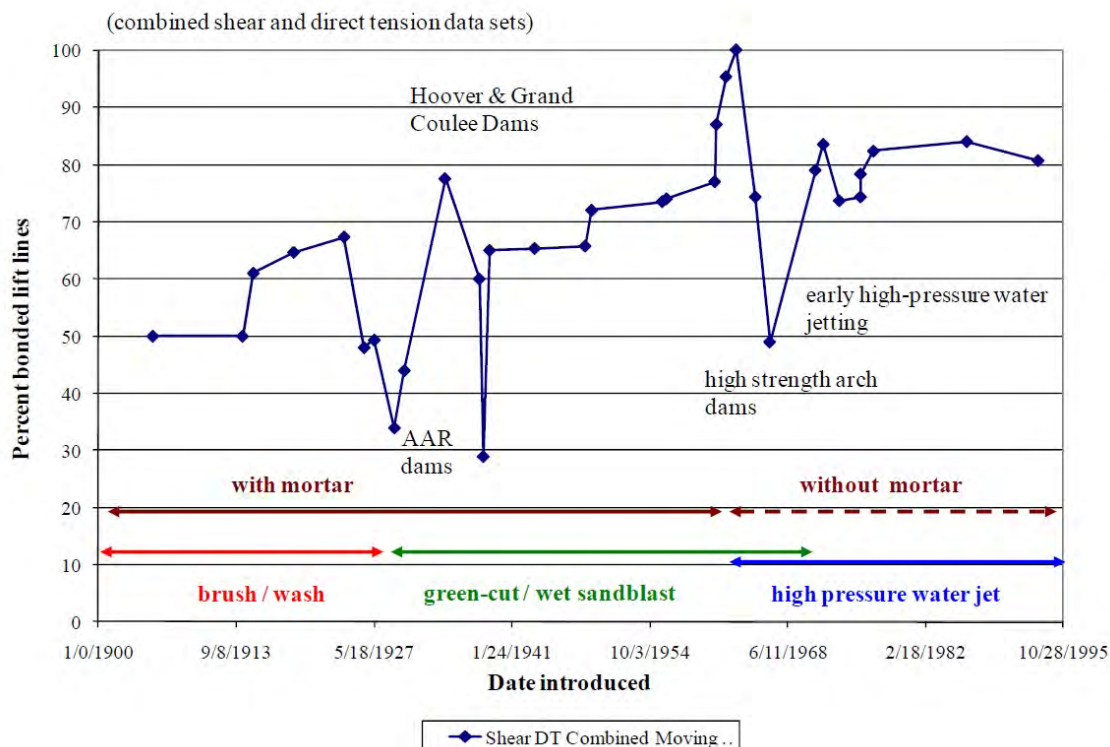


Figure 3.48: Moving average of estimated percent bonded lift lines for mass concrete dams constructed from 1905 to 1993; Dolen (2011)

Year Constructed	Average bond percent	Range low percent	Range high percent
1905 - 1933	50	9	83
1933 - 1964	85	66	100
1965 - 1993	74	23	96
1965 - 1993 *	83	66	96
AAR** 1925 - 1938	40	12	89

* Average for 1965 to 1993 not including early development of high-pressure water blasting, lift surface cleaning technology.

** Alkali aggregate reaction affected dams constructed between 1925 and 1938.

Figure 3.49: Estimate of percent bonded lift lines observed from drilled cores of Bureau of Reclamation concrete dams; Dolen (2011)

- Dams suffering from AAR have differing strength input parameters. In addition, these dams have the potential for a significant percentage of un-bonded lift lines. Even AAR dams with high lift line bond show degrading lift line strength where the reaction is more severe. In these instances, the dam should be analyzed assuming no tensile strength across lift lines.
- Lift line properties for dams suffering from AAR were noticeably lower than comparable dams of that generation.
- Figure 3.50 summarizes the average direct tensile properties of mass concrete suffering from AAR. The tests are compared to other dams constructed during the same time frame not suffering from AAR.

	Average strength	Standard deviation	Minimum	Number of tests
	lb/in ²	lb/in ²	lb/in ²	
AAR parent mass concrete 1925 - 1938	100	50	10	81
AAR bonded lift lines 1925 - 1938 [40] *	70	60	30	9
No AAR** parent mass concrete 1925 - 1938	225	90	90	9
No AAR** bonded lift lines [80]	235	85	100	17

* [Estimated percent bonded lift lines].

** Results of tests from comparable dams with no AAR.

Figure 3.50: Direct tensile strength of parent mass concrete and bonded lift lines with and without AAR; Dolen (2011)

- The average direct tensile strength of AAR-affected parent concrete is about 40%, of the non-affected concrete. Lift line strength of AAR-affected dams is about 30% of comparable non-affected ones.
- A few dams suffering from AAR with comparatively good lift line bond also seemed to be de-bonding in specific areas with the more severe reaction and expansion.
- Figure 3.51 shows the shear and sliding friction properties of lift lines for AAR affected dams compared to unaffected dams built between 1925 and 1938.
- The cohesion is about 70% of comparable concrete, and the internal friction angle is reduced by about 10%.

Lift lines	Average cohesion	90 percent exceeding	Internal friction (phi)	Number of tests
	lb/in ²	lb/in ²	degrees	
AAR 1925-1938 [40]*	365	200	49	28
No AAR** 1925-1938 [80]	505	275	56	23
AAR sliding friction 1925 - 1938	(C _a)		(phi _a)	
	65		47	88

* [Estimated percent bonded lift lines].

** Results of tests from comparable dams with no AAR.

Figure 3.51: Direct shear, “break-bond”, and sliding friction properties of AAR affected lift lines and comparable unaffected mass concrete, 1925 to 1938; Dolen (2011)

- Figure 3.52 summarizes the weighted average compressive strength and elastic properties of mass concrete dams for different construction eras. The weighted average takes into account the average strength for various test programs weighted by the number of tests for each program.
- The average compressive strength and elastic properties of early 20th century dams is about two-thirds of those completed after the Hoover Dam, indicating better quality concrete and improved construction methods.

- The properties of AAR affected dams are compared to unaffected dams constructed from about 1925 to 1938. The average compressive strength and modulus of elasticity of AAR affected concrete is about 30% lower than unaffected mass concrete.

	Average Strength lb/in ²	Modulus of Elasticity 10 ⁶ lb/in ²	Poisson's ratio	Number of tests
All concrete	4550	4.14	0.19	565
1905 - 1933	3680	3.16	0.20	256
1934 - 1964	5040	5.19	0.19	185
1965 - 1972	5940	4.73	0.20	63
1973 - 1993	5300	4.51	0.16	63
AAR dams 1925 - 1938	4230	3.21	0.11	399
No AAR ** dams 1925 - 1938	5800	4.62	0.23	23

* Results of tests from comparable dams with no AAR.

Figure 3.52: Weighted average compressive strength and elastic properties of mass concrete, 1905 to 1993, and with or without alkali aggregate reaction, 1925 to 1938; Dolen (2011)

3.33 Donghi, G. and Marcello, C. and Sainati, F. (year=2013)

```
@inproceedings{
donghibehaviourpoglia2013},
label={donghibehaviourpoglia2013},
booktitle={9th ICOLD European Club Symposium},
title={Behaviour of the Poggia dam after 7 years from the completion of remedial
works, carried out in order to reduce the effects of AAR process},
author={Donghi, G. and Marcello, C. and Sainati, F.},
year=2013
Keywords={}
```

- The Poggia Dam, built between 1949-50, is located in a narrow valley and is mainly fed through a free-flow tunnel.
- The Dam rests on a metamorphic formation.
- The total Dam height is 50 m, and the crest length is 137 m.
- Poggia Dam consists of four hollow diamond-head buttresses and two solid lateral gravity shoulders.
- The right wing gravity shoulder turns upstream because, along the main axis of the structure, the rock is at a considerable depth and originally an additional spillway was foreseen.
- In the first stage, the main instrumentation was: 1) deflection, 2) temperatures.
- Since the 1970s, the Dam began to exhibit an anomalous behavior detected by collimation, pendulums, and leveling.

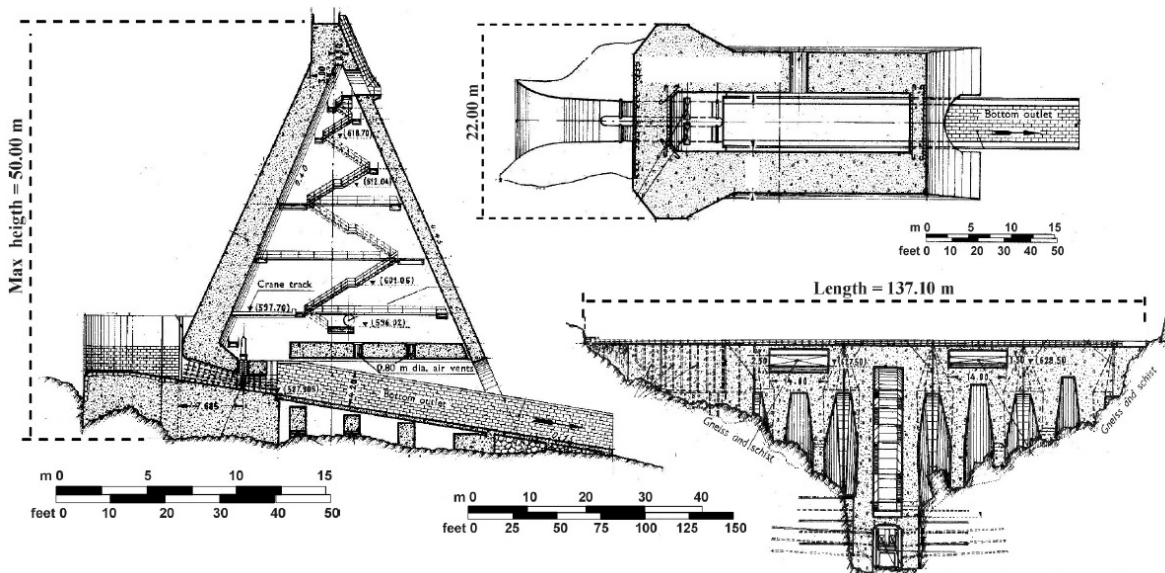


Figure 3.53: Sectional elevation, cross-section, and horizontal section of the Dam; Donghi, Marcello, and Sainati (2013)

- In particular, a drift in the displacements was observed both in the upstream-downstream direction and in the vertical direction.
- In order to ascertain the presence of AAR and to assess the present and future concrete characteristics, a set of laboratory tests was conducted both on specimens already at disposal from investigations made in the 1980s and on newly extracted core samples.
- In order to ascertain the stress state of the Dam in locations of particular interest, a set of local measurements were recorded.
- Numerical analyses were conducted with the computer code CANT-SD, Figure 3.54 (left). This is a 3D linear and nonlinear static and dynamic analysis.

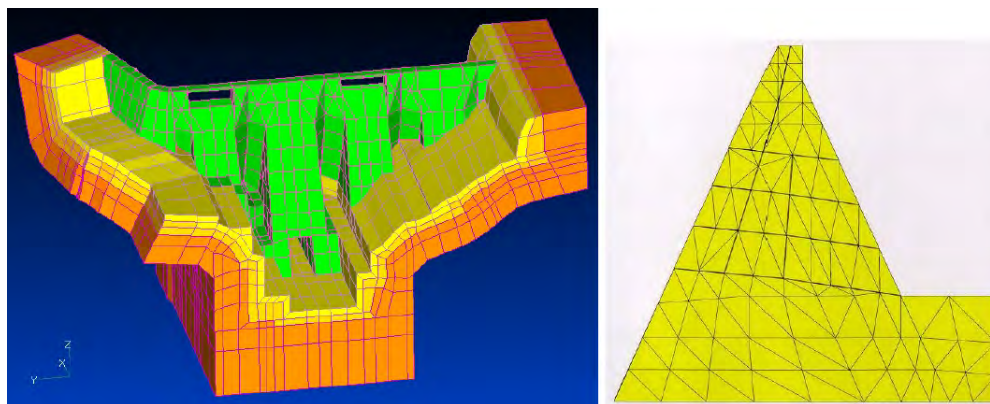


Figure 3.54: Finite element model; Donghi, Marcello, and Sainati (2013)

- The analysis of the stress distribution in the Dam's body has allowed finding a possible

explanation of the cracking pattern that can be observed in the inner cavity of the main block.

- After the cutting of the joints, the blocks will remain in the same state as they were just after construction. Accounting for the presence of the cracking pattern in the inner part of the main block, it was decided to use a limit equilibrium analysis against sliding, Figure 3.54 (right).
- The hypothetical collapse load was found with an incremental procedure in which the hydrostatic load was increased step by step up to the limit equilibrium state.
- Following the numerical analyses, the remedial works were performed.

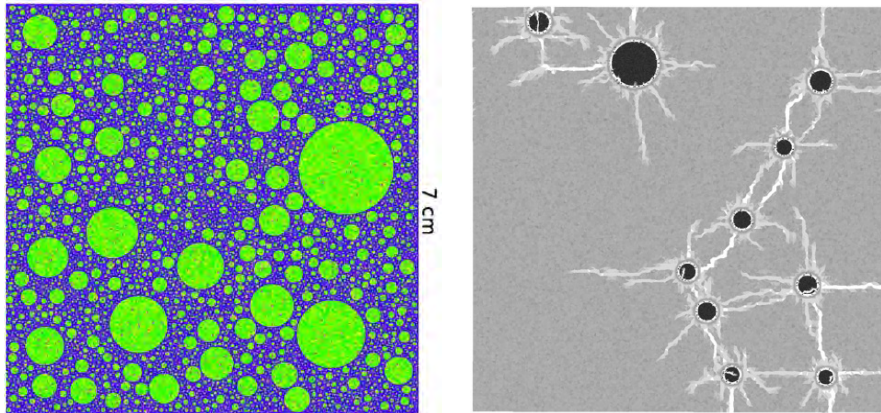
3.34 Dunant, Cyrille F and Scrivener, Karen L (2010)

URL

```
@article{
dunant2010micro},
label={dunant2010micro},
title={Micro-mechanical modelling of alkali--silica-reaction-induced degradation
using the AMIE framework},
author={Dunant, Cyrille F and Scrivener, Karen L},
journal={Cement and Concrete research},
volume={40},
number={4},
pages={517--525},
year={2010},
publisher={Elsevier}
Keywords={Laboratory; Blocks; Expansion monitoring; Quantified; Crack Index; Temp
38oC (100oF); Beams-Panels }
```

- A combined finite element/extended finite element framework was designed to analyze microstructural simulations due to ASR.
- Macroscopic free expansion and degradation of mechanical properties are linked to the extent of reaction.
- The connection between microscopic and macroscopic measurements (simulated by the model) supports the hypothesis that damage is induced by growing gel pockets in the aggregates.
- For the simulation of ASR, a typical simulation is as follows:
 - From a particle size distribution, aggregates are generated and placed in a sample.
 - Reactive zones are generated and placed in each aggregate .
 - The framework then generates the discrete representation of the setup.
 - At each step, boundary conditions are applied, and the reactive zones are caused to expand.
 - The damage caused by this expansion is computed, and the macroscopic properties are extracted.

- The process then repeats a specified number of steps.
- A sample of simulated concrete is shown in Figure 3.55(a). Spherical aggregates are used for simplicity.



(a) Simulated concrete with aggregates and mortar (b) Crack patterns produced by an expansive ring of gel

Figure 3.55: Proposed model based on Dunant and Scrivener (2010)

- The microstructure is generated using a random packing algorithm which allows a packing density of 63% of the volume with aggregates to be achieved.
- The influence of the varied nature of the aggregate is simulated by randomly varying the distribution of the mechanical properties of the elements in the aggregates. A random Weibull variable is used for this purpose.
- Both aggregates and paste are assumed to be linear elastic with damage.
- Gel pockets are modeled using a soft-discontinuity type of enrichment, simulating a perfect contact between two materials of distinct mechanical properties.
- The crack pattern of such a model is illustrated in Figure 3.55(b).

3.35 Dunant, Cyrille F and Scrivener, Karen L (2012)

[URL](#)

```

@article{
dunant2012effects},
label={dunant2012effects},
title={Effects of uniaxial stress on alkali--silica reaction induced expansion of
concrete},
author={Dunant, Cyrille F and Scrivener, Karen L},
journal={Cement and concrete research},
volume={42},
number={3},
pages={567--576},
year={2012},
publisher={Elsevier}
Keywords={Laboratory; Blocks; Expansion monitoring; Quantified; Temp 38oC (100oF);
Beams-Panels }

```

- A set of experimental tests were conducted using sensors embedded in reactive and non-reactive samples loaded on modified creep frames.
- Numerical analysis was used to link the microstructural damage under the load to the expansion.
- For numerical simulations, a set of aggregates with the correct size distribution was generated. Then, the aggregates are placed in the virtual sample slice using a random placement algorithm.
- The geometry is meshed and mechanical behaviors are attributed to each element. The behaviors are slightly randomized in each element to reproduce the inhomogeneities of the cement paste and aggregates.
- Gel pockets are distributed randomly in each aggregate. The gel pocket density is approximately constant and based on microscopic observations. The gel pockets are ideally-bonded elastic inclusions with an imposed isotropic strain.
- Load influences the microcrack propagation which changes the shape of the expansion curve.
- The stress around the gel pockets, calculated by elastic numerical simulation, is in the order of 1 GPa. This very high stress is due to the small size of the gel pockets and the quasi-incompressible behavior.
- When damage is taken into account, this stress never exceeds the tensile limit of the aggregate (at which point it is relieved by fracture). The stress and strain fields are oriented by the load, and, unlike initiation, the crack propagation direction is affected. The most important consequence is that aggregates are more prone to splitting along the load axis, Figure 3.56, which explains the faster lateral expansion measured at larger loads.
- The expansion is not redistributed, but the applied load forces the orientation of the microcracks at the microstructural level.
- It is not possible to consider damage along the principal axes independently when considering concrete as a homogeneous material; the expansions along each axes must be computed together.

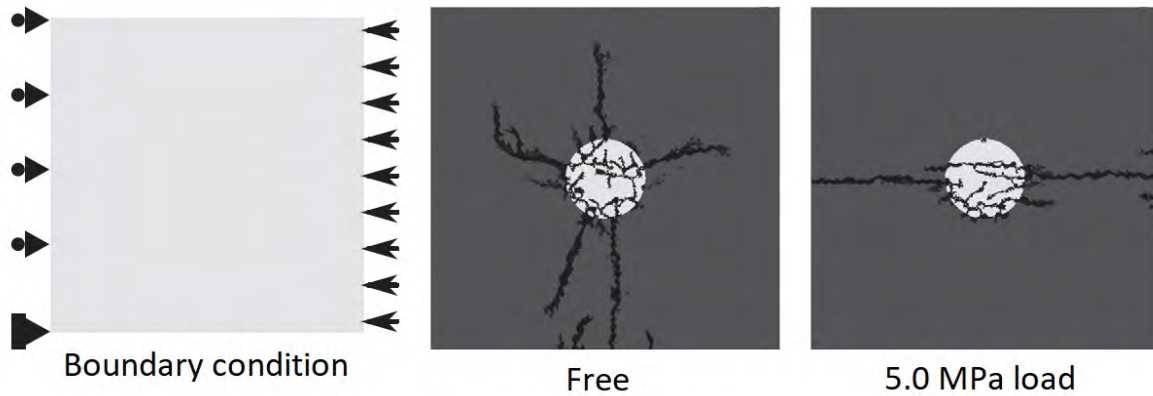


Figure 3.56: Crack pattern of a numerical sample with a single inclusion in unloaded and loaded conditions. The cracks are mainly in the paste (dark grey), which is in tension as there are no other expanding aggregates to keep it in compression. The aggregate (light grey) is partly cracked around the gel pockets, from tension and also from cracks which propagated from the paste; Dunant and Scrivener (2012b)

- The lower expansion observed in the lateral direction when longitudinal load is applied is qualitatively and quantitatively reproduced for low stresses by the numerical model.

3.36 Dunant, Cyrille F and Scrivener, Karen L (2012)

URL

```
@article{
dunant2012effects2},
label={dunant2012effects2},
title={Effects of aggregate size on alkali--silica-reaction induced expansion},
author={Dunant, Cyrille F and Scrivener, Karen L},
journal={Cement and concrete research},
volume={42},
number={6},
pages={745--751},
year={2012},
publisher={Elsevier}
Keywords={Laboratory; Cylinder; Expansion monitoring; Reinforcement; fiber
reinforced polymer }
```

- The effects of aggregate size on ASR induced expansion is studied.
- There are two main methods in which the size of the aggregates can affect damage evolution: 1) the propagation of cracks in aggregates of different sizes and the interactions between expanding, and 2) non-expanding aggregates in a densely packed micro-structure.
- Both the experimental and numerical simulations are investigated.
- For experimental tests, two aggregate sizes were used: reactive and non-reactive. Both are mixed-mineralogy alpine aggregates.

- Prismatic concrete samples of $7 \times 7 \times 28$ cm were prepared with embedded stainless steel studs. Three samples were prepared for each experimental condition.
- On the other hand, the numerical model is similar to 3.55(a) Figure 1.
- For a case of using single aggregates embedded in a cement-like matrix, Figure 3.57, the simulations were performed in non-periodic boundary conditions, with only a pin and a roller used to inhibit free body movements.

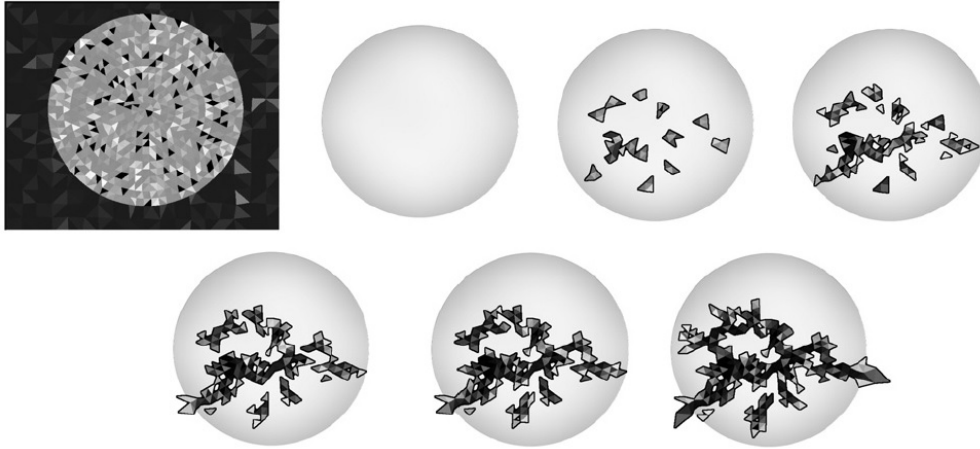


Figure 3.57: Montage of the progressive formation of a crack network in a single inclusion. States at the bottom right show cracked paste; Dunant and Scrivener (2012a)

- The results showed that without external loads, the expansion happens in two phases: first, the damage is confined within the aggregates, and the deformation of the surrounding paste is essentially elastic. In the second phase, cracks propagate in the paste, and much larger expansions are observed.
- They found that the effects of individual size fractions are related to the failure behavior of individual aggregates. This suggests that the expansion curves of ASR affected concretes are the product of three different causes.
 - First, the expansion is caused by the cracking of the aggregates and the elastic deformation of the paste.
 - Then during a transition period, both aggregate and paste cracking drive the expansion.
 - Finally, the expansion is driven by paste cracking and the exhaustion of reactive materials.
- Laboratory studies on slowly-reactive aggregates exhibit typically low expansions, as only the first and second phases occur within the time-frame of the experiment.
- Studies on rapidly-expanding aggregates may on the contrary miss the first phases, and result in expansion curves which depend mostly on the mechanical properties of the cement.

3.37 Dunant, Cyrille F and Scrivener, Karen L (2016)

URL

```
@article{
dunant2016physically},
label={dunant2016physically},
title={Physically based models to study the alkali--silica reaction},
author={Dunant, Cyrille F and Scrivener, Karen L},
journal={Proceedings of the Institution of Civil Engineers-Construction Materials},
volume={169},
number={3},
pages={136--144},
year={2016},
publisher={Thomas Telford Ltd}
Keywords={Laboratory; Expansion monitoring; Blocks; }
```

- A general overview on the activities at EPFL was provided.
- A strategy was outlined to produce a look-up table of ASR development at the microscale under all relevant load and restraint boundary conditions.
- The results can easily be integrated with existing concrete models and should be usable for prognosis.

3.38 Esposito, Rita and Anaç, Caner and Hendriks, Max AN and Çopuroğlu, Oğuzhan (2016)

URL

```
@article{
esposito2016influence},
label={esposito2016influence},
title={Influence of the alkali-silica reaction on the mechanical degradation of
concrete},
author={Esposito, Rita and Anaç{c}, Caner and Hendriks, Max AN and
çopuroğ{u}lu, Oğuzhan},
journal={Journal of Materials in Civil Engineering},
volume={28},
number={6},
pages={04016007},
year={2016},
publisher={American Society of Civil Engineers}
Keywords={}
```

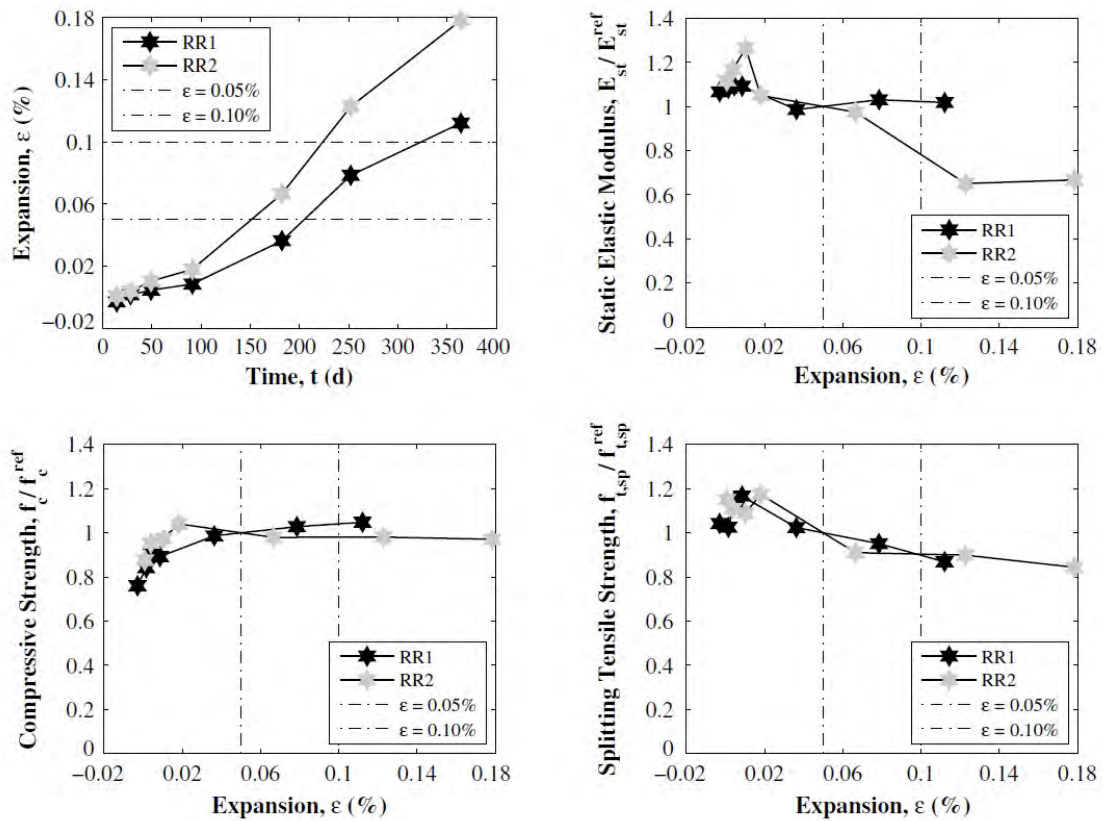
- For a detailed description, please refer to the section about the modulus of elasticity, under Esposito et al. (2016).
- The splitting tensile strength of two concrete mixtures cast with Dutch and Norwegian aggregates are reported in Figure 3.61.

- The splitting tensile strength reported a similar trend for both mixtures. After a relatively small initial increment, a degradation was observed which reached a maximum value of 23% for concrete mixture RR1 and of 26% for concrete mixture RR2.
- A large database of the experimental tests was collected, and a detailed statistical analysis was performed to determine trends in the degradation behavior.
- With reference to Figure 3.62:
 - The tensile behavior of ASR-affected concrete was found to be sensitive to the test method.
 - Whereas the splitting and flexural tests show an important decrease in the strength for high-expansion values, the direct tensile strength appears to be less sensitive.
 - In the low-expansion zone, the normalized values of all three tensile strengths are close to unity.
 - After the data clusters spread out, both the splitting tensile strength and the modulus of rupture drastically decrease.
 - The direct tensile strength exhibits a relevant degradation only in the extreme-expansion zone.
 - The three strengths exhibit a maximum degradation in the extreme-expansion zone: a reduction of 53% for the splitting tensile strength, 89% for the modulus of rupture, and 38% for the direct tensile strength.
- With reference to the third row of Figure 3.63 (left side):
 - Since the test type has a strong influence on the resulting strength, it is more appropriate to consider each test method separately.
 - The S-curve based on the splitting tensile strength data provides the best fitting of the data with an error of 8%. Its normalized value can range between 1.01 and 0.60. The degradation becomes pronounced after a latency expansion of 0.35%.
 - The modulus of rupture (represented by the thin continuous line) begins to degrade at approximately the same expansion level (i.e. 0.37%); it can reach a maximum deterioration of 76%. The estimation error is 20% which is relatively high.
 - The direct tensile strength (represented by the thin dash-dotted line) exhibits a maximum degradation of 30%. The degradation starts at a latency expansion of 2.15%. The estimation error is 12%.
- With reference to the third row of Figure 3.63 (right side):
 - The piecewise linear curve exhibited similar trends and estimation error with respect to the S-shaped curve for the splitting tensile strength.
 - It is able to capture the slight increase in strength observed for the modulus of rupture in the moderate-expansion zone.
- The normalized compressive strength exhibited a pronounced initial increase from 0.76 to 0.90 for RR1 concrete and from 0.88 to 0.97 for RR2 concrete. After the initial increase, both concrete mixtures tend to the asymptotic value of 1.

- A large database of experimental tests was also collected and a detailed statistical analysis was performed to determine trends in the degradation behavior.
- With reference to Figure 3.62:
 - Compressive strength is not a good indicator of the initiation or progress of ASR.
 - In the low-expansion zone, the normalized value of compressive strength ranged between 0.59 and 1.62 with an average of 0.92.
 - Owing to the low alkali content and the non-accelerated storage conditions, it can be hypothesized that the ASR did not lead to a significant concrete expansion, and the increase in strength can be attributed to the hydration process.
 - Excluding these data sets, the maximum normalized value in the low-expansion zone equals 1.04.
 - In the moderate-expansion zone, the data cluster narrows, and the normalized value of the compressive strength increases to 1.28.
 - For expansion values greater than 0.15% the majority of the concrete mixtures exhibit a degradation in terms of strength; however, the data show a substantial number of exceptions.
 - The maximum degradation is obtained in the extreme-expansion zone with a reduction of 46%.
- With reference to the second row of Figure 3.63 (left side):
 - Owing to the nature of the formulation, the initial increase in strength cannot be captured; the maximum normalized value is 1.00, and the latency expansion is 0.51%.
 - The S-shaped curve exhibits an asymptote at 0.64. The estimation error is 15%.
- With reference to the second row of Figure 3.63 (right side):
 - For the compressive strength, this curve shows an increase in the moderate-expansion zone.
 - The total estimation error decreases slightly to 13%; however, considering the moderate-expansion zone only, the estimation error is reduced from 20 to 13%.

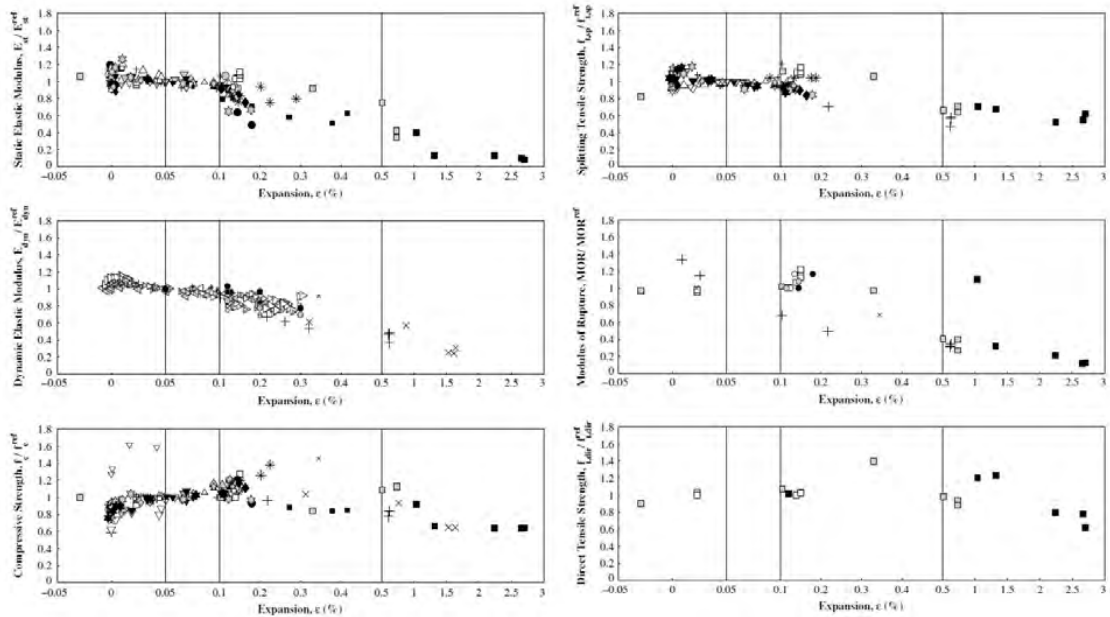
Time (d)	RR1						RR2					
	Cast	ε (%)	E_{st} (GPa)	ν	f_c (MPa)	f_{tsp} (MPa)	Cast	ε (%)	E_{st} (GPa)	ν	f_c (MPa)	f_{tsp} (MPa)
14	4-4	-0.002	42.1	0.19	45.7	3.95	5-5	0.001	29.2	0.20	53.7	4.45
28	4-1	0.002	42.7	0.20	50.6	3.90	5-3	0.004	30.5	0.21	58.5	4.30
49	4-1	0.005	43.1	0.26	54.3	4.30	5-3	0.011	33.0	0.29	59.7	4.20
91	4-1	0.009	43.1	0.20	53.7	4.40	5-3	0.018	27.4	0.24	63.7	4.55
182	4-2	0.037	38.9	0.28	59.4	3.85	5-6	0.067	25.5	0.25	60.0	3.50
252	4-2	0.079	40.7	0.18	61.8	3.60	5-6	0.123	17.0	0.27	60.1	3.50
364	4-2	0.113	40.1	0.18	63.0	3.30	5-6	0.179	17.4	0.25	59.5	3.30
Calculated reference value		0.05	39.5	0.24	60.11	3.76	—	0.05	26.1	0.25	61.23	3.85

(a)

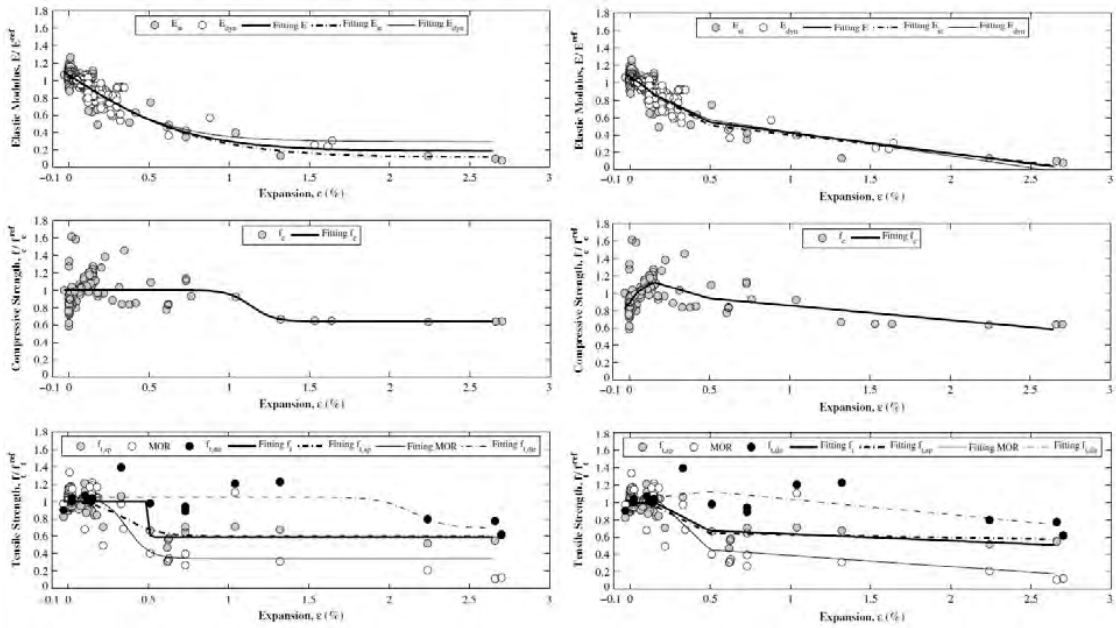


(b)

Figure 3.58: Results by Esposito et al. (2016)



(a)



(b)

Figure 3.59: Results by Esposito et al. (2016)

3.39 Esposito, Rita and Hendriks, Max AN (2016)

URL

```
@article{
  esposito2016multiscale},
  label={esposito2016multiscale},
  title={A multiscale micromechanical approach to model the deteriorating impact of
    alkali-silica reaction on concrete},
  author={Esposito, Rita and Hendriks, Max AN},
  journal={Cement and Concrete Composites},
  volume={70},
  pages={139--152},
  year={2016},
  publisher={Elsevier}
  Keywords={}
```

- The main experimental program is reported by Anaç et al. (2012). The test was conducted at Delft University of Technology. The scope of this research was to investigate the damage effects induced by the ASR in concrete from the microscopic to the macroscopic scales.
- The current paper reports the results for the macroscopic scale. It highlights the importance of mechanical degradation in relation to ASR-induced concrete expansion.
- Two comparable concrete mixtures were adopted throughout the study using Dutch and Norwegian aggregates.
- Concrete mixtures cast with Dutch and Norwegian aggregates are respectively classified as RR1 and RR2 mixtures.
- Owing to the large number of samples needed, the samples were cast in six sessions. Each session includes one control specimen with no ASR.
- Mechanical tests were performed on prisms and cubes stored at 38°C and a relative humidity greater than 96%.
- The specimens were tested at 14, 28, 49, 91, 182, 252, and 365 days.
- Time dependent quantitative results are provided in Figure 3.60 for expansion, modulus of elasticity, Poisson's ratio, compressive strength, and tensile splitting test.
- The normalized material properties are also presented as a function of percentage expansion as shown in Figure 3.61. Each normalized value was obtained as the ratio between the current property value and its reference value. The latter was estimated at a reference expansion of 0.05%, the value used to discriminate between nonreactive and potentially reactive concrete.
- The mechanical properties exhibited a slight increase during the first 90 days, followed by a degradation trend.
- The static elastic modulus of concrete mixture RR1 exhibited minor variations and ranged between 99 and 107% of its reference value. Conversely, the concrete mixture RR2 exhibited a maximum degradation of 35%.

Time (d)	RR1						RR2					
	Cast	ε (%)	E_{st} (GPa)	ν	f_c (MPa)	$f_{t,sp}$ (MPa)	Cast	ε (%)	E_{st} (GPa)	ν	f_c (MPa)	$f_{t,sp}$ (MPa)
14	4-4	-0.002	42.1	0.19	45.7	3.95	5-5	0.001	29.2	0.20	53.7	4.45
28	4-1	0.002	42.7	0.20	50.6	3.90	5-3	0.004	30.5	0.21	58.5	4.30
49	4-1	0.005	43.1	0.26	54.3	4.30	5-3	0.011	33.0	0.29	59.7	4.20
91	4-1	0.009	43.1	0.20	53.7	4.40	5-3	0.018	27.4	0.24	63.7	4.55
182	4-2	0.037	38.9	0.28	59.4	3.85	5-6	0.067	25.5	0.25	60.0	3.50
252	4-2	0.079	40.7	0.18	61.8	3.60	5-6	0.123	17.0	0.27	60.1	3.50
364	4-2	0.113	40.1	0.18	63.0	3.30	5-6	0.179	17.4	0.25	59.5	3.30
Calculated reference value		0.05	39.5	0.24	60.11	3.76	—	0.05	26.1	0.25	61.23	3.85

Figure 3.60: Experimental Results and Calculated Reference Values for Normalization Procedure; Esposito et al. (2016)

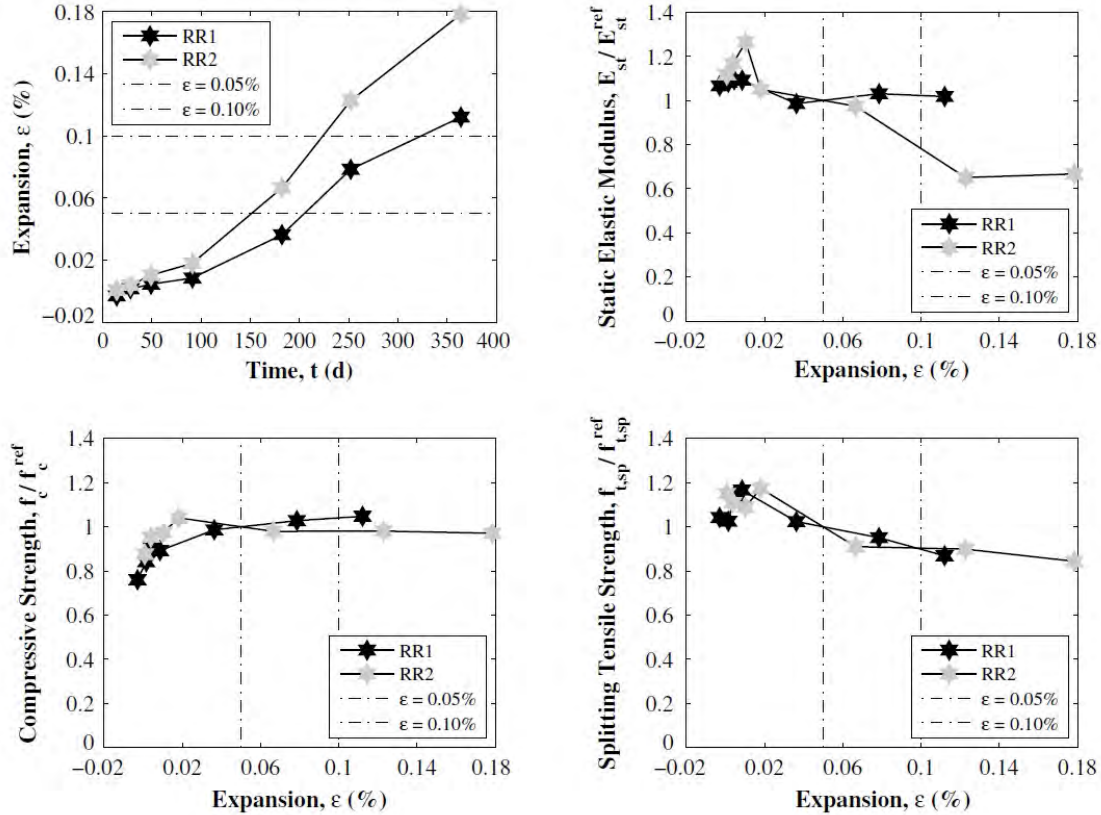


Figure 3.61: Variation of expansion dependent mechanical properties; Esposito et al. (2016)

- A large database of the experimental tests was collected and a detailed statistical analysis was performed to determine trends in the degradation behavior.
- Figure 3.62 reports the variations in the mechanical properties as functions of the concrete expansion (gathered from literature).
- Four zones were defined: low-expansion zone ($\varepsilon < 0.05\%$), moderate-expansion zone ($0.05\% \leq \varepsilon < 0.10\%$), high-expansion zone ($0.10\% \leq \varepsilon < 0.50\%$), and extreme-expansion zone ($\varepsilon \geq 0.50\%$).
- Each data point is an average of the two or three specimens.

- It was found that the elastic modulus was subjected to a significant degradation.
- Both the static and dynamic elastic moduli marginally increase for expansion values up to 0.03%. Subsequently, a slight degradation is observed in the low- and moderate-expansion zones; however, their mean values remain close to unity in these zones. For expansion values greater than 0.10%, both of the stiffness properties decreased at a similar rate. The maximum degradation was obtained in the extreme-expansion zone, with a reduction of 92% for the static elastic modulus and 86% for the dynamic elastic modulus.

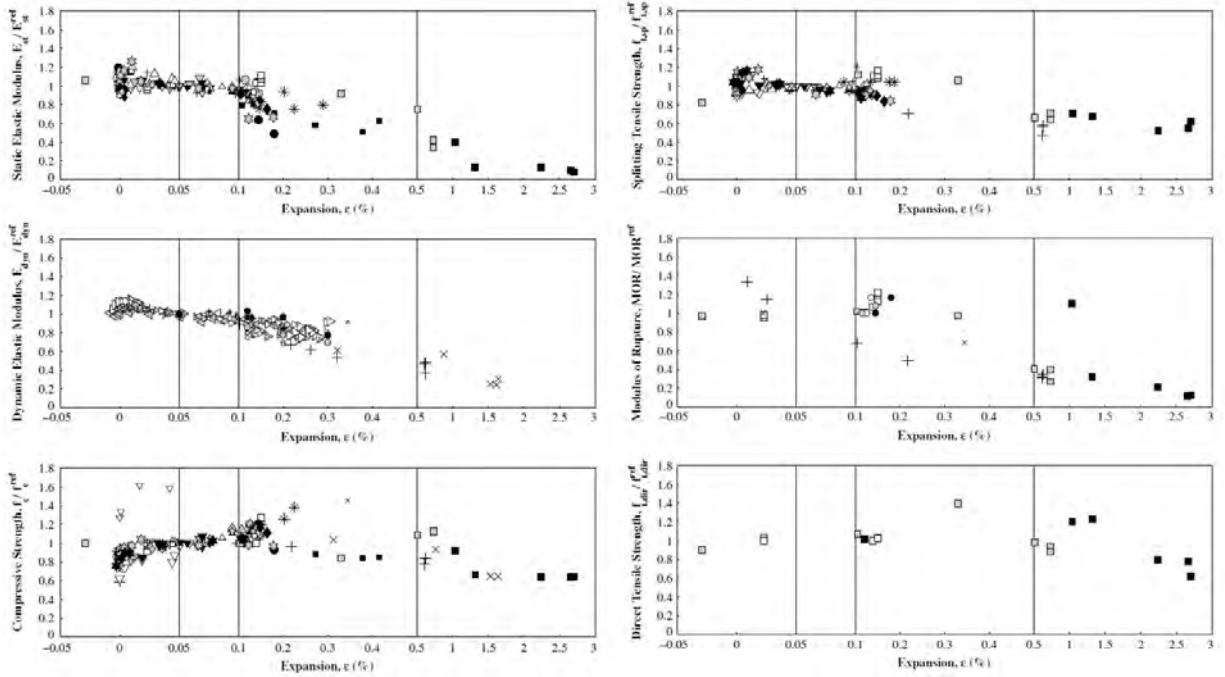


Figure 3.62: Experimental data from the literature; a nonuniform scale for the expansion axis is used; Esposito et al. (2016)

- Next, a statistical analysis was performed to determine the degradation behavior of the mechanical properties induced by the ASR under free-expansion, Figure 3.63.
- The normalized data were fitted using two formulations: an S-shaped and a piecewise linear curve.
- The S-shaped curve is a revised version of the degradation law proposed by Saouma and Perotti (2006):

$$\beta_P = \frac{P}{P^{\text{ref}}} = \beta_0 - (\beta_0 - \beta_\infty) \frac{1 - \exp\left(-\frac{\varepsilon}{\varepsilon_c}\right)}{1 + \exp\left(-\frac{\varepsilon - \varepsilon_l}{\varepsilon_c}\right)} \quad (3.7)$$

where P and P^{ref} are current and reference values of the chosen property, respectively; β_0 and β_∞ normalized property values at zero expansion and at the asymptotic expansion, respectively; and ε_l and ε_c latency and characteristic expansion values, respectively.

- With reference to Figure 3.63 (left side):

- The S-Curves exhibit a minor difference only in the extreme-expansion zone. The estimation error is 7%. The resulting latency time ε_l is extremely small (on the order of 10^{-14}), which confirms the fast stiffness degradation starting in the low-expansion zone. The maximum, β_0 , and the minimum, β_∞ , normalized values of the elastic modulus equal 1.06 and 0.19, respectively.

- Next a continuous piecewise linear function is used in the form of:

$$\beta_P = \frac{P}{P^{\text{pref}}} = \begin{cases} q_1 + m_1\varepsilon & \varepsilon \leq 0.05\% \\ q_m + m_m\varepsilon & 0.05\% < \varepsilon \leq 0.1\% \\ q_h + m_h\varepsilon & 0.1\% < \varepsilon \leq 0.5\% \\ q_e + m_e\varepsilon & \varepsilon > 0.5\% \end{cases} \quad (3.8)$$

where q and m are linear coefficients for each zone. Note that owing to the continuity condition, the number of unknown coefficients reduces from 8 to 5.

- With reference to Figure 3.63 (right side):

- For the elastic modulus degradation, the estimation error and the degradation rate, which were evaluated in the high-expansion zone, provide results that are similar to those obtained from the S-shaped curve fitting.
- For expansion values greater than 2.60%, this formulation provides unrealistic negative normalized values; therefore, zero residual stiffness should be considered after this limit.

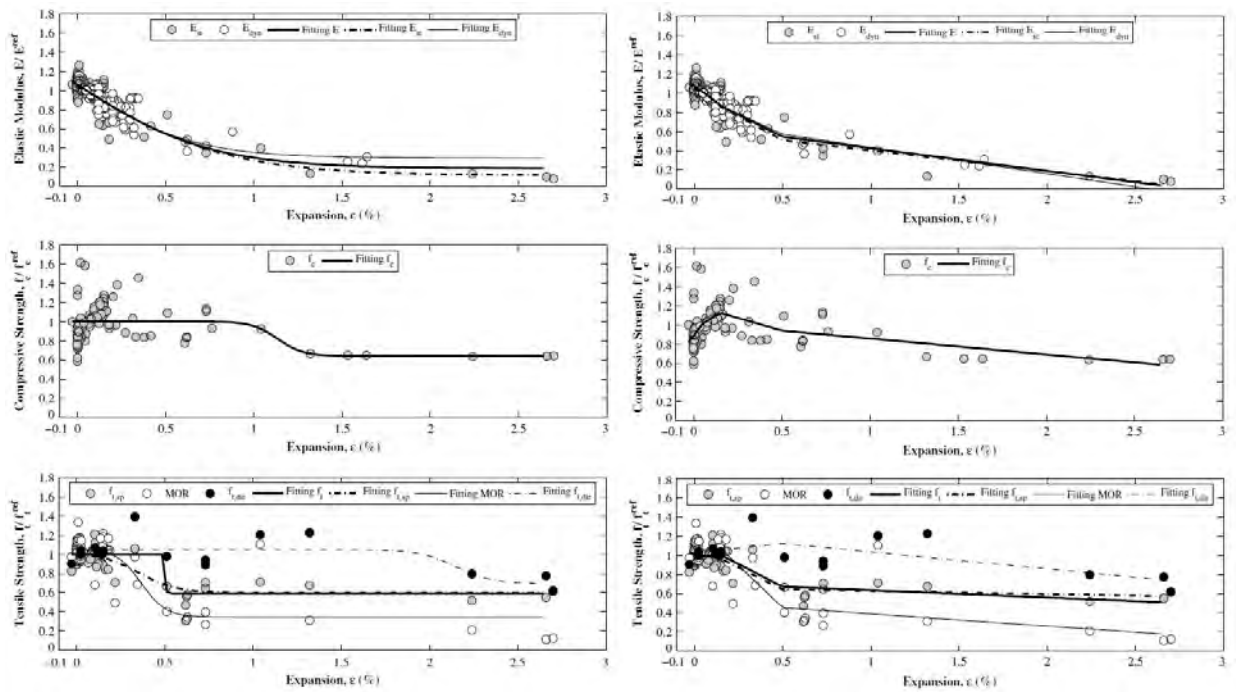


Figure 3.63: Fitting adopting S-shaped curve (left column) and fitting adopting piecewise linear curve (right column); Esposito et al. (2016)

3.40 Esposito, R and Hendriks, MAN (2017)

URL

```
@article{
esposito2017literature,
label={esposito2017literature},
title={Literature review of modelling approaches for ASR in concrete: a new
perspective},
author={Esposito, R and Hendriks, MAN},
journal={European Journal of Environmental and Civil Engineering},
pages={1--21},
year={2017},
publisher={Taylor \& Francis},
Keywords={},
DisplayPdf={0},
url={https://www.tandfonline.com/doi/abs/10.1080/19648189.2017.1347068}
```

- A literature review of the main modelling approaches for ASR in concrete is presented within a new perspective.
- Models are categorised on the basis of their input and output parameters, instead of adopting the classical classification on the base of the scale (e.g. micro, meso and macro).
- The main aim of the review is to understand to which extent the available models are able to describe the deteriorating impact induced by ASR in concrete material and if the approaches can ultimately be extended to structural analyses.
- An excellent and comprehensive literature survey on numerical models

Table 1. Overview of modelling approaches for ASR in concrete.

Input Scope Demonstration Experimental validation	Reaction products level		Aggregate level		Concrete level		Structural level			
	Ions & water	Gel	Swelling	Damage	Swelling	Damage	Mech. Prop.	Lab specimens	Members	Structures
Charlwood (1994)					█					█
Léger et al. (1996)							█			█
Capra and Bournazel (1998)						█				█
Malla and Wieland (1999)							█			█
Ulm et al. (2000)							█			█
Li and Coussy (2002)							█			█
Capra and Sellier (2003)							█			█
Farage et al. (2004), Fairbairn et al. (2004)							█			█
Bangert et al. (2004)							█			█
Saouma and Perotti (2006)							█			█
Winnicki and Pietruszczak (2008)							█			█
Comi et al. (2009)							█			█
Pesavento et al. (2012)							█			█
Esposito and Hendriks (2012)							█			█
Bažant et al. (2000)			█	█						
Dormieux et al. (2004)			█	█						
Schlangen and Van Breugel (2005)			█	█						
Çopuroğlu & Schlangen (2007), Anaç et al. (2012)			█	█						
Comby-Peyrot et al. (2009)			█	█						
Reinhardt and Mielich (2011)			█	█						
Wu et al. (2014)			█	█						
Esposito (2016), Esposito and Hendriks (2016)			█	█						
Ulm et al. (2002)	█									
Lemarchand (2001)	█									
Grimal et al. (2008a, 2008b)	█									
Dunant and Scrivener (2010)	█									
Giorla et al. (2015)	█									
Pignatelli et al. (2013)	█									
Charpin and Ehrlicher (2014)	█									
Bažant and Steffens (2000)	█									
Suwito et al. (2002)	█									
Poyet et al. (2007)	█									
Multon et al. (2009), Sanchez et al. (2014)	█									
Puatatsananon and Saouma (2013)	█									
Alnaggar et al. (2013)	█									
Liuaudat et al. (2014)	█									
Nguyen et al. (2014)	█									
Bažant and Rahimi-Aghdam (2016)	█									
Multon and Sellier (2016)	█									
Alnaggar et al. (2017)	█									

parameters as: models based on concrete expansion (Section 3), models based on internal pressure (Section 4), models based on the gel production (Section 5) and models based on the ions diffusion–reaction mechanisms (Section 6). The attention is focused on understanding to which extent the available models are able to capture the multiscale nature of ASR in concrete, are able to describe its deteriorating impact on concrete material and if the approaches can ultimately be extended to structural analyses.

Table 2. Models based on concrete expansion.

	Model type	Imposed strains dependent on	No. input parameters					Reactivity	Validation (V)/Demonstration (D)
			Mechanical	Temp.	RH	Stress state			
Charlwood (1994); Thompson et al. (1994)	Phenomenological	Stress state	2	1	-	2	-	Powerhouse (V)	
Léger et al. (1996)	Phenomenological with reduction of stiffness and tensile strength	Stress state, temperature, moisture, reactivity	6	2	2	2	1	2D FEA spillway pier (V)	
Capra and Bournazel (1998)	Phenomenological with probabilistic fracture mechanics	Stress state, temperature, moisture, reactivity	1	2	1	2	3	Lab specimens (D)	
Malla and Wieland (1999)	Phenomenological with linear elastic fracture mechanics	-	2	1	-	-	-	3D FEA arch-gravity dam (V)	
Ulm et al. (2000)	Thermo-chemo-plastic with kinetics law	Temperature	5	7	-	-	1	2D FEA dam and bridge box girder (D)	
Li and Coussy (2002, 2004)	Thermo-chemo-plastic with kinetics law	Temperature, moisture	5	4	1	-	1	2D FEA bridge pier (D), 3D FEA bridge pylon (D)	
Capra and Sellier (2003)	Thermo-hygro-chemo-damage with kinetics law	Temperature, moisture, reactivity	11	1	1	-	-	2D FEA of lab specimens (V) and of RC beam (D)	
Farage et al. (2004), Fairbairn et al. (2004)	Thermo-chemo-cracking with kinetics law	Temperature	8	2	-	-	1	3D FEA lab specimen (V) and 2D FEA dam (V)	
Bangert et al. (2004)	Thermo-hygro-chemo-damage based on mixture theory	Temperature, moisture	10	3	2	-	-	2D FEA lab specimens and beam (D)	
Saouma and Perotti (2006)	Thermo-hygro-chemo with kinetics law and reduction of stiffness and tensile strength	Stress state, temperature, moisture	8	5	-	1	1	2D FEA lab specimens (V) and dam (D)	
Winnicki and Pietruszczak (2008), Winnicki et al. (2014)	Thermo-hygro-chemo-plastic for RC with kinetics law	Stress state, temperature, moisture	11	3	1	1	1	Lab specimens (V) and 2D FEA dam (V)	
Comi et al. (2009)	Thermo-chemo-damage with kinetics law	Stress state, temperature	18	5	-	-	1	2D FEA lab specimens and dam (V)	
Pesavento et al. (2012)	Thermo-hygro-chemo-damage based on mixture theory	Temperature, moisture	3	7	5	-	2	2D FEA lab specimens (V)	
Esposito and Hendriks (2012)	Thermo-chemo-cracking rheological-based	Temperature	6	5	-	-	3	Lab specimens (V)	

Figure 3.65: Models based on concrete expansion

3.41 Fairbairn, Eduardo MR and Ribeiro, Fernando LB and Lopes, Luciana E and Toledo-Filho, Romildo D and Silvos, Marcos M (2006)

URL

```
@article{
fairbairn2006modelling},
label={fairbairn2006modelling},
title={Modelling the structural behaviour of a dam affected by alkali--silica
reaction},
author={Fairbairn, Eduardo MR and Ribeiro, Fernando LB and Lopes, Luciana E and
Toledo-Filho, Romildo D and Silvos, Marcos M},
journal={International Journal for Numerical Methods in Biomedical Engineering},
volume={22},
number={1},
pages={1--12},
year={2006},
publisher={Wiley Online Library}
Keywords={Mega; New Const. Model; Thermal Anal.; Finite Element; Dam Gravity; }
```

- An ASR thermo-chemo-mechanical expansion model was proposed with the main feature of representing the stress-induced anisotropy by means of a classical smeared cracking model.
- The model includes the influence of temperature and humidity.
- The model was applied to the 3D simulation of a real gravity dam located in the southeast region of Brazil.
- The dam began to operate in 1963.
- In 1976, the dam presented signs of AAR: cracking at the top of the spillway columns; blocks of anchorage of the forced conduits, surface of the jump ski, and powerhouse; misalignment of the crowning between the central wall and adjacent blocks.
- The simulated structure is the left central wall of 35 m height. It is located between the intake dam and the spillway. Its width varies from 5.8 m upstream to 12.0 m downstream.
- The determination of the thermal and humidity fields was based on simplified averaged assumptions. A constant ambient temperature and a constant reservoir level were assumed.
- Some of the AAR kinetics parameters are assumed from literature (e.g. activation energy and initial temperature). Other parameters are initially assumed to a dummy number and later updated from inverse analysis (e.g. latency and characteristics times).
- Figure 3.66 shows the vertical displacement of a point located at the top of the wall and its experimental counterpart monitored for the last 25 years.
- There is good agreement between the measurements and simulation results.

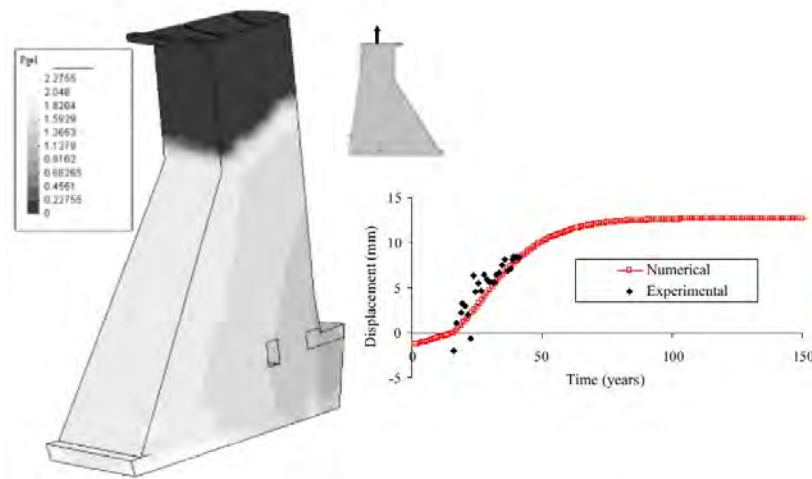


Figure 3.66: Results for the ASR simulation: gel pressure for 40 years and the displacements at the crest of the dam; Fairbairn et al. (2006)

3.42 Fan, Shenfu and Hanson, John M (1998)

URL

```
@article{
  fan1998effect,
  label={fan1998effect},
  title={Effect of alkali silica reaction expansion and cracking on structural
    behavior of reinforced concrete beams},
  author={Fan, Shenfu and Hanson, John M},
  journal={ACI Structural Journal},
  volume={95},
  pages={498--505},
  year={1998},
  publisher={Citeseer}
  Keywords={}
```

- A laboratory study was carried out to investigate the effect of deleterious ASR expansion on the structural behavior of reinforced concrete beams.
- The specimens were conditioned by immersion in a cyclically-heated alkali solution for one year to accelerate ASR.
- To simulate in-service conditions, several beams were held under load that caused flexural cracking while being conditioned.
- In total, six beams were cast: three reactive (R) and three nonreactive (N).
- In one beam they used 2@#3 bars, and for two others they used 2@#5 bars.
- Dimension of beams are: 1500 mm long, with a 150 × 250 mm rectangular cross-section. The beams were designed as singly-reinforced.

- Stirrups made with D-5 wire were placed in the shear spans of all the beams.
- Due to the restraint from the reinforcement, the longitudinal expansion at the level of the reinforcement was greatly reduced. Expansion in the transverse direction was also reduced.
- Cracking development and growth is shown in Figure 3.67.
- Cracks were first observed on top of the beams after 6 months of conditioning and were oriented in the direction parallel to the reinforcement.

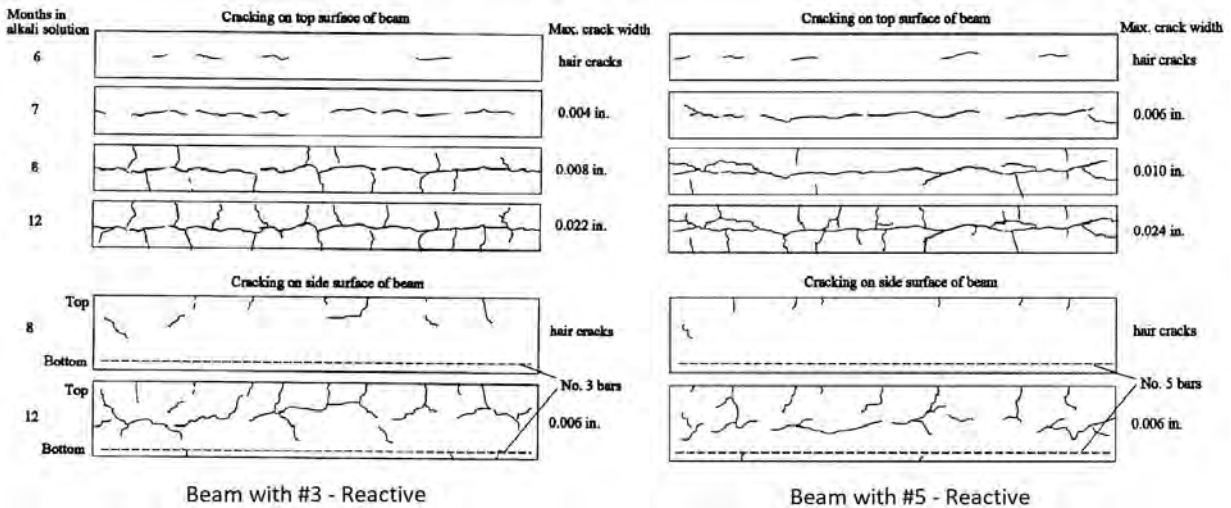


Figure 3.67: Comparison of cracking between; Fan and Hanson (1998)

- Alongside this experiment, a total of 80 100×200 mm cylinders of reactive (R) and nonreactive (N) concrete were cast (half reactive and half nonreactive).
- The specimens were conditioned by immersion in a cyclically-heated alkali solution for one year to accelerate ASR.
- The average strength of the reactive and nonreactive concrete at 28 days were 34.7 and 35.9 MPa with a standard deviation of 0.46 and 0.41 MPa, respectively.
- The compressive strength, splitting tensile strength, and dynamic modulus were not affected significantly after 90 days.
- At an age of 125 days, however, just after the ASR cracks were found, the concrete mechanical properties were greatly reduced.
- At an age of 180 days, the loss of the compressive strength, splitting tensile strength, and dynamic modulus of the cylinders was 24%, 38%, and 31%, respectively, compared to the corresponding 28-day values.
- It was also observed that the reduction of the splitting tensile strength was higher than that of the compressive strength and dynamic modulus.
- At an age of one year, further reduction of the mechanical properties was small.

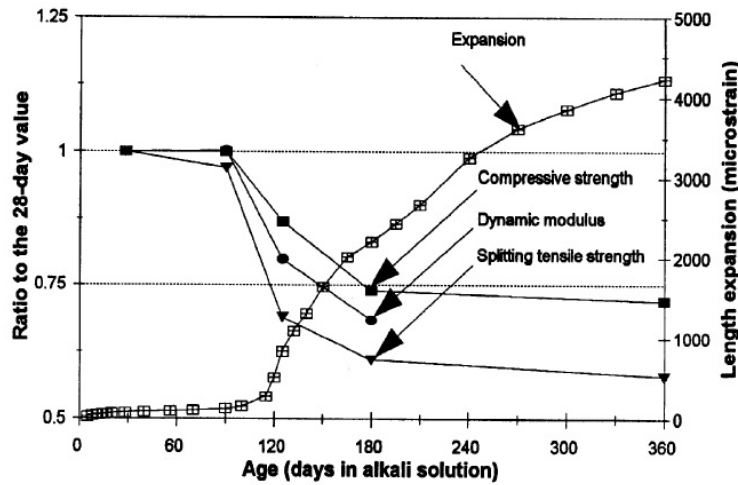


Figure 3.68: Change in mechanical properties of reactive cylinders with ASR expansion; Fan and Hanson (1998)

- The load-carrying capacity of reactive and nonreactive beams were tested under the four-point bending test.
- Beams include rebar near the bottom face.
- The load-deflection curves for one beam with rebar #3 and two beams with rebar #5 are shown in Figure 3.69.

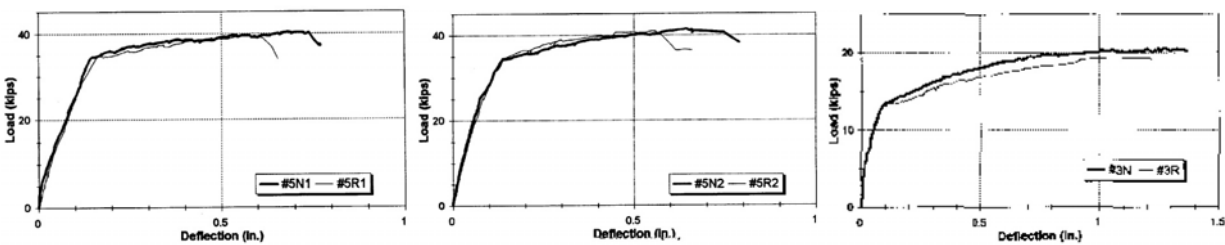


Figure 3.69: Results of flexural loading tests; Fan and Hanson (1998)

- After conditioning for one year, the flexural strength of the reactive (R) beams which experienced ASR cracking was nearly the same as that of the nonreactive (N) concrete beams.
- The effect of ASR on flexural strength of the pre-loaded and cracked beams was also reported to be insignificant.

3.43 Ferche, Anca C and Panesar, Daman K and Sheikh, Shamim A and Vecchio, Frank J (2017)

URL

```

@article{
  ferche2017toward},
  label={ferche2017toward},
  title={Toward Macro-Modeling of Alkali-Silica Reaction-Affected Structures},
  author={Ferche, Anca C and Panesar, Daman K and Sheikh, Shamim A and Vecchio,
    Frank J},
  journal={ACI Structural Journal},
  volume={114},
  number={5},
  pages={1121},
  year={2017},
  publisher={American Concrete Institute}
  Keywords={}

```

- Six different ASR expansion models were implemented in the finite element programs developed at the University of Toronto for the analysis of reinforced concrete structures.
- Those models are: 1) uniform in all directions, 2) Charlowood model (Charlowood, Solymar, and Curtis, 1992), 3) Curtis model, 4) Saouma and Perotti model (Saouma and Perotti, 2006), 5) Sellier model (Sellier et al., 2009), and 6) Gautam model. (Gautam, 2016)
- The implemented Saouma and Perotti (2006) model was validated versus the experimental test already conducted by Fan and Hanson (1998). Results are shown in Figure 3.70.

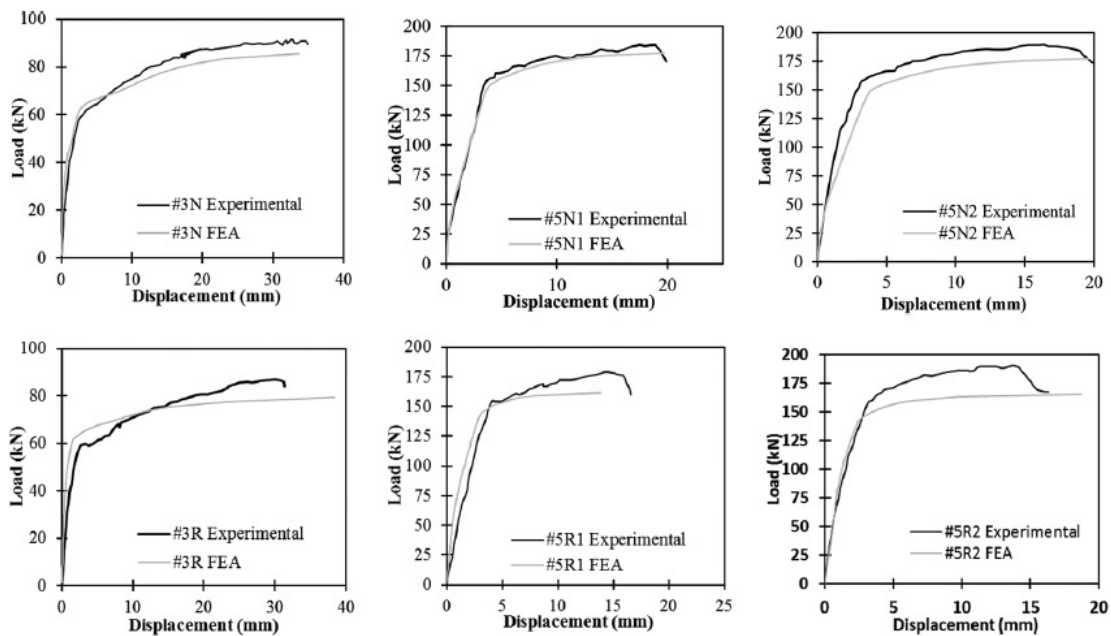


Figure 3.70: Load-deformation responses of Fan and Hanson (1998) beam specimens; Ferche et al. (2017)

3.44 Fernandes, Isabel and Noronha, Fernando and Teles, Madalena (2004)

URL

```
@article{
fernandes2004microscopic},
label={fernandes2004microscopic},
title={Microscopic analysis of alkali--aggregate reaction products in a
50-year-old concrete},
author={Fernandes, Isabel and Noronha, Fernando and Teles, Madalena},
journal={Materials Characterization},
volume={53},
number={2-4},
pages={295--306},
year={2004},
publisher={Elsevier}
Keywords={}
```

- The microscopic analysis of AAR products in an old concrete dam was studied.
- The Cabril Dam is a thin concrete arch dam built in the 1950s in the Zezere River, Central Portugal.
- The Dam is 136 m high. It has four horizontal internal galleries and a drainage gallery in the abutments which are close to the foundation.
- Cracking was observed shortly after the first reservoir impounding at the upper levels of the downstream face. These cracks were mainly horizontal and were due to structural causes related to the high rigidity of the crest and its geometry which was modified to support a road not included in the original design.
- The inspection of the galleries inside the Dam showed the existence of exudations similar to alkali-silica gel.
- According to Braga Reis, Silva, and Santos Silva (1996), deterioration of concrete was due to the following:
 - Slow alkali-aggregate reactions,
 - Reactions between sulfate and alumina from the alteration products of the aggregates,
 - And reactions between sulfate and hydrated calcium silicates from the cement paste.
- The authors performed microscopic examinations using scanning electron microscopy (SEM) and energy dispersive spectrometry analyses (EDS) in the identification and characterization of secondary products originated from reactions within the concrete.
- In the 293.65 m level gallery, only a few exudations were collected from the ceiling, Figure 3.71.
- Most of the exudations were in a solid state, but some showed a transparent viscous appearance.

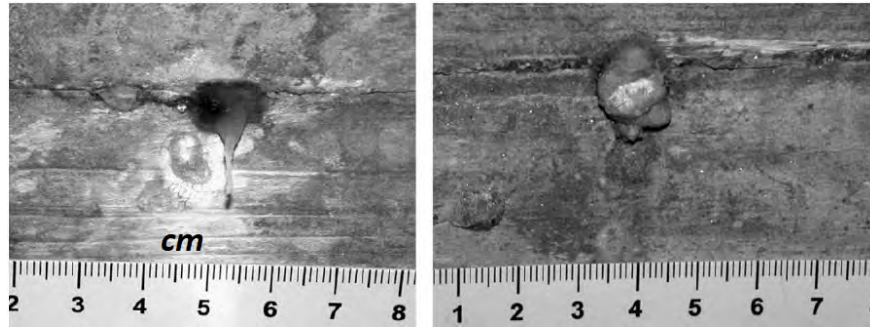


Figure 3.71: Different types of exudations from the top-level gallery. In the left panel, translucent droplets are present in the exudation; Fernandes, Noronha, and Teles (2004)

- Examination under SEM showed that the exudations are mainly composed of alkali-silica gel. In the semi-quantitative analysis obtained by EDS, no calcium was found.
- The transparent gel maintained a viscous behavior when examined by SEM, creating bubbles from inside the solid surface as the vacuum was applied.
- From the petrographic examination of thin polished sections, the presence of alkali-silica gel in voids or cracks within the concrete was not, however, identified.
- The analysis by EDS pointed to the possible coexistence of alkali-silica gel and ettringite acicular crystals in some voids, but it could not be concluded that there was a relation between their origins.

3.45 Fernandes, Isabel and Noronha, Fernando and Teles, Madalena (2007)

URL

```
@article{
fernandes2007examination},
label={fernandes2007examination},
title={Examination of the concrete from an old Portuguese dam: texture and
composition of alkali--silica gel},
author={Fernandes, Isabel and Noronha, Fernando and Teles, Madalena},
journal={Materials Characterization},
volume={58},
number={11-12},
pages={1160--1170},
year={2007},
publisher={Elsevier}
Keywords={}
```

- The texture and composition of alkali-silica gel from an old concrete dam was studied.
- Alto Rabagao is a concrete dam built in the early 1960s in an asymmetrical valley in northern Portugal.

- Due to the width of the valley and the mechanical characteristics of the rock foundation, the dam is composed of two types of structures: 1) an arch dam in the main valley and 2) two gravity dams.
- One of the gravity profiles was built in a secondary valley on the right bank, and the other closes the left bank of the main valley. There are also artificial concrete abutments linking each gravity section to the arch dam, Figure 3.72.

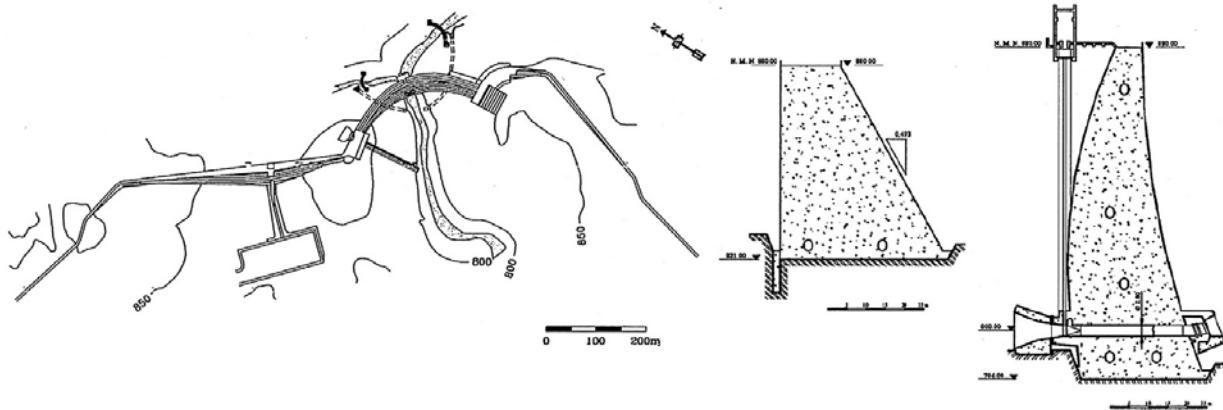


Figure 3.72: Schematic of the Alto Rabagao in Portugal (left); Concrete abutments (right); Fernandes, Noronha, and Teles (2007)

- There are three internal horizontal galleries across the arch dam and a drainage gallery along the arch and gravity structures close to the foundation.
- The dam was inspected, and, in places where signs of deterioration were found, samples were collected for characterization in the laboratory. Samples of concrete were also extracted by diamond drilling.
- In the site investigation of the interior galleries of the dam, different manifestations of alkali-silica reactions were detected.
- The use of SEM/EDS allowed the inspectors to assume that the products found in exudations and pop-outs correspond to alkali-silica gel with a variable morphology and composition.

3.46 Ferreira, Anna Paula Guida and Farage, Michèle Cristina Resende and Barbosa, Flávio de Souza (2013)

```
@article{
  ferreira2013modelling},
label={ferreira2013modelling},
title={Modelling of the mechanical behavior of concrete affected by
  alkali-aggregate reaction},
author={Ferreira, Anna Paula Guida and Farage, Mich{\`e}le Cristina Resende and
  Barbosa, Fl{\`a}vio de Souza},
journal={Rem: Revista Escola de Minas},
volume={66},
number={1},
pages={35--40},
year={2013},
publisher={SciELO Brasil}
Keywords={}
```

- The paper consists of the incorporation of AAR-stress coupling to the uncoupled model firstly proposed by Farage, Alves, and Fairbairn (2004) based on Ulm et al. (2000), so as to extend its application to structures under more sophisticated loading and boundary conditions.
- The model was implemented in a program developed in FORTRAN for nonlinear analysis of 2D problems using triangular plane strain elements.
- This coupled model is applied to simulate the mechanical behavior of a dam wall subjected to AAR.
- The dam height is 100 m and the base is 70 m. The dam is fixed at the bottom, and a hydrostatic load is applied in the upstream face. The mesh comprises 1,474 nodes and 2779 elements.
- The adopted AAR curve parameters are: $\varepsilon_{\infty} = 0.196$, $\tau_l = 3.34$ and, $\tau_c = 8.29$ years.
- Figure 3.73 compares the gel pressure evolution in the concrete wall evaluated via the uncoupled and the coupled models. The following ages were chosen with respect to the AAR evolution:
 - 10 years: when there is no evidence of AAR effects in an actual structure,
 - 40 years: when, in general, AAR cracking is more obvious,
 - 48 years: when, supposedly, a stabilization occurs.
- The coupled model accounts for the reducing effect of confinement stresses on the reaction evolution as reflected by the lower gel pressure values in the confined regions and, as a consequence, by a decrease on the amount of cracked finite elements.
- This figure also shows the cracking pattern obtained from the two models at 48 years. Cracking spreads more widely when the uncoupled model is applied. For the coupled model, cracking is mostly concentrated around the free surface.

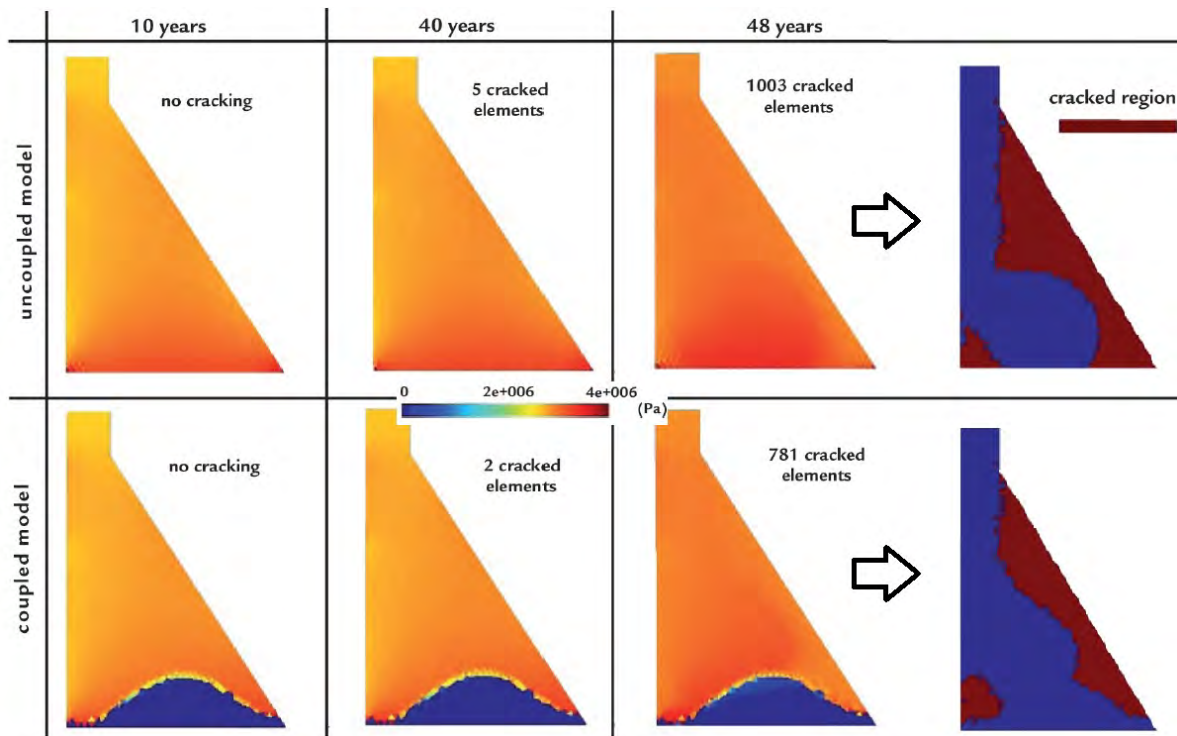


Figure 3.73: Gel pressure evolution in the concrete wall via the uncoupled (above) and the coupled (below) models; Ferreira, Farage, and Barbosa (2013)

3.47 FHWA (2010)

URL

```

fhwa2010,
title={Report on the Diagnostis, Prognosis, and Mitigation of Alkali-Silica
  Reaction (ASR) in Transportation Structures},
author={{FHWA}},
institution={{F}ederal {H}ighway {A}dministration},
year={2010},
number={FHWA-HIF-09-004},
url={https://www.fhwa.dot.gov/pavement/concrete/pubs/hif09004/hif09004.pdf}
}

```

- A major document from FHWA widely referenced.
- Written by Fournier, Bérubé, Folliard and Thomas.

Abstract

Alkali-aggregate reaction (AAR) is only one of the many factors that might be fully or partly responsible for the deterioration and premature loss in serviceability of concrete infrastructure. Two types of AAR reaction are currently recognized depending on the nature of the reactive mineral; alkalisilica reaction (ASR) involves various types of reactive silica (SiO₂) minerals and

alkali-carbonate reaction (ACR) involves certain types of dolomitic rocks ($\text{CaMg}(\text{CO}_3)_2$). Both types of reaction can result in expansion and cracking of concrete elements, leading to a reduction in the service life of concrete structures.

This document described an approach for the diagnosis and prognosis of alkali-aggregate reactivity in transportation structures. A preliminary investigation program is first proposed to allow for the early detection of ASR, followed by an assessment (diagnosis) of ASR completed by a sampling program and petrographic examination of a limited number of cores collected from selected structural members. In the case of structures showing evidence of ASR that justifies further investigations, this report also provides an integrated approach involving the quantification of the contribution of critical parameters with regards to ASR.

3.48 FHWA (2013)

URL

```
fhwa2013,  
title={Alkali-Aggregate Reactivity (AAR) Facts Book},  
author={{FHWA}},  
institution={{F}ederal {H}ighway {A}dministration},  
year={2013},  
number={FHWA-HIF-13-019},  
url={https://www.fhwa.dot.gov/pavement/concrete/asr/pubs/hif13019.pdf}  
}
```

- A major document from FHWA widely referenced.
- Written by Thomas, Fournier and Folliard.

Abstract

This document provides detailed information on alkali-aggregate reactivity (AAR). It primarily discusses alkali-silica reaction (ASR), covering the chemistry, symptoms, test methods, prevention, specifications, diagnosis and prognosis, and mitigation. Alkali-carbonate reaction (ACR) is also addressed.

3.49 Fournier, Benoit and Bérubé, Marc-André (2000)

URL

```

@article{
  fournier2000alkali,
  label={fournier2000alkali},
  title={Alkali-aggregate reaction in concrete: a review of basic concepts and
    engineering implications},
  author={Fournier, Benoit and B{\'e}rub{\'e}, Marc-Andr{\'e}},
  journal={Canadian Journal of Civil Engineering},
  volume={27},
  number={2},
  pages={167--191},
  year={2000},
  publisher={NRC Research Press},
  Keywords={},
  DisplayPdf={0},
  url={http://www.nrcresearchpress.com/doi/abs/10.1139/199-072}
}

```

- Presents theoretical and applied state-of-the-art information in the field of alkali-aggregate reactivity (AAR) in concrete:
 1. Basic concepts of the reaction and expansion mechanisms.
 2. conditions conducive to the development and the sustainability of AAR in concrete.
 3. field and laboratory investigation programs for evaluating the potential alkali-reactivity of concrete aggregates.
 4. selection of preventive measures against AAR.
 5. management of structures affected by AAR (including diagnosis of AAR in existing concrete structures and mitigation measures).
- RH distribution and its relevance of

Fournier and Bérubé

Fig. 7. Summer and winter relative humidity profiles in a bridge column exposed to arid desertic climate (from Stark 1990).

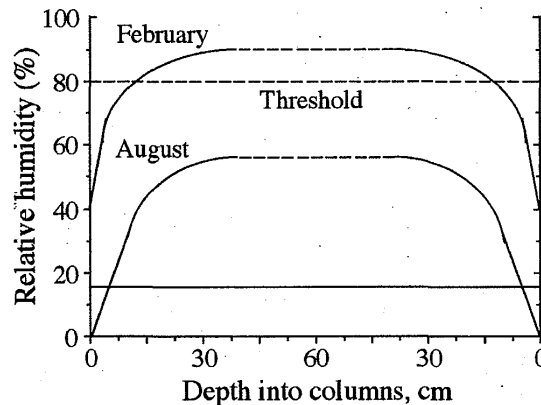


Fig. 8. Sketch showing typical features of surface map-cracks and subparallel cracks in concrete affected by ASR. Stresses due to ASR grades from horizontal tension near the surface to horizontal compression and vertical tension with depth (from A221.1R-98 1998).

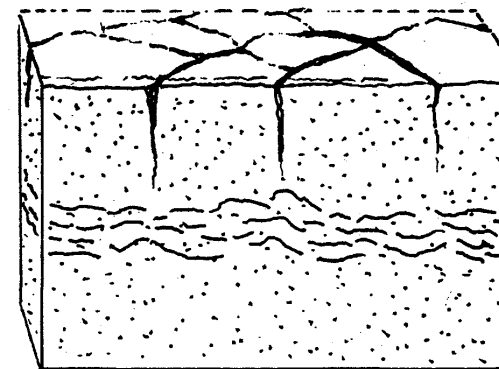


Fig. 9. Effect of compressive stress on expansion due to ASR (from ISE 1992).

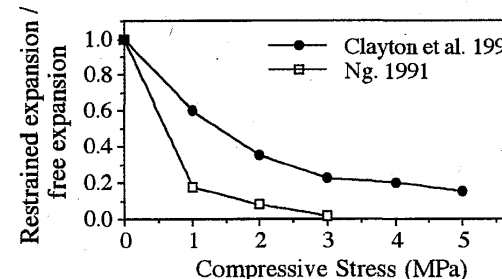


Figure 3.74: Summer and winter relative humidity profiles in a bridge column exposed to arid desertic climate (from Stark 1990).

• The structures should have been made with only portland cement since the use of supplementary cementing materials can prevent deleterious expansion and cracking due to AAR in concrete.

- The structures should have been made with an alkali supply from the cement that is similar to, or greater than, that proposed in the new structure to be built.
- The structures should have been exposed to environmental conditions, especially the availability of moisture, that are at least as severe as those to which the proposed structure(s) will be subjected.

Typical visual and petrographic symptoms of AAR affecting concrete structures are discussed later in this paper. The minimum number of structures required may vary according to the extent to which the above criteria are met for each of the structures examined; however, such a diagnostic evaluation is unlikely to be based on fewer than three structures meeting most of the criteria listed before.

issues. The source is then geologically mapped to de

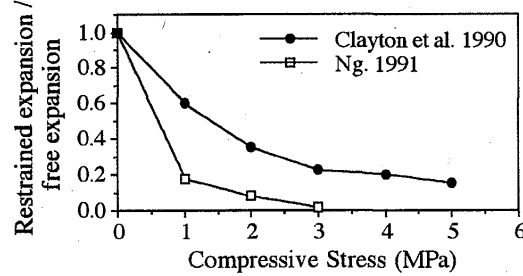
structures should have been made with only portland cement since the use of supplementary cementing materials can prevent deleterious expansion and cracking due to AAR in concrete.

structures should have been made with an alkali supply from the cement that is similar to, or greater than, that proposed in the new structure to be built.

structures should have been exposed to environmental conditions, especially the availability of moisture, that are at least as severe as those to which the proposed structure(s) will be subjected.

typical visual and petrographic symptoms of AAR affected concrete structures are discussed later in this paper. The minimum number of structures required may vary according to the extent to which the above criteria are met for each of the structures examined; however, such a diagnostic evaluation is unlikely to be based on fewer than three structures meeting most of the criteria listed above.

Fig. 9. Effect of compressive stress on expansion due to AAR (from ISE 1992).



Alkali-aggregate reactivity investigation program of concrete aggregate

Figure 10 illustrates a global approach for the evaluation of potential alkali-reactivity of aggregate sources based on detailed field and laboratory investigations. Even if the proposed program is based on Canadian experience, it is likely to apply to most aggregates produced worldwide.

Geological investigation and sampling of aggregate sources

The first step in the proposed investigation program is in examining the existing data from regional/local geological and (or) laboratory test reports where available. These bring most useful preliminary information on potential existing aggregate sources, while often allowing to better define the scope of further investigations.

Identifying aggregate sources — A visit to the source with a mining engineer and (or) the person in charge of the quarrying/aggregate processing operations will help in rapidly identifying the main geological, structural and mineralogical features of the source, as well as the basic safety

Fig. 10. Effect of compressive stress on expansion due to AAR (from ISE 1992).

issues. The source is then geologically mapped to describe the vertical and lateral distribution of the constituent rock types, the structural characteristics of the deposit and the presence of geological discontinuities (e.g., faults, folding, dykes and shear or tectonic zones) and the mining pattern in the source. Special attention is given to specific geological or petrographic features related to the presence and distribution of potentially alkali-reactive material in the rock bodies and alluvial deposits (Table 2). Samples are collected from the affected cross section illustrating the above characteristics of the source is prepared (Fig. 11a and b), which will eventually form the basis for sampling.

For detailed AAR investigations, composite face samples are collected directly from the quarrying or excavation faces of the source to obtain material representative of the distinct rock types or petrographic facies in the deposit (Fig. 12). A significant change in petrographic facies will generally correspond to a change in sample Rock AAR and sulfate attack sequences containing two or several petrographic facies that irregularly or regularly alternate in a specific exploitation level may be sampled stress which when noticeable lateral variations are observed within an individual exploitation level or deposit, two or several sampling locations should be established. The distribution of composite samples is defined on the geological cross section of the source (Fig. 11).

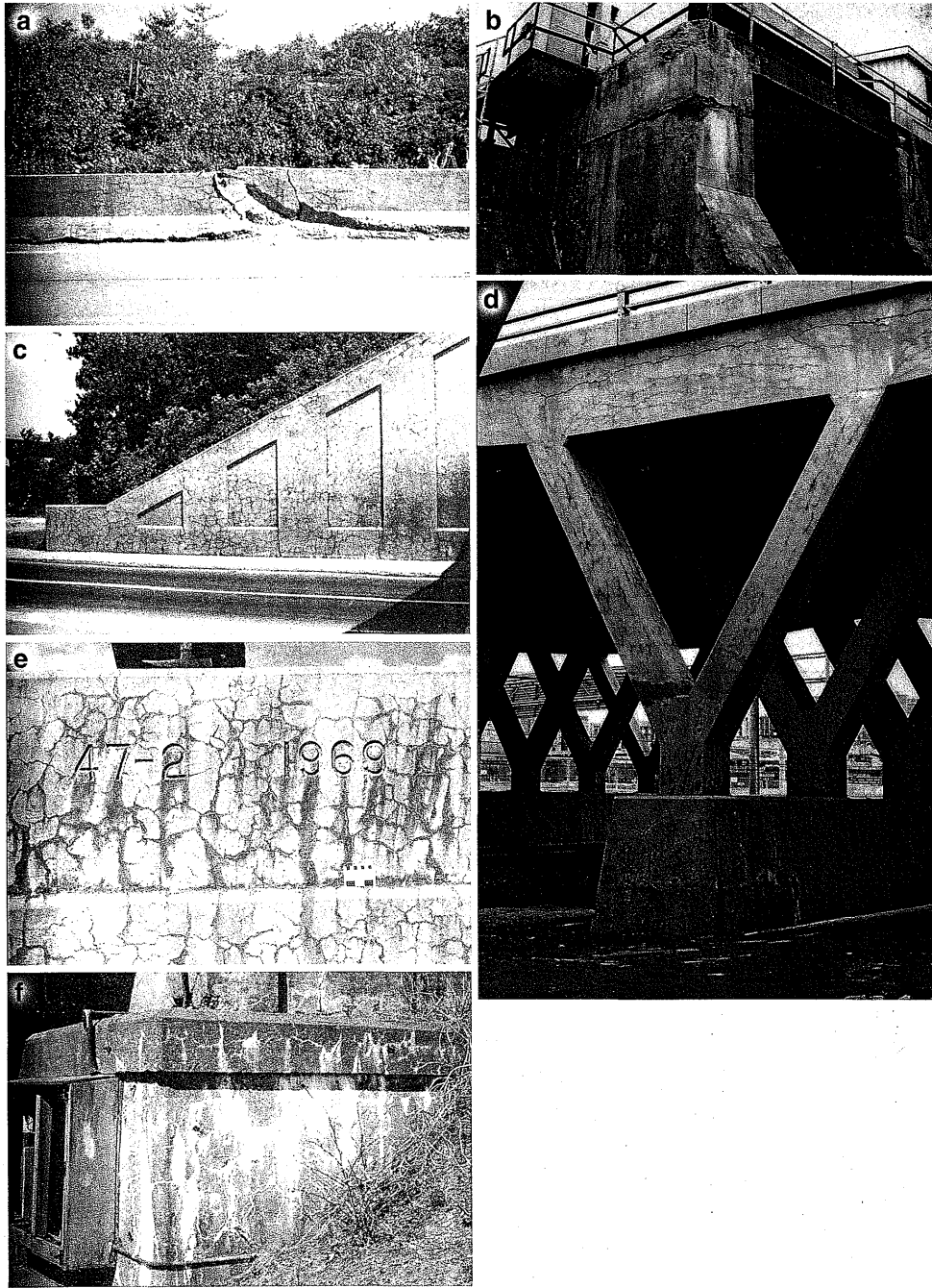
© 2000 NRC Canada

many other researcher who collected from the affected as the major cause of the distress observed. This is the basis for sampling. For detailed AAR investigations, composite face samples are collected directly from the quarrying or excavation faces of the source to obtain material representative of the distinct rock types or petrographic facies in the deposit (Fig. 12). A significant change in petrographic facies will generally correspond to a change in sample Rock AAR and sulfate attack sequences containing two or several petrographic facies that irregularly or regularly alternate in a specific exploitation level may be sampled stress which when noticeable lateral variations are observed within an individual exploitation level or deposit, two or several sampling locations should be established. The distribution of composite samples is defined on the geological cross section of the source (Fig. 11).

Map-cracking" typically stress fields or poorly reinforced and sulfate attack can also result in a similar pattern of cracking. In reinforced concrete members or under loading conditions, the cracking pattern will generally reflect the arrangement of the underlying steel or the direction of the major stress fields (Fig. 3.76-d). Surfaces of concrete elements affected by AAR and exposed to sun, moisture, and frost action usually show more extensive cracking and deterioration. Surface macrocracking due to AAR rarely penetrates more than 25 to 50 mm of the exposed surface (in rare cases \geq 100 mm) (Fig. 8). The width of surface macrocracks ranges from 0.1 to 10 mm in extreme cases.

4. Surface discoloration - Cracks caused by ASR are often bordered by a broad brownish zone, thus giving the appearance of permanent dampness (Fig. 3.76-e).
5. Gel exudation - Surface gel exudation is a common and characteristic feature of ASR-affected concrete (Fig. 3.76-f). It is usually associated with leaching of carbonated lime (efflorescence).
6. Pop outs - The expansion of unsound aggregate particles due to frost action is the main factor responsible for the development of pop outs in Canada. Alkali-reactive aggregate particles undergoing expansion near the concrete surface may also induce pop outs, or open channels for the water to penetrate and freeze, thus promoting detachment of a conical portion of concrete.
7. Sampling of concrete structures affected by alkali-aggregate reactivity.

- Laboratory experiments addressed
 1. petrographic examination.



© 2000 NRC Canada

Figure 3.76: Field symptoms of AAR: (a) Severe spalling of a 20-year old median highway barrier under expansive thrust due to ASR; (b) relative movement of concrete pier caused by the expansive forces generated by the adjacent concrete section affected by ASR; (c) map-cracking in a wingwall of a 30-year old railway bridge affected by ASR; (d) longitudinal cracks on the edge of the deck and in the columns of a 20-year old highway bridge severely affected by ASR; (e) map-cracking due to AAR affecting the parapet wall of a 25 year-old highway structure; (j) exudations of alkali-silica gel and efflorescence at the surface of a concrete foundation affected by ASR.

2. Quantitative petrographics assessment of internal damage.
 3. water-soluble alkali content of concrete.
 4. Expansion tests of concrete cores.
 5. Mechanical testing of specimens.
- In-situ monitoring and structural investigation
 1. Relative humidity measurements with depth in various concrete elements or components to establish the position of the internal equilibrium zone.
 2. Mapping of surface cracks, recording pattern, size, and width in various concrete elements, and with time.
 3. Measurements of movements, deflections, and deformations using Demec gauges and (or) metallic references, glass plates crossing surface macrocracks, invar wire extensometers, inclinometers, vibrating cords, overcoring, inverted pendulums, or levelling techniques.
 4. In situ stress measurements in the reinforcing steel and the adjoining concrete.
 5. Field loading tests where the criteria for load tests are based on some limiting deflection criteria and recovery of the deflection with time (CSA 2000);
 - Finite element analysis is barely mentioned.

3.50 Fournier, Benoit and Ideker, Jason H and Folliard, Kevin J and Thomas, Michael DA and Nkinamubanzi, Pierre-Claver and Chevrier, Ray (2009)

URL

```
@article{
fournier2009effect},
label={fournier2009effect},
title={Effect of environmental conditions on expansion in concrete due to
alkali--silica reaction (ASR)},
author={Fournier, Benoit and Ideker, Jason H and Folliard, Kevin J and Thomas,
Michael DA and Nkinamubanzi, Pierre-Claver and Chevrier, Ray},
journal={Materials Characterization},
volume={60},
number={7},
pages={669--679},
year={2009},
publisher={Elsevier}
Keywords={}
```

- Moderately- to highly-reactive aggregates were used to make concrete specimens of different alkali contents, with and without air-entrainment, that were subjected to comparative field and laboratory investigations.
- The reactive aggregates investigated were found to respond sometimes quite differently to the various conditions investigated (e.g. alkali contents, air entrainment in field specimens, etc.);

however, the results suggest that “deleterious” ASR expansion (i.e. inducing an expansion level $>0.04\%$) could be observed between 4 and 5 times faster under “warmer” climatic conditions compared to “cooler” climatic conditions.

- Consequently, a certain protection level against ASR may potentially be efficient for 75 years in one location, but only for, perhaps, 40-50 years at another location within a same country such as the USA.

3.51 Gao, Xiao Xiao and Multon, Stéphane and Cyr, Martin and Sellier, Alain (2011)

URL

```
@article{
gao2011optimising},
label={gao2011optimising},
title={Optimising an expansion test for the assessment of alkali-silica reaction
in concrete structures},
author={Gao, Xiao Xiao and Multon, St{\'e}phane and Cyr, Martin and Sellier,
Alain},
journal={Materials and structures},
volume={44},
number={9},
pages={1641--1653},
year={2011},
publisher={Springer}
Keywords={}
```

- A new procedure was developed for laboratory expansion tests since the usual test procedures appear to be difficult to use in expert assessment.
- The development involves optimizing the storage conditions and the sizes of the specimen and aggregate.
- Existing literature emphasizes the importance of the concept of stress intensity factor, K_I , in the development of ASR expansion in concrete. The larger the K_I is, the faster cracks appear and, the cracking always leads to reduction of the expansion through gel permeation and exudation.
- Therefore, for several expansion tests, the K_I has to be constant to maintain comparable mechanical conditions.
- Three sizes of specimens were studied ($20 \times 20 \times 160$, $40 \times 40 \times 160$ and $70 \times 70 \times 280$ mm) and four sizes of aggregates (0-315, 315-630, 630-1,250 and 1,250-2,500 μm).
- Next, the accelerated test was performed on the specimens. Figure 3.77 shows the ASR expansions on prismatic specimens. All the curves show a high and increasing initial rate of swelling with time, followed by a decrease of the rate until a long-term asymptote is reached.

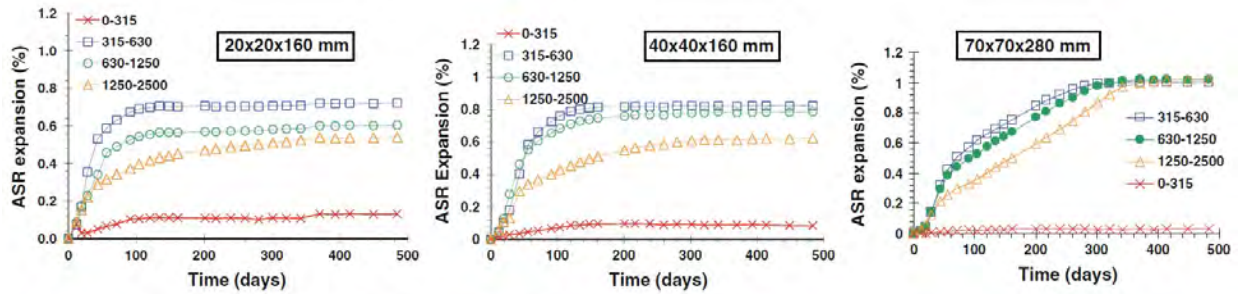


Figure 3.77: ASR expansions on prismatic specimens with siliceous limestone aggregate kept in NaOH solution; Gao et al. (2011)

- Figure 3.78 shows the cracking patterns observed during the expansion as well as the crack widths measured at 290 days with a video-microscope.
- No cracking was observed for the reference prisms nor for the prisms containing the particles of size C1 (0-315 μm) which is in accordance with the small expansion.
- For the other specimens, the largest specimens presented the widest cracks. The differences between crack widths of mortars containing different aggregate sizes were not significant.

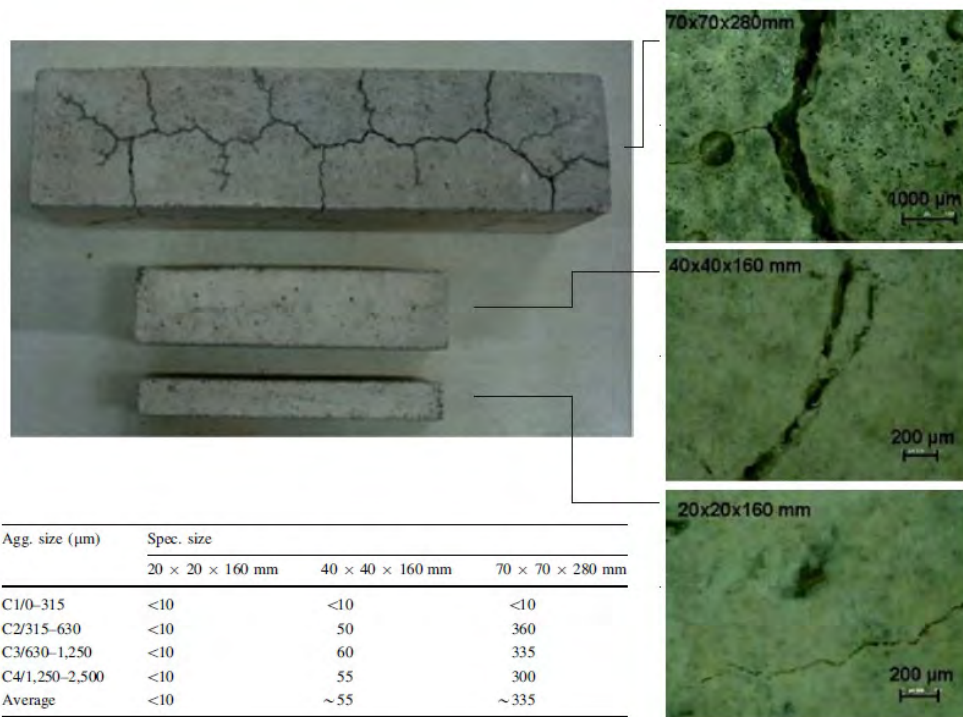


Figure 3.78: Cracking patterns of specimens cast with siliceous limestone; Gao et al. (2011)

- A combined effect of the aggregate and specimen sizes on ASR expansion is important. For a given mortar, the expansion is lower in small specimens than in large specimens.

- The ratio “specimen size/aggregate size” has to be sufficiently high to decrease this scale effect and obtain relevant measurements.
- For the same size of aggregate, small prisms needed the shortest time to achieve final expansions.
- For the same size of specimen, small-sized aggregate took the shortest time to reach the final expansions (which can be attributed to the faster diffusion of ionic species into the porosity of small prisms and into the aggregate).
- Even with a “specimen size/aggregate size” ratio higher than 100, the scale effect still exists. This can be explained by the proportion of ASR gels that permeate out of the specimens, causing a decrease of the gel pressure and thus reducing the induced expansion.
- The most relevant, fast, and convenient tests should use small reactive particles (315-630 μm) and small specimens (20×20×160 mm). But in this condition, the results should be analyzed through the concept of K_I .

3.52 Gao, XX and Cyr, M and Multon, S and Sellier, A (2013)

[URL](#)

```
@article{
gao2013comparison,
label={gao2013comparison},
title={A comparison of methods for chemical assessment of reactive silica in
concrete aggregates by selective dissolution},
author={Gao, XX and Cyr, M and Multon, S and Sellier, A},
journal={Cement and Concrete Composites},
volume={37},
pages={82--94},
year={2013},
publisher={Elsevier}
}
```

3.53 Gao, XX and Cyr, M and Multon, S and Sellier, A (2013)

[URL](#)

```

@article{
gao2013comparison,
label={gao2013comparison},
title={A comparison of methods for chemical assessment of reactive silica in
concrete aggregates by selective dissolution},
author={Gao, XX and Cyr, M and Multon, S and Sellier, A},
journal={Cement and Concrete Composites},
volume={37},
pages={82--94},
year={2013},
publisher={Elsevier},
Keywords={},
DisplayPdf={0},
url={https://www.sciencedirect.com/science/article/pii/S0958946512002387}

```

- Presents a a method that uses chemical methods to evaluate the proportion of reactive silica in different types of aggregates: opal, siliceous limestone, quartzite and quartz aggregate.
- Evaluation includes
 1. mineralogical studies (XRD and petrography) to characterise the reactive sites,
 2. chemical methods using acid and/or basic attacks (NaOH–HCl, HCl–KOH, HF) to measure the reactive site content.

When these methods are discussed and compared, HF (hydrofluoric acid) attack is found to give relevant results in short periods of time.

3.54 Gao, Xiao Xiao and Cyr, Martin and Multon, Stéphane and Sellier, Alain (2013)

URL

```

@article{
gao2013three},
label={gao2013three},
title={A three-step method for the recovery of aggregates from concrete},
author={Gao, Xiao Xiao and Cyr, Martin and Multon, St{\`e}phane and Sellier,
Alain},
journal={Construction and Building Materials},
volume={45},
pages={262--269},
year={2013},
publisher={Elsevier}
Keywords={}

```

- A very comprehensive classification of the methods used for separating aggregates from cement paste in existing concretes was summarized.

- In general, those methods can be categorized into three main groups based on their application:
 - Recycling aggregate
 - * Mechanical crushing (Eguchi et al., 2007; Nagataki et al., 2004)
 - Experiments: Crushing concrete mainly with mechanical grinder, sometimes equipped with vibrating screens and magnetic separators
 - Remarks: Effective to recycle aggregate from construction waste for industry use but not “pure” enough for laboratory tests
 - * Electrical disintegration method (Yoshimi et al., 2002)
 - Experiments: Crushing concrete with apparatus supplying a high voltage impulse
 - Remarks: Feasible to separate components of different resistivity
 - * Acid attack (Tam, Tam, and Le, 2007)
 - Experiments: Treatment of recovered aggregate through immersing in 0.1 M HCl, H₂SO₄ or H₃PO₄ solution at room temperature
 - Remarks: Improvement in mechanical properties of recovered aggregates
 - * Soundness tests (Abbas et al., 2007)
 - Experiments: Immersing the samples in 26% NaSO₄ solution then five cycles of freezing ($\sim -17^{\circ}\text{C}$) and thawing ($\sim 80^{\circ}\text{C}$)
 - Remarks: Effective for aggregate size >4.75 mm, applicable to limestone
 - * Thermal treatment (De Juan and Gutiérrez, 2009)
 - Experiments: Applying several cycles of soaking in cold water and drying at 500°C
 - Remarks: Effective to remove the attached mortar from recovered aggregates (4-16 mm), applicable to all kinds of aggregates
 - Determination of the cement content in concrete
 - * Flotation method (Nägele and Hilsdorf, 1980)
 - Experiments: Flotation process with organic sulfates as collectors, alkali hydroxides as regulators and heptanol as frothing agent
 - Remarks: Effective to separate cement and aggregate <1 mm
 - * Microwave heating (Figg, 1974)
 - Experiments: Soaking the samples in water, then performing microwave heating for 5-30 min
 - Remarks: Time-saving and effective to weaken the adherence force between aggregate and cement paste but does not remove cement paste completely
 - * Acid attack (Alvarez et al., 1999; Cardoso et al., 2009; Deloye, Maire, and Buisson, 1979)
 - Experiments: Immersing the samples in cold diluted HCl or HNO₃ solution
 - Remarks: May attack limestone aggregate
 - * Organic attack (Li, Roy, and Kumar, 1985; Ohsawa et al., 1985)
 - Experiments: Immersing the samples in solution with organic acid and anhydrous methanol
 - Remarks: Selective dissolution of cement paste

- Recovery of aggregates for re-qualification of ASR
- Freeze-thaw treatment (Grattan-Bellew, 1995)
 - * Experiments: Cycles of freezing in liquid nitrogen and thawing in a microwave oven
 - * Remarks: Effective to degrade the cement paste, especially for coarse particles
- Concentrated HCl solution (Sellier et al., 2009)
 - * Experiments: Immersing in concentrated HCl solution
 - * Remarks: Not applicable to limestone aggregate
- A method to recover aggregates from existing concrete was developed in the framework of evaluating the ASR reactivity of these recovered aggregates.
- They claimed that the method should guarantee recovery of the maximum amount of all sizes of aggregates and should dissolve the hydrated cement as completely as possible without altering the composition of the aggregate.
- A three-step methodology is proposed:
 - Rough crushing of the concrete: To augment the surface of contact for the following steps, the concrete was first crushed carefully and mildly with a hammer. The crushed size was maintained around 50 mm to avoid destroying the aggregates, considering that the largest natural aggregates used in the concrete were around 20 mm. The pieces were collected for the next step.
 - Separation of cement paste from aggregates through a thermal treatment: Two physical treatments were compared: a soundness test (ST) and liquid nitrogen-microwave oven cycles (LNMO).
 - Dissolution of the remaining attached mortar by chemical attack: The process was organic chemical attack in salicylic acid. The solution was prepared with 180 g salicylic acid dissolved in 1 L of methanol.
- This whole procedure is schematically shown in Figure.
- An efficiency of 90-92% was obtained on quartzite and siliceous limestone with very high recovery rates for particles larger than 1 mm.

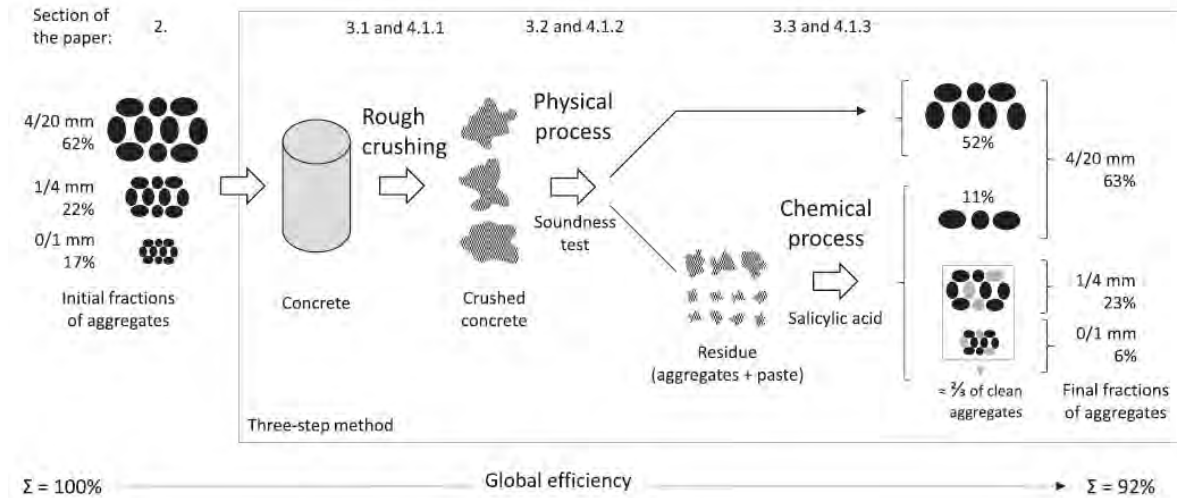


Figure 3.79: Three-step method for the recovery of aggregates and overall efficiency (for aggregate SL).; Gao et al. (2013a)

3.55 Garcia-Diaz, E and Riche, J and Bulteel, D and Vernet, C (2006)

URL

```
@article{
  garcia2006mechanism},
  label={garcia2006mechanism},
  title={Mechanism of damage for the alkali--silica reaction},
  author={Garcia-Diaz, E and Riche, J and Bulteel, D and Vernet, C},
  journal={Cement and Concrete Research},
  volume={36},
  number={2},
  pages={395--400},
  year={2006},
  publisher={Elsevier}
  Keywords={}
```

- A novel mechanism for the damage induced by ASR was proposed.
- Two reaction steps were taken into account:
 - The Q_3 tetrahedrons formation by breaking up siloxane bonds
 - The dissolution of these Q_3 tetrahedrons
- The formation of Q_3 tetrahedrons causes a swelling and a microcracking of the aggregate, and a significant increase of the aggregate pore volume was observed.
- A model based on a volume balance between the aggregate expansion and the swelling of mortar bars was proposed, enabling researchers to measure an amplification factor of the aggregate swelling.

- The observations in a practical damage mechanism detection were implemented. The swelling curve was divided into four parts as seen in Figure 3.80 where the vertical axis presents the mortar volume change.

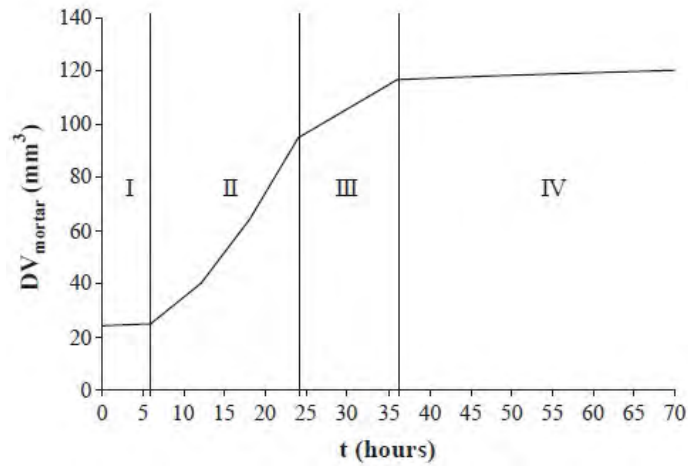


Figure 3.80: Schematic subdivision of the swelling curve; Garcia-Diaz et al. (2006)

- Period I (the first 6 hours of autoclaving): The reaction is a dissolution precipitation process. The mortar bar does not swell during this period.
- Period II (between hour 6 and hour 24 of autoclaving): One observes a regular increase in Q₃ tetrahedrons in the aggregate during this period. The pore volume of the aggregate increases five fold. The aggregate swelling is amplified by cracking in the cement paste. There is a linear relationship between the mortar swelling and the aggregate swelling.
- Period III (between hour 24 and hour 36 of autoclaving): The swelling mechanism occurs, but the dissolution-precipitation process described in period I starts again. The new products fill part of the cracks generated by the swelling.
- Period IV (beyond hour 36 of autoclaving): The swelling is asymptotic even though the reaction continues. It is a cicatrisation period where the pore volume of the aggregate decreases because of the filling of the cracks.

3.56 Gautam, Bishnu P and Panesar, Daman K (2017)

[URL](#)

```

@article{
  gautam2017effect},
  label={gautam2017effect},
  title={The effect of elevated conditioning temperature on the ASR expansion,
    cracking and properties of reactive Spratt aggregate concrete},
  author={Gautam, Bishnu P and Panesar, Daman K},
  journal={Construction and Building Materials},
  volume={140},
  pages={310--320},
  year={2017},
  publisher={Elsevier}
  Keywords={Mega; New Const. Model; Thermal Anal.; Moisture Anal.; Mathematical;
    Finite Element; Dam Gravity; }

```

- The effects of elevated temperature were evaluated by comparing expansion, damage rating index, and mechanical properties of concrete made with Spratt aggregate conditioned at 38°C and 50°C.
- The concrete prism specimens conditioned at $38 \pm 2^\circ\text{C}$ are referred to as the concrete prisms, while those kept under $50 \pm 0.5^\circ\text{C}$ are referred to as the accelerated concrete prism tests (ACPT).
- The Damage Rating Index (DRI) method was used to quantify the extent of damage in the concrete.
- Two prisms were tested for DRI at each test age. For each prism, one slice near the middle and one slice near the end were taken and polished for the microscopic observation.
- Figure 3.81 shows the DRI values for the reactive prisms in the CPT and ACPT against the longitudinal expansion.
- The DRI value increased with an increase in expansion, showing a fairly linear trend.

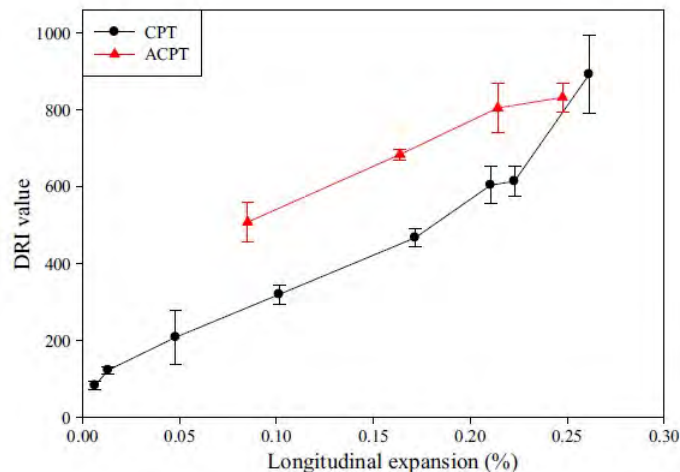


Figure 3.81: DRI value versus longitudinal expansion for the reactive prisms in CPT and ACPT; Gautam and Panesar (2017)

- Average longitudinal expansions of the concrete prisms in the CPT and ACPT are presented in Figure 3.82. The error bar represents one standard deviation.

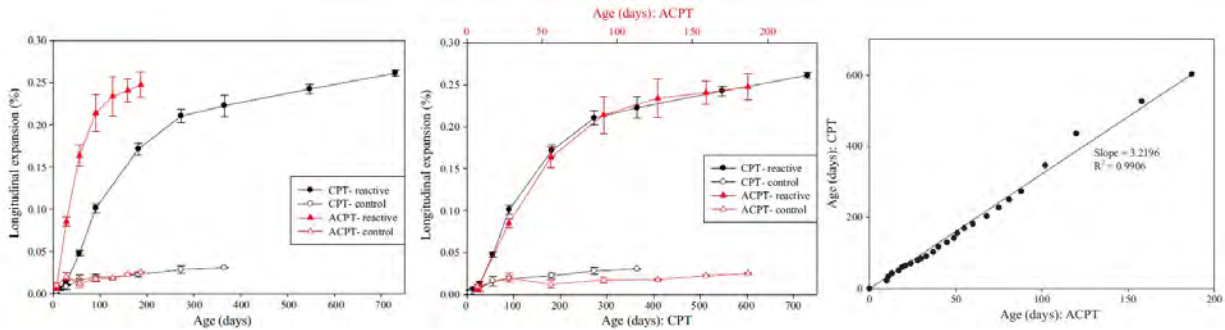


Figure 3.82: Longitudinal expansion of concrete prisms in CPT and ACPT, original scales (left), different time scales (middle), and days required by reactive prisms in CPT and ACPT for identical expansion (right); Gautam and Panesar (2017)

- The total expansion and the trend of expansion for the reactive prisms were similar in both the CPT and ACPT; however, the rate of expansion was significantly faster in the ACPT.
- Contrary to the literature (Fournier et al., 2004; Ideker et al., 2010), no reduction in expansion was observed due to the increase in temperature. One possible explanation could be that, at 50°C, the sulfate ions had minimal effect on reducing the pH of the concrete pore solution unlike at 60°C where the effect was reported as a possible reason for having reduced expansion.
- The expansion vs. age data were re-plotted in the middle plot with different lower and upper horizontal scales for the ages, such that 3.22 days for the CPT corresponded to 1 day for the ACPT.
- Increasing the temperature to 50°C from 38°C can shorten the test duration by more than three times with little effect on the response of concrete.
- The effects of elevated temperature were evaluated by comparing expansion, damage rating index, and mechanical properties of concrete made with Spratt aggregate conditioned at 38°C and 50°C.
- The concrete prism specimen conditioned at $38 \pm 2^\circ\text{C}$ are referred to as the concrete prisms, while those kept under $50 \pm 0.5^\circ\text{C}$ are referred to as the accelerated concrete prism tests (ACPT).
- Fundamental transverse resonant frequency of the prisms was measured as per ASTM C215 as a non-destructive method of estimating the degradation of dynamic modulus of elasticity.
- The dynamic modulus of elasticity, E_d (Pa), was calculated by using the formula given in ASTM C215 as $E_d = CMn^2$, where M is the mass of the prism specimen, n (Hz) is the fundamental transverse resonant frequency and C (m^{-1}) is a parameter that depends on the size, shape, and the dynamic Poisson's ratio of the concrete specimen.
- Figure 3.83 shows the dynamic modulus of elasticity for the prism specimens.

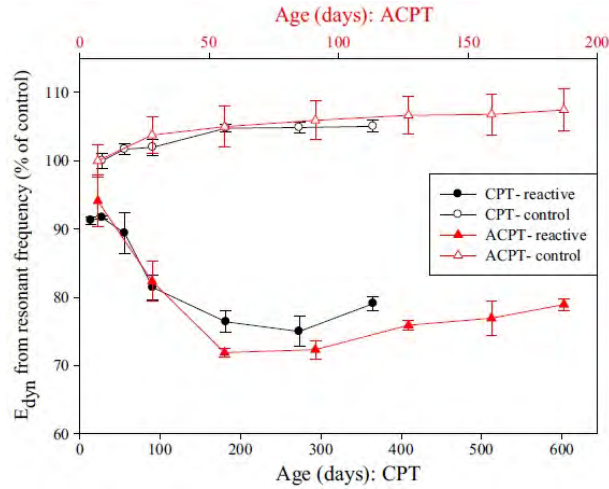


Figure 3.83: Variation in dynamic modulus of elasticity of concrete over time using different time scales; Gautam and Panesar (2017)

- The results are presented relative to the control prisms. E_d for the CPT specimens was normalized to the 28-day value of control prisms in the CPT. For the ACPT specimens, E_d was normalized to the 7-day value of control prisms in the ACPT.
- For the control prisms, E_d showed a slight and gradual increase over time. This increase can be attributed to the continued hydration of cement.
- For the reactive concrete, E_d in the CPT increased from 14 to 28 days and reduced thereafter until 273 days. The maximum reduction of 18% is reported. Partial recovery in E_d was observed at the end.
- In the ACPT specimens, E_d reduced by 12% from 7 to 28 days. The maximum reduction of 24% was observed at 56 days. After that, partial recovery was observed similar to that in the CPT specimens.
- The prisms were tested by third-point loading as outlined in ASTM C78.
- The modulus of rupture, R (MPa), is calculated as $R = \frac{PL}{bd^2}$, where L is the span length, d is the depth, b is the average width of the prism, and P is the maximum applied load.
- Figure 3.84 shows the modulus of rupture of concrete prism specimens for CPT and ACPT at different test ages.
- R for the control specimens varied between 6 and 8 MPa.
- Relatively larger scatter was observed in the control specimens than in the reactive specimens.
- R for the reactive prisms in CPT increased initially to attain its peak at 28 days. By 91 days, it reduced to approximately 50%. After 91 days, it reduced at a relatively slower rate until 365 days to reach 42% of its 28-day value.
- R for the reactive specimens in the ACPT followed a similar trend as specimens in the CPT except that the trend occurred faster.

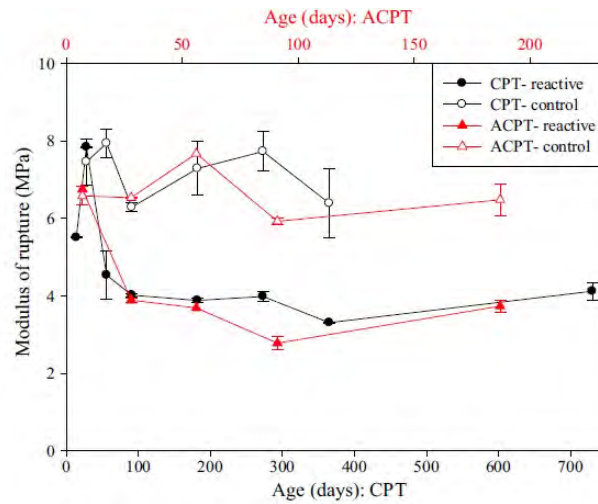


Figure 3.84: Variation in modulus of rupture of concrete prism specimens over time using different time scales; Gautam and Panesar (2017)

- Partial recovery of the R was also observed which was consistent with other literatures (Ahmed et al., 2003; Bektas and Wang, 2012; Kagimoto, Yasuda, and Kawamura, 2014; Swamy and Al-Asali, 1988).
- Dynamic Poisson’s ratios for the reactive and control concrete were estimated by measuring the pulse velocities of P- and S-waves in cube specimens using a “Pundit Lab” ultrasonic equipment.
- The values of dynamic Poisson’s ratios were obtained as 0.276 and 0.267, respectively, for the reactive and non-reactive concrete specimens conditioned at 23 ± 3 °C for 6 months of casting.

3.57 Gholizadeh-Vayghan, Asghar and Rajabipour, Farshad (2017)

URL

```
@article{
gholizadeh2017influence},
label={gholizadeh2017influence},
title={The influence of alkali--silica reaction (ASR) gel composition on its
hydrophilic properties and free swelling in contact with water vapor},
author={Gholizadeh-Vayghan, Asghar and Rajabipour, Farshad},
journal={Cement and Concrete Research},
volume={94},
pages={49--58},
year={2017},
publisher={Elsevier}
Keywords={Laboratory; aggregate Micro; Nonlinear ; }
```

- Synthetic ASR gels with 20 different chemical compositions similar to those found in field concretes were produced, and the effects of composition (i.e., Ca/Si, Na/Si and K/Si) on their

hydrophilic and swelling behavior were investigated.

- A Design of Experiments (DOE) based response surface methodology (RSM) is developed including the linear, second order, and interaction terms.
- DEO is based on central composite design (CCD) in which the three variables are combined according to the Figure 3.85 in three orthogonal directions.

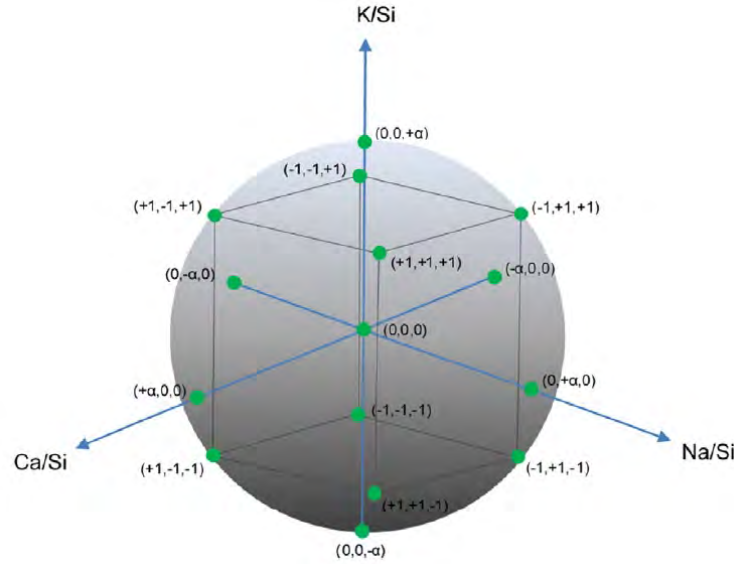


Figure 3.85: Graphical demonstration of RSM data point selection for the 3 variables case ($\alpha = 1.682$); Gholizadeh-Vayghan and Rajabipour (2017)

- According to CCD, 20 experiments are sufficient for estimating the linear and quadratic effects of the three composition variables.
- The results suggest that higher Na/Si and K/Si increase the free swelling. Ca/Si showed a multi-episode effect on the swelling.
- A RSM is proposed in the following form:

$$\varepsilon(\%) = 7.28 - 207.8 \frac{\text{Ca}}{\text{Si}} + 11.05 \frac{\text{Na}}{\text{Si}} + 12.31 \frac{\text{K}}{\text{Si}} + 823 \left(\frac{\text{Ca}}{\text{Si}} \right)^2 - 937 \left(\frac{\text{Ca}}{\text{Si}} \right)^3 \quad (3.9)$$

3.58 Giaccio, G and Zerbino, R and Ponce, JM and Batic, Oscar R (2008)

URL

```
@article{
giaccio2008mechanical},
label={giaccio2008mechanical},
title={Mechanical behavior of concretes damaged by alkali-silica reaction},
author={Giaccio, G and Zerbino, R and Ponce, JM and Batic, Oscar R},
journal={Cement and Concrete Research},
volume={38},
number={7},
pages={993--1004},
year={2008},
publisher={Elsevier}
Keywords={}
```

- The failure mechanism of concrete in compression is clearly affected by ASR. Furthermore, the shape of the stress-strain curves reflects the presence of internal fissures showing that the capability of controlling crack propagation decreases.
- Differences in the crack pattern are also reflected in the shape of the load-deflection curves in tension; damaged concretes show an increased non-linearity and a more gradual softening.
- The modifications in the mechanical properties cannot be directly associated with a level of expansion as the behavior depends on the component materials and mechanisms involved in the reaction.
- Four types of concrete were prepared:
 - C1: control concrete with coarse aggregate and the non-reactive natural siliceous sand and the granitic crushed stone.
 - R2: the non-reactive sand is replaced by the reactive sand.
 - R3: incorporated 10% of the very reactive siliceous orthoquartzite and 90% of the granitic crushed stone as coarse aggregate.
 - R4: 100% of the slow-reactive granitic crushed stone as coarse aggregate.
- The following tests were performed:
 - Stress-strain behavior in compression
 - Load-displacement and load-crack mouth opening displacement (CMOD) behavior in flexure on notched beams
 - Optical and microscopic observations on concrete slices.
- Table 3.86 presents typical characteristics of the crack pattern obtained from microscope observations.
- A general analysis indicates that although the measured expansions were similar for concretes R2 to R4, the effects on strength and stiffness can be very different depending on the source of ASR damage.
- Figure 3.87 shows the behavior of concrete in tension where typical load-deflection and load-CMOD curves are presented.

Concrete	Age (days) Specimen type	f_c	E	f_c	E	f_{crit}		f_{init}		Poisson's ratio	Expansion ^a (%) Prisms
		(MPa)	(GPa)	(MPa)	(GPa)	(MPa)	(%)	(MPa)	(%)		
		Cylinders (diameter-height)									
		100×200 mm		150×300 mm							
C1	28	28.6 (4) ^b	35.7	–	–	–	–	–	–	–	–0.006
	75	39.5 (1)	38.2	39.1 (4) ^b	38.7	37.6	96	33.2	85	0.19	0.004
	250	47.4 (3)	37.9	46.2 (2)	39.7	44.5	96	38.1	83	0.22	0.007
R2	745	49.4 (8)	37.4	47.6 (9)	39.6	44.8	94	40.5	85	0.22	0.054
	28	27.8 (11)	32.0	–	–	–	–	–	–	–	–0.001
	200	37.8 (16)	17.1	37.3 (6)	19.9	29.6	79	24.2	65	0.18	0.145
R3	250	29.1 (2)	13.1	33.6 (8)	12.1	22.5	67	20.6	61	0.19	0.180
	28	30.2 (9)	24.1	–	–	–	–	–	–	–	0.073
	75	30.8 (11)	25.1	28.9 (14)	19.0	17.6	61	15.9	55	0.17	0.115
R4	120	32.8 (3)	21.7	29.7 (8)	18.4	20.7	70	16.6	56	0.11	0.145
	28	36.5 (6)	38.1	–	–	–	–	–	–	–	–0.002
	485	51.2 (5)	31.3	49.8 (5)	33.0	48.8	98	41.5	83	0.22	0.125
	745	48.2 (2)	30.1	49.7 (7)	28.8	46.0	93	38.4	77	0.21	0.135

f_c : Compressive strength.
 E : Modulus of elasticity.
 f_{crit} : Critical stress.
 f_{init} : Initiation stress.
^a Interpolated from Fig. 1 data.
^b COV (%).

Figure 3.86: Compression test results; Giaccio et al. (2008)

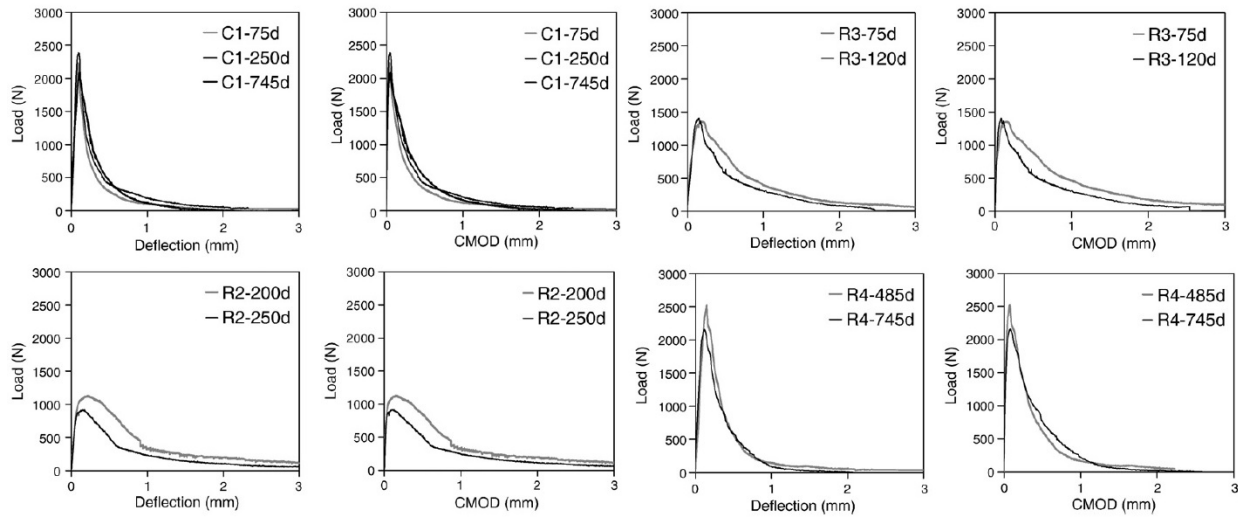


Figure 3.87: Results of flexural loading tests; Giaccio et al. (2008)

- The shape of the curves reflects the differences in the crack pattern between sound and damaged concretes.
- A linear behavior is seen up to the peak load in concrete C1; the development of the cracks starts just before the maximum load is achieved. In this case, although there is interface cracking before loading, the amount and magnitude is very limited.
- In ASR damaged concrete, extensive cracking is present before loading both at the interfaces and at the matrix. This is especially noted in concretes R2 and R3 which show an increased nonlinearity before the peak and a more gradual softening in the descending branch.
- Figure 3.88 represents the variation of the modulus of elasticity.
- In this case, the decrease in stiffness is in accordance with the increase in expansion.

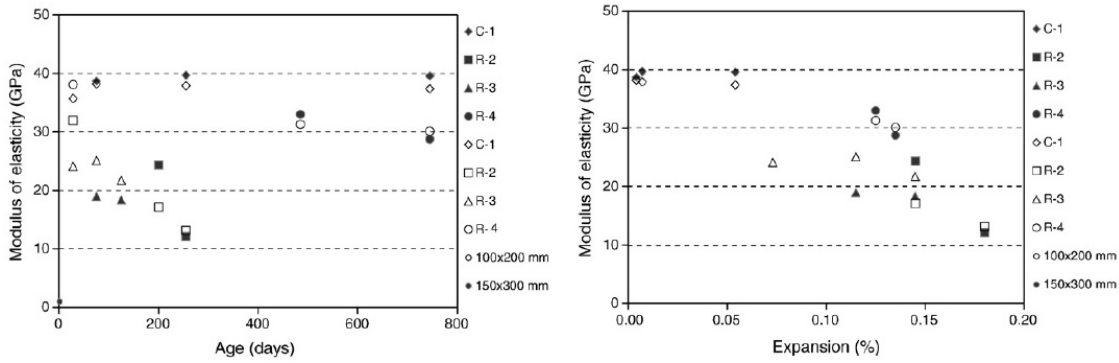


Figure 3.88: Variation of modulus of elasticity with age and expansion; Giaccio et al. (2008)

- Figure 3.89 plots the results of compressive strength vs. time, and compressive strength vs. expansion.
- A comparable expansion level not necessarily corresponds to a similar effect on compressive strength.

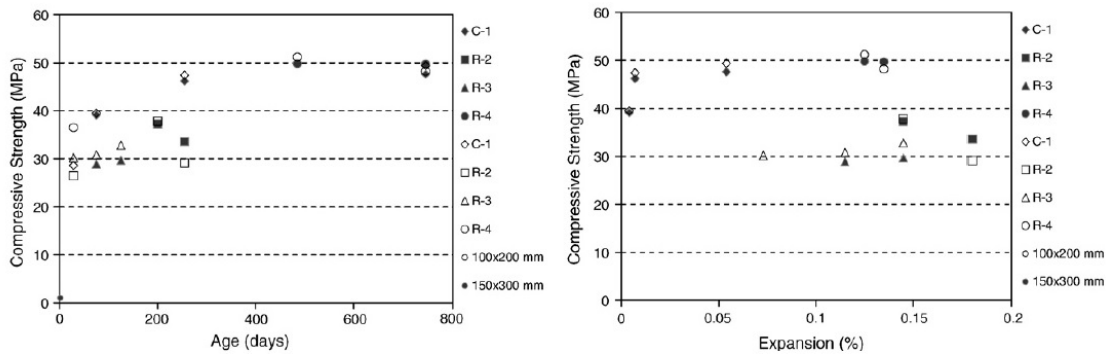


Figure 3.89: Variation of compressive strength with age and expansion; Giaccio et al. (2008)

- The most damaged concrete shows an increased nonlinearity before the peak and a more gradual softening in the descending branch, indicating that extensive meandering and branching of cracks is occurring.
- The extensive presence of cracks in the mortar and interfaces were associated with a decrease in strength and an increase in the size of the fracture zone.
- Contrarily, concrete R4 (with a slow rate ASR coarse aggregate), shows no significant effects both on the energy of fracture and the tensile strength.
- Figure 3.90 represents the variation of the modulus of elasticity.

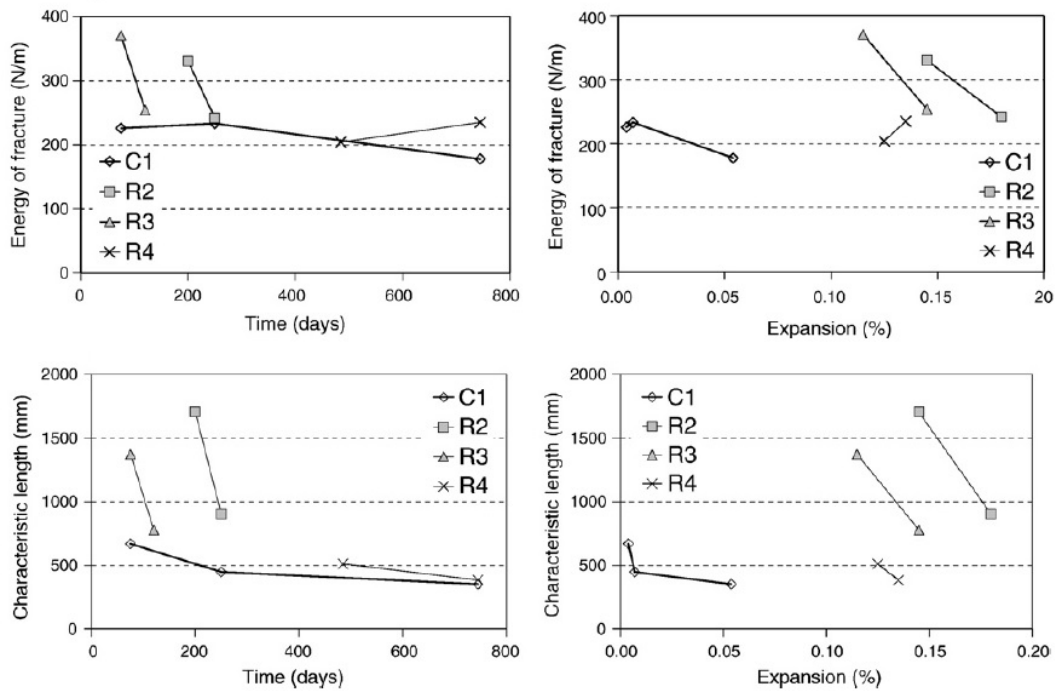


Figure 3.90: Variation of the energy of fracture and characteristic length with age and expansion; Giaccio et al. (2008)

3.59 Giorla, Alain B and Scrivener, Karen L and Dunant, Cyrille F (2015)

URL

```
@article{
  giorla2015influence},
  label={giorla2015influence},
  title={Influence of visco-elasticity on the stress development induced by
    alkali--silica reaction},
  author={Giorla, Alain B and Scrivener, Karen L and Dunant, Cyrille F},
  journal={Cement and Concrete Research},
  volume={70},
  pages={1--8},
  year={2015},
  publisher={Elsevier}
  Keywords={}
```

- A micro-mechanical model was proposed based on an explicit representation of the microstructure to simulate the role of creep on the expansion and damage induced by the reaction.
- The model accounts for the coupling between damage propagation and stress relaxation in the cement paste.
- The finite element discretization leads to the formulation of a nonlinear, time-dependent

problem. The growth of the gel pockets will progressively increase the damage in the surrounding aggregates and paste. This damage can be interpreted as cracks propagating in the microstructure.

- The mesh and boundary conditions are shown in Figure 3.91 where the microstructure has been randomly generated.

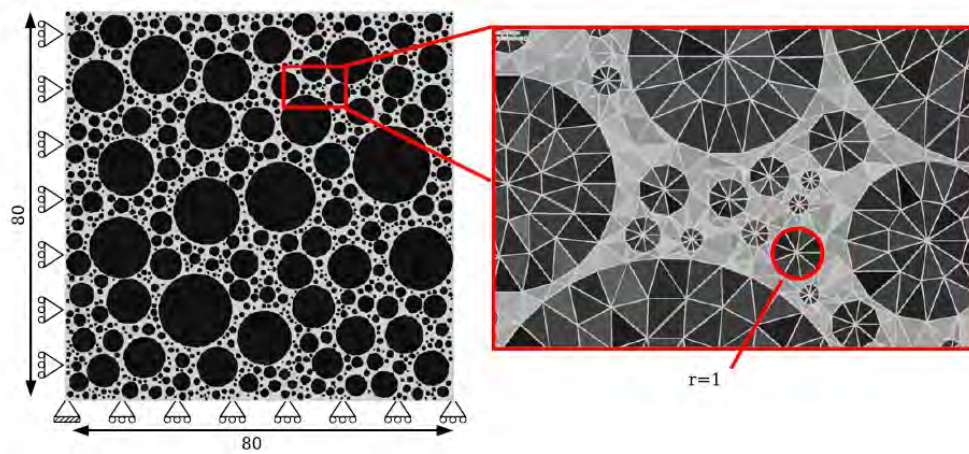


Figure 3.91: Microstructure and boundary conditions for the ASR simulation (dimensions in mm). Gel pockets are not represented. Grey level indicates the stiffness of the elements. The contrast has been enhanced in the mesh detail to highlight the distribution of the mechanical properties element by element; Giorla, Scrivener, and Dunant (2015)

- Three time lengths were studied:
 - 100 days for ultra-accelerated tests on concrete or mortar (3 months)
 - 1,000 days for accelerated tests on concrete cylinders (3 years)
 - 10,000 days for field conditions (30 years)
- The degree of damage in the aggregates and in the paste is plotted against the degree of reaction in Figure 3.92.
- First, the damage in the aggregates rises quickly until a plateau around 10% of the total aggregate surface is reached. As the evolution of damage slows down in the aggregates, it picks up pace in the paste.
- The propagation of the damage from the aggregates to the paste occurs at lower degrees of reaction for faster reaction rates.
- Also, based on the right plot in Figure 3.92, at the low degree of reaction (below the 0.10–0.15% reaction), the damage remains concentrated in the aggregates and the paste remains sound.
- At the higher degree of reaction, the cracks have propagated in the cement paste.
- It is shown that creep can explain the comparatively low amount of damage in the cement paste as observed experimentally.

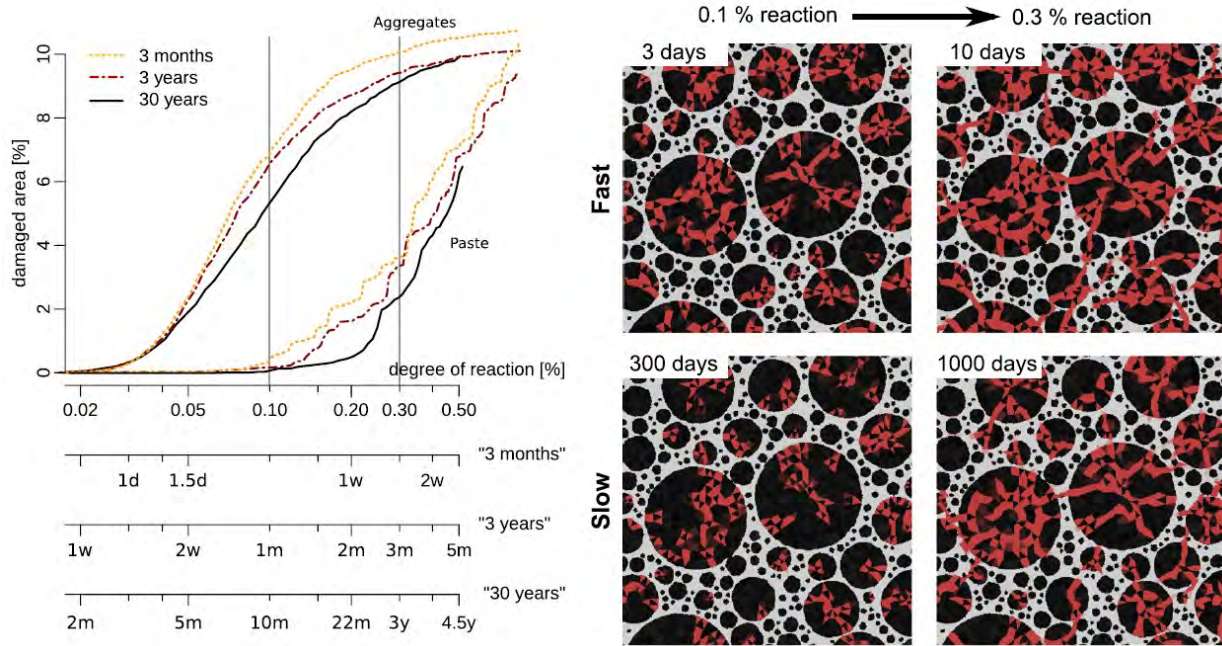


Figure 3.92: Fraction of damage in the aggregates and the cement paste as a function of the degree of reaction (left); Damage progression as a function of degree of reaction and time (right); Giorla, Scrivener, and Dunant (2015)

- Creep also increases the amount of damage in the aggregates when the rate of reaction increases.
- The results presented in this paper indicate that accelerated experiments may not be representative of the degradation in the field at equivalent degrees of reaction.

3.60 Gocevski, V. and Yildiz, E. (2017)

```
@incollection{
gocevski2017numerical},
label={gocevski2017numerical},
booktitle={Swelling Concrete in Dams and Hydraulic Structures: DSC 2017},
editor={Sellier, Alain and Grimal, {\'}E}tienne and Multon, St{\'}e}phane and
Bourdarot, Eric},
year={2017},
title={Numerical Analysis of AAR Affected Structures with Slot-Cuts},
author={Gocevski, V. and Yildiz, E.},
publisher={John Wiley \& Sons},
Keywords={Field; Rehabilitation; Mega; Damage Mechanics; Finite Element; Gravity
dam; Intake tower; },
DisplayPdf={0},
```

- AAR expansion causes an accumulation of displacements and stresses within the structure. As a remedy, slot-cutting of the concrete has been used on many structures to reduce the

stress and control the displacements.

- The simulation techniques of slot-cuts and their effects on long-term behavior are discussed.
- The numerical studies of the long-term effects of slot-cutting require the simulation of the loss of volume of concrete within the model.
- This is relatively easy in an implicit approach. Since the inertial forces are absent from the analysis in the implicit approach, the sudden release of stresses do not introduce instabilities to the model as it would in the case of an explicit analysis.
- In case of the explicit analysis, a sudden removal of a boundary condition of a stressed material would cause an effect similar to an impact load, inducing large kinetic energy and vibrations to the structure.
- A new user material was developed to simulate slot-cutting in an explicit analysis. This material's stiffness is reduced gradually following a smooth step function.
- Since AAR is a time-dependent process, Figure 3.93 shows how the expansion is interrupted during the cutting.

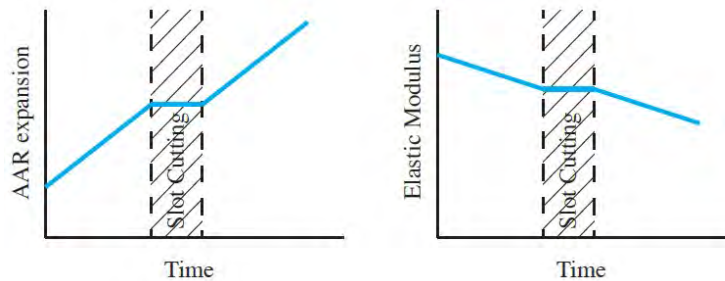


Figure 3.93: Interruption of AAR's time-dependent properties for slot-cutting duration: (left) AAR expansion and (right) Elastic modulus degradation; Gocevski and Yildiz (2017)

- The powerhouse presented in Figure 3.94 was commissioned in 1960.
- The cracking due to the AAR concrete swelling before the slot-cutting in 1981 is shown in Figure 3.95. The significant increase in cracking five years after the slot-cutting is also presented in this Figure. The analytical results obtained for the same period had no slot cutting been performed is presented in Figure d.

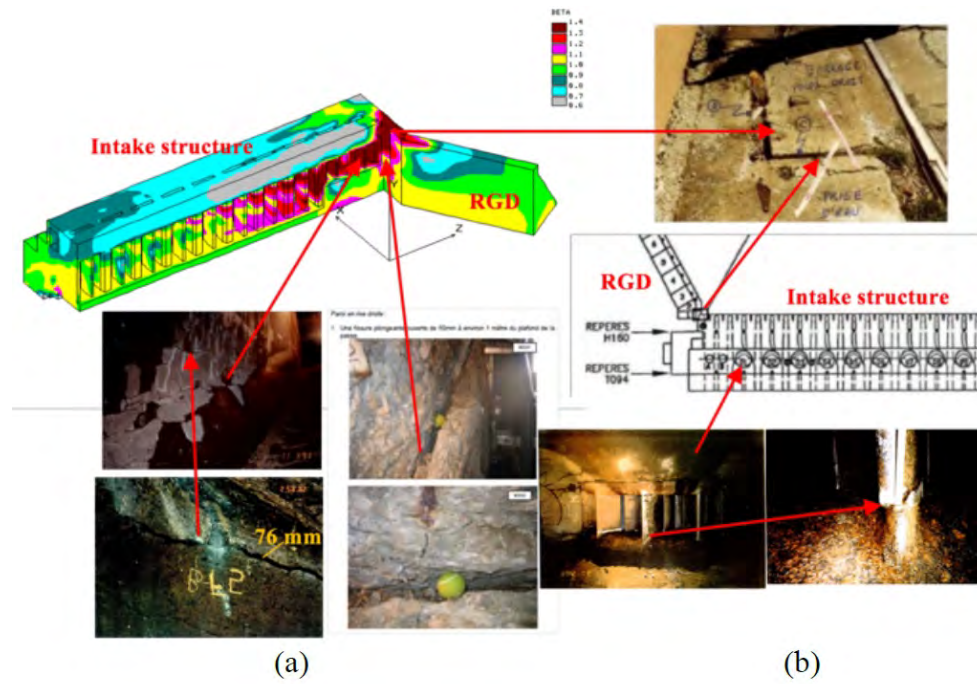


Figure 3.94: The location of the 1972-73 slot-cutting and the concrete damage as a consequence of this intervention: (a) the increased macrocracking in the water passage of group A of the intake structure and (b) sheared stay wanes of units A and B following the slot-cutting at the junction of the intake structure and the right gravity dam; Gocevski and Yildiz (2017)

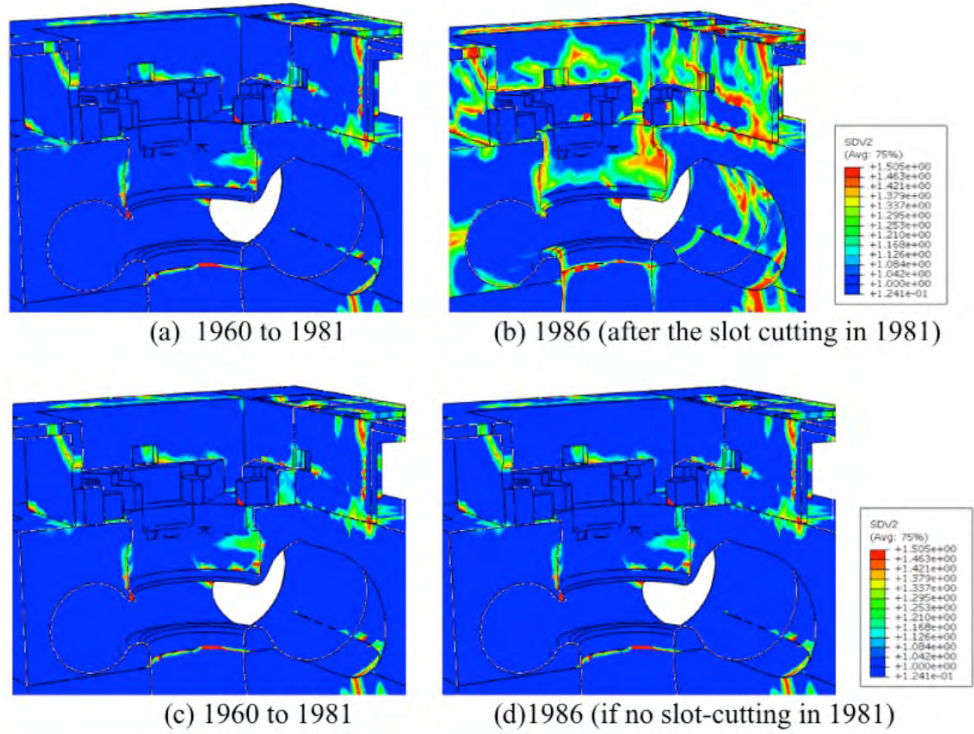


Figure 3.95: Slot-Cutting - between the units 35 and 36 (1980-1981); development of extensive concrete cracking in unit 36 five years after the slot-cutting in 1981; Gocevski and Yildiz (2017)

3.61 Godart, B and Mahut, B and Fasseu, P and Michel, M (2004)

URL

```
@article{
godart2004guide,
label={godart2004guide},
title={The guide for aiding to the management of structures damaged by concrete
expansion in France},
author={Godart, B and Mahut, B and Fasseu, P and Michel, M},
ijournal={Proceedings of the 12th ICAAR, Beijing, China},
pages={1219--1228},
year={2004},
Keywords={Literature survey; Diagnosis; Laboratory; Prognosis; },
DisplayPdf={1},
url={http://www.ifsttar.fr/Utils/librairie/getdocument.php?d=GuideTechnique-LCPC-GONFLIN.pdf}
```

Excellent and comprehensive LCPC report assisting engineers in the maintenance of structures affected by concrete swelling. Describes a methodology to organize the follow up of structures: diagnosis, root cause, prognosis, possible solutions to slow the evolution.

3.62 Godart, Bruno and de Rooij, Mario Robert and Wood, Jonathan GM (2013)

URL

```
@book{godart2013guide,
title={Guide to diagnosis and appraisal of AAR damage to concrete in structures},
author={Godart, Bruno and de Rooij, Mario Robert and Wood, Jonathan GM},
year={2013},
publisher={Springer},
url={https://link.springer.com/content/pdf/10.1007/978-94-007-6567-2.pdf}
}
```

A RILEM State of the Art Report (STAR) of great relevance.

- 1 Introduction
 - 1.1 Why the Need for a Diagnosis Document
 - 1.2 Scope
 - 1.3 Definitions
- 2 Alkali-Aggregate Reaction
 - 2.1 Introduction
 - 2.2 Alkalis
 - 2.3 Aggregates
 - 2.4 Water
 - 2.5 Pessimism Behaviour
 - 2.6 Summary
- 3 Symptoms of an Expansive Reaction during Routine Inspection
 - 3.1 General Inspection Remarks
 - 3.2 Review of Existing Records

- 3.3 Planning of a Comprehensive On-Site Inspection
 - 3.3.1 Field Equipment and Materials
 - 3.3.2 Personnel and Expertise
- 3.4 The Routine On-Site Inspection
- 3.5 Concrete Surface Features Suggestive of AAR
 - 3.5.1 Crack Pattern
 - 3.5.2 Displacements and Deformations
- 3.6 First Assessment of Field Observations
- 4 Confirmation Investigation
 - 4.1 Introduction
 - 4.2 Available Methods, Personnel and Expertise
 - 4.3 Approach for Diagnosis of AAR in Structures
 - 4.4 On-Site Sampling for AAR Confirmation
 - 4.4.1 Cores
 - 4.4.2 Fragments
 - 4.4.3 Drilled Powdered Material
 - 4.4.4 Efflorescence and Exudations
 - 4.4.5 Number of Samples
 - 4.4.6 Preservation of Samples
 - 4.5 Visual Examination of Cores
 - 4.5.1 Receipt of Cores and Documentation
 - 4.5.2 First Visual Description of Cores
 - 4.5.3 Photography and Core-Scanning
 - 4.5.4 Visual Examination and Stereomicroscopy Aid
 - 4.5.5 Selection of Specimens for Further Testing
 - 4.5.6 Cutting and Grinding
 - 4.6 Petrographic Examination
 - 4.6.1 Introduction
 - 4.6.2 Detailed Aspects from Optical Microscopy
 - 4.7 Additional Tests
 - 4.7.1 SEM Observation
 - 4.7.2 EPMA Analysis
 - 4.7.3 Determination of Soluble Alkali Content
 - 4.7.4 Tests to confirm Aggregate Reactivity
 - 4.7.5 Uranyl Acetate Test
 - 4.7.6 Estimation of Cement Content
- 5 Severity Investigation
 - 5.1 Introduction
 - 5.2 Field Investigation
 - 5.2.1 Quantification and Recording of Cracks in Structures
 - 5.3 Laboratory Tests
 - 5.3.1 Expansion Tests on Concrete Cores
 - 5.3.2 Mechanical Properties from Concrete Cores
 - 5.3.3 Quantification at the Microstructure Level
 - 5.3.4 Determining Damage Ratios at the Microstructure Level
 - 5.4 Summary of Diagnosis
- 6 Reporting
 - 6.1 Purpose

- 6.2 Scope
- 6.3 Objectives of the Investigation
- 6.4 Information Concerning the Structures
- 6.5 Methods and Techniques Used
- 6.6 Interpretation of Results
- 6.7 Conclusions
- 6.8 Author

References

Appendix 1. Proceedings of ICAAR

Appendix 2. Diagnosis of AAR within an Overall Investigation

3.63 Gong, Fuyuan and Takahashi, Yuya and Maekawa, Koichi (2017)

URL

```
@article{
gong2017strong,
label={gong2017strong},
title={Strong coupling of freeze-thaw cycles and alkali silica
reaction-multi-scale poro-mechanical approach to concrete damages},
author={Gong, Fuyuan and Takahashi, Yuya and Maekawa, Koichi},
journal={Journal of Advanced Concrete Technology},
volume={15},
number={7},
pages={346--367},
year={2017},
publisher={Japan Concrete Institute},
Keywords={},
DisplayPdf={0},
url={https://www.jstage.jst.go.jp/article/jact/15/7/15_346/_article/-char/ja/}
```

- One of the very few publications addressing the coupling between AAR and freeze-thaw cycles (FTC).
- Focuses on gel intrusion, ice formation in micro-pores and crack gaps.
- A complex numerical scheme is developed with no experiments reported.
- It show that ASR can reduce the FTC expansion for non-air-entrained case, but increase the frost damage for air-entrained concrete.
- FTC damaged concrete will have a simial expansion for non air-entrained case, but a greater expansion when air-entrained admixture agent is dosed.
- Good correlation between numerical simulation and past experiments is reported.

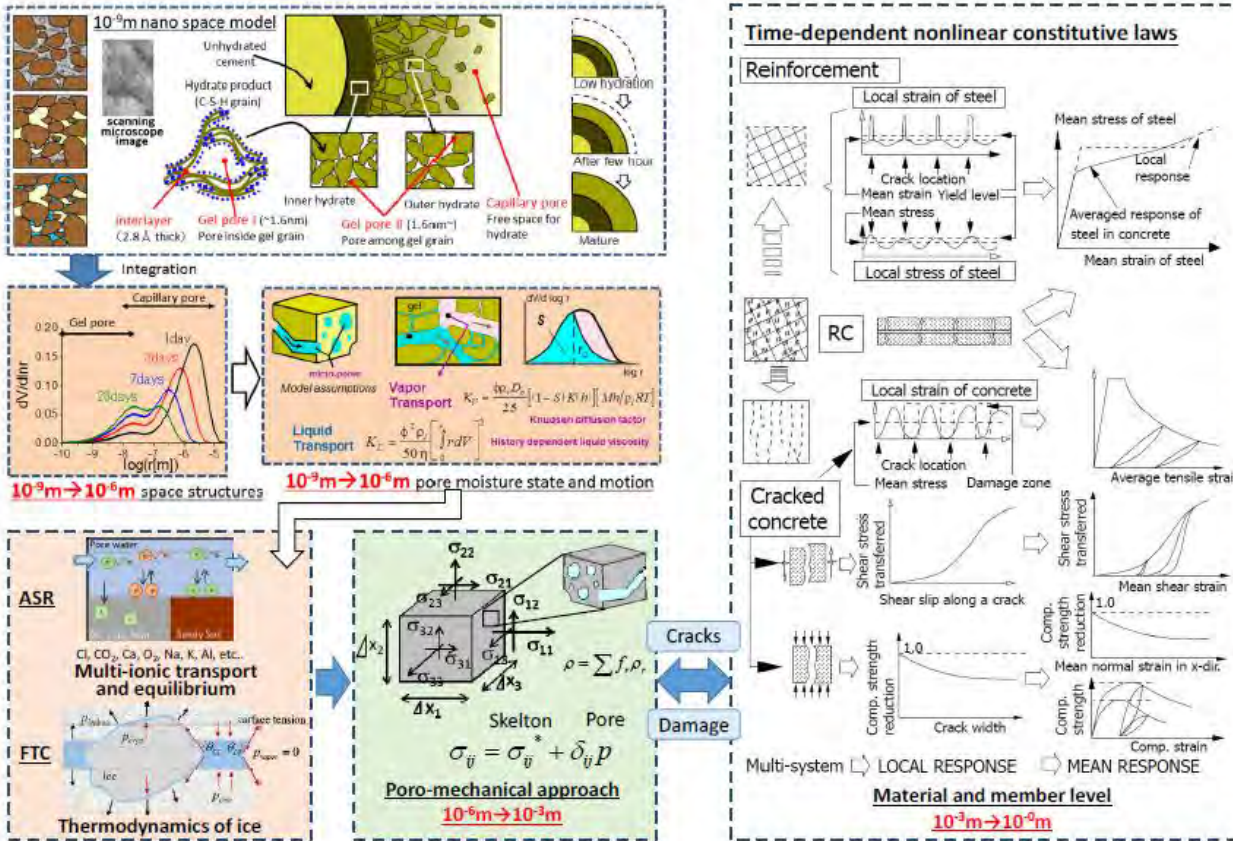


Fig. 1 Multi-scale simulation scheme of ASR and FTC induced deformation. (Maekawa *et al.* 2008)

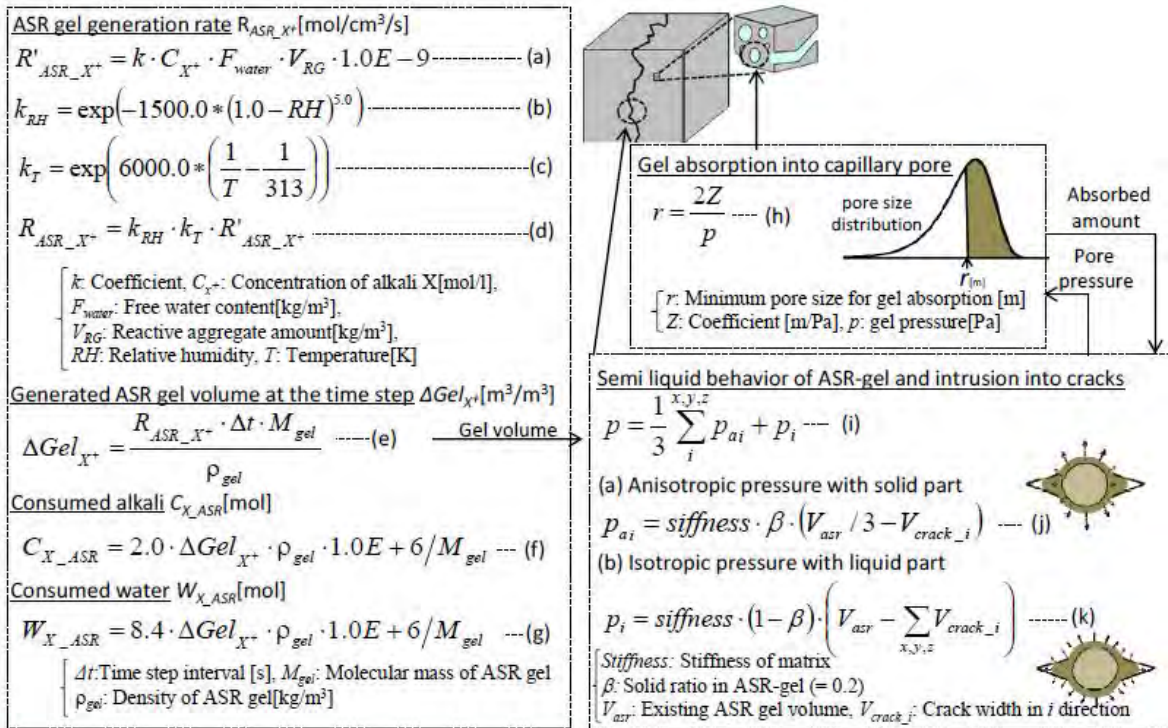


Figure 3.96: Calculation scheme for ASR gel generation and stress formation

3.64 Grimal, 'Etienne and Sellier, Alain and Le Pape, Yann and Bourdarot, 'Eric (2008)

URL

```
@article{
  grimal2008creep,
  label={grimal2008creep},
  title={Creep, shrinkage, and anisotropic damage in alkali-aggregate reaction
    swelling mechanism-Part I A constitutive model},
  author={Grimal, {'E}tienne and Sellier, Alain and Le Pape, Yann and Bourdarot,
    {'E}ric},
  journal={ACI Materials Journal},
  volume={105},
  number={3},
  pages={227},
  year={2008},
  publisher={American Concrete Institute},
  Keywords={},
  DisplayPdf={0},
  url={https://www.concrete.org/publications/internationalconcreteabstractsportal/m/details/id/19818}
```

- Modeling of alkali aggregate reaction (AAR) damaged concrete is made complex by the large number of elementary physical phenomena to be taken into account (concrete reactivity, thermal activation, moisture dependence, concrete rheology, and damage interaction).
- This paper presents the elementary physical principles that lead to the formulation of a visco-elasto-plastic orthotropic damage model including chemical pressure induced by AAR.
- Particular attention is also paid to the modeling of moisture effects on AAR development and on drying shrinkage.
- The constitutive modeling proposed is developed into the framework of an anisotropic damage theory to realistically model the strong cracking anisotropy and swelling observed on affected reinforced beams.

3.65 Guilloteau, T. and Martinot, F. and Sausse, J. (2017)

```
@incollection{
guilloteau2017long},
label={guilloteau2017long},
booktitle={Swelling Concrete in Dams and Hydraulic Structures: DSC 2017},
editor={Sellier, Alain and Grimal, {\'E}tienne and Multon, St{\'e}phane and
Bourdarot, Eric},
year={2017},
title={Long-Term Behaviour of EDF Dams Regarding Concrete Swelling Structures},
author={Guilloteau, T. and Martinot, F. and Sausse, J.},
publisher={John Wiley \& Sons},
Keywords={Field; Expansion Assessment/monitoring Rehabilitation; Gravity dam; Arch
dam; Buttress dam; },
DisplayPdf={0},
```

- EDF operates 156 monitored concrete dams. The studies of this large panel discovered that at least 20% of them are potentially affected by swelling reactions, considering at least dams with a medium ratio higher than $2\mu\text{m}/\text{m}/\text{year}$ (only 5 dams have a medium ratio above $30\mu\text{m}/\text{m}/\text{year}$).
- All of these dams were built between 1930 and 1960 (aged from 60 to 90 years) and are mainly gravity and single-curvature arch dams.
- According to the 2007 study:
 - Among the 54 dams equipped with vertical displacement devices, 20 show an irreversible expansion with a maximum rate varying from 2 to $70\mu\text{m}/\text{m}/\text{year}$.
 - High levels of expansion (more than $30\mu\text{m}/\text{m}/\text{year}$) are very rare and concern only 5 dams among the 150 studied (less than 5%).
 - The distinction between maximal rate and the medium rate underlines some homogeneous swellings and heterogeneous swellings. The dam in Figure 3.97 shows the most heterogeneous swelling studied: only few concrete lifts are affected by ISR phenomena.
 - Irreversible movements towards the upstream can be the sign of the swelling reaction of arch dams if this displacement is the consequence of an arc elongation. 15 arch dams show an arc elongation greater than $2\mu\text{m}/\text{m}/\text{year}$.
 - The identification of dams affected by swelling reactions underlines the arch and gravity dams as the more concerned types.
 - Effectively, gravity dams show horizontal displacements towards the upstream, when the number of contraction joints per meter is limited or when their joints are closed. At the opposite, when joints are numerous and opened, the horizontal displacements due to swelling reactions is lower and could be oriented downstream in some cases.
- According to the 2014 study:
 - Based on a statistical model (using a polynomial law of time fitted between t and $t^{2.5}$), whole time series were rebuilt to estimate accumulated effects. This model appears like an approximation of the “initiation” part of the theoretical “S” curve.

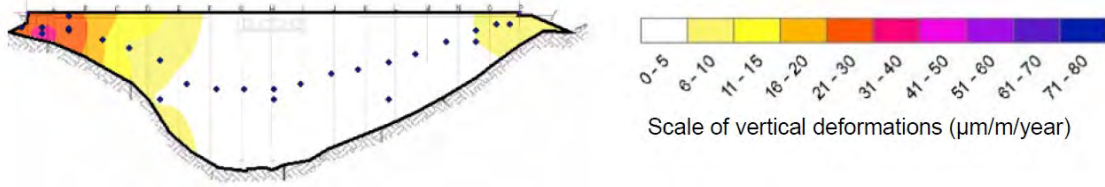


Figure 3.97: Vertical swelling rates observed on dam n-18; Guilloteau, Martinot, and Sausse (2017)

- Quantification of total strains since the date of first detection is shown in Figure 3.98. The total estimated strain values in vertical and horizontal directions are calculated.
- Shapes of kinetics are generally better explained with a linear law of time (t) for vertical strains, and with a polynomial function (with a degree upper than 2) for arc elongations.

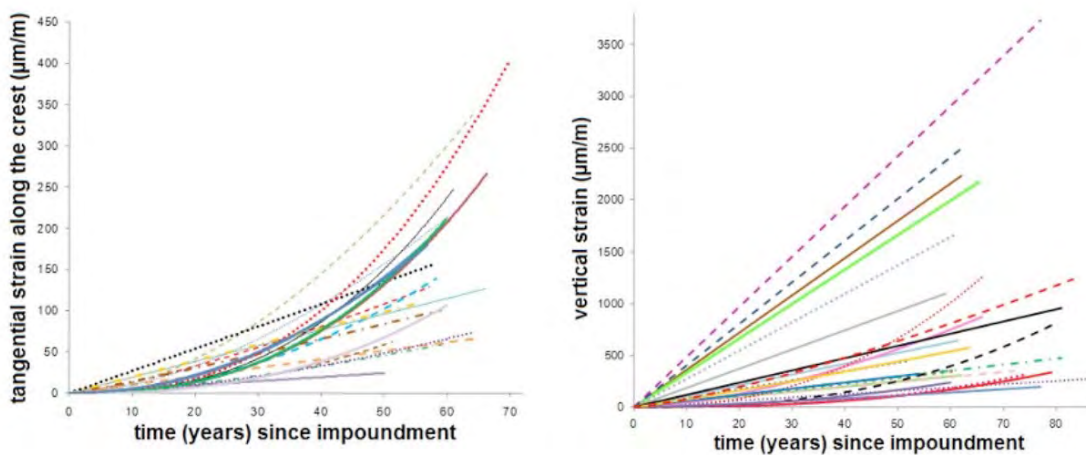


Figure 3.98: Tangential and vertical strains modeled since the first impoundment on 30 dams; Guilloteau, Martinot, and Sausse (2017)

- For an appropriate and valid evaluation of the kinetics of swelling on a dam, it is recommended to:
 - * Orient measurements in directions where the phenomenon can freely expand and generate maximum displacements and strain, generally following a vertical orientation;
 - * Adapt the monitoring system to its type and geometry, to its different structures (central and abutments blocks, spillways, etc), and to the possible heterogeneity of concrete;
 - * Perform regular and accurate measurements to quantify the progress of evolutions.

3.66 Gunn, R. and Scrivener, K. and Leemann, A. (2017)

```
@incollection{
gunn2017identification},
label={gunn2017identification},
booktitle={Swelling Concrete in Dams and Hydraulic Structures: DSC 2017},
editor={Sellier, Alain and Grimal, {\'}Etienne and Multon, St{\'}eplane and
Bourdarot, Eric},
year={2017},
title={The Identification, Extent and Prognosis of Alkali-Aggregate Reaction
Related to Existing Dams in Switzerland},
author={Gunn, R. and Scrivener, K. and Leemann, A.},
publisher={John Wiley \& Sons},
Keywords={Laboratory; Field; Expansion Assessment/monitoring Petrography; Finite
Element; Arch dam; Crack Index; },
DisplayPdf={0},
```

- Based on visual observations, instrumentation monitoring, and subsequent behavioral evaluations of the structure, a campaign of in-situ testing with specific short, medium, and long term goals may be undertaken.
- A series of test procedures and methods that provide the necessary quality information needed to assess AAR within dams is proposed.
- Factors influencing the identification of AAR in existing dams are shown in Figure 3.99.
- The following strategy is proposed for the investigation of AAR in existing dams:
 - Phase 1: AAR stage tests, material source(s) (e.g. quarries), visual inspection, and core sampling should cover all stages of the AAR process in the short, medium, and long term of the structures service life, including information needed for numerical modeling.
 - * Classification of AAR tests by: category, location, phase, type, sample type, classification, reliability, quality of information, and sample preparation.
 - * Influencing Factors: specimen size, quantity of cement, additives, relative humidity, temperature, time, and cost.
 - * Results and Conclusions: Standard limits above which AAR is deemed to be potentially deleterious.
 - Phase 2: AAR monitoring and data analysis. Using statistical, deterministic, and hybrid data analysis techniques to capture the potential zones of AAR swelling and, hence, perform analyses to assess the behavior and safety of the dam.
 - Phase 3: AAR follow-up tests should be systematically performed every 5 years from the onset of AAR.
 - Figure 3.100 summarizes the proposed strategy for dam AAR identification.
 - This approach defines three expansion/crack displacement and opening indexes that schematically illustrate AAR affected zones of different magnitude and importance throughout the entire dam body. Knowledge of these AAR zones with their respective extents allows test core samples to be selectively targeted in the dam body. Moreover,

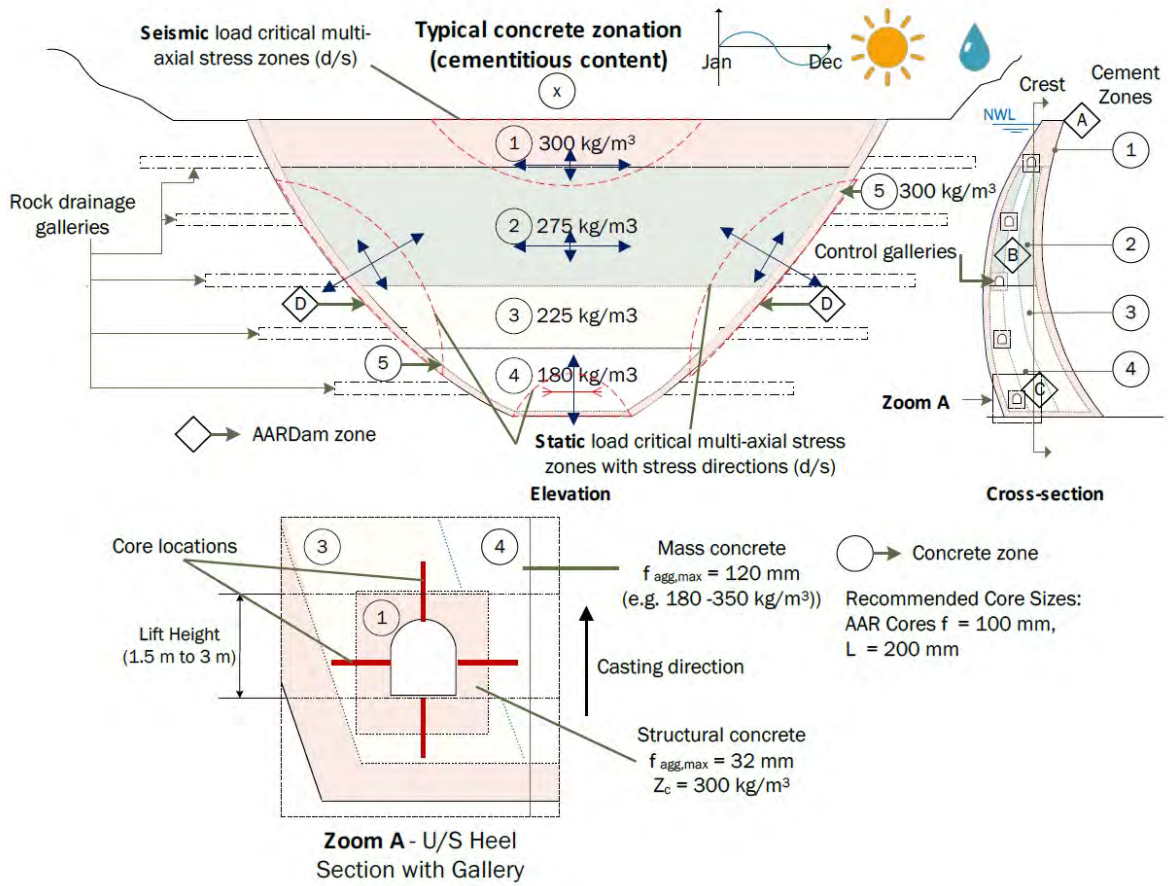


Figure 3.99: Schematic view of elements affecting the selection of AAR testing core samples; Gunn, Scrivener, and Leemann (2017)

the method defines fictitious temperatures that allow correlation tests to be performed against laboratory residual expansion tests enabling the long-term effects of AAR and hence appropriate rehabilitation works to be estimated.

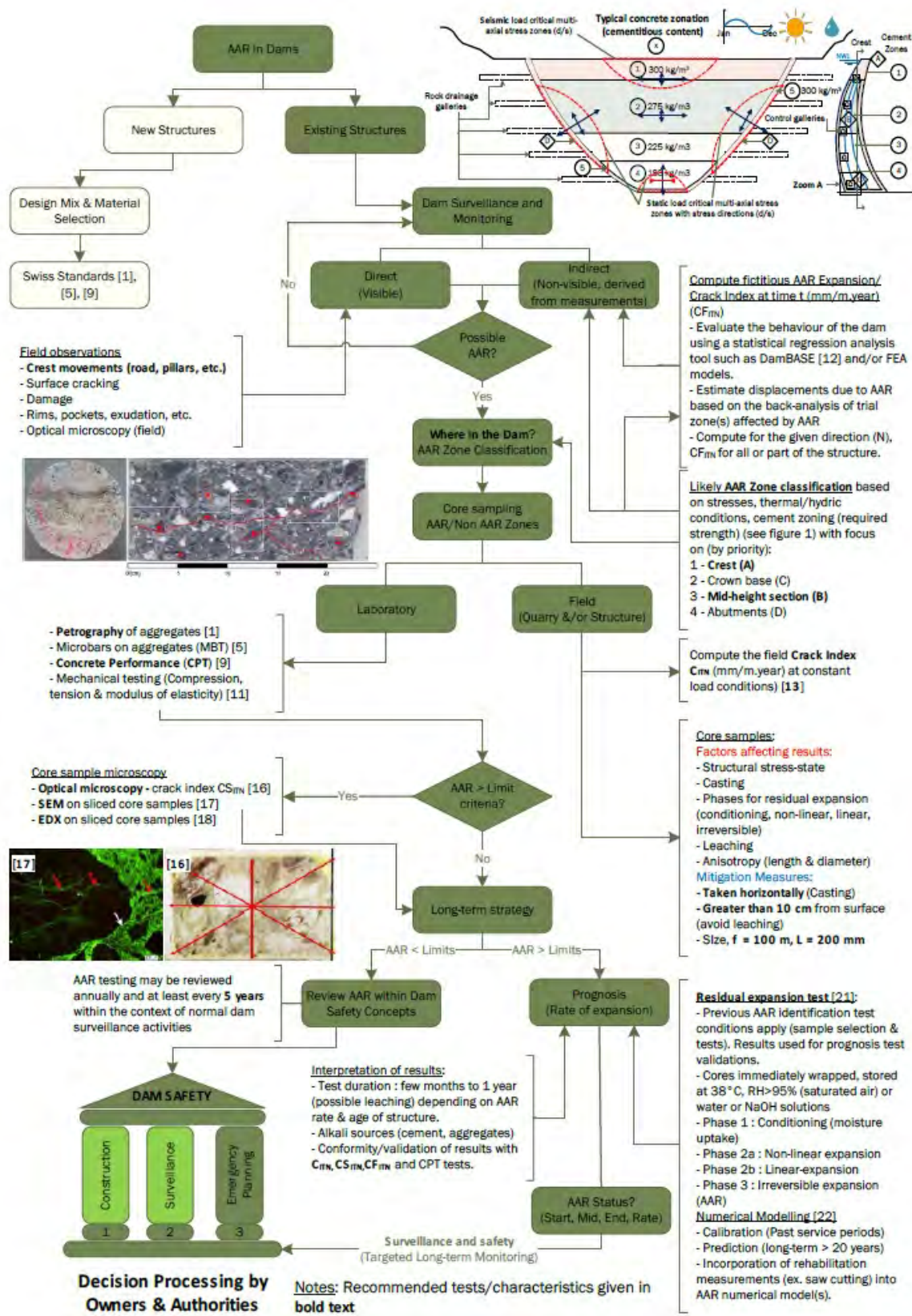


Figure 3.100: Proposed strategic method for dam AAR identification, Extent and Prognosis Evaluations; Gunn, Scrivener, and Leemann (2017)

3.67 Haha, M Ben and Gallucci, Emmanuel and Guidoum, Amor and Scrivener, Karen L (2007)

URL

```
@article{
haha2007relation},
label={haha2007relation},
title={Relation of expansion due to alkali silica reaction to the degree of
reaction measured by SEM image analysis},
author={Haha, M Ben and Gallucci, Emmanuel and Guidoum, Amor and Scrivener, Karen
L},
journal={Cement and Concrete Research},
volume={37},
number={8},
pages={1206--1214},
year={2007},
publisher={Elsevier}
Keywords={}
```

- Scanning Electron Microscopy (SEM) image analysis was used to quantify the degree of ASR in affected micro-bars, mortar, and concrete prisms.
- The image analysis sequence is shown in Figure 3.101.
- The degree of reaction gave a unique correlation with the macroscopic expansion for three different aggregates, stored at three temperatures and with two levels of alkali.
- The relationships found for the concretes and the mortars overlap when normalized by the aggregate content.
- This relationship is linear up to a critical reaction degree which coincides with crack initiation within the reactive aggregates.
- Figure 3.102 (left) presents the relationships obtained between the expansion and the degree of reaction for both mortar and concrete samples.
- The results show a strong correlation between the expansion and the degree of reaction.
- The predominant factor is the cement to aggregate ratio (C/A). The normalized curve is illustrated in Figure 3.102 (right).
- A linear domain is observed which corresponds to a constant expansion rate in terms of degree of reaction (up to approximately a reaction degree of 0.3%) followed by wider nonlinear domain.
- At this critical degree of reaction, the average corresponding expansion is around 0.03% and 0.06% for mortar and concrete samples respectively.

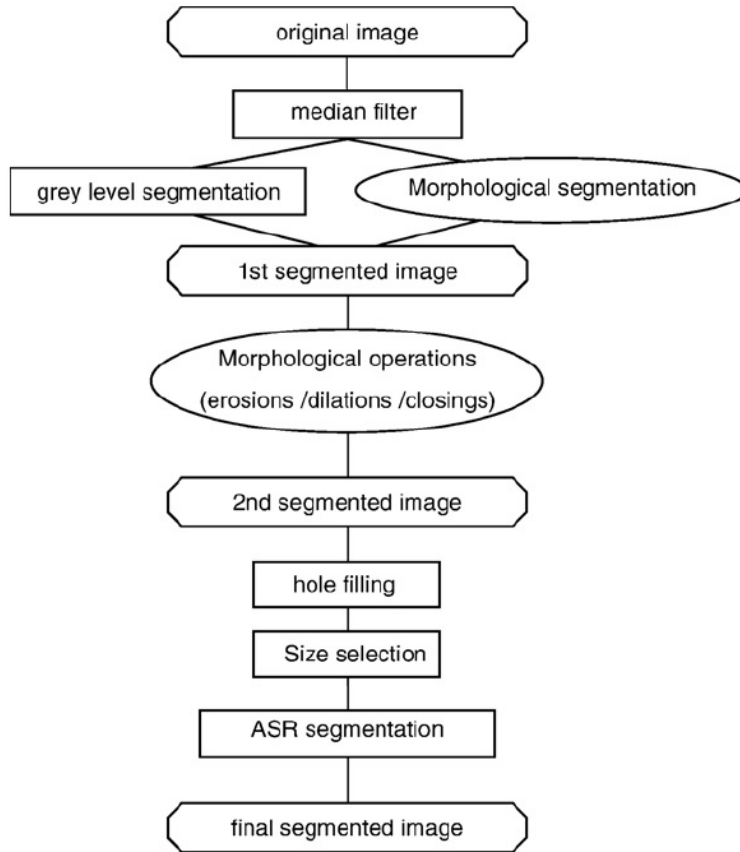


Figure 3.101: Image analysis sequence; Haha et al. (2007)

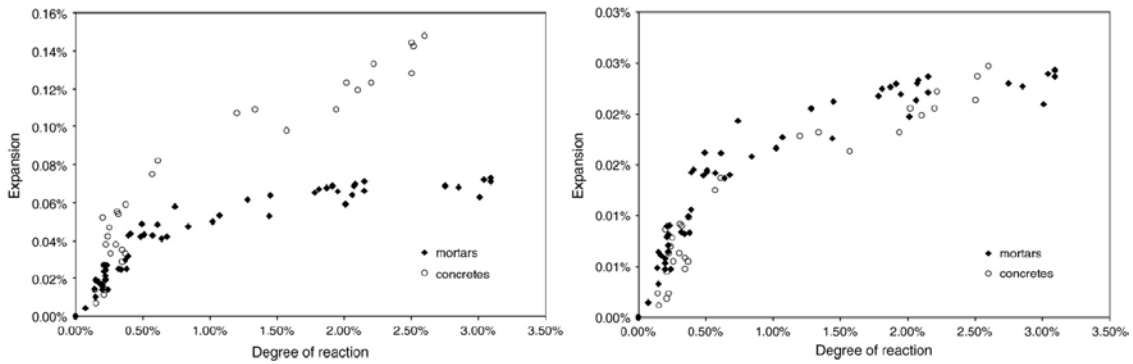


Figure 3.102: Image analysis sequence; Haha et al. (2007)

3.68 Hariri-Ardebili, Mohammad Amin and Saouma, Victor E and Merz, Christine (2018)

URL

```

@article{
hariri2018risk},
label={hariri2018risk},
title={Risk-Informed Condition Assessment of a Bridge with Alkali-Aggregate
Reaction.},
author={Hariri-Ardebili, Mohammad Amin and Saouma, Victor E and Merz, Christine},
journal={ACI Structural Journal},
volume={115},
number={2},
year={2018}
Keywords={}

```

- A computational framework that assesses the integrity of a bridge structure suffering from AAR was proposed.
- First, a detailed field observation and laboratory tests are reported, followed by comprehensive numerical simulations.
- All analyses are in the context of risk-informed condition assessment and probabilistic models.
- Preliminary results (deformation and stress field) were completely unintuitive and highlighted the complexity of the impact of AAR on a structural response.
- The prepared 3D finite element model employs the smeared crack model in which many of the parameters are assumed to be random variables (RVs). Those are modulus of elasticity, tensile and compressive stresses, fracture energy, etc.
- Depending on the RV, a normal or uniform truncated distributional model is adopted.
- In addition, many of the parameters in the AAR model are also assumed to be RV:
 - The distributional model and range of truncation for some of the RVs, e.g. activation energy, are best estimated using engineering judgment.
 - For some other RVs the range of variation is reported by photographer, e.g. final AAR expansion.
 - For the rest of the RVs, the variation is computed using several available measurements combined by optimization techniques, e.g. characteristics and latency time, reduction factor for the modulus of elasticity and tensile strength, Figure 3.103.
- The procedure to quantify the uncertainty in the final value and shape of the expansion curves can be summarized as follows:
 - Define the construction time as the starting point with no expansion.
 - Determine the “current uncertainty” (at the present time) using the petrography information.
 - Determine the future uncertainty.
 - * There is uncertainty in time: When is the expansion curve is going to plateau?
 - * Final expansion for this specific expansion

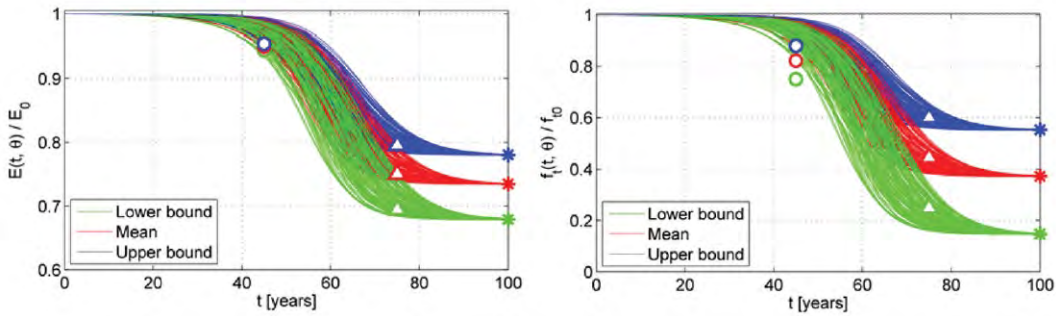


Figure 3.103: Predicting degradation of E and f_t based on optimization of experimental tests; Hariri-Ardebili, Saouma, and Merz (2018)

- One may note that the increasing time increases the uncertainty in the expansion value. Thus, the future uncertainty takes a trapezoidal form, Figure 3.104 (left plot).
- Next, several uniformly distributed points are selected from the generated trapezoidal plot. This step is similar to the Latin Hypercube Sampling.
- Using optimization techniques, the best expansion curves are generated from three points: 1) the origin point, 2) one random point from current uncertainty, and 3) one random point from future uncertainty. This is shown in Figure 3.104 (right plot).

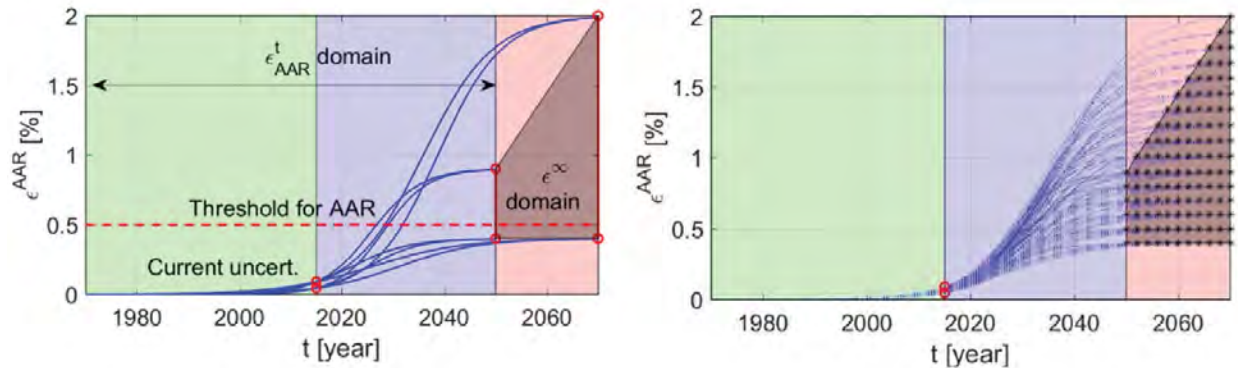


Figure 3.104: Domain of investigation for AAR expansion and the LHS based sampling approach; Hariri-Ardebili, Saouma, and Merz (2018)

- The generated expansion curves are used as input parameters in finite element simulations, along with other randomness in material properties.
- Results of N_{sim} simulations are then summarized to present them in forms of 16%, 50% and 84% fractiles.
- There are two representations of the summary curves: 1) time—EDP and 2) EDP—time, where EDP stands for engineering demand parameter such as displacement or damage index. This is shown schematically in Figure 3.105. One may note that the discrete date point along the “time” or EDP follow the log-normal distributional model.

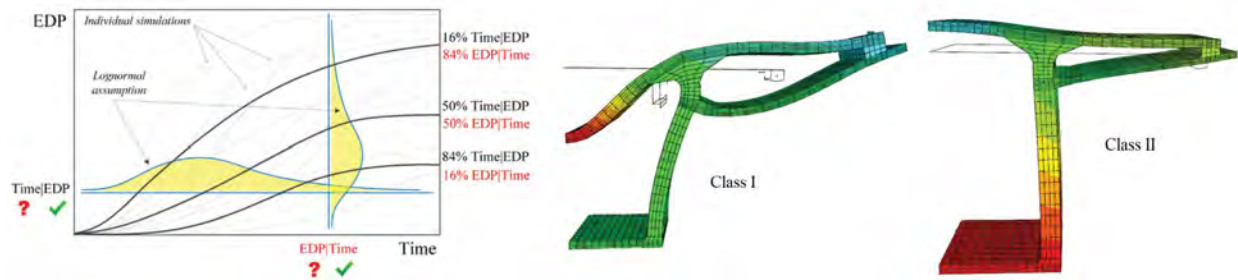


Figure 3.105: Interpretation of probabilistic analyses results based on summarized curves; Hariri-Ardebili, Saouma, and Merz (2018)

- The importance of non-uniform expansion was emphasized. Two different types of deformation were identified: class I and II where the main response can be observed in the web or deck respectively (See Figure 3.105).
- The fragility function is defined as a continuous function showing the probability of exceedance of a certain limit state (LS) for specific time:

$$\text{Fragility} = P [LS|T = t] \quad (3.10)$$

where $P[A|B]$ is the conditional probability that A occurs given that B is equal to a particular value.

3.69 Hariri-Ardebili, Mohammad Amin and Saouma, Victor E (2018)

URL

```
@article{
hariri2018sensitivity},
label={hariri2018sensitivity},
title={Sensitivity and uncertainty analysis of AAR affected reinforced concrete
shear walls},
author={Hariri-Ardebili, Mohammad Amin and Saouma, Victor E},
journal={Engineering Structures},
volume={172},
pages={334--345},
year={2018},
publisher={Elsevier}
Keywords={}
```

- The shear behavior of a shear wall was studied with and without AAR effects.
- The wall is a scaled down model already built and tested in the University of Toronto.
- Both the sound and AAR affected models are examined under reversed cyclic displacement.
- The model includes a shear wall with one layer of reinforcement in vertical and horizontal directions, as well as two columns (in the left and right sides) and two beams holding all the system together at the top and bottom.

- The analyses are performed in the context of the probabilistic methods.
- The uncertainty stems from randomness in material properties and unknown parameters in the AAR model.
- For the web and the columns, it is assumed that the material properties are nonlinear using the smeared crack model. The top and bottom beam are modeled as a linear elastic material. The observed failure also supports this assumption as there was not damage to the beam while the web and columns were extensively damaged (Jurcut, 2015).
- Since the authors were provided by partial data available after 260 days, an optimization based method is developed to estimate the unknown parameters at 1,000 days (the day in which the shear response was going to be tested).
- The estimated expansion curves, as well as the degraded material after 1,000 days, are shown in Figure 3.106.

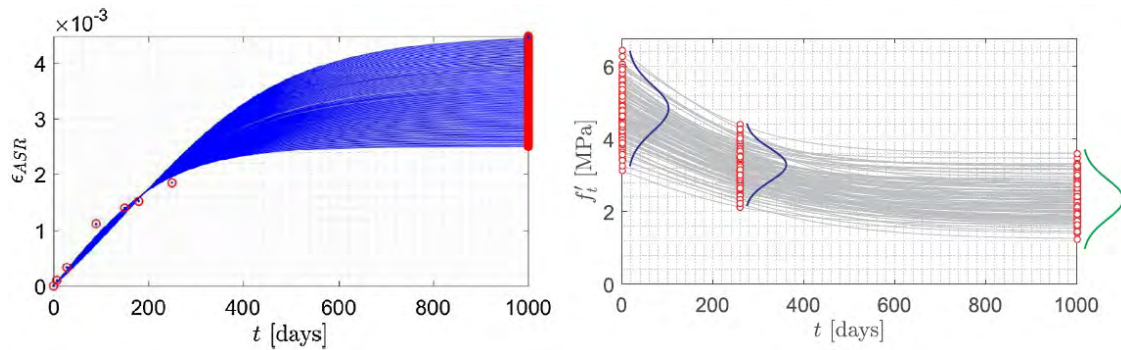


Figure 3.106: Optimization-based curve fitting to find the future expansion and estimation of residual coefficients; Hariri-Ardebili and Saouma (2018)

- In order to perform an effective probabilistic analysis, first a sensitivity analysis was performed and the corresponding Tornado diagram was plotted.
- The sensitivity analysis procedure is rooted in the Taylor's Series-Finite Difference Estimation.
- Having N random variables, a classical sensitivity analysis requires $2N + 1$ analyses to get the capacity functions and the Tornado diagram. This is shown in Figure 3.107.
- Next, the uncertainty quantification is performed. One hundred realizations with different combinations of material properties and AAR models are generated and applied to the finite element model. Each model is analyzed and the results are extracted in the form of load-displacement (i.e. capacity) curves.
- To be used in the context of probabilistic methods, these individual curves need to be summarized to some central values, i.e. 16%, 50% and 84% curves. This is shown in Figure 3.108 (Left).
- Having the results at 260 days, the objective was to predict the results at 1,000 days based on probabilistic models. This is shown in the Figure 3.108 (right) and in the context of the cumulative density function. The vertical axis represents the probability of non-exceedance for any particular value of the maximum shear force at the failure point (P_{max}).

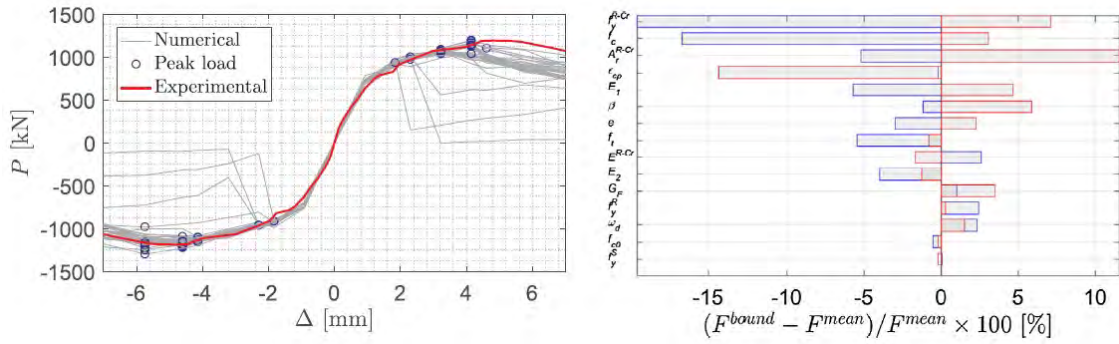


Figure 3.107: Results of sensitivity analysis on concrete constitutive model, capacity curves (left) and Tornado diagram (right); Hariri-Ardebili and Saouma (2018)

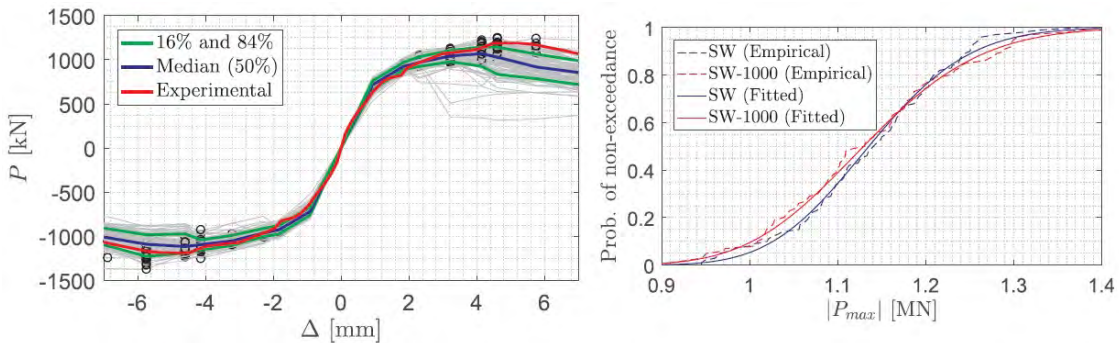


Figure 3.108: Probabilistic presentation of capacity curves (left) and cumulative density functions (right); Hariri-Ardebili and Saouma (2018)

3.70 Hattingh, L. and Oosthuizen, C. and Tembe, I. and Mahlabela, C. (2017)

```
@incollection{
hattingh2017important},
label={hattingh2017important},
booktitle={Swelling Concrete in Dams and Hydraulic Structures: DSC 2017},
editor={Sellier, Alain and Grimal, {\'}E}tienne and Multon, St{\'}e}phane and
Bourdarot, Eric},
year={2017},
title={Important Lessons Learnt from the Proper Surveillance of Swelling Concrete},
author={Hattingh, L. and Oosthuizen, C. and Tembe, I. and Mahlabela, C.},
publisher={John Wiley \& Sons},
Keywords={Field; Expansion Assessment/monitoring Confined; Arch dam; },
DisplayPdf={0},
```

- The uncertainties in safety assessment of ASR affected dams are:
 - the current extent of reaction/swelling

- the rate and prediction of future reaction/swelling (in other words, when, if at all, will the swelling reaction stop, if at all?)
 - 3D swelling behavior of the structure
 - the impact of openings on swelling behavior
 - changes in stress profile within the structure
- A proper surveillance system of a dam should monitor both loads and responses. For an arch dam, this typically includes the following:
 - Loads:
 - * hydrostatic (water levels)
 - * temperature (air and concrete)
 - * foundation piezometric pressures
 - Responses (both static and dynamic):
 - * ground motion
 - * displacements and rotations (relative and absolute)
 - * strains
 - * stress
 - * seepage
 - * pore pressure
 - * dynamic responses
- Cahora Bassa Dam, a 170 m high double curvature concrete arch dam, is located in South Africa. Construction was finished in 1976.
 - Upon close examination of the monitoring results, signs of ASR were evident soon after its completion in the early 1980s.
 - The annual vertical swelling strain rate of the top part in the center of the Dam (the closest to the free strain rate) is around 30μ strain/year. It decreases with depth.
 - The vertical swelling strain rates of 19 and 23 micro strain/year observed at the installations between the peripheral gallery and the rock interface.
 - From the “no stress” strain gauges close to the top of the wall annual vertical swelling strain rates of between 20 and 35 micro strain are evident, Figure [3.109](#).
 - Using the strain results of the different monitoring systems a quite clear picture of the strain behavior of Cahora Bassa Dam is evident, especially as a result of the swelling due to ASR. Of particular importance is the observed impact of openings on the strain behavior of the concrete, especially in the vicinity of the galleries, as well as the impact of confinement on strain (strain rates significantly decrease with an increase of confinement).
 - The results highlight the importance of having redundancy measurements with different types of instruments that can provide similar results, even if some manipulation may be required to ensure confidence in the measurements.
 - In the case of Cahora Bassa Dam, it was possible to compare all the results by converting them to strain rates from displacements and strains respectively.

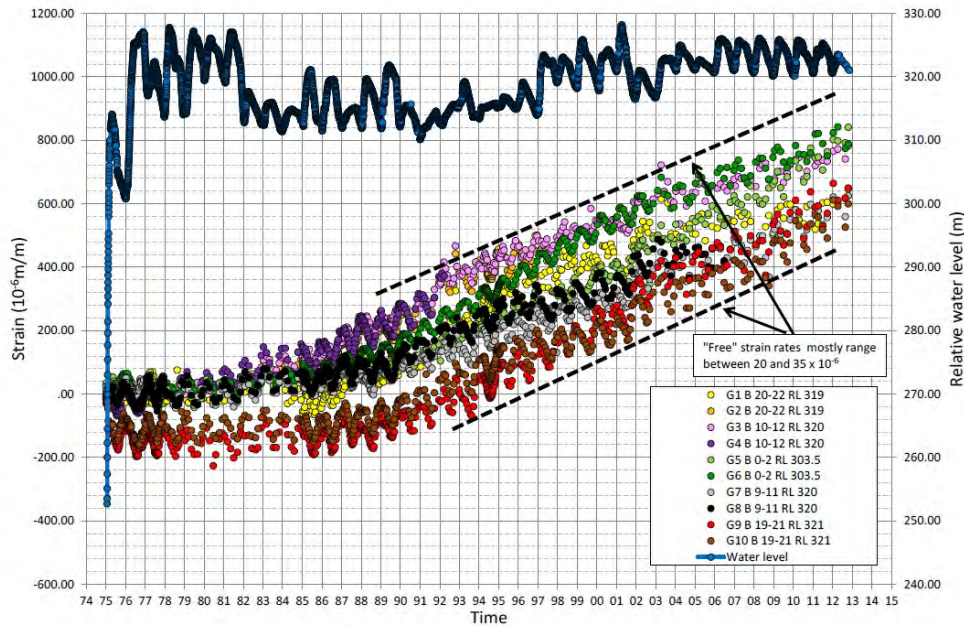


Figure 3.109: Cahora Bassa Dam: Carlson strain gauges: “Stress free” strain at the top of the dam wall above RL 300 m; Hattingh et al. (2017)

- The 69 m high Kouga Dam (a double curvature arch dam) is located in South Africa. The Dam was completed in 1969.
- Since 1972, some form of concrete swelling became clear. Some inelastic movement of the right flank followed a few years later that further complicated the behavior model of the structure.
- 3D-crack gauges across major joints and major cracks on the non-overspill crest were added in 1991.
- From the Kouga Dam example, it is evident that only monitoring the behavior of the central cantilever or vertical displacement of the crest will, in many instances, not provide a correct interpretation of the behavior of the structure to draw conclusions on the current as well as future swelling behavior of the concrete.

3.71 Hayes, Nolan Wesley and Gui, Qiang and Abd-Elssamd, Ammar and Le Pape, Yann and Giorla, Alain Benjamin and Le Pape, Sihem and Giannini, Eric R and Ma, Zhongguo John (2018)

URL


```

@article{
  hayes2018monitoring},
  label={hayes2018monitoring},
  title={Monitoring Alkali-Silica Reaction Significance in Nuclear Concrete
    Structural Members},
  author={Hayes, Nolan Wesley and Gui, Qiang and Abd-Elssamd, Ammar and Le Pape,
    Yann and Giorla, Alain Benjamin and Le Pape, Sihem and Giannini, Eric R and
    Ma, Zhongguo John},
  journal={Journal of Advanced Concrete Technology},
  volume={16},
  number={4},
  pages={179--190},
  year={2018},
  publisher={Japan Concrete Institute}
  Keywords={}

```

- Concrete cylinders were cast with reaction and non-reaction (CTRL) conditions. Reaction concrete is allowed to undergo free expansion (UASR) or is confined in a metallic mold (CASR).
- After 28 days, all the concrete show a similar modulus of elasticity.
- The modulus of elasticity is not affected by addition of sodium hydroxide (unlike compressive strength).
- The modulus of elasticity collected on the reactive sample specimen show a rapid decrease at a relatively young age.
- The UASR specimens exhibit a higher decrease in the modulus of elasticity than the confined specimens.
- Figure 3.110 (left) shows the changes in modulus of elasticity.

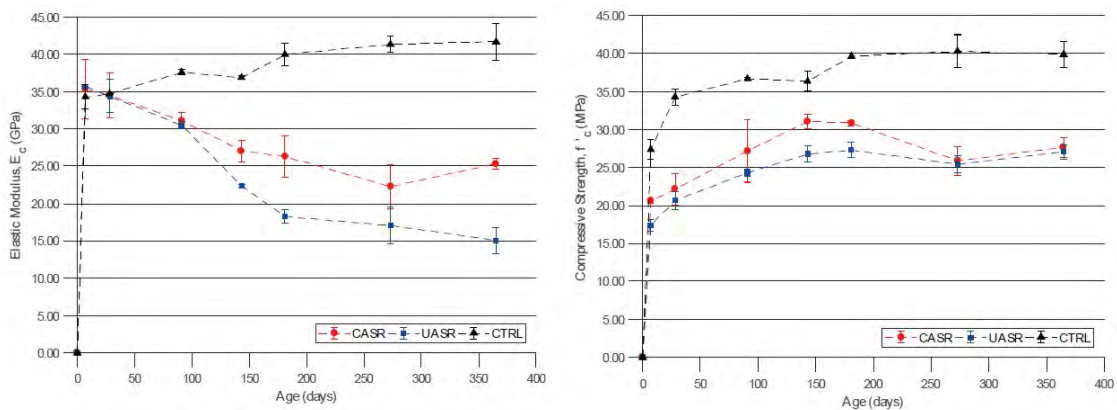


Figure 3.110: Variation of modulus of elasticity (left) and compressive strength (right); Hayes et al. (2018)

- The CTRL shows a much higher gain in the strength at a lower age.

- The difference in compressive strength can be attributed to the addition of sodium hydroxide to the reactive concrete mix. Addition of sodium hydroxide reduces the compressive strength due to the formation of porous cement paste.
- Following a hardening until about 200 days, the compressive strength measured on the CASR and UASR specimen exhibit a decrease apparently independent of the confinement.
- Figure 3.110 (right) shows the changes in compressive strength.

3.72 Hefny, A and Lo, KY and Adeghe, L (2001)

URL

```
@article{
hefny2001measurements,
label={hefny2001measurements},
title={Measurements of laboratory rates of concrete expansion and their
comparisons with field rates},
author={Hefny, A and Lo, KY and Adeghe, L},
journal={Canadian Journal of Civil Engineering},
volume={28},
number={3},
pages={402--410},
year={2001},
publisher={NRC Research Press},
Keywords={},
DisplayPdf={0},
url={http://www.nrcresearchpress.com/doi/abs/10.1139/101-003}
```

- A laboratory test methodology for measuring the residual expansion rate in dams with simulation of field environment has been developed.
- Describes the test principles and method of interpretation of the different tests developed.
- Results of various expansion tests performed on samples recovered from the R.H Saunders dam (Canada) are presented. Results showed that the expansion rates measured in laboratory are consistent with those measured by extensive instrumentation in the field (in situ rebar tests, levelling data, stress meters, and in situ overcoring data).
- It is believed that the test methodology developed provides the necessary and inexpensive tools for measuring the stress-dependent residual expansion potentials in concrete dams.

3.73 Heidarzadeh, N and Samadzad, M and Shekarchi, M and Mirghaderi, SR (2017)

URL

```

@article{
heidarzadeh2017long},
label={heidarzadeh2017long},
title={LONG-RUN EFFECT OF ALKALI-SILICA REACTIONS ON THE STRUCTURAL INTEGRITY OF A
MULTI-STORY REINFORCED CONCRETE BUILDING},
author={Heidarzadeh, N and Samadzad, M and Shekarchi, M and Mirghaderi, SR},
journal={ASIAN JOURNAL OF CIVIL ENGINEERING (BHRC)},
volume={18},
number={8},
pages={1315--1328},
year={2017}
Keywords={}

```

- The effect of ASR on the integrity of a multistory (thirty-year-old half-built) reinforced concrete building was studied.
- The building has undergone two construction phases. The first phase occurred from 1975 to 1977 (only the four basements were constructed). Then, the construction was stopped for 16 years. The second phase was from 1993 to 1995 (during which the four parking floors were constructed above the basements). The construction was stopped again until 2006.
- Between the first and second construction phases, the structure was exposed to environmental conditions, such as freeze-thaw, moisture due to the ponding of rainwater on the slabs, carbonation reaction due to air pollution, and temperature change.
- 52 concrete cores of 100 mm diameter were taken from the columns and retaining walls and tested. The mean compressive strength is estimated 33.3 MPa with a standard deviation of 10.6 MPa. The coefficient of variation is very large due to the lack of an elaborate quality control system at the time of the construction.

3.74 Helene, Paulo and Carvalho, Mariana and Pacheco, Jéssika (2017)

URL

```

@article{
helene2017engineering},
label={helene2017engineering},
title={Engineering field tests for alkali-aggregate reaction},
author={Helene, Paulo and Carvalho, Mariana and Pacheco, J{\`e}ssika},
journal={Structural Concrete},
volume={18},
number={2},
pages={349--355},
year={2017},
publisher={Wiley Online Library}
Keywords={}

```

- The Paulo Guerra Bridge in Recife, Brazil, was constructed in 1977.

- The Bridge is subjected to marine spray, as well as wet and dry cycles.
- After about 15 years, some pathological symptoms appeared (e.g. map cracking, concrete expansion, steel corrosion, and leaching stains).
- Several inspections were conducted on the bridge, including visual observation of the foundation blocks (pile caps), core extraction, ultrasonic pulse velocity tests, carbonation tests, measurements of chloride concentration, electrochemical resistivity, corrosion potential, compressive strength, modulus of elasticity and X-ray diffraction, and microscopy evaluations.
- The results confirmed the existence of generalized AAR on the pile caps, as well as steel corrosion, Figure 3.111.



Figure 3.111: Signs of deterioration at the Paulo Guerra Bridge (left); severe steel corrosion (right); Helene, Carvalho, and Pacheco (2017)

- The original project specified a compressive strength of 20 MPa for the pile caps with an expected modulus of elasticity of 21 GPa.
- The compressive strength and modulus of elasticity values taken from cores are shown in Table 3.112. There is a large scatter of results and the obtained modulus of elasticity is very low.

Block	Core no.	Compressive strength (MPa)	Expected modulus of elasticity ²	Measured modulus of elasticity ³¹
01	01	19.1	20.7	10.4
	02	23.6	23.0	17.2
	03	35.4	23.9	24.4
10	01	13.1	17.1	8.0
	02	23.6	23.0	13.2
	03	28.6	25.3	16.6

Figure 3.112: Results of the modulus of elasticity tests and the compressive strength; Helene, Carvalho, and Pacheco (2017)

- Once AAR was confirmed, many corrective alternatives were studied, including induced carbonation and injection of lithium salts. Considering the local conditions and the advanced deterioration, confinement of the blocks appeared to be the best alternative.

3.75 Herrador, Manuel F and Martínez-Abella, Fernando and Dopico, Juan Ramón Rabuñal (2008)

URL

```
@article{
herrador2008experimental},
label={herrador2008experimental},
title={Experimental evaluation of expansive behavior of an old-aged ASR-affected
dam concrete: methodology and application},
author={Herrador, Manuel F and Mart{\'i}nez-Abella, Fernando and Dopico, Juan
Ram{\'o}n Rabu{~n}al},
journal={Materials and Structures},
volume={41},
number={1},
pages={173--188},
year={2008},
publisher={Springer}
Keywords={}
```

- A series of tests were performed to obtain meaningful data for mechanical characterization of an existing, old ASR-affected dam concrete.
- A specific methodology is developed including procedures for test design, mechanical loading and data acquisition in harsh environmental non-laboratory conditions.
- First, a table was compiled showing the relationship between external pressure (i.e. inhibition pressure) and ASR kinetics. Table 3.113 shows those results of experimental tests on different types of structures.
- According to this table, inhibition pressure may range between 3 MPa and 10 MPa, falling within the range of ordinary concrete service stresses.

Pressure	Estimation procedure
3 MPa	Saunders Dam specimens submitted to various compression levels
5 MPa	Maximum value of induced compression while forcing 0 strains in creep frame
2.2—10.3 MPa	Theoretical value obtained from Double-Layer model
10 MPa	Theoretical value obtained from Fracture Mechanics model
7.5 MPa	Numerically calibrated value for Saunders Dam structural model
6 MPa	Laboratory specimens submitted to various compression levels
8 MPa	Numerically calibrated value for Mactaquac Dam structural model
10 MPa	Extrapolated value obtained from reinforced concrete expansive specimens
5 MPa	Nanteuil bridge specimens submitted to various compression levels
3 MPa	Laboratory specimens submitted to various compression levels
4 MPa	Beams in laboratory

Figure 3.113: Typical values of ASR inhibition pressure; Herrador, Martínez-Abella, and Dopico (2008)

- Belesar, a 600 m long and 129 m high concrete arch dam built across the Sil river Canyon, Spain, between 1957 and 1963.

- Belesar Dam was first diagnosed with ASR in 1994 after showing irreversible displacements since monitoring measures began in 1963.
- The map-like fissures on a concrete wall can be seen in Figure 3.114.



Figure 3.114: Map-like fissures on a concrete wall in the Belesar Dam; Herrador, Martínez-Abella, and Dopico (2008)

- Tests are consistent mainly in long term measurement of free and confined expansions of core-drilled specimens extracted from different locations in the dam.
 - Load-free expansion testing: characterization of expansive potential and expansion velocity of concrete in its present state.
 - Constant load testing under different loads: characterization of long term behavior and detection of inhibition pressure value.
 - Variable load testing: observation of behavior under realistic load speeds for dam concrete.
 - Instantaneous mechanical testing: standard characterization of resistance and longitudinal modulus.
- Conclusions about the possibility of ASR-expansion mitigation through confinement are drawn from experimental data.

3.76 Huang, M and Pietruszczak, S (1996)

[URL](#)

```
@article{
huang1996numerical},
label={huang1996numerical},
title={Numerical analysis of concrete structures subjected to alkali-aggregate
reaction},
author={Huang, M and Pietruszczak, S},
journal={Mechanics of Cohesive-frictional Materials: An International Journal on
Experiments, Modelling and Computation of Materials and Structures},
volume={1},
number={4},
pages={305--319},
year={1996},
publisher={Wiley Online Library}
Keywords={}
```

- A simple continuum theory is applied to describe the mechanical effects of the AAR in concrete structures.
- The junction between the right-wing dam and the water intake structure of the Beauharnois Powerhouse situated in Quebec (Canada) is analyzed using nonlinear 3D finite element analysis.
- The Powerhouse was constructed in three stages. The construction started in 1928 and was completed in 1961.
- The total length of the concrete structures (including gravity dams) is 1034 m. The height of the intake structure and the right and left gravity dams is 29, 22 and 19.5 m, respectively.
- For the right wing dam, the average values of recorded vertical strain rates were of the order of 0.0001/year.
- Overall, the studies show that the reaction will continue with the same rate for the next several decades.
- In the prepared finite element model, the first two blocks of the dam and the first unit of intake structure were considered.
- The model includes 4360 3D solid elements for concrete and 764 shell elements for reinforcement.
- First, the solution due to the self-weight of the structure and the pressure exerted by water and backfill soil was obtained. For this phase, no kinematic constraints were imposed along vertical boundaries due to the existence of expansion joints between units at early stages of operation.
- The second phase of the analysis was the simulation of the effect of AAR, continuing for a period of 25 years.
- The rock foundation at the bottom of the structure was considered to be rigid (prescribed zero displacements).
- The free expansion of 0.005775 is used for analysis.

- Figure 3.115 presents the contours of all displacement components after 25 years of reaction.
- The results indicate that the crest of the dam is rising with an average rate of 2.4 mm/year which is consistent to the field measurements.

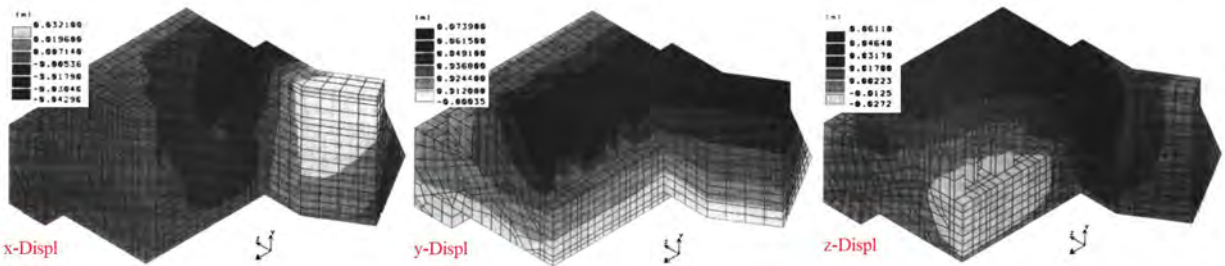


Figure 3.115: Contours of displacement components after 25 years of the reaction; Huang and Pietruszczak (1996)

- Figure 3.116 illustrates the distribution of the stress intensity factor, β , along the faces of the considered section. $\beta > 1$ corresponds to the failure mode associated with the formation of macrocracks.
- The most severe damage occurs in the region adjacent to the surface and confined to some specific locations within the water intake structure.
- The structural integrity of the entire section, which is basically a gravity structure, is certainly not at risk. If the reaction is continued for the next few decades, however, the local damage may result in serious operational problems.

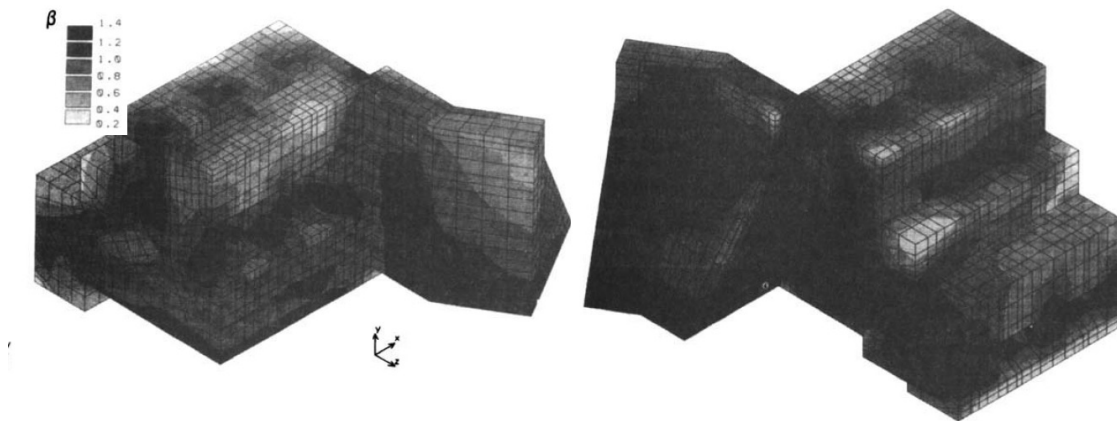


Figure 3.116: Distribution of the stress intensity factor, β , after 25 years of continuing AAR; Huang and Pietruszczak (1996)

3.77 Huang, Maosong and Pietruszczak, S (1999)

URL


```

@article{
huang1999modeling},
label={huang1999modeling},
title={Modeling of thermomechanical effects of alkali-silica reaction},
author={Huang, Maosong and Pietruszczak, S},
journal={Journal of engineering mechanics},
volume={125},
number={4},
pages={476--485},
year={1999},
publisher={American Society of Civil Engineers}
Keywords={}

```

- This research is a follow up for Huang and Pietruszczak (1996).
- Again, the Beauharnois power plant (Quebec, Canada) is used as case study. A large portion of the structure is analyzed.
- The free expansion is mentioned to be 0.057. This value 10 time larger than the previously reported value Huang and Pietruszczak (1999). It is not clear if this is typo or change in formulation.
- The extended finite element model includes more than 23,000 tetrahedral elements.
- Figure 3.117 shows the distribution of the damage factor $\bar{\beta}$ corresponding to 25 years of ASR expansion.
- It is evident that the most severe damage occurs in the first unit (unit A/B) of the intake structure due to significant distortion.

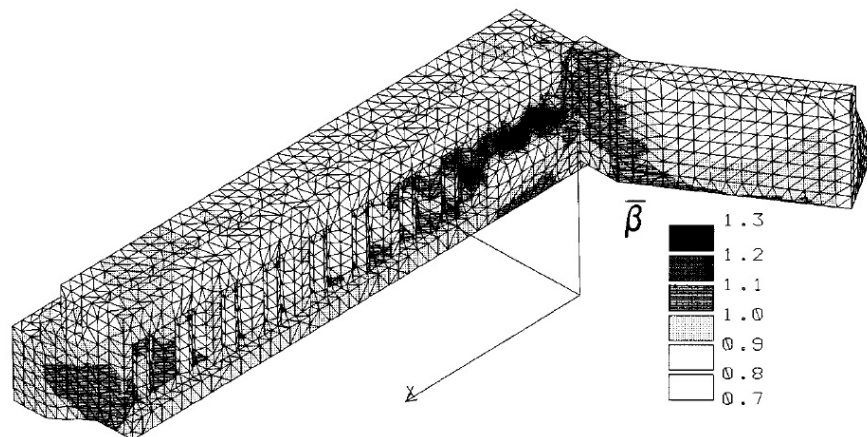


Figure 3.117: Distribution of damage factor $\bar{\beta}$ after 25 years of reaction; Huang and Pietruszczak (1999)

- Next, the refined finite element mesh of the section was critical using about 25,000 tetrahedral elements.

- The most severe damage occurs in the region adjacent to the channels in the intake structure, which is consistent with the on-site observation.
- The current findings are different from previous research (Huang and Pietruszczak, 1999). These differences are attributed to different kinematic boundary conditions. The solution given in the recent paper employs a numerical interpolation, whereas the one provided in the old paper corresponds to a simpler linear distribution of displacements.
- The south wing dam is a gravity structure, 115.44 m long and 22.10 m high. The dam is founded on a firm rock.
- The structure has been divided into two zones with different expansion rates, Figure 3.118. The expansion rate in the concrete adjacent to the exposed surfaces was assumed to be 30% of the maximum rate.
- The problem has been considered as 2D and the finite element mesh with about 1,100 triangular elements is developed, Figure 3.118.

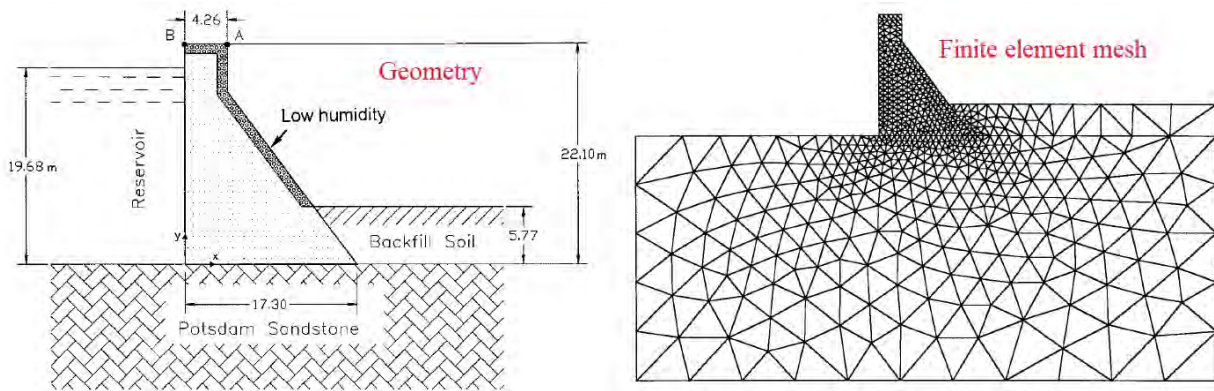


Figure 3.118: Geometry and finite element mesh of dam-foundation system; Huang and Pietruszczak (1999)

- A separate heat transfer analysis was performed, and the resulting temperature distribution was used for the mechanical analysis.
 - Dam-Air Interface:
 - * Only the convection and radiation boundary conditions were considered while the externally supplied heat flux from the sun was neglected.
 - * The evolution of the air temperature was described by a sine function.
 - Ground Surface Boundary: The temperature history at the ground surface was described by a sine curve from $P/4$ to $3P/4$, where P is the period and was taken to be 365 days.
 - Dam-Reservoir Interface: The reservoir temperature was assumed to follow a periodic seasonal fluctuation. The ice period was assumed to be approximately from $3P/4$ to next year's $P/4$.
 - Foundation Bottom Boundary: In general, the penetration depth of annual temperature oscillations beneath the ground surface is ~ 10 m; therefore, the temperature at the base of the foundation may be considered as constant.

- Both the isothermal and nonisothermal analyses were performed over a period of 25 years of continuing reaction. Results are shown in Figure 3.119.
 - Under isothermal formulation, the extent of structural damage is quite limited: The macro-cracks form only near the exposed surface which is primarily due to a lower humidity of concrete in this region.
 - Under nonisothermal formulation, the values of $\bar{\beta}$ are high near the exposed surfaces and lower near the dam-reservoir interface. On the exposed surfaces, the macro-cracking is much more severe than that predicted by the isothermal formulation.

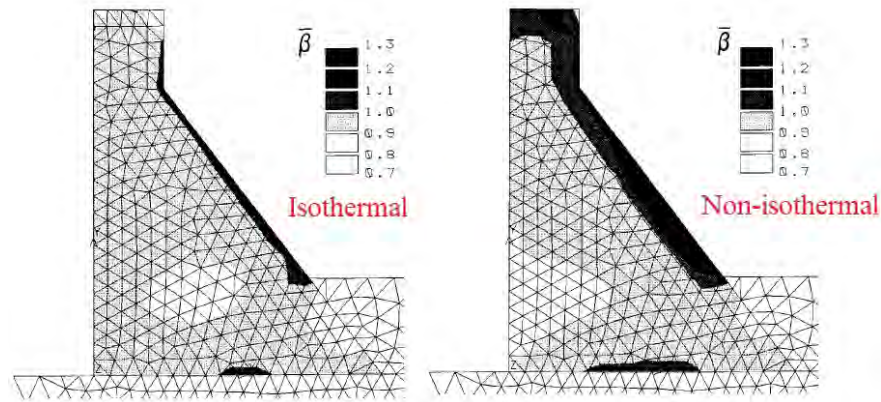


Figure 3.119: Distribution of Damage Factor $\bar{\beta}$ after 25 Years of Reaction with two types of thermal analyses; Huang and Pietruszczak (1999)

- Figure 3.120 compares the horizontal and vertical displacement histories at the crest of the dam. In general, the predictions based on thermo-mechanical analysis are more consistent with on site measurements.

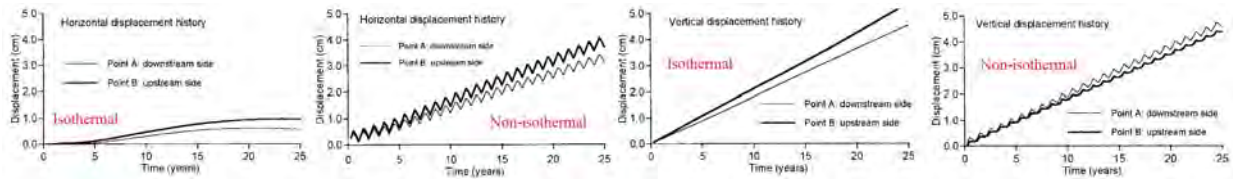


Figure 3.120: Comparison of displacements at crest of dam; Huang and Pietruszczak (1999)

3.78 Huang, H and Spencer, BW and Cai, G (2015)

URL

```
@techreport{
huang2015grizzly,
label={huang2015grizzly},
title={Grizzly model of multi-species reactive diffusion, moisture/heat transfer
and alkali-silica reaction in concrete},
author={Huang, H and Spencer, BW and Cai, G},
year={2015},
institution={Technical Report INL/EXT-15-36425, Idaho National Laboratory, Idaho
Falls, ID},
url={https://www.osti.gov/biblio/1484297}
```

- Reports on the Idaho National Laboratory (INL) effort in developing a fully coupled thermo-hydronechanical-chemical (THMC) concrete model, referred as Grizzly, with the ultimate goal of reliably simulating and predicting the long-term performance of concrete structures subjected to various aging and degradation mechanisms.
- Paper presents a fully coupled concrete model implemented in Grizzly code for simulating coupled moisture/heat transfer, stress dependent ASR swelling and elastic/inelastic mechanics.
- Model based on Saouma and Perotti stress dependency.
- Example simulation results and preliminary model validation results against experimental data reported in the literature are provided.
- Close matches between the simulation results and experiments clearly reveal the potential of the fully coupled solution strategy for solving tightly coupled THMC concrete models.
- Rate-dependent damaging mechanics model for simulating the ASR swelling induced degradation of concrete structures is also presented along with its feedback to moisture and heat transport processes.

3.79 Huang, Hai and Spencer, Benjamin W (2016)

```
@techreport{
huang2016grizzly2},
label={huang2016grizzly2},
title={Grizzly model of fully coupled heat transfer, moisture diffusion,
alkali-silica reaction and fracturing processes in concrete},
author={Huang, Hai and Spencer, Benjamin W},
year={2016},
institution={Idaho National Lab.(INL), Idaho Falls, ID (United States)},
Keywords={Mega; Nonlinear; Damage Mechanics; Moisture analysis; Thermal analysis;
Finite Element; Gravity dam; },
DisplayPdf={0},
```

- Idaho National Laboratory (INL) developed a fully coupled thermo-hydro-mechanical-chemical (THMC) concrete model, referred to as Grizzly, for concrete structures subjected to various aging and degradation mechanisms.

- This program is based on the stress-dependent ASR model proposed by Saouma and Perotti (2006).
- The program also includes a rate-dependent isotropic damage mechanics model to simulate the softening behavior of degraded concrete.
- The concrete gravity dam model of Ulm et al. (2000) was used to implement the fully coupled implicit model.
- The height of the dam and the base's width are 52 and 41 m, respectively.
- The based is fixed.
- Temperature and moisture boundary conditions are: upstream: $T=8^{\circ}\text{C}$, $H=1.0$; downstream: $T=15^{\circ}\text{C}$, $H=0.25$; Initial: $T=8^{\circ}\text{C}$, $H=1.0$.
- Figure 3.121 illustrates simulated damage and vertical stress fields at about 8.2 years. The simulated damage pattern is very consistent with the stress field prior to the occurrence of the damage.
- The mostly damaged region within the concrete dam is ahead of the ASR reaction front. Damage releases the tensile stress within the dam.
- The Figure also shows the moisture diffuseness and relative humidity fields. The damage process has significantly influenced them. Note the small moisture diffuseness right next to the downstream surface.

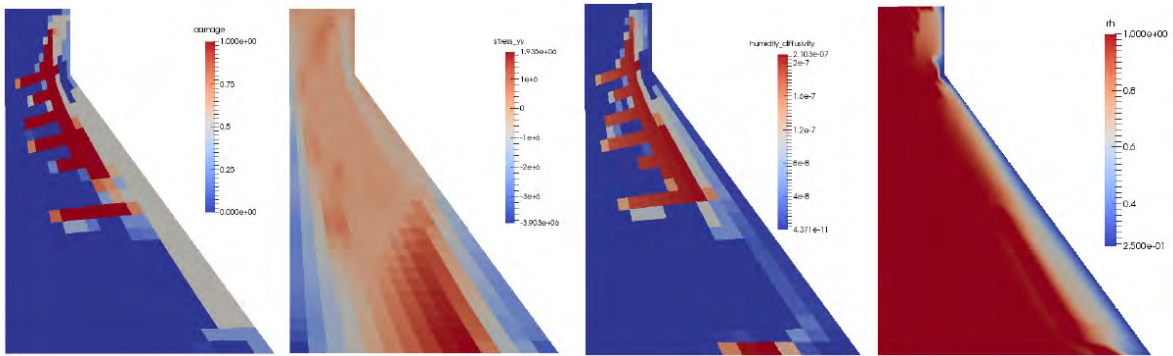


Figure 3.121: Simulated results from ASR; Huang and Spencer (2016)

3.80 Ichikawa, Tsuneki and Kimura, Takahide (2007)

URL

```

@article{
  ichikawa2007effect,
  label={ichikawa2007effect},
  title={Effect of nuclear radiation on alkali-silica reaction of concrete},
  author={Ichikawa, Tsuneki and Kimura, Takahide},
  journal={Journal of Nuclear Science and Technology},
  volume={44},
  number={10},
  pages={1281--1284},
  year={2007},
  publisher={Taylor & Francis},
  url={https://www.tandfonline.com/doi/abs/10.1080/18811248.2007.9711372}
}

```

- Aggregates containing plagioclase as one of the major minerals become sensitive to the ASR by absorbing nuclear radiations.
- The critical dose for making the plagioclase ASR-sensitive is estimated to be 100 MGy for β - and γ -rays.
- Critical dose for fast neutron irradiation has not been measured, but it can be estimated from the radiation-induced amorphization of α -quartz, that is, 1×10^{12} Gy for β - or γ -irradiation and 1×10^{20} n/cm² for fast neutron (> 0.1 MeV) irradiation)
- The rate of the ASR is determined not only from the reactivity of aggregates but also from the moisture content and chemical composition of cement paste.
- Although concrete structures near the pressure vessels are potentially subjected to dry conditions, since they have no external supply of moisture and nuclear radiations decompose water into H₂ and O₂, they may still maintain humid conditions because of their massive structures.
- Irradiation of concrete composed of plagioclase-rich aggregates, such as andesite and alkali-rich cement, may therefore cause the ASR even if the aggregates are initially inert to the alkali-silica reaction.
- Concrete surrounding the pressure vessel of a nuclear reactor as a shielding material receives the highest radiation dose among concrete structures in nuclear power plants.
- The maximum dose rates for the concrete in commercial PWR power plants are approximately 2×10^7 Gy/year for β - and γ -rays and 1×10^{18} n/cm²/year for fast neutrons.
- Concrete structures surrounding the pressure vessels have a possibility of suffering from the radiation-induced ASR shortly after the operation of the power plants, though the radiation effect decreases with increasing distance from the pressure vessels.
- Concrete structures around the pressure vessels are highly reinforced by many iron bars. It should therefore be noted that the acceleration of the ASR does not necessarily mean the loss of the soundness of the concrete structures.

3.81 Islam, Mohammad S and Ghafoori, Nader (2015)

URL

```
@article{
islam2015relation},
label={islam2015relation},
title={Relation of ASR-induced expansion and compressive strength of concrete},
author={Islam, Mohammad S and Ghafoori, Nader},
journal={Materials and Structures},
volume={48},
number={12},
pages={4055--4066},
year={2015},
publisher={Springer}
Keywords={}
```

- The aim is to determine the loss in compressive strength of concrete cylinders due to ASR.
- The expansions of 14 aggregate groups, obtained from the accelerated mortar bar and modified concrete prism tests at various immersion ages, were correlated to the loss in compressive strength of the companion concrete cylinders at the immersion ages of 4 and 28 weeks.
- The mortar bar specimens of dimensions $25.4 \times 25.4 \times 254$ mm were prepared according to ASTM Standards C1260.
- Concrete prisms of dimensions $75 \times 75 \times 250$ mm from each trial aggregate were also prepared according to the requirements of ASTM C 1293.
- For each of the 14 aggregate sources, twelve 102×204 mm cylinders were cast.
- Table 3.122 shows the 4- and 26-week water- and alkali-cured compressive strength and the loss in compressive strength (LICS) of the alkali-cured cylinders at 4 and 26 weeks.
 - Once the immersion age of the water-cured specimens was extended from 4 to 26 weeks, the gain in strength due to increased hydration was greater than the potential loss in strength due to ASR.
 - For the alkali-cured cylinders, the net gain/loss in strength due to increased hydration with an increase in the immersion age from 4 to 26 weeks and the loss due to ASR varied depending upon aggregate source and the extent of ASR-based expansion.
 - The loss in strength of the cylinders made with reactive aggregates was more than the gain in strength due to increased hydration.
 - At the test duration of 4 weeks, the increase in the curing temperature from 20°C to 80°C resulted in about a 10.2% gain in the compressive strength of alkali-cured cylinders.
 - When the immersion age increased from 4 to 26 weeks, depending on the aggregate source and degree of alkali-silica reactivity, the strength gain decreased or strength loss increased with an increase in curing temperature from 20°C to 80°C .
- Next, the failure criteria for ASR-induced loss in compressive strength was determined. For this purpose, the percent loss in the ultimate compressive strength is compared.

Agg. ID	Water-cured cylinders at 20 °C			Alkali-cured cylinders at 80 °C			LICS of alkali-cured cylinders at 4 weeks ^b (%)	LICS of alkali-cured cylinders at 26 weeks ^b (%)
	4-Week average comp. strength, MPa (SD ^a)	26-Week average comp. strength, MPa (SD ^a)	LICS between 4 and 26 weeks (%)	4-Week average comp. strength, MPa (SD ^a)	26-Week average comp. strength, MPa (SD ^a)	LICS between 4 and 26 weeks (%)		
SN-A ^{I₁I₂}	41.04 (1.48)	49.35 (0.49)	-20.2	43.99 (0.77)	58.09 (0.73)	-32.1	-7.2	-17.7
SN-B ^{I₁R₂}	39.46 (1.36)	47.09 (0.33)	-19.3	41.09 (0.85)	41.587 (0.3)	-1.2	-4.1	11.7
SN-C ^{R₁R₂}	29.61 (0.06)	36.74 (0.16)	-24.1	31.56 (0.46)	28.08 (0.65)	11.0	-6.6	23.6
SN-D ^{I₁I₂}	38.75 (1.38)	44.60 (0.19)	-15.1	42.93 (0.9)	45.91 (0.74)	-6.9	-10.8	-2.9
SN-E ^{I₁I₂}	37.32 (1.32)	44.25 (0.85)	-18.6	41.28 (1.23)	58.13 (0.36)	-40.8	-10.6	-31.4
SN-F ^{R₁R₂}	36.82 (0.27)	44.50 (0.61)	-22.2	40.97 (0.65)	36.53 (1.00)	10.8	-11.2	18.8
SN-G ^{R₁R₂}	34.22 (0.59)	40.67 (1.30)	-18.9	35.64 (0.79)	22.33 (0.24)	37.3	-4.2	45.1
SN-H ^{I₁I₂}	37.72 (0.25)	45.08 (0.58)	-19.5	45.68 (2.86)	47.15 (1.58)	-3.2	-21.1	-4.6
SN-I ^{I₁I₂}	32.32 (0.32)	38.28 (0.48)	-18.4	34.63 (0.29)	38.98 (0.94)	-12.6	-7.1	-1.8
SN-J ^{R₁R₂}	33.72 (1.14)	39.67 (0.12)	-17.6	38.75 (2.24)	35.02 (0.16)	9.6	-14.9	11.7
NN-A ^{I₁I₂}	43.01 (1.27)	52.03 (0.61)	-21.0	48.26 (0.49)	53.53 (1.17)	-10.9	-12.2	-2.9
NN-B ^{R₁R₂}	34.86 (0.45)	41.65 (0.16)	-19.5	27.16 (0.87)	23.63 (0.51)	13.0	22.1	43.3
NN-C ^{R₁R₂}	33.14 (0.64)	39.14 (0.52)	-18.1	34.65 (0.47)	28.99 (0.56)	16.3	-4.5	25.9
NN-D ^{R₁R₂}	33.62 (0.31)	40.09 (0.74)	-19.3	39.49 (1.18)	38.79 (0.55)	1.8	-17.5	3.2

Negative sign (-) indicates gain in compressive strength; 1 MPa = 145.0378 psi

I₁ and I₂ innocuous based on the extended failure limits of mortar bars and alkali-cured prisms, respectively

R₁ and R₂ reactive based on the extended failure limits of mortar bars and alkali-cured prisms, respectively

^a Standard deviation of three cylinders

^b Compared with water-cured cylinders

Figure 3.122: Percent loss in compressive strength (LICS) of concrete cylinders; Islam and Ghafoori (2015)

- Failure criteria of the 26-week LICS of alkali-cured cylinders is studied.
- First, it is correlated by expansions of the mortar bars containing companion aggregates at the ages of 14, 28, and 56 days. An equation is proposed as:

$$\text{LICS} = a + b \times (\text{MEXP})^2 + \frac{c}{(\text{MEXP})^2} \quad (3.11)$$

where LICS is loss in compressive strength in percentage; MEXP is mortar expansion (%); a , b and c are the regression parameters (Table 3.123).

- Next, it is correlated with the expansions of the alkali-cured prisms at the ages of 4, 8, 13, and 26 weeks. An equation is proposed as:

$$\text{LICS} = a + b \times (\text{MEXP}) + c \times (\text{MEXP})^{0.5} \quad (3.12)$$

where the regression parameters are based on Table 3.124.

- Results concluded that the compressive strength generally was not sensitive to ASR at early age; however, it was significantly impacted at the extended immersion age when excessive expansions and cracks were experienced.

Variables	Immersion age (weeks)		
	2	4	8
Regression parameters			
<i>a</i>	10.44003	7.01019	6.441354
<i>b</i>	33.43641	15.56001	9.92697
<i>c</i>	-0.02984	-0.07821	-0.14051
Prob(<i>t</i>) of regression parameters			
<i>a</i>	0.01750	0.14265	0.27919
<i>b</i>	0.00117	0.00296	0.01201
<i>c</i>	0.00073	0.00654	0.03287
Prob(<i>F</i>)	0.00013	0.00002	0.00034
R^2	0.89	0.88	0.75
Expansion limits of mortar bars (%)	0.10	0.33 (0.28)	0.48 (0.47)
Failure criteria of the 26-week loss in compressive strength of alkali-cured cylinders (%)	7.8	8.0 (7.2)	8.1 (8.0)

Figure 3.123: Statistical parameters of Eq. 3.11; Islam and Ghafoori (2015)

Variables	Immersion age (weeks)			
	4	8	13	26
Regression parameters				
<i>a</i>	-63.54455	-45.04291	-57.02533	-51.43838
<i>b</i>	-356.61172	-48.73734	-79.50510	-19.99951
<i>c</i>	382.40086	157.41135	190.13714	122.07975
Prob(<i>t</i>) of regression parameters				
<i>a</i>	0.00129	0.00740	0.02244	0.02347
<i>b</i>	0.02886	0.57476	0.43492	0.75187
<i>c</i>	0.00272	0.04997	0.07172	0.11531
Prob(<i>F</i>)	0.00011	0.00008	0.00094	0.00031
R^2	0.90	0.88	0.83	0.83
Expansion limits of ASTM C 1,293 M (%)	0.040	0.105	0.165	0.285
Loss in compressive strength of alkali-cured cylinders at 26 weeks (%)	-1.3	8.5	7.1	8.0

Figure 3.124: Statistical parameters of Eq. 3.12; Islam and Ghafoori (2015)

3.82 Jensen, Viggo (2004)

URL

```

@article{
jensen2004alkali},
label={jensen2004alkali},
title={Alkali--silica reaction damage to Elgeseter Bridge, Trondheim, Norway: a
review of construction, research and repair up to 2003},
author={Jensen, Viggo},
journal={Materials characterization},
volume={53},
number={2-4},
pages={155--170},
year={2004},
publisher={Elsevier}
Keywords={}

```

- Elgeseter Bridge was built from 1949 to 1951 and is a unique design for Norwegian construction in this era.
- It is a continuous, 200 m long, reinforced concrete bridge with only one expansion joint at its northern end.
- Norwegian standard valid in 1950 requires two concrete qualities: A: 31.9 MPa, and AA:39.6 MPa.
- Concrete quality in abutments and beams, as well as foundations, should be “A”, while concrete quality should be “AA” in the columns.
- The field measurements revealed a mean f'_c of 34.2 MPa with a coefficient of variation of 12.3% for abutments/beams; a 39.1 MPa mean with a COV of 7.1% for the foundation; and a mean of 40.8 MPa with a COV of 16.2% for the columns.
- In the early 1990s, deleterious ASR was investigated. The reaction explains the observed expansions and concrete cracking.
- Damage due to ASR occurred most severely on the western face of the structural elements which are exposed to the middle of the river.
- Relative humidity is generally high (100%), and cracks expand at a maximum rate of 0.15 mm/year.
- Between 1990 and 1991, lab investigations were performed. Three cores with diameter of 100 mm, 300 mm, and 400 mm in length were taken from different columns.
- Figure 3.125 (left) shows the percentage of cracked aggregates in cores related to the maximum crack width in the structure. There is large uncertainty in the data with a relatively poor coefficient of determination for the polynomial.
- Figure 3.125 (right) plots percentage of the cracked aggregate vs. cracks in cement paste. The Figure shows an acceptable correlation; therefore, it can be inferred that ASR has caused most of the cracks which occur in the paste.

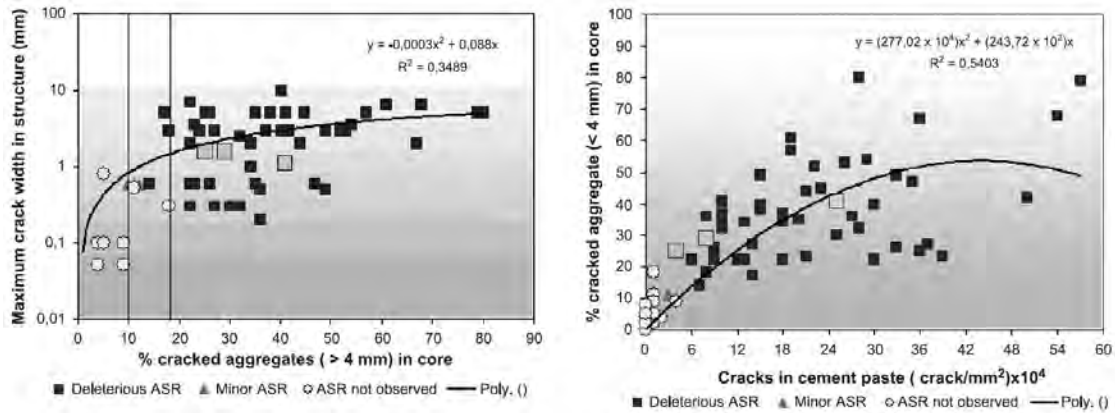


Figure 3.125: Percentage of cracked aggregates and the relation with the maximum crack width in the structure and the cracks in cement paste; Jensen (2004)

- In the Elgeseter Bridge, the relative humidity varies from 100% to 87%. RH is significantly higher on the western faces exposed to rainwater relative to the eastern faces. Rainwater is, therefore, suggested to be the most important source of water in concrete structures exposed to Norwegian climatic conditions.
- A survey of the crack distribution in columns shows that crack widths vary from 0.05 to 3 mm and the number of cracks in the columns varies from 5 to 19.
- Impregnation with monosilane reduces the concrete's relative humidity 50 mm from the surface, even if the columns are massive and ASR occurs in an advanced stage.
- Since the only expansion joint is reduced to near zero in 2003, renovation of the bridge is urgent.

3.83 Jensen, Viggo (2012)

```
@article{
jensen2012reclassification},
label={jensen2012reclassification},
title={Reclassification of alkali aggregate reaction},
author={Jensen, Viggo},
journal={Proc. 14th ICAAR},
volume={1},
pages={031111},
year={2012},
Keywords={Laboratory; Field; Expansion Assessment/monitoring Aggregate; Grain size
},
DisplayPdf={0},
```

- A new classification system based on “reactivity rate” and “negative lists” of reactive constituents with aggregates designated “very fast reactive AAR”, “fast reactive ASR”, and “slow reactive ASR” is presented.

- It suggests that the reaction mechanism for slow reactive aggregates are different compared to fast reactive aggregates and occur in five stages.
- The group “very fast reactive AAR” includes argillaceous dolomitic limestone supposed to be Alkali Carbonate Reactive (ACR) and certain very unstable siliceous constituent suggested to be Alkali Silica Reactive (ASR). “Very fast reactive AAR” is not recommended to be used in concrete without special precautions.
- For the groups “fast reactive ASR” and “slow reactive ASR”, precautionary measures are suggested as guidance.
- AAR is traditionally subdivided into 3 subgroups based on supposed different reaction mechanisms and expansion mechanisms, namely 1) Alkali Silica Reaction (ASR), 2) Alkali Silicate Reaction (ASiR) and 3) Alkali Carbonate reaction (ACR).
- The traditional explanation of the reaction mechanism of the two last reactions (ASiR) and (ACR) are questioned today and supposed to none exist or not to be the mechanism causing expansion of concrete.
- Various characteristics of three reactions are summarized in Figures 3.126 to 3.128.

TABLE 1: Reactive minerals and rock types, <i>list from RILEM AAR-1 2003, ANNEX A.1.2 and A.1.3 [1]</i>		
Reaction type	Reactive minerals	Reactive rock types
Very fast reactive AAR	<i>fine dolomite crystals?, expansive clay minerals?, disseminated sub microscopic opal/quartz/chalcedony, certain siliceous volcanic glass (hydrated or devitrified), certain artificial glass and possibly in rare cases also cristobalite and tridymite.</i>	certain argillaceous dolomitic limestone (ACR), certain rhyolite, tuff and siliceous volcanic rock with volcanic siliceous glass, artificial alkali-silica rich glass and <i>undispersed silica dust</i>
Fast reactive ASR	opal, opaline silica, chalcedony, chalcedonic silica, certain volcanic and artificial glass and cryptocrystalline quartz. Possible alkali contribution from feldspar	siliceous limestone, <i>metamarl</i> , opaline sandstone, rhyolite, andesite, basalt with glass or opal, <i>porous flint</i> , certain chert and flint or any rock containing sufficient content of the reactive minerals.
Slow reactive ASR	cryptocrystalline and microcrystalline quartz, highly strained quartz with sub grain development and re-crystallized quartz. Possible alkali contribution from feldspar.	sandstone, siltstone, clay stone, phyllite, argillite, quartzite, mylonite, cataclasite, metarhyolite, certain greywacke, certain hornfels, certain granite and gneiss or any rock containing sufficient content of the reactive minerals.
<i>Cursive not included in RILEM AAR-1, ANNEX A.1.2 and A.1.3 [1]</i>		
Note 1: Alkali Carbonate Reaction might be alkali silica reaction which exclude dolomite crystals and expansive clays		
Note 2: Many of the slow reactive rock types were formerly included “Alkali Silicate Reaction” (ASiR) and SLEASS		

Figure 3.126: Reactive minerals and rock types; Jensen (2012)

Reaction type	Behaviour in concrete	Microscopic characteristic
Very fast reactive AAR	<u>Alkali carbonate reaction (ACR):</u> Reaction caused by coarse particles. Pessimism relation not observed. Rapid expansion in concrete expansion tests. <u>Silicious constituents:</u> same as fast reactive ASR, see next	<u>Alkali carbonate reaction (ACR):</u> Fine dolomite rhombs. Peripheral calcite rim and outer calcite rim in contact zone to cement paste. Reaction products difficult to observe in thin section (but sometimes possible). Internal cracking and cracks running out in cement paste. SEM/EDX analyses recommended <u>Silicious constituents:</u> see fast reactive ASR
Fast reactive ASR	Reaction caused mostly by fine particles and less coarse particles? Pessimism relation caused by varying content of reactive constituents and particle size. Rapid expansion in expansion tests.	Amorphous (sometimes recrystallized) gel in aggregate and cement paste. "Portland free" zone around reacted aggregates and gel filled cracks. Internal cracking and cracks running out in cement paste. Dissolution of constituents internal in reacted aggregates.
Slow reactive ASR	Reaction caused by coarse particles (> 1 mm). Pessimism relation not observed. Delayed expansion in expansion tests.	Cryptocrystalline reaction products in aggregates. Amorphous (sometimes recrystallized) gel in cement paste and contact zone. Dense peripheral rim in reacted aggregates. Internal cracking and cracks running out in cement paste. Dissolution of constituents in reacted aggregates. Main crack in aggregate.

Figure 3.127: Behaviours in concrete and microscopic characteristics; Jensen (2012)

Reaction type	eq. Na ₂ O	kg eq. Na ₂ O/m ³ concrete	Low lime fly ash, blast furnace slag
Very fast reactive AAR	<i>No limits can be recommended</i>	<i>No limits can be recommended</i>	<i>No precautionary measures are known For some argillaceous dolomitic limestone high replacement of blastfurnace slag</i>
Fast reactive ASR	Max 0,6 %	<i>Min. 2.5 – 3.0</i>	<i>Min. 40 % fly ash replacement Min. 50 % blastfurnace slag replacement</i>
Slow reactive ASR	Max 0,8 %	<i>Min. 3.0 – 3.5</i>	<i>Min. 25 % fly ash replacement Min. 40 % blastfurnace slag replacement Min. 8 % silica fume replacement Min. 15 % metakaolin replacement</i>
<i>Low reactivity (correspond to non-reactive in RILEM AAR-O)</i>	No requirement	<i>None required</i>	<i>Any fly ash replacement Any fly slag replacement</i>

Limits from RILEM AAR-7.1(cursive) [22]. Fast reactive ASR values from "high reactivity aggregates" and slow reactive ASR values from "medium reactivity aggregates". RILEM AAR-7.1 specifies not which types of aggregate are highly reactive or medium reactive so the values shall be used with care.

Figure 3.128: Precautionary measures, cements (eq. Na₂O) and kg eq. Na₂O/m³ concrete and additive replacement of cement contents; Jensen (2012)

3.84 Ju, Taeho and Achenbach, Jan D and Jacobs, Laurence J and Guimaraes, Maria and Qu, Jianmin (2017)

URL

```
@article{
ju2017ultrasonic,
label={ju2017ultrasonic},
title={Ultrasonic nondestructive evaluation of alkali--silica reaction damage in
concrete prism samples},
author={Ju, Taeho and Achenbach, Jan D and Jacobs, Laurence J and Guimaraes, Maria
and Qu, Jianmin},
journal={Materials and Structures},
volume={50},
number={1},
pages={60},
year={2017},
publisher={Springer},
url={https://link.springer.com/article/10.1617/s11527-016-0869-6}
```

- Presents a study that used ultrasonic techniques to nondestructively evaluate (NDE) the damage induced by alkali-silica reaction (ASR) in concrete.
- Study was conducted on concrete prism samples that contained reactive aggregates and were subjected to different ASR conditioning.
- The ultrasonic NDE techniques used in the study included measuring wave speed, attenuation and the amplitude of mixed wave in order to accurately calculate the acoustic nonlinearity parameter.
- Results of the study show that ASR damage reduces wave speed and increases the wave attenuation in concrete.
- Neither wave speed nor attenuation is sensitive enough to ASR damage to be considered a good measure for the quantitative NDE of ASR damage in concrete.
- The acoustic nonlinearity parameter, on the other hand, shows a greater sensitivity to ASR damage, and can thus be used to nondestructively track ASR damage in concrete.
- Due to the significant attenuation caused by ASR induced microcracks and scattering by the aggregates, attenuation measurements also need to be conducted in order to accurately measure the acoustic nonlinearity parameter.
- Destructive tests were conducted to measure the compressive strength of the concrete prisms subjected to different ASR conditioning. It was found that the measured acoustic nonlinearity parameter is well-correlated with the reduction of the compressive strength induced by ASR damage.

3.85 Kagimoto, Hiroyuki and Yasuda, Yukihiro and Kawamura, Mitsunori (2014)

URL

```
@article{
kagimoto2014asr},
label={kagimoto2014asr},
title={ASR expansion, expansive pressure and cracking in concrete prisms under
various degrees of restraint},
author={Kagimoto, Hiroyuki and Yasuda, Yukihiro and Kawamura, Mitsunori},
journal={Cement and Concrete Research},
volume={59},
pages={1--15},
year={2014},
publisher={Elsevier}
Keywords={}
```

- The characteristics of expansive pressure in concrete prisms ($100 \times 100 \times 400$ mm) were studied under various degrees of uniaxial restraint.
- Two concrete mixtures were studied in which the maximum aggregate size is identical while the w/c ratio and sand ratio vary. The mixtures are named as C_A and C_B . Various amounts of NaOH were added to produce concretes with alkali contents of 3.6, 5.4, 6.0, 6.4, 7.2, 9.0 and 9.6 kg/m³.
- Relationships between expansive pressure and the degree of restraint in concretes with various alkali contents were nearly linear in the range of low degree of restraint.
- Increased rates in expansive pressure with the degree of restraint were drastically reduced above a critical degree of restraint.
- In Figure 3.129 (left), longitudinal expansions were plotted against transversal expansions measured in all the concrete specimens (under restraint). An anisotropy coefficient obtained as the slope of regression line was 3.07. Expansions in the concretes under restraint are found to be anisotropic.
- Plotting all of the expansions measured in the transversal direction against those in the longitudinal direction after the release of restraint gives Figure 3.129 (right). This figure clearly indicates that the former expansions were greater than the latter ones in most concretes. An anisotropy coefficient as the slope of regression line was 1.46.
- This slope (1.46) is less than previous one (3.07). Thus, an anisotropic coefficient for concretes under restraint was greater than that for concretes after the release of restraint.
- Expansions were promoted in a direction perpendicular to the restraining direction.
- After the release of restraint, concrete prisms continued to expand for several months, and ultimate expansions in the transversal direction were greater than those in the longitudinal direction.

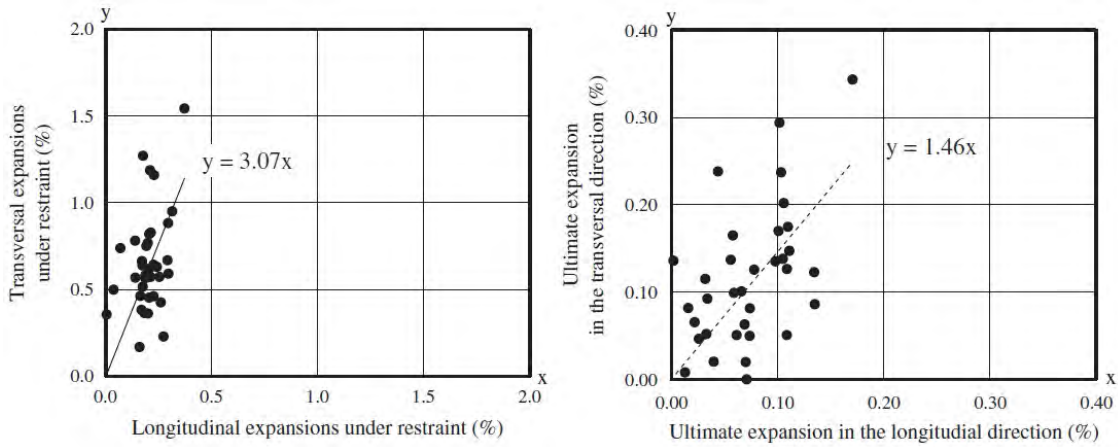


Figure 3.129: Schematic subdivision of the swelling curve; Kagimoto, Yasuda, and Kawamura (2014)

- Surface cracks appeared in concrete prisms under restraint oriented toward the direction of restraint. Some of internal cracks were visible on the surfaces of the concrete prisms.
- Figure 3.130 shows time-dependent changes in compressive strength and the modulus of elasticity.
- Compressive strength and modulus of elasticity decrease with increasing amounts of alkali.
- Compressive strength of concretes with alkali contents of 3.6 and 5.4 kg/m³ increased with age up to 28 days, and even thereafter rose a little; however, compressive strength of concretes with alkali contents greater than 6.6 kg/m³ rose only a little or decreased with age. Reductions in the modulus of elasticity in concretes with alkali contents greater than 6.0 kg/m³ after 28 days were especially remarkable.

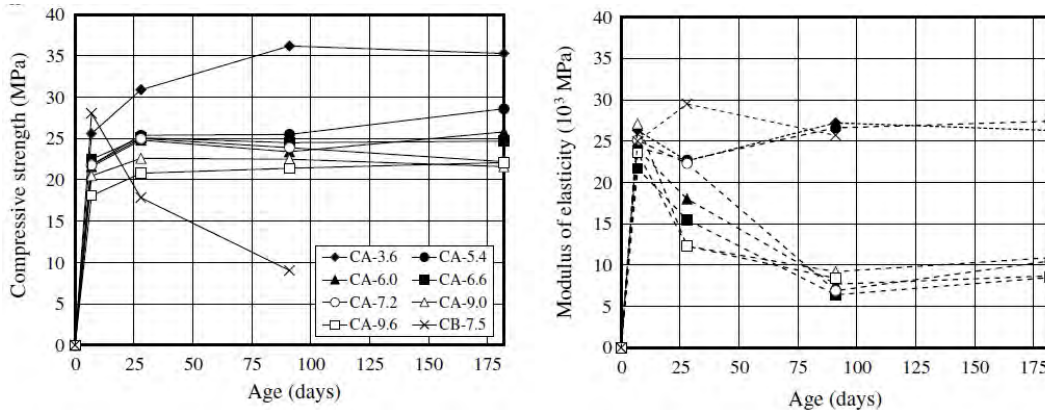


Figure 3.130: Changes in compressive strength and modulus of elasticity with age in concretes; Kagimoto, Yasuda, and Kawamura (2014)

3.86 Kobayashi, Kazuo and Inoue, Susumu and Yamasaki, Takao and Nakano, Kin-ichi (1988)

URL

```
@article{
kobayashi1988alkali},
label={kobayashi1988alkali},
title={Alkali aggregate reaction in prestressed concrete beams},
author={Kobayashi, Kazuo and Inoue, Susumu and Yamasaki, Takao and Nakano,
Kin-ichi},
journal={International Journal of Cement Composites and Lightweight Concrete},
volume={10},
number={4},
pages={233--240},
year={1988},
publisher={Elsevier}
Keywords={Mega; New Const. Model; Nonlinear ; Finite Element; Dam Gravity;
Expansion monitoring; }
```

- Time-dependent strains are measured on a total of ten pre-stressed concrete beams.
- The tested beams had rectangular cross sections 10×20 cm and lengths of 160 cm.
- Two levels of prestress, each corresponding to approximately 4.90 MPa and 9.80 MPa at the lower fiber of the cross section, were introduced by tensioning an 11/15 mm diameter prestressing bar.
- Both the sound (named as mix-I) and ASR affected (mix-II and mix-III) concretes are studied.
- An accelerated curing condition of 40°C and 100% RH is used.
- The shear span to effective depth ratio of 2.5 and 4.0 are studied.
- The four-point bending test was conducted to determine the load carrying capacity.
- The compressive strength, tensile strength, and elastic modulus of mix-III ASR concrete was reduced by approximately 60%, 50% and 45%, respectively, of mix-I normal concrete after curing under 40°C and 100% RH. Those of mix-II ASR concrete, however, showed very little decrease.
- Longitudinal ASR expansion can be restrained by introduction of a prestressing force, yet the effect depends strongly on the amount of the prestress.
- All mix-III ASR beams, as well as mix-I normal and mix-II ASR beams, failed finally in flexure irrespective of shear span to effective depth ratio of 2.5 and 4.0.
- The reduction in the ultimate strength of the ASR beam is about 10% compared to that of the normal beam.
- No remarkable differences in the overall shape of the load-deflection curve up to failure were observed among the comparable beams of the three types of mixes.
- Failure models are shown in Figure 3.131.



Figure 3.131: Failure modes; Kobayashi et al. (1988)

3.87 Kubat, Thamer and Al-Mahaidi, Riadh and Shayan, Ahmad (2016)

URL

```
@article{
kubat2016strain},
label={kubat2016strain},
title={Strain development in CFRP-wrapped circular concrete columns affected by
alkali-aggregate reaction},
author={Kubat, Thamer and Al-Mahaidi, Riadh and Shayan, Ahmad},
journal={Construction and Building Materials},
volume={113},
pages={603--612},
year={2016},
publisher={Elsevier}
Keywords={}
```

- Fiber reinforced polymer (FRP) is one of the materials that can be used for the rehabilitation of concrete columns affected by AAR.
- A number of cylindrical columns 200 mm in diameter and 500 mm in height were fabricated from reactive concrete using fused silica and additional alkali in its ingredients.
- At different periods during AAR development (i.e., 7, 15, 30, 45, 60, 90 and 120 days after casting) external confinement by carbon fiber reinforced polymer (CFRP) was applied.
- Results indicate that the efficiency of CFRP application in reducing AAR expansion depends on the time of CFRP wrapping and on the number of CFRP layers applied to the columns.
- The rate of radial and axial expansion could be reduced by CFRP confinement; however, the expansion still continued (i.e. AAR expansion did not cease by CFRP wrapping).
- The CFRP confinement of columns at early ages shows improved performance in reducing expansion than CFRP confinement at later ages.
- The use of two layers of CFRP at the ages 30 and 60 days is more effective in restraining AAR expansion than one layer of CFRP due to the increase in stiffness which causes increased confinement pressure on the expanding concrete.
- The maximum deformations values reached at one year of age did not exceed the 15% and 17% of strain capacity of one and two layers of CFRP, respectively; the potential efficiency of using CFRP wrapping to improve the strain capacity of the confined affected columns by AAR under loadings.

- The efficiency of reducing AAR expansion depends upon the time of CFRP wrapping and on the number of CFRP layers applied to the column.
- The efficiency of CFRP wrapping would be larger when natural aggregates of lower expansion capacity are used compared to the fused silica.

3.88 Lamea, M and Mirzabozorg, H (2015)

URL

```
@article{
lamea2015evaluating},
label={lamea2015evaluating},
title={Evaluating Sensitivity of an AAR-Affected Concrete Arch Dam to the Effects
of Structural Joints and Solar Radiation},
author={Lamea, M and Mirzabozorg, H},
journal={Strength of Materials},
volume={47},
number={2},
pages={341--354},
year={2015},
publisher={Springer}
Keywords={}
```

- The impact of AAR on static analysis of a high arch dam was studied.
- Dez Dam was used as case study. The Dam's height is 203 m from the foundation and 190 m from the riverbed. The thicknesses at the crest elevation and base of the Dam's crown cantilever are 4.5 and 21 m, respectively.
- The Dam's body and saddle (Pulvino) were modeled using 648 and 144 elements.
- Concrete was assumed to be linear elastic.
- Contraction joints were modeled with node-to-node contact elements.
- ANSYS commercial finite element code was used for all the simulations.
- Results of initial thermal analysis included the solar radiations effect as reported in Mirzabozorg et al. (2014).
- The displacement time history of the crest for different simulations is shown in Figure 3.132.
- Based on horizontal displacement:
 - The solar radiation does not significantly affect crest displacements in US/DS direction.
 - On the other side, joints tend to move the crest downstream;
 - These effects are mitigated when AAR damages the Dam's body.
 - AAR causes some deviation of the crest upstream; this is more distinguished when contraction joints are present in the conducted analysis.

- Based on vertical displacement:
 - Same as horizontal displacement.
- Solar radiation effect is not disregarable in the first half of the history duration pertinent to AAR-affected cases.
- In contrast to the horizontal displacements, in all of the AAR-affected cases, the vertical displacements are not considerably affected by modeling none of the solar radiation or the contraction joints.

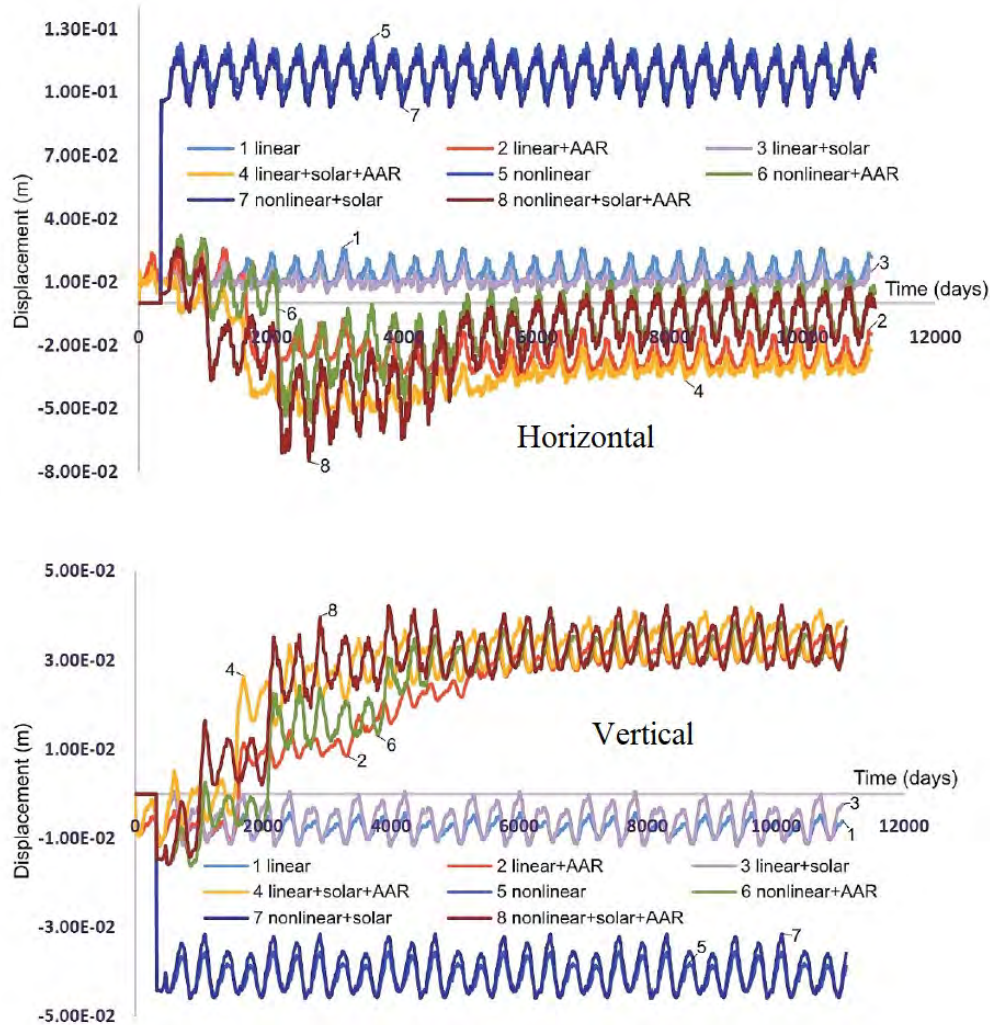


Figure 3.132: Comparison of displacements at crest of the Dam; Lamea and Mirzabozorg (2015)

- Figure 3.133 shows the contours of the 1st principal stresses on the downstream face for 1800 days for different assumptions.
- Effects of solar radiation and vertical joints are obvious.
- The final results demonstrate the high importance of both solar radiation and joints when stresses are evaluated; however, the effect of solar radiation is disregarable when only crest

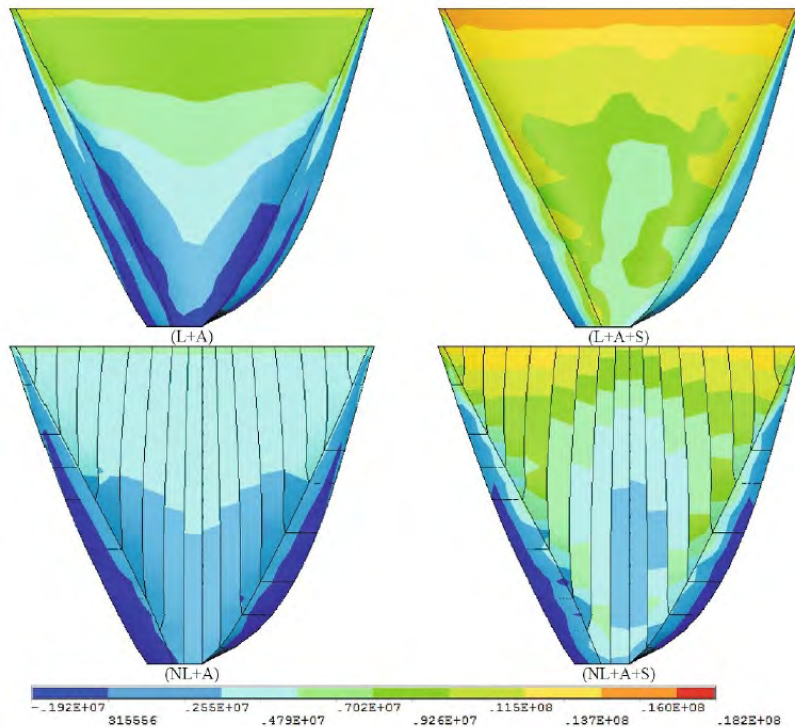


Figure 3.133: Contours of the 1st principal stresses on downstream face for the time of 1800 days (L: Linear; A: AAR; NL: Joint); Lamae and Mirzabozorg (2015)

displacements are considered. The deduction is somehow different, though, when responses of a middle step are compared.

3.89 author="Lancon, H. and Piot, S. (2011)

```
@incollection{
lancon2011new},
label={lancon2011new},
booktitle={Dams and reservoirs under changing challenges},
editor={Schleiss, Anton J and Boes, Robert M},
year={2011},
title="A new approach for large structures monitoring: SCANSITES 3D",
author="Lancon, H. and Piot, S.",
publisher={CRC press},
Keywords={Field; Gravity dam; Arch dam; },
DisplayPdf={0},
```

- Two monitoring devices and methodologies are widely used for large dams' safety management: visual inspection and geometric survey.
- A new approach is introduced using an exhaustive and numeric method called "SCANSITES 3D".

- It is based on the combination of an advanced tool (to provide numeric defects inspection on large structures) and new wide ranged Lidar technologies (aiming to deliver geometric exhaustive mapping, and photogrammetric coverage).

3.90 Leemann, Andreas and Merz, Christine (2013)

URL

```
@article{
leemann2013attempt},
label={leemann2013attempt},
title={An attempt to validate the ultra-accelerated microbar and the concrete
performance test with the degree of AAR-induced damage observed in concrete
structures},
author={Leemann, Andreas and Merz, Christine},
journal={Cement and Concrete Research},
volume={49},
pages={29--37},
year={2013},
publisher={Elsevier}
Keywords={}
```

- This research is conducted to validate the ultra-accelerated microbar and the concrete performance test with the degree of AAR-induced damage observed in concrete structures.
- Aggregates used in structures damaged by AAR were analyzed with the microbar test and the concrete performance test.
- Next, the samples were examined using optical and scanning electron microscopy.
- The agreement of measured expansion, reacted rock types, and the composition of the reaction products between the on-site concrete and the reproduced concrete subjected to the CPT clearly indicates that the reaction mechanisms in the structure and in the concrete performance test are comparable.
- Comparing the expansions determined with the microbar test (MBT) and the CPT reveals the limitations of the former:
 - There is no correlation between microbar expansion and expansion in the CPT. Even the use of aggregates classified as non-reactive in the MBT can result in concrete expansion exceeding the limit value (called false positives).
 - Ultra-accelerated expansion tests like the MBT must be examined very critically.
 - Reproducing the concrete of damaged structures, testing it with the CPT, and analyzing it with microscopy allow a validation of the accelerated test:
 - * The majority of the lab concrete mixtures exceeds the limit value for expansion at a cement content of 300 kg/m³ while all concrete mixtures, except the non-reactive reference, exceed it at a cement content of 400 kg/m³.
 - * Expansion rates determined with crack measurements on structures in advanced state of AAR and expansion in the CPT show a good correlation.

- * The same rock types react frequently (above average) in on-site concrete but rarely (below average) in lab concrete.
 - * The chemical composition of the reaction products is very similar in both on-site and lab concrete.
- The concrete performance test appears to be an appropriate tool to test the potential reactivity of specific concrete mixtures.

3.91 Leemann, Andreas and Griffa, Michele (2013)

URL

```
@article{
leemann2013diagnosis,
label={leemann2013diagnosis},
title={Diagnosis of alkali-aggregate reaction in dams},
author={Leemann, Andreas and Griffa, Michele},
journal={EMPA, Materials Science \& Technology},
year={2013},
publisher={Citeseer}
```

- Excellent comprehensive study on the diagnosis of AAR in dams.
- Full report can be freely downloaded.

1. INTRODUCTION
 - 1.1 GENERAL INFORMATION5
 - 1.2 DIAGNOSIS
2. STUDIES IDENTIFYING AAR IN DAMS
3. METHODS FOR AAR IDENTIFICATION
 - 3.1 INTRODUCTION
 - 3.2 VISUAL INSPECTION
 - 3.2.1 On-Site
 - 3.2.2 Cores
 - 3.3 OPTICAL MICROSCOPY
 - 3.3.1 Introduction
 - 3.3.1.1 General information
 - 3.3.1.2 Sample selection
 - 3.3.1.3 Sample preparation
 - 3.3.2 Diagnosing AAR
 - 3.3.2.1 Crack patterns
 - 3.3.2.2 AAR products
 - 3.4 SEM COMBINED WITH EDX
 - 3.4.1 Introduction
 - 3.4.2 Characteristics of the reactions products
 - 3.4.2.1 Advanced stage of AAR
 - 3.4.2.2 Initial stage of AAR
 - 3.5 SOME REMARKS ABOUT ALKALI-CARBONATE REACTION

3.6 SOME REMARKS ABOUT ETTRINGITE FORMATION AND IRON SULFIDE OXIDATION
3.7 CONCLUSIONS AND OUTLOOK
4. METHODS FOR ASSESSING THE EXTENT OF AAR
4.1 INTRODUCTION
4.2 MACROSCOPIC MEASUREMENTS
4.3 MICROSCOPY
4.4 MECHANICAL TESTS
4.5 NON-DESTRUCTIVE EVALUATION (NDE)
4.5.1 NDE with linear sound/ultrasounds
4.5.2 NDE with nonlinear sound/ultrasounds
4.5.3 NDE with X-ray tomographic microscopy
4.6 CONCLUSIONS AND OUTLOOK
5. PROGNOSIS
6. RELATION BETWEEN DIAGNOSIS AND MODELING
7. SUMMARY
8. REFERENCES

3.92 Leemann, A and Lura, P (2013)

URL

```
@article{
leemann2013modulus},
label={leemann2013modulus},
title={E-modulus of the alkali--silica-reaction product determined by
micro-indentation},
author={Leemann, A and Lura, P},
journal={Construction and Building Materials},
volume={44},
pages={221--227},
year={2013},
publisher={Elsevier}
Keywords={}
```

- The modulus of elasticity of the ASR product determined by micro-indentation was studied.
- As a side result, Vickers hardness and indentation are also determined on undried, polished concrete samples taken from a structure damaged by ASR.
- Both the indentation tests and the chemical analysis by EDX performed on the ASR product in different aggregates indicate that the concrete is relatively homogeneous.
- The studied concrete originates from a 45 year old ASR-affected bridge in Switzerland.
- The compressive strength of the concrete is between 70 and 80 MPa.
- The E -modulus was calculated from the indentation modulus, E_i , using $E = \frac{E_i}{1-\nu^2}$. A Poisson's ratio of 0.18 was assumed in this equation.

- To assess the influence of load level, the indentation was performed running with four loading levels ranging from 6 to 50 mN. The E -modulus decreases when decreasing the load from 50 mN to 12 mN, Figure 3.134 (left). No further decrease is observed when decreasing the load from 12 mN to 6 mN.
- An increase in E -modulus of about 20% while increasing the load from 6 and 12 mN to 50 mN was observed.

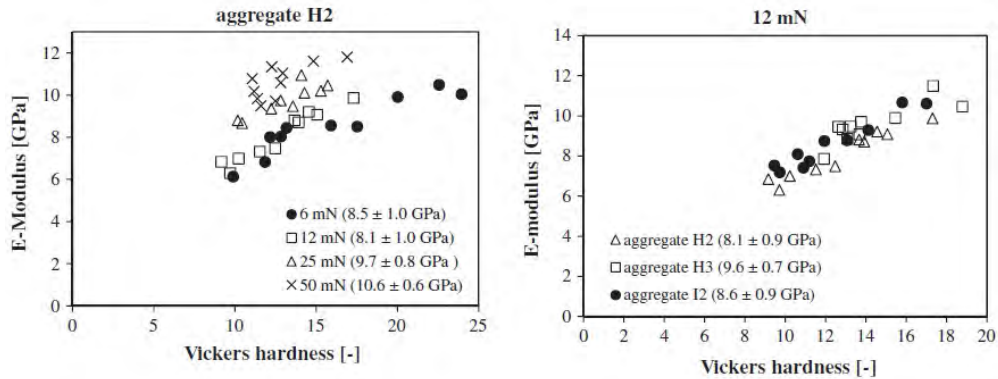


Figure 3.134: E -modulus as a function of Vickers hardness of the reaction product different loading levels (left); In the central area of three different aggregates tested with a load of 12 mN (right); Leemann and Lura (2013)

- The variation of the average E -modulus from aggregate to aggregate is lower than the variation of single measurements within one aggregate, Figure 3.134 (right).
- In contrast to the E -modulus, there is no systematic change in Vickers hardness with increasing load. The determined values range from 10 to 19.
- E -modulus varies between 7 and 9 GPa.
- Toward the edge of the aggregates the values for Vickers hardness and E -modulus increase.

3.93 author="Leroy, R. and Boldea, L.I. and Seignol, J.F. and Godart, B. (2011)

```
@incollection{
  leroy2011reassessment},
label={leroy2011reassessment},
booktitle={Dams and reservoirs under changing challenges},
editor={Schleiss, Anton J and Boes, Robert M},
year={2011},
title="{Re-assessment and treatment-design of an ASR-affected gravity dam}",
author="Leroy, R. and Boldea, L.I. and Seignol, J.F. and Godart, B.",
publisher={CRC press},
Keywords={Mega; Sensitivity; Parametric; Finite Element; Gravity dam; Field;
  Expansion Assessment/monitoring },
DisplayPdf={0},
```

- The abnormal crest displacements due to ASR in a gravity dam is studied over 50 years.
- The polygonal shape of the dam amplifies the effect of concrete expansion in the bends and could result in excessive stresses.
- Numerical modeling with ASR effects is investigated.
- The Salanfe Dam in Switzerland is selected as case study.
- It is a concrete dam classified in the gravity-dam category. The upstream face is vertical and the downstream face has a slope of 1:0.742, and 1:0.2 (crest level).
- The crest length can be divided into 4 straight sections. The total length at the crest is 616.65 m; the maximum height above the foundations is 52 m. The Dam consists of 42 blocks which are, for the most part, 14 m long and separated by construction joints.
- The Dam is equipped with several monitoring systems as pendulums, extensometers, a geodetic, and a leveling network.
- The Dam is deformed due to concrete swelling noticeable since 1970.
- In 2001 the presence of ASR was confirmed, having observed relatively important cracking, particularly around the left bank bend, as well as irreversible upstream displacements of the structure.
- The numerical model used to assess ASR-affected concrete structures is implemented in the ALKA modulus in FEM-software CESAR-LCPC.
- A chemo-mechanical model is used for concrete.
- Both 2D and 3D models are studied.
- Preliminary tests on 2D-models lead to the following conclusions, Figure 3.135:
 - Although the Dam was built with different concrete mix-designs (with various cement quantities), the global behavior was best represented by considering a homogeneous expansion potential.
 - The ASR-induced deformation and its kinetics are poorly influenced by temperature variations and temperature-field heterogeneity, as long as these variations remain in a reasonable range (tests were conducted with mean temperature varying from 4 to 8°C according to locations).
 - Global upward and upstream crest displacement are better obtained with homogeneous moisture field in the Dam.
 - The 2D-models seem unable to correctly represent the real structure behavior since a large part of the observed displacement is due to the “arched” shape of the Dam.
- Next, 3D FE model is prepared:
 - The mesh is composed of 28,589 quadratic elements and a total of 128,861 nodes, Figure 3.136.
 - The rock around the Dam is considered to be of uniform quality and therefore consisting of a single material.

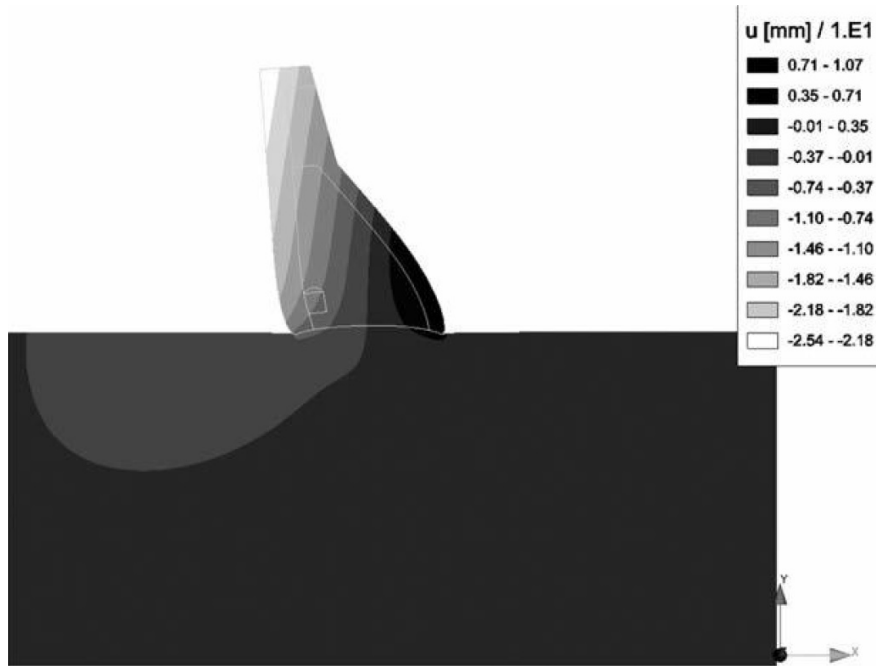


Figure 3.135: Deformation of a 2D-slice of the Dam after 40 years with upstream-downstream displacement mapping (navy blue represents upstream displacement above 20 mm); Leroy et al. (2011)

- The body of the Dam is separated into several groups to allow to take into account the various different qualities of concrete if necessary.
- Model fitting to the monitoring data is used to determine the correct values for the three parameters: τ_l , τ_c and ε_∞ .
- The temperature and moisture fields in the structure are considered as homogeneous.
- More than 30 parametric analyses are performed for 60 years of ASR expansion, and the computed crest displacement in blocks 13 and 23 are compared to the upstream-downstream displacements monitored on the Dam, Figure 3.136.

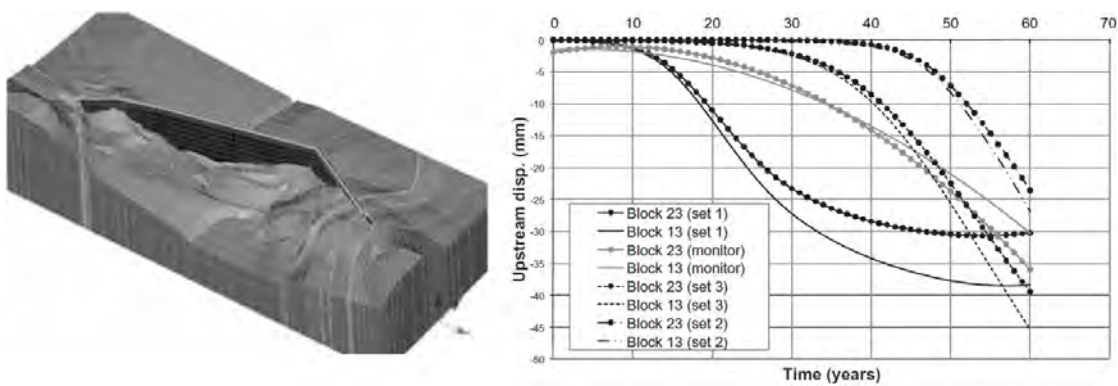


Figure 3.136: Views of the mesh, and Downstream displacement at the crest of the Dam; Leroy et al. (2011)

- The rehabilitation project is conducted on the Dam to reestablish an acceptable level of stress and deformation.
- Sawing the upper part of the Dam to release stress and decrease the arching effect, which has been amplified by the Dam's elbow, is a good option to achieve this goal.
- A numerical model of the Dam, accounting for ASR-development, is a good tool to answer different questions about slot-cutting.
- Specific contact elements have been used. Figure 3.137 represents the evolution of computed transverse stress in a test-case dam block after a 10 mm-wide slot-cutting.

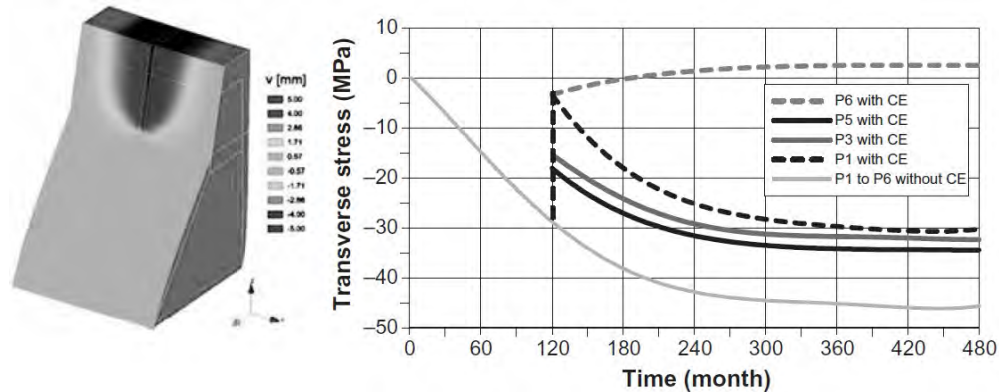


Figure 3.137: Transverse stress versus time at different heights (P1 is the top of the slot-cutting, P6 its bottom) and transverse displacement mapping just after slot-cutting; Leroy et al. (2011)

3.94 Leńnicki, Krzysztof J and Kim, Jin-Yeon and Kurtis, Kimberly E and Jacobs, Laurence J (2011)

URL

```
@article{
lesnicki2011characterization},
label={lesnicki2011characterization},
title={Characterization of ASR damage in concrete using nonlinear impact resonance
acoustic spectroscopy technique},
author={Le{\'}snicki, Krzysztof J and Kim, Jin-Yeon and Kurtis, Kimberly E and
Jacobs, Laurence J},
journal={NDT \& E International},
volume={44},
number={8},
pages={721--727},
year={2011},
publisher={Elsevier}
Keywords={}
```

- The nonlinear impact resonance acoustic spectroscopy (NIRAS) technique was applied for the characterization of progressive damage due to ASR in standard concrete specimens.

- NIRAS is a non-destructive evaluation (NDE) technique that is highly sensitive to defects, especially to small cracks in materials.
- The microcracks and debonded interfaces act to increase the nonlinearity of concrete.
- The response of the specimen to impact loading is analyzed to obtain a nonlinearity parameter. This parameter is then used as a measure of damage.
- Using the phenomenological model for hysteresis and classical nonlinear constitutive relations, the elastic modulus can be represented as follows:

$$E = E_0 (1 + \beta\varepsilon + \delta\varepsilon^2 + \alpha(\Delta\varepsilon + \varepsilon \operatorname{sgn}(\dot{\varepsilon}))) \quad (3.13)$$

where E_0 is the linear elastic modulus (modulus for small deformation), β is the parameter for quadratic anharmonicity, δ is the parameter for cubic anharmonicity, ε is strain, $\Delta\varepsilon$ is the strain amplitude, $\dot{\varepsilon}$ is strain rate, and $\operatorname{sgn}(\dot{\varepsilon}) = 1$ if $\dot{\varepsilon} > 0$, -1 if $\dot{\varepsilon} < 0$ and 0 if $\dot{\varepsilon} = 0$. The hysteresis nonlinearity parameter, α , is a measure of the material hysteresis.

- The nonlinear resonance frequency shift occurs with an increased level of strain excitation for a damaged state of the material. The relationship between strain and frequency shift is:

$$\frac{f_0 - f}{f_0} = \alpha' \Delta\varepsilon \quad (3.14)$$

where the parameter α' is proportional to the hysteresis non-linearity parameter, α ; f_0 is the linear resonance frequency; and f is the resonance frequency at increased excitation amplitude.

- With the NIRAS technique, a specimen is vibrated in its fundamental flexural mode using a low amplitude hammer impact.
- Three aggregates with varying reactivity are examined.
 - S1: coarse aggregate: reactive, fine aggregate: nonreactive
 - S2: coarse aggregate: nonreactive, fine aggregate: reactive
 - S3: coarse aggregate: nonreactive, fine aggregate: potentially reactive
- The results from the expansion test are compared with those from the NIRAS measurements.
- For potentially reactive aggregate, the NIRAS technique offers a more definitive assessment of the damage state of the specimen and can be used to distinguish marginally reactive aggregates.
- Figure 3.138 shows the test setup, as well as the measure expansion for three specimen and the degree of nonlinearity. Both techniques demonstrate a general trend of increased standard deviation with increasing damage.
- The NIRAS results not only demonstrate a clear distinction between non-reactive and reactive aggregates using the nonlinearity parameter, but also the capability to quantitatively track ASR-induced damage in concrete.

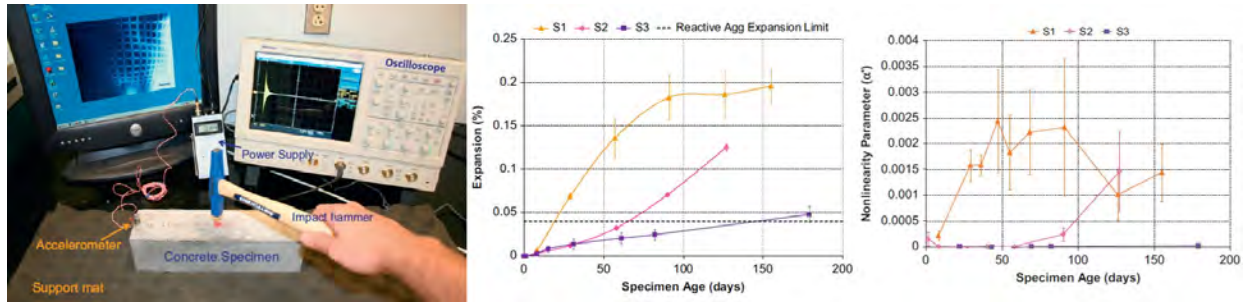


Figure 3.138: Experimental setup; Expansion of specimen and the measured nonlinearity; Leśnicki et al. (2011)

3.95 Leśnicki, Krzysztof J and Kim, Jin-Yeon and Kurtis, Kimberly E and Jacobs, Laurence J (2013)

URL

```
@article{
lesnicki2013assessment},
label={lesnicki2013assessment},
title={Assessment of alkali--silica reaction damage through quantification of
concrete nonlinearity},
author={Le{\'}snicki, Krzysztof J and Kim, Jin-Yeon and Kurtis, Kimberly E and
Jacobs, Laurence J},
journal={Materials and structures},
volume={46},
number={3},
pages={497--509},
year={2013},
publisher={Springer}
Keywords={}
```

- This research is along the previous research reported in Leśnicki et al. (2011).
- Again, the NIRAS is applied to concrete specimens suffering from ASR.
- NIRAS can distinguish reactive from nonreactive aggregates without ambiguity.
- The concept of the accumulated damage (integration of area under the nonlinearity-time curve) was employed to present the NIRAS results more quantitatively. This can be completed with the application of a Riemann sum:

$$\eta_c \approx \frac{1}{2} \sum_{i=2}^N (t_i - t_{i-1}) (\eta(t_i) + \eta(t_{i-1})) \quad (3.15)$$

where t is time (days).

- Figure 3.139 plots the results for accumulated nonlinearity.
- The results allow even greater differentiation between reactive and nonreactive specimens.

- Among the five aggregates examined, the classification of aggregate reactivity was found to be coincident with that from expansion measurements with one exception.

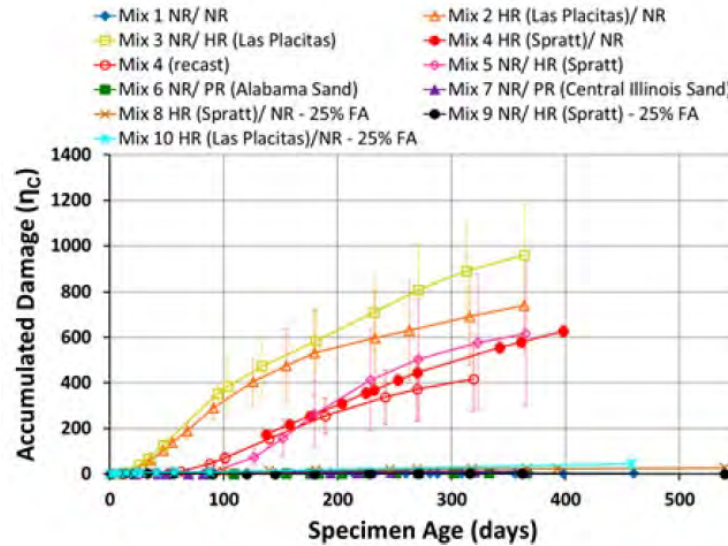


Figure 3.139: NIRAS results for accumulated damage; Leśnicki et al. (2013)

- The NIRAS method appears to be generally insensitive to aggregate gradation on nonlinearity measurements (unlike the expansion test).
- The NIRAS technique can be applied to core samples to test the state of structures currently in the field, potentially eliminating the need for time consuming and costly petrographic analysis.

3.96 Liaudat, Joaquín and Martínez, A and López, CM and Carol, Ignacio (2015)

URL

```
@incollection{
  liaudat2015numerical,
  label={liaudat2015numerical},
  title={Numerical modelling of ASR expansions in concrete},
  author={Liaudat, Joaquín and Martínez, A and López, CM and Carol,
    Ignacio},
  booktitle={CONCREEP 10},
  pages={445--454},
  year={2015},
  url={https://ascelibrary.org/doi/abs/10.1061/9780784479346.054}
```

- Results of a series of tests on specimens with a single interface between aggregate and cement paste, and the comparison to the numerical results of a simplified diffusion-reaction Finite Element model are presented.

- Tests are conceived as the simplest test to characterize the basic constituent reactions of the process.

reaction model already formulated and in the process of implementation.

to its higher porosity or the presence interfacial cracks, preexistent or originated by the ASR. In spite of its relative simplicity, the model described seems capable of reproducing the experimental observations with specimens tested under different diffusion boundary conditions.

- and provides a satisfactory b:
 - Set #2: Specimens with complete lateral sealing
 - Set #3: Specimens with lateral sealing of 10mm (glass), the ITZ and the immediate HCP.

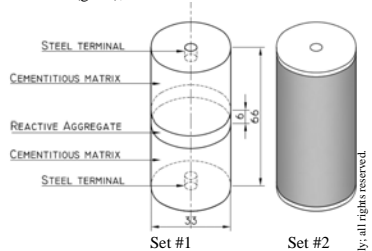


Figure 1. Configuration of AAR-INTER active specimens and schematic representation of the three sets of specimens tested with different lateral sealing.

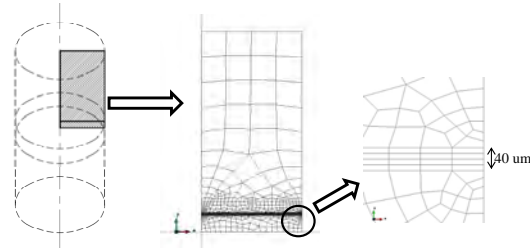


Figure 5. Model geometry and FE mesh.

The specimens were elaborated with cement paste as cementitious matrix and 6mm width soda-lime glass as reactive aggregate. Each set consisted in 4 specimens and 4 control (without glass) specimens. The cement used was 42.5R (UNE-EN 125) and the water/cement ratio was 0.37. Sodium Hydroxide was added to the mixing water in order to raise the equivalent sodium dioxide content to 1.1% of the cement weight. The lateral sealing was realized with self-curing rubber tape once the curing period was end, just before putting the recipients into the oven.

3.9.7 Liaudat, Joaquín and Carol, Ignacio and López, Carlos M and Saouma, Victor E (2017)

URI

From the length change measurements of active and control specimens during the exposition stage, the expansions d , corresponding to the ASR reaction products

```
@article{
  liaudat2017asr},
  label={liaudat2017asr},
  title={ASR expansions in concrete under triaxial confinement},
  author={Liaudat, Joaquín and Carol, Ignacio and López, Carlos M and Saouma, Victor E},
  journal={Cement and Concrete Composites},
  year={2017},
  publisher={Elsevier}
  Keywords={}
```

- Results of experimental ASR tests are presented in terms of expansion curves obtained from cubical concrete specimens subjected to three different triaxial stress states by means of a new testing machine especially designed for this purpose.
- The results confirm that the volumetric ASR expansion rate is reduced as the applied volumetric compressive stress is increased.
- There is an increase in the expansion rate in the less compressed direction to the detriment of the expansion rate in the most compressed direction.
- The Alkali-Aggregate Reaction Triaxial Machine (AARTM) was originally constructed at the University of Colorado Boulder, Figure 3.140.

- The AARTM consists of a triaxial load frame which can deliver up to 9 MPa confining stress on each axis of a 150×150×150 mm cubical specimen.

- Specimen deformation is measured using three displacement sensors on each of the three axes.
- The apparatus is designed to be capable of raising and maintaining the specimen temperature at a pre-set value between 30°C and 70°C.
- The faces of the loading plates in contact with the specimens are crossed by grooves for a solution to circulate in order to keep the specimen wet and supply reactants (alkalis).

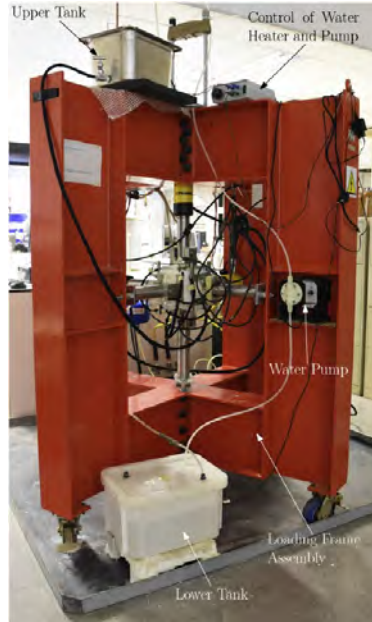


Figure 3.140: General view of the AARTM; Liaudat et al. (2017)

- Two different concrete mixtures were tested under the same conditions, one reactive (with crushed soda-lime glass aggregate) and one non-reactive.
- Three nominal load cases were studied with the AARTM:
 - Case 1-1-1: $\sigma_x = \sigma_y = \sigma_z = -1$ MPa.
 - Case 9-9-9: $\sigma_x = \sigma_y = \sigma_z = -9$ MPa.
 - Case 9-9-1: $\sigma_x = \sigma_y = -9$ MPa, $\sigma_z = -1$ MPa.
- Basic creep was accounted for my monitoring the time-dependent deformations measured on control (non-reactive) specimens.
- The observations were in good agreement with the model previously proposed in Saouma and Perotti (2006), although a correction is proposed for the dependency of total volumetric expansion with volumetric stress.
- The revised formula to predict the observed ASR volumetric expansion rate under compressive stresses is:

$$\dot{\epsilon}_v^{ASR} = \Gamma_c(\sigma_v)\dot{\epsilon}_{v,free}^{ASR} \quad (3.16)$$

where $\dot{\varepsilon}_{v,free}^{ASR}$ is the rate of volumetric ASR expansion without applied stresses, and Γ_c is a dimensionless factor that accounts for the reduction of $\dot{\varepsilon}_v^{ASR}$ under compressive stresses. Γ_c is assumed to be a function of the volumetric stress σ_v as:

$$\Gamma_c = \begin{cases} 1 & \sigma_v \geq 0 \\ 1 - \left(\frac{\sigma_v}{\bar{\sigma}_v}\right)^2 & \bar{\sigma}_v \leq \sigma_v < 0 \\ 0 & \sigma_v < \bar{\sigma}_v \end{cases} \quad (3.17)$$

where $\bar{\sigma}_v$ is a parameter that stands for the volumetric stress under which ASR expansion would be totally suppressed.

- Results of experimental ASR tests are presented in terms of expansion curves obtained from cubical concrete specimens subjected to three different triaxial stress states by means of a new testing machine especially designed for this purpose.
- The results obtained from material test are summarized in Figure 3.141.

Type	Id.	E [GPa]	f_c [MPa]	f_t [MPa]	G_f^I [J/m ²]
Cured for 15 weeks					
Control	TM25	41.5	42.5	–	–
Reactive	TM30	21.5	26.8	–	–
Control	TM26	–	–	2.8	74.6
Reactive	TM31	–	–	2.4	144.1
Cured for 47 weeks					
Control	TM18	40.0	60.5	–	–
Reactive	TM24	19.0	24.9	–	–
Cured for 63–67 weeks and tested 9-9-9 for 3 weeks					
Control	TM16	40.3	54.3	–	–
Reactive	TM22	25.5	34.4	–	–
Cured for 14 weeks and tested 0-0-0 for 36 weeks					
Control	TM07	41.7	52.6	–	–
Reactive	TM13	5.6	8.5	–	–

Figure 3.141: Results of the performed mechanical tests; Liaudat et al. (2017)

- Four curing times are studied.
- Results from the specimens cured for 15 weeks without ASR testing:
 - The E and f_c measured for the control concrete are significantly higher than those measured on reactive concrete.
 - In contrast, the G_f^I measured on reactive concrete is practically twice that measured on control concrete while the estimated f_t values are similar.
 - These differences can be attributed to the flaky shape and the smoothness of the crushed glass particles.
- When considering the remaining results, it seems that curing and testing history only have an influence on the measured values of f_c and E on reactive concrete but not on control concrete.

- Comparison of results with curing times of 15 and 47 weeks suggests that ASR degradation occurring at curing conditions was not significant, even when some signals of occurring ASR were detected on the specimen cured for 47 weeks.

3.98 Lindgård, Jan and Nixon, Philip J and Borchers, Ingmar and Schouenborg, Björn and Wigum, Børge Johannes and Haugen, Marit and Åkesson, Urban (2010)

URL

```
@article{
lindgaard2010eu,
label={lindgaard2010eu},
title={The EU ‘PARTNER’ Project-European standard tests to prevent alkali
reactions in aggregates: final results and recommendations},
author={Lindg{\aa}rd, Jan and Nixon, Philip J and Borchers, Ingmar and
Schouenborg, Bj{\o}rn and Wigum, B{\o}rge Johannes and Haugen, Marit and
{\AA}kesson, Urban},
journal={Cement and Concrete Research},
volume={40},
number={4},
pages={611--635},
year={2010},
publisher={Elsevier},
Keywords={},
DisplayPdf={0},
url={https://www.sciencedirect.com/science/article/pii/S0008884609002440}
```

- Presents the main findings in the EU PARTNER Project (2002–2006) providing the basis for a unified European test approach for evaluating the potential alkali-reactivity of aggregates.
- Project evaluated the tests developed by RILEM and some regional tests for their suitability for use with the wide variety of aggregates and geological types found across Europe.
- Project had 24 partners from 14 countries, covering most of Europe, from Iceland to Greece. 22 different types of aggregates from 10 different European countries were evaluated.
- Major conclusions: in most cases the RILEM tests could successfully identify the reactivity of the aggregates tested. They were most successful with normally reactive and nonreactive aggregates, but with aggregates that react very slowly an extended test period may be necessary for some of the RILEM methods. Overall, the accelerated mortar bar test and the accelerated concrete prism test seemed most effective and to have the best precision.
- Detailed conclusions:
 - In the majority of cases, all the RILEM test methods were able to correctly identify the potential alkali-reactivity of each of the individual aggregates or aggregate combinations (a total of 22) investigated in this study. The tests were particularly successful in identifying aggregates that react in “normal” time scales (i.e. 5 to 20 years) and in identifying non-reactive aggregates. There was less certainty in identifying “slowly”

reactive aggregates, i.e. those that react in greater than 15–20 years. Whether these experiences can be applied to all European regions will have to be verified by additional local examinations.

- Where there were discrepancies between the results of the tests and field experience, these can usually be attributed to either uncertainties about the field results, to variability in the aggregate source or to pessimum effects.
- Overall, the accelerated mortar bar test (AAR-2) and the accelerated concrete prism test (AAR-4, reactor version) seemed the most effective of the RILEM methods across the whole range of European aggregates investigated, including the identification of “slowly” reactive aggregate combinations. Moreover, these methods have the advantage of producing (relatively) rapid results. To get comparable results from both prism sizes allowed for in AAR-2, it seems necessary to continue the test to 28 days. However, critical limits after 14 days are suggested.
- The petrographic RILEM AAR-1 method can produce an even quicker result. The averaged results for this method seem quite effective at identifying reactive materials, but can conflict with field experience when pessimum effects operate. The consistency of individual results for this method is the main issue, however, due to a rather large spread in results between many of the laboratories.
- Overall, the results from the petrographic analyses confirm the necessity of education and round robin testing. Petrographers need to get acquainted with the potentially reactive components in aggregates from different countries in order to use the most appropriate analytical techniques and to make a relevant assessment. Education, in combination with proficiency trials of individual laboratories, is therefore the way forward for future constructive development in this area. An improvement of the common understanding between petrographers really calls for extensive and repeated workshops, e.g. as arranged as part of the PARTNER project. The petrographic atlas developed in the project will also be a good tool to help the petrographers to recognise potentially reactive rock types and to differentiate these from rock types that will be resistant to alkali reactions.
- Precision statements for the four RILEM methods have been made. These confirm the poor precision of the petrographic method, unless the laboratories carrying out the test are familiar with the materials being evaluated. The precision of the expansion methods is much better, and the results confirm the conclusion that the AAR-2 and AAR-4 methods are the most repeatable and reproducible despite some non negligible within and between laboratory variations.
- The field site tests were carried out in various climate zones representative for Europe in order to take into account the influence of different environmental conditions. However, the results indicate that a deleterious ASR occurs in the same way in northern and in southern Europe with the difference that with some aggregates the reaction may occur earlier in southern Europe, probably due to the higher mean temperature.
- Specimens were stored alongside a highway in Sweden to study the additional influence of alkali supply under severe conditions. So far, there is no difference in the performance of the concrete cubes stored in a nearby forest (without alkali supply) and alongside the highway (with alkali supply).

3.99 Lindgård, Jan and Andiç-Çakır, Özge and Fernandes, Isabel and Rønning, Terje F and Thomas, Michael DA (2012)

URL

```
@article{
lindgaard2012alkali,
label={lindgaard2012alkali},
title={Alkali--silica reactions (ASR): literature review on parameters influencing
laboratory performance testing},
author={Lindg{\aa}rd, Jan and Andi{\c{c}}--{\c{C}}ak{\i}r, {"0}zge and Fernandes,
Isabel and R{\o}nning, Terje F and Thomas, Michael DA},
journal={Cement and Concrete Research},
volume={42},
number={2},
pages={223--243},
year={2012},
publisher={Elsevier},
Keywords={},
DisplayPdf={0},
url={https://www.sciencedirect.com/science/article/pii/S0008884611002687}
```

- Utilisation of potentially alkali–silica reactive aggregates requires reliable performance tests to evaluate the alkali–silica reactivity of various aggregate combinations, including their alkali threshold dependence on binder type.
- Several such performance tests have been used worldwide for more than 15 years, but none of the methods have proven to be reliable for use with all aggregate types and all binders.
- Several parameters may influence the results obtained in an accelerated performance test compared to the field behaviour.
- Based on a state of the art literature review, paper discusses which parameters must be considered to be able to develop reliable ASR performance testing methods and provides some tentative recommendations.
- The internal humidity in the test specimens, the extent of alkali leaching and the storage temperature are of particular importance.

Major Conclusions and Recommendations

Precautions dependent on type of aggregate

- When dealing with aggregates showing a possible pessimum, this must be accounted for during performance testing, e.g. by performing several concretes mixes with different percentages of reactive constituents.
- The aggregate fractions used in structures should also be used in the laboratory tests, since the aggregate size causing the highest ASR expansion is dependent on the nature and composition of the aggregate. Concrete prism tests are thus recommended instead of mortar bar tests. It should also be kept in mind that crushing some certain types of aggregates may affect their reactivity.

- Testing and assessment of alkali release from aggregates should preferably be taken into account during performance testing, since the extent of alkali release might vary with the test conditions, e.g. with the exposure temperature. However, the first and urgent step is to agree on a test method for measurement of alkali release representative of that occurring in practice and corresponding interpretation criteria.
- The ASR aggregate test methods and the corresponding interpretation criteria (maximum allowed expansion) have been developed for normal weight aggregates and are not necessarily applicable for lightweight aggregates (oven dry particle density less than 2000 kg/m³) or heavy weight aggregates (oven dry particle density greater than 3500 kg/m³). Also the weight increase should be taken into consideration since experiences show that the ASR gel (if developed) initially accumulates in voids in the LWAs and primarily contributes to a weight increase but only a moderate length increase. After the gel has accumulated in and partly filled the voids in the LWAs, the rate of expansion might increase

Precautions dependent on type of binder

- The same type of OPC cement should be used in performance testing as planned to be used in the structure. The reason is that some concrete mixtures produced with cements having similar Na₂O_{eq} but different K/Na ratios have been observed to expand considerably differently in accelerated laboratory tests. However, there are contradictory findings in the literature about this issue.
- The type of cement and the type and amount of any SCMs incorporated influence the parameters related to ASR, including composition of hydration products, porewater composition and permeability. This should be taken into account when testing the concrete performance, during mix design, pre-curing and exposure, as further discussed below.
- It is recommended to test the actual binder composition in combination with the actual aggregate to be used in the structure. Even though the chemical composition of e.g. two fly ashes is quite similar, their ASR mitigation properties might differ significantly.
- If the aim is to document the ability of a commercial binder (e.g. a fly ash cement) to prevent ASR for a number of aggregate types within a region, a possible alternative approach is to test the binder in combination with an assumed “worst case reference aggregate” (e.g. as described in the Norwegian ASR regulations).
- An acceptable performance test method requires an approach that accelerates the pozzolanic reaction and the ASR to the same extent, since an extensive acceleration of the pozzolanic reaction might lead to less ASR expansion in the laboratory testing (not conservative). This might be of particular interest when testing fly ash containing cements, in which the pozzolanic reaction and thus the alkali binding starts after a period of approximately 28 days when cured at 20m³C.
- Performance testing of silica fume containing concretes needs a prolonged testing time (at least two years) in order to detect a possible increased alkali level with time when the alkali–silica gel continuously reacts with calcium. Thus, at least part of the alkalis becomes available for alkali–silica reaction.

Important factors to take into account during mix design

- The w/cm ratio influences the concrete properties, and thus the outcome of an ASR performance test. Decreasing the w/cm ratio on the one hand might lead to increased ASR expansions (due to increased OH⁻ concentration in the pore solution), while on the other hand may reduce the ASR expansions (due to a denser paste, and thus slower and less transport and ingress of water or solutions, and due to a higher degree of self-desiccation and thus a reduced internal RH). As a consequence, the authors suggest that the net influence of a reduced w/cm ratio should be investigated further, before executing commercial accelerated laboratory performance testing of concretes with w/cm ratio below 0.40.
- As a conservative approach, pre-saturated aggregates might be used to counteract self-desiccation to a certain extent (might be particularly effective for highly porous aggregates).
- The alkali content of the concrete is often boosted to ensure that there are sufficient alkalis present to identify reactive aggregates and to compensate for alkali leaching. Nonetheless, extensive alkali boosting is not in general recommended for performance testing because it masks the critical role of the alkali content of the job mixture. Additionally, there are several other concerns regarding alkali boosting (e.g. added alkalis might influence the behaviour of the concrete and thus affect the ASR properties). However, there are contradictory findings in the literature on the influence of some alkali boosting, thus calling for more research.
- It is recommended that the entrained air content of the performance test is the same as that intended for the job mixture. Alternatively, one might use lower air content in the laboratory test prisms, since this is a conservative approach. Whereas it is generally agreed that entrained air will not prevent or delay ASR expansion, there is some evidence that it can reduce expansion with some aggregates by accommodating ASR gel.
- In the case of using lithium to reduce the risk of ASR, it is essential that the lithium to alkalis (sodium and potassium) molar ratio, $[Li] / [Na+K]$, in the performance test is equal to that of the job mixture being tested.
- The “pre-storage conditions” (i.e. moisture conditions during prestorage and the length of the pre-storage period at ambient temperature) and the ASR exposure conditions (i.e. moisture conditions, type of container, prism size, wrapping (if any), storage temperature, storage period and any external alkalis added) might have significant influence on vital “ASR parameters” (i.e. prism internal humidity, composition of the concrete pore solution, aggregate reactivity, properties of hydration products formed and properties of any reaction products formed) and thus on the outcome of a performance test.
- A laboratory performance test should be designed to subject the prisms to “worst-case humidity conditions”, while considering the problems related to increased alkali leaching. As a quality control measure, the mass of prisms should always be measured, evaluated and reported.
- When using a relatively low w/cm ratio, e.g. as in high performance concrete, the self-desiccation will increase and, as a consequence, the internal RH will decrease. Several parameters might increase the influence of self-desiccation (e.g. the prism size and the micro climate in the storage containers) and thus contribute to maintain a “rather low” internal RH in the concrete prisms. A good laboratory performance test should take into account these parameters to avoid a too low internal RH in the concrete prisms.

- It is essential to keep the internal prism temperature constant during all measurements, because the recorded expansion is rather sensitive to a moderately deviating prism temperature at the time of measuring compared with the temperature during the reference readings. The time of reading the prism reference length might also be of importance, in particular for concretes showing some shrinkage in the early age (e.g. when testing binders with high extent of self-desiccation).
- The extent of alkali leaching, one of the biggest challenges during accelerated ASR testing in the laboratory, should be minimised. It is important to account for alkali leaching when drawing conclusions based on a performance test.
- The rate and extent of alkali leaching are heavily influenced by the storage and exposure conditions. The following parameters are of particular importance:
 - Reduced alkali leaching occurs with larger prism size, lower concrete permeability, lower exposure temperature and less moisture condensing on the prism surfaces.
 - Increased alkali leaching occurs when prisms are submerged in water or exposed to extreme moisture conditions (e.g. fog chamber), prisms wrapped in wet cotton cloth or prisms subjected to drying and wetting cycles (e.g. during cooling before measuring).
- To make a performance test more practical, there is a need to find a way to accelerate the reaction, e.g. by elevating the storage temperature. However, exposing the prisms to 60m³C during ASR testing might be questionable due to several reasons:
 - Lack of experience with respect to laboratory-field correlation.
 - Higher rate of silica dissolution and alkali release from aggregates.
 - The concentration of sulphates in the concrete pore water increases with increasing temperature, and thus the concentration of OH⁻ is reduced correspondingly.
 - The influence of the pre-curing conditions (e.g. length of curing at ambient temperature before starting the ASR test) on the prism expansion might be of higher importance, dependent on the type of binder.
 - The alkali binding capacity is influenced by the exposure temperature.
 - The pozzolanic reactivity of the SCMor the ggbs used might be accelerated significantly, and thus contribute to a poorer laboratory/ field correlation.
- To build up experience with ASR testing at 60m³C and collect data for evaluation of the laboratory/field correlation, research laboratories are encouraged to keep on testing various concretes by use of the RILEM AAR-4.1 test method and cast concrete cubes for outdoor exposure. Also the extent of alkali leaching should be documented.
- In a performance test, exposure of the test prisms to temperatures above 60m³C should be avoided. At such high temperatures, some other deterioration mechanisms may occur, e.g. DEF.

3.100 Lindgård, Jan and Sellevold, Erik J and Thomas, Michael DA and Pedersen, Bård and Justnes, Harald and Rønning, Terje F (2013)

[URL](#)


```
@article{
lindgaard2013alkali,
label={lindgaard2013alkali},
title={Alkali--silica reaction (ASR)--performance testing: influence of specimen
pre-treatment, exposure conditions and prism size on concrete porosity,
moisture state and transport properties},
author={Lindg{\aa}rd, Jan and Sellevold, Erik J and Thomas, Michael DA and
Pedersen, B{\aa}rd and Justnes, Harald and R{\o}nning, Terje F},
journal={Cement and Concrete Research},
volume={53},
pages={145--167},
year={2013},
publisher={Elsevier},
Keywords={},
DisplayPdf={0},
url={https://www.sciencedirect.com/science/article/pii/S0008884613001348}
```

- Assesses the suitability of the concrete prism tests (CPTs) for general ASR performance testing of concrete.
- Presents the background for the choice of test procedures and results on how variations in specimen pre-treatment, ASR exposure conditions and prism size influence concrete porosity, moisture state and transport properties.
- For ordinary Portland cements and with water-to-cementitious-materials ratio (w/cm) 0.45 and higher it was found that the internal moisture state is sufficiently high in all the assessed procedures to produce ASR expansion.
- For less permeable concretes lack of internal moisture and lower rate of diffusion can significantly reduce the rate and extent of ASR expansion during laboratory performance testing.

Major Conclusions and Recommendations

Based on the comprehensive laboratory study, including 58 test series with modified versions of five concrete prisms tests (CPTs), the following conclusions can be drawn:

- The internal moisture state and the transport properties of a given concrete may be significantly influenced by the specimen “pre-treatment”, “ASR exposure conditions” and prism cross-section. The influence depends on the concrete composition, i.e.w/cm and cement type. Consequently, the results of applying a performance test to a given concrete might differ depending on the details of the test method.
- During the ASR exposure, the concrete properties are altered. The general tendency is increased suction porosity and increased internal moisture state with increased ASR expansion, but the alteration depends on the binder composition. The change in macro porosity is negligible. Moreover, a relation exists between water uptake and expansion, i.e. concrete expansion leads to increased porosity that takes up water. However, more water is taken up than the volume corresponding to the increased porosity.
- With respect to the specimen ”pre-treatment”, the main findings are:

- From a “moisture point of view”, the 0.5 h submersion after de-moulding described in several CPTs seems unnecessary (has little effect beyond the first weeks of exposure).
 - The length of pre-storage at 20°C before exposure to elevated temperature might marginally influence the internal moisture state in the first period of exposure, but not at later ages. However, exposure to 60°C directly after de-moulding significantly increase the relative diffusion coefficient (RelD) for CEM I binders, making the internal transport of water and ions easier.
 - Prisms wrapped in moist cotton cloth and plastic sheets absorb significantly more water than unwrapped prisms displaying similar expansions in ASR tests. During the first weeks of exposure, this behaviour is particularly pronounced at 60°C. For prisms exposed to 38°C, the wrapping also leads to slightly higher DCS and internal RH after 4 weeks of exposure.
- With respect to the “exposure conditions” and prism cross-section, the main findings are:
 - The “exposure parameter” confirmed to have the highest impact on the internal moisture state and the transport properties of concrete is the temperature. The prism cross-section can also significantly influence the internal moisture state. For both parameters, the influence depends on the binder composition.
 - Generally for CEM I binders, exposure to 60°C leads to considerably higher water absorption during the first weeks compared with corresponding test series exposed at 38°C. The internal RH is also significant higher for the test series exposed to 60°C, both at early age and later. This RH-increase is probably primarily related to the coarsening of the pore structure produced by the elevated temperature and, of course, more water.
 - At the end of the ASR exposure, the total prism water uptake and the internal moisture state is to a high extent influenced by the extent of ASR and thus the extent of internal cracking and amount of ASR-gel produced. Also the electrical resistivity is influenced—increased ASR expansion tends to decrease the electrical resistivity.
 - In general for CEM I binders exposed to 38°C, increased prism cross-section leads to less absorbed water in the interior of the prisms, in particular during the first period of the exposure. A pronounced RH gradient is present for test series with the “dense” binder (w/c of 0.30) during the entire exposure period. A similar, but less distinct, gradient is observed in prisms with the “fly ash” binder (w/cm of 0.45).
 - With respect to influence of binder composition (i.e. w/cm and cement type), the main findings are:
 - No systematic difference in the degree of capillary saturation (DCS) between binders of different composition can be found, neither at 4 weeks nor at the end of the exposure.
 - For the CEM I test series, one of the most important properties of the “dense” binder (w/c of 0.30) compared with higher w/c is the much lower internal RH, in particular when exposed to 38°C (RH in the range of 82–90%). The reason is primarily the higher extent of self-desiccation. Furthermore, the relative diffusion coefficient is substantially lower also due to a finer pore structure so that the water uptake is slower. Additionally, an assumed higher concentration of ions in the porewater might contribute to reduce the RH.

- Several concrete properties of the test series with the “fly ash” binder deviate from the CEM I series. Firstly, most concrete properties for the “fly ash” binder seem to be more or less independent of both the specimen pre-treatment and the storage conditions during testing. Secondly, concrete prisms with the “fly ash” binder generally absorb less water compared with prisms with the CEM I binders at the same w/cm, presumably due to the lower “permeability” (measured as a low RelD and a higher electrical resistivity) and less water bound by the hydration products incorporating fly ash. Thirdly, the internal RH is considerably lower in the “fly ash” test series compared with CEM I series with equal w/cm. Fourthly, the general increase in RH seen for the CEM I binders during the ASR exposure is not observed for the “fly ash” binder. Note that all test series are subjected to elevated temperature which is very favourable for the pozzolanic reaction.
- It is likely that the comparatively low RH found for the “dense” binder and probably also for the “fly ash” binder after 4 weeks of exposure contributes together with the measured lower relative diffusion coefficients to reduce the rate and extent of ASR. This is particularly true for the test series exposed to 38°C. Additionally, less amount of available (evaporable) water in the “dense” CEM I concrete (w/c of 0.30) might contribute to the lower extent of ASR observed compared with the CEM I concretes with higher w/c.
- For all test series with the CEM I binders with higher w/c (0.45 or 0.60), RH is regarded to be sufficient for ASR to initiate (well over 90% RH after 4 weeks). Thus, it appears that for these binders all the specimen pre-treatment and test procedures provide sufficient moisture contents for ASR to proceed. The consequences of the present results for alkali leaching and prisms expansion are treated in a separate paper. A number of practical details and recommendations on the test procedures are given in the appendix to the thesis.

3.101 Lindgård, Jan and Thomas, Michael DA and Sellevold, Erik J and Pedersen, Bård and Andiç-Çakır, Özge and Justnes, Harald and Rønning, Terje F (2013)

URL

```
@article{
lindgaard2013alkali2,
label={lindgaard2013alkali2},
title={Alkali--silica reaction (ASR)-performance testing: influence of specimen
pre-treatment, exposure conditions and prism size on alkali leaching and prism
expansion},
author={Lindg{\aa}rd, Jan and Thomas, Michael DA and Sellevold, Erik J and
Pedersen, B{\aa}rd and Andi{\c{c}}-{\c{C}}ak{\i}r, {\"}zge and Justnes,
Harald and R{\o}nning, Terje F},
journal={Cement and Concrete Research},
volume={53},
pages={68--90},
year={2013},
publisher={Elsevier},
Keywords={},
DisplayPdf={0},
url={https://www.sciencedirect.com/science/article/pii/S0008884613001312}
```

- Assesses whether concrete prism tests developed for assessment of alkali–silica reactivity of aggregates might be suitable for general ASR performance testing of concrete.
- Discusses how variations in specimen pre-treatment, ASR exposure conditions and prism size influence the rate and amount of alkali leaching and prism expansion, together with a discussion of consequences for ASR test procedures.
- Results from some complementary tests are included.
- Generally, a remarkably high proportion of the in-mixed alkalis were leached out of the concrete prisms during the ASR exposure.
- For prisms exposed to 60°C, the rate and amount of alkali leaching is the main controlling factor for the prism expansion.
- For less permeable concretes exposed to 38°C, lack of internal moisture and lower rate of diffusion contributes to reduce the rate and extent of ASR expansion.

Major Conclusions

Main findings

Based on the comprehensive laboratory study, including 58 test series with modified versions of five concrete prisms tests (CPTs), the following conclusions can be drawn:

- The rate of alkali leaching during the first weeks of exposure is the parameter shown to have highest impact on the prism expansion.
- A modified wrapping procedure developed (cotton cloth added alkalis) might be a promising tool to reduce the amount of alkali leaching during accelerated laboratory testing. Increasing the prism cross-section also decreases the rate and amount of alkali leaching considerably.
- The results clearly show that the amount of alkali leaching and the prism expansion is significantly influenced by the specimen “pre-treatment”, “ASR exposure conditions” and prism cross-section. Most test conditions are by no means extreme, but represent test procedures used in various “commercial” CPTs. The extent of the impact depends on the concrete quality, i.e. w/cm and cement type. Consequently, the conclusion from a concrete performance test will differ depending on the test procedure used.
- Generally, a very substantial proportion of the in-mixed alkalis was leached out of the concrete prisms during the ASR exposure; 3–20% during the first 4 weeks of exposure and 10–50% at the end of the exposure of the CEM I test series (w/c of 0.30–0.60) with an initial alkali content 3.7 kg Na₂O_{eq} per m³ of concrete. For the test series submerged in de-ionised water, a substantial higher portion of alkalis was leached out of the concrete during exposure.
- A very good correlation is found between the amount of alkali leaching during the first 4 weeks and the final prism expansion, in particular for the test series exposed to 60°C. At this exposure temperature, the rate and amount of alkali leaching is the main controlling factor for the prism expansion. Consequently, to be able to mirror what will happen in a real concrete structure with minor or no alkali leaching, minimisation of the rate and amount of alkali leaching during accelerated laboratory performance testing is crucial.

- In principle, the expansion curves and the internal ranking between the various “open” binder test series (CEM I, w/c of 0.60) are comparable with the “basis” binder test series (CEM I, w/c of 0.45) with equal alkali content. This is valid for both exposure temperatures.
- For less permeable concretes (i.e. the “dense” binder (CEM I, w/c of 0.30) and the “fly ash” binder (CEM II/A-V, w/cm of 0.45)) exposed to 38°C, it is not only the alkali leaching that controls the prism expansion, but the internal moisture state and the diffusion properties also play a role. Thus, the two exposure temperatures produce different expansions. When exposed to 60°C, the internal RH is a little higher during the ASR exposure, contributing to the higher measured expansion (compared with 38°C). In a follow-up project, the field behaviour of some of these test series will be evaluated: one main aim is to assess which test procedure is best able to foresee the field behaviour of various concrete mixtures.

Effect of varying the specimen “pre-treatment”

With respect to variations in the specimen “pre-treatment”, the main findings are:

- During the 0.5 h submersion period in water after de-moulding (standard procedure for some of the CPTs), 3–4% of the alkalis mixed in the concrete prisms leached out into the water. Since this submersion period had little effect on the internal moisture state of the prisms beyond the first weeks of exposure, it is recommended to eliminate this submersion sequence from the ASR testing procedures.
- Wrapping of concrete prisms by use of moist cotton cloths and plastic sheets caused leaching of considerable quantities of alkalis during the first 4 weeks, significantly more than measured for the unwrapped prisms. The result was a dramatic reduction of the prisms expansion for the wrapped test series exposed to 60°C, while the effect was far less pronounced (not statistically significant) for the wrapped test series exposed to 38°C. “Traditional” wrapping of concrete prisms with a damp cotton cloth, applied in some test methods primarily with the aim to secure a high moisture content surrounding the prisms, is thus not recommended. (Comment: This advice is already adopted by RILEMTC 219-ACS based on this study; the Alternative wrapped version of the AAR-4.1 CPT (60°C) is no longer recommended, and the revised version of the RILEM AAR-3 CPT (38°C) use unwrapped prisms similar as the ASTM C 1293 CPT).
- The wrapping procedure is also of high importance for the amount of alkali leaching, in particular for test series exposed to 60°C. Less water added to the cotton cloth significantly reduced the early age alkali leaching and correspondingly increased the expansion. Opposite, removal of the polyethylene bag increased the alkali leaching and reduced the expansion.
- To try to reduce the amount of alkali leaching, some prisms were wrapped with a cotton cloth saturated with a basic solution of either pH = 14.2 or 13.2. For both exposure temperatures, the measurements indicates a small uptake of alkalis by the concrete prisms from the “pH 14.2 wrapping” during the exposure period, corresponding to about 15% (60°C) and 20% (38°C), respectively, of the in-mixed alkali content of the “basis” binder concrete. During the full exposure period, the wrapped prisms exposed to 60°C consequently expanded about 25 prisms after 26 and 39 weeks of exposure and up to 3.5 times more than the prisms wrapped with de-ionised water. This “modified wrapping procedure” might thus be a promising tool to reduce the amount of alkali leaching during accelerated laboratory testing.

- The less alkaline wrapping (pH 13.2) was not able to significantly prevent alkali leaching from the concrete prisms during the ASR exposure. Consequently, the effect on the prism expansions was practically negligible.
- With a few exceptions, neither the pre-storage length at ambient temperature nor the “simulated field curing” did significantly influence the alkali leaching properties of the test series exposed to 38°C, neither at early age nor later during the exposure period. Likewise for the test series exposed to 60°C, no general influence on the rate of alkali leaching at early age was observed when varying the length of pre-storage at ambient temperature. However, pro-longed pre-storage tends to somewhat decrease the final amount of alkali leaching from unwrapped prisms. However, none of these small differences in amount of alkali leaching directly influenced the expansion of the AAR-4.1 prisms.

Effect of varying the exposure conditions

With respect to variations in the “exposure conditions”, the main findings are:

- In general, elevating the exposure temperature from 38°C to 60°C does not influence the amount of alkali leaching during the first 4 weeks, neither for wrapped nor for unwrapped prisms. Furthermore, throughout the full exposure period, the rate and amount of alkali leaching from the unwrapped AAR-4.1 prisms (60°C) and the unwrapped ASTM prisms (38°C) are comparable for almost all corresponding test series, even though the relative diffusion coefficient is considerably increased with increasing temperature. The main reason for this is assumed to be that the “sink capacity” is the limiting factor, not the rate of diffusion.
- In contrast, the temperature dependency for the alkali leaching is more evident (and more as expected) for wrapped prisms in the period beyond 4 weeks of exposure; those exposed to 60°C have a considerably higher rate of alkali leaching compared with those exposed 38°C, probably due to higher “sink capacity” for wrapped prisms (compared with unwrapped prisms) and thus more influence of differences in diffusion properties.
- For all binders, increasing the prism size cross-section from 70 x 70 mm (RILEM size) to 100 x 100 mm (Norwegian size) decreases the rate and amount of alkali leaching considerably. For many test series, the amount of alkali leaching is practically halved. As a result of this, the final expansion increases substantially. An obvious consequence of this finding is that one effective measure to reduce the amount of alkali leaching during performance testing is to increase the prism cross-section.
- Pre-cooling the prisms before every periodic reading of length and mass increases the amount of alkali leaching. The assumed mechanism is that cooling results in drying which again concentrates alkalis near the surface—making them easier to be washed away. However, no significant differences in expansion were found between pre-cooled test series and corresponding test series measured “warm”.
- For the Norwegian CPT and the ASTM C 1293 CPT, both using an absorbing lining inside the storage containers in order to maintain a high humidity, 25 to 30% of the total amounts of alkalis leached out from the concrete prisms have on average been absorbed by the lining (same type of cotton cloth) during the exposure period. The remaining alkalis were found in the water in the bottom of the containers. Thus, it is important to measure all alkalis that have leached out from the concrete prisms.

Influence of binder composition on alkali leaching

The binder composition, i.e. cement type and w/cm, have different effects on alkali leaching and prism expansion. With respect to the influence of binder composition on alkali leaching, the main findings are:

- At both exposure temperatures, the rate and amount of alkali leaching are less dependent on the w/c of the CEM I binders than expected, despite the huge differences between the measured relative diffusion coefficients of water vapour (RelD). This demonstrates that not only diffusion properties, but also other parameters, for example concentration of alkalis in the pore water and “sink capacity”, influence the rate and amount of alkali leaching.
- For unwrapped prisms exposed to 38°C, the rate of alkali leaching is as expected a little less during the first 6 months of exposure of test series with the “dense” binder (CEM I, w/c of 0.30) compared with corresponding test series with higher w/c (0.45 and 0.60), probably due to the lower rate of diffusion. However, relatively more alkalis are leached out from the “dense” 38°C test series with time, assumed to primarily be caused by higher concentration of alkalis in the pore water and thus a higher “driving force” for alkali leaching.
- For unwrapped prisms exposed to 60°C, the rate of alkali leaching is significantly higher for the “open” binder compared with the two CEM I binders with lower w/c, which exhibit comparable alkali leaching throughout the full exposure period.
- For wrapped prisms, the rate of alkali leaching the first 4 weeks of exposure seems to be independent of the w/c for both exposure temperatures.
- As a consequence of the higher alkali content of the “fly ash” binder (9.0 kg Na₂O_{eq} per m³ of concrete, after boosting it from the initial 5.0 kg/m³), the relative alkali leaching ratio between the CEM I test series (3.7 kg Na₂O_{eq} per m³ of concrete) and the “fly ash” test series depends on how the results are presented. In absolute terms (e.g. in kg/m³ of alkalis) more alkalis are leached from the “fly ash” test series. However, when expressed as a proportion of the initial alkali content, the alkali leaching for the “fly ash” test series is considerably less than that for the CEM I test series.
- The ratio between alkali leaching from the “fly ash” binder and the CEM I binders is similar for all the concrete prism tests.

Influence of binder composition on prism expansion

With respect to the influence of binder composition (cement type and w/cm) on prism expansion, the main findings are:

- At both temperatures, corresponding test series with the “basis” binder and the “open” binder show comparable expansion.
- Similarly, the expansion curves for the “dense” binder test series (w/c of 0.30) exposed to 60°C are comparable with the corresponding results obtained at higher w/c. Furthermore, the “fly ash” binder test series expand almost as much as the CEM I test series at this exposure temperature, in contrast to what is observed at 38°C. One assumed reason for this behaviour is that a higher internal RH is obtained for these less permeable concretes when exposed to 60°C compared with 38°C. One cannot rule out that also other parameters that

might influence the development of ASR are slightly different at 60°C compared with 38°C, e.g. the properties of the fly ash reaction product and the pore solution chemistry.

- When exposed to 38°C, the rate of expansion and the final expansion for the less permeable test series with the “dense” binder and the “fly ash” binder are dramatically reduced relative to 60°C and compared with the CEM I test series with higher w/c exposed to 38°C. This behaviour indicates that it is not only the alkalinity of the pore solution and the alkali leaching that controls the prism expansion when exposing these less permeable binders to 38°C, but also the internal moisture state and the diffusion properties. To avoid any “false negative results” during accelerated performance testing, a fixed w/cm of 0.50 could be used (assumed to be conservative) until more research possibly documents that a lower (and more realistic) w/cm is safe to use; i.e. without resulting in a possible lower moisture state in the laboratory prisms compared with real concrete structures exposed to very high humidity.
- Another observation supporting the “lack of moisture theory” is that the wrapped “dense” binder test series exposed to 38°C expands a little more than the corresponding unwrapped test series in the period after 26 weeks of exposure, the opposite to what was found for the CEM I test series with higher w/c. This finding contradicts the observation that the wrapped test series results in more alkalis being leached out during the first period of the ASR exposure. The main reason for this inconsistency is assumed to be that the internal moisture state is slightly higher in the wrapped “dense” binder test series than in the unwrapped prisms.
- The “fly ash” test series exposed to either 1 day or 28 days at ambient temperature prior to ASR exposure produce comparable expansions at both exposure temperatures.
- When exposed to 60°C, the CEM I binders expand a little more than the “fly ash” binder. Also when exposed to 38°C, the “fly ash” test series exhibit the least expansion after 2 years of exposure. This is remarkable taking into account that the in-mixed alkali content is 9.0 kg/m³ Na₂O_{eq} for the “fly ash” binder (after boosting it from the initial 5.0 kg/m³) compared with only 3.7 kg/m³ for the other CEM I binders. However, this finding is as expected and demonstrates the favourable effect on the development on ASR of substituting cement by only about 20% of class F fly ash.

Complementary testing

The main conclusions from the complementary testing are:

- Measurement of alkali release from the aggregates indicated that only a minor (insignificant) amount of alkalis would be released from the aggregates under the conditions of the tests.
- A new method for the measurement of “cracking intensity” (given as area-% of cracks in an impregnated polished section) based on image analysis has been developed. This method has been used successfully to compare the extent of cracking due to ASR in concretes, both internally within one plane polished section and between different test series.
- The image analyses of the 16 fluorescence impregnated plane polished sections confirm the results from the alkali leaching measurements. The main reason for the lower crack intensity in the outer/upper/lower parts of the prisms compared with the interior is assumed to be the higher amount of alkali leaching in these areas of the prisms.

- A very good linear correlation is found between “cracking intensity” and prism expansion ($R^2 = 0.89$), and this seems valid for all strength levels tested. This implies that the image analysing technique is sufficiently good to use the method as a tool to analyse the degree of ASR damage in larger concrete samples, at least for post-documentation of the internal cracking in laboratory exposed samples.

3.102 Liu, Kai-Wei and Mukhopadhyay, Anol K (2015)

URL

```
@article{
liu2015accelerated},
label={liu2015accelerated},
title={Accelerated Concrete-Cylinder Test for Alkali--Silica Reaction},
author={Liu, Kai-Wei and Mukhopadhyay, Anol K},
journal={Journal of Testing and Evaluation},
volume={44},
number={3},
pages={1229--1238},
year={2015},
publisher={ASTM International}
Keywords={}
```

- The concrete-prism test (CPT) has been considered as the best index for ASR field performance, but alkali leaching and test duration are still of concern. Reduction of test duration by increasing testing temperature (e.g., 60 °C) was an option to develop an accelerated version of the concrete-prism test (ACPT); however, it has been discovered that there is a significant reduction in expansion associated with more alkali leaching in the ACPT compared to CPT.
- The authors proposed an accelerated concrete-cylinder test (ACCT) with no involvement of errors because of operation and temperature change along with arresting alkali leaching.
- The linear expansion of the ACCT measured at a temperature of 60 °C over a period of 1 month have been correlated with the one-year ASTM C1293 test to evaluate the ASR reactivity of aggregates.
- Cylinders made with highly reactive borosilicate glass balls were tested first in order to validate the proposed approach before any concrete-cylinder testing occurred.
- The results indicate that:
 - An expansion limit of 0.04% using 0.82% Na₂O equivalent (Na₂O_e) cement without alkali boosting after a testing period of 28 days is proposed for the ACCT to diagnose ASR aggregate reactivity.
 - The proposed method can serve as an alternative to validate the ASR-resistant mix design (e.g., fly ash contents).
- The ACCT procedure is briefly described below:

- A 27.9 cm (11 inch) stainless steel threaded rod was embedded (2.54 cm depth) on top of each concrete cylinder (7.6 cm × 15.2 cm) during specimen casting. After casting, the molds were covered with plastic foil and kept inside a 100% RH chamber at 25 °C ± 62 °C for 7 days.
- After 7 days, the concrete cylinders were de-molded and placed inside the VCMDs, which were filled with a soak solution with chemical content equal to the pore solution chemistry of each mix (each mix has a specific level of alkalis).
- Each VCMD was tightly closed and placed inside an oven at 60 °C.
- Expansion measurements were recorded every 15 min automatically through a data-acquisition computer system over time.

3.103 Lu, Duyou and Zhou, Xiaoling and Xu, Zhongzi and Lan, Xianghui and Tang, Mingshu and Fournier, Benoit (2006)

URL

```
@article{
  lu2006evaluation},
  label={lu2006evaluation},
  title={Evaluation of laboratory test method for determining the potential alkali
    contribution from aggregate and the ASR safety of the Three-Gorges dam
    concrete},
  author={Lu, Duyou and Zhou, Xiaoling and Xu, Zhongzi and Lan, Xianghui and Tang,
    Mingshu and Fournier, Benoit},
  journal={Cement and concrete research},
  volume={36},
  number={6},
  pages={1157--1165},
  year={2006},
  publisher={Elsevier}
  Keywords={}
```

- The releasable alkali from granite (used in the Three-Gorges concrete dam project in China), gneiss, and feldspar was estimated by extraction in distilled water and super-saturated Ca(OH)₂ solution.
- Since non-reactive aggregate and low calcium fly ash were used in the Three-Gorges dam concrete, ASR would not be an issue for the dam, despite the release of alkali from the aggregate into the concrete.
- In order to prevent thermal cracking, a medium-heat, low-alkali cement combined with low-alkali, low-calcium fly ash were used. The total alkali content of the concrete was limited to <2.5kg/m³, even in the structural parts of the dam. All these measures assure sufficient protection against potential ASR in the concrete.

3.104 Marzouk, H and Langdon, S (2003)

URL

```

@article{
marzouk2003effect},
label={marzouk2003effect},
title={The effect of alkali-aggregate reactivity on the mechanical properties of
high and normal strength concrete},
author={Marzouk, H and Langdon, S},
journal={Cement and Concrete Composites},
volume={25},
number={4-5},
pages={549--556},
year={2003},
publisher={Elsevier}
Keywords={}

```

- The objective is to identify the impact of alkali aggregate reactivity on the mechanical properties of concrete specimen.
- Other properties, like compressive strength and modulus of elasticity, are also explained.
- The results of the direct tension test are more sensitive to any changes in the C-S-H gel than the compressive strength tests.
- The effect of specimen size on the results of the tension test, however, is more profound than that on the compression test results.
- Normal strength concrete:
 - A decrease in the tensile strength was noted after 12 weeks of exposure.
 - In the specimens exposed to the NaOH solution, the tensile strength decreased by 37% and 31% in the specimens prepared with moderately reactive highly reactive and moderately reactive aggregates, respectively.
 - No apparent loss in the tensile strength was noted in the specimens prepared with moderately reactive aggregates and placed in the deionized water for 12 weeks.
 - The specimens prepared with highly reactive aggregates showed a slight decrease in the tensile strength of approximately 7% over 12 weeks.
- High strength concrete:
 - The change in the tensile strength using the highly reactive aggregates was 4.9%.
 - The samples exposed to NaOH solution experienced a continual decrease in the tensile strength throughout the testing duration.
 - At the end of the 12 week test period, the tensile strength had decreased approximately by 25% for the highly reactive aggregate.
 - The same trend of tensile strength reduction, due to exposure time, was observed in the specimens containing moderately reactive aggregates.
 - Both the potentially high and moderate reactive aggregates (identified by accelerated mortar bar testing and petrographic examination) were used to prepare concrete specimen with normal and high strength.

- After the initial 28 day curing period, the specimens were equally divided and submerged in a holding tank containing either a solution of a sodium hydroxide or deionized water at 80°C for a period of 12 weeks.
- Normal strength concrete specimens containing the potentially highly reactive aggregate and exposed to the sodium hydroxide solution experienced more losses in mechanical properties than the concrete specimens prepared with potentially moderately reactive aggregates.
- In high strength concrete specimens exposed to the sodium hydroxide solution, however, there was a minimal loss in mechanical properties for both of the specimens containing the highly reactive or moderately reactive aggregates.
- The superior performance of high strength concrete can be explained by the improved microstructure and decreased permeability due to the formation of secondary calcium silicate hydrate formed as a result of the pozzolanic reaction.
- The effect of ASR on the compressive strength of concrete is a function of time.
- The cylinder compressive strength and the secant modulus of elasticity at different exposure periods are summarized in Figure 3.142. The secant modulus of elasticity was determined by dividing the concrete stress at a stress level equal to 0.45 of the ultimate compressive strength by the corresponding concrete strain.

Aggregates	Period of exposure	Normal strength concrete				High strength concrete			
		Cured in water		Exposed to NaOH solution		Cured in water		Exposed to NaOH solution	
		f'_c (MPa)	E_c (GPa)	f'_c (MPa)	E_c (GPa)	f'_c (MPa)	E_c (GPa)	f'_c (MPa)	E_c (GPa)
Highly reactive	28 days	41.25	39.14	41.25	39.14	77.70	30.59	77.70	30.59
	12 weeks	46.60	28.78	30.42	–	95.59	35.67	79.98	25.97
Moderately reactive aggregate	28 days	47.98	33.46	47.98	33.46	74.52	31.75	74.52	31.75
	12 weeks	57.93	53.95	48.70	23.04	93.64	44.17	91.69	37.28

f'_c : Ultimate compressive strength of concrete cylinder, E_c : secant modulus of elasticity.

Figure 3.142: Compressive strength and modulus of elasticity of normal and high strength concretes; Marzouk and Langdon (2003)

- Normal strength concrete:
 - Maximum reduction in compressive strength was noted for the normal strength concrete prepared with the highly reactive aggregates.
 - For specimens exposed to NaOH solution, an overall reduction of 24% in the compressive strength and 81% in the modulus of elasticity was observed after 12 weeks of exposure.
 - In the specimens stored in deionized water, an overall increase in strength of 14% was observed after the same exposure period. This can be attributed to the elevated storage temperature (80°C) probably accelerated the hydration of cement.
 - Despite an increase in the compressive strength of specimens exposed to deionized water, the modulus of elasticity of normal strength concrete decreased with exposure time for the specimens containing highly reactive aggregate.
 - For specimens exposed to the NaOH solution and containing moderately reactive aggregates, the compressive strength of the specimens after 12 weeks stayed virtually the same; whereas, the modulus of elasticity was reduced at the same period of exposure.

- Both the compressive strength and modulus of elasticity were increased during the same exposure period for the specimens subjected to deionized water due to increased maturity of concrete.
- High strength concrete:
 - High strength concrete specimens exposed to NaOH solution exhibited 3% and 23% increase in compressive strength for highly reactive and moderately reactive aggregates, respectively.
 - The modulus of elasticity of the highly reactive specimens indicated a decrease during the same exposure period, despite the small increase in the compressive strength.
- The test is based on ASTM C293 on the prism samples with central point loading.
- Normal strength concrete:
 - Samples containing highly reactive aggregates exposed to the NaOH solution experienced a decrease in the modulus of rupture from 4.56 to 4.16 MPa.
 - A similar trend was observed for the specimens containing moderately reactive aggregates.
 - All specimens exposed to the deionized water experienced a small increase in the modulus of elasticity after a 12 week period of exposure due to the increased maturity of concrete.
- High strength concrete:
 - Samples containing highly reactive and moderately reactive aggregates placed in the NaOH solution experienced an increase in the modulus of rupture of 10% and 21%, respectively.
 - Samples exposed to deionized water experienced an overall increase in the modulus of rupture throughout the testing period.

3.105 Merz, Christine and Leemann, Andreas (2013)

URL

```
@article{
merz2013assessment,
label={merz2013assessment},
title={Assessment of the residual expansion potential of concrete from structures
damaged by AAR},
author={Merz, Christine and Leemann, Andreas},
journal={Cement and concrete research},
volume={52},
pages={182--189},
year={2013},
publisher={Elsevier},
url={https://www.sciencedirect.com/science/article/pii/S0008884613001622}
```

- Determination of the residual expansion potential can provide important information on the prognosis of AAR in concrete structures.

- There are still uncertainties about the test protocol and data analysis.
- In this study, residual expansion of cores from several concrete structures damaged by AAR was measured.
- Expansion during the test can be divided into different phases with different expansion rates.
- Results indicate that the expansion in the first phase, that takes place after sample conditioning but before a linear expansion rate is reached, is specific for each concrete and proportional to the further expansion of the cores during the test.
- It can be used to distinguish concrete with different residual expansion potentials.
- Residual expansion correlates both with the expansion rates on the investigated structures and the expansion of lab concrete, having a similar composition as the on-site concrete, determined with a concrete performance test.

Major Conclusions

The residual expansion potential of cores with diameters of 50 and 100 mm taken from structures damaged by AAR was determined. The determined expansions during the different phases were compared and discussed to improve and confirm the methodical approach. Additionally, the results were compared with the crack-index of strongly damaged parts of the investigated structures and with the expansion of concrete, having a similar composition as the on-site concrete, determined with the CPT to further assess the significance of the residual expansion test. The following conclusions can be drawn in regard to the different expansion phases:

- The expansion during the water saturation of the samples (phase 1) is partially irreversible indicating AAR-induced expansion in addition to expansion caused by moisture uptake.
- The non-linear expansion (rate and duration) after the water saturation and at the beginning of the storage is specific for each concrete and depends on the temperature condition. It influences the following linear expansion rates, respectively the irreversible expansion reached at the end of the test. Additionally, it correlates with the expansion obtained in the concrete performance tests.
- The following linear expansion rate of the samples is independent of temperature and sample diameter, but it levels off rapidly for small samples likely due to alkali leaching. High linear expansion rates indicate the presence of an internal source of alkalis in the concrete.
- The irreversible expansion is determined by drying the cores back to their initial mass at the start of phase 1. It includes the part of the expansion reached during phase 1 which is not caused by the increase of water saturation but likely by AAR and the expansion during phase 2.

Recommendations

The following recommendations for conducting the residual expansion potential test can be given:

- During the non-linear expansion phase, the longitudinal expansions are independent of the core diameter in contrast to the diametral expansion. Therefore, it is recommended to use the longitudinal expansion for assessing the residual expansion potential.

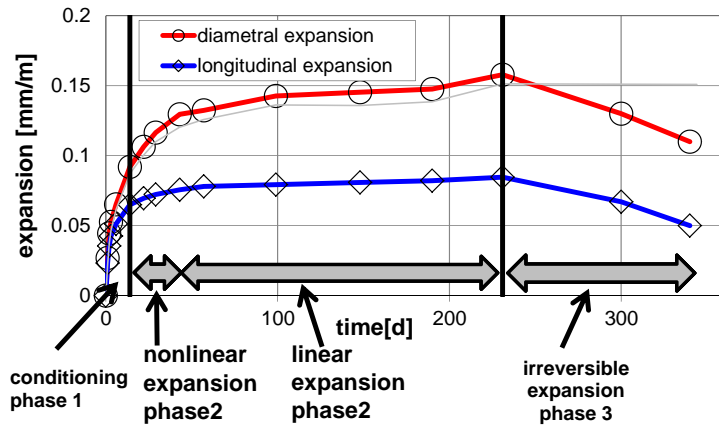


Fig. 2. Different phases of expansion during the residual expansion measurements in longitudinal and diametral directions of cores

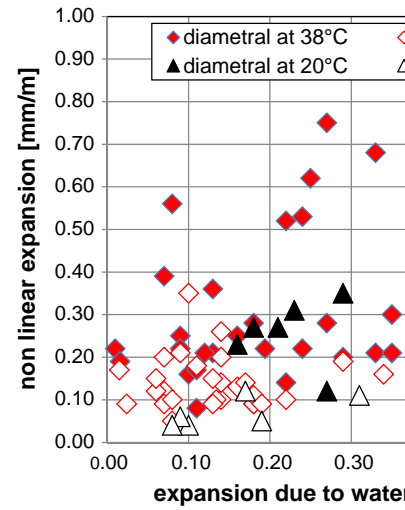


Fig. 4. Non-linear expansion at the beginning of water adsorption during conditioning of the sam

Figure 3.143: Different phases of expansion during the residual expansion measurements in longitudinal and diametral directions of cores.

- Cores with a large diameter are less prone to alkali leaching. Therefore, 100 mm cores are better suited for the residual expansion test than 50 mm cores. A core length of 200 mm has proven to provide the needed accuracy in the length measurements and to be easy enough to handle in the laboratory.
- Expansion rates are faster at a temperature of 38°C compared to 20°C. As results are obtainable within a shorter time period, a temperature of 38°C is recommended. Different parameters permit to assess expansion rates and the residual expansion potential:
- Both the non-linear and the linear expansion during phase 2 permit an assessment of expansion rate of a specific concrete if the latter shows no levelling off.
- It is preferable to use the expansion during phase 2 for assessing the residual expansion potential.
- If the expansion of the 100 mm cores levels off before the end of the test after one year, the expansion potential is exhausted and the measured expansion represents the residual expansion potential of a specific concrete. If this happens with 50 mm cores it can either be caused by leaching or by the exhaustion of the expansion potential. The residual expansion potential is a valuable tool to assess the further development of AAR in a structure. However, more data are needed to support the conclusions of this study.

3.106 Metalssi, Othman Omikrine and Seignol, Jean-François and Rigobert, Stéphane and Toutlemonde, François (2014)

URL

```

@article{
  metalssi2014modeling},
  label={metalssi2014modeling},
  title={Modeling the cracks opening--closing and possible remedial sawing operation
    of AAR-affected dams},
  author={Metalssi, Othman Omikrine and Seignol, Jean-Fran{\c{c}}ois and Rigobert,
    St{\`e}phane and Toutlemonde, Fran{\c{c}}ois},
  journal={Engineering Failure Analysis},
  volume={36},
  pages={199--214},
  year={2014},
  publisher={Elsevier}
  Keywords={}

```

- The AAR effect in a concrete dam was studied including the nonlinearity and contact elements.
- Displacements and stresses at the contact elements zone were computed and compared with results of the dam computations without contact elements.
- The results show that the creation of the slot cutting leads to a decrease of the compressive stresses in the structure, confirming a favorable effect of this stress release technique to address AAR affected structures.
- The contact elements can be used in 2D and 3D conditions.
- The nodes of the contact elements are common, for half of them, to one of the solid elements, element E1, and the second half also belongs to the second solid element, element E2. It is then possible to define a relative displacement between E1 and E2. The stress field in the contact element can also be written as the sum of a normal and a shear stresses.
- As long as the normal displacement u_N remains strictly positive, the contact element is inactive. When $u_N \leq 0$, the element is activated.
- Active contact elements can be assigned a tensile strength f_t . As long as the normal stress, σ_N , fulfills the tensile criterion $\sigma_N < f_t$, normal displacement is prescribed. When the tensile criterion is no longer satisfied, the contact element is deactivated.
- Coulomb friction criterion is considered for shear response.
- The basic principle of modeling cutting lines consists in creating a thin void in the structure and allowing the compressive stress to re-close this slot until contact occurs. This technique is rejected in this case study since it requires a very fine mesh and makes the problem unrealistic.
- In the case of classical contact elements, the cutting of concrete with a saw cut of width w would be represented by opening the contact element, hereby, prescribing the normal stress σ_N to zero and giving an initial value of relative displacement $u_N = w > 0$.
- A simplified model, which might represent an idealized part of an AAR-affected gravity dam (20 m long, 5.0 to 18.9 m wide and 26 m high), is used as case study.
- The concrete behavior is linear elastic.

- 51 year time-steps were used for the simulation.
- The mesh counts 650 3D elements, 25 frictionless contact elements, and 3392 nodes.
- The main geometrical characteristics are illustrated in Figure 3.144.
- The model is supposed to be homogeneous.
- Characteristics and latency times are assumed to be 6 years. Maximum AAR expansion is 0.0015.

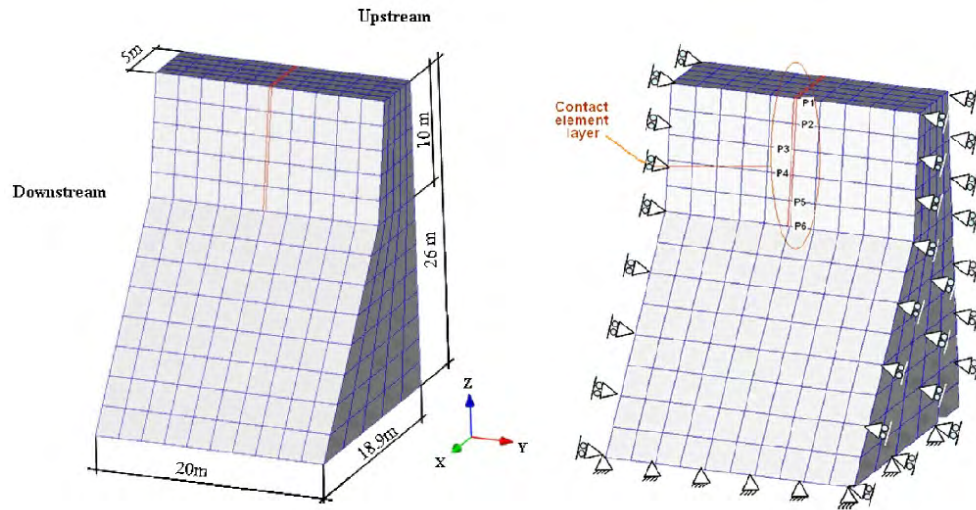


Figure 3.144: Geometrical characteristics of the idealized dam and finite element mesh including contact elements and boundary conditions; Metalssi et al. (2014)

- Displacement and stress at different points along the joint are shown in Figure 3.145. Results are presented for both before and after sawing.
- Transverse displacements are zero for points until 10 years for reasons of symmetry. After sawing ($e = 1$ cm), the notch closes instantaneously due to the decompression of surrounding concrete, and cumulated displacements on both sides of this notch reach exactly the value of the sawing thickness. The notch remains open only at point P6 (top).
- For the reference case, the transverse stress increases with time until its stabilization at a value of 45 MPa (the theoretical maximum stress). While in the case of the slot cutting, the stresses decrease instantaneously just after sawing but then increase again with time until stabilization at values of 30 to 35 MPa (the theoretical values calculated at the end of the swelling).
- The vertical displacements decrease instantaneously after sawing and increase again, but these displacements stay about 5% lower than the vertical displacements of the reference case (without sawing).
- Effect of stresses on anisotropy of expansion:

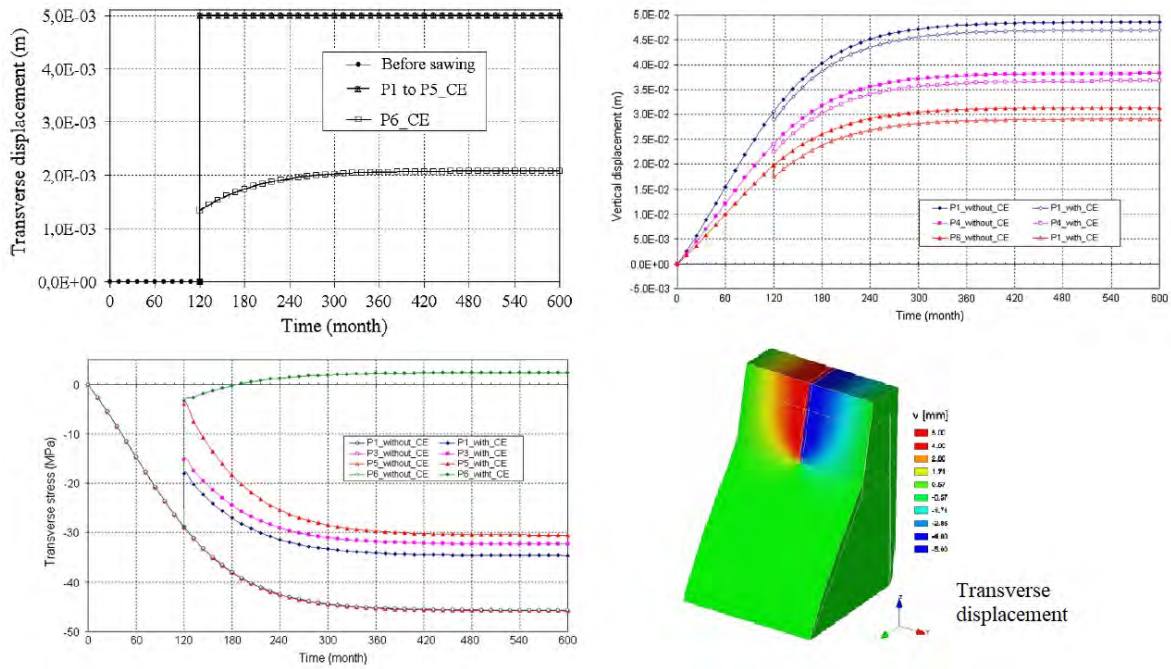


Figure 3.145: Displacement and stress vs. time before and after sawing; Metalssi et al. (2014)

- Considering anisotropy effects reduces the vertical displacement during the first 12 years because of the influence of stresses caused by the weight of the dam. After this time, however, this vertical displacement becomes more important.
- The stress-induced anisotropy effect is more important in the direction of the stream because of the influence of the model's shape and the boundary conditions. In fact, as the two sides in this direction are free, the displacement becomes more important when the effect of anisotropy is considered.
- Without sawing, the transverse stress becomes more important by considering the anisotropy effect during the 15 first years, and it stabilizes rapidly after this time. After the creation of the notch in the studied dam, however, the difference between the maximum transverse stresses becomes small.

3.107 Miyagawa, Toyoaki and Seto, Kaoru and Sasaki, Kazunori and Mikata, Yasuhiro and Kuzume, Kazuhiro and Minami, Toshikazu (2006)

URL

```
@article{
miyagawa2006fracture},
label={miyagawa2006fracture},
title={Fracture of Reinforcing Steels in Concrete Structures Damaged by
Alkali-Silica Reaction},
author={Miyagawa, Toyoaki and Seto, Kaoru and Sasaki, Kazunori and Mikata,
Yasuhiro and Kuzume, Kazuhiro and Minami, Toshikazu},
journal={Journal of Advanced Concrete Technology},
volume={4},
number={3},
pages={339--355},
year={2006},
publisher={Japan Concrete Institute}
Keywords={}
```

- The safety of a structure becomes questionable when the confinement of concrete becomes degraded due to the fracture of reinforcing steel bars.
- It is important to clarify the mechanism of the fracture of reinforcing steel bars and develop methods for detecting steel bar fractures and strengthening concrete structures damaged by ASR.
- The examined concrete member is a PC beam of a T-shaped pier constructed 1979.
- The pier was repaired twice (in 1989 and 1992) by applying surface protective coating and crack injection.
- In 1999, it is realized that the compressive strength is about 10-15 MPa lower than the specified compressive strength (35 MPa). Also, the modulus of elasticity was half that of sound concrete.
- Chipping inspection of the corner of the beam crown is conducted, and the fracture was discovered at the bent section of the stirrups.



Figure 3.146: Chipping inspection of pier beam (left); Fractured steel bar (right); Miyagawa et al. (2006)

- Based on a series of extensive laboratory experiments and the results of field measurements, several general conclusions were provided:

- In piers with few reinforcing bars, many steel fracture at the dens of steels have been reported when deterioration due to ASR is severe at locations where the weather readily attacks the structures.
- The steel bar rib shape and the bending radius are considered to have a significant influence on steel bar fracture due to ASR.
- Non-destructive tests (such as electromagnetic tests) can be used to determine the progress of deterioration causing steel bar fracture in the case when the cover is less than 10 mm thick.

3.108 Moranville-Regourd, Michelle (1997)

URL

```
@article{
moranville1997modelling},
label={moranville1997modelling},
title={Modelling of expansion induced by ASR-New approaches},
author={Moranville-Regourd, Michelle},
journal={Cement and Concrete Composites},
volume={19},
number={5-6},
pages={415--425},
year={1997},
publisher={Elsevier}
Keywords={}
```

- ASR expansion mechanism is studied by thermodynamics and kinetics of the chemical reaction considering the diffusion law and by probabilistics of random gradients of alkalis and silica reactive sites and local formation of gel.
- Induced mechanical effects are based on:
 - The capillary pressure relating the volume of expansive gels dissipated in connected porous zones to the initiation of cracks the linear fracture mechanics applied to the propagation and orientation of initiated cracks
 - A law of proportionality between confinement, temperature, relative humidity, and reactivity describing the nonuniform anisotropic 3D distribution of the AAR expansion
- The probabilistic approach accounts for the localization, size, and degree of reactivity of silica as well as the probability of local and global presence of Na^+ , K^+ , and OH^- ions.
- The numerical model was adopted from Roelfstra, Sadouki, and Wittmann (1985) and, representing the heterogeneity of the material by discretization, has been applied to two gravity dams by Carol (1994).
- The mechanical behavior of concrete is represented by a constitutive model based on the theory of plasticity.
- The finite element model uses 698 standard elements (383 of which represent mortar), and 155 joint elements correspond to the aggregate-mortar interface.

- The parametric model is a finite element structural analysis of dams altered by AAR. Parameters influencing the concrete expansion are confinement, temperature, moisture, and reactivity, Figure 3.147.

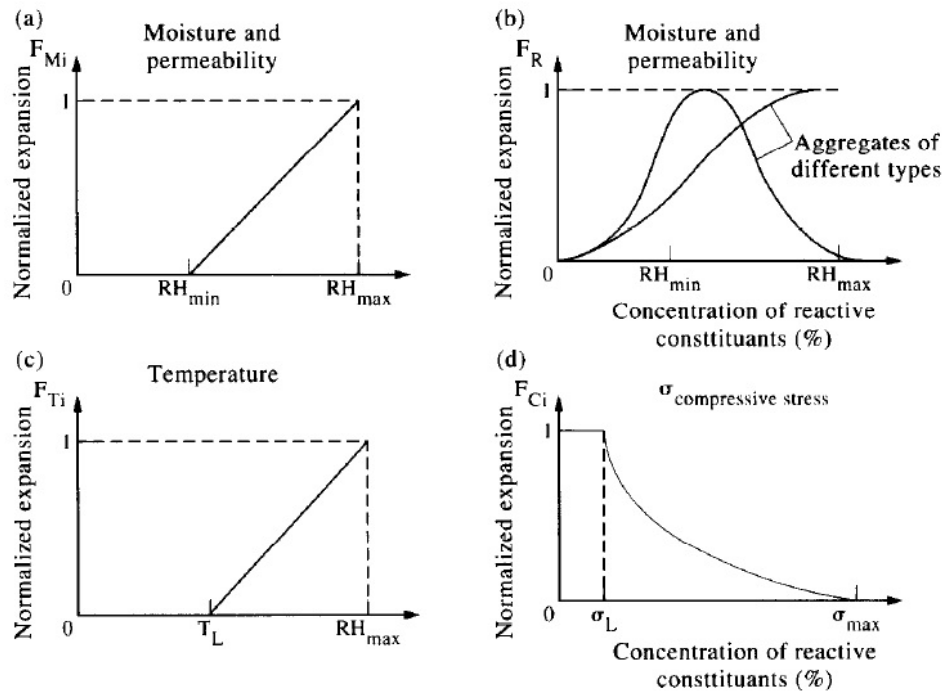


Figure 3.147: Factors influencing AAR related concrete expansion; Moranville-Regourd (1997)

- Numerical results are very close to experimental data for the pessimum content of reactive silica, the evolution of linear expansions vs. the consumed alkali, and the benefit of an isotropic confinement on expansion.
- The anisotropic nonuniform character of AAR is considered in a new law which calls for a closer combination with the physical processes involved.

3.109 Morenon, Pierre and Multon, Stéphane and Sellier, Alain and Grimal, Etienne and Hamon, François and Bourdarot, Eric (2017)

URL

```

@article{
morenon2017impact},
label={morenon2017impact},
title={Impact of stresses and restraints on ASR expansion},
author={Morenon, Pierre and Multon, St{\`e}phane and Sellier, Alain and Grimal,
Etienne and Hamon, Fran{\c{c}}ois and Bourdarot, Eric},
journal={Construction and Building Materials},
volume={140},
pages={58--74},
year={2017},
publisher={Elsevier}
Keywords={}

```

- The impact of applied stresses and restraint due to reinforcement or boundary conditions on ASR expansion and induced anisotropic cracking was studied.
- First, a poro-mechanical model is proposed. Next, it is validated.
- In this model, the cracks created by ASR are represented by plastic strains.
- Numerical results were compared to the results of Multon's tests (Multon and Toutlemonde, 2006) to validate the proposed model.
- The impact of restraint is studied by modeling a cube. It was restrained in from one to three directions as in Figure 3.148. In order to analyze the concrete behavior under ASR pressure only, the tests were calculated without shrinkage.

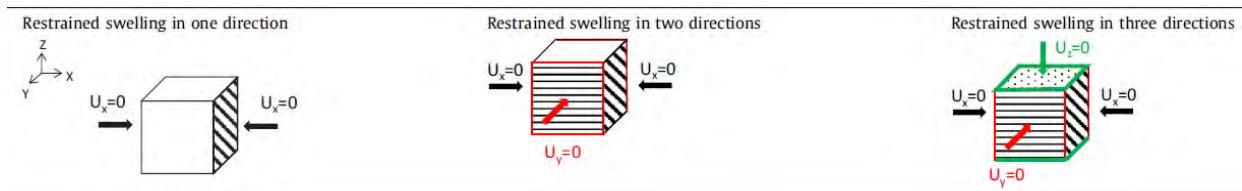


Figure 3.148: Boundary conditions of theoretical tests; Morenon et al. (2017)

- Expansion is assumed to be 0.3%, and different restrains were applied to the cube, Figure 3.149.
- Strain in the free directions increased by 25%, compared to stress free expansion when the cube was restrained in one direction, and by 65% when it was restrained in two directions.
- The stress in restrained conditions could be described in two phases: a slow increase of the stress before first cracking (0 to 80 days) and then a fast increase after the first ASR damage.
- For these conditions of perfect restraint, the maximum stress lay between 3 and 7 MPa of compression (for 1-3 restrained directions). For specimens with 2 or 3 restrained directions, the maximum compressive stress increased, reaching 4 and 7 MPa respectively.

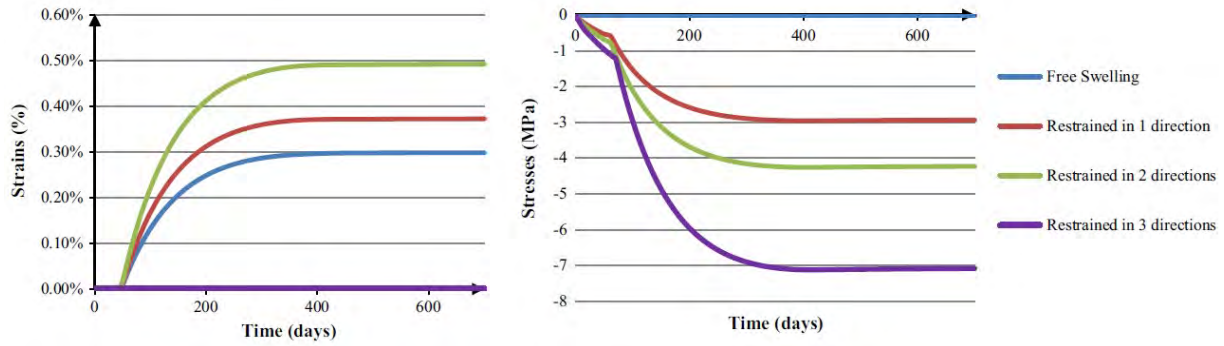


Figure 3.149: Comparison of strains and stresses in free swelling and restrained tests; Morenon et al. (2017)

- For the specimen restrained in one direction, induced stresses were between 0 and 3 MPa. Figure 3.150 (left) shows the strains obtained for different loads in the stress direction. The larger the applied stress, the smaller the final strain.
- Above 1 MPa of compressive stress, the latency period depended on the stress state because creep strains were larger than the strains induced by the gel pressure.
- ASR damage (right plot) is not linearly proportional to the stress applied. It weights ASR plastic strains when calculating ASR damage.

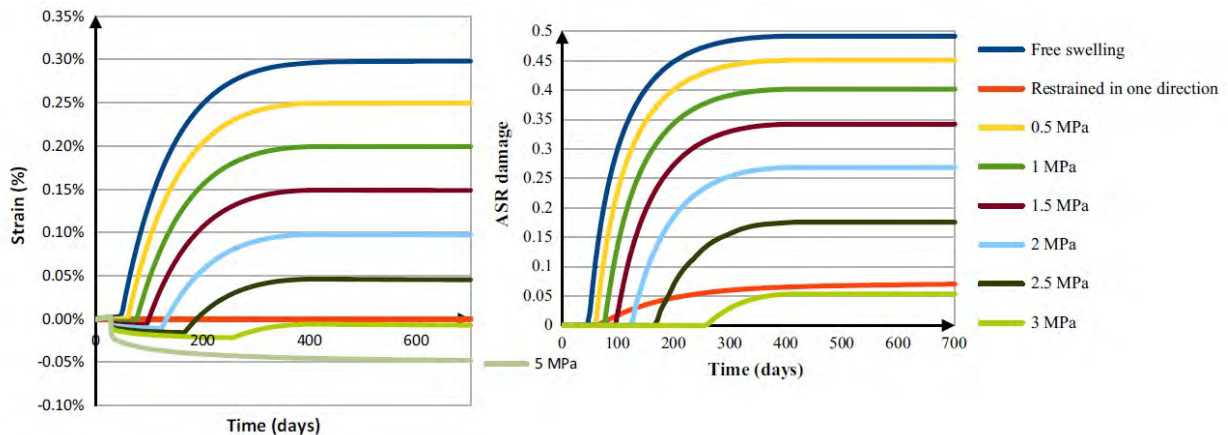


Figure 3.150: Strains and damage (in loading direction) in loaded or restrained direction; Morenon et al. (2017)

- Figure 3.151 shows the damage in the loaded and free directions for the 3 MPa loading test (one direction loaded).
- The first damage was in the unloaded direction, and then the loaded direction was slightly damaged.
- There was a delay between the start of cracking in the different directions. The free direction was less damaged than the loaded direction. This represents the effect of compressive stress on the anisotropy of cracking due to ASR expansion.

- The difference depends directly on the applied stress. For a smaller stress, the damage perpendicular to the loaded direction is greater while, for a stress higher than about 3 MPa, no damage is expected perpendicular to the loaded direction.
- As damage directly affects the Young's modulus, the material becomes anisotropic; the Young's modulus will be smaller in the free direction while the mechanical performances are less affected in the loaded directions.

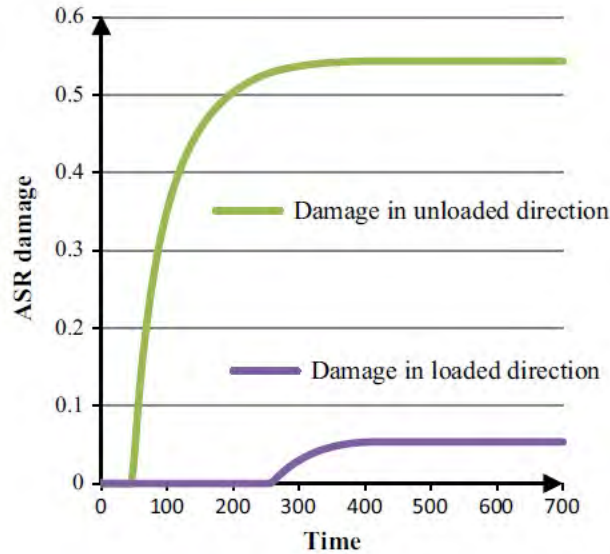


Figure 3.151: ASR damage in the 3 MPa test (applied in one direction); Morenon et al. (2017)

- Simulated unloading tests during swelling showed that specimens extracted from a structure could crack rapidly due to the relaxing of stress and, thus, would impact future prognostic tests.
- Tension stresses during ASR swelling could lead to premature and greater expansion.

3.110 Morenon, P. and Grimal, E. and Kolayer, P. and Sellier, A. and Multon, S. (year=2018)

```
@article{
morenonmodelling18},
label={morenonmodelling18},
title={Modelling, assessment and rehabilitation of a dam affected by an internal
swelling reaction (ISR)},
author={Morenon, P. and Grimal, E. and Kolayer, P. and Sellier, A. and Multon, S.},
journal={Dam Engineering},
year=2018
Keywords={Laboratory; Expansion monitoring; Dam Gravity; Dam Arch; }
```

- The first part of the paper describes a poro-mechanical model for internal swelling reaction (ISR) and its implementation in the finite elements code Code-Aster.

- The constitutive model is based on a global rheological scheme which considers the porous pressures that come from shrinkage (water pressure) or ISR (gel pressure), external loading, and the solid concrete matrix as a representative elementary volume where the coupling between the swelling, creep, and anisotropic damage occurs (Grimal et al., 2008).
- The model was calibrated and validated upon several experiments and structures (Grimal et al., 2008; Morenon et al., 2017).
- Chambon Dam is a concrete gravity dam located in France and is used as case study. It was built 1929-1935.
- Its height is 137 m above the sub-glacial, deep, narrow channel (88 m above the river bed); and the crest is 294 m long and 5 m wide.
- The first disorders were observed in 1958, with cracks mainly located on lift joints on the upstream and downstream faces, as in the galleries.
- The first monitoring results indicated an atypical mechanical behavior with an upstream tilting of the crest on the left curved part.
- Several laboratory tests performed (1967 and 1996) showed signs of AAR. The heterogeneity of the location, intensity, and potential expansion of reactive sites within the dam were noted.
- Later, several remedial works were performed between 1990 and 1997 (i.e. crack grouting, new spillway, PVC membrane on the upstream face, and slot cutting).
- 10 years later (in 2007), the Dam was analyzed with new model.
- The Dam's structure is composed of different types of concrete.
- The temperature of the Dam was assumed to remain uniform and constant throughout computation. The chosen temperature is the average Dam temperature since its construction (8°C).
- The global methodology is summarized Sellier et al. (2009) and is repeated in Figure 3.152.
- Two complementary stages are recommended in this global methodology: 1) laboratory tests on drilled specimens allows the kinetics parameter to be obtained; 2) a finite elements inverse analysis of displacement and crack pattern allows the maximal swelling amplitude to be determined.
- As a result of the application of this method, Figure 3.153 shows the right representation of the radial, tangential and vertical displacements at the crest of the other cantilever.
- The model allows for the appreciation of the evolution of the stresses, which have increased since 1940, especially in the area of contact with the foundation rock.
- Several works have been implemented to treat each identified pathology and to extend the life of the Dam:
 - Sawing
 - Anchoring and upstream face reinforcement
- Anchoring density was completed by a “nest” formed with carbon fiber strips in order to prevent the fall of possible isolated blocks.

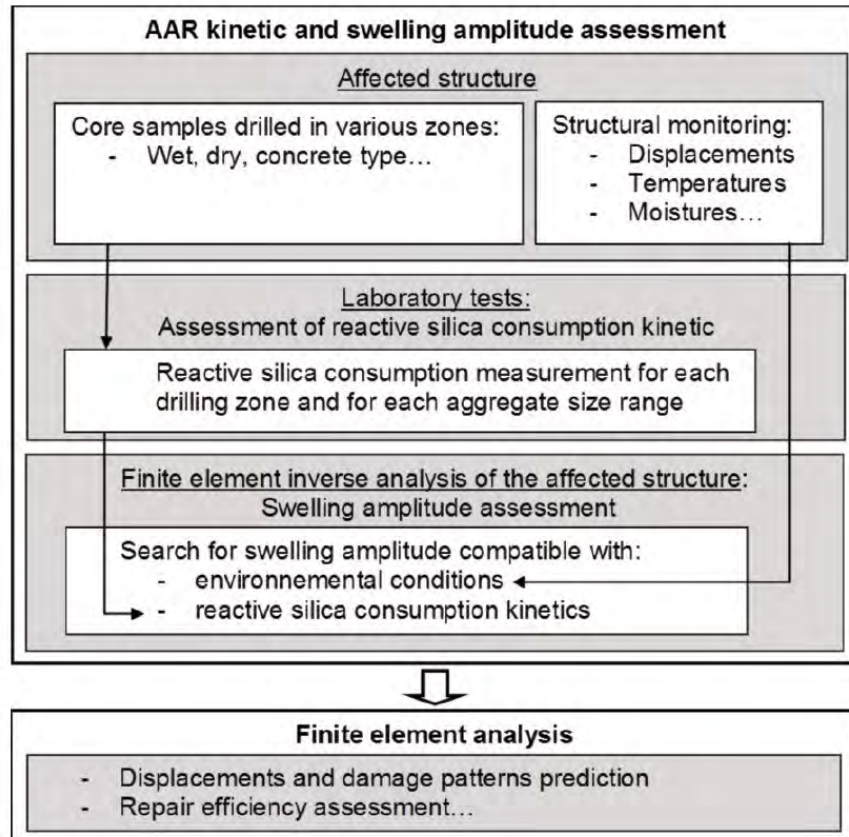


Figure 3.152: Global methodology summary; Morenon et al. (2018)

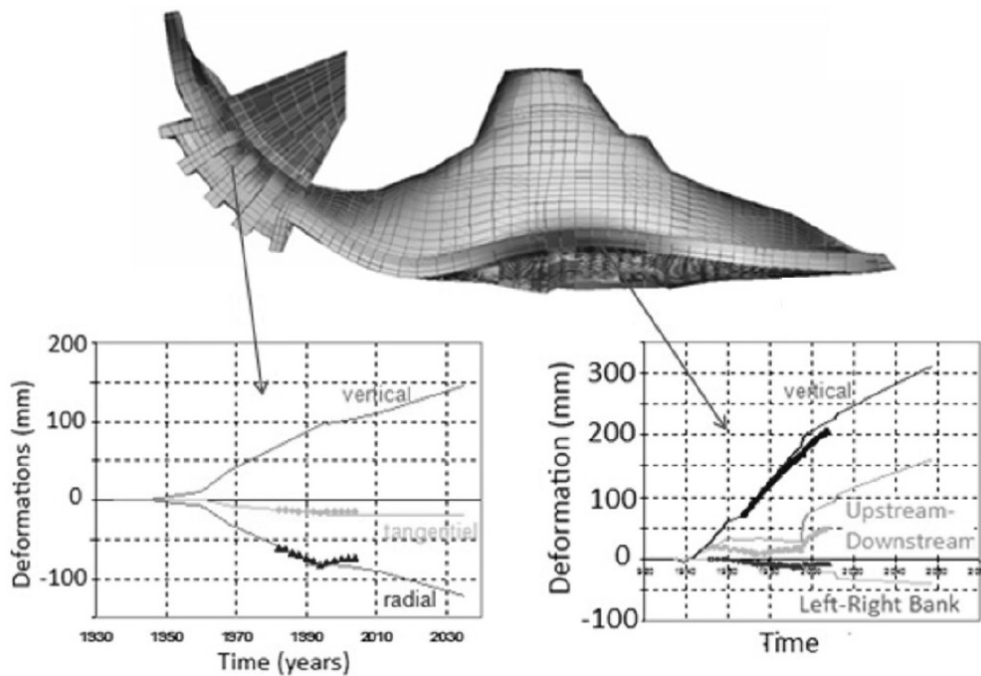


Figure 3.153: Comparison of measured and computed deformations in 3D; Morenon et al. (2018)

3.111 Mukhopadhyay, Anal and Shon, Chang-Seon and Zollinger, Dan (2006)

```
@article{
mukhopadhyay2006activation},
label={mukhopadhyay2006activation},
title={Activation energy of alkali-silica reaction and dilatometer method},
author={Mukhopadhyay, Anal and Shon, Chang-Seon and Zollinger, Dan},
journal={Transportation Research Record: Journal of the Transportation Research
Board},
number={1979},
pages={1--11},
year={2006},
publisher={Transportation Research Board of the National Academies}
Keywords={}
```

- Certain initial conditions related to material alkalinity, aggregate reactivity, humidity, and temperature conditions are known to initiate ASR.
- A key factor in the prediction of ASR in concrete over time is the reactivity of the aggregate.
- A performance-based approach is proposed that can address the ASR potential of concrete at levels of alkali, temperature, and moisture that are realistic and representative of actual field conditions.
- The concept of ASR-related activation energy is introduced as a representative single parameter of the ASR.
- An attempt was made to introduce the dilatometer test method as part of a performance-based testing protocol.
- It is observed that this method can categorize minerals and aggregates based on their reactivity within a short period.
- The use of the activation energy provides a unique parameter for evaluating ASR susceptibility of minerals and aggregates.
- The proposed performance-based approach for predicting ASR is given by the following equation:

$$\varepsilon = \lambda \varepsilon_0 \exp \left(- \left(\frac{\alpha}{t_e} \right)^\beta \right) \quad (3.18)$$

where ε is concrete expansion, ε_0 ultimate ASR expansion of the concrete, λ supplementary cementitious material adjustment factor, α and β are concrete parameters, and t_e is equivalent age and is computed as:

$$t_e = \gamma_H \sum_0^t \exp \left(- \frac{E_a}{R} \left(\frac{1}{273 + T} - \frac{1}{273 + T_r} \right) \right) \cdot \Delta t \quad (3.19)$$

where γ_H is relative humidity factor, E_a ASR activation energy of aggregate, T temperature ($^{\circ}\text{C}$), T_r reference temperature ($^{\circ}\text{C}$), R universal gas constant (8.314 J/mol.K), and Δt is time.

- Determination of the ASR activation energy (E_a) of aggregates is accomplished through a series of steps:
 - First, the rate constant and ultimate expansion are determined.
 - The second step is to determine the activation energy (E_a) that characterizes the ASR susceptibility of aggregate.
- Increasing temperature of the test solution accelerates the rate of expansion caused by ASR regardless of mineral and aggregate reactivity.
- Activation energy appears to be a useful measure for categorizing different form of silica minerals based on their reactivity. The degree of crystallinity of different forms of silica minerals matches with the activation energy results.
- The ASR potential of mineral-aggregate can be determined by dilatometry within a short period of time (e.g., 2 to 3 days). It is, however, necessary to verify whether the predicted later age results based on the early age fitted curve correlates well to the actual measured later age data (e.g., 14 days).
- The E_a of different forms of silica will be useful to validate the E_a of different aggregates containing those minerals in different proportions.
- Activation energy can serve as an overall indicator of ASR potential and can be used as a potential screening parameter as a minimum for ASR in-the-field performance. This method is potentially useful, therefore, for both practitioners and researchers.

3.112 Mullick, AK (1988)

URL

```
@article{
mullick1988distress},
label={mullick1988distress},
title={Distress in a concrete gravity dam due to alkali silica reaction},
author={Mullick, AK},
journal={International Journal of Cement Composites and Lightweight Concrete},
volume={10},
number={4},
pages={225--232},
year={1988},
publisher={Elsevier}
Keywords={}
```

- Multidisciplinary investigations were conducted to identify the causes of distress in case of a concrete gravity dam and powerhouse structure.
- Visual observations of the damaged concrete in the dam, as well as elaborate instrumental analyses of the concrete samples, established the occurrence of ASR after nearly 25 years of service.

- Granitic aggregates containing strained quartz with UE angle varying from 25 to 30° and alkali feldspars (used with cements of moderate to high alkali content) gave rise to deleterious reactions.
- Although the structural stability of the dam was not endangered, the serviceability was seriously affected.
- Repair measures provided for future movements in the reinforced concrete frame structure due to continued ASR.
- Cracks at the upstream faces were to be sealed with epoxy grout, followed by epoxy painting to minimize ingress of water.
- Chemical grouting was recommended to be completed in the mass of the structures to effectively fill up the cracks and restore their monolithic behavior.
- In the powerhouse structure where reinforcement had snapped in the concrete columns, additional reinforcement was provided and then jacked with steel plates. For accommodating future expansion, the fixed joints in the penstock gallery frame were to be released.

3.113 Multon, S and Seignol, J-F and Toutlemonde, F (2005)

[URL](#)

```
@article{
multon2005structural},
label={multon2005structural},
title={Structural behavior of concrete beams affected by alkali-silica reaction},
author={Multon, S and Seignol, J-F and Toutlemonde, F},
journal={Materials Journal},
volume={102},
number={2},
pages={67--76},
year={2005}
Keywords={}
```

- A large experimental program about ASR was carried out on beam specimens.
- 3D deformations were measured on five 3 m-long plain or reinforced concrete beams undergoing partial drying over a period of 14 months. The beam specimens had a cross section of 0.25 × 0.50 m and were simply supported. The upper face was exposed to air at 30% relative humidity.
- The effect of a moisture gradient over the depth of the beams and the influence of reinforcement on the development of ASR-induced expansions were studied.
- The temperature within the beams was constant at 37±1°C.
- The methodology for the assessment of ASR-affected structures is based on the potential expansion of the material (which directly depends on the concrete mixture and on the environmental conditions).

- Two concrete mixtures were studied: one with reactive coarse aggregate and nonreactive sand and one with nonreactive aggregate only.
- The two mixtures were designed to have close rheological and mechanical properties.
- Tests on companion specimens (160 × 320 mm cylinders and 140 × 140 × 280 mm prisms) were completed to measure the material expansion and mechanical characteristics.
- Mechanical characteristics of two concrete mixtures are shown in Figure 3.154. Every mechanical property was measured on three specimens for every time-step.
- The mean Young's modulus of the reactive concrete, measured on three specimens, decreased approximately 20% between the 90th and the 365th exposure days.

Test time-steps		28th day	90th day	6th month	1 year
Reactive concrete	f_c , MPa	38.4	42.4	41.8	42.1
	E , MPa	37,300	37,200	30,100	29,700
	ν	0.22	0.24	—	—
	f_t , MPa	3.2	3.4	3.0	3.3
Nonreactive concrete	f_c , MPa	35.5	40.6	40.4	41.8
	E , MPa	38,700	38,400	37,800	40,700
	f_t , MPa	3.4	3.8	3.2	3.8

Notes: f_c = mean compressive strength on cylinders (diameter: 160 mm; height: 320 mm). E = Young's modulus on cylinders (diameter: 160 mm; height: 320 mm). ν = Poisson's ratio. f_t = mean splitting tensile strength on cylinders (diameter: 110 mm; height: 220 mm).

Figure 3.154: Mechanical characteristics; Multon, Seignol, and Toutlemonde (2005)

- The anisotropy of ASR-induced expansions has been verified with vertical swellings twice as large as horizontal swellings.
- Significant ASR expansions (0.10%) can occur without an external water supply and lead to significant structural degradation.
- An increase in ASR expansions with an external water supply has been quantified.
- Transverse and vertical measurements of the nonreactive beams showed expected strain ranges compared with the profile of mass variations and the relative humidity measurements, validating moisture input data for the analysis.
- For the reactive beams, the water distribution induced large expansions from 0.17 to 0.50 m along the transverse and vertical directions, smaller expansions at the depth of 0.08 m, and shrinkage on the drying face. The dominant influence of water supply on ASR-induced expansion was thus confirmed and quantified on beam specimens submitted to local intense drying.
- The effect of reinforcement on ASR-induced strains was quantified on beams; it was highly significant along the longitudinal direction (with a large decrease of strains and deflections for

Beams	Mixtures	Percent area of longitudinal steel
B1	Reactive	0
B2	Nonreactive	0
B3	Reactive	0.45
B4	Reactive	1.80
B5	Nonreactive	0.45

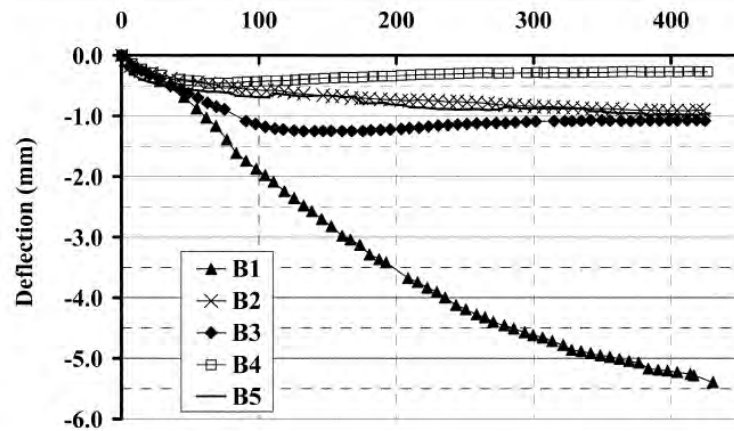


Figure 3.155: Mean deflection of five beams at midspan; Multon, Seignol, and Toutlemonde (2005)

the reinforced concrete beams compared to the plain beam) while the local effects of stirrups were hardly significant on vertical and transverse deformations.

3.114 Multon, Stéphane and Seignol, Jean-François and Toutlemonde, François (2006)

URL

```
@article{
  multon2006chemomechanical},
  label={multon2006chemomechanical},
  title={Chemomechanical assessment of beams damaged by alkali-silica reaction},
  author={Multon, St{\'e}phane and Seignol, Jean-Fran{\c{c}}ois and Toutlemonde,
    Fran{\c{c}}ois},
  journal={Journal of materials in civil engineering},
  volume={18},
  number={4},
  pages={500--509},
  year={2006},
  publisher={American Society of Civil Engineers}
  Keywords={}
```

- Chemo-mechanical calculations were formulated to investigate the assumption of modeling ASR-induced expansions as imposed strains.
- The input data for the model includes the moisture distribution in the damaged structures,

ASR-induced potential strains, and the influence of ASR on the concrete mechanical properties.

- The results of calculations were compared to experimental data obtained from ASR-damaged beam specimens.
- The role of water supply and reinforcement has been analyzed by comparing the deformations of plain and reinforced concrete beams subjected to a moisture gradient.
- Calculations show that cracking and compressive stresses (induced by steel reinforcement) have a large influence on the anisotropy of the ASR swellings. This induced anisotropy is one of the main factors that should be considered while predicting the mechanical behavior of ASR-damaged structures.
- The uncertainty of the calculations result from uncertainty in the moisture distribution and in the large scatter of the ASR-induced strains measured on the specimens.

3.115 Multon, Stéphane and Toutlemonde, François (2006)

[URL](#)

```
@article{
multon2006effect},
label={multon2006effect},
title={Effect of applied stresses on alkali--silica reaction-induced expansions},
author={Multon, St{\'e}phane and Toutlemonde, Fran{\c{c}}ois},
journal={Cement and Concrete Research},
volume={36},
number={5},
pages={912--920},
year={2006},
publisher={Elsevier}
Keywords={}
```

- The mechanical effects of ASR were modeled to assess the deterioration level and the stability of ASR-damaged concrete structures.
- The effect is so significant that assessment models must account for the modification of ASR expansions due to applied stresses and the consequential mechanical response of damaged structures.
- Measurements performed on concrete specimens subjected to several states of stress were analyzed along the three directions (due to applied stresses and to passive restraints).
- Mechanical calculations show that the volumetric expansion imposed by ASR is constant regardless of the stress conditions.
- “Expansion transfer” occurs along the directions which are less compressed; the effect of stresses on ASR expansions anisotropy can be precisely quantified.

- Two concrete mixtures with a 0.5 water/cement ratio and a 410 kg/m³ cement content is used: one “reactive” mixture with siliceous limestone aggregate containing reactive silica and one “reference” mixture with aggregate without reactive silica.
- After 28 days of curing, nine different states of stresses were applied to cylindrical specimens (130 mm in diameter and 240 mm in height) during 450 days.
- The axial stresses were applied by a flat hydraulic jack within closed frames which are usually used as creep devices.
- The radial stresses resulted from lateral restraint provided by steel rings (3- or 5-mm-thick), Figure 3.156.
- Reactive concrete was submitted to all combinations of three axial stresses (0, 10, and 20 MPa) and three transverse restraint levels (no rings, 3-mm-thick rings, 5-mm-thick rings). The reference concrete was only submitted to axial loading (due to insufficient lateral strains for inducing measurable restraint). Four specimens were tested for each condition, Figure 3.156.

		Restraint		
		None	3 mm	5 mm
Applied stresses	0 MPa	4R+4NR	4R	4R
	10 MPa	4R+4NR	4R	4R
	20 MPa	4R+4NR	4R	4R

R: reactive concrete, NR: non-reactive concrete.

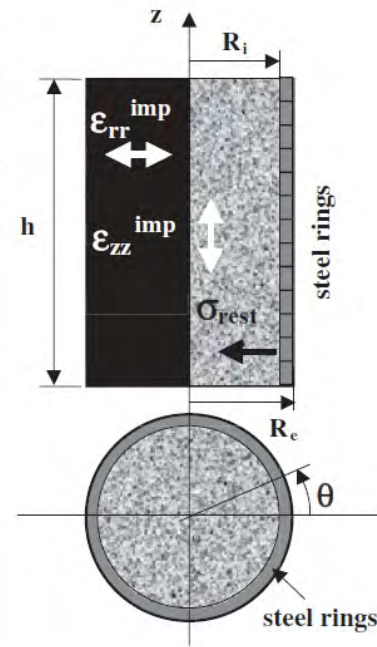


Figure 3.156: Characteristics of the 48 specimens including the steel rings and strain measurements by an automated device; Multon and Toutlemonde (2006)

- During the experiment, the deformations were measured on reference sealed specimens which were subjected to shrinkage and/or to basic creep, Figure 3.157. On the free-expanding reference specimens, large shrinkage strains were observed during the first 60 days (before stabilization).
- The long term Young’s modulus was obtained by dividing the instantaneous Young’s modulus by 4.

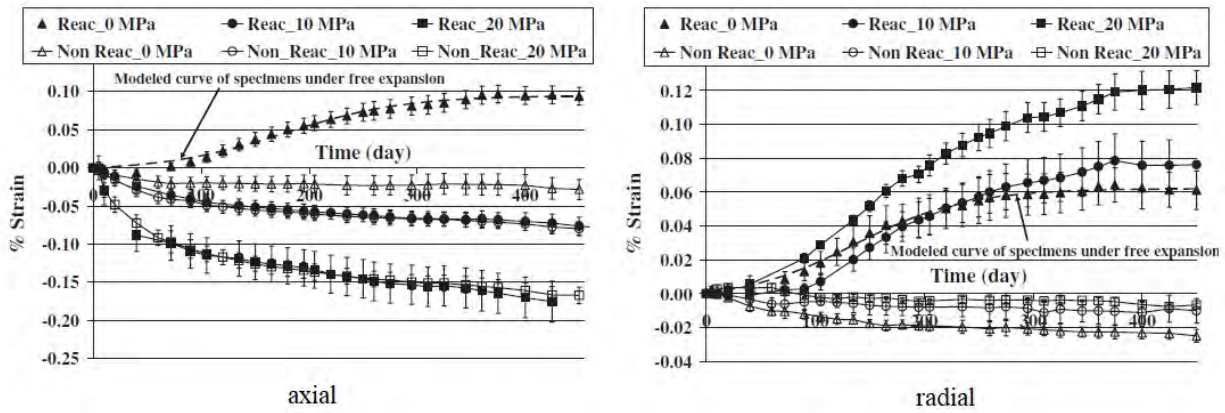


Figure 3.157: Measured axial and radial strains of the reactive and reference specimens under axial loading only; Multon and Toutlemonde (2006)

- Anisotropy of ASR-imposed strains appears to be constant during free expansion tests without externally applied loading, Figure 3.158. Anisotropy was about 1.15 - which is quite close to unity and far from previously reported values (about 2 in (Multon, Seignol, and Toutlemonde, 2005)).
- Mass losses were observed in (*ibid.*), so evaporation through watertight cover can be suspected. Such evaporation caused heterogeneity in the conditions of the specimens and can explain a larger value (about 2) of anisotropy than in the present study.
- Large ASR expansions caused more cracks and can cause a larger ASR anisotropy.

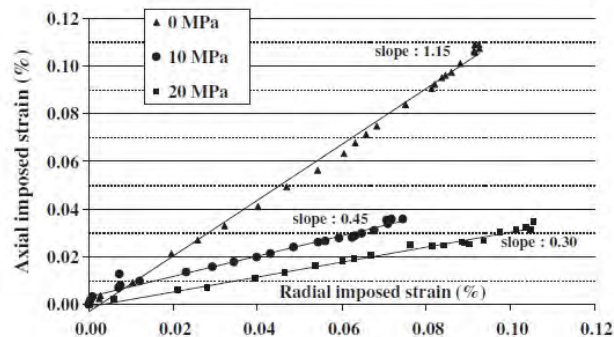


Figure 3.158: Axial imposed strains versus radial imposed strains for the reactive specimens without restraint; Multon and Toutlemonde (2006)

- Present investigations have validated the consistency of the approach which represents the ASR-induced expansions as isotropic imposed strains.
- Careful analysis of the “stress-free” expansion test is mandatory in order to consider the Poisson’s effect on 3D free expansion.
- The ASR volumetric imposed strain can be considered as constant regardless of the stress state.

- In loaded and/or restrained concrete, ASR-induced expansions are transferred in the less compressed direction.

3.116 Multon, Stéphane and Cyr, Martin and Sellier, Alain and Leklou, Nordine and Petit, Laurent (2008)

URL

```
@article{
  multon2008coupled},
  label={multon2008coupled},
  title={Coupled effects of aggregate size and alkali content on ASR expansion},
  author={Multon, St{\`e}phane and Cyr, Martin and Sellier, Alain and Leklou,
    Nordine and Petit, Laurent},
  journal={Cement and Concrete Research},
  volume={38},
  number={3},
  pages={350--359},
  year={2008},
  publisher={Elsevier}
  Keywords={}
```

- Experimental results were reported concerning the effect of particle size of an alkali-reactive siliceous limestone on mortar expansion.
- These results show that ASR expansion is seven times larger for coarse particles (1.25-3.15 mm) than for smaller ones (80-160 μm).
- In mortars for which the two size fractions were used, ASR expansion increased in almost linear proportion to the amount of coarse reactive particles for two different alkali contents.
- An empirical model is proposed to study correlations between the measured expansions and parameters such as the size of aggregates and the alkali and reactive silica contents.
- Starting with the procedure for calibrating the empirical model using the experimental program combined with results from the literature, it is shown that the expansion of a mortar containing different sizes of reactive aggregate can be assessed with acceptable accuracy.
- The cement used was a standard CEM I 52.5R (specific gravity: 3.1, surface area (Blaine): 400 m^2/kg).
- Six mortar mixtures were studied with different proportions of reactive and non-reactive aggregates from the three size fractions F1 to F3 (Figure 3.159). Only fractions F1 and F3 were used as reactive aggregates in order to study reactive particle sizes which were significantly different.
- Figure 3.160 (left) shows the final ASR expansion (after about 150 days at 60 °C) of mixtures containing only reactive particles from size fractions F1 and F3 (mortars M5 and M1).

Size fraction	Weight fraction (%) of the sand					
	F1 (80–160 μm)		F2 (315–630 μm)		F3 (1.25–3.15 mm)	
Nature	R	NR	R	NR	R	NR
Reference	0	30	0	40	0	30
M1	0	30	0	40	30	0
M2	5	25	0	40	25	5
M3	15	15	0	40	15	15
M4	25	5	0	40	5	25
M5	30	0	0	40	0	30

Figure 3.159: Grading of aggregates of mortar mixtures; Multon et al. (2008a)

- For the two alkali contents and for the same amount of reactive aggregate in the mortars, the expansion decreased by about 90% when aggregate fraction F1 was used (0.08-0.16 mm) instead of aggregate fraction F3 (1.25-3.15 mm). The sole difference in soluble silica between fractions F1 (9.4%) and F3 (12.4%) cannot easily explain these variations of expansion.

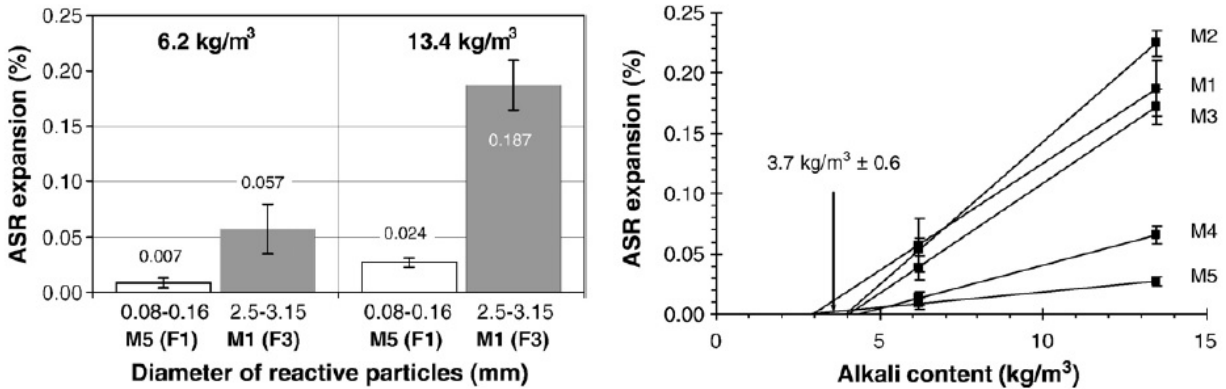


Figure 3.160: Effect of particle size of reactive aggregate on mortar expansion (M5 and M1) (left); Effect of the alkali contents on expansions of mortars M1 to M5 (right); Multon et al. (2008a)

- A decrease of about 70% to 80% of the expansion was obtained when the alkali content of mortar mixtures was reduced from the higher value (13.4 kg/m³) to the lower value (6.2 kg/m³).
- Figure 3.160 (right) presents the ASR-expansion of the mortars as a function of their alkali content. A linear relationship was assumed between the expansion and the alkali content.
- The results for mortar prisms M1 to M5 lead to a threshold value to be defined for alkali content, ranging between 2.9 kg/m³ and 4.4 kg/m³ with a mean value of 3.7 kg/m³.
- Next, a model was proposed to interpret the results and to describe the relationship between the amount of alkali and reactive silica and the final ASR expansion for mortar cast with reactive siliceous limestone.
- The empirical model is based on the summation of the ASR expansion values of the different size fractions and on the amounts of available and required alkali which react with the reactive silica, assessed from Poyet's experimental study (Poyet, 2003).

3.117 Multon, Stéphane and Barin, François-Xavier and Godart, Bruno and Toutlemonde, François (2008)

URL

```
@article{
multon2008estimation},
label={multon2008estimation},
title={Estimation of the residual expansion of concrete affected by alkali silica
reaction},
author={Multon, St{\`e}phane and Barin, Fran{\c{c}}ois-Xavier and Godart, Bruno
and Toutlemonde, Fran{\c{c}}ois},
journal={Journal of Materials in Civil Engineering},
volume={20},
number={1},
pages={54--62},
year={2008},
publisher={American Society of Civil Engineers}
Keywords={}
```

- An experimental research program was carried out in order to validate a methodology for the mechanical assessment of structures damaged by ASR.
- Long-term deformations of specimens kept under varied environments were measured.
- Results were collected according to the French methodology for measuring residual expansion on cores drilled from cylinders and prisms made of the same concrete materials.
- Numerous testing conditions were intended to check the experimental robustness of the most significant input data for structural assessment.
- Omitting the measured expansion of the specimens during a rather long period (60 days), as presently recommended, can lead to an unsafe estimation of ASR-residual expansions, especially when the core is drilled during the active phase of ASR development.
- The strains of the specimens during the first days of the test are caused by the superimposition of concrete expansion due to water sorption and additional ASR expansions. Evolutions and improved conditions of application relative to the French standard method for estimating residual expansion of ASR-affected concrete are proposed.
- The expansion must be evaluated through several measurements due to the large heterogeneity of ASR expansions.
- The core locations must be carefully chosen in order to be representative of the structure under study (direction of coring compared to casting direction and/or cracking, saturation level within the structure at the coring sites).
- Residual expansion tests must begin as soon as possible after coring to limit the non-measured expansion between coring and the first deformation measurements.
- The cores must be immediately sealed after coring until being tested in order to prevent any drying. The residual expansion tests must begin as soon as possible to avoid neglecting ASR expansions.

- Small containers are strictly required in order to obtain a correct control of the environment close to 100% RH.
- The expansion rate between 8 and 52 weeks, used in the French methodology for evaluation of the residual expansion on cores, appears to be too optimistic by neglecting the expansion occurring during the first 8 weeks of testing.
- It is absolutely necessary to consider the previous, present, and future conditions of water supply and moisture conditions of the zones of the considered concrete structures and of the samples used for identifying the whole time evolution of ASR expansions which shall be used in order to assess the behavior of the damaged structures.

3.118 Multon, Stéphane and Sellier, Alain and Cyr, Martin (2009)

URL

```
@article{
multon2009chemo,
label={multon2009chemo},
title={Chemo--mechanical modeling for prediction of alkali silica reaction (ASR)
expansion},
author={Multon, St{\`e}phane and Sellier, Alain and Cyr, Martin},
journal={Cement and Concrete Research},
volume={39},
number={6},
pages={490--500},
year={2009},
publisher={Elsevier},
url={https://www.sciencedirect.com/science/article/pii/S0008884609000702}
```

- Presents a microscopic model to analyze the development of ASR expansion of mortars containing reactive aggregate of different sizes.
- The attack of the reactive silica by alkali was determined through the mass balance equation, which controls the diffusion mechanism in the aggregate and the fixation of the alkali in the ASR gels.
- Mechanical part of the model is based on the damage theory in order to assess the decrease of stiffness of the mortar due to cracking caused by ASR and to calculate the expansion of a Representative Elementary Volume (REV) of concrete.
- Parameters of the model were estimated by curve fitting the expansions of four experimental mortars.
- Paper shows that the decrease of expansion with the size of the aggregate and the increase of the expansion with the alkali content are reproduced by the model, which is able to predict the expansions of six other mortars containing two sizes of reactive aggregate and cast with two alkali contents.

3.119 Multon, Stéphane and Cyr, Martin and Sellier, Alain and Diederich, Paco and Petit, Laurent (2010)

URL

```
@article{
multon2010effects,
label={multon2010effects},
title={Effects of aggregate size and alkali content on ASR expansion},
author={Multon, St{\`e}phane and Cyr, Martin and Sellier, Alain and Diederich,
Paco and Petit, Laurent},
journal={Cement and Concrete Research},
volume={40},
number={4},
pages={508--516},
year={2010},
publisher={Elsevier},
url={https://www.sciencedirect.com/science/article/pii/S0008884609002038}
```

- Attempts to model ASR expansion are usually limited by the difficulty of taking into account the heterogeneous nature and size range of reactive aggregates.
- This work is a part of an overall project aimed at developing models to predict the potential expansion of concrete containing alkali-reactive aggregates.
- Paper gives measurements in order to provide experimental data concerning the effect of particle size of an alkali-reactive siliceous limestone on mortar expansion.
- Results show that no expansion was measured on the mortars using small particles (under 80 μm) while the coarse particles (0.63–1.25 mm) gave the largest expansions (0.33%).
- When two sizes of aggregate were used, ASR-expansions decreased with the proportion of small particles.
- Models are proposed to study correlations between the measured expansions and parameters such as the size of aggregates and the alkali and reactive silica contents.
- Pessimum effect of reactive aggregate size is assessed and the consequences on accelerated laboratory tests are discussed.

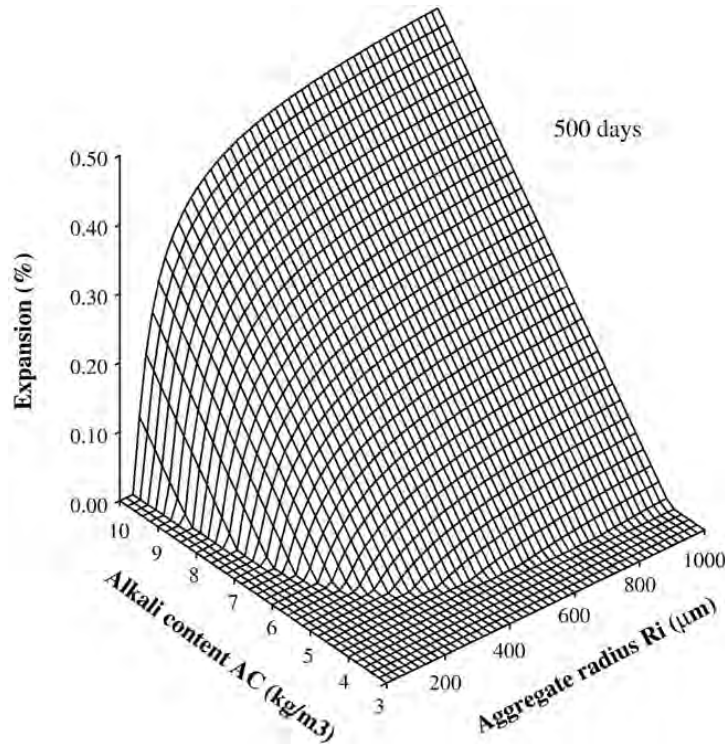


Fig. 9. Long-term expansion ($t=500$ days) versus aggregate radius (R) and initial alkali content (AC) in mortars, calculated using the asymptotic expansion model (data: $k=1$, $l_c=11 \mu\text{m}$, $\phi_{ref}^{gel}=0.066$, $\phi^{void-mortar}=0.17$, $AC_0=8.1 \text{ kg/m}^3$, $AC_{th}=3.5 \text{ kg/m}^3$).

Figure 3.161: Long-term expansion ($t=500$ days) versus aggregate radius (R) and initial alkali content (AC) in mortars, calculated using the asymptotic expansion model (data: $k=1$, $l_c=11 \mu\text{m}$, $\phi_{ref}^{gel}=0.066$, $\phi^{void-mortar}=0.17$, $AC_0=8.1 \text{ kg/m}^3$, $AC_{th}=3.5 \text{ kg/m}^3$).

reactive aggregates. Finally the expansion is reduced or suppressed. However, it should be noted that this explanation is not satisfactory in all cases: alkali-referenced aggregates sometimes only retard it (e.g. high alkali fly ashes).

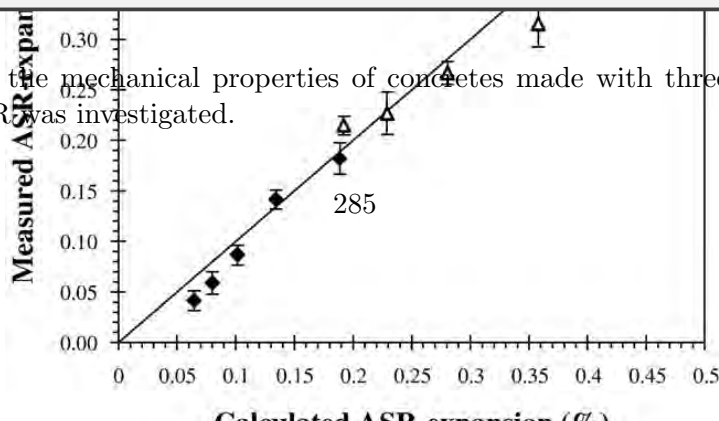
3.120 Na, Okpin and Xi, Yunping and Ou, Edward and Saouma, Victor E. (2016)

URL

```

@article{
na2016effects},
label={na2016effects},
title={The effects of alkali-silica reaction on the mechanical properties of
concretes with three different types of reactive aggregate},
author={Na, Okpin and Xi, Yunping and Ou, Edward and Saouma, Victor E},
journal={Structural Concrete},
volume={17},
number={1},
pages={74--83},
year={2016},
publisher={Wiley Online Library}
Keywords={}
    
```

- Degradation of the mechanical properties of concretes made with three types of aggregate affected by ASR was investigated.



for the largest particle was about (Fig. 7). The overestimation of the leads to an overestimate of the mixtures of fine and coarse aggregate.

The model uses only proportion volume of gel, alkali content appears to be efficient for assessing which mix designs and environmental known.

4.2. Time-dependent expansion model

In order to improve the model dependent model which allows the pessimism effect of coarse aggregate is chosen, which does not consider different sizes.

The simplest way to introduce model is to model the alkali penetration phenomenological function. For example square root of the time is used for penetration from the paste to the aggregate by Eq. (7).

With:

- $x(t)$: thickness of alkali penetration from the center of the aggregate
- R_{ref} : radius of the aggregate reference time t_{ref} is fitted
- t_{ref} : time necessary for alkali penetration of radius R_{ref} , fitted

of radius R_{ref} , fitted $= R_{ref}$. In our case $236 \mu\text{m}$ (mortar M) assumed that the of the aggregate of the asymptotic

2). on of test duration t , the volume by the reaction

$$= \frac{R_i^3 - (R_i - x(t))^3}{R_i^3}$$

The combination of Eqs. (1)–(3) reactive particles leads to the time

$$\begin{aligned}
 \epsilon_{ASR}(t) &= k \cdot \phi_i^{agg} \cdot e_i^{agg}(t) \\
 &= k \cdot \phi_i^{agg} \cdot \frac{\langle V_i^{gel} \cdot f(t) - V_i^{po} \rangle}{V_i^{agg}} \\
 &= k \cdot \phi_i^{agg} \cdot \left[\langle \phi_i^{gel} \cdot f(t) - \phi_i^{po} \rangle \right]
 \end{aligned}$$

With $\phi_i^{gel} = \phi_{ref}^{gel}$ (Eq. (5)) since $AC = AC_{ref} = 8.1 \text{ kg/m}^3$ and ϕ_i^{agg} .

- Three standard testing methods (ASTM C289, JASS 5N T-603 and ASTM C1260) were used to identify the reactivity of ASR of the three aggregates selected.
- The test results show that all three aggregates are potentially deleterious.
- A new acceleration method based on JASS 5N T-603 and ASTM C1260 was proposed for concrete specimens.
- In this method, cylindrical concrete specimens were used, additional alkali material was added to the concrete mixture and the specimens were stored under conditions similar to ASTM C1260.
- The preconditioned concrete specimens were used for evaluating the mechanical properties of the ASR-affected concrete in terms of strength and stiffness.
- The test results demonstrate that special attention must be paid to the effects of two opposing mechanisms on the strength and stiffness of concrete: hydration reactions and ASR.
 - Hydration reactions enhance the mechanical properties,
 - ASR does the opposite.
- The compressive strength was obtained from the maximum stress in a stress-strain curve (these curves were tested at different times - different acceleration periods).
- Figure 3.162 (left) shows compressive strength of the ASR-affected concrete specimens in terms of the immersion times and reactive aggregates. The right plot shows the strains corresponding to the peak stresses at different immersion times. During the first four weeks, the concrete strength gradually increased and then decreased although the total variation in compressive strength is not large for different immersion times.
- Figure 3.162 (middle) shows the stiffness of concrete affected by ASR, characterized by the modulus of elasticity. The trend for stiffness is similar to that for the strength. In the first four weeks, the slightly increased stiffness can be explained by the dominant hydration reactions, whereas the decreased stiffness after the first four weeks indicates that the detrimental effect of ASR became more significant.

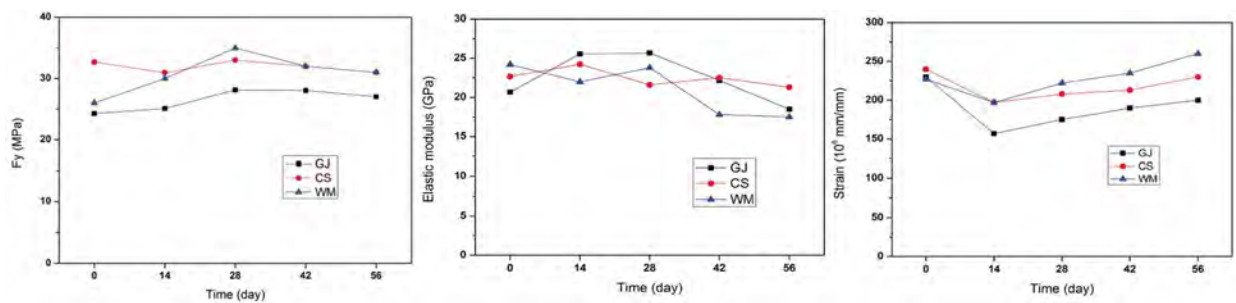


Figure 3.162: Mechanical properties vs. immersion time; Na et al. (2016)

- The changes in length of concrete specimens were also measured, demonstrating that the basic trends for change in length and mechanical properties may be different.

- The size and reactivity of the aggregate are very important factors for the mechanical properties of ASR-affected concretes.
- Within the two-month testing period, the reactive fine aggregate might cause ASR expansion and the reactive coarse aggregates might not.

3.121 Noret, C. and Laliche, K. (2017)

```
@incollection{
noret2017bimont},
label={noret2017bimont},
booktitle={Swelling Concrete in Dams and Hydraulic Structures: DSC 2017},
editor={Sellier, Alain and Grimal, {\`E}tienne and Multon, St{\`e}phane and
Bourdarot, Eric},
year={2017},
title={Bimont Dam Case; Studies and Investigations Inside the Dam Body},
author={Noret, C. and Laliche, K.},
publisher={John Wiley \& Sons},
Keywords={Field; Reinforcement; Rehabilitation; Finite Element; Nonlinear; Arch
dam; },
DisplayPdF={0},
```

- The Bimont Dam is a concrete, double-curved, arch-type structure measuring 86.50 m in height and 180 m in crest length. It consists of 15 cantilevers, and its thickness ranges from 4 m at its crest to 13 m at its foot.
- Located in the south of France, the Bimont Dam was first brought into service in 1952.
- The Bimont Dam developed a network of cracks in some cantilevers soon after construction.
- The following investigations showed that specific areas of concrete were affected by Delayed Ettringite Formation (DEF).
- This phenomenon caused changes in the Dam's equilibrium, resulting in the formation of superficial and internal cracks.
- A numerical model of the Dam with elasto-plastic features ran in parallel with two special investigation campaigns. These measures allowed for a more in-depth understanding of how the network of cracks was formed, its spatial extent, and its probable future evolution, information which proved invaluable for the design of the Dam's renovation program.
- The finite element model represented the arch dam and its immediate foundation, Figure 3.163 (left).
- The zones of swelling concrete were identified in the model. Joint elements were placed along the line of contact between the foundation and the Dam, and along some construction joints and along the main crack between the swelling zones of cantilevers 2 and 4.
- The swelling phenomenon was reproduced using the nonlinear and anisotropic law.

- Numerical simulations showed that the cracks are a direct result of swelling due to the mechanism explained in Figure 3.163 (right). The zones affected by these cracks are weakened, and there is a major impact on stress distribution with possible consequences on the Dam's overall resistance.

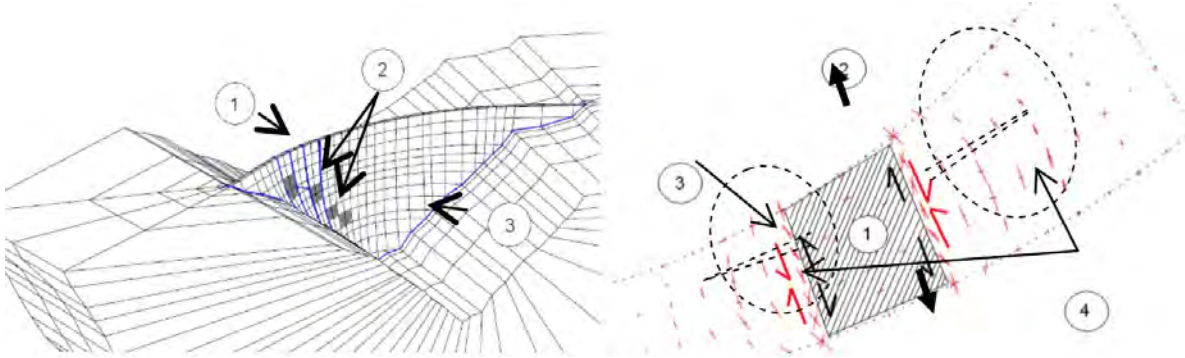


Figure 3.163: (left): Dam mesh: (1) Joint between two blocks, (2) Swelling areas, and (3) Joint along the dam footprint; (right): Cracking mechanism around swelling areas: (1) P4 Swelling area of P4, (2) Increase of the swelling bloc, (3) Shear stress at the origin of cracks, and (4) Plastic strain; Noret and Laliche (2017)

- The Dam had a renovation plan which aimed to restore its monolithism. It will be able to handle the full reservoir load once more.
- The project involves mainly the treatment by cement grouting of the cracks and joints and the waterproofing of the Dam's upstream face.

3.122 Orbovic, N. and Panesar, D. and Sheikh, S. and Vecchio, F. and Lamarche, C.P. and Blahoianu, A. (2015)

```
@inproceedings{
  orbovic2015alkali},
  label={orbovic2015alkali},
  title={Alkali Aggregate Reaction in Nuclear Concrete Structures: Part 1: A
    Holistic Approach},
  author={Orbovic, N. and Panesar, D. and Sheikh, S. and Vecchio, F. and Lamarche,
    C.P. and Blahoianu, A.},
  booktitle="{Proceedings of the 23rd Conference on Structural Mechanics in Reactor
    Technology (SMiRT23)}",
  year={2015},
  Keywords={Laboratory; Expansion Assessment/monitoring Det. E; Det f'c; Det. V;
    Beams-Panels; },
  DisplayPdF={0},
```

- The response of ASR affected concrete is studied.

- Concrete cylinder tests were performed as unconfined compressive strength, split tensile strength, Poisson's ratio, and static modulus of elasticity tests. The results are presented in Figure 3.164.
- Dog bone specimen tests are performed in order to determine concrete tensile strength with direct tensile tests. The results indicate that the regular concrete with tensile capacity of 4.76 MPa has 47% higher capacity than the AAR concrete with tensile strength of 3.24 MPa.

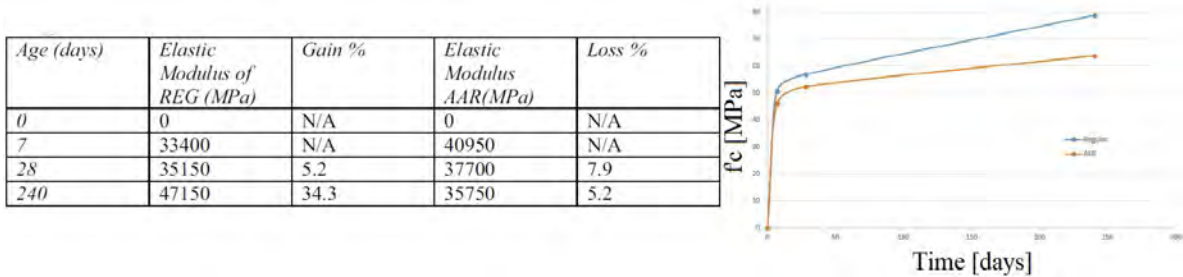


Figure 3.164: ASR effects on material tests; Orbovic et al. (2015)

- A destructive examination is also performed to determine mechanical characteristics such as: ultimate resistance, ultimate displacement, ductility, and residual strength of walls with AAR. The examination also correlates the level of damage in terms of crack spacing and crack width with the structural drift.
- Two actuators with 1000 kN capacity are used in this test, Figure 3.165.

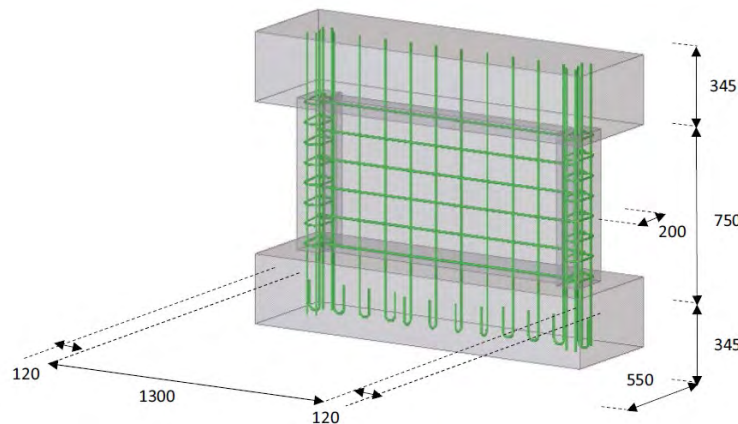


Figure 3.165: Geometry and reinforcement of shear wall specimen; Orbovic et al. (2015)

- The wall is anchored to the strong floor with the help of two high strength bolts.
- Axial load is maintained throughout the test with the help of an 800 kN jack.
- A regular shear wall was tested at the age of 220 days and the AAR impacted shear wall at the age of 260 days.
- Both specimens failed in shear after developing diagonal cracks.

- The maximum capacity of the regular shear wall was recorded as 1180 kN and the maximum capacity of the AAR shear wall was recorded as 1354.5 kN. Therefore, the AAR shear wall showed 14.8% higher capacity than the regular shear wall.
- Modal analysis showed lower resonant frequencies (-8.1%), consistent with the lower modulus of elasticity (-24%), and higher damping of the wall with AAR. However, the destructive structural tests showed higher capacity (+14.8%) of the shear wall with AAR than the regular one. Therefore, the code relations between the material properties (e.g. unconfined compressive strength) and the structural capacity (e.g. shear capacity) are not valid for shear walls with boundary elements affected by AAR and with approximately 0.18% expansion.

3.123 Ostertag, Claudia P and Yi, ChongKu and Monteiro, Paulo JM (2007)

URL

```
@article{
ostertag2007effect},
label={ostertag2007effect},
title={Effect of confinement on properties and characteristics of alkali-silica
reaction gel},
author={Ostertag, Claudia P and Yi, ChongKu and Monteiro, Paulo JM},
journal={ACI materials journal},
volume={104},
number={3},
pages={276},
year={2007},
publisher={American Concrete Institute}
Keywords={}
```

- The degree of damage depends on the amount of local confinement existing in the material.
- Steel microfibers can generate confinement of the resulting ASR gel. The effect of confinement on formation and characteristics of the ASR gel was investigated.
- The ASR products near the reaction sites were present in both solid and liquid form.
- The chemical composition of these products was determined by microprobe analysis and by inductive coupled plasma spectroscopy for the solid and liquid products, respectively.
- Viscosity measurements of the liquid alkali-silicate solution were performed.
- This type of confinement not only reduces the volumetric expansion but also reduces the formation of the ASR gel and the reactivity of the reactive aggregate.

3.124 Pan, JW and Feng, YT and Wang, JT and Sun, QC and Zhang, CH and Owen, DRJ (2012)

URL

```
@article{
pan2012modeling,
label={pan2012modeling},
title={Modeling of alkali-silica reaction in concrete: a review},
author={Pan, JW and Feng, YT and Wang, JT and Sun, QC and Zhang, CH and Owen, DRJ},
journal={Frontiers of Structural and Civil Engineering},
volume={6},
number={1},
pages={1--18},
year={2012},
publisher={Springer},
url={https://link.springer.com/article/10.1007/s11709-012-0141-2}
```

- Presents a comprehensive review of modeling of alkali-silica reaction (ASR) in concrete.
- Concept of ASR and the mechanism of expansion are first outlined, and the state-of-the-art of modeling for ASR, is then presented in detail.
- Modeling includes theoretical approaches, meso- and macroscopic models for ASR analysis.
- The theoretical approaches dealt with the chemical reaction mechanism and were used for predicting pessimum size of aggregate.
- Mesoscopic models have attempted to explain the mechanism of mechanical deterioration of ASR-affected concrete at material scale.
- Macroscopic models, chemomechanical coupling models, have been generally developed by combining the chemical reaction kinetics with linear or nonlinear mechanical constitutive, and were applied to reproduce and predict the long-term behavior of structures suffering from ASR.

3.125 Pan, JianWen and Feng, YunTian and Xu, YanJie and Jin, Feng and Zhang, ChuHan and Zhang, BingYin (2013)

URL

```
@article{
pan2013chemo},
label={pan2013chemo},
title={Chemo-damage modeling and cracking analysis of AAR-affected concrete dams},
author={Pan, JianWen and Feng, YunTian and Xu, YanJie and Jin, Feng and Zhang,
ChuHan and Zhang, BingYin},
journal={Science China Technological Sciences},
volume={56},
number={6},
pages={1449--1457},
year={2013},
publisher={Springer}
Keywords={}
```

- A chemo-damage model for cracking analysis of concrete dams affected by AAR is proposed, combining the plastic-damage model for concrete with the AAR kinetics law.
- This model is first verified by a stress-free AAR expansion test. The expansion deformation obtained from the simulation was in good agreement with the measurement.
- Next, the expansion deformation and cracking process of the AAR-affected Fontana Gravity Dam is analyzed.
- The Dam, completed in 1944, is located on the Little Tennessee River in North Carolina, United States. It is a concrete gravity dam with a maximum height of 147 m and length of 720 m.
- Only after 4 years of completion, network cracks were observed in the parapets, and continued extending over time. An increasing upstream deflection of the structure was also found according to plumb lines.
- The petrographic examination found deposits of alkali-silica gels and microcracks in the aggregates, revealing that AAR had occurred in the Dam.
- A series of remedial measures have been performed to slow down the AAR development and strengthen the structure:
 - Spraying cold reservoir water onto the downstream face of the Dam.
 - Post-tensioning the cracked blocks and grouting the cracks.
 - Wide expansion slots which interrupted the longitudinal thrust across the upper portion of the Dam were cut to release stresses in the Dam caused by AAR.
- A 2-m-thick slice of Block-35 of the Dam is analyzed. Downstream-filled soil is considered in the model for possibly realistic boundary conditions of the Dam during operation.
- 3D 8-node-brick elements are used. The mesh surrounding the galleries is refined with an element size of 0.2 m \times 0.2 m and is coarser in the other regions of the Dam with the average size of 0.4 m \times 0.4 m. The mesh size in the foundation varies gradually from 0.4 m \times 0.4 m in the near field to 4.0 m \times 4.0 m in the far field.
- The foundation rock and downstream filled-soil are assumed to be linear elastic in the analysis.
- A transient thermal analysis of the dam-foundation system is first performed to determine the varying temperature field in the Dam during the AAR process.
- Following the transient thermal analysis, a mechanical simulation is performed. The gravity load of the Dam is first applied, followed by the varying hydrostatic pressure and the temperature load.
- Figure 3.166 illustrates the AAR extent distribution in the Dam at the selected time instants. In the earlier period, AAR mainly occurs in the upper portion and downstream face in which the concrete exposes in air with a higher temperature and the reaction rate is faster compared with the concrete in the lower part of the Dam.

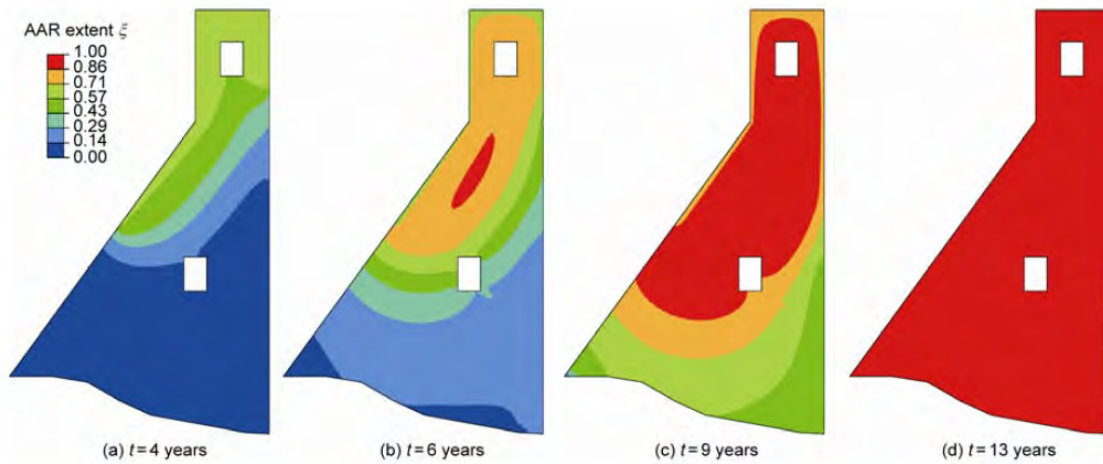


Figure 3.166: AAR extent of the Fontana Dam; Pan et al. (2013a)

- Figure 3.167 shows the cracking propagation and damage pattern of the Dam during the AAR process. Cracking initially occurs in the walls of the foundation drainage gallery inside the Dam after $t=4$ years. The crack extends diagonally upward towards the downstream face where a new crack appears in $t=5$ years. These cracks form an inclined plane intersecting the section between the gallery and the downstream face after $t=13$ years.

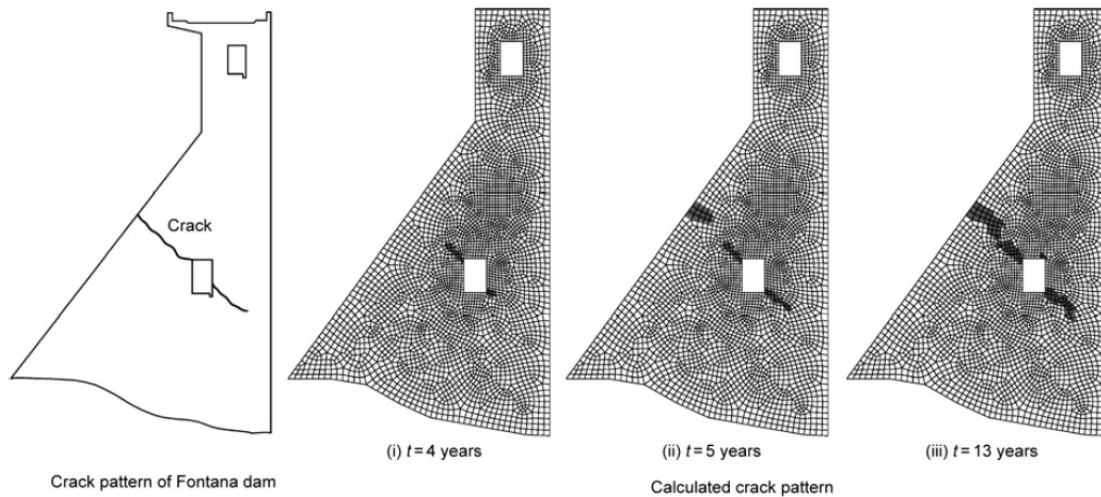


Figure 3.167: Comparison of crack patterns of Fontana Dam between field inspection and simulation; Pan et al. (2013a)

- Figure 3.168 shows the displacement time history of the crest point on the upstream face. These increasing deflections of the Dam are induced by the AAR expansion with time. The horizontal crest displacement of the AAR-affected Dam is rapidly increased before $t=6$ years but decreased at the peak value of 2.6 cm. It finally remains at a permanent displacement around 1.6 cm. The vertical crest displacement is increased gradually and reaches its maximum value of 3.6 cm after about 13 years.

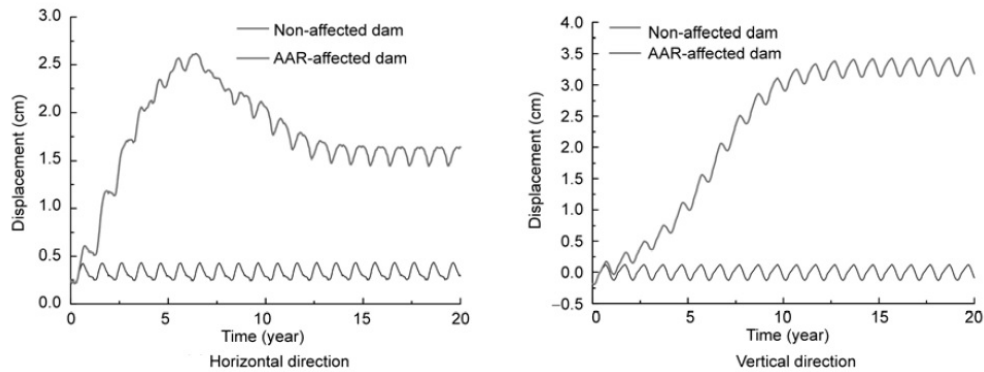


Figure 3.168: Yearly variation of crest displacement with time; Pan et al. (2013a)

3.126 Pan, Jianwen and Feng, YT and Jin, Feng and Zhang, Chuhan (2013)

URL

```
@article{
pan2013numerical,
label={pan2013numerical},
title={Numerical prediction of swelling in concrete arch dams affected by
alkali-aggregate reaction},
author={Pan, Jianwen and Feng, YT and Jin, Feng and Zhang, Chuhan},
journal={European Journal of Environmental and Civil Engineering},
volume={17},
number={4},
pages={231--247},
year={2013},
publisher={Taylor & Francis}
Keywords={}
```

- A chemo-damage model was presented for anisotropic swelling analysis of concrete arch dams affected by AAR.
- The model combines the AAR kinetics and the plastic-damage model, and the chemical and mechanical phases are coupled.
- A redistributing weight function, determined by the applied stresses in the concrete, is introduced to control the AAR-induced anisotropic expansion of the concrete.
- Creep strain is also included in the approach using the Kelvin-Voigt model.
- Accelerated tests, in which the specimens are confined with steel rings and subjected to axial loads, are first analyzed using the proposed model. The computed strains of the specimens were in good agreement with the experimental measured strains.
- This procedure is applied to the AAR-affected Kariba Dam, completed in 1959, located in Zimbabwe.

- The height of the Dam is 128 m above the foundation.
- The dam-foundation system is discretized with 20-node brick elements and 15-node prism elements. The foundation rock is assumed linear elastic.
- The AAR kinetics parameters of the concrete are determined based on inverse analysis. The vertical displacements measured at some monitoring points at the crest near the left abutment are used to fit the AAR kinetics parameters.
- The self-weight of the Dam is first applied with the assumption of independent cantilevers and joint grouting at a uniform temperature equal to the average ambient air temperature. The water pressure exerted on the upstream face of the Dam is varied with the reservoir water level during the impounding and operation periods.

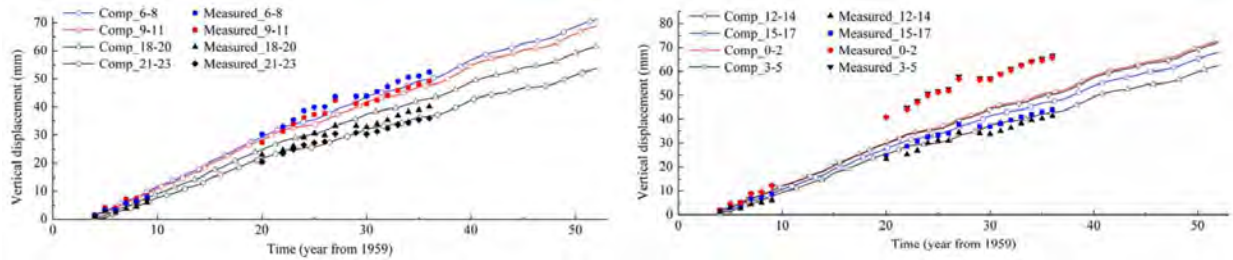


Figure 3.169: Vertical displacements at the monitoring points; Pan et al. (2013b)

- Figure 3.169 presents the vertical displacements at the monitoring points. The displacements obtained from the simulation in 1963 are initialized to zero and the subsequent values are adjusted accordingly.
- The vertical displacements increase gradually during the AAR process. The expansion deformation is larger in the central portion compared to the Dam blocks on both sides.
- The principal stress distributions of the Dam in 1963 and 2012 are shown in Figure 3.170. The maximum principal stresses in the central portion of the downstream face and the dam heel are found to be large in 1963; however, the maximum principal stresses reduce even to negative (compressive state) in 2012. The maximum principal stresses on the downstream face of the Dam near the dam-foundation interface significantly increase in 2012 compared to those in 1963. Regarding the minimum principal stresses within the Dam, it can be found that the stresses become much smaller.
- Severe cracking and damage appear to occur in the dam heel and the downstream face on both sides of the dam-foundation interface.

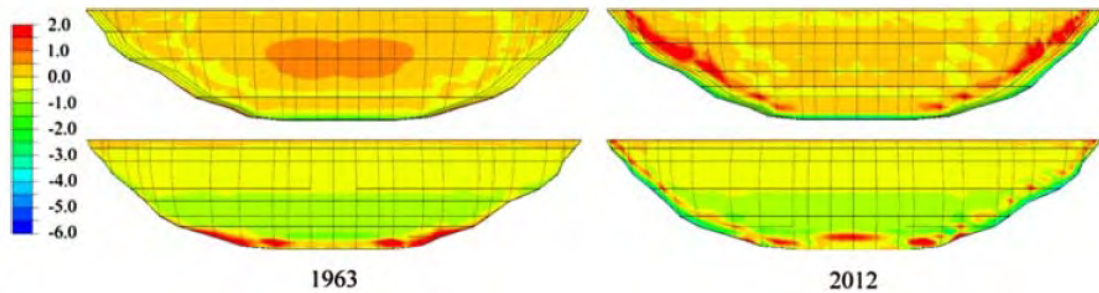


Figure 3.170: Distribution of the maximum principal stress (MPa) on the downstream and upstream faces; Pan et al. (2013b)

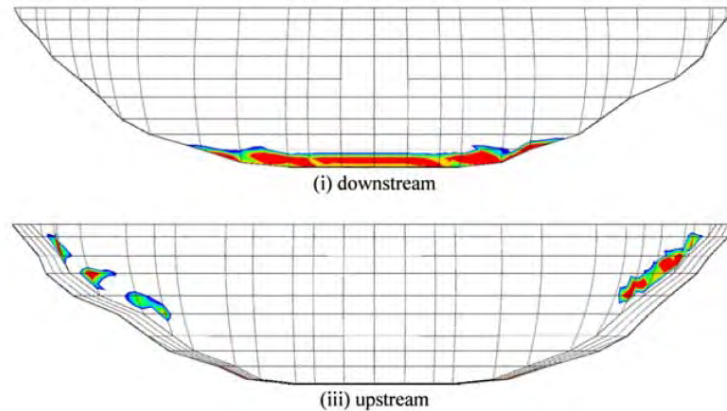


Figure 3.171: Predicted crack patterns of the Kariba Dam in 2012; Pan et al. (2013b)

3.127 Parvini, M and Pietruszczak, S and Gocevski, V (2001)

URL

```
@article{
parvini2001seismic,
label={parvini2001seismic},
title={Seismic analysis of hydraulic structures affected by alkali-aggregate
reaction: a case study},
author={Parvini, M and Pietruszczak, S and Gocevski, V},
journal={Canadian Journal of Civil Engineering},
volume={28},
number={2},
pages={332--338},
year={2001},
publisher={NRC Research Press}
Keywords={}
```

- A hydraulic structure subjected to seismic load suffering from AAR was numerically analyzed.
- First, a numerical procedure for the description of mechanical effects of AAR in concrete structures was outlined.

- Subsequently, a single unit of the Beauharnois Power Plant, situated in Quebec (Canada), is analyzed in the context of seismic excitation.
- The Power Plant consists of a powerhouse, a water intake structure, and right and left wing gravity dams. The total length of the concrete structures, including gravity dams, is 1034 m. The height of the intake structure and the right and left gravity dams is 29, 22, and 19.5 m, respectively.
- The construction of Powerhouse 1 began, and Powerhouse 3 was completed in 1961. Since the early 1940s, the powerhouse has been experiencing concrete expansion and progressive deterioration.
- A network of monitoring instruments was installed in 1970 and 1991 to quantify the displacements of different substructures.
- A finite element mesh for the structure was developed which consists of 2664 3D solid (8-node) elements, 347 beam elements (representing the steel superstructure), and 55 gap elements (along the interface with rock foundation).
- The vertical boundaries were restrained in the direction of the longitudinal axis of the structure. This appears to be a reasonable approximation for units located sufficiently far from the junction with gravity dams.
- The water pressure at the upstream face and the self-weight of the structure were considered in the analysis.
- Two simulations were carried out, one corresponding to a fixed bottom boundary and the other using the gap elements. The gap elements used here were simple 2-node elements placed between adjacent nodes of the bodies coming into contact.
- The simulations were conducted in two basic steps.
 - First, a transient analysis evaluating the effect of up to 100 years of continuing reaction was performed.
 - Second, the seismic event was analyzed.
- The stability of the structure was computed using a so-called safety factor (the normalized value of the second rate of work). Results for the cases with and without 100 years of AAR are shown in Figure 3.172.
- The distribution of damage is plotted in Figure 3.173. The left plot shows the extent of damage for the case when the unit was not affected by AAR. The middle and right plots show the cases with 50 years of AAR (before and after the earthquake), respectively.
- The extent of damage due to the earthquake alone is not very significant.
- The lower part of the structure does not experience any significant redistribution of damage. At the same time, the propagation of damage in the upper part of the structure is quite limited.

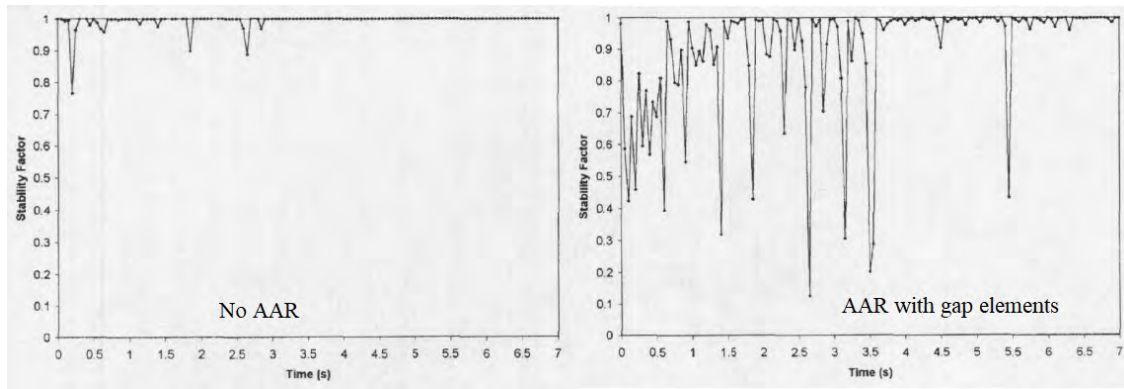


Figure 3.172: Evolution of the stability factor; Parvini, Pietruszczak, and Gocevski (2001)

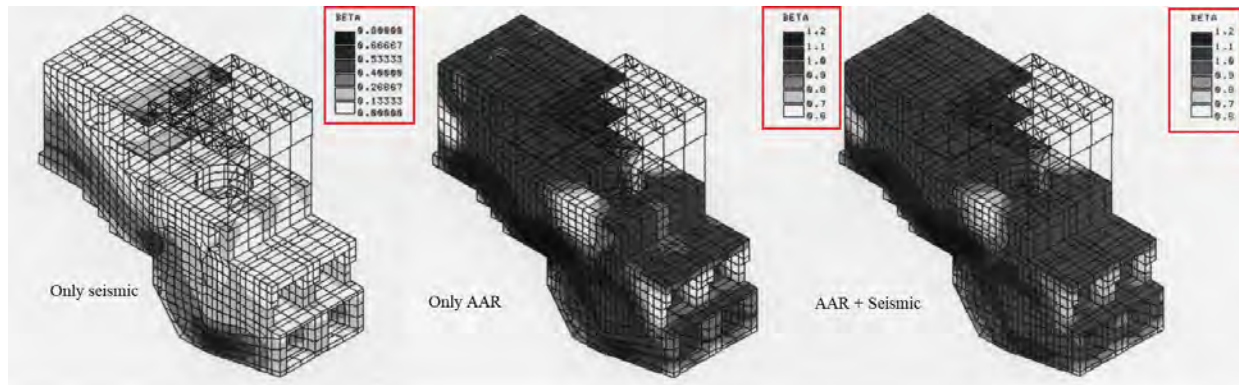


Figure 3.173: Distribution of the damage factor; Parvini, Pietruszczak, and Gocevski (2001)

3.128 Plusquellec, G and Geiker, MR and Lindgård, J and De Weerd, K (2018)

URL

```
@article{
plusquellec2018determining},
label={plusquellec2018determining},
title={Determining the free alkali metal content in concrete--Case study of an
ASR-affected dam},
author={Plusquellec, G and Geiker, MR and Lindg{\aa}rd, J and De Weerd, K},
journal={Cement and Concrete Research},
year={2018},
publisher={Elsevier}
Keywords={}
```

- In concrete affected by ASR, aggregates react in the high pH environment and cause deleterious expansion and cracking of the concrete. Leaching of alkali metals from the concrete might therefore locally reduce ASR.
- The goal is to document the alkali metal leaching and to generate an alkali inventory (the

amount in the solid and in the solution as well as and the amount released by the aggregates) in a full-scale structure.

- The 50-year-old Votna I Dam in Norway is studied, Figure 3.174. It is a double-curved arch dam connected to a slab dam via an abutment wall. The Dam's total length is 185 m and its maximum height is 55 m. The thickness of the arch Dam is 4 m at the bottom decreasing to 0.95 m at the top.
- The water level in the reservoir reaches the top of the Dam during summer/autumn and is gradually lowered during winter/spring.

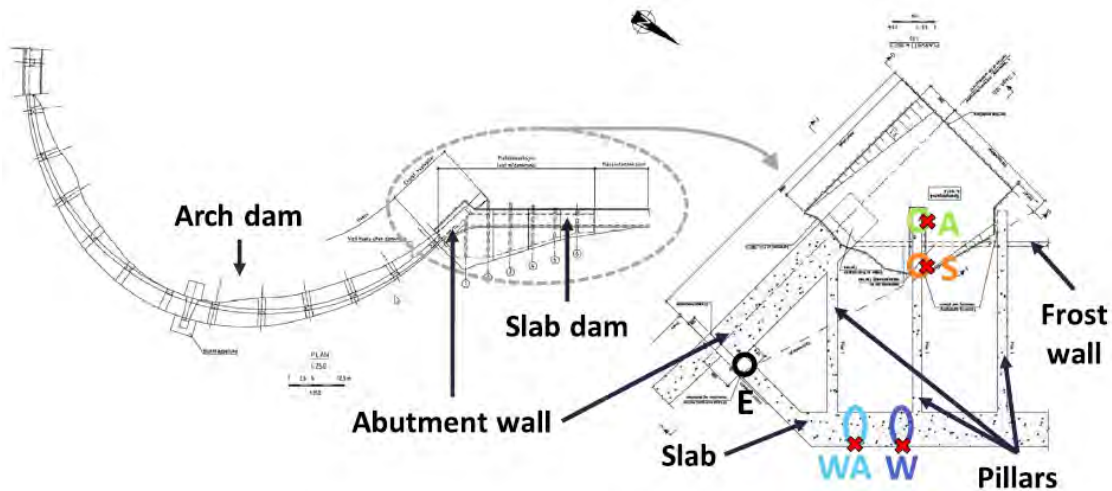


Figure 3.174: Grading of aggregates of mortar mixtures; Plusquellec et al. (2018)

- The first indications of ASR in the Dam were observed in the years 1987-1988: typical map cracking in the arch Dam coupled with deformations at the top.
- The Dam has been investigated several times based on 1) deformation measurements, 2) laboratory investigations of drilled cores for moisture measurement, 3) Crack Index, 4) gel observation, and 5) the testing of mechanical properties (Larsen et al., 2008).
- Several plots from different map cracking and ASR sign are shown in Figure 3.175.
- Free alkali metal profiles were determined on cores taken at four locations with different exposure conditions: 1) permanently immersed, 2) periodically immersed, 3) exposed to rain, or 4) sheltered.
- Alkali leaching was observed at all four locations up to a depth of 100 mm. The leached zone exhibited less intense cracking than the non-leached concrete, indicating that the alkali leaching might be limiting ASR.
- The acid dissolution was unable to measure the alkali content due to the partial dissolution of the aggregates. Cold water extraction (CWE), however, enabled to determine the free alkali metal content.
- The exposure conditions have an impact on the free alkali metal content:



Figure 3.175: Photos of the Votna I Dam: a) map cracking at the rail of the Dam; b) map cracking inside the slab ; c) presence of ASR gel in a bore hole; d) humidity inside the slab; e) aggregates visible on the surface; f) upstream face after drilling; Plusquellec et al. (2018)

- The external surfaces of the cores permanently submerged or periodically submerged were affected by alkali metal leaching.
 - The external surfaces exposed to atmospheric conditions were affected by leaching but to a lesser extent than the submerged surfaces.
 - For one of the internal surfaces, an accumulation of alkali was observed which might indicate wick action.
- The alkali metal profiles correspond relatively well to the crack density profiles.

3.129 Poyet, Stéphane and Sellier, Alain and Capra, Bruno and Thèvenin-Foray, Geneviève and Torrenti, Jean-Michel and Tournier-Cognon, Hélène and Bourdarot, Eric (2006)

URL

```

@article{
poyet2006influence},
label={poyet2006influence},
title={Influence of water on alkali-silica reaction: Experimental study and
numerical simulations},
author={Poyet, St{\`e}phane and Sellier, Alain and Capra, Bruno and
Th{\`e}venin-Foray, Genevi{\`e}ve and Torrenti, Jean-Michel and
Tournier-Cognon, H{\`e}l{\`e}ne and Bourdarot, Eric},
journal={Journal of Materials in civil Engineering},
volume={18},
number={4},
pages={588--596},
year={2006},
publisher={American Society of Civil Engineers}
Keywords={}

```

- Water is very important for ASR; the more available water, the more expansion and degradation occurs.
- A new law for modeling the influence of water on ASR was presented.
- Two series of experiments were undertaken.
 - In the first one (subsequently called RH-constant), the external relative humidity remains constant.
 - In the second one (called RH-variable), the specimens undergo cyclic changes in relative humidities. Furthermore, two types of cycles are studied:
 - * Short cycles
 - * Long cycles
- The specimens are cylindrical with 16 cm height and diameters of 2 cm.
- Specimens are cast and kept vertically. ASR expansion is measured vertically, as well.
- Two compositions are cast including different aggregates: a reactive limestone sand and an innocuous limestone sand.
- The specimens are removed from their mold after 10 days at 20 °C and wrapped in a sealing film. Afterwards, they are kept at 60 °C and submitted to the desired external relative humidity.
- Figure 3.176 (left) shows the ASR expansion for constant RH. The higher the external RH, the more and faster the ASR expansion. There is a clear correlation between water intake and ASR expansion.
- For constant RH, the expansion generated by ASR for the specimens with RH=100% is inferior to the one for RH=96%.
- Figure 3.176 (right) shows the ASR expansions. Expansions are quite similar for both cycles up to 80 days. Afterwards, expansion for the short cycles seems to stop.

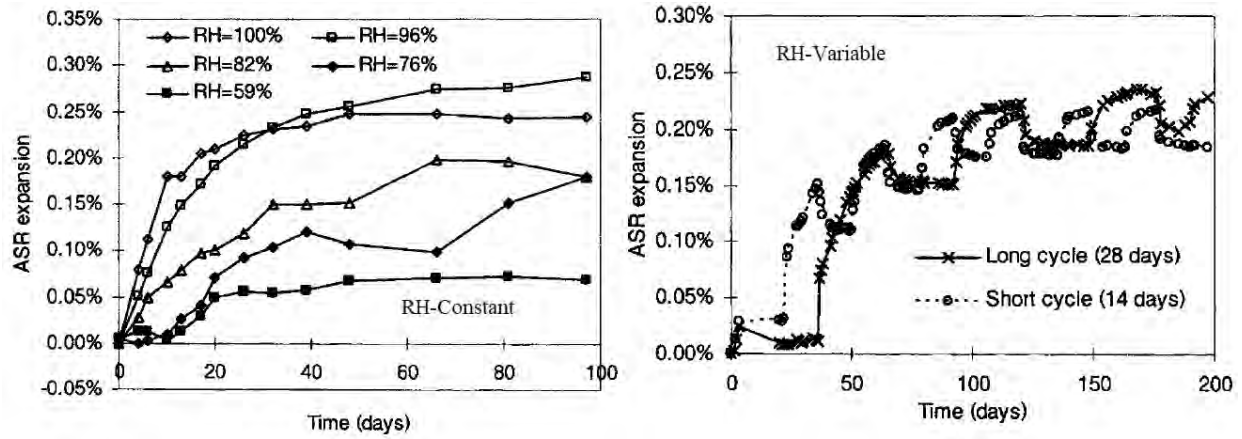


Figure 3.176: ASR expansion for constant RH (left); ASR expansions (right); Poyet et al. (2006)

- ASR deformations for cyclic samples are always higher than those for constant 59% RH and lower than those of constant 96% RH.
- Next, a numerical model was proposed to describe the available water within the affected concrete by the means of the saturation ratio, S_r . It represents the pore water filling percentage.
- To use this modeling, one has first to fit three swelling parameters. These are material parameters that define the swelling properties of the studied reactive material.
- The results of a first series of experiments (cylindrical samples maintained within constant RH at six different levels), were used to fit the modeling constitutive laws which do not depend on the studied material.

3.130 Rajabipour, Farshad and Giannini, Eric and Dunant, Cyrille and Ideker, Jason H and Thomas, Michael DA (2015)

URL

```
@article{
  rajabipour2015alkali,
  label={rajabipour2015alkali},
  title={Alkali--silica reaction: current understanding of the reaction mechanisms
    and the knowledge gaps},
  author={Rajabipour, Farshad and Giannini, Eric and Dunant, Cyrille and Ideker,
    Jason H and Thomas, Michael DA},
  journal={Cement and Concrete Research},
  volume={76},
  pages={130--146},
  year={2015},
  publisher={Elsevier},
  Keywords={},
  DisplayPdf={0},
  url={https://www.sciencedirect.com/science/article/pii/S0008884615001611}
```

- Despite decades of study, the underlying chemical and physical reaction mechanisms of ASR remain poorly understood, especially at molecular to micro-scale levels, and this has resulted in the inability to efficiently assess the risk, predict the service life, and mitigate deterioration in ASR-susceptible structures.
- Paper intends to summarize the current state of understanding and the existing knowledge gaps with respect to reaction mechanisms and the roles of aggregate properties (e.g., composition, mineralogy, size, and surface characteristics), pore solution composition (e.g., pH, alkalis, calcium, aluminum), and exposure conditions (e.g., temperature, humidity) on the rate and magnitude of ASR.
- Current state of computer modeling as an alternative or supplement to physical testing for prediction of ASR performance is discussed.

Major Conclusions

- ASR is a result of a number of sequential reactions: dissolution of silica, formation of sol, formation of gel, and swelling of the gel. The underlying chemical reactions along with some thermodynamic information were presented in this paper. However, more research is needed to better quantify the thermodynamics and kinetics data, especially in conditions more similar to concrete's interior; e.g., accounting for aggregate composition and heterogeneity, local pore solution composition at silica surface, and effects of temperature, pressure/restraint, and humidity on the reaction parameters. This knowledge could be very powerful in developing more efficient ASR inhibiting admixtures, and ability to predict and optimize service life through computer models and laboratory and field experiments.
- Aggregate reactivity depends not only on the type of silica mineral it contains, but also on the size/distribution of these minerals within aggregate structure. Reactive aggregate size and content have documented effects on ASR expansion, and often an intermediate particle size (i.e., the “pessimum” size) and intermediate content (i.e., the “pessimum” content) result in the highest expansion. Also, it is important to note that contrary to a common belief, ASR does not always occur at the aggregate–cement paste interface, but may only occur in the interior of some aggregates.
- Internal alkali release from non-portland cement sources in concrete can be a significant contributor to ASR in structures with long service lives and/or low cement alkali loadings. Standardized methods for measuring the potential releasable alkalis from aggregates and SCMs are needed. These methods must include criteria for interpreting results in a manner relevant to field performance.
- LiNO₃ has emerged as the preferred lithium compound for controlling ASR, as many other lithium salts increase the pH of pore solution. However, not a single prescribed Li dosage or [Li]/[Na + K] molar ratio is effective against aggregates of different reactivity. Future research on the long-term efficacy of LiNO₃, in better correlating laboratory and field data to determine an optimum Li dosage, and in better understanding of the mechanisms of ASR mitigation by Li is beneficial.
- Presence of calcium is required for formation of ASR gel; otherwise the dissolved silica could remain innocuously in the pore solution. In addition, Ca plays two specific roles with respect

to ASR: (a) it can replace alkalis in ASR gel (i.e., recycle alkalis back into pore solution), and thus maintain a high pH in the pore solution, and (b) it impacts the properties (e.g., viscosity, yield strength, swelling capacity) of ASR gel.

- There is evidence that presence of soluble Al in pore solution helps in mitigating ASR. The exact mechanisms are unknown, but the effects could be due to reducing silica dissolution, improving alkali binding and reducing the pH, consuming portlandite, reducing swelling of the gel, or densifying the pore structure and reducing the permeability of concrete.
- Limited qualitative information is available on the composition versus rheological and swelling properties of ASR gels. Research is needed to quantify the effect of gel composition, temperature, humidity, and pressure/restraint on the gel's structure, moisture uptake, and swelling.
- There is a strong need for synthesis, development, and assessment of new ASR mitigation methods (e.g., new or unconventional SCMs, new chemical admixtures, and innovative treatment methods) applicable to new and, more importantly, to existing structures.
- Considerable progress has been made in understanding the micromechanics of ASR. This has led to predictive models valid for samples of laboratory size. Much is still needed to integrate the chemical aspects of the reaction in these models. There are also a number of well-established macroscopic models, used for the management of real structures. These are unfortunately largely empirical and need to be constantly amended to track the observed changes in the field. In future, reactive-transport and micromechanical models should serve as a base for formulating more robust macroscopic predictive models.

3.131 Reinicker, B. and Duke, W. and Cima, J. and Charlwood, R. (2010)

```
@inproceedings{
reinicker10alkali-silica},
label={reinicker10alkali-silica},
title={Alkali-Silica Reactivity At Roanoke Rapids Dam
Unique Remedial Design Challenges},
author={Reinicker, B. and Duke, W. and Cima, J. and Charlwood, R.},
booktitle={USSD 2010 Conference},
address={Sacramento, CA},
pages={367--390},
year={2010}
Keywords={}
```

- This paper is focused on ASR in Roanoke Rapids Dam and its remedial challenges.
- The Dam is a 72 foot high, 3,050 foot long concrete gravity dam located in North Carolina.
- The Dam was constructed in 1955 and has performed satisfactorily for most of its life.
- Recent instrumentation history indicated accelerated deformation, increased seepage, and increases in uplift pressure in the south non-overflow section (SNOS).

- A two-phased research program was then started (2006-2008). The investigation discovered significant cracking along several monoliths of the upstream face of the curved portion of the SNOS and concluded that the Dam was experiencing concrete growth due to ASR.
- The partial sections of the affected monoliths above the cracking were determined to be unstable during the design flood (PMF).
- Low pressure grouting of the cracks and installing high-capacity, post-tensioned anchors in selected SNOS monoliths to improve the long-term stability were the recommended remedial solutions.
- Several significant challenges were identified early in the design process. One challenge was the severe horizontal cracking and downstream bowing of the upper portions of the SNOS structure.
- The horizontal cracking was the result of longitudinal expansion in the SNOS.
- The stability of the upper sections was, therefore, strongly dependent on the clamping effect of the longitudinal thrust.
- The cracking had been assumed to propagate from the measured crack locations on the upstream face through the structure and terminate prior to reaching the downstream face, Figure 3.177.
- Another design challenge was the presence of the 5 foot wide gallery which continues through three adjacent blocks (which will also receive anchors) and into the powerhouse.
- 2D stability analyses were used as an initial conservative basis to establish the anchor position and minimum anchor load required to meet conventional stability criteria. The stability analyses evaluated the upper portion of the structure above the open lift joints.
- The decision was made by the project design team to perform crack grouting prior to anchor installation.
- Design of the crack grouting and post-tensioned rock anchors was performed based on the assumption that the expansion mechanism would continue at the present rate for the foreseeable future.

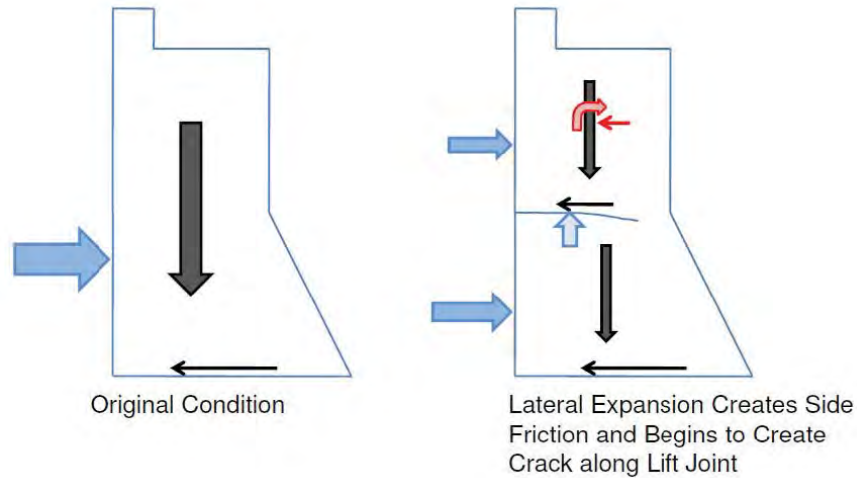


Figure 3.177: Assumed cracking pattern; Reinicker et al. (2010)

3.132 Reinicker, B. and Abedzadeh, F. and Charlwood, R. and Cima, J. (2013)

```
@inproceedings{
reinicker13advanced},
label={reinicker13advanced},
title={An Advanced Model for Simulation of ASR Behavior at Roanoke Rapids Dam},
author={Reinicker, B. and Abedzadeh, F. and Charlwood, R. and Cima, J.},
booktitle={USSD 2013 Conference},
address={Phoenix, AZ},
pages={127--147},
year={2013}
Keywords={}
```

- This paper is focused on ASR in Roanoke Rapids Dam and its remedial challenges.
- It is a 72 foot high, 3,050 foot long concrete gravity dam located in North Carolina.
- The Dam was constructed in 1955 and has performed satisfactorily for most of its life.
- This paper summarizes the stage I model development and analyses.
- A 3D ASR model of the Dam from the south abutment to the north including all monoliths of the structure and part of the rock foundation is modeled. It does not include details such as galleries or the opening in the powerhouse.
- Simulations include: transient thermal analysis, temperature dependent ASR expansion rates, anisotropic stress dependent ASR expansion rates, visco-elastic creep model, and separation and opening along preexisting cracks.
- The computer program ANSYS ID used for modeling.



Figure 10. Typical Section of Key Instrument Locations at SNOS.

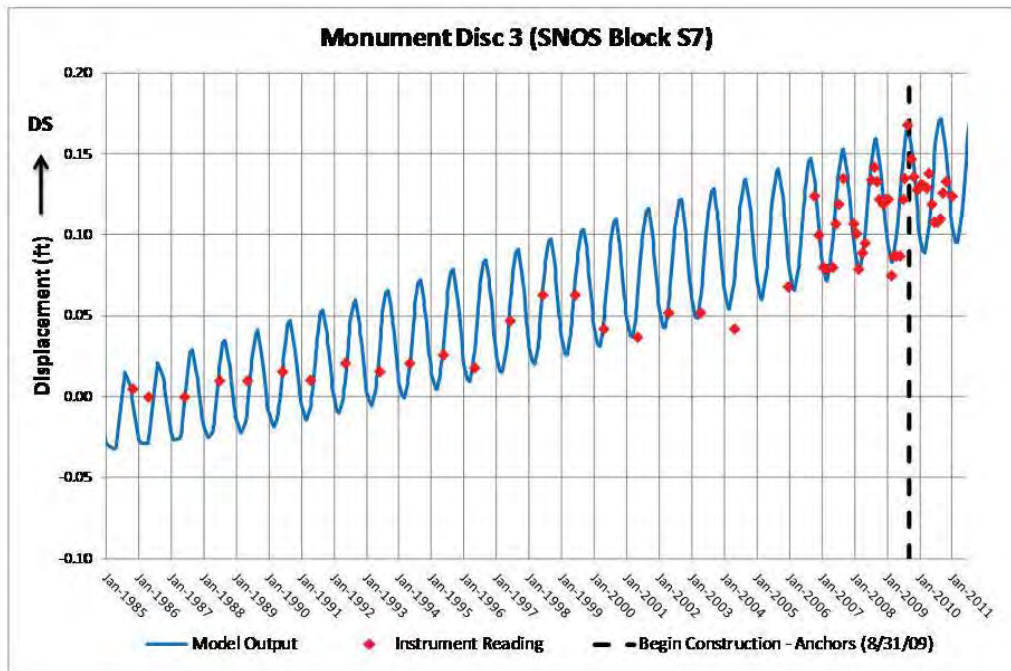


Figure 178. Finite Element Simulation vs. measured Reinforcement (2013)

3.133 Rivard, Patrice and Fournier, Benoit and Ballivy, Gérard
 142 (2000) **Managing Aging Infrastructure**

URL

```
@article{
  rivard2000quantitative,
  label={rivard2000quantitative},
  title={Quantitative petrographic technique for concrete damage due to ASR:
    experimental and application},
  author={Rivard, Patrice and Fournier, Benoit and Ballivy, G{\'}e{rard}},
  journal={Cement, Concrete and Aggregates},
  volume={22},
  number={1},
  pages={63--72},
  year={2000},
  publisher={ASTM International},
  url={http://www.astm.org/DIGITAL_LIBRARY/JOURNALS/CEMENT/PAGES/CCA10465J.htm}
```

- An automatic petrographic test procedure for quantifying damage in concrete affected by alkali-silica reaction (ASR) is presented.

- A computer image analysis program was designed to quantify the degree of microcracking and the amount of silica gel resulting from ASR.
- Procedure involves the petrographic examination at a magnification of 320 of polished concrete sections impregnated with fluorescent epoxy resin for cracking and uranyl acetate coated sections for the determination of their silica gel content.
- Data were compared to the results obtained from a semi-quantitative petrographic method, i.e., the Damage Rating Index commonly used in Canada for evaluating the condition of concrete affected by ASR.
- Petrographic examination was first carried out on laboratory sections cut and polished from concrete prisms incorporating two different aggregate types, the Spratt limestone and the Potsdam sandstone.
- Both methods were also applied to specimens prepared from a core collected from a large dam affected by ASR.
- Good correlation was obtained between analytical parameters derived from the image analysis method and the expansion levels of the laboratory test prisms; however, no explicit relation was found to date between the amount of gel as measured in this study and the expansion level.

3.134 Rivard, Patrice and Fournier, Benoit and Ballivy, Gérard (2002)

URL

```
@article{
rivard2002damage,
label={rivard2002damage},
title={The damage rating index method for ASR affected concrete-a critical review
of petrographic features of deterioration and evaluation criteria},
author={Rivard, Patrice and Fournier, Benoit and Ballivy, G{\'}e{rard}},
journal={Cement, concrete and aggregates},
volume={24},
number={2},
pages={1--11},
year={2002},
publisher={ASTM International},
Keywords={},
DisplayPdf={0},
url={http://www.astm.org/DIGITAL_LIBRARY/JOURNALS/CEMENT/PAGES/CCA10465J.htm}
```

- Damage Rating Index method has recently been used with success in several cases of damage evaluation in structures affected by alkali-silica reaction in Canada and in Brazil.
- Although this petrographic method is starting to be widely used and is in the process of becoming integrated as a Canadian standard, it has not been modified yet from the original design.

- An evaluation of the method is presented.
- According to data obtained from many petrographic examinations, the number of cracks in coarse aggregates (filled or not with silica gel) seemed to show to best correlation with the expansion measured on laboratory concrete specimens made with Spratt limestone.
- The reaction rim is not a real “damage” feature and should not be considered as one but as a “degree of reaction” feature.
- A attempt to improve the DRI method for assessing damage related to ASR is made, and a new parameter should be introduced, which takes into account cracks running from aggregate particles to cement paste.
- The geological nature of the rock used as concrete aggregate may influence the reaction mechanism as well as the petrographic features related to ASR.
- Comparing concrete specimens subjected to ASR, which incorporate different aggregate types may, in some instances, be influenced by the type of reaction produced by the various reactive rocks and minerals in each aggregate.

3.135 Rivard, Patrice and Saint-Pierre, François (2009)

URL

```
@article{
rivard2009assessing},
label={rivard2009assessing},
title={Assessing alkali-silica reaction damage to concrete with non-destructive
methods: From the lab to the field},
author={Rivard, Patrice and Saint-Pierre, Fran{\c{c}}ois},
journal={Construction and Building Materials},
volume={23},
number={2},
pages={902--909},
year={2009},
publisher={Elsevier}
Keywords={}
```

- A relation between physical and mechanical properties was studied in order to evaluate the effectiveness of non-destructive (ND) testing procedures on damaged concrete structures.
- Three ND methods were applied for the evaluation of concrete cores drilled from a large hydraulic structure affected by ASR.
- The investigated site is a hydraulic structure located in southern Canada. The concrete is 50-years old and is affected by ASR, detected about 20 years after the structure’s construction. The current horizontal expansion rate is estimated to be about 1.6 mm/year.
- Cores of 80 mm in diameter were collected along two vertical boreholes running through the structure down to the bedrock.
- Three ND methods were:

- Ultrasonic wave velocities: The P-wave and S-wave velocities were measured for different mixtures.
 - Dynamic Young’s modulus measured with resonant frequency: The results indicated that there was a general increase of about 4% during the test period for the non-reactive specimens. On the other hand, a reduction of about 12% was observed for the reactive specimens, indicating a loss of concrete rigidity.
 - Electrical resistivity: The electrical resistivity of both concrete specimens (reactive and non-reactive) showed a decrease during the first twelve weeks in storage condition (which may be associated with the water gained by the concrete exposed to humid air). After about sixteen weeks, the electrical resistivity remains quite constant.
- The concrete was tested for its mechanical properties as well as petrographic examinations.
 - ND results were compared to those obtained from concrete specimens made in the lab which showed various levels of deterioration associated with ASR.
 - Results from all methods (except electrical resistivity) demonstrated the overall condition of the concrete remains of good quality, in spite of the significant expansion rates measured on the structure.
 - Damage is mainly located within the first two meters from the surface. Figure 3.179 shows that there is no clear relation between compressive and indirect tensile strength with depth while the static Young’s modulus is higher at depth.
 - Dynamic Young’s modulus and ultrasonic pulse velocity yielded better results than electrical resistivity.
 - The best correlation was found between the P-wave velocities and the static Young’s modulus.
 - It is claimed that laboratory results cannot be directly extrapolated to field results.
 - No significant trend was observed in dynamic Young’s modulus.
 - Petrographic results are shown in Figure 3.180 (right). The most deteriorated zones correspond to the first meters from the surface. The concrete from the lower part of the boreholes showed lower damage which is also in accordance with mechanical and ND results.

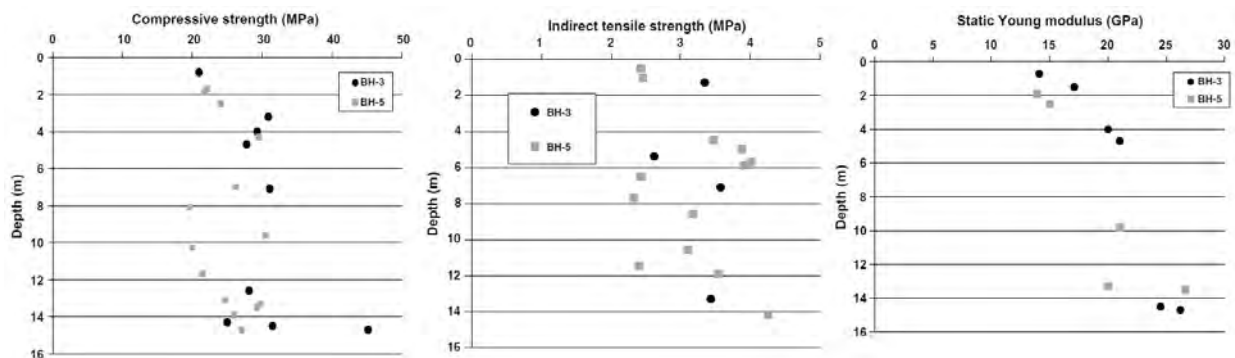


Figure 3.179: Material properties with depth; Rivard and Saint-Pierre (2009)

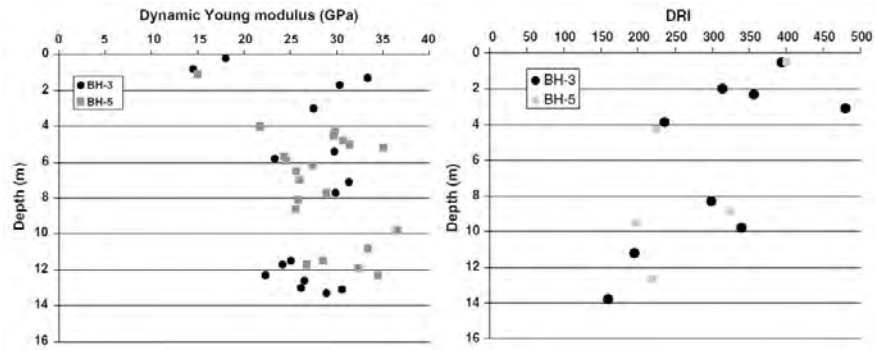


Figure 3.180: Dynamic material properties and DRI with depth; Rivard and Saint-Pierre (2009)

3.136 Rivard, Patrice and Ballivy, Gérard and Gravel, Clermont and Saint-Pierre, Francois (2010)

URL

```
@article{
  rivard2010monitoring},
  label={rivard2010monitoring},
  title={Monitoring of an hydraulic structure affected by ASR: A case study},
  author={Rivard, Patrice and Ballivy, G{\'e}rard and Gravel, Clermont and
    Saint-Pierre, Francois},
  journal={Cement and concrete research},
  volume={40},
  number={4},
  pages={676--680},
  year={2010},
  publisher={Elsevier}
  Keywords={}
```

- A program aiming at assessing the condition of a hydraulic structure affected by ASR was presented.
- The structure has been exhibiting signs of ASR for more than 30 years and shows various levels of damage.
- The study was conducted on a large hydraulic structure located in eastern Canada. It was built nearly 50 years ago and is affected by various degrees of ASR which was first detected approximately 20 years after construction.
- The ASR in this structure is due to the use of a reactive crushed siliceous limestone as coarse aggregate in the concrete.
- Horizontal displacements related to the expansion of concrete vary between 0.1 mm/year and 1.6 mm/year.
- The program encompassed different components, consisting of: 1) stress measurement, 2) evaluation of concrete condition by non-destructive methods without drilling (seismic tomog-

raphy), and 3) the evaluation of the mechanical, physical, and petrographic properties of the concrete determined from cores recovered from full-length boreholes.

- Seismic tomography enables the mapping of sections in order to visualize the distribution of the concrete quality in 2D.
- The variations of velocity are mainly related to the mechanical properties of the concrete as well as the presence of large defects, such as cracks or voids.
- The configurations used for data acquisition are shown in Figure 3.181. Each straight line represents the supposed path followed by P-waves between the impact and the receiver.
- The velocities calculated from the inversion vary between approximately 2000 and 4500 m/s.
- Since the variations are significant, low velocities are assumed to be caused by cracks in the concrete rather than by a reduction in the modulus of elasticity.
- It is suggested that a velocity above 3000 m/s is indicative of a good quality concrete which is in accordance with the ASTM C 597.
- The results suggest that ASR may generate relatively little damage in structures, and that the concrete mechanical properties do not seem to be significantly affected despite high expansion levels measured in this structure.
- A major crack was localized with the seismic tomography.

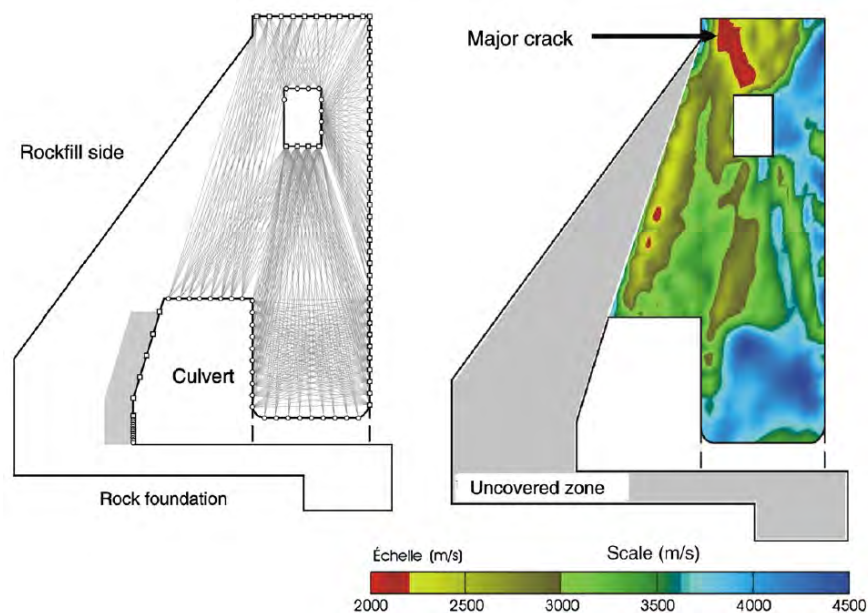


Figure 3.181: Cross-section of investigated structure and P-waves velocity tomography; Rivard et al. (2010)

- Mechanical properties of this paper are already summarized in Rivard and Saint-Pierre (2009).

3.137 Sanchez, LFM and Fournier, B and Jolin, M and Bastien, J (2014)

URL

```
@article{
  sanchez2014evaluation},
  label={sanchez2014evaluation},
  title={Evaluation of the stiffness damage test (SDT) as a tool for assessing
    damage in concrete due to ASR: test loading and output responses for concretes
    incorporating fine or coarse reactive aggregates},
  author={Sanchez, LFM and Fournier, B and Jolin, M and Bastien, J},
  journal={Cement and concrete research},
  volume={56},
  pages={213--229},
  year={2014},
  publisher={Elsevier}
  Keywords={}
```

- The damage's degree of concrete affected by ASR was evaluated using stiffness damage test (SDT).
- The assessment of some parameters (test loading and output responses) on the efficiency of the method was presented.
- The analyses were conducted with three types of concrete (25, 35, and 45 MPa) and two highly-reactive aggregates.
- The results showed that the SDT should be carried out with a percentage of the design strength (ideally 40%) instead of working with a fixed load.
- Parameters, such as the hysteresis area, the plastic deformation over the five cycles of loading/unloading, and the average modulus of elasticity of the second and the third cycles, seem to give quite good correlations with the amount of expansion reached by the concrete.
- Chrisp, Waldron, and Wood (1993) proposed the following as the diagnostic parameters for determining the extent of damage in a specimen:
 - Modulus of elasticity (E_c): Average modulus of elasticity value of the last four cycles as concrete samples of damaged concretes presented lower secant modulus of elasticity than undamaged samples;
 - Hysteresis area (H , in J/m^3): Area of the hysteresis loops averaged over the last four cycles as damaged concrete samples showed greater energy loss (or hysteresis areas) than undamaged samples;
 - Nonlinearity index (NLI): It represents the ratio of the slope of the stress response at half the maximum load over the secant E_c . This parameter provided information about either the extent of damage or the crack patterns of the samples.
- The results of the most critical output parameters are presented in Figure 3.182, for stiffness damage tests carried out at the four different loading levels (15 to 40% of the 28-day/design

strength) and four expansion levels (up to 0.30%) in the 25 MPa concretes incorporating the reactive Texas sand (first row) and reactive New Mexico gravel (second row).

- For concrete mixtures incorporating the TX and NM reactive aggregates, clear differences in the hysteresis area and plastic deformation responses with increasing expansion in the test specimens can be observed only at loading levels corresponding to 30% and 40% of the 28-day design strength.

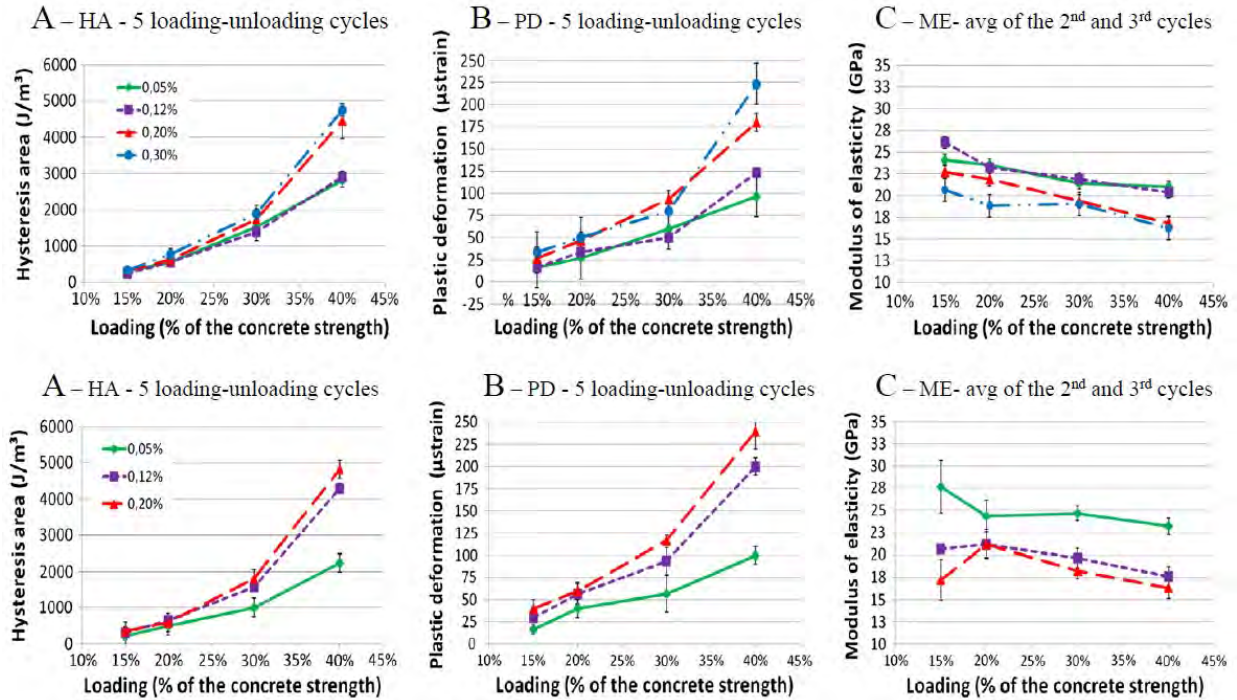


Figure 3.182: Responses of selected SDT output parameters versus the loading applied (% of the 28-day/design strength) for 25 MPa concrete mixtures (first row: Tx sand; second row: NM gravel); Sanchez et al. (2014)

- The stiffness damage test can provide a reliable assessment of the effects of ASR expansion on damage generation in different types of concretes.
- Carrying out the SDT with percentages of loading of less than 30% (and preferably 40%) of the concrete mix-design strength does not make the SDT a diagnostic tool for assessing the degree of expansion attained by ASR-affected concretes.
- The hysteresis area and the plastic deformation over the complete five loading/unloading cycles, as well as the average value of the modulus of elasticity obtained in the second and third cycles, were found to be the best parameters to use as output responses when the test is carried out up to a load corresponding to 40% of the mix-design (28-day) strength.
- Even when using 40% of the concrete mix-design strength, the SDT seems to maintain its non-destructive character, as seen in the results of the microscopic examination of the test specimens carried out through the damage rating index (DRI).

- In general, the greater the concrete mix design strength, the greater the hysteresis area obtained through the SDT for the same aggregate type.

3.138 Sanchez, LFM and Fournier, B and Jolin, M and Bastien, J (2015)

URL

```
@article{
  sanchez2015evaluation},
  label={sanchez2015evaluation},
  title={Evaluation of the Stiffness Damage Test (SDT) as a tool for assessing
    damage in concrete due to alkali-silica reaction (ASR): Input parameters and
    variability of the test responses},
  author={Sanchez, LFM and Fournier, B and Jolin, M and Bastien, J},
  journal={Construction and Building Materials},
  volume={77},
  pages={20--32},
  year={2015},
  publisher={Elsevier}
  Keywords={}
```

- The Stiffness Damage Test (SDT) was used for assessing damage in concrete affected by ASR.
- The use of fixed loading over the test limits the Test's ability to reliably appraise the distress level of concrete samples, mainly when different concrete strengths and aggregate types are used.
- A critical evaluation of several input parameters of the SDT were presented, including the core's environmental conditions, the samples' characteristics, and the samples' conditioning history.
- Different types of surface preparation and the specimens' size (i.e. diameter) did not seem to clearly modify the test analyses.
- When a damage assessment is carried out on an aging concrete structure/element potentially affected by ASR, the environmental characteristics of the specimens extracted should be considered, such as the core depth from the surface and the exposure condition of the element investigated.
- Significantly different values for all the SDT output parameters are obtained for cores extracted from exposed and unexposed portions of the structure investigated, confirming a greater damage in the sections exposed to moisture.
- Using cores with length-to-diameter ratios smaller than 2.0 can significantly affect the results of stiffness damage testing, especially the Hysteresis Area and Plastic Deformation parameters.
- The moisture condition of the specimens prior to testing can largely influence the responses over SDT. Drying of the cores/test specimens increases their stiffness and elastic modulus

while decreasing both the Hysteresis Area and the Plastic Deformation values measured over SDT.

- The different types of end surface preparation (capping vs. grinding) do not seem to influence significantly the responses over SDT.

3.139 Sanchez, LFM and Fournier, B and Jolin, M and Duchesne, Josée (2015)

URL

```
@article{
  sanchez2015reliable,
  label={sanchez2015reliable},
  title={Reliable quantification of AAR damage through assessment of the Damage
    Rating Index (DRI)},
  author={Sanchez, LFM and Fournier, B and Jolin, M and Duchesne, Jos{\`e}},
  journal={Cement and Concrete Research},
  volume={67},
  pages={74--92},
  year={2015},
  publisher={Elsevier},
  Keywords={},
  DisplayPdf={0},
  url={https://www.sciencedirect.com/science/article/pii/S0008884614001665}
```

- Presents the results of the condition assessment of twenty concrete mixtures incorporating ten different reactive aggregates through the Damage Rating Index (DRI), a microscopic and semi-quantitative petrographic tool, with the aim of verifying the development of distress due to alkali-aggregate reaction (AAR) as a function of the specimen's expansion (i.e. from 0.05 to 0.30%).
- The DRI was found to provide a reliable assessment of the degree of damage in the concretes incorporating reactive fine or coarse aggregates.
- An envelope of DRI damage assessments against the expansion level of the affected materials is proposed. For all alkali-silica reactive aggregates investigated, the progress in counts and proportions of opened cracks in the aggregate particles and in the cement paste, with and without gel, as well as the crack density parameter, were found to be diagnostic petrographic features for quantifying ASR progress.
- A qualitative ASR distress model in concrete was defined.

Major Conclusions

- The DRI output final value can provide a reliable assessment of the degree of expansion in AAR-affected specimens when the deleterious reaction comes either from a reactive sand or a reactive coarse aggregate. However, the use of the DRI number only does not give further

information about the exact nature/cause of the specimen's damage and is consequently not meant to replace the conventional petrographic examination;

- A similar progress in DRI values was observed for concretes of different strengths or incorporating different reactive rock/aggregates types, which allowed obtaining an envelope of DRI results against the expansion level of the concrete specimens. However, exceptions could be seen for an alkali-carbonate reactive rock (King) and a siliceous sandstone (Pots), which displayed somewhat different reaction mechanisms or kinetics than that observed for most other reactive quartz-bearing rocks investigated;
- For the aggregates investigated, no significant differences in the development of petrographic features of deterioration were observed between 25 and 35MPa concretes at similar expansion levels. However, the cracking pattern was more difficult to identify and also seemed slightly different for the 45 MPa mixtures, especially in the early stages of the chemical reaction where damage degrees higher than that observed in the 25 and 35 MPa concretes were obtained. Moreover, the presence of gel was found to be greater for 45 MPa concrete mixtures for all expansion levels;
- For all alkali-silica reactive aggregates investigated, the counts and proportions of opened cracks in the aggregate particles, as well as cracks in the cement paste, with and without gel, increased with increasing expansion in the test specimens. They were found to be indicative petrographic features of the development of AAR in the concrete specimens. Opened cracks are likely to develop inside the reactive aggregate particles in the early stages as a result of the chemical reaction process and potentially initiating from closed cracks induced through aggregate processing operations. With the progress of ASR, the number and importance (i.e. length and width) of those opened cracks increase and cracks formed inside the aggregate particles extend into the cement paste for higher expansion levels ($\simeq 0.12\%$). Exceptions were seen for the mixture King + Lav where a largely different damage pattern was found for all the expansion levels studied;
- The crack density (CD) (counts of opened cracks in the aggregate particles and cracks in the cement paste/surface area examined (cm^2)) was confirmed as an interesting supplementary information of the DRI procedure. CD values were typically found to increase almost linearly as a function of increasing expansion in the test specimens and formed a data envelope that could be used for estimating the AAR expansion in the test specimens. Once again, the King and Pots aggregates were excluded from the above relationship because of their somewhat different reaction mechanism/kinetics;
- The analyses of the counts of the different petrographic features of deterioration, in absolute and relativeways, help to better understand the development of ASR distress in the concrete specimens and also how this chemical reaction progresses as a function of the expansion level of the samples;
- A model for the development of ASR damage in concrete as a function of expansion in concrete was defined, mainly based on the development of two cracking types commonly found in the concrete specimens. Sharp (Type A) and/or Onion skin/en echelon (Type B) cracks were found to form in the aggregates particles in the early stages of the reaction, then extending into the cement paste with increasing expansion to eventually connect reactive aggregate particles in an extensive cracking network. Type A and Type B cracks are not necessarily

present at the same time in the affected aggregate particles. Their presence will be a function of rock type characteristics;

- A different pattern of damage generation is observed with the alkali– carbonate reactive aggregate King. In this case, extensive cracking in the cement paste develops in the early stages of the reaction/ expansion process, with cracking also developing, but to a lesser extent, within the aggregate particle;
- The petrographic investigations carried out in this study suggest that the development of cracking within individual alkali–silica reactive aggregate particles does not follow a linear pattern as a function of expansion in concrete. It is proposed that a significant number of new cracks will form in the early stages of the chemical reaction until some of them reach given critical length and width. Following the minimum energy law, it will then be easier for the expanding system to propagate those “critical” cracks instead of creating new ones. Thus, the rate of crack generation within the aggregate particles will start slowing down;
- Finally, the Damage Rating Index (DRI) was found to be a powerful tool for evaluating damage in concrete specimens affected by ASR incorporating reactive fine or coarse aggregates. However, this procedure still needs to prove its efficiency in assessing damage in concrete cores extracted from ASR-affected aging concrete structures and, in a second step, for assessing other distress mechanisms (e.g. delayed ettringite formation, freezing and thawing). Moreover, a careful analysis and assessment of the weighing factors would give even more impact on the DRI final results;
- A comparative analysis of the impact of ASR on the mechanical properties of concrete, as a function of expansion, and the development of petrographic features obtained through the DRI is in progress to confirm the reliability of the latter as a global damage assessment tool for ASR-affected concrete structures.

and its amount depends on the aggregate's nature and concrete characteristics.

At very high expansion levels (e.g. $\geq 0.30\%$), type A cracks link to other cracks formed at other location in the concrete, either due to ASR within adjacent reactive aggregate particle or non reactive aggregate particles or the cement paste resulting from ASR pressure developing within the concrete matrix, as described in the previous sections. A more or less extensive network of cracking will then link several

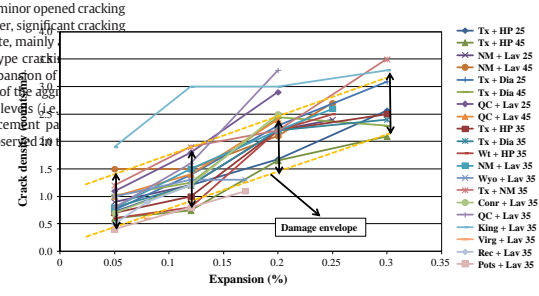
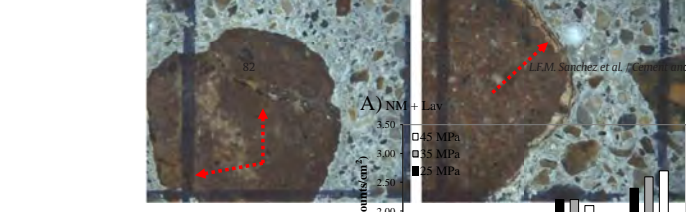
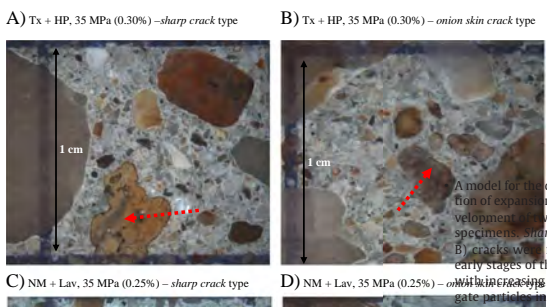


Fig. 17. Crack density (CD) assessment envelope.

A model for the development of ASR damage in concrete as a function of expansion was defined, mainly based on the development of two cracking types commonly found in the concrete specimens: sharp (Type A) and/or Onion skin/en echelon (Type B) cracks were found to form in the aggregates particles in the early stages of the reaction, then extending into the cement paste with increasing expansion to eventually connect reactive aggregate particles in an extensive cracking network. Type A and Type

B cracks are not necessarily present at the same time in the affected aggregate particles. Their presence will be a function of rock type characteristics;

- A different pattern of damage generation is observed with the alkali-carbonate reactive aggregate King. In this case, extensive cracking in the cement paste develops in the early stages of the reaction/expansion process, with cracking also developing, but to a lesser extent, within the aggregate particle;

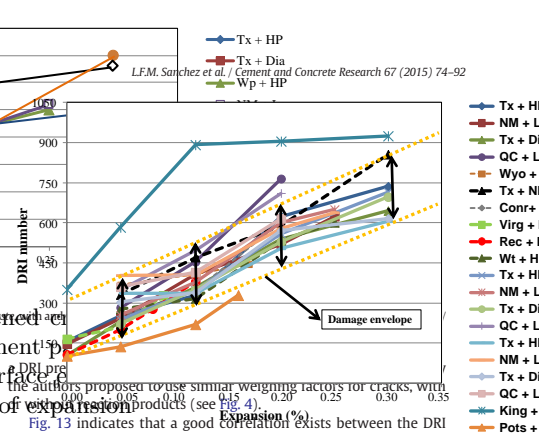
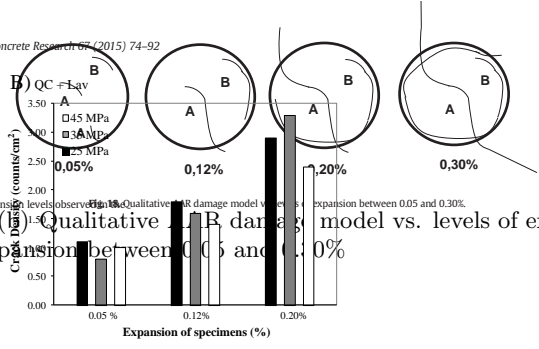


Fig. 13. Crack density (sum of opened particles and cracks in the cement paste) as a function of expansion.

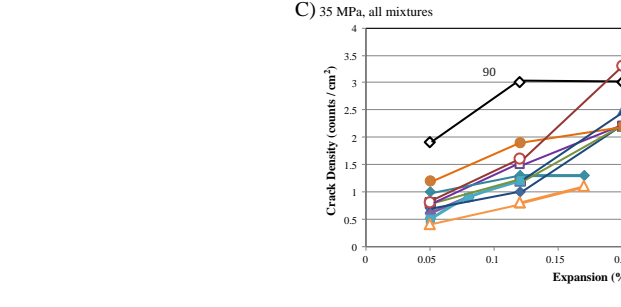
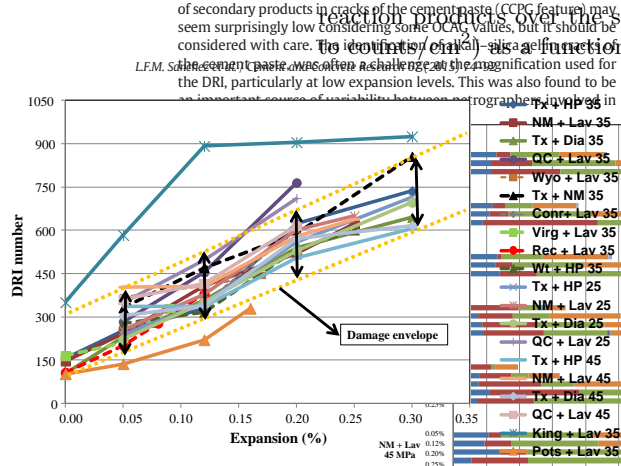


Fig. 9. Crack density (sum of opened particles and cracks in the cement paste) as a function of expansion.



(d) DRI damage assessment envelope

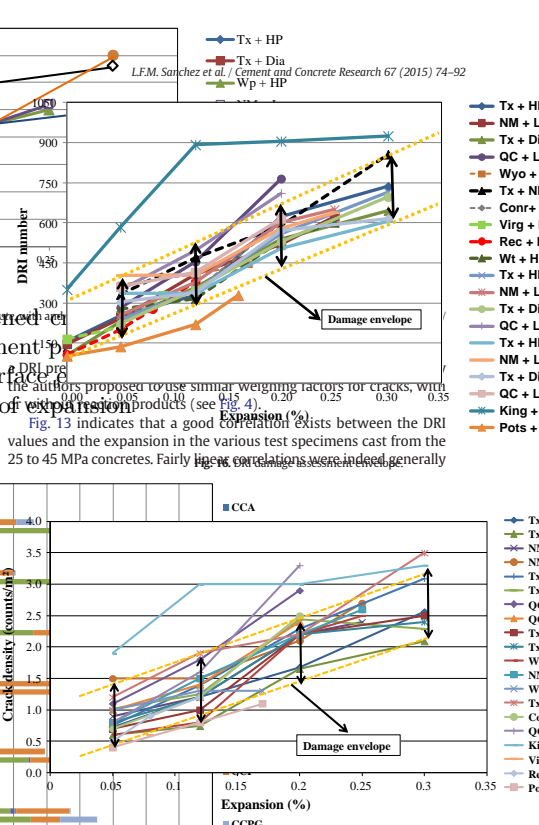


Fig. 17. Crack density (CD) assessment envelope.

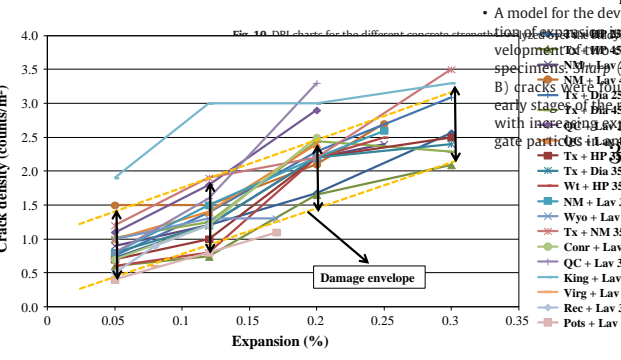
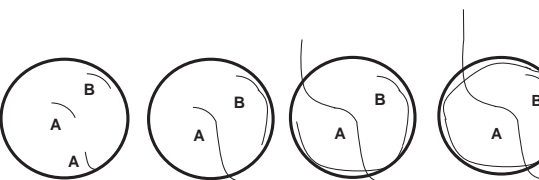


Fig. 10. DRI charts for the different concrete specimens.

A model for the development of ASR damage in concrete as a function of expansion was defined, mainly based on the development of two cracking types commonly found in the concrete specimens: sharp (Type A) and/or Onion skin/en echelon (Type B) cracks were found to form in the aggregates particles in the early stages of the reaction, then extending into the cement paste with increasing expansion to eventually connect reactive aggregate particles in an extensive cracking network. Type A and Type

B cracks are not necessarily present at the same time in the affected aggregate particles. Their presence will be a function of rock type characteristics;

- A different pattern of damage generation is observed with the alkali-carbonate reactive aggregate King. In this case, extensive cracking in the cement paste develops in the early stages of the reaction/expansion process, with cracking also developing, but to a lesser extent, within the aggregate particle;



3.140 Sanchez, LFM and Fournier, B and Jolin, M and Bastien, J and Mitchell, D (2016)

URL

```
@article{
  sanchez2016practical},
label={sanchez2016practical},
title={Practical use of the Stiffness Damage Test (SDT) for assessing damage in
  concrete infrastructure affected by alkali-silica reaction},
author={Sanchez, LFM and Fournier, B and Jolin, M and Bastien, J and Mitchell, D},
journal={Construction and Building Materials},
volume={125},
pages={1178--1188},
year={2016},
publisher={Elsevier}
Keywords={}
```

- The Stiffness Damage Test (SDT) was used to assess damage in concrete affected by ASR.
- The use of a fixed loading level for stiffness damage testing limits the SDT's ability to reliably appraise the distress level of concrete samples, especially when different concrete strengths and aggregate types are used.
- The use of output indices (i.e. SDI and PDI) instead of absolute output values makes the procedure more diagnostic and less influenced by practical assumptions (e.g. choice of the loading level for stiffness damage testing).
- Figure 3.183 illustrates the proposed procedure for concrete damage assessment using stiffness damage testing.
- The flowchart is divided into 9 steps:
 - First, cores are extracted from damaged and non-damaged locations of interest in the structure (step 1).
 - Then, the specimens are prepared and conditioned in order to decrease the variability among companion samples (steps 2-6).
 - Once the conditioning is performed and the test samples are ready to be tested, a compressive strength test is performed on cores extracted from non-damaged (or less damaged) portions of the structure. Forty % of this value is used to run the SDT on the damaged cores.
 - Finally, the results are evaluated and reported, representing the last step of the proposed procedure.

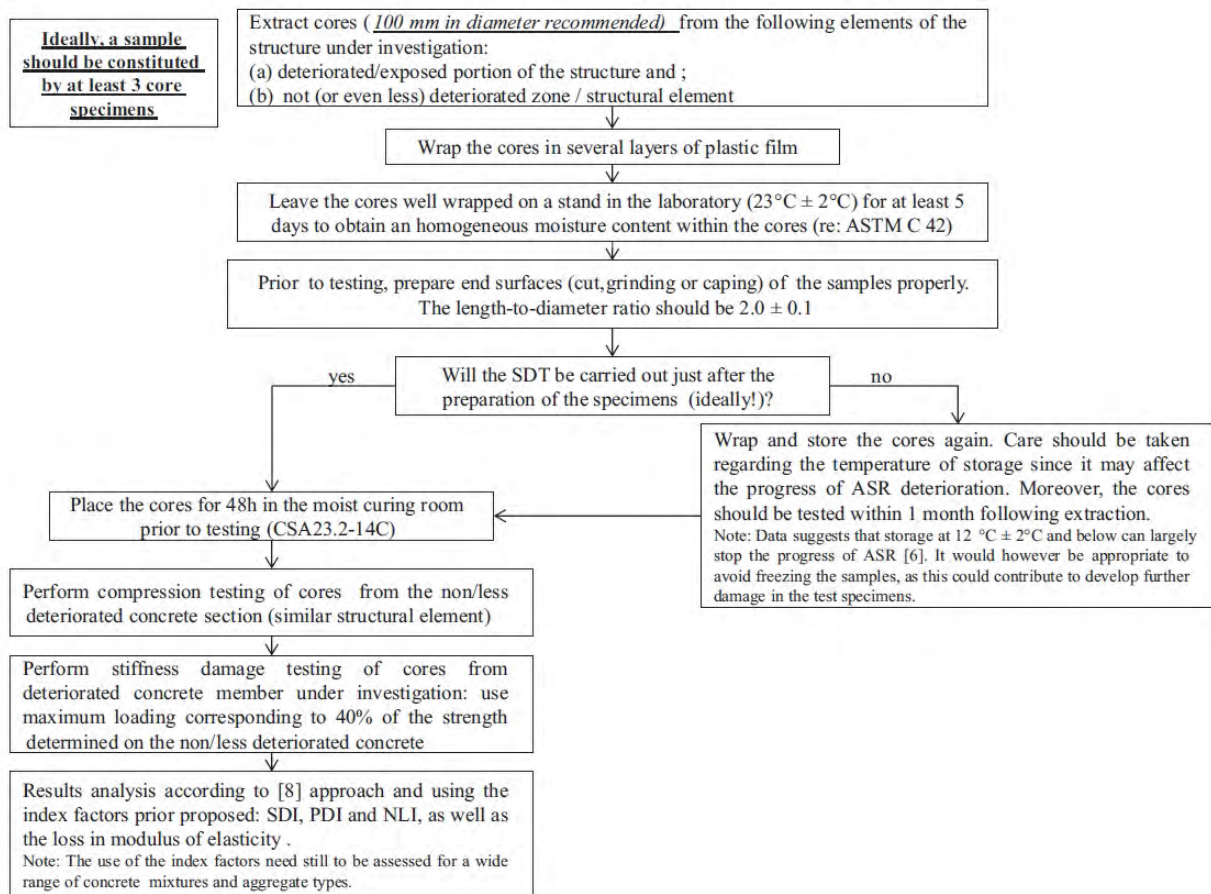


Figure 3.183: Proposed procedure for concrete damage assessment using stiffness damage testing; Sanchez et al. (2016a)

3.141 Sanchez, LFM and Fournier, B and Jolin, M and Bedoya, MAB and Bastien, J and Duchesne, J (2016)

URL

```
@article{
  sanchez2016use,
  label={sanchez2016use},
  title={Use of Damage Rating Index to Quantify Alkali-Silica Reaction Damage in Concrete: Fine versus Coarse Aggregate.},
  author={Sanchez, LFM and Fournier, B and Jolin, M and Bedoya, MAB and Bastien, J and Duchesne, J},
  journal={ACI Materials Journal},
  volume={113},
  number={4},
  year={2016},
  Keywords={},
  DisplayPdf={0},
  url={https://www.concrete.org/publications/internationalconcreteabstractsportal.aspx?m=details&ID=511}
```

- The Damage Rating Index (DRI), a microscopic and semi-quantitative petrographic tool, is a method that has increasingly been used in North America and Europe because it can answer questions regarding the nature and the degree of damage in concrete affected by deleterious mechanisms such as alkali-aggregate reaction (AAR).
- Paper presents the results of the condition assessment, using the DRI, of concrete mixtures of different strengths and incorporating different reactive aggregate types (fine versus coarse aggregate) with the aim of verifying both how alkali-silica reaction (ASR) develops against its expansion levels and how the DRI could be used to better quantify damage in concrete due to ASR.
- Concrete specimens cast from a series of concrete mixtures of different strengths (25, 35, and 45 MPa [3626, 5076, and 6527 psi]) and incorporating reactive coarse or fine aggregates were examined at expansion levels ranging from 0.05 to 0.30% to determine their internal damage through the use of the DRI. The following conclusions can be drawn from the results obtained in this study:
 - The DRI number was found to be very effective for assessing damage in concrete distressed due to ASR. For each of the different expansion levels selected in this study, no significant differences in the DRI values were obtained between the 25 and 35 MPa (3626 and 5076 psi) concrete mixtures.
 - DRI results were found to be similar for ASR coming from different reactive aggregate types (sand versus coarse aggregate) because no significant variations in the microscopic results were obtained. However, the cracking pattern is somewhat more sparsely distributed within the concrete matrix when ASR comes from reactive sands compared to cracking generated in the coarse aggregate fraction.
 - Further important information can also be obtained through the analysis of DRI bar charts, counts of cracks, crack density, and cracks lengths and/or widths; all these parameters were found to be linked to ASR development.
 - DRI seems to be a powerful tool for evaluating damage in concrete affected by ASR incorporating reactive fine or coarse aggregates. More research is needed to verify its efficiency in assessing other distress mechanisms and concrete cores extracted from affected structures in the field.

Petrographic features		Weighing factors	
		Original values ³	This study ²
Crack in coarse aggregate	CCA	0.25	0.25
Opened crack in coarse aggregates	OCA	--	2
Crack with reaction product in coarse aggregate	OCAG	2	2
Coarse aggregate debonded	CAD	3	3
Crack in cement paste	CCP	2	3
Crack with reaction product in cement paste	CCPG	4	3
Air void lined/filled with gel	AVG	0.5	--
Reaction rim around aggregate	RR	0.5	--
Disaggregate/corroded aggregate particle	DAP	--	2

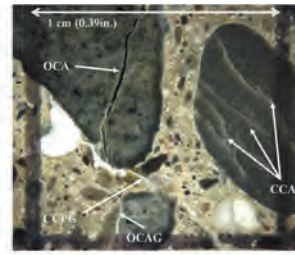


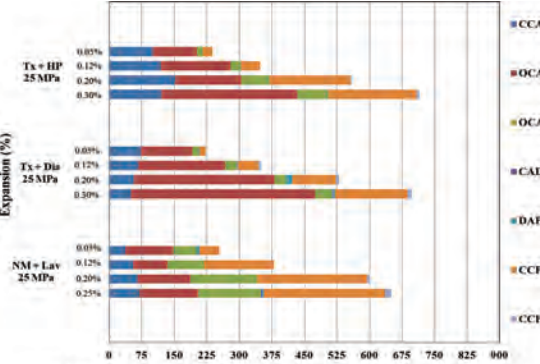
Fig. 1—Damage Rating Index Method. Micrograph B shows 1 cm² (0.155 in.²) section where most petrographic features to be noted in DRI (as listed in A) can be observed and identified. Distance between two vertical lines is 1 cm (0.3937 in.).

found that eliminating the counts of the number of voids with reaction products in the cement paste and reaction rims from the calculation of the DRI values also contributes to reducing the variability between the are not really direct indicators. The fact of classifying types of secondary reaction particles (factor of 2) or v 3), may result in overestimating damage from other divers. It is important to the goal of the DRI approach to appraise the cause of "overall distress level, or regarding the mechanism(s) i proper assessment of the c addressed through, for ex: tion of the concrete follow

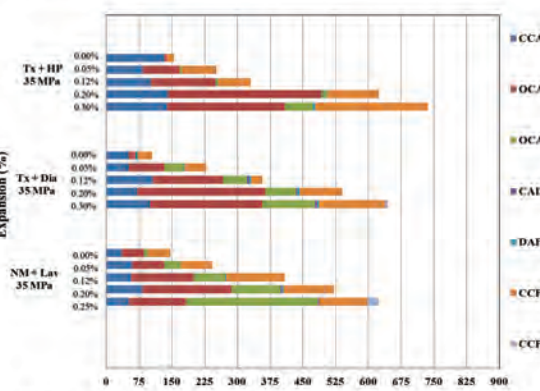
Because the process o through the type of reac coarse aggregate, lithotyp the nature and degree o: them with either the exp: concrete or, ideally, with l Such information is, howe over, although the differe distressed concrete specim microscope,²⁴⁻²⁶ there is c tion based on DRI values, high damage levels in con is important to mention th used by several researche test procedure available to

In view of eventually c for the DRI, it appears th: be answered?:

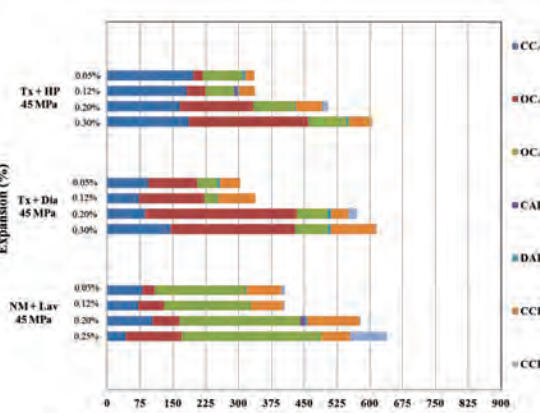
- Should/can the DRI representing a damage distress mechanism?
- Does the type/nature versus coarse aggregate results of the DRI for



(a) 25 MPa mixtures



(b) 35 MPa mixtures



(c) 45 MPa mixtures

Fig. 7—DRI charts for all concrete mixtures (that is, Tx + HP, Tx + Dia, NM + Lav): (a) 25 MPa (3626 psi); (b) 35 MPa (5076 psi); and (c) 45 MPa (6527 psi) concretes. Full definition of petrographic features is given in Fig. 1.

3.142 Sanchez, LFM and Fournier, B and Jolin, M and Mitchell, D and Bastien, J (2017)

URL

```
@article{
sanchez2017overall},
label={sanchez2017overall},
title={Overall assessment of Alkali-Aggregate Reaction (AAR) in concretes
presenting different strengths and incorporating a wide range of reactive
aggregate types and natures},
author={Sanchez, LFM and Fournier, B and Jolin, M and Mitchell, D and Bastien, J},
journal={Cement and Concrete Research},
volume={93},
pages={17--31},
year={2017},
publisher={Elsevier}
Keywords={Micro; Expansion monitoring; Damage Mech.; }
```

- Twenty concrete mixtures of different strengths (i.e. 25, 35, and 45 MPa) and incorporating ten different reactive aggregate types/natures were selected for this study.
- The coarse aggregates ranged from 5 mm to 20 mm in size. Non-reactive fine (Lav) and coarse (HP or Dia) aggregates were used in combination with the reactive aggregates.
- A minimum of 35 cylinders, 100 mm by 200 mm in size, were cast from each of the twenty concrete mixtures manufactured in the laboratory.
- Figure 3.184 presents the average expansion value from each 35 MPa concrete mixture vs. time. A wide range of expansion kinetics and amplitudes was obtained as a function of the reactive aggregate tested. In general, the mixtures containing the reactive TX sand presented faster reactivity.
- Next, the mechanical properties reduction of the various concretes were investigated as the ratio of values obtained at each selected free expansion level against the values obtained on concrete specimens of equivalent maturity.
- The modulus of elasticity correspond to the average values obtained from the 2nd and 3rd cycles of stiffness damage testing.
- The compressive strengths were determined on the test specimens that were previously subjected to stiffness damage testing while the tensile strengths were obtained on a separate set of test cylinders at each selected expansion levels.
- Modulus of elasticity (ME):
 - Globally, ME losses presented a “concave” trend of reductions towards AAR development.
 - It is ranging from 5-30% at low expansions to 40-65% at high levels.
 - Similar trends were found for the 25 and 45 MPa mix.

- Tensile strength (TS):
 - TS losses ranged from 12-70% and from 50-70% for low (i.e. 0.05%) and high expansion levels (0.20% and 0.30%), respectively.
 - At low expansion levels, the range of results was greater than for high levels of damage.
 - 25 and 45 MPa presented roughly the same trend.
- Compressive strength (CS):
 - In general, CS was found to decrease in a somewhat modest way with increasing expansion.
 - Despite some variations from one reactive aggregate combination to another, similar trends in CS reductions were obtained for the various mixtures investigated (25 to 45 MPa).
 - Maximum CS losses reaching about 10% at 0.05% expansion, 10-20% at 0.12% expansion and 20-30% at expansions greater than 0.20%.

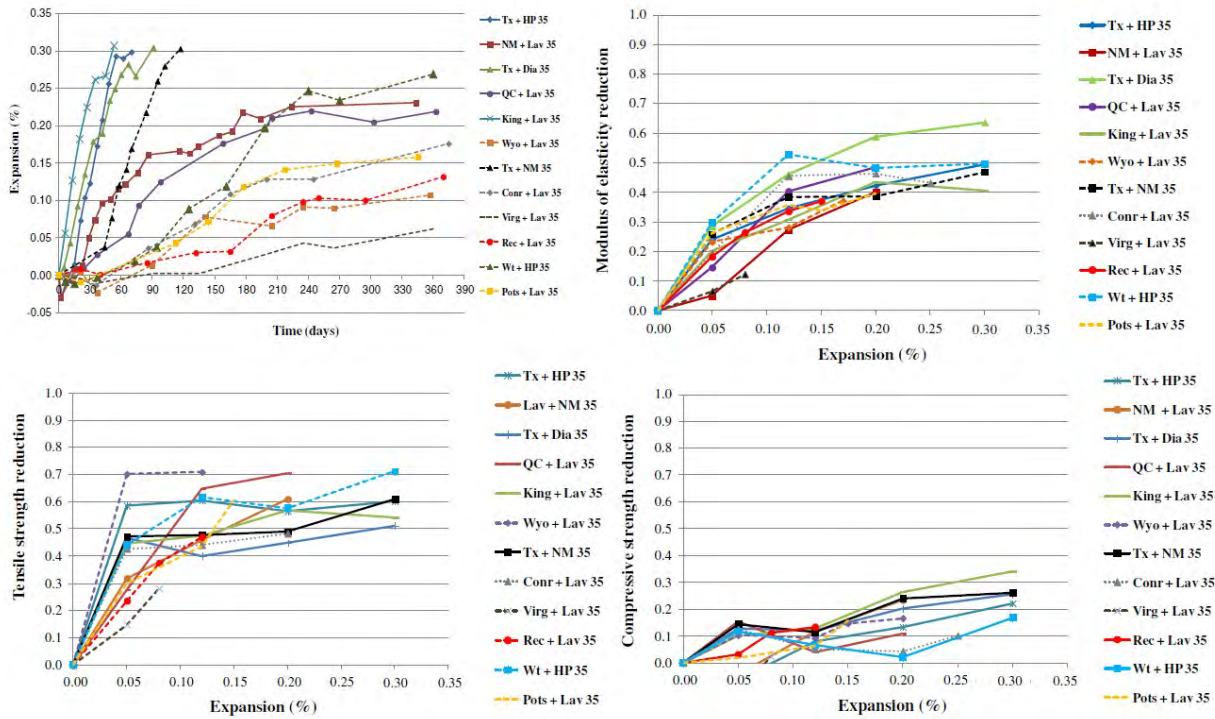


Figure 3.184: AAR kinetics and material properties for the 35 MPa concrete mix; Sanchez et al. (2017)

3.143 Saouma, Victor and Perotti, Luigi (2006)

URL


```
@article{
saouma2006constitutive},
label={saouma2006constitutive},
title={Constitutive model for alkali-aggregate reactions},
author={Saouma, Victor and Perotti, Luigi},
journal={ACI materials journal},
volume={103},
number={3},
pages={194},
year={2006},
publisher={American Concrete Institute}
Keywords={}
```

- A new constitutive model for AAR expansion was presented.
- This thermo-chemo-mechanical model was rooted in the chemistry, physics, and mechanics of concrete.
- The major assumptions in this model are related to the volumetric expansion of the gel and redistribution on the basis of weights related to the stress tensor.
- This three-component model is an anisotropic model.
- The model is developed based on the kinetics of the reaction.
- This model is combined by the parameter identification technique to analyze laboratory tests on triaxially confined concrete cylinders.
- A detailed 2D analysis of an arch gravity dam is presented.
- First, the seasonal pool elevation variation (for both thermal and stress analysis) and the stress free temperature (typically either the grouting temperature or the average yearly temperature) are identified.
- Next, a transient thermal analysis is performed for which only the heat transfer by conduction is accounted. Convection and radiation are approximated through an additional temperature.
- The total simulation time was 50 years with the selected incremental time of 2 weeks.
- Following the thermal analysis, the computed temperature must be transferred to another model (built for stress analysis) as, in general, we do not have the same finite element mesh (foundations, joints, and cracks are typically not modeled in the thermal analysis).
- A comprehensive input data file was prepared for the stress analysis:
 - Gravity load (first increment only);
 - Incremental temperature load;
 - Stress-free referenced temperature;
 - Cantilever and dam/foundation joint characteristics;
 - Uplift load characteristics; and

– AAR data characteristics.

- For the plane strain analysis, a 2D central section of the arch gravity dam is selected.
- Note that, creep is not accounted for in this analysis.
- Results are compared with the method proposed by Charlwood, Solymar, and Curtis (1992). To do so, final volumetric expansion was calibrated to yield identical vertical crest displacement after 50 years, Figure 3.185 (left), where the proposed model nonlinearity in the crest displacement is caused by the kinetics model and its latency time in particular.
- Despite equal final crest displacements, internal field stresses are drastically different. Those determined from Charlwood’s model are substantially lower than those predicted by the proposed model, Figure 3.185 (right).
- The large discrepancy in stresses is partially caused by the plane strain (which inhibits redistribution in the third direction) assumption of the proposed model.

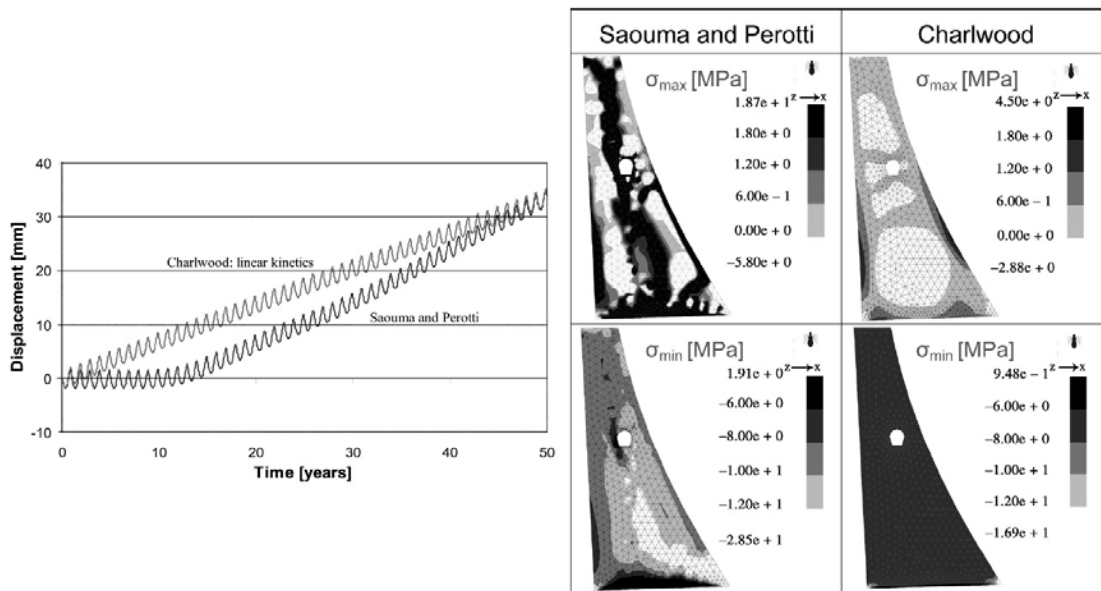


Figure 3.185: Comparison of yearly vertical displacement, and principal stress fields in two models; Saouma and Perotti (2006)

3.144 Saouma, Victor and Perotti, Luigi and Shimpo, Takashi (2007)

[URL](#)

```

@article{
saouma2007stress},
label={saouma2007stress},
title={Stress analysis of concrete structures subjected to alkali-aggregate
reactions},
author={Saouma, Victor and Perotti, Luigi and Shimpo, Takashi},
journal={ACI structural journal},
volume={104},
number={5},
pages={532},
year={2007},
publisher={American Concrete Institute}
Keywords={}

```

- The paper first briefly summarizes the key ingredients of the proposed model.
- A methodology is described for analysis and system identification of important AAR parameters.
- The general framework proposed in this paper includes: 1) thermal analysis, 2) stress analysis, and 3) system identification.
- Thermal analysis:
 - Because of the temperature dependency, and to obtain a temporal map of the internal temperature, a transient thermal analysis must be performed.
 - At this stage, there is no need to model the rock base in such analysis.
 - Required data for this stage are:
 - * The air temperature variation (including the grouting temperature),
 - * The spatial (along the depth) and temporal (at least 12 or 24 increments a year) variation of the water temperature,
 - * The pool elevation variation during a typical year,
 - * And the concrete thermal properties.
- Stress analysis:
 - The stress analysis is then performed, and an effective E_{eff} is used to account for long-term creep ($E_{eff} = \frac{E_i}{1+c_t}$, where c_t is the specific creep coefficient and E_i is the initial modulus).
 - Detailed FE model including the joints, foundation, etc. should be used.
 - It should be kept in mind that the stress analysis requires the temperature difference with respect to the stress-free temperature.
 - A correct pool elevation (upstream and downstream), uplift pressures, and internal nodal temperatures should be applied for each increment.
- System identification:
 - AAR problems are prime candidates for system identification.

- The field recorded (usually crest) displacements are denoted by $u(t)$, the kinetic (and possibly other) parameters as x , the finite element operator $f(\cdot)$, and computed results by $u(t, x)$.
 - Hence, $f(x) = u'(t, x) \neq u(t)$.
 - The goal is to minimize the objective function $\omega(x) = (u - u')^T(u - u')$. The trust region method can be used to solve the problem.
 - A weight function can be used to assign importance to the last data field which usually has a major absolute value and, thus, better represents the irreversible effect of the AAR expansion with respect to the effect of normal loads.
- Several FE analyses were performed.
 - First, analyses are performed for a 2D case. Due to the complex interplay among temperature, stresses, and expansion, the internal core of the dam constrains the expansion of the external layer which produces tensile stresses in the inner part.
 - The proposed model (state-of-the-art) was compared with the state-of-the-practice model.
 - The state-of-the-practice model greatly underestimates the magnitude of the tensile stresses.

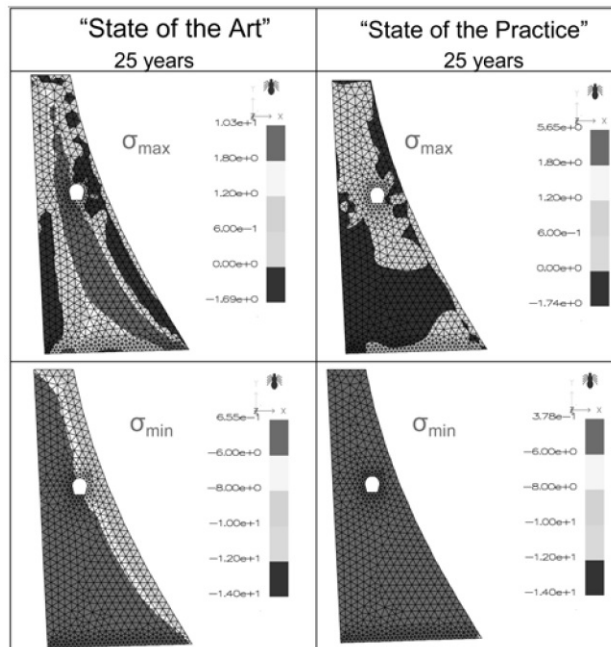


Figure 3.186: Comparison of principal stress fields in two models; Saouma, Perotti, and Shimpo (2007)

- Next, a 3D analysis of an arch gravity dam is performed.
- First, a thermal analysis is performed, followed by a parametric identification study of the dam, and a final predictive analysis using AAR parameters from the previous step.

- Figure 3.187 (left) shows that the computed crest displacement is well within the seasonal variations of the numerical final predictions.
- Figure 3.187 (right) shows the internal AAR induced maximum principal stresses. The maximum principal stress field inside the dam can explain the cracks discovered along the upper gallery of the analyzed dam.

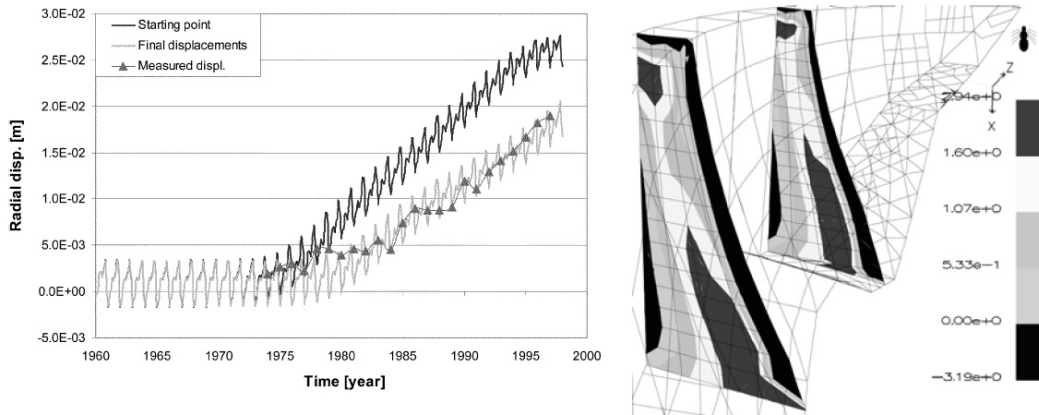


Figure 3.187: Comparison between first guess analysis and final analysis with optimized parameters (left), Internal AAR-induced maximum principal stresses in MPa (right); Saouma, Perotti, and Shimpo (2007)

- The other example includes a hollow-gravity dam composed of two lateral gravity dams and four hollow diamond-head-buttrass central elements.
- Following the thermal analysis, a stress analysis is conducted using a mesh that included the dam, the foundation, and the interface joints between the rock and concrete.
- The 3D finite element mesh had 6,145 nodes and 24,133 elements.
- Figure 3.188 shows the vertical and horizontal crest displacements. The following observations can be made:
 - The final maximum crest vertical displacement is approximately 30 mm.
 - The seasonal variation of the displacements is not negligible compared to the total AAR irreversible one.
 - The kinematics of the displacement is not yet satisfactorily captured.
 - The horizontal displacements are substantially smaller than the vertical displacements due to the lateral constraints.
- The last example investigated is the effect of AAR expansion in a massive reinforced concrete structure that supports a high-voltage transmission tower.
- A single frame of the structure was modeled through a 3D mesh.
- The effect of humidity variation was neglected and left for future studies.

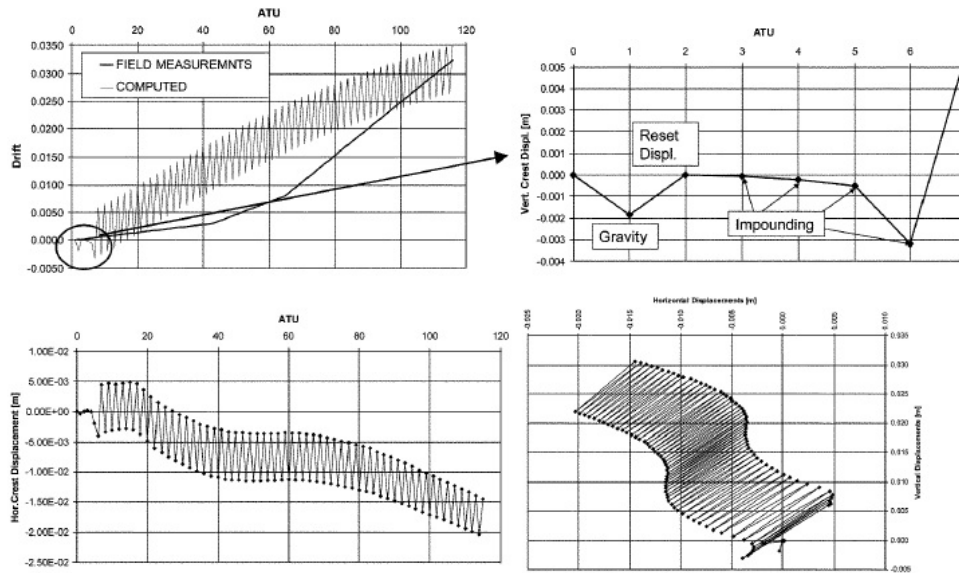


Figure 3.188: Crest vertical and horizontal displacements versus ATU; vertical versus horizontal displacements; Saouma, Perotti, and Shimpo (2007)

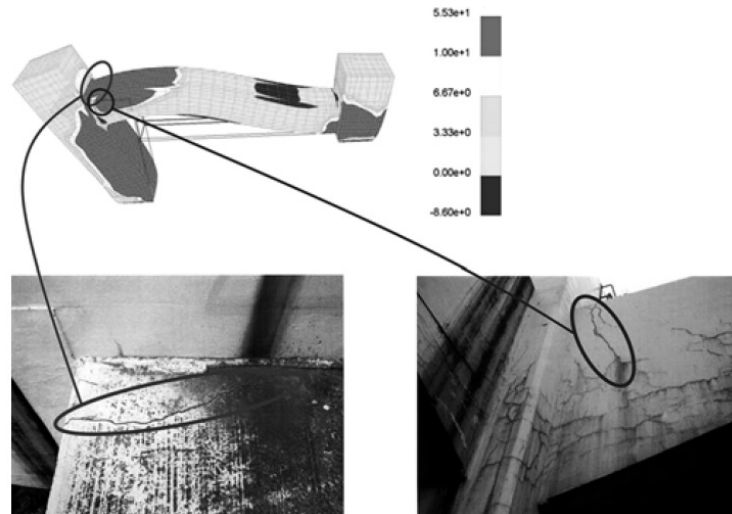


Figure 3.189: Correlation between AAR finite element simulation and observed cracks; Saouma, Perotti, and Shimpo (2007)

- Following a 50-year simulation (Figure 3.189), it was observed that zones of high tensile stresses do indeed correspond to the location of the observed cracks in the field. The high tensile zone, however, seems to be isolated to the external part of the beam.

3.145 Saouma, Victor E and Hariri-Ardebili, Mohammad A (2014)

URL

```
@article{
saouma2014proposed},
label={saouma2014proposed},
title={A proposed aging management program for alkali silica reactions in a
nuclear power plant},
author={Saouma, Victor E and Hariri-Ardebili, Mohammad A},
journal={Nuclear Engineering and Design},
volume={277},
pages={248--264},
year={2014},
publisher={Elsevier}
Keywords={}
```

- An aging management program for ASR in the Seabrook Nuclear Power Plant was proposed.
- The following actions were suggested as a comprehensive framework to deal with the structures suffering from ASR:
 - Minimize the importance of surface crack measurements.
 - Perform one-time tests to measure the internal relative humidity (gauges exist to measure both RH and temperature) and free chloride concentration.
 - Conduct long-term (multiple years) monitoring (especially away from the surface) of:
 - * Dynamic elastic properties through any of the most appropriate and/or feasible means: pulse velocity, impact echo, or other,
 - * In situ stresses,
 - * Out-of-plane surface deformation (possibly through laser measurements),
 - * Strains in rebar (by simply scraping the concrete surface and installing a few strain gauges with a long life span).
 - Perform tests in an attempt to measure the residual expansion (both magnitude and kinetics).
 - Completely ignore compressive strength tests and instead rely exclusively on tensile strength, Young's modulus, and, most importantly, on fracture energy.
 - Conduct a coupled heat/moisture transport analysis of both the large-scale testing specimen and the wall at Seabrook to better correlate ASR expansion to local conditions. A separate analysis may also include the chloride diffusion to address possible corrosion.
 - Conduct a nonlinear finite element analysis, keeping in mind that serviceability is of primary interest for shear and failure on the anchors. The code should first be validated with benchmark problems. Then, and only then, can the result be “trusted”.
- A new paradigm of performance based engineering was proposed, Figure 3.190, in terms of both anticipated gel expansion multiplier of a reference value X and complexities of the prognosis studies.

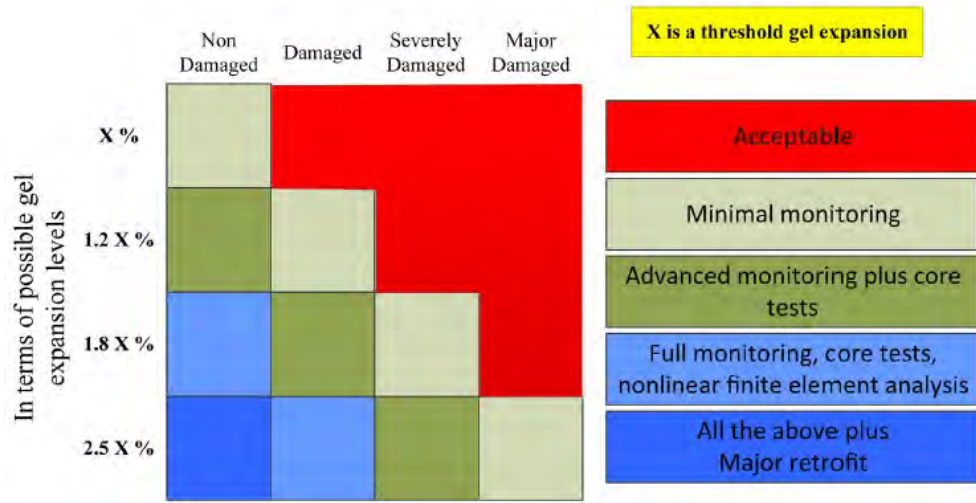


Figure 3.190: Proposed paradigms for proper aging management studies; Saouma and Hariri-Ardebili (2014)

3.146 Saouma, Victor E and Martin, Ruth A and Hariri-Ardebili, Mohammad A and Katayama, Tetsuya (2015)

URL

```
@article{saouma2015mathematical,
title={A mathematical model for the kinetics of the alkali--silica chemical reaction},
author={Saouma, Victor E and Martin, Ruth A and Hariri-Ardebili, Mohammad A and Katayama, Tetsuya},
journal={Cement and Concrete Research},
volume={68},
pages={184--195},
year={2015},
publisher={Elsevier},
url={https://www.sciencedirect.com/science/article/pii/S000888461400218X}
}
```

- Starting from the chain of three chemical reactions which characterize the alkali-silica reaction (ASR), this paper attempts to develop a mathematical framework through which the reaction kinetics can be better understood.
- A petrographic support is given to better understand the physical implications of these equations, and to provide a reasonable support for the choice of the reaction rates.
- First an analytical solution is sought. Though one was not found, three new conservation laws were derived.
- Then a numerical solution is applied, and important observations are made.

- First, and foremost, the role of water is confirmed, and then the outcome of the reaction when different concentrations of alkali and silica are used is derived.
- The temporal evolution of the expansive gel formation is contrasted with both macro-kinetics model, and diffusion based meta-model for the concrete expansions are compared.

Major Conclusions

- Model is only a first attempt to improve our fundamental understanding of the kinetics of the chemical reaction governing ASR. It is hampered by a lack of data (kinetic rates), inconclusive basic understanding (the governing chemical reaction), and some simplifying assumptions (ignoring the effect of temperature and stoichiometry), yet some interesting results are obtained. More precisely:
 - Three nonintuitive conservation laws (M_i , $i = 1, 2, 3$) are derived.
 - Depending on the initial concentrations of the alkali and silica, estimates of the residual concentrations of these reactants at the end of the reaction are provided.
 - The importance of the initial concentration of water in gel formation is confirmed.
 - It is determined that the relative initial concentrations of the alkali, silica, and water in the system lead to four possible distinct estimates of the final concentration of the alkali silicate gel.
 - When alkali are in smaller supply than silica, a smaller amount of expanded gel is produced.
 - Qualitative similarities (sigmoidal curve) between the concentration of gel (chemical reaction) and the expansion of concrete under the ASR (physical macroscopic laboratory observations and diffusion based meso-models) are observed.
 - The parametric study indicates that results are relatively robust with respect to the choice of selected reaction rates.
- In general, there are two major groups on the micromechanical model of ASR in concrete. They stemmed from the difference in the type of the reactive aggregates, i.e. the early-expansive ASR with pronounced reaction rims and the late-expansive ASR without reaction rims but with localized reactions inside the aggregate. Such a difference in the reactivity of the aggregates yielded various models for expansion. However, our study covers both the early- and the late-expansive ASR, which serves as a “Grand-Unifying” model. It is hoped that this small effort will stimulate further studies into the kinetics of the ASR, as it is absolutely critical to be able to ultimately predict the rate (and exhaustion) of the reaction. Finally, it would be highly desirable if a “Grand-Unifying” multi-scale/physico-chemical model be capable of reconciling meso-based diffusion models, macro-based observed bar expansions, and chemical based kinetics models. The first two models address the volumetric expansion, and the last model addresses the rate of gel formation. Such a model would be of great importance to assess the residual expansion of structures suffering from ASR.

3.147 Saouma, Victor E and Hariri-Ardebili, Mohammad Amin and Le Pape, Yann and Balaji, Rajagopalan (2016)

URL

```
@article{
saouma2016effect},
label={saouma2016effect},
title={Effect of alkali--silica reaction on the shear strength of reinforced
concrete structural members. A numerical and statistical study},
author={Saouma, Victor E and Hariri-Ardebili, Mohammad Amin and Le Pape, Yann and
Balaji, Rajagopalan},
journal={Nuclear Engineering and Design},
volume={310},
pages={295--310},
year={2016},
publisher={Elsevier}
Keywords={}
```

- A set of statistical analysis was performed on the numerical models of concrete components affected by ASR.
- Three set of physical models are studied: 1) three-point full beams, 2) truncated beam model, and 3) concrete panels.
- Each of those three includes two sets of boundary conditions: 1) during long term ASR progress and 2) during the short term shear load.
- Each of those two major boundary conditions are sub-divided into three groups: 1) unrestrained models, 2) partially restrained models, and 3) fully restrained models.
- In general, 18 different geometrical-BC-load models are prepared.
- Two sizes are used for the finite element models: small and large.
- Two orthogonal sets of reinforcements are used at the top and bottom of the concrete specimen. The longitudinal and transverse ones correspond to the vertical and hoop reinforcement in the nuclear containment structure.
- A full bond is assumed between rebar and concrete, and reinforcement is modeled by altering the stiffness matrix of crossed finite elements.
- An elasto-plastic constitutive model is used for rebar.
- A rotating crack model is used for concrete.
- ASR was applied through the first 73 increments while incremental shear was applied from increment 74 through 174 (for 100 increments).
- Variables in the FE modelling are: geometry, boundary condition, thickness, reinforcement ratio, ASR expansion, residual elastic modulus, and residual tensile strength.

- All the combinations led to 648 FE models for the case of ASR+shear and 54 models for the case of only shear analysis (no ASR).
- The capacity curve is computed for all the finite element simulations which is the plot of shear force vs. displacement.

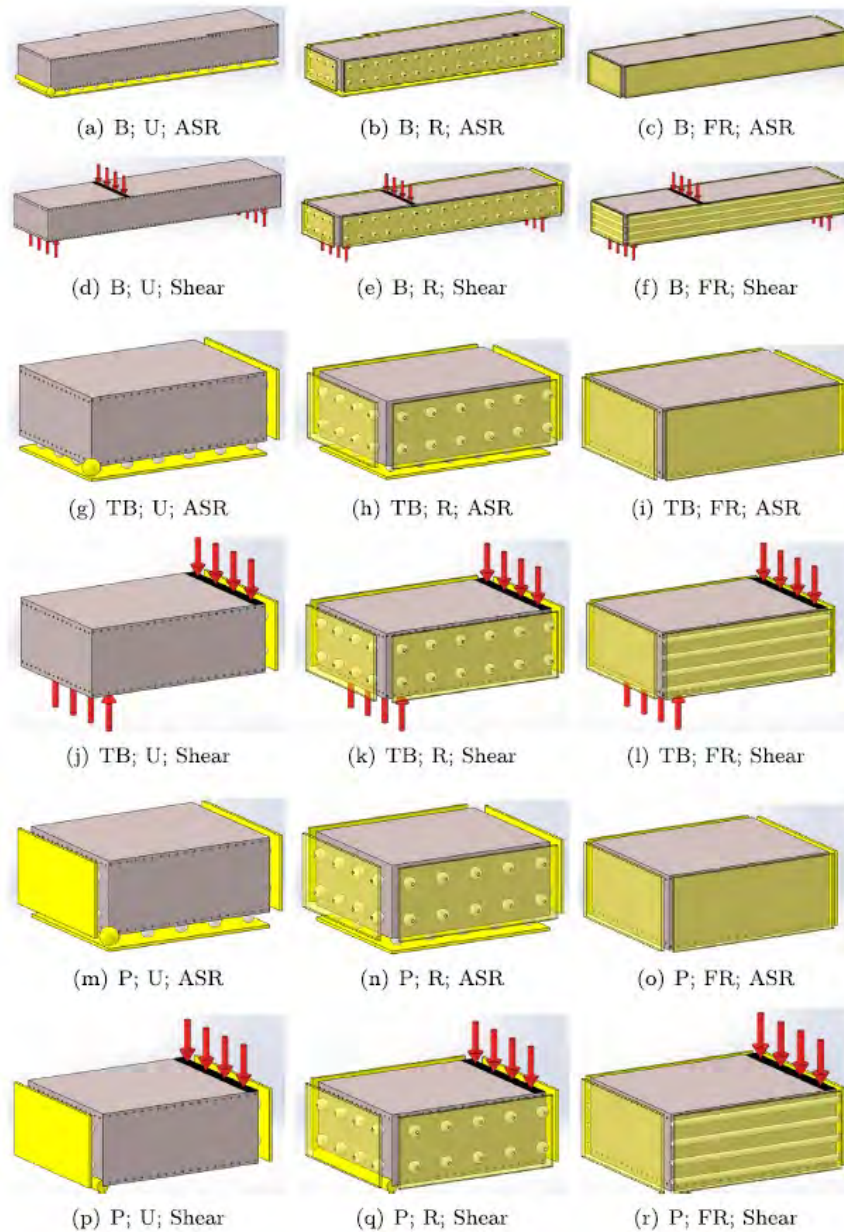


Figure 3.191: Unrestrained (U), Restrained (R), and Fully Restrained (FR) boundary conditions for the Beam (B), Truncated Beam (TB), and Panel (P) models; (Single orb = vertex restriction; group of orbs = restriction in perpendicular direction on surface; single rod = edge restriction; group of rods = roller boundary conditions on surface); Saouma et al. (2016)

- In order to understand the ASR effects, the models ASR+Shear and Shear-only are compared.

- Among the full set of 648 analyses, 53% resulted in an overall shear strength decrease, and 47% in increase.
- Next, a set of statistical analyses are performed.
- A total of 18 input variables are detected.
- Three fitting models are considered: 1) full set, 2) Increased shear strength change data set, and 3) Decreased shear strength change data set.
- For each one, three models are used:
 - General model: considering all variables,
 - Best model based on Akaike Information Criterion (AIC): filters the final sub-variables based on AIC, and
 - Best model based on Bayesian Information Criterion (BIC): filters the final sub-variables based on BIC.
- Figure 3.192 presents the boxplots relative to increasing shear strength. Similar plots exist in the paper for other cases.

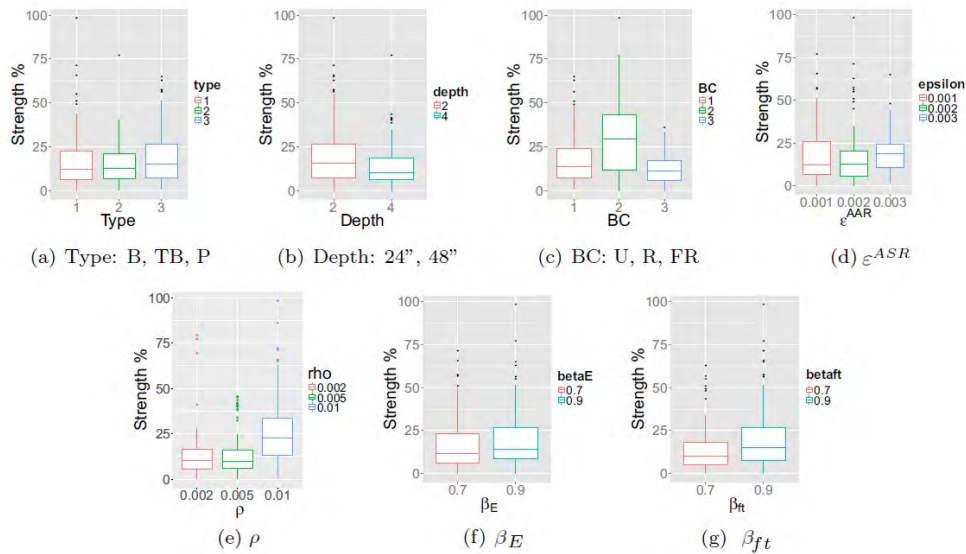


Figure 3.192: Boxplots for Shear Strength Increase in terms of each of the seven variables; Saouma et al. (2016)

- Statistically speaking (mean and deviation), highest gains of structural shear strength are achieved for greater reinforcement ratio and restrained boundary conditions while highest losses are observed for the same boundary conditions and higher ASR expansions.
- In terms of variation (mean values), it was found that 1) the highest gains of shear resistance are obtained with the lowest reinforcement ratio, 2) multi-linear regression and parameter selections analysis show that minimal loss of concrete tensile strength has a significant impact on potential gain in structural resistance, 3) the loss shear capacity amplitude is extremely scattered, and 4) the greater losses appear to result from large ASR expansions and, non-intuitively, high reinforcement ratios.

3.148 Sargolzahi, Maryam and Kodjo, Serge A and Rivard, Patrice and Rhazi, Jamal (2010)

URL

```
@article{
sargolzahi2010effectiveness},
label={sargolzahi2010effectiveness},
title={Effectiveness of nondestructive testing for the evaluation of
alkali--silica reaction in concrete},
author={Sargolzahi, Maryam and Kodjo, Serge A and Rivard, Patrice and Rhazi,
Jamal},
journal={Construction and Building Materials},
volume={24},
number={8},
pages={1398--1403},
year={2010},
publisher={Elsevier}
Keywords={}
```

- The application of various test methods for monitoring the progression of ASR in laboratory concrete mixtures was investigated.
- Concrete specimens were stored at 38°C in a high humidity environment.
- Two concrete mixtures were studied: reactive concrete (RC) and nonreactive concrete (NRC).
- Mechanical properties were assessed with a conventional destructive test and with nondestructive tests (ultrasonic pulse velocity, dynamic modulus of elasticity, and nonlinear acoustics).
- Petrographic examination was performed to confirm damage associated with ASR.
- Compressive strength and ultrasonic pulse velocity were slightly affected by ASR expansion.
- Both static and dynamic moduli of elasticity were significantly affected by ASR expansion.
- Nonlinear acoustics yielded the best correlation with expansion.
- The measurement of the static modulus of elasticity, Figure 3.193 (bottom left), appeared to be relevant for the characterization of an ASR-affected concrete structure. A difference of about 40% was observed between the reactive and nonreactive mixtures after 23 months at 38°C. Compressive strength was not, however, affected by ASR during the same period.
- The dynamic modulus of elasticity, Figure 3.193 (bottom right), calculated from the transversal resonant frequency was strongly affected by ASR. The higher sensitivity of dynamic modulus compared with pulse velocity indicates that the effect of ASR on stiffness is more critical than the effect on microcracking.

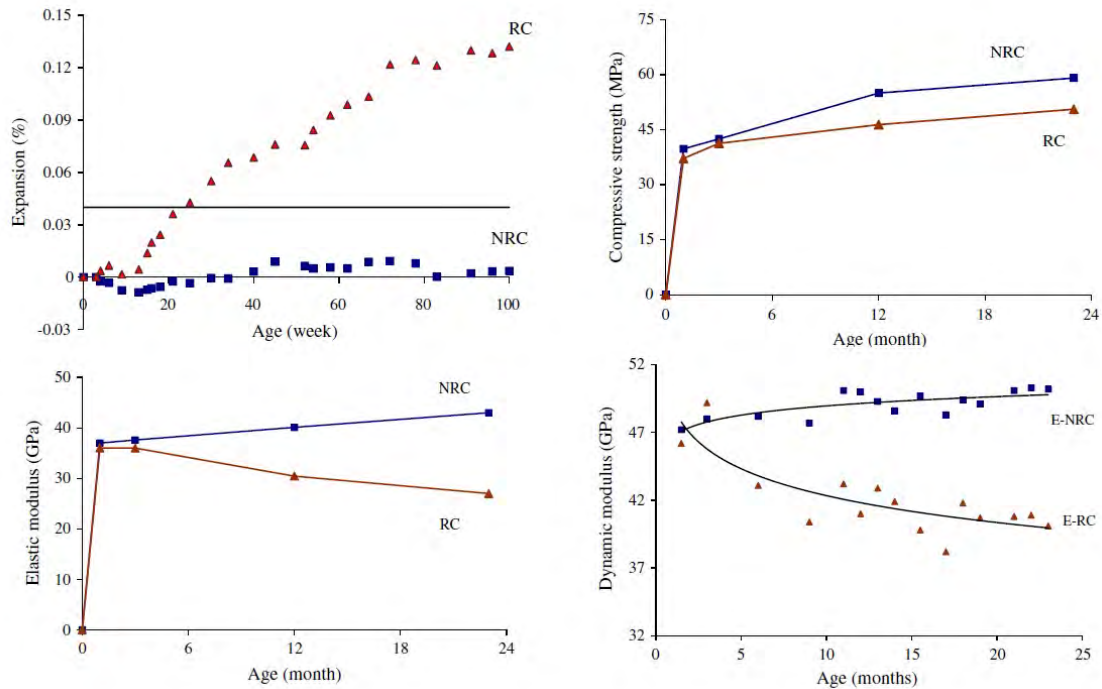


Figure 3.193: Evolution of the mechanical characteristics of the RC and NRC with time; Sargolzahi et al. (2010)

3.149 Sausse, J and Fabre, JP (2011)

```
@inproceedings{
  sausse2011diagnosis},
  label={sausse2011diagnosis},
  title={Diagnosis of dams affected by swelling reactions: lessons learned from 150
    monitored concrete dams in France},
  author={Sausse, J and Fabre, JP},
  booktitle={6th International Conference on Dam Engineering. Lisbon, Portugal},
  pages={156--157},
  year={2011}
  Keywords={Laboratory; Expansion monitoring; Det. E; Petrography; SEM }
```

- Nearly 150 concrete dams in France were studied, about 120 dams higher than 20 m and about 30 other smaller dams.
- Of these dams, 130 are equipped with mechanical monitoring devices, principally represented by: topometry in X,Y, and Z axis; pendulum measuring displacements on X, Y, and Z axis; embedded vibrating wire extensometers; surfacing long-base extensometers; and crack/joint meters.
- The 30 concrete dams (20%) at least are concerned by swelling, and 40% are not monitored satisfactorily to discover their potential to be affected.

- The identification of dams affected by swelling reactions underlines arch and gravity dams as the more concerned types. The other types with thinner structures present higher reinforcement, limiting the effects of the expanding cement.
- The analysis of swelling arch dams shows that most of the swelling cases are single curvature (cylindrical) arches. In other terms, it has been observed that double curvature arches generally show irreversible movements toward the downstream due to a more important part of creep of these thin structures, Figure 3.194.
- The number of dams bringing to light a vertical inflation is maximum in the decade 1951-1960, but this is also the period when the most dams were built in France.

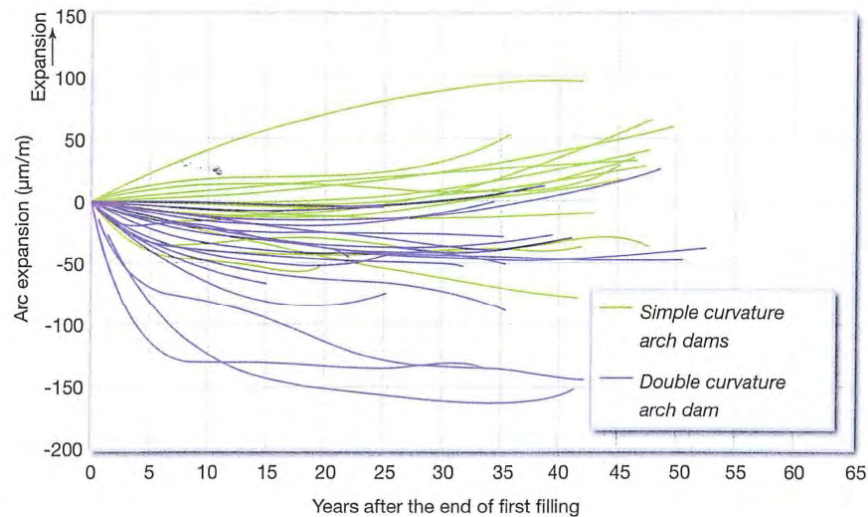


Figure 3.194: Deformation of the crest of arch dams; Sausse and Fabre (2011)

- The poor quality of cements produced during the Second World War and the difficulties of supply during this period could explain this important percentage of swelling dams aged 60 to 80 years.
- Geology is also an important factor. Most of the affected dams are located in the mountain “Massif Central” where the geology shows a predominant part of igneous and magmatic rocks which are able to liberate alkali.

3.150 Sbarigia, M. and Zinetti, F. and Maugliani, V. and Palmitelli, G. and Mazzolani, S. (2013)

```
@inproceedings{
sbarigia13slot},
label={sbarigia13slot},
title={Slot Cutting Of The Lago Colombo Dam, Affected By Swelling
Deformation, To Bring The Behaviour Back From Arch To Gravity},
author={Sbarigia, M. and Zinetti, F. and Maugliani, V. and Palmitelli, G. and
Mazzolani, S.},
booktitle={9th ICOLD European Club Symposium},
year={2013}
Keywords={Reinforcement; Mega; Nonlinear ; Damage Mech.; Mathematical; Finite
Element; None; }
```

- The paper studies the rehabilitation and maintenance of the Lago Colombo Dam. It was built in 1924-1928 for hydropower generation.
- It is a 31 m high gravity dam with some particular design features:
 - No vertical joints
 - A concrete upper part with significant curvature ($R_c = 80$ m)
 - A narrow masonry lower part (about 40 m wide), embedded between rock abutments
- The dam crest is about 140 m long.
- The dam foundation consists of compact slate.
- Since the end of eighties, the dam crest began to show irreversible displacement toward upstream. Besides slight cracking started growing on the Dam's downstream face.
- A main horizontal crack developed roughly between the concrete upper part and the masonry lower part of the Dam.
- In 20 years (1990-2010), the crack extending itself to 100 m onto downstream face. The crack was investigated in 2002 and a 4 m depth was estimated, Figure 3.195.
- The drift of the crest displacement was about 1.5 mm/year.
- The laboratory tests evaluated a swelling deformation of 0.05-0.06% in a year.
- The results of the simulation of the Dam's behavior as monolithic with numerical models showed that in the crack area there were tensile stresses, even if small.
- The main crack area ideally divides the wide concrete upper part from the narrow masonry lower part, and that area could have been affected by a low tensile strength.
- The rehabilitation design was then performed to restore the structural continuity of the weak and cracked region to reduce the stress in the Dam and to stop the growth of cracking, bringing the Dam's behavior back from arch to gravity, according to the original structural scheme.

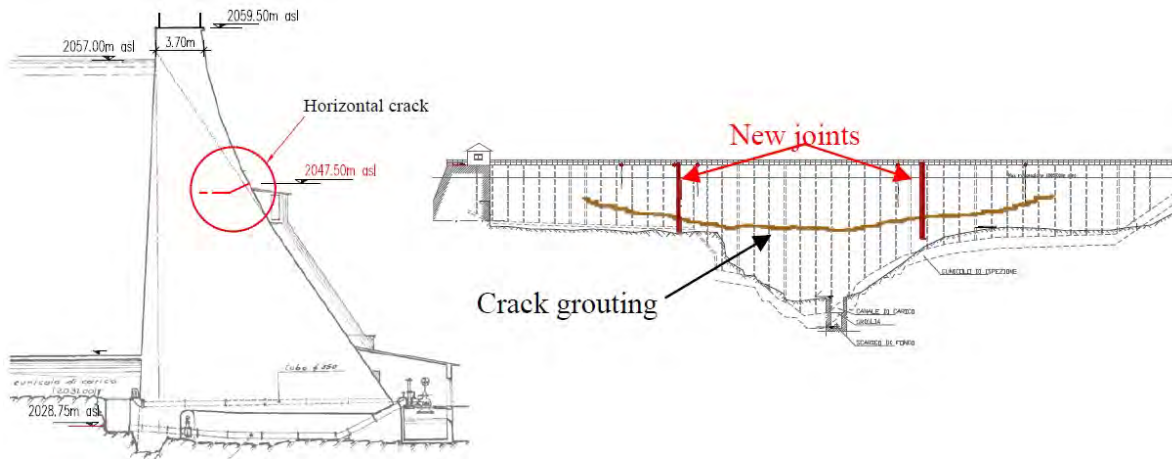


Figure 3.195: The extension and the direction of the main crack; Sbarigia et al. (2013)

- Two main actions were designed:
 - Grouting of the crack and nearby region by means of special self-compacting mineral mortar
 - Two new vertical structural joints build by means of slot cutting (2 cm wide) with diamond wire taking in account the following factors:
 - * The residual potential of swelling deformation
 - * Seasonal opening/closing extent
 - * Instant elastic release at the cutting
- The monitoring system played a key role before, during, and after the works.

3.151 Sbarigia, M and Zinetti, F and Hernandez-Bagaglia, M (2016)

```
@inproceedings{
sbarigia2018slot},
label={sbarigia2018slot},
title={Slot Cutting of the Lago Colombo Dam, Affected by Swelling Deformation, to
Bring the Behavior Back from Arch to Gravity},
author={Sbarigia, M and Zinetti, F and Hernandez-Bagaglia, M},
booktitle={Conference on Italian Concrete Days},
pages={496--511},
year={2016},
organization={Springer},
Keywords={Field; Laboratory; Expansion Assessment/monitoring Reinforcement;
Rehabilitation; Gravity dam; },
DisplayPdf={0},
```

- The rehabilitation and maintenance of the Lago Colombo Dam is studied. It was built in 1924-1928 for hydropower generation.

- The Dam's crest is about 140 m long. The 31 m high Dam was built as a gravity structure with some particular design features:
 - no vertical joints
 - a concrete upper part with significant curvature ($R_c = 80$ m)
 - a narrow masonry lower part (about 40 m wide) embedded between rock abutments
- The Dam had a regular behavior, with seasonal fluctuations of about 15 mm, until the end of the 1980s when the Dam crest began to show an irreversible displacement toward upstream.
- Besides slight cracking started growing on the Dam's downstream face, a main horizontal crack developed roughly between the concrete upper part and the masonry lower part of the Dam.
- The investigations found some evidence of slight ASR and chemical produced gel with high Ca/Si ratio. The laboratory tests evaluated a swelling deformation of 0.05-0.06% per year.
- The rehabilitation design was completed: the original gravity behavior was restored and the arch effect was reduced.
- The final solution consisted in the crack grouting with special self-compacting mineral mortar and in the carrying out of two new vertical structural joints by means of slot cutting (20 mm-wide) with diamond wire taking in account the following factors, Figure 3.196:
 - the residual potential of swelling deformation
 - seasonal opening/closing extent
 - instant elastic release at the cutting
- Two reinforced concrete beams were designed to sustain and protect the sealing device of the joint. The sealing device was designed to be removable for future re-cutting.
- The Dam's behavior after rehabilitation confirms the fulfillment of the design targets. The measures of the crest displacements no longer show the historical irreversible drift towards upstream.



Figure 3.196: The slot cutting from downstream face. On the left, the kerb of the crest; on the right, the wire in the middle of the cutting; Sbarigia, Zinetti, and Hernandez-Bagaglia (2016)

3.152 author="Scuero, A. and Vaschetti, G. (2011)

```
@incollection{
scuero2011development},
label={scuero2011development},
booktitle={Dams and reservoirs under changing challenges},
editor={Schleiss, Anton J and Boes, Robert M},
year={2011},
title="{Development of geomembrane systems for watertightness of dams in Europe}",
author="Scuero, A. and Vaschetti, G.",
publisher={CRC press},
Keywords={Field; Expansion Assessment/monitoring Rehabilitation; Gravity dam; },
DisplayPdf={0},
```

- Some significant recent or historical projects that are representative of the possible numerous applications of geomembrane systems to the rehabilitation of existing dams are presented.
- Illsee is a 25 m high gravity dam in the Swiss Alps, with temperatures ranging from -30°C to $+35^{\circ}\text{C}$, freeze-thaw cycles in the order of 100 per year, and maximum ice thickness 1.0 m.
- Displacements that could not be related to hydrostatic or thermal stresses were ascertained as being caused by AAR.
- Installation of a new impervious layer on the upstream face was deemed mandatory to stop water penetration inside the dam.

- A drained PVC geomembrane system was preferred to shotcrete and to reinforced concrete solutions for its superior performance in cold climates and its draining capability.
- From its completion in 1997, the geomembrane system has been providing continuous good performance.

3.153 Seignol, Jean François and Godart, Bruno (2012)

```
@inproceedings{
seignol2012collective},
label={seignol2012collective},
title={A collective effort to propose practical guidance on the use of numerical
models to re-assess AAR-affected structures},
author={Seignol, Jean Fran{\c{c}}ois and Godart, Bruno},
booktitle={14th ICAAR-International Conference on Alkali-Aggregate Reaction},
pages={10p},
year={2012},
Keywords={Laboratory; Field; Mathematical; Finite Element; },
DisplayPdf={0},
```

- The purpose of this report is to propose practical guidance on the use of numerical models as a tool for managing AAR-affected structures.
- This guide is organized in four main chapters: the role of numerical modeling, a tentative typology of models, a compendium of existing numerical tools, and practical advice on how to use these models.
- As for tools used to re-assess a structure's present state and its long-term evolution, three types of recommendations can be mentioned:
 - The ones which do not mention specific tools but put the stress on the importance of re-assessing structural state,
 - The ones which propose to adapt classical methods developed for sound concrete structures, such as engineering methods or FEM-numerical models with modified material parameters,
 - And, the ones which recommend to use numerical models specifically designed to represent AAR-affected concrete structures behavior.
- The numerical models must take into account:
 - Over-tensions in rebars and tendons which restrain concrete expansion;
 - Reciprocally, the compressive stress induced in the affected concrete by the rebars' resistance;
 - The complex stress-states which can result from strain gradients (due to heterogeneous water ingress, temperature gradients, various alkali content, or dispersion in material properties);
 - Complexity of multi-physics coupling which influence occurring and development of AAR such as thermal history;

- Second order effects or occurring of eccentricity in compressive forces due to excessive strains in structural elements;
 - And, in the case of statistically indeterminate structures, strain-induced redistribution of reactions.
- Different numerical models can be classified according to the scale(s) at which they represent the material and the structure:
 - Microscopic models (where the characteristic length is far smaller than the largest aggregate) allow for instance to explicitly represent cracks occurring in an aggregate core due to AAR-gel growth and micro-structure of the material;
 - Material models (where the characteristic length is similar to the aggregates size);
 - Structure models (where concrete is assumed to be a homogeneous continuous media) allow the representation of an entire bridge, building, or dam with a limited number of finite elements.
 - A compendium for different models is developed which tend to provide the following information:
 - Scope of the model;
 - Theoretical background;
 - Description of main equations;
 - Fitting of the various parameters involved in the model description and, if any, laboratory tests or in-situ measurements used to obtain appropriate values;
 - Numerical implementation;
 - And validation with an example on simple test-case.
 - The correct choice model type implies a good balance between necessary sophistication (to achieve a fair simulation of the complex physical, chemical, and mechanical interactions occurring in AAR-affected concrete) and limiting the complexity of the model, unless it could be impossible to correctly fit it due to the lack of available data, Figure 3.197.
 - Choosing the appropriate model is a required condition of success, but is not sufficient. Adjusting the model with adequate parameters is essential to correctly represent the studied structure and its evolution.
 - Choosing sample cores
 - Representativity and size effect
 - From residual expansion to total expansion
 - * Inverse-problem techniques
 - * Relation between AAR-development and Young modulus decrease
 - * Evaluation of micro-cracking due to previous AAR

Name	Scale	AAR-effect
Bažant <i>et al.</i>	M	E
Comby <i>et al.</i>	M	E
Comi <i>et al.</i>	S	P
Curtis <i>et al.</i>	S	E
Dunant <i>et al.</i>	μ	E
Farage <i>et al.</i>	S	P
Gomes <i>et al.</i>	S	E
Gonzalez <i>et al.</i>	μ	nr
Grimal <i>et al.</i>	S	P
Léger <i>et al.</i>	S	E
Li <i>et al.</i>	S	E
Meghella <i>et al.</i>	S	E
PAT-ASR project	M	nr
Poyet <i>et al.</i>	M/S	P
Saouma <i>et al.</i>	S	E
Winnicki <i>et al.</i>	S	E

Figure 3.197: Alphabetically sorted list of models to be included in compendium. Scales are denoted by μ (micro), M (material), and S (structure); AAR-effects can be represented by P (pressure) or E (prescribed expansion); nr stands for “not relevant”; Seignol and Godart (2012)

3.154 Sellier, Alain and Bourdarot, Eric and Multon, Stéphane and Cyr, Martin and Grimal, Etienne (2009)

URL

```
@article{
  sellier2009combination},
  label={sellier2009combination},
  title={Combination of structural monitoring and laboratory tests for assessment of
    alkali-aggregate reaction swelling: application to gate structure dam},
  author={Sellier, Alain and Bourdarot, Eric and Multon, St{\`e}phane and Cyr,
    Martin and Grimal, Etienne},
  journal={ACI materials journal},
  volume={106},
  number={3},
  pages={281},
  year={2009},
  publisher={American Concrete Institute}
  Keywords={}
```

- The Temple-sur-Lot Dam, located in southwest France, has been operating since 1951. The Dam was cast with two types of concrete mixtures: C250 with a cement content of 250 kg/m³ and containing siliceous aggregates of sizes 0 to 100 mm, and C350 with a cement content of 350 kg/m³ containing the same aggregate but with sizes 0 to 30 mm.
- As early as 1963, an inspection revealed the existence of cracks on the upstream part of the Dam’s piers.

- Initially, conventional residual expansion tests were conducted, consisting of measuring the longitudinal expansion and the mass variation of core samples drilled from the Dam and stored in a controlled environment.
- The swelling rate is estimated approximately $100 \mu\text{m}/\text{m}$ per year. According to the LPC recommendations, this corresponds to a negligible AAR phenomenon, in disagreement with the in-place observations of the Dam.
- The same swelling rate was obtained from both wet and dry concretes which was an unexpected situation. The interpretation of the swelling rates by the LPC recommendations, therefore, seemed unsuitable for this dam.
- It was assumed that a substitution process between alkali and calcium in the AAR gel could explain this long-term behavior. As the calcium substitution phenomenon is very slow, it cannot be detected using a conventional residual swelling test, so an original method to assess the AAR kinetics and the residual swelling capability is proposed.
- This method first involved a laboratory test dealing with the silica consumption kinetics and, second, a numerical finite element inverse analysis of the Dam which included the consumption kinetics measured in the laboratory.
- A global methodology for finding the AAR kinetics independently of the gel nature is proposed and summarized in Figure 3.198 which is based on the assessment of reactive silica consumption.
 - The reactive silica consumption kinetics is determined for each aggregate size range.
 - The amplitude of final swelling is not measured from laboratory expansion tests but assessed from an FE inverse analysis of the affected structure.
 - The FE modeling used is summarized in the following: It combines the advancement kinetics deduced from laboratory tests and the final AAR swelling which is the only parameter to be fitted with the structural FE inverse analysis.
 - Once the final swelling was obtained by curve fitting, the numerical model is tested to compare its results with other expansion measurements conducted on the Dam and not used for the determination of the fitted parameter.
 - If the results are good, calculations can be carried out to predict the future structural behavior.
- A procedure is also proposed to assess the chemical advancement for each aggregate size of the concrete. This process splits the problem into two phases, Figure 3.199:
 - Phase 1:
 - * Aggregates of the affected concrete are first extracted by chemical attack and sifted.
 - * Then, the residual reactive silica content is assessed for each reactive aggregate size.
 - * Several types of mortar containing only one aggregate size from the dam concrete are cast.
 - * The aggregates are crushed to obtain the same aggregate size distribution in each mortar.

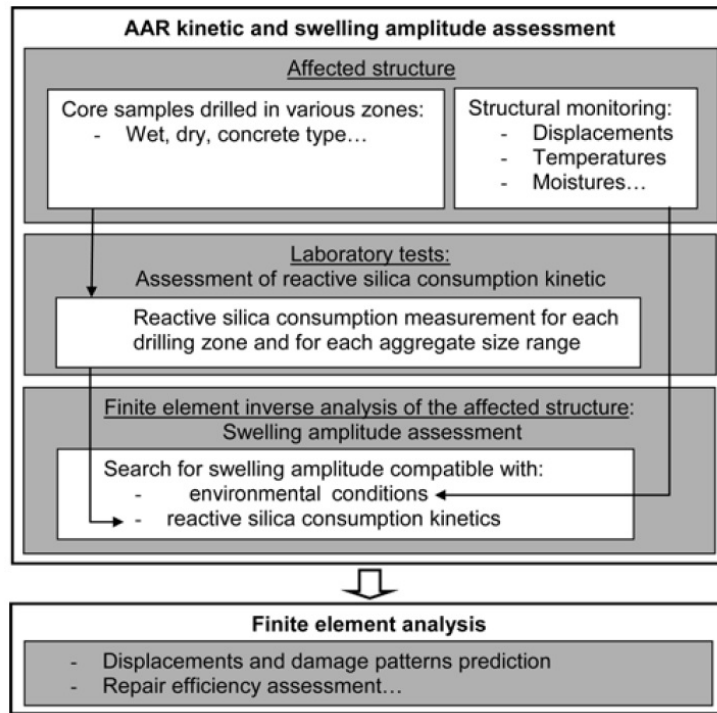


Figure 3.198: Global methodology summary; Sellier et al. (2009)

- * A sufficient amount of alkali is added to the mortar cement paste to be sure that all the residual reactive silica contained in the crushed aggregates will be consumed during the tests.
 - * The total swelling measured for each mortar depends only on the residual reactive silica contained in the reactive aggregate.
- Phase 2:
- * The constant representing the kinetics of in-place chemical advancement is deduced from both the chemical advancements measured for each aggregate size and the environmental conditions.
- For the case study, the variation of the lateral displacement measured at Point PC of the dam was used to fit the unknown parameter. Then, the vertical displacements of PC and the horizontal displacement of PA could be simulated with good accuracy.
 - Also, a good agreement was found between the computed damage and the crack pattern with the lightest zones corresponding to the observed cracks.

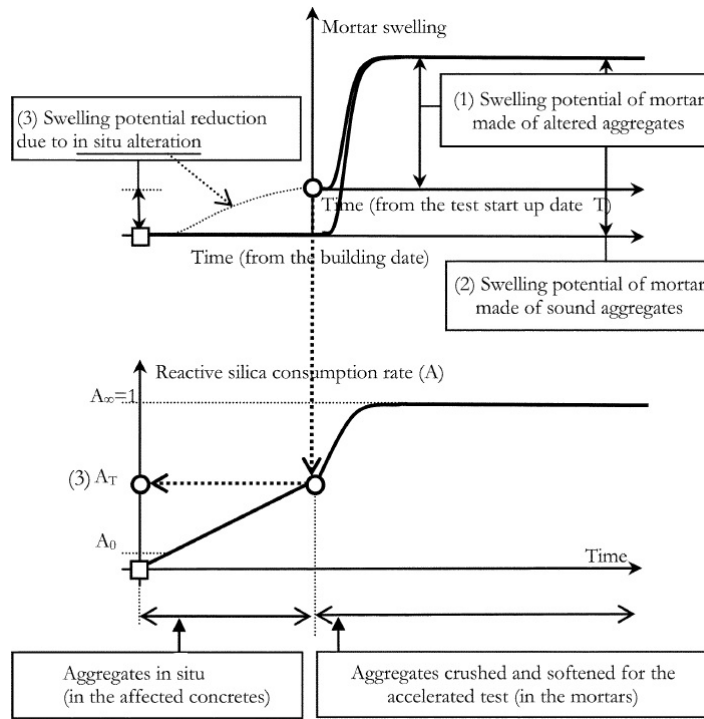


Figure 3.199: Principle of chemical advancement assessment; Sellier et al. (2009)

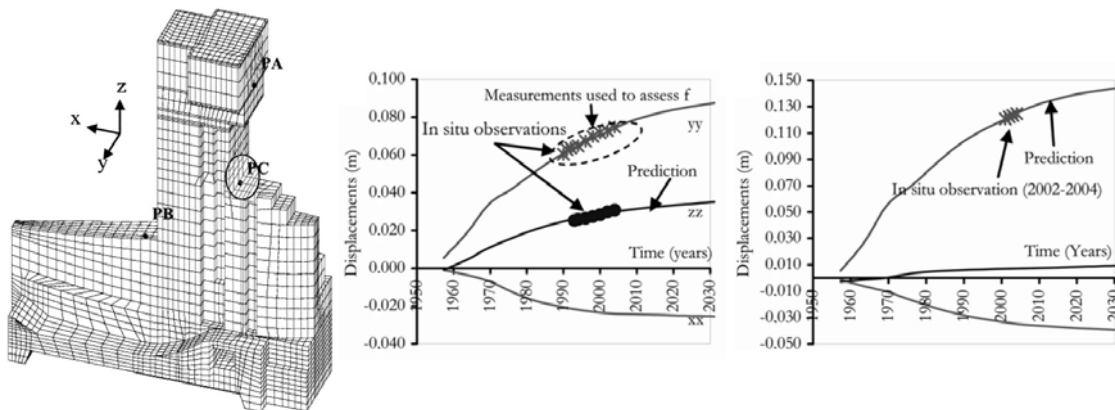


Figure 3.200: Finite element mesh (left plot); fitting of swelling amplitude on structural displacements (Point PC, direction yy), prediction for PC directions zz and xx, future extrapolation (middle plot); PA displacements, comparison with in-place observations and future prediction (right plot); Sellier et al. (2009)

3.155 Shayan, Ahmad and Grimstad, Jack (2006)

URL

```
@article{
shayan2006deterioration},
label={shayan2006deterioration},
title={Deterioration of concrete in a hydroelectric concrete gravity dam and its
characterisation},
author={Shayan, Ahmad and Grimstad, Jack},
journal={Cement and Concrete Research},
volume={36},
number={2},
pages={371--383},
year={2006},
publisher={Elsevier}
Keywords={}
```

- The case study is of a concrete gravity dam in the Snowy Hydro network that exhibits signs of concrete distress in the form of cracking in some sections of the dam wall and vertical movements in the wall.
- Concrete elements of the associated power station had also shown some degree of distress in the form of cracking.
- AAR was considered as a likely cause of cracking.
- Core samples ranging in length from 0.3 m to 10 m were extracted and investigated for the presence of AAR, its extent, likelihood of continuing reaction, residual expansion potential, and effect on the strength of concrete.
- The cores were inspected and segments allocated to different examinations and tests. These included visual and petrographic examination; scanning electron microscopy (SEM) and energy dispersive X-ray (EDX) analysis; residual alkali content; residual expansion; and mechanical properties of concrete.
- The aggregate was used for the following tests:
 - Accelerated mortar bar test (AMBT) according to the RTA Test Method T363, at four NaOH concentrations (0.7 M-1.0 M).
 - Concrete prism test (CPT) according to the ASTM C-1293 test method, at alkali contents of 1.0%, 1.25%, 1.5%, and 1.8% by mass of cement.
- There is mild AAR in some sections of the wall of the power station but not in the floor where drying shrinkage could have caused the cracking.
- Mild AAR was also present in sections of the dam wall with minor visible cracking, but AAR was stronger and more widespread in the badly cracked area.

3.156 Shayan, Ahmad (2016)

[URL](#)

```
@article{
shayan2016effects},
label={shayan2016effects},
title={Effects of alkali--aggregate reaction on concrete and structures},
author={Shayan, Ahmad},
journal={Proceedings of the Institution of Civil Engineers-Construction Materials},
volume={169},
number={3},
pages={145--153},
year={2016},
publisher={Thomas Telford Ltd}
Keywords={}
```

- A general overview is provided of the changes that occur in the mechanical and durability properties of AAR-affected concrete elements.
- It has been shown that higher expansion levels cause larger reductions in strength properties. This effect was demonstrated by Kubat, Al-Mahaidi, and Shayan (2014a,b) who produced highly expansive concretes using fused silica as reactive aggregate. Their strength properties were then measured at different levels of expansion, Figure 3.201 (left). The largest loss in strength occurred at the lower levels of expansion.
- The results of Shayan, Xu, and Andrews-Phaedonos (2003), who employed different natural aggregates to generate different magnitudes of expansion, showed the adverse effects of expansion on these strength properties. Flexural strength significantly dropped with increasing expansion, Figure 3.201 (right), which shows that it is sensitive to AAR-induced expansion and deteriorates even at low levels of expansion (but particularly beyond 0.10%).

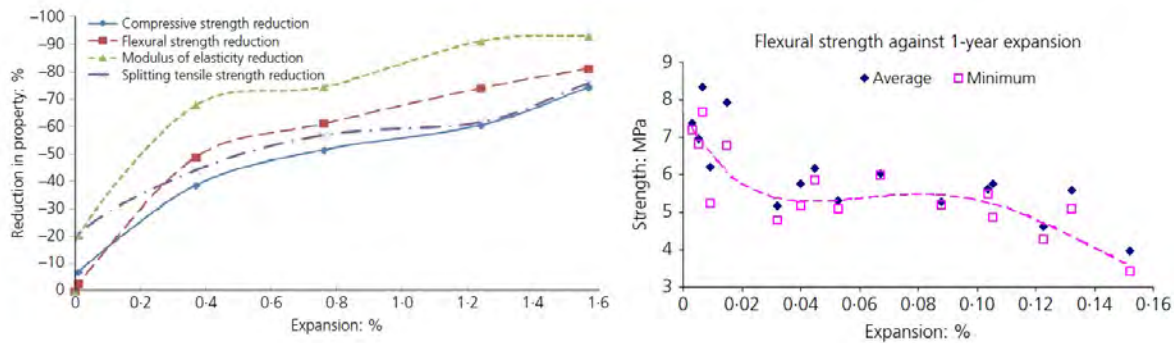


Figure 3.201: Reduction in strength at different levels of expansion (left); Reduction in flexural strength at different levels of expansion (right); Shayan (2016)

3.157 Helmuth, R. and Stark, D. and Diamond, S. and Moranville-Regourd, M. (2013)

URL

```
shrp1993,  
title={Alkali-Silica Reactivity: An Overview of Research},  
author={Helmuth, R. and Stark, D. and Diamond, S. and Moranville-Regourd, M.},  
institution={Strategic Highway Research Program},  
year={2013},  
number={FHWA-HIF-13-019},  
url={http://onlinepubs.trb.org/onlinepubs/shrp/SHRP-C-342.pdf}  
}
```

- A major document from FHWA widely referenced.
- Written by Thomas, Fournier and Folliard.

Abstract

Part I of this report is a synthesis of our knowledge of mechanisms of damage to concrete by alkali-silica reactivity. Alkali-silica reaction gels are composed of two-component mixtures of alkali-calcium-silicate hydrate and alkali-silica sols of nearly fixed compositions. Cracking may be initiated by swelling of aggregate particles before copious production of gel and large expansions of cracks caused by swelling of gel occurs. External restraint reduces expansions and cracking, increases stress and the rate of dissolution of silica at reaction sites, reduces osmotic swelling of gel and causes gel to flow or creep from reaction sites, and causes creep of the matrix in compression. In practice the process is complicated by the effects of drying and growth of shrinkage cracks in exposed surfaces. The presence of chloride salts accelerates alkali-silica reactions. Formation of Friedel's salt and other complex chloride containing salts complicates test results.

Part II identifies 10 specific gaps in our knowledge of alkali-silica reactions in concrete that limit our ability to control these reactions or to predict performance of concrete with reactive aggregates. These involve rapid and reliable test methods; moisture conditions in highway structures; effects of salts, role of sulfate reactions accompanying expansions caused by reactivity; measurement of aggregate reactivities; effect of restraint on kinetics; mechanisms by which pozzolans prevent expansion; test methods and specifications for pozzolans; and inhibition of reactivity by chemical agents..

3.158 Siegert, D and Multon, S and Toutlemonde, F (2005)

[URL](#)

```
@article{
siegert2005resonant},
label={siegert2005resonant},
title={Resonant frequencies monitoring of alkali aggregate reaction (AAR) damaged
concrete beams},
author={Siegert, D and Multon, S and Toutlemonde, F},
journal={Experimental Techniques},
volume={29},
number={6},
pages={37--40},
year={2005},
publisher={Wiley Online Library}
Keywords={}
```

- The six tested concrete beams (P1, P2, . . . , P6) were made of reactive or non-reactive aggregates.
- Three beams were plain concrete and three were reinforced concrete beams.
- The beams were all 3 m long and 2.80 m in span with a rectangular cross section area of $0.5 \times 0.25 \text{ m}^2$.
- After 28 days of moist curing, the specimens were placed for two years in a climate controlled room with an ambient temperature of 38°C and a relative humidity fixed at 30%.
- The lower sides of the beams were first immersed in water as the upper side was exposed to the 30% RH air for a period of 14 months. Moisture exchange between the beam and the environment through the lateral sides was prevented by a watertight cover.
- The resonant frequencies of the tested beams were periodically measured to evaluate the feasibility of vibration-based health monitoring in realistic but well controlled conditions.
- The aim was to detect the global changes of the physical properties, such as the Young's modulus of the damaged concrete or the loss of the bending rigidity of the AAR damaged beams.
- Figure 3.202 displays the time variations of the measured resonant frequencies related to the first bending mode for the tested specimens P1-6.
- The resonant frequencies of the nonreactive specimens are fairly constant within the dispersion prior to the water immersion of the upper side. The subsequent increase in the range of 2% to 3% of the resonant frequencies might be explained by the effect of free water content in the voids of the cement paste on the value of the Young's dynamic modulus.
- The results in Figure 3.202 show that the resonant frequencies of the reactive specimens first decrease to reach a minimum value between 6% and 10% lower than the initial value. The observed reduction of the resonant frequencies is a result of the loss of rigidity induced by the AAR expansion progressing at the lower side of the reactive beams.
- The experimental values of Young's modulus for reactive and nonreactive specimens are reported in Figure 3.202 (right).

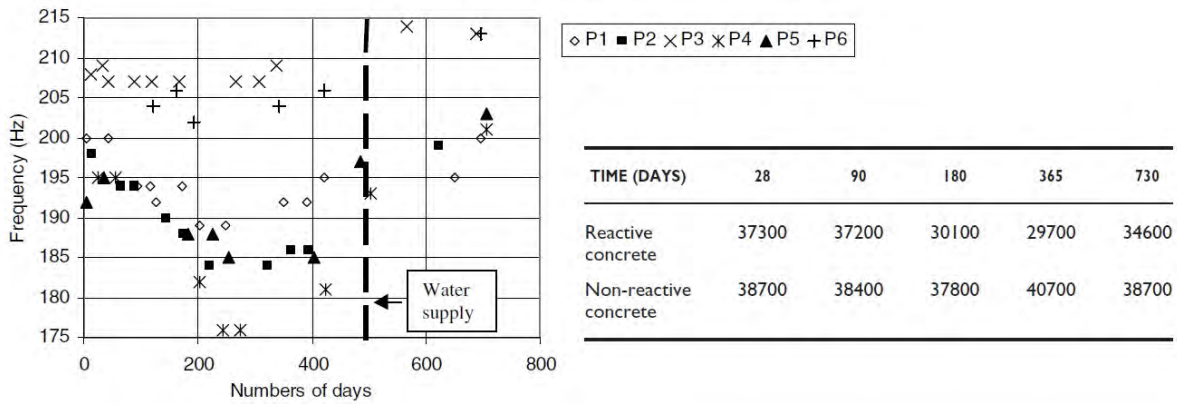


Figure 3.202: Resonant frequency monitoring of the tested specimens (left); Measures of Young's modulus (MPa) of the concrete specimens; Siegert, Multon, and Toutlemonde (2005)

- The loss of stiffness measured in compressive static test conditions on reactive specimens reached 20%, which corresponds to the maximum reduction of bending rigidity measured with the beams P2 and P4.

3.159 Smaoui, Nizar and Bérubé, Marc-André and Fournier, Benoit and Bissonnette, Benoit and Durand, Benoit (2004)

URL

```
@article{
smaoui2004evaluation},
label={smaoui2004evaluation},
title={Evaluation of the expansion attained to date by concrete affected by
alkali--silica reaction. Part I: Experimental study},
author={Smaoui, Nizar and B{\`e}rub{\'e}, Marc-Andr{\`e} and Fournier, Benoit and
Bissonnette, Benoit and Durand, Benoit},
journal={Canadian Journal of Civil Engineering},
volume={31},
number={5},
pages={826--845},
year={2004},
publisher={NRC Research Press}
Keywords={}
```

- Three methods were used to evaluate the expansion to date of the concrete from a structure affected by ASR: 1) stiffness damage test (SDT), 2) damage rating index (DRI), and 3) surface cracking.
- Several concrete cylinders were made using different types of coarse and fine reactive aggregates and at 38°C and RH_i95%.
- At various expansion levels, the specimens were subjected to SDT and DRI tests.
- Very similar relationships were obtained between the expansion due to ASR and the SDT.

- The correlation between the ASR expansion and the DRI was not as similar but still of interest.
- Adopted from Chrisp et al. 1989, the two parameters used to evaluate the damage undergone by the concrete are:
 - The modulus of elasticity during the first loading,
 - The average energy dissipated during the last four cycles (cycles 2-5) of loading-unloading.
- The modulus of elasticity was measured during the first loading cycle at 10 MPa, on cylinders from the five tested concretes, at different expansion levels, Figure 3.203. This plot shows that the modulus of elasticity is significantly reduced by ASR.

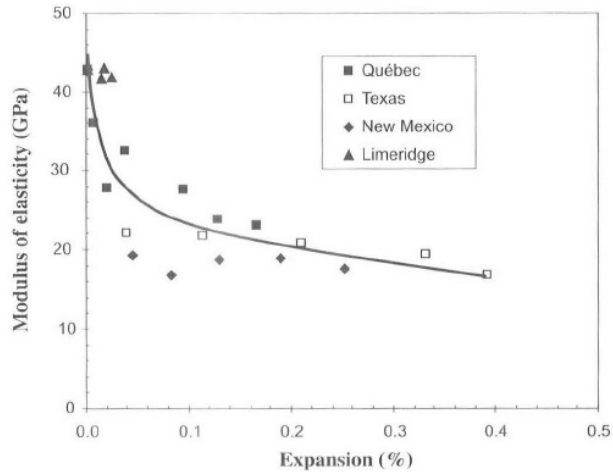


Figure 3.203: Modulus of elasticity measured on cylinders during the first loading of the modified SDT test as a function of expansion due to ASR; Smaoui et al. (2004a)

- Figure 3.204 shows an enlargement of the hysteresis loop of the first loading-unloading cycle and the increase of the plastic axial deformation accumulated over the course of the five cycles with an increase in ASR expansion.
- The area of the first hysteresis is obtained from the difference between the areas limited by the two third-degree polynomial stress-strain relationships corresponding to the loading and unloading curves for the first cycle.
- The plastic deformation after the five loading-unloading cycles is measured directly after the last cycle.
- The correlations obtained between the dissipated energy during the first cycle and the expansion are very good, Figure 3.205.
- The relationships between the plastic deformation after the 5 cycles and the expansion are also very good for the Québec City limestone and Texas Sand.
- The correlations obtained depended, to a certain extent, on the type of reactive aggregate used.

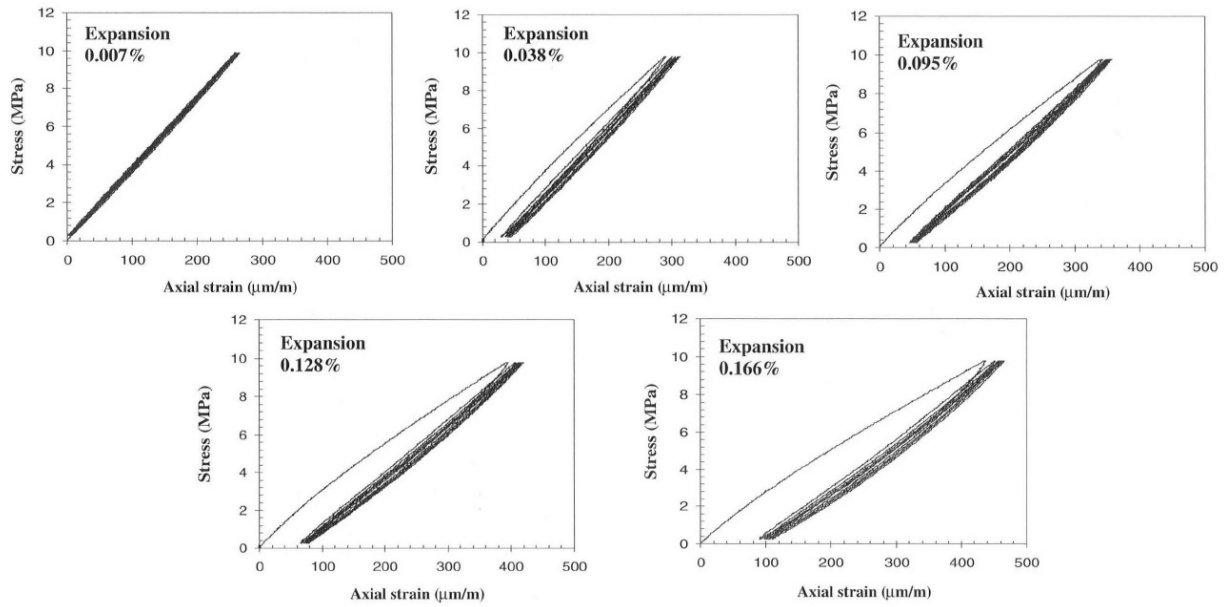


Figure 3.204: Results of the modified SDT tests at different expansion levels for cylinders made with the Quebec City limestone; Smaoui et al. (2004a)

- The modified SDT was found to be promising in the evaluation of the expansion generated by other expansion mechanisms such as freezing-thawing.

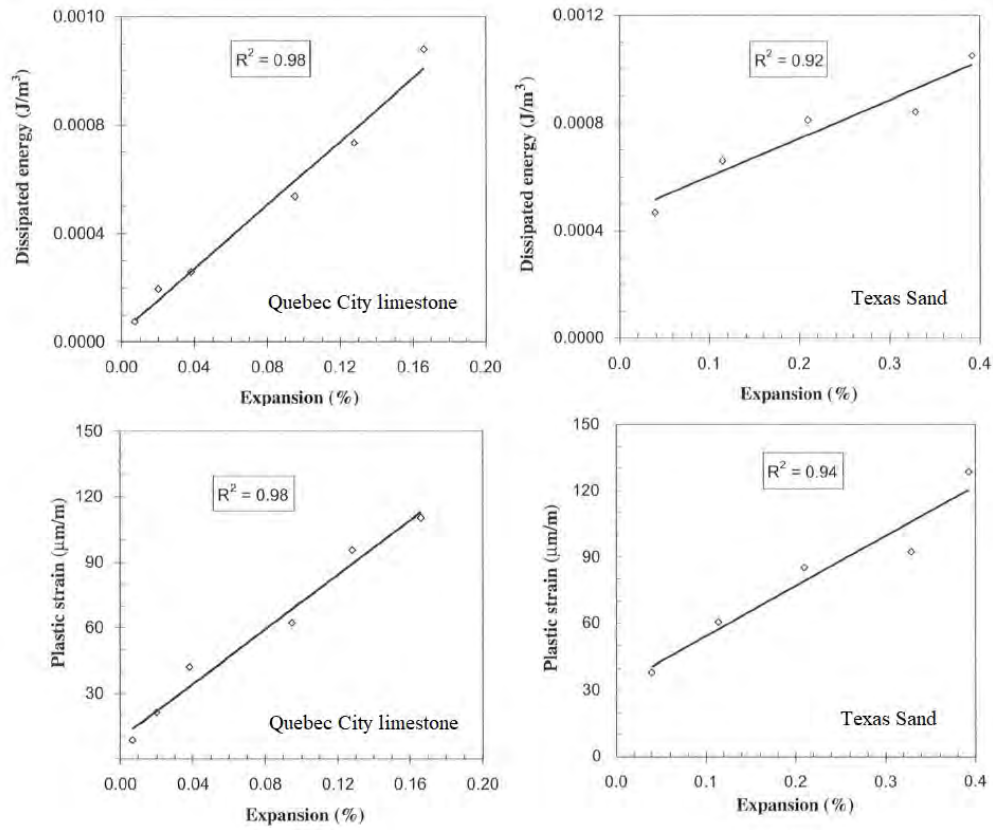


Figure 3.205: Relationships between the expansion of cylinders and the energy dissipated during the first cycle and the plastic strain accumulated after the five cycles of the modified SDT test; Smaoui et al. (2004a)

3.160 Smaoui, Nizar and Fournier, Benoit and Bérubé, Marc-André and Bissonnette, Benoit and Durand, Benoit (2004)

[URL](#)

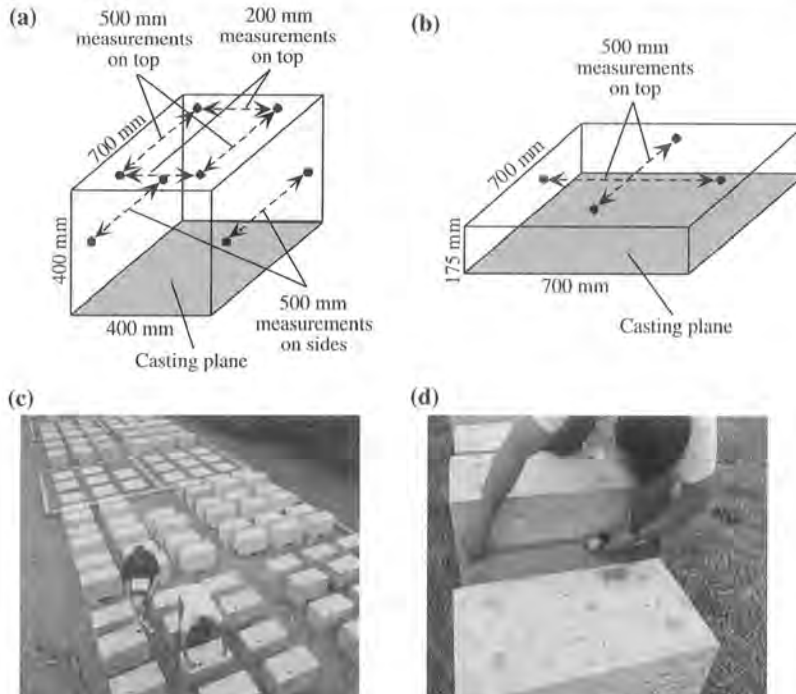
```

@article{
smaoui2004evaluation2,
label={smaoui2004evaluation2},
title={Evaluation of the expansion attained to date by concrete affected by alkali
silica reaction. Part II: Application to nonreinforced concrete specimens
exposed outside},
author={Smaoui, Nizar and Fournier, Benoit and B{\`e}rub{\`e}, Marc-Andr{\`e} and
Bissonnette, Benoit and Durand, Benoit},
journal={Canadian Journal of Civil Engineering},
volume={31},
number={6},
pages={997--1011},
year={2004},
publisher={NRC Research Press},
Keywords={},
DisplayPdf={0},
url={http://www.nrcresearchpress.com/doi/abs/10.1139/104-074}

```

- The objective is to verify the validity of the relationships for concrete elements made in the laboratory but exposed outside.
- On average for the 51 blocks and 14 slabs tested, the surface cracking increased with ASR expansion and approached the measured expansion in the case of the most severely exposed sections of the specimens tested.
- The ratio between the expansion estimated from the surface cracking and the measured expansion varied greatly from one specimen to another (between 0 and 4.:1), however.
- Taking into account the type of reactive aggregate involved did not explain the situation despite a variety of reactive aggregates. a quite good relationship (coefficient of linear regression $R^2 = 0.59$) was obtained between the DRI and the ASR expansion for the six blocks cored and tested for DR! and SDT.
- This relationship is significantly different from those obtained in the laboratory, however.
- The exposed concretes clearly differ from the laboratory concretes regarding the most important defects observed in the DRI test.
- As in the laboratory, the results obtained from the SDT seem to depend on the type of reactive aggregate involved.
- Nevertheless, this test globally supplied results with the best agreement with the measured expansion.

Fig. 1. Concrete specimens exposed outside: (a) block; (b) slab; (c) exposure site near Ottawa (Ontario, Canada); and (d) expansion measurement on the side of one block.



4. Result

4.1. Concrete

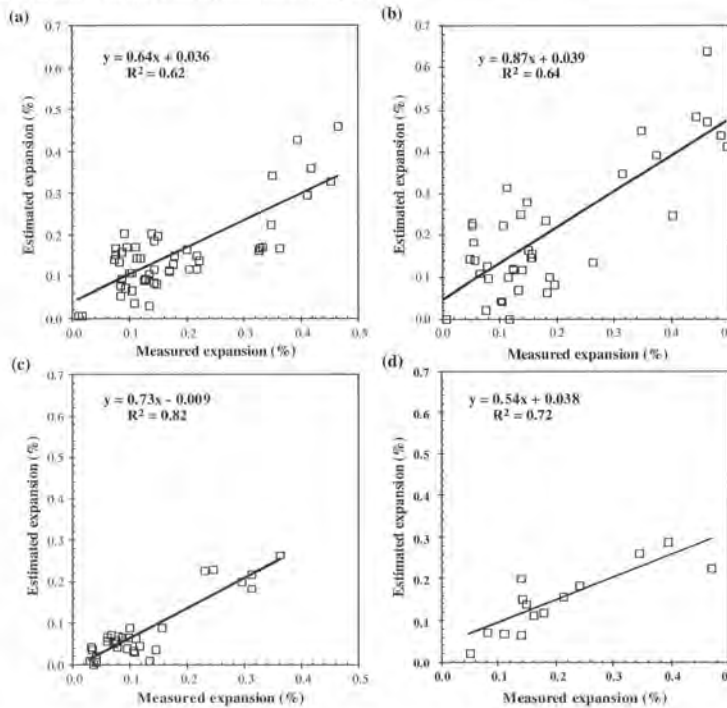
In the case between the gate to another reactivity; (i) same aggregate variability; fact that the always been type of measurement versus explained, at conditions. On 500 mm longitudinal measurements on top of the blocks; results that measurement average), with sides of the weather, are notes also that (0.201% on expansion measurement for the long together, but

Smaoui et al.

1003

the fabric-gravel

Fig. 2. Relationships between the expansion estimated from the surface cracking and that measured for the blocks and slabs exposed outside: (a) longitudinal measurements on top of the blocks; (b) transverse measurements on top of the blocks; (c) longitudinal measurements on sides of the blocks; and (d) measurements on top of the slabs.



(b) Relationships between the expansion estimated from the surface cracking and that measured for the blocks and slabs exposed outside: (a) longitudinal measurements on top of the blocks; (b) transverse measurements on top of the blocks; (c) longitudinal measurements on sides of the blocks; and (d) measurements on top of the slabs.

The cracking is also less developed on the concrete slabs (average ratio of 0.76) and lower in the case of the measurements taken on the tops of the blocks (average ratio of 0.76). The same effect has also been observed, however, in laboratory conditions, whose faces are assumed to be exposed to the same well-controlled conditions, i.e., 38 °C and 95% RH (Smaoui et al. 2004) (Table 1). The differences observed between the measurements taken on the tops of the blocks (average ratio of 1.12 for all longitudinal and transverse measurements) and on the tops of the slabs (average ratio of 0.76) are surprising at first glance,

cracking that in the estimated expansions use of the variable at the top of the primary indentation of separated measurements, top, and in the case of the results measurements

measured expansion with and individual

RC Canada

Reproduced with permission of the copyright owner. Further reproduction prohibited without permission.

3.161 Smaoui, Nizar and Bérubé, Marc-André and Fournier, Benoit and Bissonnette, Benoit (2004)

URL

```
@article{
smaoui2004influence},
label={smaoui2004influence},
title={Influence of specimen geometry, orientation of casting plane, and mode of
concrete consolidation on expansion due to ASR},
author={Smaoui, Nizar and B{\'e}rub{\'e}, Marc-Andr{\'e} and Fournier, Benoit and
Bissonnette, Benoit},
journal={Cement, concrete and aggregates},
volume={26},
number={2},
pages={1--13},
year={2004},
publisher={ASTM International}
Keywords={}
```

- Concrete specimens of different sizes and shapes were made with various reactive aggregates and stored under conditions favorable to the development of ASR. Expansion was measured with time along three directions.
- The specimens were cast vertically (cylinders and prisms) or horizontally (prisms and larger blocks) using a vibrating table, a vibrating needle, or rodding.
- The expansion due to ASR was always greater in the direction perpendicular to the casting plane.
- The higher the number of flat and elongated particles in the reactive aggregate, the higher the coefficient of anisotropy (the ratio between the expansions perpendicular and parallel to the casting plane).
- This coefficient of anisotropy was constant through the course of the expansion.
- The coefficient was generally higher for the cylinders than for the prisms, and it was lower for larger blocks.
- Consolidation by rodding induced anisotropy coefficients distinctly smaller than consolidation using a vibrating table, and a vibrating needle induced intermediate values; however, all methods produced constant volumetric expansion at least up to an important expansion level.
- For prisms cast horizontally and measured axially, consolidation using rodding induced long term (axial) expansions greater by 71% compared with consolidation using a vibrating table.
- When evaluating field concrete affected by ASR, it appears important to consider the orientation with respect to the casting plane of the core samples subjected to mechanical or residual expansion tests.

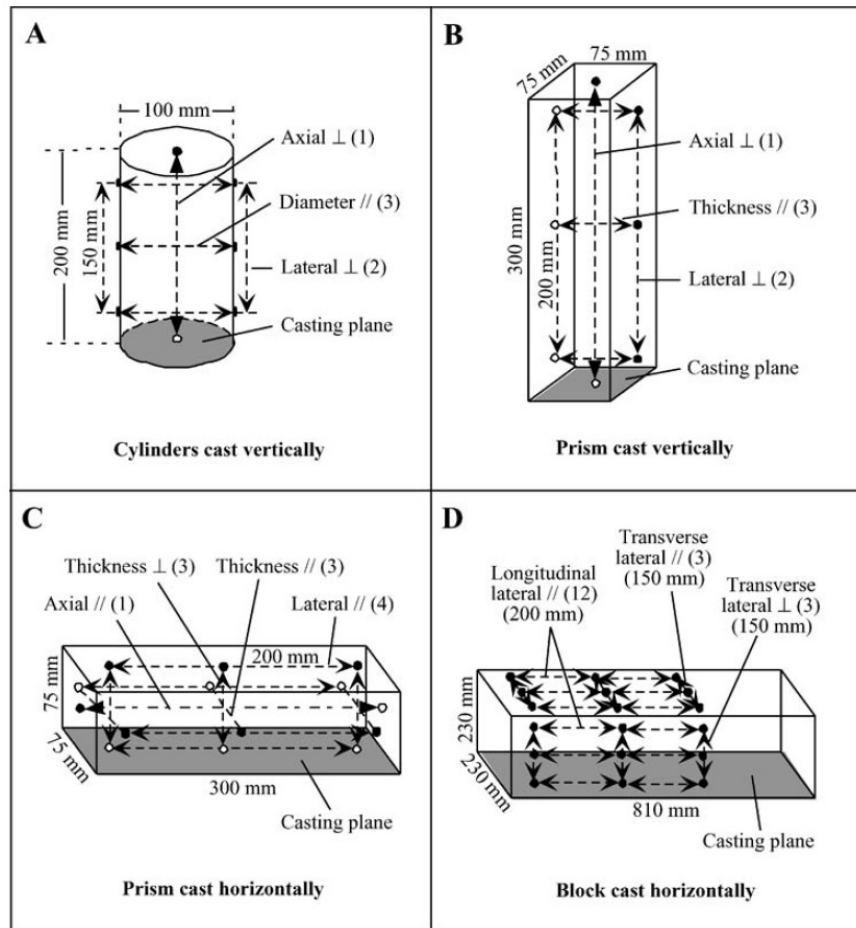


Figure 3.206: Diagrams illustrating the various types of specimens manufactured and the various types of measurements taken on each of them; Smaoui et al. (2004c)

- Longitudinal measurements (i.e., parallel to the long axis of the specimens) also gave results comparable to transverse measurements (i.e., parallel to the short axis), as long as both types of measurements were oriented in the same manner with respect to the casting plane.
- The expansion of an ASR-affected concrete element may vary in the three-dimensional space with respect to the orientation of the casting plane, in addition to the directions of the in-situ constraints.
- When evaluating field concrete elements affected by ASR, it is thus necessary to plan and note the orientation of the core samples subjected to mechanical or residual expansion tests, as well as the directions of the in-situ expansion measurements with respect to the orientation of the casting plane.
- In the case of residual expansion tests on cores, it is recommended to take axial and diameter measurements along the three directions. Of course, the direction of the maximal expansion on cores that are free of all constraints will not be necessarily the same direction in the corresponding elements in the field due to the positive effect of the in-situ compressive stresses on the expansion due to ASR.

3.162 Smaoui, N and Bérubé, MA and Fournier, Benoit and Bissonnette, B and Durand, B (2005)

URL

```
@article{
smaoui2005effects},
label={smaoui2005effects},
title={Effects of alkali addition on the mechanical properties and durability of
concrete},
author={Smaoui, N and B{\'e}rub{\'e}, MA and Fournier, Benoit and Bissonnette, B
and Durand, B},
journal={Cement and concrete research},
volume={35},
number={2},
pages={203--212},
year={2005},
publisher={Elsevier}
Keywords={Laboratory; aggregate Beams-Panels }
```

- The impact of alkali addition on the mechanical properties and durability of concrete was studied.
- Increasing the concrete alkali content from 0.6% to 1.25% of Na_2O_e of the cement mass by adding NaOH to the mixture water has harmful effects on most mechanical properties (compressive, splitting, direct tensile, and flexure strengths) of concrete made with a water-to-cement (w/c) ratio of 0.41 and limestone aggregates not susceptible to ASR; however, it was not harmful to the elasticity modulus measured under compression or direct tension.
- Shrinkage tests at 50% RH and 23°C started after 7 days at 100% RH and 23°C show that the low-alkali concrete shrinks more than the high-alkali concrete, despite similar water losses.
- Freeze-thaw tests performed on air-entrained concretes demonstrate that the two concretes resist freezing and thawing while showing similar air-void systems.
- When examined under the scanning electron microscope (SEM), the hydrates in the two concretes present similar microstructures; however, the high-alkali concrete shows a more reticular and porous micro-texture (which could explain the reduction in strength).
- Compressive strength and modulus of elasticity under compression:
 - Raising the alkali content in concrete resulted in significant reductions of the compressive strength.
 - The main reduction with respect to the low-alkali system was obtained at 3 days, and the differences remained somewhat similar afterwards (i.e., up to 180 days), Figure 3.207.
 - When maintained in the moist curing room at 23°C, the two concretes showed continuous strength gains during the 180-day testing period.
 - The modulus of elasticity is lower for the high-alkali concrete up to 28 days, whereas both concretes gave similar modulus values in the long term.

- Tensile strength and modulus of elasticity under tension:
 - The addition of alkalis to concrete resulted in a noticeable reduction in the tensile strength.
 - The main reduction was observed at 3 days while the difference remained about the same afterwards.
 - The modulus of elasticity under tension was not significantly affected by the increase in the alkali content (with differences generally within ± 2 GPa).
 - Despite some scattering in the test results, the addition of alkalis to the concrete mixture resulted in reduction in the splitting tensile strength from 5% to 16% over the 180-day testing period.
- Modulus of rupture:
 - Increasing the alkali content in concrete resulted in reductions of about 8% in the modulus of rupture up to 28 days; afterwards, both high- and low-alkali concretes showed similar values.

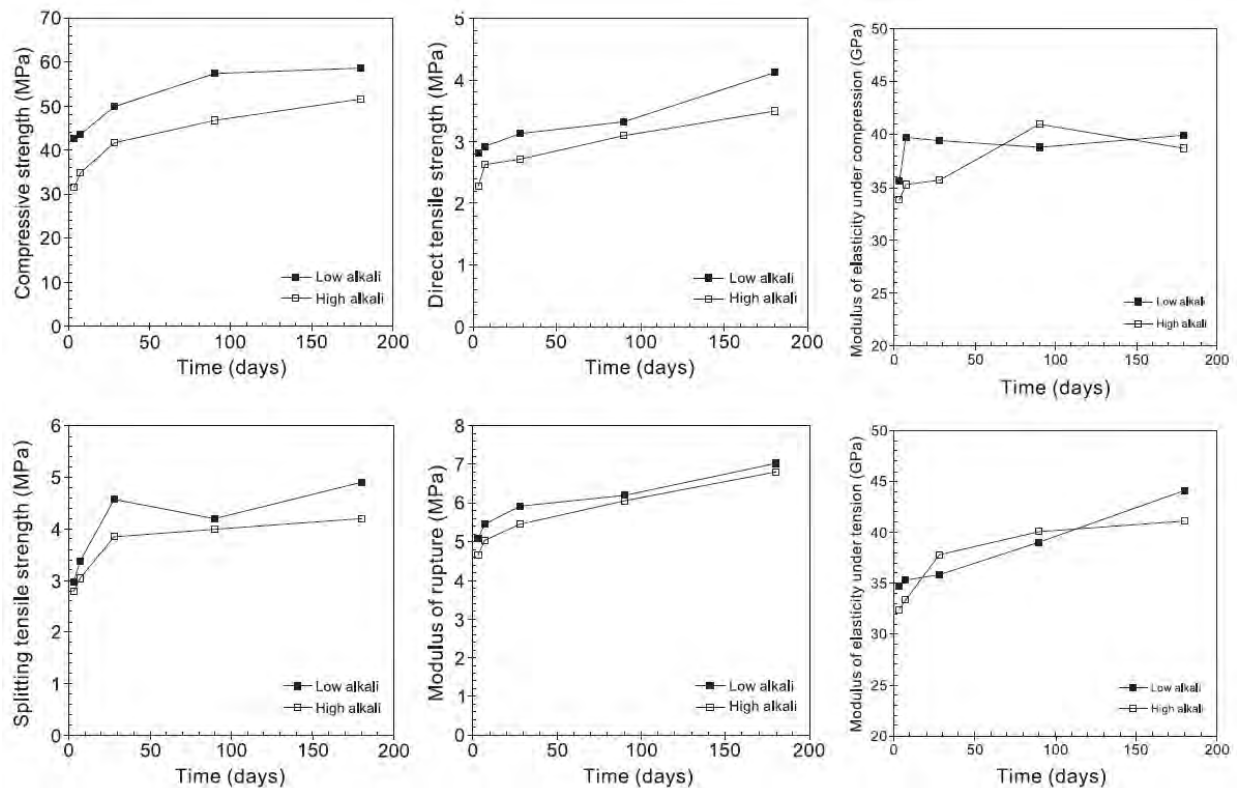


Figure 3.207: Results of mechanical testing as a function of time; Smaoui et al. (2005)

- Drying shrinkage tests show that the low-alkali concrete shrinks slightly more than the high-alkali concrete even though the two concretes lost the same amount of water.
- The two concretes resist freeze-thaw tests; moreover, additional alkalis do not modify the characteristics of the air-void system.

3.163 Stanton, Thomas E (2008)

URL

```
@article{
  stanton2008expansion,
  label={stanton2008expansion},
  title={Expansion of concrete through reaction between cement and aggregate},
  author={Stanton, Thomas E},
  journal={ASCE},
  number={SP-249-1},
  year={2008},
  Keywords={},
  DisplayPdf={0},
  url={https://trid.trb.org/view/868520}
```

- Seminal paper by Stanton.
- Probably the most cited paper on ASR (721 and counting).
- This is where it all started, no need to summarize.
- ~~Wonderfully written~~ ~~tribute~~ ~~written~~ ~~by~~ ~~Michael~~ ~~Tomas~~

Chapter 1 – Introduction



Figure 3.208. Figure 1. Thomas Stanton of the California State Division of Highways and a Bridge Parapet Wall that is Showing Signs of Damage due to Alkali-Silica Reaction. From *Alkali-Aggregate Reactivity (AAR) Fact Book*; (FHWA, 2013)

Alkali carbonate reaction (ACR) was first discovered by Swenson (1957a) as the cause of concrete deterioration in Canada at about the same time that ASR was first documented in the same country (Swenson 1957b). ACR was subsequently implicated in cases of degradation of concrete structures in the USA (Hadley 1961) and alleged cases of ACR have now occurred in Virginia, West Virginia, Kentucky, Missouri, Tennessee, Iowa, Illinois, Indiana, and New York, as well as England, Bahrain, Iraq, and China (Ozol 2006). However, unlike ASR, problems with ACR are still restricted to a few isolated locations worldwide. Consequently, there has been comparatively little research conducted on this topic.

A series of international conferences on alkali-aggregate reaction (IGAAR) in concrete began in

3.164 Steffens, Alexander and Li, Kefei and Coussy, Olivier (2003)

URL

```
@article{
  steffens2003aging},
label={steffens2003aging},
title={Aging approach to water effect on alkali--silica reaction degradation of
  structures},
author={Steffens, Alexander and Li, Kefei and Coussy, Olivier},
journal={Journal of engineering mechanics},
volume={129},
number={1},
pages={50--59},
year={2003},
publisher={American Society of Civil Engineers}
Keywords={}
```

- The role of water at both the reaction and the material level was discussed. A comprehensive mechanical model was proposed for the material swelling employing a hydro-chemo-mechanical approach.
- The proposed model adopts a two-stage mechanism for the swelling kinetics, consisting of the formation of an amorphous gel for which a characteristic time of reaction is identified and of the combination of important quantities of water by the gel.
- Because the combination of water shows an aging effect, a second reaction with a characteristic time of aging is introduced.
- Furthermore, the initial phase of the material swelling is explained by the filling process of internal pores by the swollen gel.
- At a structural level, a characteristic ASR water diffusion length is proposed to evaluate the concrete surface delamination depth. Its range is calculated by means of a 1D analysis of ASR swelling activated by water diffusion.
- As a case study, a reactive retaining wall is analyzed, Figure 3.209. This structure serves as the joint piece between the road structure and the bridge structure with the back side filled with soil and sand.
- The wall is supposed to be subject to a typical humidity history initiated by a drying process after completion of the structure ($t = 0$) with the internal humidity higher than the external humidity. At a certain instant ($t = 5$ years), due to a defect in the waterproof layers of the road structure, external water penetrates into the soil and sand body, reaching the foot of the retaining wall.
- The ambient RH is supposed to be 60% and the initial internal humidity of the concrete 80%.
- The internal humidity of the concrete is expressed by the relative humidity with the conversion from relative humidity to water content.

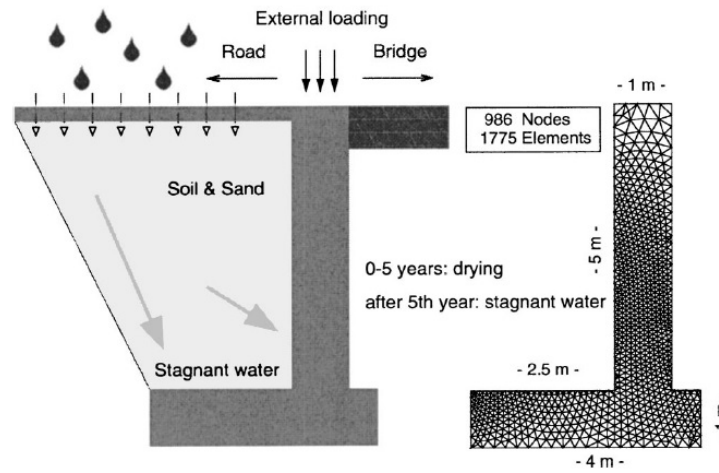


Figure 3.209: Reactive concrete retaining wall and its finite element mesh; Steffens, Li, and Coussy (2003)

- In order to demonstrate the structural behavior explicitly, an elasto-plastic calculation is realized on the retaining wall.
- The pushing force arising from the soil and sand body is neglected, and the structure is loaded by its dead load and the external vertical loads from the road and the bridge.
- The retaining wall is calculated for a 15 year period from its structural completion.
- Observations at:
 - End of the drying process ($t = 5$ year): Until this instant, the retaining wall is well protected from water by the road structure. Due to the drying of the outer parts of the structure the reaction is more advanced in the inner part.
 - Just after the attack of stagnant water ($t = 5.5$ years): the high humidity of 100% at the wall-soil interface changes the humidity gradient. The wall starts to sustain substantial plastic strain corresponding to the microcracking. Delamination cracking acts as the main degradation in the vertical wall, and both delamination cracking and longitudinal cracking in the foot can be observed.
 - Total material degradation ($t = 6$ years): The surface delamination develops rapidly to attain a total surface delamination. For the wall considered, a humidity of 80% substantially reduces the ASR-induced material swelling compared to the swelling at 100%.

3.165 Swamy, RN and Al-Asali, MM (1986)

```
@incollection{
swamy1986influence},
label={swamy1986influence},
title={Influence of alkali-silica reaction on the engineering properties of
concrete},
author={Swamy, RN and Al-Asali, MM},
booktitle={Alkalies in concrete},
year={1986},
publisher={ASTM International},
Keywords={Laboratory; Expansion Assessment/monitoring Det. E; Det f't; Det f'c;
Crack Index; },
DisplayPdf={0},
```

- Several experiments were performed to quantify the effect of ASR on the properties of concrete. Two reactive aggregates were used.
- At 0.1% expansion, concrete containing 5.2 kg/m³ equivalent sodium oxide showed a loss of 12% compressive strength and 50% tensile strength, Figure 3.210.
- The compressive strength was not found to be a good indicator of ASR, but the modulus of rupture test proved to be a sensitive and reliable test to identify the progress of the reaction, Figure 3.210.
- Dynamic modulus and pulse velocity also appear to be good indicators of ASR.
- The tests suggest that fused silica is an ideal reactive aggregate to simulate expansion due to ASR, and that it provides an effective means of determining the deterioration in concrete properties and in evaluating mineral admixtures to control expansion.
- The ASTM limit of 0.1% expansion over six months may need modification if it is to be applied to field structures.
- The pulse velocity tests show that the core of the concrete is as much affected by ASR as the outer surfaces.
- Whilst the concrete surface demonstrates visible cracking, which penetrates into the body of the concrete, the core does not show any cracking due to swelling; however, its properties appear to be affected in the same way as the external surfaces.

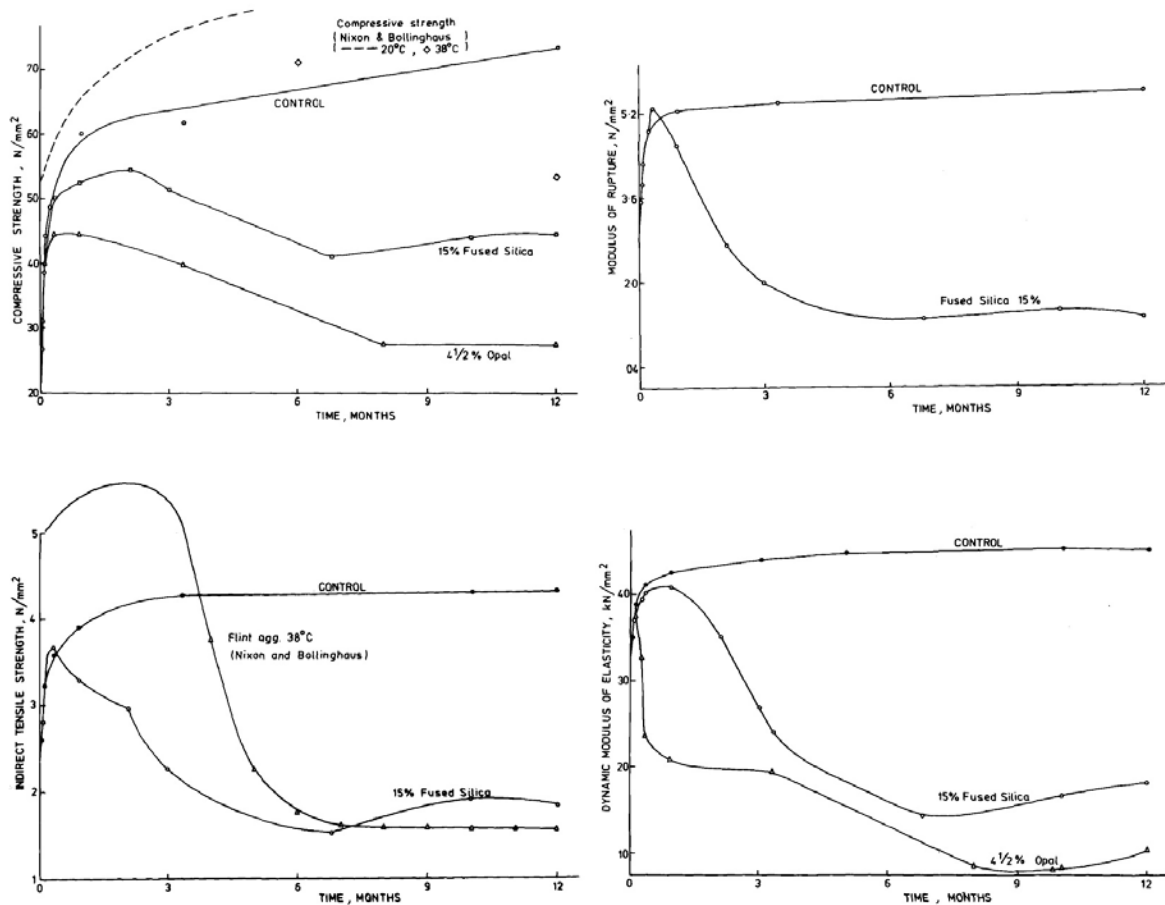


Figure 3.210: Variation of mechanical properties with time due to ASR; Swamy and Al-Asali (1986)

3.166 Swamy, R Narayan and Wan, WM Raymond (1993)

URL

```
@article{
swamy1993use},
label={swamy1993use},
title={Use of dynamic nondestructive test methods to monitor concrete
deterioration due to alkali-silica reaction},
author={Swamy, R Narayan and Wan, WM Raymond},
journal={Cement, Concrete and Aggregates},
volume={15},
number={1},
pages={39--49},
year={1993},
publisher={ASTM International}
Keywords={}
```

- The use of dynamic nondestructive test methods, such as pulse velocity and dynamic modulus,

to monitor the initiation and progress of ASR in concrete is described.

- Several parameters were studied: two different types of reactive aggregates; varying environments; concretes with and without mineral admixtures such as fly ash, ground-granulated blast-furnace slag, and silica fume; and concrete beams with and without reinforcement.
- The results show that both pulse velocity and dynamic modulus are sensitive to material and structural changes arising from ASR.
- The results of the tests at $20 \pm 1^\circ\text{C}$ and $96 \pm 2\%$ RH are shown in Figure 3.211.
- These data demonstrate that both pulse velocity and dynamic modulus are highly sensitive to changes occurring in the internal structure of the concrete arising from material damage due to ASR.
- There is no unique relationship between expansion and loss in pulse velocity or loss in dynamic modulus.
- Since losses in engineering properties do not occur at the same rate or in proportion to expansion, unique relationships between expansion and pulse velocity or loss in pulse velocity or dynamic modulus cannot be expected.

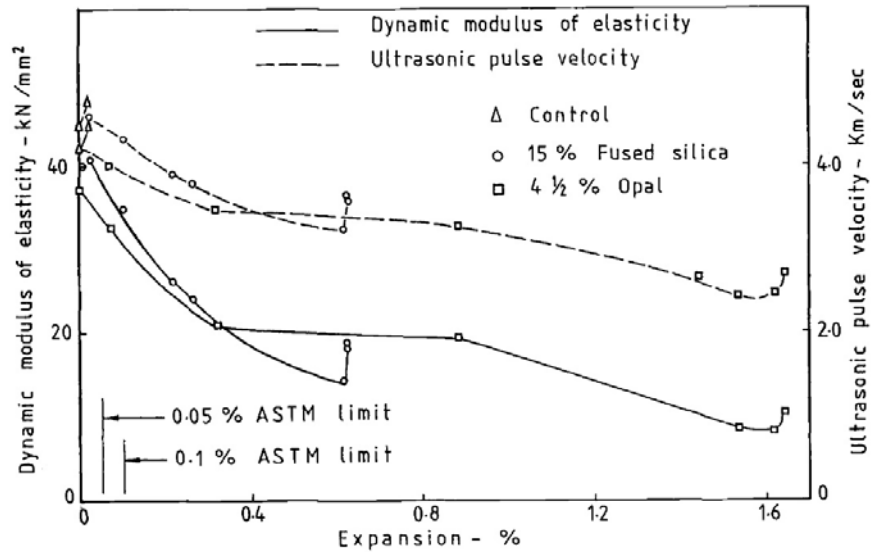


Figure 3.211: Effect of ASR expansion on pulse velocity and dynamic modulus; Swamy and Wan (1993)

- Dynamic modulus values are generally more sensitive than pulse velocity measurements.

3.167 Takakura, Takeo and Masuda, Hirotaka and Murazumi, Yasuyuki and Takiguchi, Katsuki and Masuda, Yoshihiro and Nishiguchi, Isoharu (2007)

```
@inproceedings{
takakura2007structural},
label={takakura2007structural},
title={Structural soundness for turbine-generator foundation affected by
alkali-silica reaction and its maintenance plans},
author={Takakura, Takeo and Masuda, Hirotaka and Murazumi, Yasuyuki and Takiguchi,
Katsuki and Masuda, Yoshihiro and Nishiguchi, Isoharu},
year={2007},
booktitle="{Proceedings of the 23rd Conference on Structural Mechanics in Reactor
Technology (SMiRT19)}",
publisher={IASMiRT},
Keywords={Expansion Assessment/monitoring Petrography; Rehabilitation; Nuclear
power plants; },
DisplayPdf={0},
```

- Ikata No.1 nuclear power station is constructed by Shikoku Electric Power Company.
- The Turbine Generator foundation of Unit 1 is the reinforced concrete structure which supports the turbine and generator located inside the turbine building.
- An abnormal setting condition and movement different than the turbine generator installation value were confirmed between the generator, the rotor, and their bearings during the first annual inspection in 1979.
- ASR cracks were observed on the TG foundation and were confirmed by various test results, such as the core sampling test.
- It was confirmed that the TG foundation had expanded in the longitudinal direction due to the affect of ASR, and the maximum expanded rate was about 1000 micro.
- The TG foundation has confirmed that it has sufficient bearing capacity to the design seismic load, even now.
- The various monitoring tests for comprehension of the TG foundation condition such as the development of ASR and keeping structure soundness have been executed.
- Monitoring items are as follows:
 - Monitoring items which would have indicated some changes to the TG foundation due to ASR development:
 - * Table deck expansions
 - * Reinforcement strain
 - * Cracking conditions on the exterior surface of the TG foundation
 - * The TG foundation vibration character measurement
 - * Enjoinment temperature and humidity around the table deck

- Monitoring items which are kept continuously for safe operation of the TG against ASR development:
 - * Monitoring Shaft vibration
 - * Monitoring Bearing metal temperature
- Planned additional monitoring items:
 - * Nondestructive concrete tests
 - * Deformation measurements of the TG foundation

3.168 Talley, Kimberly G and Kapitan, Jacob G and Breen, John E (2016)

URL

```
@article{
talley2016method},
label={talley2016method},
title={Method for approximation of ASR/DEF damage in concrete columns},
author={Talley, Kimberly G and Kapitan, Jacob G and Breen, John E},
journal={ACI Structural Journal},
volume={113},
number={1},
pages={105},
year={2016},
publisher={American Concrete Institute}
Keywords={}
```

- By mechanically cracking reinforced concrete columns, the method used to approximate the damage caused by ASR and delayed ettringite formation (DEF) . is derived
- The structural capacity of a series of columns with varying crack widths was compared to two columns specially cast and exposed to trigger ASR and/or DEF expansion.
- All specimens had identical dimensions but varied in initial damage levels: undamaged control, three widths of mechanically induced pre-cracking, and ASR/DEF expansion.
- Four conventionally constructed scale column specimens were used for an undamaged control, and three mechanically cracked columns with different through-section crack widths were fabricated. These columns had concrete compressive strengths of 40 to 41 MPa on their respective days of testing.
- The through-section cracks were induced using stone-splitting wedges inserted in PVC voids that ran through the concrete section.
- All columns were tested under doubly eccentric axial loads and failed in bearing. The axial load was applied following the AASHTO Load Case III with two lanes.
- The ASR/DEF columns had over 1% expansion when tested and had no significant reduction in bearing capacity.

- The mechanical cracking method approximated the ASR/DEF degradation to structural capacity in significantly less time than it took to trigger ASR/DEF in laboratory specimens.
- The load-displacement behavior of all scaled column series specimens is presented in Figure 3.212.
- The load-displacement behavior of ASR/DEF Column A was truncated at 1730 kN when the concrete spalled underneath the linear potentiometer, preventing further readings of column displacement.
- This plot presents the measurements of displacement from the top of the column along the x-axis (on the short face).
- The two ASR/DEF-affected columns had different total displacements and stiffness.
- There was no significant reduction in load-carrying capacity for the two ASR/DEF specimens versus the control and 0.51 mm specimens. The average width of the major cracks on the ASR/DEF specimens was 0.51 mm.

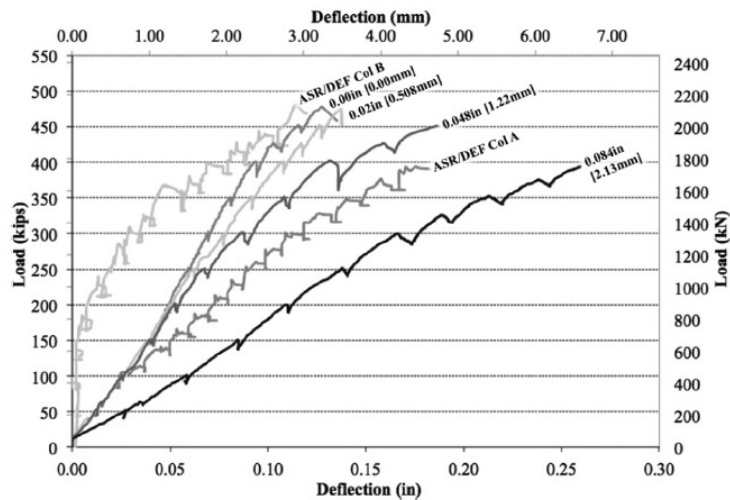


Figure 3.212: Load-displacement comparison on the short face; Talley, Kapitan, and Breen (2016)

3.169 Tcherner, Julia and Aziz, T (2009)

```
@inproceedings{
tcherner2009effects},
label={tcherner2009effects},
title={Effects of AAR on seismic assessment of nuclear power plants for life
extensions},
author={Tcherner, Julia and Aziz, T},
booktitle={Proceedings of the 20th International Conference on Structural
Mechanics in Reactor Technology (SMiRT), Espoo, Finland},
pages={9--14},
year={2009},
Keywords={Laboratory; Expansion Assessment/monitoring Reinforcement; Confined;
Det. E; Seismic; Nuclear power plants; },
DisplayPdf={0},
```

- In NPP, the containment system represents an ultimate barrier to fission product releases into the environment.
- As part of the containment system, CANDU-6 NPPs use a fully prestressed concrete Reactor Building that is designed to contain the pressure build-up that might result from accident scenarios.
- Several NPPs are approaching the end of their original design life and, as the service life is being extended, containment improvements are performed in order to meet the Probabilistic Safety Assessments (PSA) related targets.
- As part of the PSA work, Seismic Margin Assessment (SMA) is performed as seismic requirement has increased for some plants.
- New Floor Response Spectra (FRS) for the R/B containment structure need to be developed, which, in addition to new seismic requirements, should consider the current conditions of the R/B structure including possible aging-related degradation.
- AAR was identified as applicable Aging Related Degradation Mechanism (ARDM) for one of the plants, and an investigation was performed to establish the means of accounting for AAR in the development of FRS for R/B to be used in SMA work.
- AAR was identified early in the life of one of the CANDU reactor buildings. Relative humidity inside R/B is between 5% and 20%. Thus, the concrete inside the R/B is kept under very dry conditions.
- Based on this investigation, geometry, and current conditions of the post-tensioned R/B, no change in the modulus of elasticity to account for AAR is necessary for generation of seismic FRS.
- It is considered prudent to include a possible reduction in the modulus of elasticity of about 15% to account for possible local variations in material characteristics, environment of exposure, and chemical reactivity.

- Measured compressive strength of the R/B concrete (51 MPa) is higher than the strength used in original design calculations (35 MPa). Thus, an increase in the modulus of elasticity also needs to be considered for seismic FRS generation for R/B for life extension.

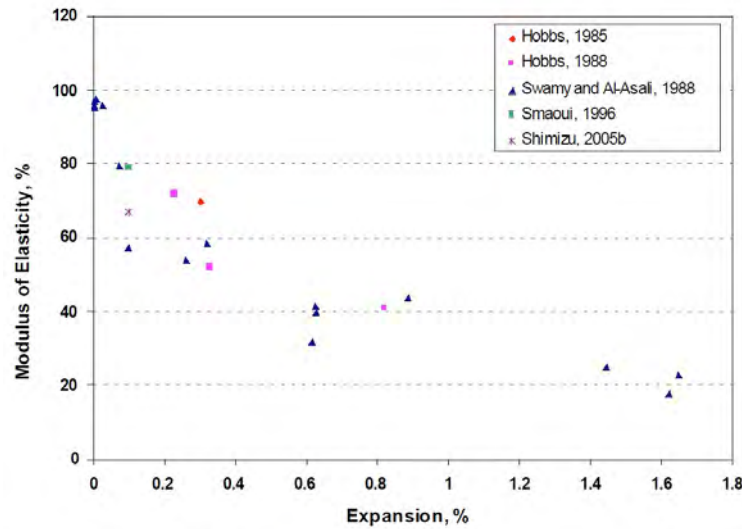


Figure 3.213: Effect of Expansion due to AAR on Elastic Modulus; Tchner and Aziz (2009)

3.170 Torii, Kazuyuki and Kubo, Tetsuji and Sannoh, Chikao and Kanitani, Maki (2016)

URL

```
@article{
  torii2016strengthening},
  label={torii2016strengthening},
  title={The Strengthening of an ASR-Affected Water Intake Tower in a Hydro-Electric
  Dam by Using Post-tensioned Tendons and the Long-term Monitoring of the Tower},
  author={Torii, Kazuyuki and Kubo, Tetsuji and Sannoh, Chikao and Kanitani, Maki},
  journal={Journal of Advanced Concrete Technology},
  volume={14},
  number={7},
  pages={384--396},
  year={2016},
  publisher={Japan Concrete Institute}
  Keywords={}
```

- An intake tower suffering from ASR and deformed due to deterioration was studied.
- The tower is located at a dam in the Japan. It is an SRC structure.
- Countermeasures were carefully considered, and post-tensioned tendons were inserted into the intake tower concrete (vertically oriented), so the power station can continue to operate safely in the future.

- This is the first challenge of its type anywhere in the world for which the deformation of a real structure caused by ASR expansion must be controlled.
- The horizontal and vertical deformations were measured at the top of the intake tower. The measurement accounts for the 8 year period of 22 to 30 years following the construction.
- The rate of horizontal and vertical changes are 5.6 mm and 2.1 mm per year, respectively.
- Deformation started 15 years after construction.
- On the surfaces of the exterior and interior walls, extensive mapping cracks were observed.
- Cracks were approximately, 0.2 mm in width at 200 to 300 mm intervals and were not severe.
- After post-tensioning, the rate of deformation is confirmed to be reduced. More specifically, the anticipated 16 mm horizontal displacement reduced to only 5 mm.
- Figure 3.214 shows the horizontal changes before and after strengthening.

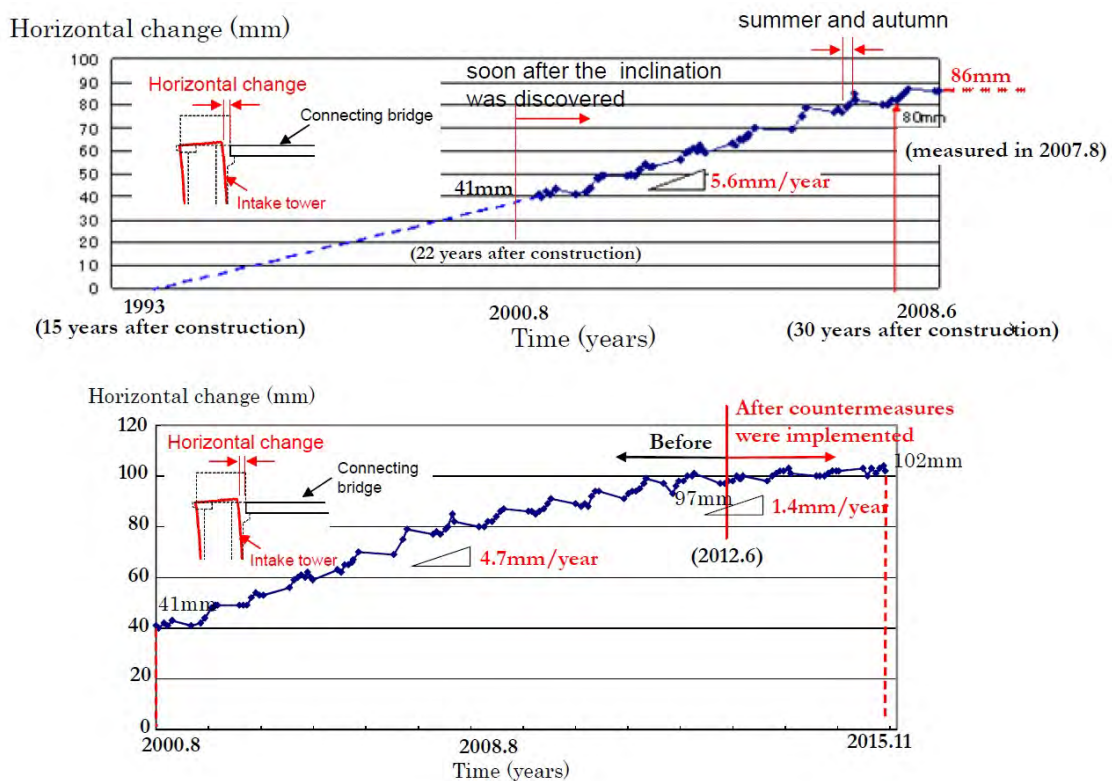


Figure 3.214: Horizontal change in distance over time at the top of the tower; Torii et al. (2016)

3.171 Ulm, Franz-Josef and Coussy, Olivier and Kefei, Li and Larive, Catherine (2000)

URL

```

@article{
  ulm2000thermo},
  label={ulm2000thermo},
  title={Thermo-chemo-mechanics of ASR expansion in concrete structures},
  author={Ulm, Franz-Josef and Coussy, Olivier and Kefei, Li and Larive, Catherine},
  journal={Journal of engineering mechanics},
  volume={126},
  number={3},
  pages={233--242},
  year={2000},
  publisher={American Society of Civil Engineers}
  Keywords={}

```

- A chemo-elastic model was developed that accounts for ASR kinetics and the swelling pressure exerted by the ASR reaction products on the skeleton.
- This model is a first-order engineering approach to capture the timescale and magnitude of ASR expansion.
- This technique was implemented through finite element case studies of ASR effects in structures: a concrete gravity dam and a bridge box girder.
- A typical, medium-sized gravity dam fixed at the base was used as the case study.
- In such structures, heat diffusion often results from the difference in surface temperature: the upstream temperature is given by the water temperature, and the surrounding air temperature determines the downstream thermal boundary conditions.
- To capture irreversible skeleton deformation related to microcracking, the three-parameter Willam-Warnke concrete-plasticity criterion is applied.
- Figure 3.215 shows, at different times, the results of the plain strain chemo-elastic-plastic analysis. On the one side The fields of ASR extents are illustrated above; the principal plastic strains representing stress-induced microcracking are pictured below.
- The initiation of microcracking induced by ASR swelling occurs in front of the ASR front; the compression induced by ASR swelling behind the ASR front is balanced by tensile stresses within the bulk of the structure.
- The initiation of ASR-induced microcracking occurs here after 8 years.
- Visible, irreversible evolutions at the surface, with surface delamination ($t = 8$ years), result from the biaxial compressive stress state parallel to the surface, generated by restrained in-plane expansion.
- With the ASR advancing, the localized surface degradation extends over the entire surface ($t = 10$ years).
- The results demonstrate that gravity dams are highly ASR heat sensitive structures.
- The second example is typical box girder for large span bridges.

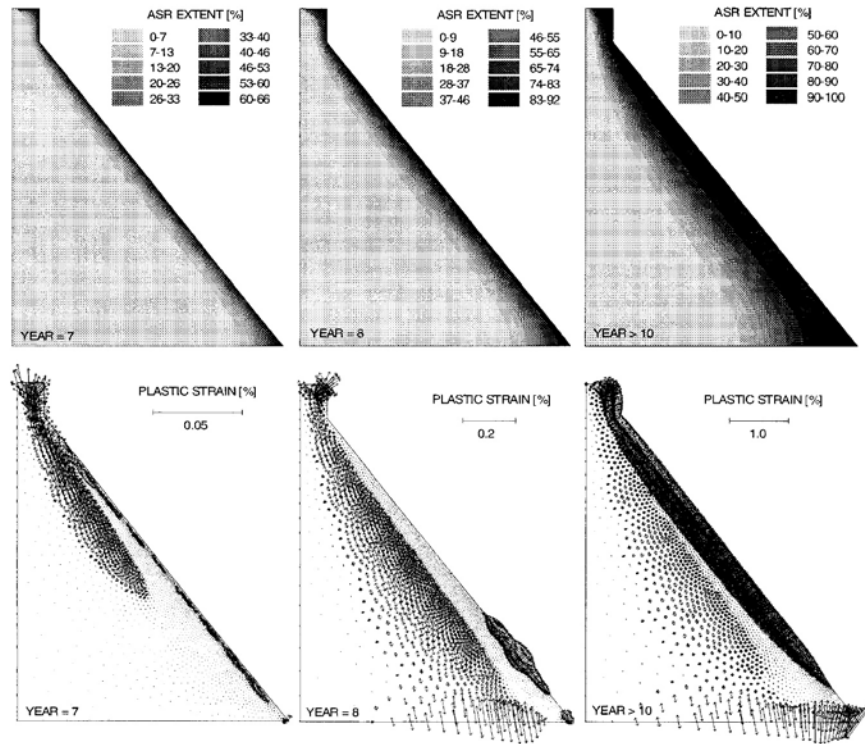


Figure 3.215: Time dependent response of dam, ASR extent, and principal plastic strain vectors; Ulm et al. (2000)

- The surfaces of the bridge section are subjected to annual thermal cycles with a sinusoidal air temperature history; the average annual air temperature is equal to 15°C on the outside, and 8°C on the inside. The surfaces are modeled by means of linear exchange elements, complying with the boundary conditions.
- The 2D analysis is conducted under the generalized bending condition.
- Structural effects induced by ASR in slender structures are limited. The slabs are exposed to a higher air temperature than the inside. Due to thermal activation, the ASR advances faster in the outer structural elements than in the section core.
- These tensile stresses can exhaust the material strength, as illustrated in Figure 3.216 which shows the isovalues of the ASR extent and the corresponding longitudinal plastic strains after a 2.5 year temperature cycle, respectively.
- These irreversible deformations associated with microcracking are the mechanical effects of ASR-induced eigen-stresses in kinematically restrained structures.

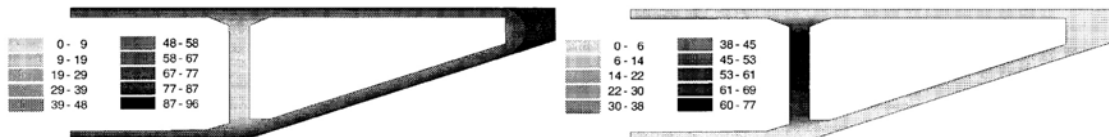


Figure 3.216: ASR extent percent and longitudinal plastic strains in box girder; Ulm et al. (2000)

3.172 Šachlová, Šárka and Příklad, Richard and Pertold, Zdeněk (2010)

URL

```
@article{
vsachlova2010alkali,
label={vsachlova2010alkali},
title={Alkali-silica reaction products: Comparison between samples from concrete
structures and laboratory test specimens},
author={{\v{S}}achlov{\`a}, {\v{S}}{\'a}rka and P{\v{r}}ikryl, Richard and
Pertold, Zden{\v{e}}k},
journal={Materials Characterization},
volume={61},
number={12},
pages={1379--1393},
year={2010},
publisher={Elsevier},
Keywords={},
DisplayPdf={0},
url={https://www.sciencedirect.com/science/article/pii/S1044580310002688}
```

- Alkali-silica gels (ASG) were investigated in concrete from bridge structures (constructed from the 1920s to 2000), as well as in experimental specimens; employing optical microscopy, petrographic image analysis, and scanning electron microscopy combined with energy dispersive spectroscopy (SEM/EDS).
- The main differences were found in the chemical composition and morphology of the ASGs.
- ASGs which had formed in older concrete samples (50–80 years old) show a partly crystalline structure and higher Ca²⁺ content, indicating their aging and maturation.
- Younger concrete samples and experimental test specimens exhibit the presence of amorphous ASG.
- The chemistry of ASG from experimental specimens reflects the chemical composition of accelerating solutions.
- ASG formed under different environmental conditions (seven up-to 84 year-old concrete samples, and experimental laboratory samples) showed significant variations in their chemical composition and morphology.
- The structure and morphology of ASG is principally affected by the process of aging and maturation.
- Partly crystallized ASGs were found in concrete samples that were 60 to 84 years old.
- An age of more than 50 years seems to be sufficient for the origination of ASG in concrete containing quartz-rich and greywacke aggregates, and long enough for the crystallization of the ASG.

- The process of aging and maturation of ASG is apparent from their high variability in chemical composition and the increase in the amount of CaO.
- More uniform composition, lower amounts of CaO, and amorphous structure are the principal characteristics of very young ASGs from the 7 yearold concretes.
- The comparison of ASGs in the experimental specimens, contrasted with those from the concrete samples, highlights two other important factors: (I) the influence of accelerating solution composition, and (II) the influence of temperature maintained during the accelerating period.
- Temperature mainly affects the total amount of originating ASG.
- The composition of the accelerating solutions affects the composition of the ASG.
- Investigation of the ASGs pointed out the importance of external factors during the aggregate laboratory tests.
- The influence of aggregates onASG formation shouldbe investigated when the influence of these external factors is suppressed

3.173 Wald, David M and Allford, Morgan T and Bayrak, Oguzhan and Hrynyk, Trevor D (2017)

URL

```
@article{
wald2017development},
label={wald2017development},
title={Development and multi-axial distribution of expansions in reinforced
concrete elements affected by alkali--silica reaction},
author={Wald, David M and Allford, Morgan T and Bayrak, Oguzhan and Hrynyk, Trevor
D},
journal={Structural Concrete},
volume={18},
number={6},
pages={914--928},
year={2017},
publisher={Wiley Online Library}
Keywords={}
```

- The development and multi-axial distribution of ASR expansions were monitored for 33 480-mm reinforced concrete cubes.
- The cubes were fabricated using three different concrete mixtures of varying reactivity and contained uniaxial, biaxial, and triaxial reinforcement layouts with different reinforcement ratio combinations.
- Four specimens were not reinforced in order to examine free expansion behavior.
- Different combinations of gross reinforcing ratios were incorporated using ASTM A615 Grade 6014 deformed steel reinforcing bars with U.S. designations.

- Reinforcement ratios of 0.5, 1.1, and 1.5% were achieved using varying amounts of No. 4, 5, 6, and 7 reinforcing bars.
- The reinforcing bars were placed in either three distributed layers spaced at 150-200 mm or in two layers at the top and bottom spaced at 360-410 mm.
- The different reinforcing schemes are illustrated in Figure 1.

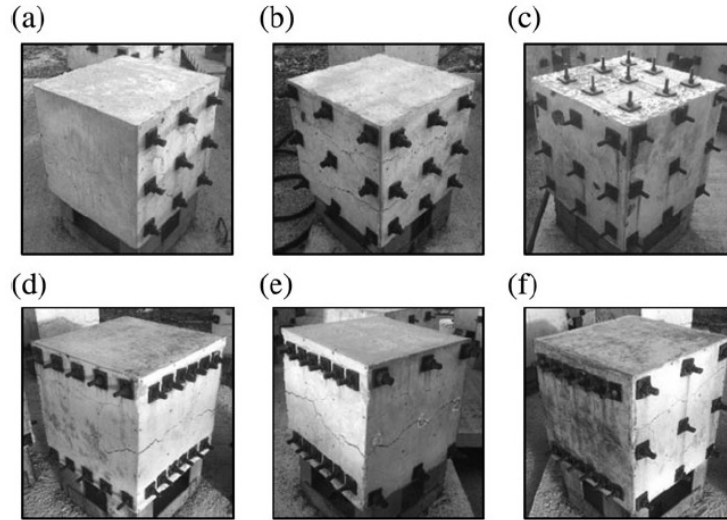


Figure 3.217: Specimen reinforcement layouts. (a) Three-layer uniaxial reinforcement; (b) Three-layer biaxial reinforcement; (c) Three-layer triaxial reinforcement; (d) Two-layer biaxial reinforcement (L1); (e) Two layer biaxial reinforcement (L2); (f) Combined two-layer/three-layer biaxial reinforcement (L3); Wald et al. (2017)

- Each cube specimen was fabricated from one of three concrete mixtures: mix-C (reactive fine aggregates with low-reactivity coarse aggregates), mix-B (nonreactive fines with highly reactive coarse aggregates), mix-A (both reactive fines and reactive coarse aggregates).
- In all cases, the cubes expanded at greater rates in the unreinforced directions than in the reinforced directions.
- Sample (and not all) expansion curves for the A1 specimens with uniaxial, biaxial, and triaxial reinforcement is shown in Figure 3.218.

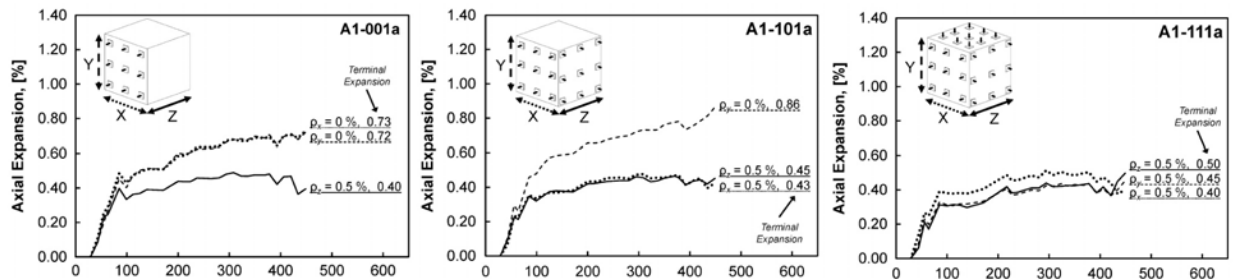


Figure 3.218: Axial expansions versus specimen age; Wald et al. (2017)

- Increasing the number of reinforced directions resulted in reduced volumetric expansion development over time and greater differences between expansions in reinforced and unreinforced directions.
- Expansions were reduced due to the presence of reinforcement; however, the actual reinforcing ratios used (0.5, 1.1, 1.5%) did not appear to significantly influence the overall development or distribution of expansions, especially in the cases of uniaxially, equal biaxially, and equal triaxially reinforced specimens.
- No correlation between reinforcing percentages and volumetric expansion development was discernible among specimens reinforced in the same number of directions.
- The multiaxial distribution of expansions for uniaxially, equal biaxially, and equal triaxially reinforced specimens were independent of the reinforcement ratios employed.
- The multiaxial distribution of expansions for unequal biaxially or triaxially reinforced specimens was only slightly dependent on the two or three reinforcement ratios used.
- Cubes with end-anchored, deformed steel reinforcing bars placed in three layers developed expansions exceeding steel yield strains in all directions.
- Cubes with bars placed in two layers exhibited differential expansions between locally reinforced concrete regions at the edges of elements and unreinforced core regions.
- Mixture reactivity and environmental conditioning influenced expansion rates but not trends of the multiaxial distribution of volumetric expansions.

3.174 Wald, David and Martinez, Gloriana Arrieta and Bayrak, Oguzhan (2017)

URL

```
@article{
wald2017expansion},
label={wald2017expansion},
title={Expansion behavior of a biaxially reinforced concrete member affected by
alkali-silica reaction},
author={Wald, David and Martinez, Gloriana Arrieta and Bayrak, Oguzhan},
journal={Structural Concrete},
volume={18},
number={4},
pages={550--560},
year={2017},
publisher={Wiley Online Library}
Keywords={}
```

- Development and multiaxial ASR distribution were quantified for a large-scale reinforced concrete beam.
- The beam has top and bottom mats of bidirectional reinforcement with no reinforcement through its depth.

- The impact of different conditioning environments and the influence of reinforcing bar size and layout on the expansion behavior of the beam were studied.
- The expansions in the reinforced directions were less than those in the unreinforced direction at all times.
- The directional distribution of volumetric expansions showed that expansion in the unreinforced direction accounted for more than one third of any given volumetric expansion.
- While all three primary orthogonal directions continued to expand, the unreinforced direction contributed approximately 50% of the volumetric expansion.
- The directional expansions were measured using calipers in each of the three monitoring zones, shown in Figure 3.219.

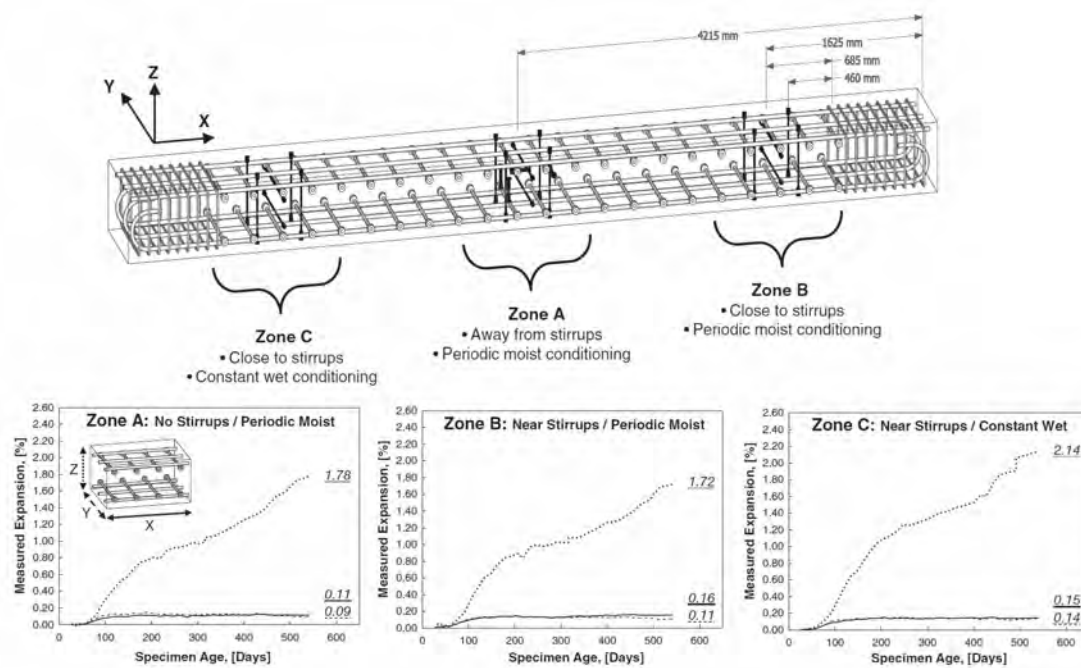


Figure 3.219: Instrumentation layout and monitoring zones; Measured directional expansions (calipers) versus specimen age; Wald, Martinez, and Bayrak (2017)

- Different types of environmental exposure conditions promoting ASR expansion affected only the rates of expansion but not the distribution of volumetric expansions among primary orthogonal directions.
- According to caliper measurements, the reinforced directions stopped expanding between 0.1% and 0.15% prior to steel yielding and before the unreinforced direction stopped expanding.
- At an expansion of 0.14%, the induced compressive stresses in concrete in these directions were computed to be 2.0 and 3.1 MPa. These values are lower than a limit between 5.0 and 10.0 MPa, above which ASR expansion does not occur.
- Expansion behavior within the biaxially reinforced portion of the specimen was not influenced by triaxial restraint conditions at nearby specimen ends.

- The closest expansion measurement zone to the end region of the specimen was sufficiently separated (by nearly 30 bar diameters) from the nearest stirrup.
- Expansion behavior in the reinforced directions was relatively uniform through the depth of the specimen. The top and bottom layers of reinforcement were spaced close enough (less than 15 bar diameters) such that the effective restraint against expansion was uniform in each direction.
- Large, mid-depth cracks formed on the specimen side surfaces due to strains in the unreinforced direction, Figure 3.220.

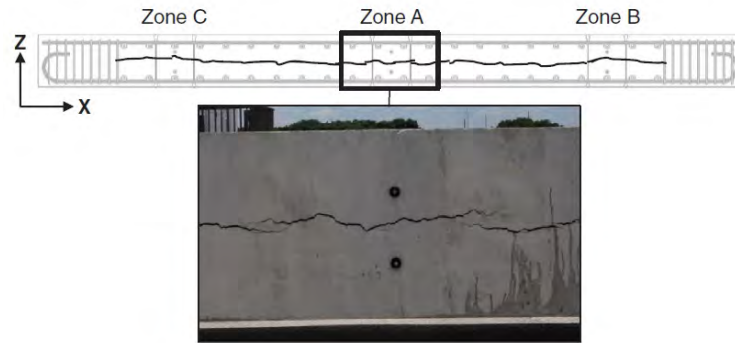


Figure 3.220: Mid-depth surface crack on x - z specimen face; Wald, Martinez, and Bayrak (2017)

- A preliminary finite element simulation was performed using VecTor2, a program capable of analyzing reinforced concrete structures in 2D with applied direction-dependent concrete pre-strains.
- Nonuniform restraint against expanding concrete in the transverse direction generated by lumped reinforcement layers resulted in tensile stresses developing in the unreinforced direction at the edges of the cross section.

3.175 Wallau, Wilma and Pirskawetz, Stephan and Volland, Katja and Meng, Birgit (2018)

[URL](#)

```

@article{
wallau2018continuous},
label={wallau2018continuous},
title={Continuous expansion measurement in accelerated concrete prism testing for
verifying ASR-expansion models},
author={Wallau, Wilma and Pirskawetz, Stephan and Volland, Katja and Meng, Birgit},
journal={Materials and Structures},
volume={51},
number={3},
pages={79},
year={2018},
publisher={Springer}
Keywords={}

```

- In situ expansion measurement was applied to accelerated concrete prism testing.
- In concrete prism testing at 60°C, the expansion is measured manually throughout the test. This work shows that the cooling-heating cycles, associated to manual measurements, effect additional expansion of the prisms, especially when undertaken during the phase of accelerated expansion.
- Automated measuring facilitates both storage (without the usually necessary interruptions for manual measurement) and acquisition of quasi-continuous expansion data.
- Conventional testing resulted in stronger expansion and leaching of alkali than automated testing.
- Two phenomenological approaches were validated with continuous expansion data of three types of aggregate, Figure 3.221.

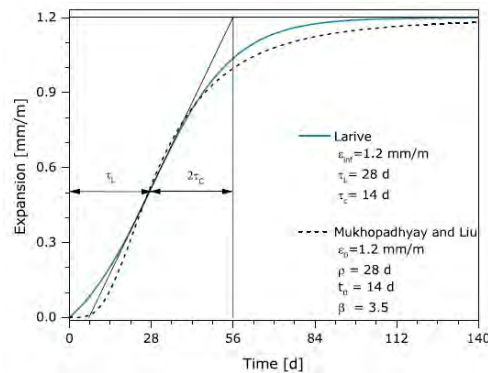


Figure 3.221: Example curves of expansion approaches; Wallau et al. (2018)

- Experimental expansion depicted S-shaped curves similar to those of the modeling approaches. Strong swelling recorded in the beginning of the test, however, was not covered by the model curves.
- Auxiliary measurement of acoustic emissions and ultrasonic velocity helped characterizing mechanisms, such as hydration and cracking which also influence prism expansion.

- Advantages of automated measuring in ASR testing include online monitoring, early notice when expansions exceed the limit value, and reduced human influence on the test result.

3.176 Wang, Jian and Morikawa, Hidenori (2012)

```
@inproceedings{
wang2012study},
label={wang2012study},
title={Study on shear behavior of deteriorated RC beams due to alkali-silica
reaction},
author={Wang, Jian and Morikawa, Hidenori},
booktitle={37th Conference on our world in concrete \& structures},
year={2012},
Keywords={Laboratory; Blocks; Expansion Assessment/monitoring Confined;
Reinforcement; Nonlinear; Finite Element; },
DisplayPdf={0},
```

- The influence of ASR on the shear failure behavior and shear capacity of RC beams is studied.
- A number of specimens were cast by adding reactive aggregate for ASR triggering and then exposed to the exterior environment.
- The specimens were evaluated by non-destructive inspections and material tests, and the loading tests of RC beams were also conducted, reflecting the shear resisting performance.
- FEM analyses were conducted to evaluate different analysis models with respect to the behavior of the beams.
- Experimental results showed that the RC beams with ASR finished in undesirable shear failure mode, and bond slip is easily occurs in RC beams with ASR induced cracks along the tensile reinforcing bars.
- Under a consideration of the chemical pre-stress induced by the expansion in concrete due to ASR, the result of an experiment can also be simulated by the FEM analysis. The analysis results showed a good agreement with the experimental data regarding to the load-displacement response (Figure 3.222), crack pattern, and rebar strain distribution.
- Two groups of beams exist:
 - Group 1 consists of one control RC beam and five deteriorated RC beams.
 - Group 2 consists of one control RC beam and two deteriorated RC beams.
- To avoid the flexural failure after exposure, deteriorated beams were strengthened with a carbon fiber reinforced polymer sheet (CFRP).
-

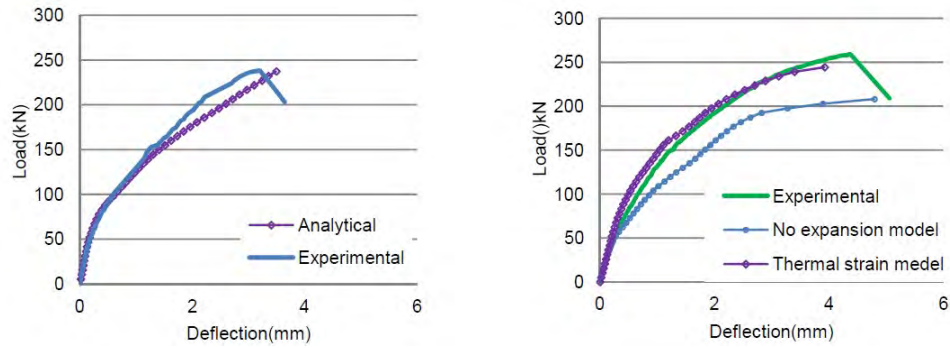


Figure 3.222: Load-deflection curves of beams; Wang and Morikawa (2012)

3.177 Winnicki, Andrzej and Serkega, Szymon (2017)

```
@inproceedings{
winnicki2017alkali},
label={winnicki2017alkali},
title={Alkali-Silica Reaction in concrete--numerical modelling: an engineering
approach},
author={Winnicki, Andrzej and Serkega, Szymon},
booktitle={2017 World Congress on Advances in Structural Engineering and
Mechanics},
year={2017}
Keywords={}
```

- The paper provides a chemo-mechanical model of ASR. Two models of first order kinetics are presented and the author's modifications to dependency of the models on variable temperature and humidity are discussed.
- A numerical algorithm, Figure 3.223, to solve chemo-mechanical problems is presented. The main advantage of this algorithm lies in that there is no need to build special FEM code in order to solve the problem.
- This model includes the effects of creep.
- The Fontana Gravity Dam was chosen for numerical analyses. It is located in North Carolina, USA, and its construction was finished in 1946.
- Three years after the end of completing, a pattern of cracking was first observed together with an upstream movement of the structure.
- Later inspections (1972) discovered large cracks inside the Dam.
- The analyzed cross-section of the Dam, together with the subsoil, is presented in Figure 3.224.
- The applied initial conditions with the imposed changes of thermal, hygral, and mechanical boundary conditions in a year period are also presented in the plot.

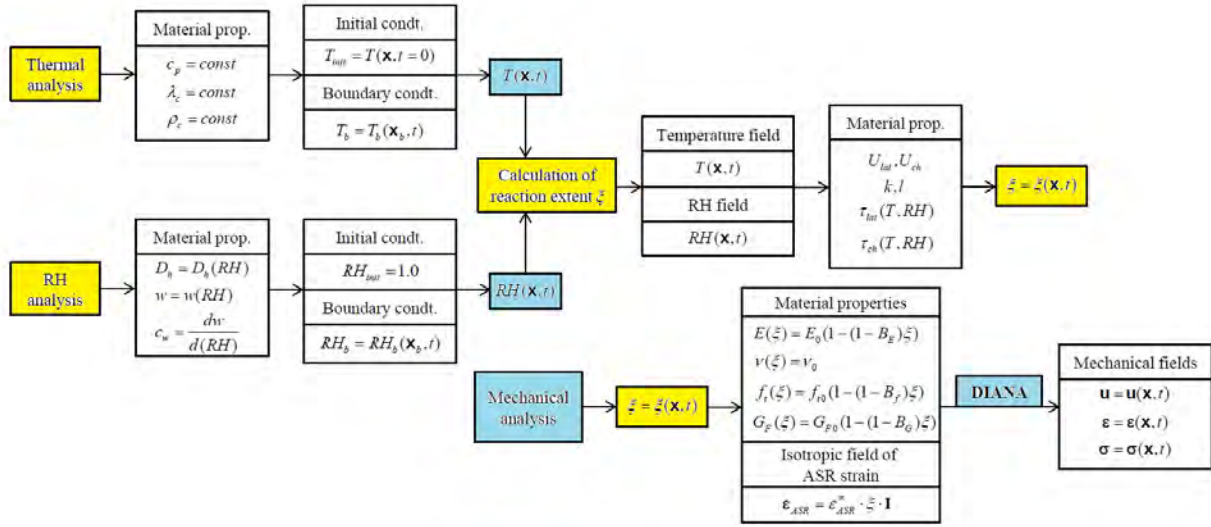


Figure 3.223: Computational algorithm; Winnicki and Serkega (2017)

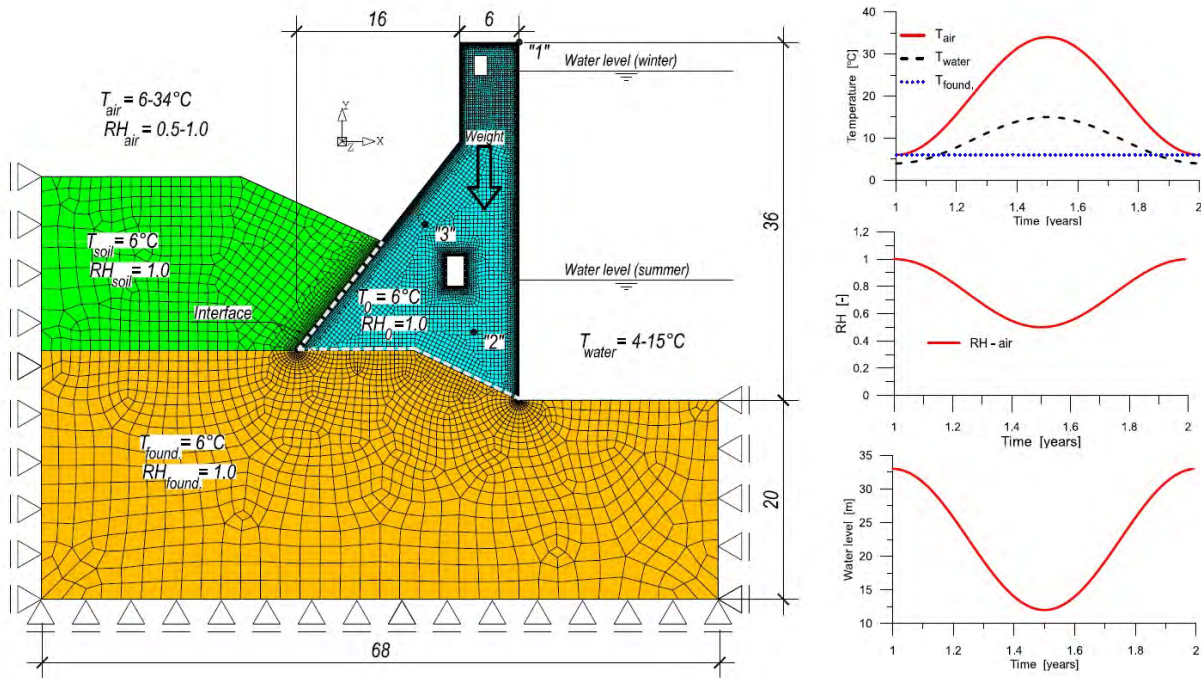


Figure 3.224: Cross section of Fontana Dam with foundation on subsoil; Winnicki and Serkega (2017)

- Analyses are in two parts: 1) the normal exploitation state of the Dam within time period of 30 years, and 2) the catastrophic situation in which the Dam is loaded until failure.
- Figure 3.225 illustrates the computed fields of relative humidity and temperature after 30 years in summer.
- The smeared crack approach in the form of a multidirectional fixed crack model is implemented

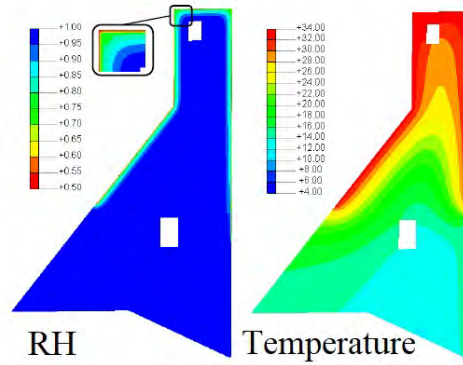


Figure 3.225: Relative humidity and temperature field after 30 years; Winnicki and Serkega (2017)

in FEM code.

- In Figure 3.226, the crack patterns after 30 years of ASR action are shown for the cases with and without creep effects. Creep effects result in reducing the cracked area mainly in the middle portion of the Dam.

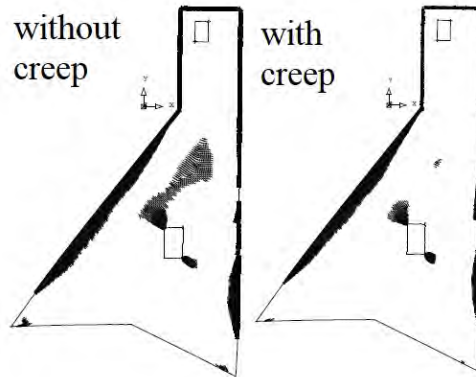


Figure 3.226: Relative humidity and temperature field after 30 years; Winnicki and Serkega (2017)

3.178 Yang, Huaquan and Li, Pengxiang and Rao, Meijuan (2017)

[URL](#)


```

@article{
yang2017long},
label={yang2017long},
title={Long term investigation and inhibition on alkali-aggregates reaction of
Three Gorges Dam concrete},
author={Yang, Huaquan and Li, Pengxiang and Rao, Meijuan},
journal={Construction and Building Materials},
volume={151},
pages={673--681},
year={2017},
publisher={Elsevier}
Keywords={}

```

- The long term behavior of AAR in Three Gorges Dam concrete was studied.
- The expansion rate of AAR is closely related to the time changes.
- The results of AAR were obtained from the observations recorded for a time period of about 20-30 years.
- The expansion rate accumulates as the age extends, and the maximum value of expansion rate can be observed only in certain periods.
- In particular, the peak in the curve of expansion rate appears in 13-16 years. Thereafter, the expansion rate of mortar has a declining trend, as shown in Figure 3.227.

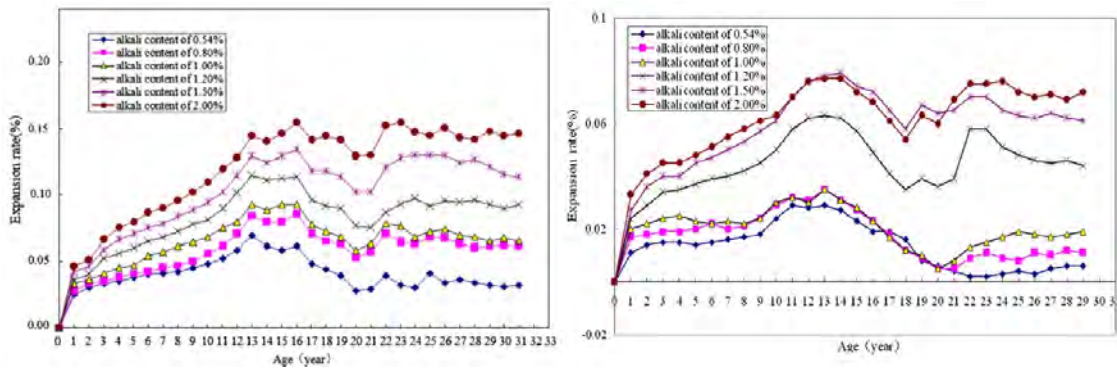


Figure 3.227: Mortar expansion curves of the plagioclase granite (left), and weakly weathered granite (right); Yang, Li, and Rao (2017)

- Micro analysis indicates that, although the expansion rate of mortar is over 0.1%, no apparent characteristics of AAR are apparent.

3.179 Zhang, Chengzhi and Wang, Aiqin and Tang, Mingshu and Wu, Bingqin and Zhang, Ningsheng (1999)

URL

```
@article{
zhang1999influence,
label={zhang1999influence},
title={Influence of aggregate size and aggregate size grading on ASR expansion},
author={Zhang, Chengzhi and Wang, Aiqin and Tang, Mingshu and Wu, Bingqin and
Zhang, Ningsheng},
journal={Cement and concrete research},
volume={29},
number={9},
pages={1393--1396},
year={1999},
publisher={Elsevier},
Keywords={},
DisplayPdf={0},
url={https://www.sciencedirect.com/science/article/pii/S000888469900099X}
```

- The influences of aggregate size and aggregate size grading on ASR expansion in the Chinese autoclave test were studied.
- The result shows that the effect of the addition of coarse aggregate on the expansion of mortar is complex.
- It may be inhibiting expansion, may have no effect, or may be promoting expansion. Its effect will change with age.
- By theoretic analysis of micromechanics, it is shown that the effect of coarse aggregate on the expansion of mortar depends on the relation between the free expansion of coarse aggregate and mortar.
- From the results of experimental and theoretic analyses, the authors suggest that for the evaluation of the alkali-reactivity of aggregate, single-size aggregate grading might be more reasonable.

Bibliography

- Abbas, Abdelgadir et al. (2007). “Proposed method for determining the residual mortar content of recycled concrete aggregates”. In: *Journal of ASTM International* 5.1, pp. 1–12.
- Ahmed, Tarig et al. (2003). “The effect of alkali reactivity on the mechanical properties of concrete”. In: *Construction and Building Materials* 17.2, pp. 123–144.
- Alnaggar, Mohammed, Gianluca Cusatis, and Giovanni Di Luzio (2013). “Lattice discrete particle modeling (LDPM) of alkali silica reaction (ASR) deterioration of concrete structures”. In: *Cement and Concrete Composites* 41, pp. 45–59.
- Alvarez, José Ignacio et al. (1999). “Methodology and validation of a hot hydrochloric acid attack for the characterization of ancient mortars”. In: *Cement and Concrete Research* 29.7, pp. 1061–1065.
- Amberg, F (2012). “A review of expanding concrete cases and consequences on dam performance”. In: *Hydro 2012 Conference, Bilbao*.
- Amberg, F, R Stucchi, and N Brizzo (2013). “The effect of temperature on the development of the Alkali Aggregate Reaction at the Pian Telesio dam”. In: *9th ICOLD European Club Symposium*.
- Amberg, Francesco (2011). “Performance of dams affected by expanding concrete”. In: *Dams and Reservoirs under Changing Challenges*, pp. 115–122.
- Amberg, Francesco et al. (2017). “Swelling Dams in Switzerland”. In: *Swelling Concrete in Dams and Hydraulic Structures: DSC 2017*, p. 40.
- Anaç, Caner et al. (2012). “A tool for concrete performance assessment for ASR affected structures: An outlook”. In: *Paper presented at: 14th International Conference on Alkali-Aggregate Reaction in Concrete, ICAAR, Austin, Texas, USA, May 20-25, 2012*.
- Bach, Finn, Torsten S Thorsen, and MP Nielsen (1993). “Load-carrying capacity of structural members subjected to alkali-silica reactions”. In: *Construction and Building Materials* 7.2, pp. 109–115.
- Bangert, F, D Kuhl, and G Meschke (2004). “Chemo-hygro-mechanical modelling and numerical simulation of concrete deterioration caused by alkali-silica reaction”. In: *International Journal for Numerical and Analytical Methods in Geomechanics* 28.7-8, pp. 689–714.
- Batista, António Lopes and J Piteira Gomes (2016). “Characteristic behaviour of the Portuguese large concrete dams built with granite aggregates and affected by ASR”. In:
- Bektas, Fatih and Kejin Wang (2012). “Performance of ground clay brick in ASR-affected concrete: Effects on expansion, mechanical properties and ASR gel chemistry”. In: *Cement and Concrete Composites* 34.2, pp. 273–278.
- Bérubé, Marc-André et al. (2002). “Laboratory assessment of alkali contribution by aggregates to concrete and application to concrete structures affected by alkali-silica reactivity”. In: *Cement and Concrete Research* 32.8, pp. 1215–1227.
- Berube, Marc-Andre et al. (2002). “Laboratory assessment of the potential rate of ASR expansion of field concrete”. In: *Cement, concrete and aggregates* 24.1, pp. 13–19.

- Bérubé, Marc-André et al. (2005). “Evaluation of the expansion attained to date by concrete affected by alkali–silica reaction. Part III: Application to existing structures”. In: *Canadian Journal of Civil Engineering* 32.3, pp. 463–479.
- Blanco, A et al. (2018). “Expansions with different origins in a concrete dam with bridge over spillway”. In: *Construction and Building Materials* 163, pp. 861–874.
- Braga Reis, MO, HS Silva, and A Santos Silva (1996). “Ocorrência de reações álcalis-inerte em Portugal”. In: *Estudos de Casos, Atas do Encontro Nacional Betão Estrutural*, pp. 2–37.
- Capra, B and J-P Bournazel (1998). “Modeling of induced mechanical effects of alkali-aggregate reactions”. In: *Cement and Concrete Research* 28.2, pp. 251–260.
- Capra, Bruno and Alain Sellier (2003). “Orthotropic modelling of alkali-aggregate reaction in concrete structures: numerical simulations”. In: *Mechanics of materials* 35.8, pp. 817–830.
- Cardoso, Fábio A et al. (2009). “Carbide lime and industrial hydrated lime characterization”. In: *Powder Technology* 195.2, pp. 143–149.
- Carles-Gibergues, André and Martin Cyr (2002). “Interpretation of expansion curves of concrete subjected to accelerated alkali–aggregate reaction (AAR) tests”. In: *Cement and concrete research* 32.5, pp. 691–700.
- Carol, I (1994). “NUMERICAL STUDIES OF TWO GRAVITY DAMS SUBJECTED TO DIFFERENTIAL EXPANSION OF THE MICROSTRUCTURE”. In:
- Charlwood, RG, SV Solymar, and DD Curtis (1992). “A review of alkali aggregate reactions in hydroelectric plants and dams”. In: *Proceedings of the international conference of alkali-aggregate reactions in hydroelectric plants and dams*. Vol. 129.
- Chen, Jun et al. (2010). “Rapid evaluation of alkali–silica reactivity of aggregates using a nonlinear resonance spectroscopy technique”. In: *Cement and Concrete Research* 40.6, pp. 914–923.
- Chrisp, TM, P Waldron, and JGM Wood (1993). “Development of a non-destructive test to quantify damage in deteriorated concrete”. In: *Magazine of Concrete Research* 45.165, pp. 247–256.
- Chulliat, O., E. Grimal, and E. Bourdarot (2017). “Chambon Dam”. In: *Swelling Concrete in Dams and Hydraulic Structures: DSC 2017*. Ed. by Alain Sellier et al. John Wiley & Sons.
- Cima, J. and B. Reinicker (2015). “Concrete Growth at Roanoke Rapis Dam”. In: *Hydro Review*.
- Comby-Peyrot, Isabelle et al. (2009). “Development and validation of a 3D computational tool to describe concrete behaviour at mesoscale. Application to the alkali-silica reaction”. In: *Computational Materials Science* 46.4, pp. 1163–1177.
- Comi, C, R Fedele, and U Perego (2009). “A chemo-thermo-damage model for the analysis of concrete dams affected by alkali-silica reaction”. In: *Mechanics of Materials* 41.3, pp. 210–230.
- Comi, Claudia, Beatrice Kirchmayr, and Rossella Pignatelli (2012). “Two-phase damage modeling of concrete affected by alkali–silica reaction under variable temperature and humidity conditions”. In: *International Journal of Solids and Structures* 49.23-24, pp. 3367–3380.
- Coubard, G. and J. Sausse (2017). “Swelling Arch Dams with Thrust Blocks”. In: *Swelling Concrete in Dams and Hydraulic Structures: DSC 2017*. Ed. by Alain Sellier et al. John Wiley & Sons.
- Criaud, A and C Defossé (1995). “Evaluating the reaction of actual compositions of concrete with respect to alkali-aggregate reactions preliminary testing at 110° C and 150° C”. In: *Materials and Structures* 28.1, pp. 32–42.
- Crouch, RS and JGM Wood (1990). “Damage evolution in AAR affected concretes”. In: *Engineering Fracture Mechanics* 35.1-3, pp. 211–218.
- Curtis, D. et al. (2005). “Updated Assessment of Concrete Growth Effects on a TVA Dam”. In: *USSD 2005 Conference, Salt Lake City, UT, June*.
- Curtis, DD (1995). *Modeling of AAR affected structures using the GROW3D FEA program*. Tech. rep. Committee on Large Dams, Denver, CO (United States).

- Custódio, J. et al. (2017). “The diagnosis and prognosis of ASR and ISR in Miranda dam, Portugal”. In: *Swelling Concrete in Dams and Hydraulic Structures: DSC 2017*. Ed. by Alain Sellier et al. John Wiley & Sons.
- De Juan, Marta Sánchez and Pilar Alaejos Gutiérrez (2009). “Study on the influence of attached mortar content on the properties of recycled concrete aggregate”. In: *Construction and Building Materials* 23.2, pp. 872–877.
- Deloye, FX, G Maire, and MJ Buisson (1979). “Analyse des bétons durcis à partir d’une attaque nitrique”. In: *BULL LIAISON LAB PONTS CHAUSS* 104.
- Diamond, S and N Thaulow (1974). “A study of expansion due to alkali-silica reaction as conditioned by the grain size of the reactive aggregate”. In: *Cement and Concrete Research* 4.4, pp. 591–607.
- Dolen, T. (2005a). “Materials Properties Model of Aging Concrete”. In: Report DSO-05-05. URL: <https://www.usbr.gov/ssle/damsafety/TechDev/DSOTechDev/DSO-05-05.pdf>.
- Dolen, TP (2005b). *Materials properties model for aging concrete. Bureau of Reclamation Dam Safety Program Report No.* Tech. rep. DSO-05-05. USBR, Colorado Google Scholar.
- (2011). “Selecting strength input parameters for structural analysis of aging concrete dams”. In: *Proceedings of the 31st USSD Annual Conference*.
- Donghi, G., C. Marcello, and F. Sainati (2013). “Behaviour of the Poggia dam after 7 years from the completion of remedial works, carried out in order to reduce the effects of AAR process”. In: *9th ICOLD European Club Symposium*.
- Dunant, Cyrille F and Karen L Scrivener (2010). “Micro-mechanical modelling of alkali-silica-reaction-induced degradation using the AMIE framework”. In: *Cement and Concrete research* 40.4, pp. 517–525.
- (2012a). “Effects of aggregate size on alkali-silica-reaction induced expansion”. In: *Cement and concrete research* 42.6, pp. 745–751.
- (2012b). “Effects of uniaxial stress on alkali-silica reaction induced expansion of concrete”. In: *Cement and concrete research* 42.3, pp. 567–576.
- (2016). “Physically based models to study the alkali-silica reaction”. In: *Proceedings of the institution of Civil Engineers-Construction Materials* 169.3, pp. 136–144.
- Eguchi, Kiyoshi et al. (2007). “Application of recycled coarse aggregate by mixture to concrete construction”. In: *Construction and Building Materials* 21.7, pp. 1542–1551.
- Esposito, R and MAN Hendriks (2017). “Literature review of modelling approaches for ASR in concrete: a new perspective”. In: *European Journal of Environmental and Civil Engineering*, pp. 1–21.
- Esposito, Rita and Max AN Hendriks (2016). “A multiscale micromechanical approach to model the deteriorating impact of alkali-silica reaction on concrete”. In: *Cement and Concrete Composites* 70, pp. 139–152.
- Esposito, Rita et al. (2016). “Influence of the alkali-silica reaction on the mechanical degradation of concrete”. In: *Journal of Materials in Civil Engineering* 28.6, p. 04016007.
- Fairbairn, Eduardo MR et al. (2006). “Modelling the structural behaviour of a dam affected by alkali-silica reaction”. In: *International Journal for Numerical Methods in Biomedical Engineering* 22.1, pp. 1–12.
- Fan, Shenfu and John M Hanson (1998). “Effect of alkali silica reaction expansion and cracking on structural behavior of reinforced concrete beams”. In: *ACI Structural Journal* 95, pp. 498–505.
- Farage, MCR, JLD Alves, and EMR Fairbairn (2004). “Macroscopic model of concrete subjected to alkali-aggregate reaction”. In: *Cement and Concrete Research* 34.3, pp. 495–505.
- Ferche, Anca C et al. (2017). “Toward Macro-Modeling of Alkali-Silica Reaction-Affected Structures”. In: *ACI Structural Journal* 114.5, p. 1121.

- Fernandes, Isabel, Fernando Noronha, and Madalena Teles (2004). “Microscopic analysis of alkali–aggregate reaction products in a 50-year-old concrete”. In: *Materials Characterization* 53.2-4, pp. 295–306.
- (2007). “Examination of the concrete from an old Portuguese dam: texture and composition of alkali–silica gel”. In: *Materials Characterization* 58.11-12, pp. 1160–1170.
- Ferreira, Anna Paula Guida, Michèle Cristina Resende Farage, and Flávio de Souza Barbosa (2013). “Modelling of the mechanical behavior of concrete affected by alkali–aggregate reaction”. In: *Rem: Revista Escola de Minas* 66.1, pp. 35–40.
- FHWA (2010). *Report on the Diagnostis, Prognosis, and Mitigation of Alkali-Silica Reaction (ASR) in Transportation Structures*. Tech. rep. FHWA-HIF-09-004. Federal Highway Administration. URL: <https://www.fhwa.dot.gov/pavement/concrete/pubs/hif09004/hif09004.pdf>.
- FHWA (2013). *Alkali-Aggregate Reactivity (AAR) Facts Book*. Tech. rep. FHWA-HIF-13-019. Federal Highway Administration. URL: <https://www.fhwa.dot.gov/pavement/concrete/asr/pubs/hif13019.pdf>.
- Figg, John (1974). “Microwave heating in concrete analysis”. In: *Journal of Applied Chemistry and Biotechnology* 24.3, pp. 143–155.
- Fournier, Benoit and Marc-André Bérubé (2000). “Alkali–aggregate reaction in concrete: a review of basic concepts and engineering implications”. In: *Canadian Journal of Civil Engineering* 27.2, pp. 167–191.
- Fournier, Benoit et al. (2004). “The accelerated concrete prism test (60 C): variability of the test method and proposed expansion limits”. In: *Proc. of the 12th Int. Conf. on AAR in Concrete, Beijing (China)*, pp. 314–323.
- Fournier, Benoit et al. (2009). “Effect of environmental conditions on expansion in concrete due to alkali–silica reaction (ASR)”. In: *Materials Characterization* 60.7, pp. 669–679.
- Gao, Xiao Xiao et al. (2011). “Optimising an expansion test for the assessment of alkali–silica reaction in concrete structures”. In: *Materials and structures* 44.9, pp. 1641–1653.
- Gao, Xiao Xiao et al. (2013a). “A three-step method for the recovery of aggregates from concrete”. In: *Construction and Building Materials* 45, pp. 262–269.
- Gao, Xiao Xiao et al. (2013b). “Alkali–silica reaction (ASR) expansion: pessimum effect versus scale effect”. In: *Cement and Concrete Research* 44, pp. 25–33.
- Gao, XX et al. (2013c). “A comparison of methods for chemical assessment of reactive silica in concrete aggregates by selective dissolution”. In: *Cement and Concrete Composites* 37, pp. 82–94.
- Garcia-Diaz, E et al. (2006). “Mechanism of damage for the alkali–silica reaction”. In: *Cement and Concrete Research* 36.2, pp. 395–400.
- Gautam, Bishnu P and Daman K Panesar (2017). “The effect of elevated conditioning temperature on the ASR expansion, cracking and properties of reactive Spratt aggregate concrete”. In: *Construction and Building Materials* 140, pp. 310–320.
- Gautam, Bishnu Prasad (2016). “Multiaxially Loaded Concrete Undergoing Alkali-Silica Reaction (ASR)”. PhD thesis. University of Toronto (Canada).
- Gholizadeh-Vayghan, Asghar and Farshad Rajabipour (2017). “The influence of alkali–silica reaction (ASR) gel composition on its hydrophilic properties and free swelling in contact with water vapor”. In: *Cement and Concrete Research* 94, pp. 49–58.
- Ghrib, Faouzi and Rene Tinawi (1995). “An application of damage mechanics for seismic analysis of concrete gravity dams”. In: *Earthquake Engineering & Structural Dynamics* 24.2, pp. 157–173.
- Giaccio, G et al. (2008). “Mechanical behavior of concretes damaged by alkali–silica reaction”. In: *Cement and Concrete Research* 38.7, pp. 993–1004.

- Giorla, Alain B, Karen L Scrivener, and Cyrille F Dunant (2015). “Influence of visco-elasticity on the stress development induced by alkali–silica reaction”. In: *Cement and Concrete Research* 70, pp. 1–8.
- Gocevski, V. and E. Yildiz (2017). “Numerical Analysis of AAR Affected Structures with Slot-Cuts”. In: *Swelling Concrete in Dams and Hydraulic Structures: DSC 2017*. Ed. by Alain Sellier et al. John Wiley & Sons.
- Godart, B et al. (2004). *The guide for aiding to the management of structures damaged by concrete expansion in France*. in French. LCPC/IFSTTAR. URL: <http://www.ifsttar.fr/Utils/librairie/getdocument.php?d=GuideTechnique-LCPC-GONFLIN.pdf>.
- Godart, Bruno, Mario Robert de Rooij, and Jonathan GM Wood (2013). *Guide to diagnosis and appraisal of AAR damage to concrete in structures*. Springer.
- Gong, Fuyuan, Yuya Takahashi, and Koichi Maekawa (2017). “Strong coupling of freeze-thaw cycles and alkali silica reaction-multi-scale poro-mechanical approach to concrete damages”. In: *Journal of Advanced Concrete Technology* 15.7, pp. 346–367.
- Grattan-Bellew, PE (1995). “Laboratory evaluation of alkali-silica reaction in concrete from Saunders Generating Station”. In: *Materials Journal* 92.2, pp. 126–134.
- Grimal, Etienne et al. (2008). “Creep, shrinkage, and anisotropic damage in alkali-aggregate reaction swelling mechanism-Part I A constitutive model”. In: *ACI Materials Journal* 105.3, p. 227.
- Guilloteau, T., F. Martinot, and J. Sausse (2017). “Long-Term Behaviour of EDF Dams Regarding Concrete Swelling Structures”. In: *Swelling Concrete in Dams and Hydraulic Structures: DSC 2017*. Ed. by Alain Sellier et al. John Wiley & Sons.
- Gunn, R., K. Scrivener, and A. Leemann (2017). “The Identification, Extent and Prognosis of Alkali-Aggregate Reaction Related to Existing Dams in Switzerland”. In: *Swelling Concrete in Dams and Hydraulic Structures: DSC 2017*. Ed. by Alain Sellier et al. John Wiley & Sons.
- Haha, M Ben et al. (2007). “Relation of expansion due to alkali silica reaction to the degree of reaction measured by SEM image analysis”. In: *Cement and Concrete Research* 37.8, pp. 1206–1214.
- Hariri-Ardebili, Mohammad Amin and Victor E Saouma (2018). “Sensitivity and uncertainty analysis of AAR affected reinforced concrete shear walls”. In: *Engineering Structures* 172, pp. 334–345.
- Hariri-Ardebili, Mohammad Amin, Victor E Saouma, and Christine Merz (2018). “Risk-Informed Condition Assessment of a Bridge with Alkali-Aggregate Reaction.” In: *ACI Structural Journal* 115.2.
- Hattingh, L. et al. (2017). “Important Lessons Learnt from the Proper Surveillance of Swelling Concrete”. In: *Swelling Concrete in Dams and Hydraulic Structures: DSC 2017*. Ed. by Alain Sellier et al. John Wiley & Sons.
- Hayes, Nolan Wesley et al. (2018). “Monitoring Alkali-Silica Reaction Significance in Nuclear Concrete Structural Members”. In: *Journal of Advanced Concrete Technology* 16.4, pp. 179–190.
- Hefny, A, KY Lo, and L Adeghe (2001). “Measurements of laboratory rates of concrete expansion and their comparisons with field rates”. In: *Canadian Journal of Civil Engineering* 28.3, pp. 402–410.
- Heidarzadeh, N et al. (2017). “LONG-RUN EFFECT OF ALKALI-SILICA REACTIONS ON THE STRUCTURAL INTEGRITY OF A MULTI-STORY REINFORCED CONCRETE BUILDING”. In: *ASIAN JOURNAL OF CIVIL ENGINEERING (BHRC)* 18.8, pp. 1315–1328.
- Helene, Paulo, Mariana Carvalho, and Jéssika Pacheco (2017). “Engineering field tests for alkali-aggregate reaction”. In: *Structural Concrete* 18.2, pp. 349–355.

- Helmuth, R. et al. (2013). *Alkali-Silica Reactivity: An Overview of Research*. Tech. rep. FHWA-HIF-13-019. Strategic Highway Research Program. URL: <http://onlinepubs.trb.org/onlinepubs/shrp/SHRP-C-342.pdf>.
- Herrador, Manuel F, Fernando Martínez-Abella, and Juan Ramón Rabuñal Dopico (2008). “Experimental evaluation of expansive behavior of an old-aged ASR-affected dam concrete: methodology and application”. In: *Materials and Structures* 41.1, pp. 173–188.
- Huang, H, BW Spencer, and G Cai (2015). *Grizzly model of multi-species reactive diffusion, moisture/heat transfer and alkali-silica reaction in concrete*. Tech. rep. Technical Report INL/EXT-15-36425, Idaho National Laboratory, Idaho Falls, ID.
- Huang, Hai and Benjamin W Spencer (2016). *Grizzly model of fully coupled heat transfer, moisture diffusion, alkali-silica reaction and fracturing processes in concrete*. Tech. rep. Idaho National Lab.(INL), Idaho Falls, ID (United States).
- Huang, M and S Pietruszczak (1996). “Numerical analysis of concrete structures subjected to alkali-aggregate reaction”. In: *Mechanics of Cohesive-frictional Materials: An International Journal on Experiments, Modelling and Computation of Materials and Structures* 1.4, pp. 305–319.
- Huang, Maosong and S Pietruszczak (1999). “Modeling of thermomechanical effects of alkali-silica reaction”. In: *Journal of engineering mechanics* 125.4, pp. 476–485.
- Ichikawa, Tsuneki and Takahide Kimura (2007). “Effect of nuclear radiation on alkali-silica reaction of concrete”. In: *Journal of Nuclear Science and Technology* 44.10, pp. 1281–1284.
- Ideker, Jason H et al. (2010). “The current state of the accelerated concrete prism test”. In: *Cement and Concrete Research* 40.4, pp. 550–555.
- Ingraffea, AR (1990). “Case studies of simulation of fracture in concrete dams”. In: *Engineering Fracture Mechanics* 35.1-3, pp. 553–564.
- Islam, Mohammad S and Nader Ghafoori (2015). “Relation of ASR-induced expansion and compressive strength of concrete”. In: *Materials and Structures* 48.12, pp. 4055–4066.
- Jensen, Viggo (2004). “Alkali-silica reaction damage to Elgeseter Bridge, Trondheim, Norway: a review of construction, research and repair up to 2003”. In: *Materials characterization* 53.2-4, pp. 155–170.
- (2012). “Reclassification of alkali aggregate reaction”. In: *Proceedings of the 14th Conference on Alkali-Aggregate Reaction in Concrete*.
- Ju, Taeho et al. (2017). “Ultrasonic nondestructive evaluation of alkali-silica reaction damage in concrete prism samples”. In: *Materials and Structures* 50.1, p. 60.
- Jurcut, Anca-Cristina (2015). “Modelling of alkali-aggregate reaction effects in reinforced concrete structures”. MA thesis. University of Toronto (Canada).
- Kagimoto, Hiroyuki, Yukihiro Yasuda, and Mitsunori Kawamura (2014). “ASR expansion, expansive pressure and cracking in concrete prisms under various degrees of restraint”. In: *Cement and Concrete Research* 59, pp. 1–15.
- Kobayashi, Kazuo et al. (1988). “Alkali aggregate reaction in prestressed concrete beams”. In: *International Journal of Cement Composites and Lightweight Concrete* 10.4, pp. 233–240.
- Kubat, T, R Al-Mahaidi, and A Shayan (2014a). “Effect of CFRP wrapping time on rehabilitation of concrete damaged by alkali aggregate reaction”. In:
- (2014b). *Rehabilitation of alkali-aggregate reaction-damaged bridge columns using CFRP composites*.
- Kubat, Thamer, Riadh Al-Mahaidi, and Ahmad Shayan (2016). “Strain development in CFRP-wrapped circular concrete columns affected by alkali-aggregate reaction”. In: *Construction and Building Materials* 113, pp. 603–612.

- Lamea, M and H Mirzabozorg (2015). “Evaluating Sensitivity of an AAR-Affected Concrete Arch Dam to the Effects of Structural Joints and Solar Radiation”. In: *Strength of Materials* 47.2, pp. 341–354.
- Lan, H. and S. Piot (2011). “A new approach for large structures monitoring: SCANSITES 3D”. In: *Dams and reservoirs under changing challenges*. Ed. by Anton J Schleiss and Robert M Boes. CRC press.
- Larsen, Svein et al. (2008). “Experiences from extensive condition survey and FEM-analyses of two norwegian concrete dams with ASR”. In: *Proceedings of the 13th International Conference on Alkali-Aggregate Reaction in Concrete*. Citeseer Trondheim, Norway.
- Leemann, A and P Lura (2013). “E-modulus of the alkali–silica-reaction product determined by micro-indentation”. In: *Construction and Building Materials* 44, pp. 221–227.
- Leemann, Andreas and Michele Griffa (2013). “Diagnosis of alkali-aggregate reaction in dams”. In: *EMPA, Materials Science & Technology*.
- Leemann, Andreas and Christine Merz (2013). “An attempt to validate the ultra-accelerated microbar and the concrete performance test with the degree of AAR-induced damage observed in concrete structures”. In: *Cement and Concrete Research* 49, pp. 29–37.
- Leroy, R. et al. (2011). “Re-assessment and treatment-design of an ASR-affected gravity dam”. In: *Dams and reservoirs under changing challenges*. Ed. by Anton J Schleiss and Robert M Boes. CRC press.
- Leśnicki, Krzysztof J et al. (2011). “Characterization of ASR damage in concrete using nonlinear impact resonance acoustic spectroscopy technique”. In: *NDT & E International* 44.8, pp. 721–727.
- (2013). “Assessment of alkali–silica reaction damage through quantification of concrete nonlinearity”. In: *Materials and structures* 46.3, pp. 497–509.
- Li, Shiqyn, Della M Roy, and Amitabha Kumar (1985). “Quantatative determination of pozzolanas in hydrated systems of cement or Ca (OH) 2 with fly ash or silica fume”. In: *Cement and Concrete Research* 15.6, pp. 1079–1086.
- Liaudat, Joaquín et al. (2015). “Numerical modelling of ASR expansions in concrete”. In: *CON-CREEP 10*, pp. 445–454.
- Liaudat, Joaquín et al. (2017). “ASR expansions in concrete under triaxial confinement”. In: *Cement and Concrete Composites*.
- Lindgård, Jan et al. (2010). “The EU “PARTNER” Project-European standard tests to prevent alkali reactions in aggregates: final results and recommendations”. In: *Cement and Concrete Research* 40.4, pp. 611–635.
- Lindgård, Jan et al. (2012). “Alkali–silica reactions (ASR): literature review on parameters influencing laboratory performance testing”. In: *Cement and Concrete Research* 42.2, pp. 223–243.
- Lindgård, Jan et al. (2013a). “Alkali–silica reaction (ASR)-performance testing: influence of specimen pre-treatment, exposure conditions and prism size on alkali leaching and prism expansion”. In: *Cement and Concrete Research* 53, pp. 68–90.
- Lindgård, Jan et al. (2013b). “Alkali–silica reaction (ASR)-performance testing: influence of specimen pre-treatment, exposure conditions and prism size on concrete porosity, moisture state and transport properties”. In: *Cement and Concrete Research* 53, pp. 145–167.
- Liu, Kai-Wei and Anol K Mukhopadhyay (2015). “Accelerated Concrete-Cylinder Test for Alkali–Silica Reaction”. In: *Journal of Testing and Evaluation* 44.3, pp. 1229–1238.
- Lu, Duyou et al. (2006). “Evaluation of laboratory test method for determining the potential alkali contribution from aggregate and the ASR safety of the Three-Gorges dam concrete”. In: *Cement and concrete research* 36.6, pp. 1157–1165.

- Marzouk, H and S Langdon (2003). “The effect of alkali-aggregate reactivity on the mechanical properties of high and normal strength concrete”. In: *Cement and Concrete Composites* 25.4-5, pp. 549–556.
- Merz, Christine and Andreas Leemann (2013). “Assessment of the residual expansion potential of concrete from structures damaged by AAR”. In: *Cement and concrete research* 52, pp. 182–189.
- Metalssi, Othman Omikrine et al. (2014). “Modeling the cracks opening–closing and possible remedial sawing operation of AAR-affected dams”. In: *Engineering Failure Analysis* 36, pp. 199–214.
- Mirzabozorg, H. et al. (2014). “Mathematical Modeling and Numerical Analysis of Thermal Distribution in Arch Dams Considering Solar Radiation Effect”. In: *The Scientific World Journal* 2014.
- Miyagawa, Toyooki et al. (2006). “Fracture of Reinforcing Steels in Concrete Structures Damaged by Alkali-Silica Reaction”. In: *Journal of Advanced Concrete Technology* 4.3, pp. 339–355.
- Moranville-Regourd, Michelle (1997). “Modelling of expansion induced by ASR-New approaches”. In: *Cement and Concrete Composites* 19.5-6, pp. 415–425.
- Morenon, P. et al. (2018). “Modelling, assessment and rehabilitation of a dam affected by an internal swelling reaction (ISR)”. In: *Dam Engineering*.
- Morenon, Pierre et al. (2017). “Impact of stresses and restraints on ASR expansion”. In: *Construction and Building Materials* 140, pp. 58–74.
- Mukhopadhyay, Anal, Chang-Seon Shon, and Dan Zollinger (2006). “Activation energy of alkali-silica reaction and dilatometer method”. In: *Transportation Research Record: Journal of the Transportation Research Board* 1979, pp. 1–11.
- Mullick, AK (1988). “Distress in a concrete gravity dam due to alkali silica reaction”. In: *International Journal of Cement Composites and Lightweight Concrete* 10.4, pp. 225–232.
- Multon, S, J-F Seignol, and F Toutlemonde (2005). “Structural behavior of concrete beams affected by alkali-silica reaction”. In: *Materials Journal* 102.2, pp. 67–76.
- Multon, Stéphane, Jean-François Seignol, and François Toutlemonde (2006). “Chemomechanical assessment of beams damaged by alkali-silica reaction”. In: *Journal of materials in civil engineering* 18.4, pp. 500–509.
- Multon, Stéphane, Alain Sellier, and Martin Cyr (2009). “Chemo–mechanical modeling for prediction of alkali silica reaction (ASR) expansion”. In: *Cement and Concrete Research* 39.6, pp. 490–500.
- Multon, Stéphane and François Toutlemonde (2006). “Effect of applied stresses on alkali–silica reaction-induced expansions”. In: *Cement and Concrete Research* 36.5, pp. 912–920.
- (2010). “Effect of moisture conditions and transfers on alkali silica reaction damaged structures”. In: *Cement and Concrete Research* 40.6, pp. 924–934.
- Multon, Stéphane et al. (2008a). “Coupled effects of aggregate size and alkali content on ASR expansion”. In: *Cement and Concrete Research* 38.3, pp. 350–359.
- Multon, Stéphane et al. (2008b). “Estimation of the residual expansion of concrete affected by alkali silica reaction”. In: *Journal of Materials in Civil Engineering* 20.1, pp. 54–62.
- Multon, Stéphane et al. (2010). “Effects of aggregate size and alkali content on ASR expansion”. In: *Cement and Concrete Research* 40.4, pp. 508–516.
- Na, Okpin et al. (2016). “The effects of alkali-silica reaction on the mechanical properties of concretes with three different types of reactive aggregate”. In: *Structural Concrete* 17.1, pp. 74–83.
- Nagataki, S et al. (2004). “Assessment of recycling process induced damage sensitivity of recycled concrete aggregates”. In: *Cement and Concrete Research* 34.6, pp. 965–971.

- Nägele, E and HK Hilsdorf (1980). “A new method for cement content determination of fresh concrete”. In: *Cement and Concrete Research* 10.1, pp. 23–34.
- Nik-Azizan, N.Z. et al. (2017). “Numerical prediction of stress and displacement of ageing concrete dam due to alkali-aggregate and thermal chemical reaction”. In: *Structural Engineering and Mechanics* 64.6, pp. 793–802.
- Noret, C. and K. Laliche (2017). “Bimont Dam Case; Studies and Investigations Inside the Dam Body”. In: *Swelling Concrete in Dams and Hydraulic Structures: DSC 2017*. Ed. by Alain Sellier et al. John Wiley & Sons.
- Ohsawa, S et al. (1985). “Quantitative determination of fly ash in the hydrated fly ash-CaSO₄”. In: *Cement and Concrete Research* 15.2, pp. 357–366.
- Orbovic, N. et al. (2015). “Alkali Aggregate Reaction in Nuclear Concrete Structures: Part 1: A Holistic Approach”. In: *Proceedings of the 23rd Conference on Structural Mechanics in Reactor Technology (SMiRT23)*.
- Ostertag, Claudia P, ChongKu Yi, and Paulo JM Monteiro (2007). “Effect of confinement on properties and characteristics of alkali-silica reaction gel”. In: *ACI materials journal* 104.3, p. 276.
- Pan, JianWen et al. (2013a). “Chemo-damage modeling and cracking analysis of AAR-affected concrete dams”. In: *Science China Technological Sciences* 56.6, pp. 1449–1457.
- Pan, Jianwen et al. (2013b). “Numerical prediction of swelling in concrete arch dams affected by alkali-aggregate reaction”. In: *European Journal of Environmental and Civil Engineering* 17.4, pp. 231–247.
- Pan, JW et al. (2012). “Modeling of alkali-silica reaction in concrete: a review”. In: *Frontiers of Structural and Civil Engineering* 6.1, pp. 1–18.
- Parvini, M, S Pietruszczak, and V Gocevski (2001). “Seismic analysis of hydraulic structures affected by alkali-aggregate reaction: a case study”. In: *Canadian Journal of Civil Engineering* 28.2, pp. 332–338.
- Plusquellec, G et al. (2018). “Determining the free alkali metal content in concrete—Case study of an ASR-affected dam”. In: *Cement and Concrete Research*.
- Poyet, Stéphane (2003). “Etude de la dégradation des ouvrages en béton atteints par la réaction alcali-silice—approche expérimentale et modélisation numérique des dégradations dans un environnement hydro-chemo-mécanique variable”. PhD thesis. Université de Marne la Vallée.
- Poyet, Stéphane et al. (2006). “Influence of water on alkali-silica reaction: Experimental study and numerical simulations”. In: *Journal of Materials in civil Engineering* 18.4, pp. 588–596.
- Rajabipour, Farshad et al. (2015). “Alkali-silica reaction: current understanding of the reaction mechanisms and the knowledge gaps”. In: *Cement and Concrete Research* 76, pp. 130–146.
- Reclamation (1941). *Alkalies in Cement and Their Effect on Aggregates and Concrete*. Tech. rep.
- Reinicker, B. et al. (2010). “Alkali-Silica Reactivity At Roanoke Rapids Dam Unique Remedial Design Challenges”. In: *USSD 2010 Conference*. Sacramento, CA, pp. 367–390.
- Reinicker, B. et al. (2013). “An Advanced Model for Simulation of ASR Behavior at Roanoke Rapids Dam”. In: *USSD 2013 Conference*. Phoenix, AZ, pp. 127–147.
- Rivard, Patrice, Benoit Fournier, and Gérard Ballivy (2000). “Quantitative petrographic technique for concrete damage due to ASR: experimental and application”. In: *Cement, Concrete and Aggregates* 22.1, pp. 63–72.
- (2002). “The damage rating index method for ASR affected concrete—a critical review of petrographic features of deterioration and evaluation criteria”. In: *Cement, concrete and aggregates* 24.2, pp. 1–11.

- Rivard, Patrice and François Saint-Pierre (2009). “Assessing alkali-silica reaction damage to concrete with non-destructive methods: From the lab to the field”. In: *Construction and Building Materials* 23.2, pp. 902–909.
- Rivard, Patrice et al. (2010). “Monitoring of an hydraulic structure affected by ASR: A case study”. In: *Cement and concrete research* 40.4, pp. 676–680.
- Roelfstra, PE, H Sadouki, and FH Wittmann (1985). “Le béton numérique”. In: *Materials and Structures* 18.5, pp. 327–335.
- Šachlová, Šárka, Richard Přikryl, and Zdeněk Pertold (2010). “Alkali-silica reaction products: Comparison between samples from concrete structures and laboratory test specimens”. In: *Materials Characterization* 61.12, pp. 1379–1393.
- Sanchez, LFM et al. (2014). “Evaluation of the stiffness damage test (SDT) as a tool for assessing damage in concrete due to ASR: test loading and output responses for concretes incorporating fine or coarse reactive aggregates”. In: *Cement and concrete research* 56, pp. 213–229.
- (2015a). “Evaluation of the Stiffness Damage Test (SDT) as a tool for assessing damage in concrete due to alkali-silica reaction (ASR): Input parameters and variability of the test responses”. In: *Construction and Building Materials* 77, pp. 20–32.
- Sanchez, LFM et al. (2015b). “Reliable quantification of AAR damage through assessment of the Damage Rating Index (DRI)”. In: *Cement and Concrete Research* 67, pp. 74–92.
- Sanchez, LFM et al. (2016a). “Practical use of the Stiffness Damage Test (SDT) for assessing damage in concrete infrastructure affected by alkali-silica reaction”. In: *Construction and Building Materials* 125, pp. 1178–1188.
- Sanchez, LFM et al. (2016b). “Use of Damage Rating Index to Quantify Alkali-Silica Reaction Damage in Concrete: Fine versus Coarse Aggregate.” In: *ACI Materials Journal* 113.4.
- Sanchez, LFM et al. (2017). “Overall assessment of Alkali-Aggregate Reaction (AAR) in concretes presenting different strengths and incorporating a wide range of reactive aggregate types and natures”. In: *Cement and Concrete Research* 93, pp. 17–31.
- Saouma, Victor and Luigi Perotti (2006). “Constitutive model for alkali-aggregate reactions”. In: *ACI materials journal* 103.3, p. 194.
- Saouma, Victor, Luigi Perotti, and Takashi Shimpo (2007). “Stress analysis of concrete structures subjected to alkali-aggregate reactions”. In: *ACI structural journal* 104.5, p. 532.
- Saouma, Victor E and Mohammad A Hariri-Ardebili (2014). “A proposed aging management program for alkali silica reactions in a nuclear power plant”. In: *Nuclear Engineering and Design* 277, pp. 248–264.
- Saouma, Victor E et al. (2015). “A mathematical model for the kinetics of the alkali-silica chemical reaction”. In: *Cement and Concrete Research* 68, pp. 184–195.
- Saouma, Victor E et al. (2016). “Effect of alkali-silica reaction on the shear strength of reinforced concrete structural members. A numerical and statistical study”. In: *Nuclear Engineering and Design* 310, pp. 295–310.
- Sargolzahi, Maryam et al. (2010). “Effectiveness of nondestructive testing for the evaluation of alkali-silica reaction in concrete”. In: *Construction and Building Materials* 24.8, pp. 1398–1403.
- Sausse, J and JP Fabre (2011). “Diagnosis of dams affected by swelling reactions: lessons learned from 150 monitored concrete dams in France”. In: *6th International Conference on Dam Engineering. Lisbon, Portugal*, pp. 156–157.
- Sbarigia, M, F Zinetti, and M Hernandez-Bagaglia (2016). “Slot Cutting of the Lago Colombo Dam, Affected by Swelling Deformation, to Bring the Behavior Back from Arch to Gravity”. In: *Conference on Italian Concrete Days*. Springer, pp. 496–511.

- Sbarigia, M. et al. (2013). “Slot Cutting Of The Lago Colombo Dam, Affected By Swelling Deformation, To Bring The Behaviour Back From Arch To Gravity”. In: *9th ICOLD European Club Symposium*.
- Scuero, A. and G. Vaschetti (2011). “Development of geomembrane systems for watertightness of dams in Europe”. In: *Dams and reservoirs under changing challenges*. Ed. by Anton J Schleiss and Robert M Boes. CRC press.
- Seignol, Jean François and Bruno Godart (2012). “A collective effort to propose practical guidance on the use of numerical models to re-assess AAR-affected structures”. In: *14th ICAAR-International Conference on Alkali-Aggregate Reaction*, 10p.
- Sellier, Alain et al. (2009). “Combination of structural monitoring and laboratory tests for assessment of alkali-aggregate reaction swelling: application to gate structure dam”. In: *ACI materials journal* 106.3, p. 281.
- Shayan, A, A Xu, and F Andrews-Phaedonos (2003). “Development of a performance measure for durability of concrete bridges”. In: *Proceedings of the 21st Biennial Conference, Concrete Institute of Australia, Brisbane. Concrete Institute of Australia, Sydney, NSW, Australia*, pp. 739–757.
- Shayan, Ahmad (2016). “Effects of alkali–aggregate reaction on concrete and structures”. In: *Proceedings of the institution of Civil Engineers-Construction Materials* 169.3, pp. 145–153.
- Shayan, Ahmad and Jack Grimstad (2006). “Deterioration of concrete in a hydroelectric concrete gravity dam and its characterisation”. In: *Cement and Concrete Research* 36.2, pp. 371–383.
- Siegert, D, S Multon, and F Toutlemonde (2005). “Resonant frequencies monitoring of alkali aggregate reaction (AAR) damaged concrete beams”. In: *Experimental Techniques* 29.6, pp. 37–40.
- Smaoui, N et al. (2005). “Effects of alkali addition on the mechanical properties and durability of concrete”. In: *Cement and concrete research* 35.2, pp. 203–212.
- Smaoui, Nizar et al. (2004a). “Evaluation of the expansion attained to date by concrete affected by alkali–silica reaction. Part I: Experimental study”. In: *Canadian Journal of Civil Engineering* 31.5, pp. 826–845.
- Smaoui, Nizar et al. (2004b). “Evaluation of the expansion attained to date by concrete affected by alkali silica reaction. Part II: Application to nonreinforced concrete specimens exposed outside”. In: *Canadian Journal of Civil Engineering* 31.6, pp. 997–1011.
- Smaoui, Nizar et al. (2004c). “Influence of specimen geometry, orientation of casting plane, and mode of concrete consolidation on expansion due to ASR”. In: *Cement, concrete and aggregates* 26.2, pp. 1–13.
- Stanton, Thomas E (2008). “Expansion of concrete through reaction between cement and aggregate”. In: *ASCE SP-249-1*.
- Steffens, Alexander, Kefei Li, and Olivier Coussy (2003). “Aging approach to water effect on alkali–silica reaction degradation of structures”. In: *Journal of engineering mechanics* 129.1, pp. 50–59.
- Swamy, R Narayan and WM Raymond Wan (1993). “Use of dynamic nondestructive test methods to monitor concrete deterioration due to alkali-silica reaction”. In: *Cement, Concrete and Aggregates* 15.1, pp. 39–49.
- Swamy, RN and MM Al-Asali (1986). “Influence of alkali-silica reaction on the engineering properties of concrete”. In: *Alkalies in concrete*. ASTM International.
- (1988). “Engineering properties of concrete affected by alkali-silica reaction”. In: *Materials Journal* 85.5, pp. 367–374.

- Takakura, Takeo et al. (2007). “Structural soundness for turbine-generator foundation affected by alkali-silica reaction and its maintenance plans”. In: *Proceedings of the 23rd Conference on Structural Mechanics in Reactor Technology (SMiRT19)*. IASMiRT.
- Talley, Kimberly G, Jacob G Kapitan, and John E Breen (2016). “Method for approximation of ASR/DEF damage in concrete columns”. In: *ACI Structural Journal* 113.1, p. 105.
- Tam, Vivian WY, Chi Ming Tam, and Khoa N Le (2007). “Removal of cement mortar remains from recycled aggregate using pre-soaking approaches”. In: *Resources, Conservation and Recycling* 50.1, pp. 82–101.
- Tcherner, Julia and T Aziz (2009). “Effects of AAR on seismic assessment of nuclear power plants for life extensions”. In: *Proceedings of the 20th International Conference on Structural Mechanics in Reactor Technology (SMiRT), Espoo, Finland*, pp. 9–14.
- Torii, Kazuyuki et al. (2016). “The Strengthening of an ASR-Affected Water Intake Tower in a Hydro-Electric Dam by Using Post-tensioned Tendons and the Long-term Monitoring of the Tower”. In: *Journal of Advanced Concrete Technology* 14.7, pp. 384–396.
- Ulm, Franz-Josef et al. (2000). “Thermo-chemo-mechanics of ASR expansion in concrete structures”. In: *Journal of engineering mechanics* 126.3, pp. 233–242.
- Wald, David, Gloriana Arrieta Martinez, and Oguzhan Bayrak (2017). “Expansion behavior of a biaxially reinforced concrete member affected by alkali-silica reaction”. In: *Structural Concrete* 18.4, pp. 550–560.
- Wald, David M et al. (2017). “Development and multiaxial distribution of expansions in reinforced concrete elements affected by alkali-silica reaction”. In: *Structural Concrete* 18.6, pp. 914–928.
- Wallau, Wilma et al. (2018). “Continuous expansion measurement in accelerated concrete prism testing for verifying ASR-expansion models”. In: *Materials and Structures* 51.3, p. 79.
- Wang, Jian and Hidenori Morikawa (2012). “Study on shear behavior of deteriorated RC beams due to alkali-silica reaction”. In: *37th Conference on our world in concrete & structures*.
- Washa, George W, Jesse C Saemann, and Steven M Cramer (1989). “Fifty-year properties of concrete made in 1937”. In: *Materials Journal* 86.4, pp. 367–371.
- Winnicki, Andrzej and Szymon Serkega (2017). “Alkali-Silica Reaction in concrete—numerical modelling: an engineering approach”. In: *2017 World Congress on Advances in Structural Engineering and Mechanics*.
- Yang, Huaquan, Pengxiang Li, and Meijuan Rao (2017). “Long term investigation and inhibition on alkali-aggregates reaction of Three Gorges Dam concrete”. In: *Construction and Building Materials* 151, pp. 673–681.
- Yoshimi, Isao et al. (2002). “Liberation of materials by electrical disintegration for recycling”. In: *International Journal of the Society of Materials Engineering for Resources* 10.1, pp. 66–70.
- Zhang, Chengzhi et al. (1999). “Influence of aggregate size and aggregate size grading on ASR expansion”. In: *Cement and concrete research* 29.9, pp. 1393–1396.